Malaria Bites and Quinoline Delights

The Discovery and Development of Novel

4-Aminoquinolines for use Against Multidrug-Resistant

Plasmodium falciparum.

Mason James Handford Ph.D.

2025-04-18

Ozzy

June 2010 – November 29th, 2025

To my steadfast and loyal companion of the last 14 years. You were there when I first met Alexandra, when I proposed, and the day we got married. You were there waiting at our home when we brought our son home from the hospital, for his first steps, and for his first words. You were a constant in my life. You did not understand or care that I got my doctorate, but I wish you were there with me the day I defended: for one last walk, for one last round of fetch, for you to rest your head in my lap one last time. You are so very missed.

"A dog does not live as long as a man and this natural law is the fount of many tears. If a boy and puppy might grow to manhood and doghood together, and together grow old, and so in due course die, full many a heartache might be avoided. But the world is not so ordered, and dogs will die and men will weep for them so long as there are dogs and men."

— Ben Ames Williams, *Bird Dog Book*, 1989

Table of Contents

Table of Contents 3
List of Tables 6
List of Figures 7
Acknowledgements 14
Foreword 15
Overview - Malaria in a Breath 16
What is Malaria? 16
What causes Malaria? 16
What cures Malaria? 17
1. Abstract 17
Part I. Introduction 18
2. Malaria - A Persistent Thorn 18
2.1. Malaria through Time 18
2.2. The “Malaria Hypothesis” and You 19
2.3. Eradication Evasion 19
3. A Bit About Bugs - Malaria Biology 20
3.1. Possessions and Bad Air 20
3.2. Plasmodium spp. Life Cycle 20
3.3. Human Infecting Plasmodium Species 23
4. From Cobwebs to Tree Bark - A History of Antimalarials 25
4.1. Barbaric Medicine 25
4.2. Quinine - Treating a Bite with a Bark 25
4.3. “Modern” Antimalarial Drugs 39
5. 4-Aminoquinolines - Successes, Failings, and Potentials 48
5.1. Historical Discovery 48
5.2. Targets, Troubling Resistance and Toxicology 52
5.3. Diversification over Abandonment 57
5.4. Bisquinolines 64
Part II. Results 67
6. Discovery of Amodiachins, a Novel Class of 4-Aminoquinoline Antimalarials Active Against Multidrug-Resistant Plasmodium falciparum. 67
6.1. Introduction 67
6.2. Chemistry 68

6.3. Results and Discussion 70
6.4. Summary and Concluding Remarks 82
7. Designing Novel Bisquinoline Antimalarials from Historical 4-Aminoquinolines to Combat Drug-Resistant Malaria 83
7.1. Introduction 83
7.2. Results and Discussion 84
7.3. Summary and Discussion 95
Part III. Conclusion 96
8. Conclusion 96
8.1. Summary 96
8.2. Contemplation 97
8.3. Future Work 98
8.4. Implications of Findings 99
References 100
Glossary 142
Part IV. Experimental Methods 145
9. Chemistry Methods 145
9.1. Materials and Methods of Chapter 6 145
9.2. Materials and Methods of Chapter 7 147
10. Biological Methods 148
10.0.1. Plasmodium falciparum Drug Sensitivity: 148
10.1. Methods used in Chapter 6 149
10.2. Methods used in Chapter 7 152
B. Malaria's many "chicken or the egg" 155
C. P. falciparum Antimalarial Resistance 157
D. Piperaquine Survival Assay 157
D.1. Methods 157
D.2. Results 158
D.3. Discussion 164
E. Synthetic Details of Presented Compounds 164
E.1. Synthetic details of Compounds presented in Chapter 6 164
E.2. Synthetic details of Compounds presented in Chapter 7 170
F. Chemical Characterization of Select Compounds 175
F.1. ^{1}H NMR of compounds presented in Chapter 6 175
F.2. ^{1}NMR of Compounds presented in Chapter 7 215

F.3. High Resolution Mass Spectrometry of Compounds presented in Chapter 6 238
F.4. High Resolution Mass Spectrometry of Compounds presented in Chapter 7 252
F.5. High Performance Liquid Chromatography of Select Compounds Presented in Chapter 6 261

List of Tables

Table 1: Human infecting Plasmodium species and key features. 24

Table 2: Antimalarial activity, cytotoxicity, and physicochemical properties of selected quinoline-based compounds. 72
Table 3: Markush structure and biological activity of select analogs 73
Table 4: Markush structure and biological activity of select analogs. 74
Table 5: Microsomal stability, parasite burden suppression, and in vivo efficacy of select amodiachins. 76
Table 6: R^5 analogs and associated activity against Pf D6 and Pf Dd2, cytotoxicity in HepG2 cells, and calculated CLogP values. 78
Table 7: Microsomal stability, parasite burden suppression, and in vivo efficacy of select amodiachins. 78
Table 8: Pharmacokinetic properties of compound 43 in male CD1 mice (n = 3) after an oral dose of 10 mg/kg and an intravenous dose of 0.5 mg/kg. 81
Table 9: Activity of bisquinolines against drug-sensitive Pf D6 and multidrug-resistant Pf Dd2 strains, cytotoxicity in HepG2 cells, and selectivity index. 88
Table 10: Activity against Pf D6 and Pf Dd2, cytotoxicity in HepG2 cells, and log selectivity index. Portrait format. 90
Table 11: Intrinsic Metabolic Stability and In Vivo Efficacy Against P. Yoelii Murine Malaria Model of Bisquinolines from Table 2.1. 91
Table 12: In vitro half-life (t1/2) determined from HPLC UV traces of drug after incubation with pooled murine liver microsomes. 92
Table 13: Pharmacokinetic properties of 69 in male CD1 mice (n = 3) after PO dose of 10 mg/kg and IV dose of 0.5 mg/kg. 94
Table 14: Detailed list of parasites used in this study and resistant/sensitive profile. 158
Table 15: IC50 and IC90 shift of PfCRT mutants against PPQ. 160
Table 16: IC50 and IC90 shift of PfCRT mutants against 54. 161
Table 17: IC50 and IC90 shifts of P. falciparum PfCRT mutants against 69. 162
Table 18: IC50 and IC90 values and shifts for P. falciparum PfCRT mutants against 70. 163

List of Figures

Figure 1: Illustration of the lifecycle of human Plasmodium spp. including the three stages. 21
Figure 2: Light microscopy images of Giemsa-stained Plasmodium falciparum Dd2 parasites during erythrocytic lifecycle stages. 22
Figure 3: Examples and illustrations of the quinine containing cinchona bush. 26
Figure 4: Oil paintings (1930) of frescos in the Ospedale di Santo Spirito in Sassia, Rome. 27
Figure 5: Historical evidence of Jesuit Priest's knowledge of cinchona bark in 17th century. 28
Figure 6: Structures of antimalarial cinchona alkaloids. 29
Figure 7: Ad for quinine bisulfate tablets found in "The prevention of malaria" by Sir Ronald Ross, 1910. 30
Figure 8: Markush structure of the four related compounds that make up the dye mauve. 31
Figure 9: Scheme 1: Woodward-Doering/Rabe-Kinder synthesis of quinine. 32
Figure 10: Structures of quinine analogs that demonstrate vinyl group modifications can exhibit a range of perturbations to antiplasmodial activity and beta-hematin formation inhibition. 33
Figure 11: Structures of quinine analogs that demonstrate alcohol group modifications can exhibit a range of perturbations to antiplasmodial activity and beta-hematin formation inhibition. 35
Figure 12: Structures of quinine analogs that demonstrate quinoline, quinuclidine, and stereochemical modifications can exhibit a range of perturbations to antiplasmodial activity and beta-hematin formation inhibition. 37
Figure 13: Structure of quinoline ring with numbering pattern. 40
Figure 14: Structures of 4-aminoquinolines derived from quinine. 40
Figure 15: Structures of 8-aminoquinolines. 41
Figure 16: Chemical structures of 4-methanolquinoline antimalarials. 42
Figure 17: Chemical structures of the arylamino-alcohol antimalarials. 43
Figure 18: Chemical structures of the acridine-related antimalarials. 44
Figure 19: Structures of antifolate antimalarials. 44
Figure 20: Structures of the some naphthoquinone antimalarials. 45
Figure 21: Structures of the antibiotic antimalarials recognized by the World Health Organization. 46
Figure 22: Structures of the antimalarial artemisinin and artemisinin derivatives currently used in artemisinin combination therapies. 47
Figure 23: Structures of antimalarials that are in or have been in Medicines for Malaria Venture's pipeline. 48
Figure 24: 4-Aminoquinoline Core. 48
Figure 25: A portrait of German chemist John (Hans) Andersag (1902–1955). 49
Figure 26: Structure of the cresol pharmacophore that exhibited antiplasmodial activity described in Burckhalter et al., (1946). 51
Figure 27: Structure of piperaquine created by Rhône-Poulenc and rediscovered during Project 533. 51
Figure 28: Hemozoin: the crystalline structure and arrangement of heme monomers in hematin and hemozoin. 54
Figure 29: Structure of possible amodiaquine oxidation product, a reactive quinone imine. 56

Figure 30: Compounds that illustrate SAR studies of the quinoline core scaffold hopping of 4-aminoquinoline and amodiaquine-analog antimalarials. 58
Figure 31: Structures of compounds that illustrate SAR studies of 4-aminoquinoline substituent pattern of amodiaquine and amodiaquine-analog antimalarials. 59
Figure 32: Structures of compounds that illustrate SAR studies of the Mannich base of amodiaquine and amodiaquine-analog antimalarials. 60
Figure 33: Structures of compounds that illustrate SAR studies of the Mannich base of amodiaquine and amodiaquine-analog antimalarials, continued. 61
Figure 34: Compounds that illustrate SAR studies of the para-hydroxyl group of amodiaquine and amodiaquine-analog antimalarials. 62
Figure 35: Compounds that illustrate SAR studies of the para-hydroxyl group of amodiaquine and amodiaquine-analog antimalarials. 63
Figure 36: Compounds that illustrate SAR studies of the para-hydroxyl group of amodiaquine and amodiaquine-analog antimalarials. 64
Figure 37: Compounds that illustrate SAR studies of bisquinoline antimalarials. 65
Figure 38: Compounds that illustrate SAR studies of bisquinoline antimalarials, continued. 66
Figure 39: Chemical structures of the antimalarials quinine and select 4-aminoquinolines. 67
Figure 40: Synthesis of initially designed amodiachins. Reagents and conditions. 69
Figure 41: Synthesis of initially designed amodiachins. Reagents and conditions. 69
Figure 42: Synthesis of compounds to explore the contribution of substituents around benzenoid ring of the quinoline core. 70
Figure 43: Synthesis of amodiachins that explored the contribution of the heterocycle. 71
Figure 44: Markush structure (above) of select analogs and associated antiplasmodial activity against PfD6 and PfDd2 and cytotoxicity in HepG2 mammalian cells. 71
Figure 45: Markush structure (above) of select analogs and associated antiplasmodial activity against Pf D6 and Pf Dd2 and cytotoxicity. 74
Figure 46: Markush Structure of Selected Antiplasmodial Analogs. 75
Figure 47: Compound activity and physicochemical properties. 76
Figure 48: Markush Structure of R^5-Substituted Antiplasmodial Analogs. 77
Figure 49: Mean plasma concentration-time profiles of 43 after IV dose at 0.5 mg/kg and PO dose at 10 mg/kg in male CD1 mice(n=3). 80
Figure 50: 43 versus P. yoelii growth suppression mouse malaria model described in Table 1.6. 81
Figure 51: Structural representations of 4-aminoquinoline antimalarials. 84
Figure 52: Structure of 43 (ADC-028) with structural variations of interest and Markush structure of bisquinoline designs. 84
Figure 53: Structure of 43 (ADC-028) with structural variations of interest and Markush structure of bisquinoline designs. 85
Figure 54: Scheme 6. Synthetic scheme used to generate compounds 51-58. 85
Figure 55: Scheme 7: Synthetic scheme used to generate compounds 60-61. 86
Figure 56: Compound 43 with the 7-chloro-N-phenylquinolin-4-amine core highlighted in blue. 86
Figure 57: Scheme 8: Synthetic scheme used to generate compounds 67-72. 87
Figure 58: Markush Structure of R^6- and R^7-Substituted Analogs. 89
Figure 59: Mean plasma concentration-time profiles of 69 after IV dose at 0.5 mg/kg and PO dose at 10 mg/kg in male CD1 mice(n=3). 93

Figure 60: Comparative IC50 of piperaquine (PPQ) against Dd2-B2, RF12, 3D7 Dd2_GC03, Dd2_PfCRT_F145I, Dd2_PfCRT_T93S, and Dd2_Dd2. IC50s for each line are presented as means ± SEMs (N, n = 2-3,2). 159
Figure 61: Combined average percent inhibition of Dd2-B2, RF12, 3D7, Dd2_GC03, Dd2_PfCRT_F145I, Dd2_PfCRT_T93S, and Dd2_Dd2 when treated with piperaquine (PPQ) on a log10 scale. 159
Figure 62: Comparative IC50 of 11 against Dd2-B2, RF12, 3D7 Dd2_GC03, Dd2_PfCRT_F145I, Dd2_PfCRT_T93S, and Dd2_Dd2. IC50s for each line are presented as means ± SEMs (N, n = 2-3,2). 160
Figure 63: Percent parasite survival against 54 (N,n = 1-4,2). 161
Figure 64: Comparative IC50 of 69 against Dd2-B2, RF12, 3D7 Dd2_GC03, Dd2_PfCRT_F145I, Dd2_PfCRT_T93S, and Dd2_Dd2. IC50s for each line are presented as means ± SEMs (N, n = 2-3,2). 162
Figure 65: Percent parasite survival against 69 (N,n = 1-4,2). Evidence of increased parasite survival against 69 is seen in RF12 and Dd2_PfCRT_F145I, both piperaquine-resistant parasites. 162
Figure 66: Comparative IC50 of 70 against Dd2-B2, RF12, 3D7 Dd2_GC03, Dd2_PfCRT_F145I, Dd2_PfCRT_T93S, and Dd2_Dd2. 163
Figure 67: 1H NMR spectra of 7. 175
Figure 68: 1H NMR spectra of 8. 176
Figure 69: ^{1}H NMR spectra of 10a. 177
Figure 70: ^{1}H NMR spectra of 10b. 178
Figure 71: ^{1}H NMR spectra of 10c. 179
Figure 72: ^{1}H NMR spectra of 11a. 180
Figure 73: ^{1}H NMR spectra of 11b. 181
Figure 74: ^{1}H NMR spectra of 11c. 182
Figure 75: ^{1}H NMR spectra of 12. 183
Figure 76: ^{1}H NMR spectra of 13. 184
Figure 77: ^{1}H NMR spectra of 14. 185
Figure 78: ^{1}H NMR spectra of 15. 186
Figure 79: ^{1}H NMR spectra of 16. 187
Figure 80: ^{1}H NMR spectra of 17. 188
Figure 81: ^{1}H NMR spectra of 20. 189
Figure 82: ^{1}H NMR spectra of 21. 190
Figure 83: ^{1}H NMR spectra of 22. 191
Figure 84: ^{1}H NMR spectra of 23. 192
Figure 85: ^{1}H NMR spectra of 24. 193
Figure 86: ^{1}H NMR spectra of 25. 194
Figure 87: ^{1}H NMR spectra of 26. 195
Figure 88: ^{1}H NMR spectra of 29a. 196
Figure 89: ^{1}H NMR spectra of 29b. 197
Figure 90: ^{1}H NMR spectra of 30a. 198
Figure 91: ^{1}H NMR spectra of 30b. 199
Figure 92: ^{1}H NMR spectra of 31. 200
Figure 93: ^{1}H NMR spectra of 32. 201
Figure 94: ^{1}H NMR spectra of 33. 202

Figure 95: ^{1}H NMR spectra of 34. 203
Figure 96: ^{1}H NMR spectra of 35. 204
Figure 97: ^{1}H NMR spectra of 36. 205
Figure 98: ^{1}H NMR spectra of 37. 206
Figure 99: ^{1}H NMR spectra of 38. 207
Figure 100: ^{1}H NMR spectra of 39. 208
Figure 101: ^{1}H NMR spectra of 40. 209
Figure 102: ^{1}H NMR spectra of 41. 210
Figure 103: ^{1}H NMR spectra of 42. 211
Figure 104: ^{1}H NMR spectra of 43. 212
Figure 105: ^{1}H NMR spectra of 44. 213
Figure 106: ^{1}H NMR spectra of 45. 214
Figure 107: ^{1}H NMR spectra of 50. 215
Figure 108: ^{1}H NMR spectra of 51. 216
Figure 109: ^{1}H NMR spectra of 52. 217
Figure 110: ^{1}H NMR spectra of 53. 218
Figure 111: ^{1}H NMR spectra of 54. 219
Figure 112: ^{1}H NMR spectra of 55. 220
Figure 113: ^{1}H NMR spectra of 56. 221
Figure 114: ^{1}H NMR spectra of 57. 222
Figure 115: ^{1}H NMR spectra of 58. 223
Figure 116: ^{1}H NMR spectra of 60. 224
Figure 117: ^{1}H NMR spectra of 61. 225
Figure 118: ^{1}H NMR spectra of 64a. 226
Figure 119: ^{1}H NMR spectra of 64b. 227
Figure 120: ^{1}H NMR spectra of 64c. 228
Figure 121: ^{1}H NMR spectra of 65a. 229
Figure 122: ^{1}H NMR spectra of 65b. 230
Figure 123: ^{1}H NMR spectra of 65c. 231
Figure 124: ^{1}H NMR spectra of 67. 232
Figure 125: ^{1}H NMR spectra of 68. 233
Figure 126: ^{1}H NMR spectra of 69. 234
Figure 127: ^{1}H NMR spectra of 70. 235
Figure 128: ^{1}H NMR spectra of 71. 236
Figure 129:^{1}H NMR spectra of 72. 237
Figure 130: HRMS trace of 7. High Resolution Mass Spectrometry using (ESI): actual m/z M + H (top) over expected m/z M + H (bottom). 238
Figure 131: HRMS trace of 8. High Resolution Mass Spectrometry using (ESI): actual m/z M + H (top) over expected m/z M + H (bottom). 238
Figure 132: HRMS trace of 12. High Resolution Mass Spectrometry using (ESI): actual m/z M + H (top) over expected m/z M + H (bottom). 239
Figure 133: HRMS trace of 13. High Resolution Mass Spectrometry using (ESI): actual m/z M + H (top) over expected m/z M + H (bottom). 239
Figure 134: HRMS trace of 14. High Resolution Mass Spectrometry using (ESI): actual m/z M + H (top) over expected m/z M + H (bottom). 240

Figure 135: HRMS trace of 15. High Resolution Mass Spectrometry using (ESI): actual m/z M + H (top) over expected m/z M + H (bottom). 240
Figure 136: HRMS trace of 16. High Resolution Mass Spectrometry using (ESI): actual m/z M + H (top) over expected m/z M + H (bottom). 241
Figure 137: HRMS trace of 17. High Resolution Mass Spectrometry using (ESI): actual m/z M + H (top) over expected m/z M + H (bottom). 241
Figure 138: HRMS trace of 20. High Resolution Mass Spectrometry using (ESI): actual m/z M + H (top) over expected m/z M + H (bottom). 242
Figure 139: HRMS trace of 21. High Resolution Mass Spectrometry using (ESI): actual m/z M + H (top) over expected m/z M + H (bottom). 242
Figure 140: HRMS trace of 22. High Resolution Mass Spectrometry using (ESI): actual m/z M + H (top) over expected m/z M + H (bottom). 243
Figure 141: HRMS trace of 23. High Resolution Mass Spectrometry using (ESI): actual m/z M + H (top) over expected m/z M + H (bottom). 243
Figure 142: HRMS trace of 24. High Resolution Mass Spectrometry using (ESI): actual m/z M + H (top) over expected m/z M + H (bottom). 244
Figure 143: HRMS trace of 25. High Resolution Mass Spectrometry using (ESI): actual m/z M + H (top) over expected m/z M + H (bottom). 244
Figure 144: HRMS trace of 26. High Resolution Mass Spectrometry using (ESI): actual m/z M + H (top) over expected m/z M + H (bottom). 245
Figure 145: HRMS trace of 31. High Resolution Mass Spectrometry using (ESI): actual m/z M + H (top) over expected m/z M + H (bottom). 245
Figure 146: HRMS trace of 32. High Resolution Mass Spectrometry using (ESI): actual m/z M + H (top) over expected m/z M + H (bottom). 246
Figure 147: HRMS trace of 33. High Resolution Mass Spectrometry using (ESI): actual m/z M + H (top) over expected m/z M + H (bottom). 246
Figure 148: HRMS trace of 34. High Resolution Mass Spectrometry using (ESI): actual m/z M + H (top) over expected m/z M + H (bottom). 247
Figure 149: HRMS trace of 35. High Resolution Mass Spectrometry using (ESI): actual m/z M + H (top) over expected m/z M + H (bottom). 247
Figure 150: HRMS trace of 36. High Resolution Mass Spectrometry using (ESI): actual m/z M + H (top) over expected m/z M + H (bottom). 248
Figure 151: HRMS trace of 38. High Resolution Mass Spectrometry using (ESI): actual m/z M + H (top) over expected m/z M + H (bottom). 248
Figure 152: HRMS trace of 39. High Resolution Mass Spectrometry using (ESI): actual m/z M + H (top) over expected m/z M + H (bottom). 249
Figure 153: HRMS trace of 40. High Resolution Mass Spectrometry using (ESI): actual m/z M + H (top) over expected m/z M + H (bottom). 249
Figure 154: HRMS trace of 41. High Resolution Mass Spectrometry using (ESI): actual m/z M + H (top) over expected m/z M + H (bottom). 250
Figure 155: HRMS trace of 42. High Resolution Mass Spectrometry using (ESI): actual m/z M + H (top) over expected m/z M + H (bottom). 250
Figure 156: HRMS trace of 43. High Resolution Mass Spectrometry using (ESI): actual m/z M + H (top) over expected m/z M + H (bottom). 251
Figure 157: HRMS trace of 44. High Resolution Mass Spectrometry using (ESI): actual m/z M + H (top) over expected m/z M + H (bottom). 251

Figure 158: HRMS trace of 45. High Resolution Mass Spectrometry using (ESI): actual m/z M + H (top) over expected m/z M + H (bottom). 252
Figure 159: HRAM/MS Chromatogram of 51. High Resolution Accurate Mass/Mass Spectrometry using positive mode ESI: [M+H]+ of [C30H20Cl2N4] = 507.11377 amu (top); observed = 507.11375 amu (bottom). 252
Figure 160: HRAM/MS Chromatogram of *52**. High Resolution Accurate Mass/Mass Spectrometry using positive mode ESI: [M+H]+ of [C30H18Cl2F2N4] = 543.09493 amu (top); observed = 543.09516 (bottom). 253
Figure 161: HRAM/MS Chromatogram of 53. High Resolution Accurate Mass/Mass Spectrometry using positive mode ESI: [M+H]+ of [C31H22Cl2N4] = 521.12942 amu (top); observed = 521.12947 (bottom). 253
Figure 162: HRAM/MS Chromatogram of 54. High Resolution Accurate Mass/Mass Spectrometry using positive mode ESI: [M+H]+ of [C30H21Cl2N5] = 522.12467 amu (top); observed = 522.12476 (bottom). 254
Figure 163: HRAM/MS Chromatogram of 55. High Resolution Accurate Mass/Mass Spectrometry using negative mode ESI: [M-H]- of [C30H20Cl2N4O] = 521.09304 amu (top); observed = 521.09434 amu (bottom). 254
Figure 164: HRAM/MS Chromatogram of 56. High Resolution Accurate Mass/Mass Spectrometry using negaitive mode ESI: [M-H]- of [C33H26Cl2N4] = 547.14507 amu (top); observed = 547.14650 (bottom). 255
Figure 165: HRAM/MS Chromatogram of 57. High Resolution Accurate Mass/Mass Spectrometry using positive mode ESI: [M+H]+ of [C30H19Cl2N5] = 520.10907 amu (top); observed = 520.10907 amu (bottom). 255
Figure 166: HRAM/MS Chromatogram of 58. High Resolution Accurate Mass/Mass Spectrometry using positive mode ESI: [M+H]+ of [C32H18Cl2F6N4O] = 659.08375 amu (top); observed = 659.08375 amu (bottom). 256
Figure 167: HRAM/MS Chromatogram of 60. High Resolution Accurate Mass/Mass Spectrometry using positive mode ESI: [M+H]+ of [C28H28Cl2N4] = 491.17637 amu (top); observed = 491.17673 amu (bottom). 256
Figure 168: HRAM/MS Chromatogram of 61. High Resolution Accurate Mass/Mass Spectrometry using positive mode ESI: [M+H]+ of [C31H34Cl2N4] = 533.22332 amu (top); observed = 533.22325 amu (bottom). 257
Figure 169: HRAM/MS Chromatogram of 67. High Resolution Accurate Mass/Mass Spectrometry using positive mode ESI: [M+H]+ of [C25H22Cl2N4] = 449.12942 amu (top); observed = 449.12952 amu (bottom). 257
Figure 170: HRAM/MS Chromatogram of 68. High Resolution Accurate Mass/Mass Spectrometry using positive mode ESI: [M+H]+ of [C29H25ClN4] = 465.18405 amu (top); observed = 465.18392 amu (bottom). 258
Figure 171: HRAM/MS Chromatogram of 69. High Resolution Accurate Mass/Mass Spectrometry using negative mode ESI: [M-H]- of [C29H24Cl2N4] = 497.12942 amu (top); observed = 497.13077 amu (bottom). 258
Figure 172: HRAM/MS Chromatogram of 70. High Resolution Accurate Mass/Mass Spectrometry using positive mode ESI: [M+H]+ of [C28H23Cl2N5] = 500.14032 amu (top); observed = 500.14042 amu (bottom). 259

Figure 173: HRAM/MS Chromatogram of 71. High Resolution Accurate Mass/Mass Spectrometry using positive mode ESI: [M+H]+ of [C29H25ClN4] = 465.18405 amu (top); observed = 465.18410 amu (bottom). 259
Figure 174: HRAM/MS Chromatogram of 72. High Resolution Accurate Mass/Mass Spectrometry using positive mode ESI: [M+H]+ of [C29H26N4] = 431.22302 amu (top); observed = 431.22282 amu (bottom). 260
Figure 175: HPLC trace spectra of 17. 261
Figure 176: HPLC trace spectra of 20. 262
Figure 177: HPLC trace spectra of 31. 263
Figure 178: HPLC trace spectra of 35. 264
Figure 179: HPLC trace spectra of 40. 265
Figure 180: HPLC trace spectra of 41. 266
Figure 181: HPLC trace spectra of 42. 267
Figure 182: HPLC trace spectra of 43. 268
Figure 183: HPLC trace spectra of 44. 269
Figure 184: HPLC trace spectra of 45. 270

Acknowledgements

Despite the lone servitude one toils away at under the demanding authority of a dissertation, the journey to arrive at this point is not a solitary one. I have been aided by the helpful hands, strong backs, kind words, and the wisdom of countless people, and without them I would not be here today. I have been fortunate enough to have met many wonderful people that have been willing to share their lives with me and guide me as I find my way through life. As much as they deserve to be immortalized in this thesis for their contributions, no matter how small, I believe it would be impossible to list every single person or every moment that guided me to the present. But I do want to pay my respects to the people who, without a shadow of a doubt, are responsible for conning me into believing a Ph.D. was a good idea.

Alexandra, you are the reason I stuck with this for as long as I did. I loathe a cliché, but you have been my rock for the last decade. You are an amazingly passionate and intelligent person, and I am so incredibly thankful to have you in my life. Your grit, determination, and integrity have inspired me to become a better person. I will forever be grateful for the grace you have given me these last several years. You have been an amazing source of inspiration for this monstrosity, and its most outspoken critic too. I cannot wait to spend the rest of my life laughing together.

Mom and Dad, you had me. That is not all I have to say on the matter of course, but that is undeniably the biggest reason I am here today. Both of you have shown me what hard work, determination, and patience are. Not through lectures, but through actions. Watching you two working a back-breaking job to support your family, and going back to school to pursue a better career, was the most inspiring thing I have ever seen. Your support and love have given me the courage to pursue this crazy dream. Thank you for everything.

Mike, I have been incredibly fortunate to have had you as my Ph.D. mentor. On a personal level, you have always been a calm, genuine, and warm person. Time and time again, I have seen you approach adversity with thoughtfulness, empathy, and kindness. In the six and a half years I have known you, I have heard you raise your voice and curse only once, and that was because the accounting office was making it difficult for you to pay the team. On a more professional level, you have always been a fierce advocate for me as a student and as a person with a life. You are a determined and driven scientist, and I hope that, having been a member of your lab, some of it has rubbed off on me. You have taught me to be confident in my own projects and ideas, and to not be afraid to pursue them.

Aaron Nilsen, you have been a gem of a mentor. I am so incredibly grateful that you always found the time to talk to me about my science, career, and my personal life. The countless times I was able to sit in on you and Mike talking shop, and later as I became a more competent chemist, joining in those conversations myself, was pivotal for my confidence as a scientist. Thank you for putting up with my messy bench and hood. I know you always said you didn't mind and that a messy hood meant I was working, but it was often quite a mess. To Rosie Dodean, Rolf Winter, Sovitj Pou, and Katherine Liebman, it has been a joy to work alongside you. The industrious labor you poured into your work has been inspiring to watch. Thank you for making me feel welcome and a part of the team.

Terry, you were such a kind and patient teacher. Without you and Yuexin, and later Wei, I would have never been able to publish. Thank you for all the work you did to help me finish. Hopefully, you were able to look past all of the times I needed a refresher on parasite culture.

To Jane, Xin, and Wei, I could not have finished my Ph.D. without your help in testing my compounds. Thank you for always finding the time to run experiments for me and translating patents. A special thanks to Jane for being another foodie in the lab, inviting me to eat at such wonderful places, and serving as a reader for my dissertation.

To the friends I have made during my time in Portland: Greg, Sarah, Omar, Katie, Sierra, Belin, Teresa, Erin, Victoria, Dan, Katy, Lindsey, and Rich, thank you so much for the wonderful memories. Pedalpalooza rides, Gin and No Juice meetups, pool, hosting dinners, and the joy of casually finding each other around town will be something I cherish forever.
Rich, I haven't yet decided if I either hate or love you for convincing me to write my dissertation using Quarto.

To my Dissertation Committee Members: Carsten Schultz, Scott Landfear, Michael Cohen, and Stone Doggett. I want to thank you for taking the time out of your schedules to meet with a trainee several times a year. Your advice, knowledge, and oversight have steered this project to what it has become. I offer my condolences to your free time these next two weeks as you read this dissertation. Thank you, Scott, for serving as my chair. A special thank you to Carsten, for being instrumental in allowing me to move to Portland. For that, I owe you immensely.

And last, and certainly least of all, to Chris and Colt. You two are just the worst.

Foreword

Dissemination of newly acquired knowledge is a fundamental principle of academia. Unfortunately, that knowledge is often packaged in a highly technical and precise language; saturated with scientific jargon, burdened by *far* too many acronyms, and written in a style that can seem almost pay-by-the-letter. All too often, the result is a dense, utilitarian prose that offers a cold and alienating experience to a casually interested reader.

With that in mind, I intend to make full use of the rare privilege afforded by writing a dissertation. To use a voice that is unencumbered by the stylistic conventions of scientific journals or grant proposals, and instead write in one that feels comfortable to me. In this way, I hope that you enjoy the narrative I have forged for you, the reader. One that will hopefully feel less like an education, and more like an informative conversation with an oddly passionate, and perhaps at times long-winded, stranger. A conversation that could be enjoyed while sipping on a well-made libation.

Hopefully.

Overview - Malaria in a Breath

To attempt to provide a full account of malaria evolution, its effects on humanity, and the progress we have made in understanding this disease would truly be a Herculean undertaking. One that is very much outside the purview of a dissertation - unless the sole purpose of the Ph.D. was to compile it in its entirety. Even so, I hope to guide you on the well-trodden path of what is necessary for understanding this work and why it was undertaken. I may have also planned a few detours along the way to share what I believe to be some of the more interesting and profound aspects of this disease and its relationship with us. Despite having a clear destination, the journey that I have planned is not a short one.

This dissertation spans not only 150 years of scientific research, but also the lore of malaria from antiquity and conjecture regarding events millions of years ago. It attempts to unravel some of the interplay of malaria and humanity. A discussion of seminal discoveries of disease function to the choices made in eradication efforts and treatment development. A tapestry that blends both the history of the disease itself and the history of our attempts to understand and control it. Rather than treating these threads separately, as I have in the introduction, I present a brief overview that weaves them together without becoming burdened by the full extent of either. All topics introduced here are discussed in further detail in the chapters that follow. The effect that malaria has on humanity is discussed in Chapter 2, and later its biology is explored in Chapter 3. Efforts made towards eradication are explored in Chapter 4, with a particular emphasis placed on the 4-aminoquinoline class of drugs in Chapter 5.

What is Malaria?

Malaria is a mosquito-borne illness that affects millions of people each year across the globe. Human-borne malaria is caused by five species of the *Plasmodium* parasite: *P. falciparum*, *P. vivax*, *P. ovale*, *P. malariae*, and *P. knowlesi*. *P. falciparum* is the deadliest and most prolific species, accounting for the vast majority of malaria cases and deaths.

What causes Malaria?

The disease is caused by a microscopic parasite that travels from the mosquito to humans and back again. Early in its jump to humans, the parasite will hide out in our liver cells so that it can replicate. Soon after becoming many parasites, they leave the liver to invade and infect our red blood cells. While in the cell, a lone parasite will scavenge most of the nutrients it needs to grow from breaking down hemoglobin, a protein that carries oxygen from your lungs to the rest of your body. As the parasite consumes the cell's contents, it will grow and eventually split into 10 to 20 individual parasites while still inside the infected cell. The increase in size will cause the red blood cell to rupture, spilling out parasites that will go on to infect other red blood cells. The cycle of infection and replication leads to the disease's characteristic periodic symptoms of chills, fever, and headaches. The disease can progress to more severe symptoms, including impaired consciousness, severe anemia, and organ dysfunction that may lead to death. Without timely intervention, the parasite can be ingested by another mosquito. Once inside the gut, the parasite will infect the mosquito, mature, and soon become able to infect another human.

What cures Malaria?

Quinine is the first antimalarial ever discovered and was found in cinchona tree bark. The exact date of its discovery has been lost to time, but it is thought to have been sometime prior to the 16th century, somewhere in today's Peru. Quinine was used heavily into the beginning of the 20th century, where it ignited the search for synthetic antimalarials. Today, there are more than 20 different antimalarials that are used to treat the illness.

One class of antimalarial drugs all shares a 4-aminoquinoline chemical core, and within the class, the most successful drugs are chloroquine, amodiaquine, and piperaquine. But the rise and spread of resistance to these drugs, and many others, threatens progress made towards global eradication of malaria. One way to slow this spread and take back what we have lost is the development of new antimalarials.

One such method of development is starting from an existing drug and systematically making small modifications to its chemical structure. These small changes are often made to improve the parent drug, often by eliminating liabilities or improving its shortcomings. To this end, this thesis describes the development of amodiaquine-like antimalarials that attempt to accomplish just that.

1. Abstract

A structure-activity relationship study was conducted to optimize metabolic stability and *in vivo* activity of amodiaquine analog antimalarials. The antiplasmodial activity of synthesized amodiachins (ADCs) was evaluated against drug-sensitive and drug-resistant strains of *Plasmodium falciparum*. Select compounds were tested in *Plasmodium yoelli* murine models. Structural modifications, including introduction of a piperidine ring and varied N-alkyl substitutions, enhanced antiparasitic activity, metabolic stability, and *in vivo* efficacy. Compound **43** (ADC-028) emerged as a standout candidate, exhibiting nanomolar activity against drug-sensitive and multidrug-resistant *P. falciparum*, minimal cytotoxicity, and favorable murine microsomal stability ($t_{1/2}$ = 48.2 min). *In vivo,* **43** achieved a non-recrudescence dose at 16 mg/kg/d and a single dose cure at 50 mg/kg. Pharmacokinetic analysis of **43** showed excellent metabolic stability ($T_{1/2}$ = 84 h) and oral bioavailability (F = 76%). This study identifies **43** as a potential candidate for further evaluation as a novel compound to overcome drug-resistant malaria. The development of **43** prompted the investigation of bisquinoline analogs featuring similar structural motifs. A follow-up structure-activity relationship study was performed guided by key chemical components of compound **43**, including the 4-anilinoquinoline core and diverse bridging linkers. Several analogs exhibited potent *in vitro* activity (IC_{50} < 20 nM) against both drug-sensitive and multidrug-resistant *P. falciparum* strains, while maintaining favorable cytotoxicity profiles. Among them, **69** demonstrated improved intrinsic metabolic stability ($t_{1/2}$ = 121 min) and potent *in vivo* efficacy (ED_{50} = 0.32 mg/kg/day), achieving complete curative protection at a reduced dose compared to ADC-028. While **69** showed moderately reduced oral bioavailability (F = 43%) and a shorter half-life ($T_{1/2}$ = 27.2 h) relative to **43**, its enhanced *in vivo* efficacy underscores its therapeutic potential. This work highlights a promising path forward in developing antimalarials that retain the efficacy of legacy compounds while overcoming modern resistance mechanisms.

Part I. Introduction

2. Malaria - A Persistent Thorn

Imagine for a moment that you are a bird.

Yes, a bird. But not the small, winged kind, that chirp in trees and soar in the sky. Not just any bird—but *the* bird. The kind that didn't have a beak, but a gaping maw full of terrible teeth. One that doesn't soar, but tramples as you stalk your prey. That kind of bird. A prehistoric apex predator.

A dinosaur.

And imagine further that you, as deadly as you are, are dying. From what, you might ask? A meteor? A bigger, *badder* dinosaur? Or comically trapped in a tar pit, like something you expect to find in the 1981 film "Caveman"? No. You, a top-of-the-food-chain predator, a 20-foot-tall killing machine, are dying from a bug bite.

A *bug bite*?

But that is ridiculous; you are a titan! I am talking about a massive prehistoric terror. How could a single mosquito bite possibly matter? You've got hundreds of gallons of blood—what's a few drops taken by a tiny *bug* to you?

No, what is killing you is much smaller than that bug. Hidden inside that bite was a microscopic killer. A tiny parasite that has smuggled itself inside of you, hijacked your organs, and is playing peakaboo in your body.
One that is multiplying at an exponential rate, greedily consuming the nutrients that keep you alive with reckless abandon. Fevers batter you in ever more intense, relentless waves. You are beginning to feel weak.

Dizzy. Nauseous. You stumble and collapse, unable to get back up. Your vision fades as you fall into a coma you won't be waking up from. You are dying—from malaria.

2.1. Malaria through Time

While this may sound strange, it casts a light on a striking reality: malaria is ancient–far older than human history, before the extinction of the dinosaurs, and even possibly predating the evolution of mammals. One of the most fascinating aspects of malaria is just how *mind-bendingly* ancient it is. The oldest fossil record of malaria dates to about 15 to 45 million years ago, found in a prehistoric mosquito encapsulated in amber. But it is speculated that the *Plasmodium* clade diverged from its apicomplexan ancestor sometime during the Jurassic period, approximately 150 million years ago, following the radiation of lizards, mammals, and birds across the globe during the Triassic Period (190-225 million years ago).

So, yes, malaria has been around for a very *very* long time; that much we can agree on. But as to when and how the parasite made the jump to humans, we are still waiting to reach a consensus.[1] Some of the earliest indications that we have long been affected by malaria comes from fossil records. Paleopathological literature considers cribra orbitalia and porotic hyperostosis found in skeletal remains as possible indicators of severe malaria anemia.[2] But a considerable amount of

skepticism ought to be applied in those cases, as these skeletal malformations are not pathognomonic of malaria. More modern studies of *Plasmodium* genomes indicates that malaria was evident in humans as early as the fourth millennia BCE. But the oldest physical evidence is 5000 year old mummies that were found to be carrying *P. falciparum* antigens. There are several historical texts, like Vedic (3,500 - 2,800 years ago) scriptures from India, that mention fevers which may be malaria, but it isn't until texts attributed to the Greek philosopher Hippocrates (460 - 377 BCE) that the descriptions of persistent periodic fevers actually appear.

2.2. The "Malaria Hypothesis" and You

Despite our inability to pinpoint when malaria began to infect humans, there is strong evidence that it has exerted strong evolutionary pressure on the human genome. In the first half of the 20th century, the famous population geneticist J. B. S. Haldane put forth the "Malaria Hypothesis". In essence, it is the idea that selection pressure of malaria is responsible for the high frequency of harmful mutations in the human genome. In Haldane's case, he was speaking specifically about thalassemia, but since then it has been proven that a number of harmful variations in the human genome offer some level of protection from malaria infection in populations originating from highly endemic areas of malaria. These genetic polymorphisms are largely found within red blood cells and, depending on if the mutations are heterozygous or homozygous, can be clinically silent to extremely harmful. Thalassemia is a disease caused by either deletion of the α-globin alleles or mutations in the β-globin gene, causing red blood cells to not function properly. Another group of mutations in β-globin results in the formation of sickle hemoglobin, which results in hemoglobin malformation and anemia. Other protective polymorphisms include glucose-6-phosphate dehydrogenase (G6PD) deficiency, O-type blood, variants of the gene for complement receptor 1, and the absence of the Duffy antigen are all found in exceptionally high frequency in populations from malaria-endemic areas.
These genetic variations are often a double edge sword, offering some type of protective mechanism against the disease but often at a cost.

2.3. Eradication Evasion

Despite thousands of years of exposure and partial genomic protections, malaria continues to cause significant human morbidity and mortality worldwide. For the last 26 years, the World Health Organization has compiled an annual report containing reports, data, and trends of global progress towards malaria elimination. In the World Malaria Report (2025), there were an estimated 282 million cases of malaria and 610,000 deaths worldwide in 2024. Among the 82 countries reporting malaria cases that year, just five in Africa (Nigeria (24.3%), the Democratic Republic of the Congo (12.5%), Uganda (4.7%), Ethiopia (4.4%) and Mozambique (3.6%)) accounted for half of all global cases and deaths. The WHO African Region alone was responsible for 94% of the estimated cases and 95% of deaths worldwide. Of the five species of human infecting *Plasmodium*, *P. falciparum* is estimated to account for 96.5% of cases reported, and *P. vivax* accounting for the remaining 3.5%.

Hopefully you are wondering why have we not been able to rout this pestilence? Antimalarial development has been successful for more than a hundred years, and we know more about the disease than ever before; why have we not eliminated this parasite? In 2024 alone, global efforts to eradicate and treat malaria are estimated to account for more than 170 million cases and 1 million deaths averted. But despite effective therapies, small molecules, and more recently,

promising vaccines, global initiatives to control and eliminate are time and time again undermined. *Plasmodium spp.* exhibit robust antigenic variation mechanisms that allow the parasite to effectively evade host immune responses. Combined with multiple stages of rapid clonal expansion in the host and past ineffective antimalarial deployment, the rise and expansion of single-drug- and multidrug-resistant *P. falciparum* reduces the effectiveness of existing drugs. Additionally, our dependence on the small number of artemisinin analogs in combination with a few select partner drugs as ACTs (see Section 4.3.5 for more) has confounded the problem. Furthermore, many current successful antimalarials exhibit troubling toxicity, tolerability, and pharmacokinetic liabilities that limit their use in mass drug administration campaigns. There are many other factors that contribute to this problem, including logistics, vector control, poverty, climate change, and other diseases. But global initiatives, resources, and research to eliminate this disease are ongoing; exploiting different methods to eliminate human malaria for good. As such, as a part of this multi-pronged approach, it is essential that we continue to develop novel small-molecule antimalarials to aid in this altruistic endeavor.

3. A Bit About Bugs - Malaria Biology

3.1. Possessions and Bad Air

The understanding that malaria is caused by a microorganism was only recently discovered. For millennia, malaria was poorly understood and, like most early medicine, was grossly mischaracterized. As an example, ancient Chinese records describe people suffering from malaria-like symptoms as being possessed by three demons. The three demons were often depicted as one carrying a hammer, another carrying a bucket of water, and the third a furnace—metaphors for headaches, chills, and fever, respectively. During the Early Roman Empire, in malaria endemic areas of Italy, it was thought that *mal'arie*, or bad air, from the swamps and marshes where the disease thrived, was indeed the cause. That notion persisted until the work started by Charles Louis Alphonse Laveran in 1880, establishing that malaria was caused by a parasite. The next piece of the puzzle was discovered by Ronald Ross in 1897, when he observed that a dissected Anopheles mosquito that had taken a blood meal from an infected patient also contained a translucent body that carried the malaria pigment.[9] Since these seminal discoveries, we have slowly pulled back the veil of what this disease truly is and how it kills us.

3.2. Plasmodium spp. Life Cycle

Plasmodium spp. are Apicomplexan protists that are parasitic in several types of hosts, including humans and other mammals, but also reptiles and birds, and, of course, the mosquito. This highly auxotrophic parasite scavenges essential nutrients from its host, as they lack the molecular machinery to do so itself.

The life cycle of *Plasmodium spp.* is complex, with a complete lifecycle involving multiple morphological changes that coincide with relocalization within two different hosts. The lifecycle can be split into three stages: the liver stage, the blood stage, and the mosquito stage.

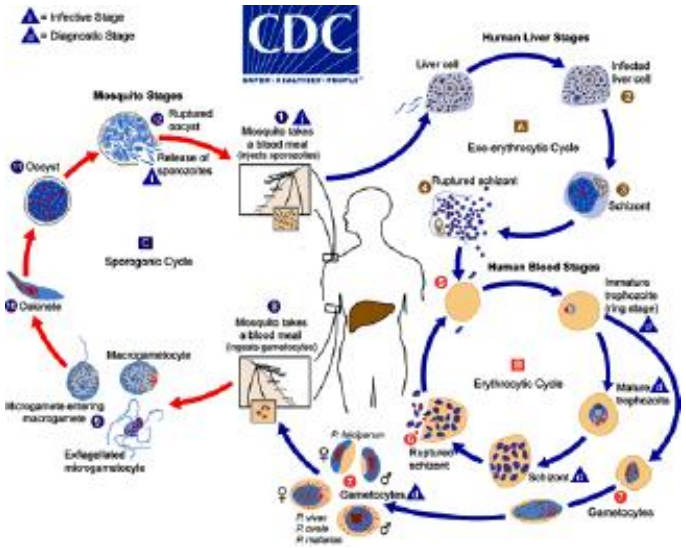

Figure 1: Illustration of the lifecycle of human Plasmodium spp. including the three stages.

(a) liver stage, (b) blood stage, and (c) mosquito stage. Image created for Center for Disease Control by National Center for Emerging and Zoonotic Infectious Diseases (NCEZID), Division of Parasitic Diseases and Malaria.

3.2.1. Liver Stage

The liver stage begins with an infected female Anopheles mosquito landing on the human host to take a blood meal. During the blood meal, mature sporozoites leave the mosquito's salivary gland and travel along the proboscis and into the bloodstream of the human host. There have been a number of studies aimed to determine the number of sporozoites inoculated given a single bite, but the inocula range varies from study to study; however, the accepted median range is from 8 to 39 sporozoites. Sporozoites will travel within the blood circulatory system until arriving at the liver through the portal vein, sometimes taking only minutes to reach their destination. They leave the vein and pass through the liver sinusoidal barrier, traversing Kupffer cells and endothelial cells, to reach hepatocytes. During invagination of the hepatocyte, the parasite forms a parasitophorous vacuole membrane—encasing itself within a shroud of host extracellular membrane. A portion of *P. vivax* and *P. ovale* sporozoites will arrest prior to schizogony and adopt a dormant morphology referred to as a hypnozoite. Weeks, months, or years will pass before the hypnozoites resume development, eventually reinfecting the host with malaria.

The length of time of sporozoite maturation into a late liver stage schizont is species dependent, but in general occurs in 6-8 days, without alerting the host immune response.[7] During liver stage maturation, a single sporozoite will undergo schizogony, repeated asexual nuclear expansion and segmentation, inside the hepatocyte to form a schizont. The result of schizogony is a schizont filled with thousands of individual parasites, called merozoites. During the final stages of development, the parasitophorous vacuole membrane disintegrates, and merozoites leak into the cytoplasm of the host cell. Once there, the merozoites are then incorporated into host cellular membrane-derived vesicles to form merosomes. When the compromised hepatocyte lyses, the merosomes will travel to the lungs, where they rupture, releasing the merozoite payload into the bloodstream.

3.2.2. Blood stage

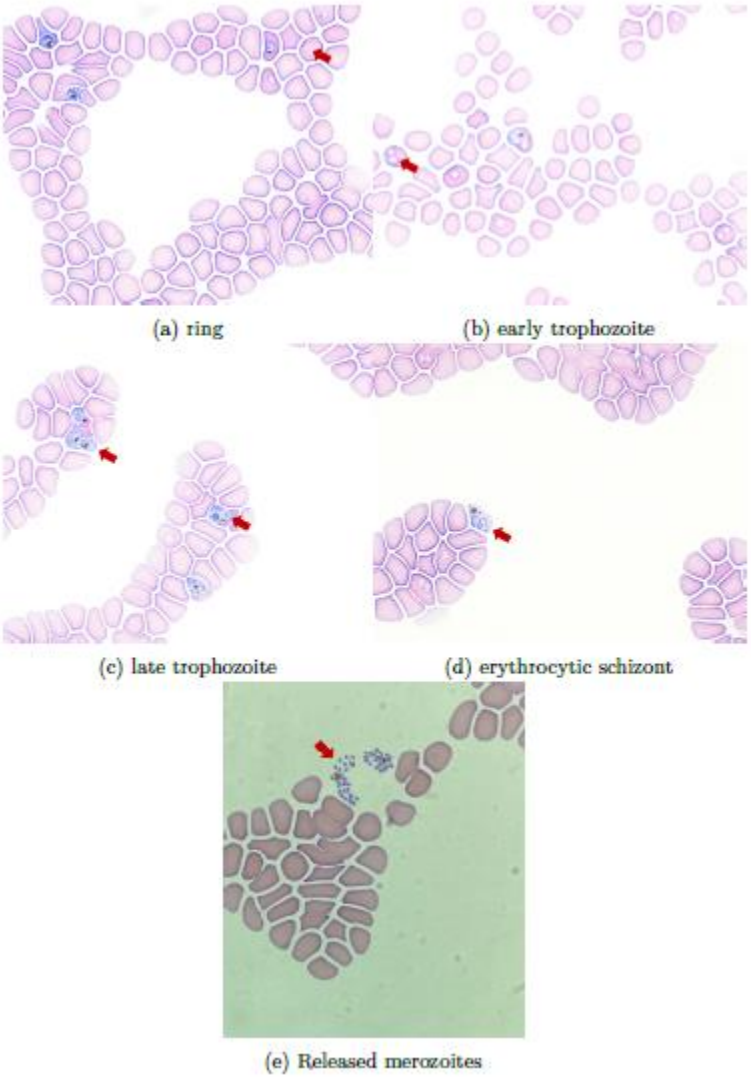

Figure 2: Light microscopy images of Giemsa-stained Plasmodium falciparum Dd2 parasites during erythrocytic lifecycle stages.

Arrows indicate respective stage from each image. Ring stage (Figure 2(a)), early- and late-trophozoites (Figure 2(b) and Figure 2(c), respectively), a fully mature schizont, and released merozoites (Figure 2(e)). Images were captured by author and coworker (Terry Riscoe) on a light microscope under 1000x magnification.

The freely circulating merozoites will quickly find their parasitic target, a red blood cell, or erythrocyte. But not all malaria is made equal, and as such, merozoite invasion exhibits species-dependent erythrocyte tropism. As *P. vivax* is primarily restricted to reticulocytes, whereas *P. falciparum* can invade erythrocytes across multiple stages of maturation, including both reticulocytes and mature erythrocytes. Upon invasion, parasites will begin the intra-erythrocytic life cycle, consisting of several developmental stages and asexual replication. The duration of the erythrocyte lifecycle is similarly species-dependent, ranging from 24 to 72 hours, with *P. falciparum* and *P. vivax* lifecycle reoccurring every 48 hours.[9] The first stage of development

within this cycle is the ring stage, Figure 2(a), followed by the early-trophozoite Figure 2(b), the late-trophozoite Figure 2(c), and then a fully mature schizont Figure 2(d). The schizont is laden with 10 to 20 newly formed merozoites, and once it bursts, the merozoites will invade other erythrocytes, often taking less than a minute to do so. This cycle commonly remains synchronized for the duration of infection, leading to periodic exponential clonal expansion of parasites.

Once the intra-erythrocytic stage begins, in roughly two weeks' time, a *P. falciparum* parasite can be found in 1 out of 10 red blood cells. Once parasitemia reaches sufficient infection of erythrocytes, the host immune system will respond by inducing a fever. Along with the fever, the host will suffer from flu-like symptoms including chills, headaches, muscle aches, nausea, vomiting, and diarrhea. Left untreated, disease progression can lead to severe anemia, kidney failure, seizures, mental confusion, coma, and death. During the intra-erythrocytic cycle, a portion of merozoites will diverge from this cyclical self-sustaining asexual pathway and develop into gametocytes.

3.2.3. Mosquito stage

Along with whole blood, circulating gametocytes are ingested by another female Anopheles mosquito during a blood meal. Several factors, including temperature, pH, and mosquito-derived co-factors, initiate gametogenesis of the two dormant male (macrogametocyte) and female (macrogametocyte) gametes, and they will begin to develop into mature gametes.[,] After maturation, two haploid gametes fuse to form a diploid zygote, which then undergoes genetic recombination. The mature zygote will form a motile ookinete and invade the midgut lumen. Ookinetes that successfully traverse the midgut epithelial barrier develop into oocysts, the only extracellular development stage of the entire parasite lifecycle. The oocyte will mature and undergo schizogony during a 10-12 day period, generating thousands of sporozoites. The sporozoites egress the oocyte and travel through the insect hemocoel, circulating throughout the entire mosquito, until arriving at the insect's salivary glands. Upon attachment to the salivary secretory system, the sporozoites undergo a final maturation that ensures mammalian infectivity and are ready to start a new lifecycle.[,]

3.3. Human Infecting Plasmodium Species

There are five human infecting *Plasmodium* species: *P. falciparum*, *P. vivax*, *P. ovale*, *P. malariae*, and *P. knowlesi*, described in Table 1. Though there are five species, the vast majority of the global burden of all malaria cases and deaths is attributed to *Plasmodium falciparum* (see Section 2.3). *P. falciparum* is primarily found in sub-Saharan Africa, but is still found in most countries that report some level of indigenous malaria. Treatment of *P. falciparum* infection is symptom-based, either considered uncomplicated - headache, chills, fever, or complicated (severe) - impaired consciousness, severe anemia, and organ disfunction. Several underlying mechanisms contribute to *P. falciparum's* enhanced lethality, including its ability to infect red blood cell stages at multiple developmental stages and infected red blood cell surface modifications. Unlike other species, *P. falciparum* may infect both mature and immature red blood cells. Due to a combination of lack of target specificity and a 48-hour replication cycle, the parasite is able to quickly increase parasitemia in the host. Evasion of pancreatic clearance through cell surface remodeling and subsequent adhesion, creating a "sticky" phenotype, aid *P.*

falciparum's ability to reach high levels of parasitemia. The parasite encodes and transports *P. falciparum* erythrocyte membrane protein 1 (*Pf*EMP1) family of proteins to the surface of the red blood cell where they facilitate adherence to vascular endothelial cells (cytoadherence), platelets and other infected or non-infected red blood cells. Cytoadherence in the microvasculature of various organs can lead to circulation obstruction, reduced tissue perfusion, lactic acidosis, and consequential organ failure and death. The brain and placenta are organs that feature extensive sequestration of *P. falciparum*. Cerebral malaria, brain sequestration, is associated with hypoxia of vessels of the microcirculation of the brain, and can lead to cognitive impairment, increased risk for seizures, coma, and death. Sequestration in the placenta during pregnancy often causes low birth weight, anemia, congenital malaria, and may result in miscarriage or stillbirth.

The two species, *P. vivax* and *P. ovale* exhibit a unique dormant developmental stage in the liver stage of infection. A portion of the sporozoites that infect the liver hepatocytes will differentiate into hypnozoites, which have arrested continued development and are clinically silent. The hypnozoites evade the host immune response for the duration of quiescence, and the mechanisms for reactivation are still unknown; and strain-specific duration of dormancy can range from a few weeks to many years after the initial infection. Though *P. malariae* doesn't have a hypnozoite stage, host infection will often be clinically silent for many years but can lead to chronic infections that can recur for decades. Interestingly, *P. knowlesi* is generally endemic to Southeast Asia, and is considered a zoonotic-mediated disease in macaques that can infect humans.

***Plasmodium* species**	**Replication cycle (hours)**	**Preferred Erythrocyte target**	**Disease severity**	**Dormancy**	**Recommended antimalarial treatment**
P. falciparum		All	Severe	No	ACT (frontline = DHAP)
P. vivax		Reticulocytes	Moderate	Yes (hypnozoites)	CQS = CQ + PMQ, CQR = ACT + PMQ
P. ovale		Reticulocytes	Mild–Moderate	Yes (hypnozoites)	CQS = CQ + PMQ, CQR - ACT + PMQ
P. malariae		Mature erythrocytes	Mild	No, but recurrent infections possible	ACT or CQ
P. knowlesi		All	Moderate–Severe	No	ACT or CQ

Table 1: Human infecting Plasmodium species and key features.

CQ - chloroquine; PMQ - primaquine; CQS - chloroquine sensitive; CQR - chloroquine sensitive; ACT - artemisinin-based combination therapy. Possible ACT treatment options include: artemether-lumefantrine (AL); artesunate-amodiaquine (AS+AQ); artesunate-mefloquine (ASMQ); dihydroartemisinin-piperaquine (DHAP); artesunate + sulfadoxine-pyrimethamine (AS+SP); artesunate-pyronaridine (ASPY). For more about current antimalarials and their uses see Section 4.3 and Chapter 5.

4. From Cobwebs to Tree Bark - A History of Antimalarials

4.1. Barbaric Medicine

Long before we discovered that malaria was a parasitic protist found in mosquitoes, we had been trying to cure it. There are only a handful of instances when a disease was cured or at least provided targeted relief, despite wrongly understanding what it was or without knowing the cause in the first place. So, it is not hard to imagine that for most of human history, attempts at treating malaria were far from effective. A brief but thorough account of historically favored treatments of fevers, as malaria was commonly diagnosed as, presented by Drs. Poser and Bruyn (1999) provides us with some insight into how ineffective they might have been. The list is quite exhaustive and goes back to ancient Greece and Rome, and all the way up to quinine's acceptance as an antimalarial, so I will only share a few of the more *interesting* "treatments".

In the sixth century, Alexander of Tralles, a Byzantine physician, recommended that to cure intermittent fevers, patients should carry hairs from a goat's chin on their person, or they should hang a little red bag containing a live dung beetle and their nail clippings from their neck. Indeed, even spiders and their webs were noted as a curative agent at this time. Patients were prescribed to capture a spider in a cloth and wear it on their left arm to cure or prevent fevers. More recently, and thus more frightening, a Dr. J. Donaldson wrote a letter published in *The Indian Medical Gazette*, recounting that oral administration of cobwebs to treat intermittent fevers in 1861 Madras, was ***more*** effective than quinine.

Along with other cure-by-bug treatment options, there have been many nostrums that focused on transferring the disease to someone or something else. One truly peculiar remedy that originated from Southern India was, in the case of intermittent fevers, to embrace a bald Brahmin widow at dawn. Or perhaps if a patient was suffering from quartan ague, they might have been prescribed the widely popular treatment around at that time and need to place their head on a copy of the fourth book of the *Iliad*, but most certainty not place the book on top of their head. If the patient lived in Bohemia, they might be thrown into a bush headfirst, for if they could remove themselves from the bramble quickly enough, the sickness would become ensnared in the bush and be left behind.

Although these are fairly harmless, save for that bush one, there were a great many treatments that can easily be considered barbaric. Forced purging (induced vomiting) and bleedings are some of the far more humane, but records of treating fevers with mercury and arsenic still exist. In several extreme and violent records, limb amputation and trepanning had been prescribed to cure the patient. Suffice it to say these "cures" for malaria were bleak, superstitious, and outright horrific. Humankind was in desperate need of finding a cure that did not rely on the supernatural, and luckily for them a *super natural* product is what they found.

4.2. Quinine - Treating a Bite with a Bark

For a disease that inspired centuries of brutality under the guise of so-called "treatment", the discovery of quinine was more than a medicine—it was a reprieve, hope, inspiration, and a catalyst for global change. As the first antimalarial, I wanted to provide a relatively in-depth discussion of its lore as a dedication to its impact on human history. Unlike other antimalarials where their discovery and development have been obscured by unpublished reports or complex patents, quinine's discovery is muddied by the passage of time.

4.2.1. Discovery

Quinine is found in the bark of the cinchona tree, a large shrub or small tree found in Andean forests and western South America; see Figure 3. The plant was later cultivated in Java, Sri Lanka, and areas in Southern India. Exactly *when* and *who* discovered the antimalarial properties of cinchona bark has been lost to the annals of time. Many historical accounts weave different legends together into their own contradictory version and thus are likely to be heavily influenced by the internal bias of whoever decided to record the event.

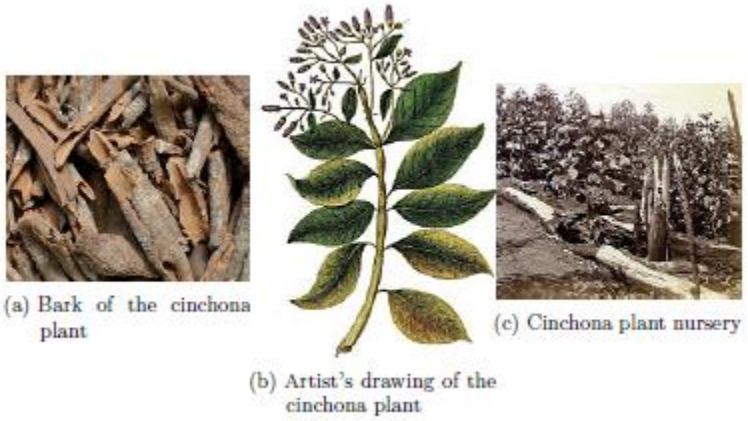

Figure 3: Examples and illustrations of the quinine containing cinchona bush.

Precolonial Peru

Due to this variety and scope of legends, in addition to how the complex nature of colonization changes written and verbal history, we will forever cast doubt on whether the therapeutic value of cinchona bark was realized before Pizarro's discovery and invasion of Peru (1513-1533). Even in the context of pre-colonial native's, the use of the bark to treat malaria prior to the 16th century is widely debated. It is instead thought to have been utilized by native healers to treat common fevers and chills. This is a largely accepted opinion, as there is considered to be no direct evidence of human malaria existing in pre-colonial South America. It is rather believed that malaria was not endemic to South America, but was rather one of many diseases unleashed by European colonizers and the slave trade onto indigenous peoples. Indeed, several genetic phenotypic studies have concluded that there are strong genetic similarities between modern strains of *P. vivax* and *P. falciparum* to ancestral European and African lineages.[»] With that being the case, it is only logical to assume that in practicing traditional medicine, native healers would have likely used medicinal plants already known to treat fevers, like cinchona bark, in their efforts to combat the ague inflicted by the colonizers.

In a more comical version of the legend of cinchona's discovery, Charles de la Condamine (1701-1774), recorded that native Peruvians had learned the medical properties of the bark by watching lions with ague eat it. This opinion was, with good reason, disputed in *Treatise of Therapeutics* in 1880 by Armand Trousseau and Hermann Pidoux. The authors offer, "[as] to the other idea that [indigenous peoples] learned of the febrifugal properties of [cinchona bark] by observing lions suffering from fever…the reader will allow us to wait in order to examine such

ineptitude, until one can confirm the existence of lions in Peru, and to what extent they have experienced tertian or quartan fever." There are legends that describe the discovery of the plant's fever-reducing properties by a native of the Andean mountains who was succumbing to a terrible fever while lost in the jungle.
In their desperation and delirium, they drank from a stagnant pool of water steeped with the bark of a nearby tree. Although their thirst was gone, the lingering bitter taste from the tainted drink led them to believe they had been poisoned. However, the fever soon disappeared, and once recovered, they found their way back to their village and shared the news of its curative properties. Though these stories exist, the most dominate tall-tale of how cinchona bark became commonplace happened a while later.

Postcolonial Peru

Other fables attribute the discovery of the power of the cinchona bark to the Countess of Chinchón. She, whilst visiting Peru, developed a fever that was only cured after ingesting the bark, Figure 4. So taken with the healing power of the plant, she returned with it on her voyage back to Spain and introduced it to Europe in 1638. It was then in 1742 that the tree was named in her honor by the botanist Carl Linnaeus. This legend was repeated many times over and persisted as a real possibility as late as 1987. Eventually, well-founded skepticism from historians eventually led to the legend's unraveling and almost complete rejection.

Figure 4: Oil paintings (1930) of frescos in the Ospedale di Santo Spirito in Sassia, Rome. Possibly of 1850, illustrating the Don Luis Jeronimo de Cabrera y Bobadilla, Count of Chinchón, persuaded in giving his wife Doña Francisca Henriquez Ribera the Countess of Chinchón, a native remedy of bark, that cured her of ague. Figure 4(a) lettering: Peruviæ collecta novis Chinconius oris accipit a servo pharmaca febrifuga. The Latin inscriptions translates to: "Collected in Peru, [the Count of] Chinchón receives from a servant the fever-curing medicine of the New World." Figure 4(b) lettering: Ægrotat Limæ Coniux Chinchonia; febrim cortice mirando pocula tincta fugant. The Latin inscription translates to: "The Lady of Chinchón falls ill in Lima; potions infused with wondrous bark drive out the fever." Figure 4(c) lettering: Purpureus Pater his solatur in Ædibus Ægros delugus limÆ cortice febrifugo. The Latin inscription translates to: "The Purple Father (referring to a high ranking figure - likely the Count) comforts the sick in these halls with a healing draught of fever-curing bark from Lima." Source: Wellcome Collection, public domain.

Some legends attribute the discovery of cinchona and its febrifugal properties to the Jesuit Priests that lived in Peru. There are several different versions; some note that a native healer cured a

priest's fever with the bark. Other stories describe that the priests practiced an old tradition of tasting the bark of felled trees, and that the taste of cinchona bark was similar to other bitter substances used to treat intermittent fevers. More reliable accounts recorded that native Peruvians working in damp and cold mines would take hot infusions of the bark to relieve themselves of shivering. From this observation, by "applying classical logic to a process of clinical observation," Jesuit priests attempted to treat the fevers and chills from malaria and found it effective. These legends might hold the truth of the discovery of the febrifugal properties of cinchona bark, as the treatment of tertian and quartan fevers with "Jesuit's bark", "cardinal's bark", or "sacred bark", was written into the historical record by Jesuit priests between 1620 and 1630, as illustrated in Figure 5.

However, after careful review of a large collection of original sources that were carefully evaluated in terms of accuracy and reliability, historian Saul Jarcho states, "[while] it is improbable that we shall ever determine the exact date at which [cinchona bark] first became known to Europeans; 1630 AD is a reasonable approximation."

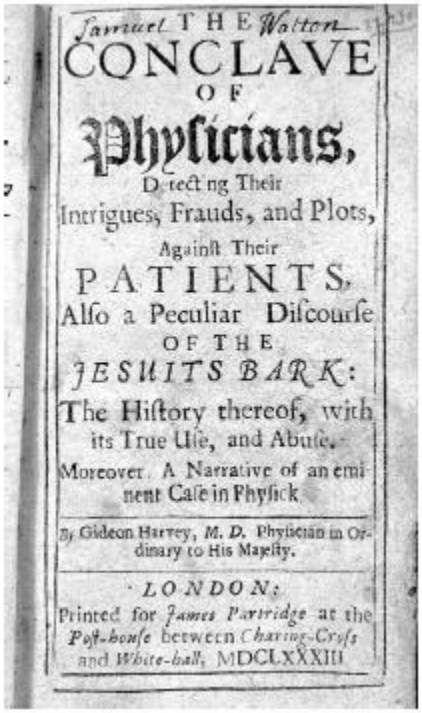
Samuel THE Walton
CONCLAVE
OF
Physicians,
Detecting Their
Intrigues, Frauds, and Plots,
Against Their
PATIENTS,
Also a Peculiar Discourse
OF THE
JESUITS BARK:
The History thereof, with
its True Use, and Abuse.
Moreover A Narrative of an eminent Case in Physick
By Gideon Harvey, M. D. Physician in Ordinary to His Majesty.
LONDON:
Printed for James Partridge at the Post-house between Charing-Cross and White-hall, MDCLXXXIII

Figure 5: Historical evidence of Jesuit Priest's knowledge of cinchona bark in 17th century.

Translation: "The conclave of physicians, detecting their intrigues, frauds, and plots, against their patients. Also a peculiar discourse of the Jesuits bark: the history thereof, with its true use, and abuse. Moreover, a narrative of an eminent case in physick By Gideon Harvey". Gideon Harvey, 1638. Source: Wellcome Collection, public domain.

4.2.2. Characteristics

Disagreement over who discovered it aside, considered the first extract to treat an infectious disease, quinine was instrumental to the future of all antimalarials, and more importantly, all of drug discovery. It wasn't until 1820, nearly 200 years after its estimated discovery, that Pierre

Pelletier and Joseph Caventou extracted the antimalarial compounds from the bark, and quinine and other antimalarial alkaloids were described (Figure 6).

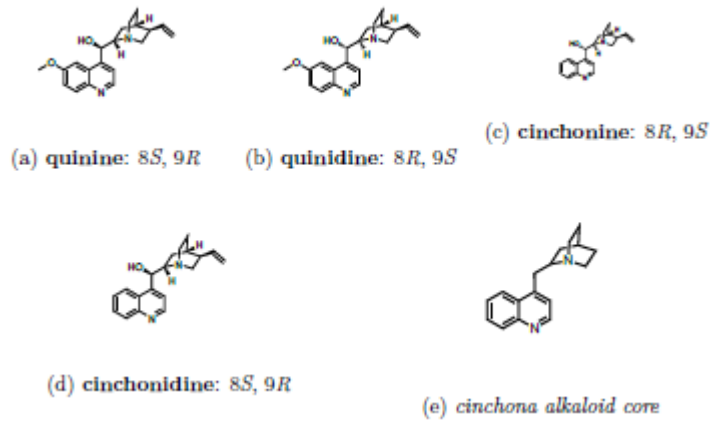

Figure 6: Structures of antimalarial cinchona alkaloids.

Quinine (Figure 6(a)), quinidine (Figure 6(b)), cinchonine (Figure 6(c)), cinchonidine (Figure 6(d)) found in the cinchona plant and their relative stereochemistry at C8 and C9. Figure 6(e) All of the cinchona alkaloids share this core pharmacophore.

Quinine belongs to the class of cinchona alkaloids structurally characterized by the presence of the cinchona pharmacophore, i.e., a quinoline connected to an azabicyclo[2.2.2]octane moiety, also referred to as a quinuclidine, depicted in Figure 6(e). As a drug, quinine is administered as a salt due to the basicity of the quinoline and quinuclidine nitrogens, $pKa_1 = 8.3$, $pka_2 = 4.2$, as seen in Figure 7.[›] The mechanism of action of quinine and other cinchona alkaloids is still not fully understood. It has been demonstrated that, similarly to other quinoline antimalarials (see Section 4.3.1 and Section 5.2.2 for more information), quinine is able to inhibit beta-hematin formation *in vitro* and by extension may inhibit hemozoin formation.[›] There is support suggesting that quinine's antimalarial activity stems from inhibition of hemoglobin metabolism.[–] But there are other reports suggesting inhibition of nucleic acid synthesis, protein synthesis, and glycolysis.[»]

Figure 7: Ad for quinine bisulfate tablets found in "The prevention of malaria" by Sir Ronald Ross, 1910.

Source: Wellcome Collection, public domain.

Total synthesis of quinine

Quinine!

During the 1860's, the estimated annual export of cinchona bark from South American ports was approximately 2 million pounds. The growing demand for quinine led to many attempts to cultivate the tree outside of its endemic area, but more importantly, the demand for quinine led researchers to develop a synthetic route to quinine. Early attempts at the total synthesis of quinine resulted in the accidental synthesis of mauve, Figure 8, the first synthetic textile dye. Synthesized by William Henry Perkin, mauve later inspired the synthesis that led to methylene blue, Figure 8(a), a histological dye turned antimalarial, and in general led to the creation of the synthetic dye industry.

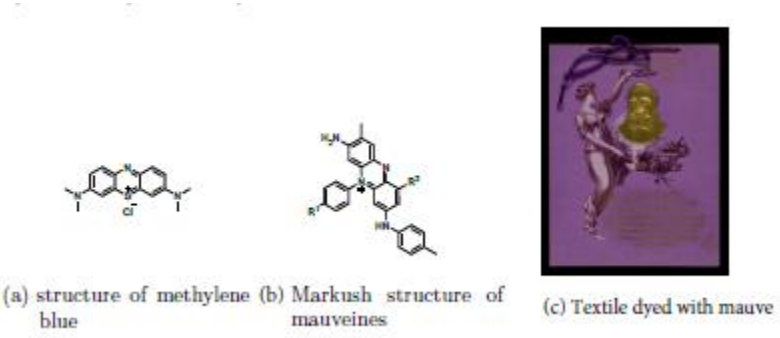

(a) structure of methylene blue (b) Markush structure of mauveines (c) Textile dyed with mauve

Figure 8: Markush structure of the four related compounds that make up the dye mauve. These include mauveine A (R^1 = H, R^2 = H), B (R^1 = H, R^2 = CH_3), B2 (R^1 = CH_3, R^2 = H), and C (R^1 = CH_3, R^2 = CH_3). The menu at a dinner held in honor of Sir William Henry Perkin, in 1906 was dyed with mauve. Source: Wellcome Collection, public domain.

And through many groundbreaking and instrumental methodologies published in pursuit of quinine, it wasn't until 1944 that a "total" (some would argue formal) synthesis of quinine was reported by esteemed chemists Robert B. Woodward and William von Eggers Doering, Scheme [schm-qn-syn].

Previous to this work, chemists Paul Rabe and Karl Kinder in 1918 reported the semisynthesis of quinine from *d*-quinotoxine.

Working from the work published by Rabe and Kinder, the Woodward-Doering/Rabe-Kinder total synthesis of quinine was reported starting from 7-hydroxyisoquine and resulted in *d*-quinotoxine. In the conclusion of the Woodward-Doering paper, it was written, "[i]n view of the established conversion of quinotoxine to quinine [(referring to Rabe-Kinder transformations)], with the synthesis of quinotoxine the total synthesis of quinine was complete." For over half a century, the Woodward-Doering/Rabe-Kinder synthesis stood as the uncontested total synthesis of quinine; however, in 2001 Gilbert Stork, an equally esteemed chemist in his own right, claimed that the synthesis of quinine by Woodward-Doering was a "…widely believed myth." Shortly thereafter, Stork published "The First Stereoselective Total Synthesis of Quinine" in the Journal of the American Chemical Society. Many chemists contested Stork's claim with historical research in hopes of proving him wrong; suffice to say there is no concrete evidence either way, but if you are interested in this debate the reviews written by Teodoro S. Kaufman and Edmundo A. Rúveda in 2005 and Jeffrey I. Seeman in 2008 perform a herculean effort to this end.[·] Regardless of who developed it, and despite the feasibility, large-scale production of synthetic quinine was never achieved. In large part, due to the discovery of synthetic antimalarials, like chloroquine (Chapter 5), that were more conducive to production-scale synthesis.

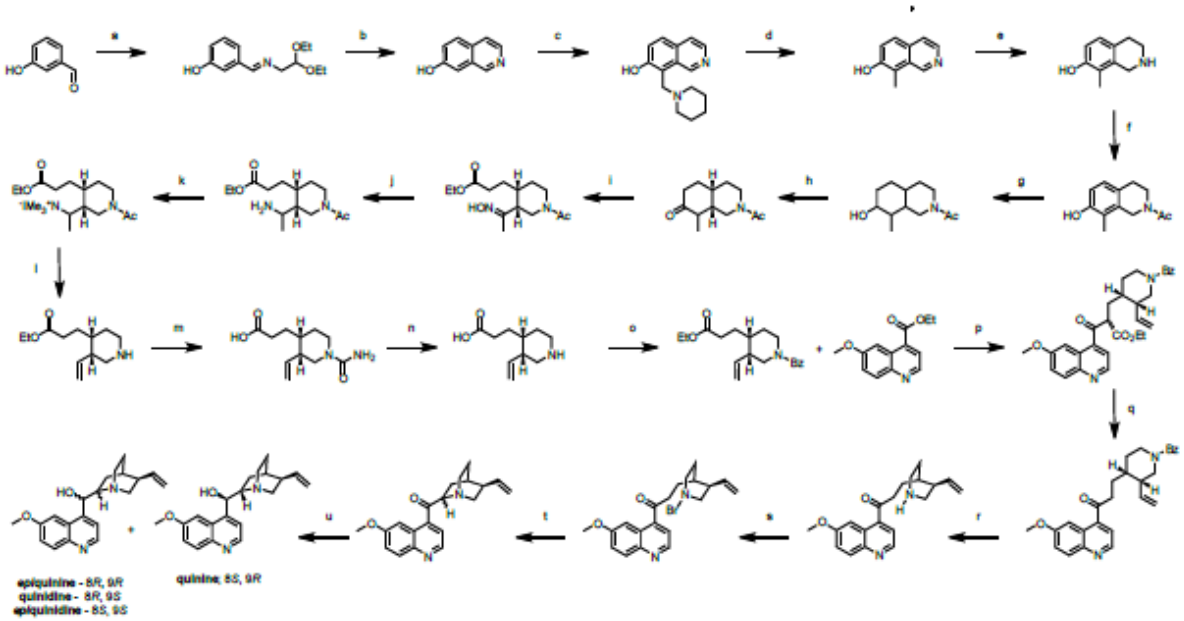

Figure 9: Scheme 1: Woodward-Doering/Rabe-Kinder synthesis of quinine.

Synthetic steps (a-r) were performed by Woodward/Doering and (s-u)were pioneered by Rabe/Kinder. Reaction conditions for the total synthesis of quinine: a) H2NCH(OEt)2; b) 1. 80 % H2SO4; 2. NaOH, crystallization then H+; c) piperidine, HCHO, EtOH; d) NaOMe, MeOH, 220 °C, 16 h; e) H2, Pt, AcOH; f) Ac2O; g)

H2, Raney nickel, EtOH, 150 °C, 205 bar, 16 h [1:1 cis(crystalline)/trans(oil)]; h) H2Cr2O7, AcOH; Et2O/H2O, diastereomer separation; i) EtO-N=O, NaOEt, EtOH; j) H2, Pt, AcOH, 1–3 bar; k) MeI, K2CO3; l) 60 % KOH, 180 °C, 1 h; m) KCNO; n) dilute HCl, EtOH, reflux; o) PhCOCl, K2CO3; p) NaOEt, 80 °C; q) 6 n HCl, reflux; r) hydrolysis; s) NaBrO; t) NaOEt/EtOH; u) Al, NaOEt/EtOH. See the Glossary for acronym definitions.

4.2.3. Structure-Activity Relationship Analysis of Quinine

As quinine was a natural product discovered hundreds of years ago, a contemporary structure-activity relationship (SAR) study is nonexistent. However, we can instead infer some structure-activity relationships of the natural product from drug discovery methods based on quinine and its other cinchona alkaloids. To this end, there is an excellent review capturing some of the more insightful SAR campaigns that aid in illuminating what structural moieties are important to quinine's antiplasmodial activity. In that review, the SAR of quinine is grouped into 3 structural modifications that are responsible for activity, but I prefer grouping the modifications into the five categories described below.

Substitutions of vinyl group

Walsh and colleagues used the vinyl group of quinine as a chemical handle to attach artemisinin (see Section 4.3.5), creating a dual antimalarial drug conjugate, the structure in Figure 10(a). The conjugate was more active than artemisinin or quinine only, as well as more potent than a 1:1 molar equivalent mixture of quinine and artemisinin in 3D7 and FcB1. Though this modification was well tolerated, this only suggests that changes to the quinuclidine vinyl group have the possibility to improve antiplasmodial activity. Further derivatization performed by Dinio and colleagues (2012) through a Heck coupling demonstrated that additions of unsubstituted and substituted aromatic rings will greatly reduce activity. The majority of compounds were far less effective, but compounds with substitutions at either the *para* or *meta* position to the alkene tempered the decrease to have only moderate activity in HB3 and Dd2, with compound QN-7 (Figure 10(b)) showing a slight reduction in potency in HB3 compared to quinine, but that activity is fairly conserved in Dd2, unlike quinine.

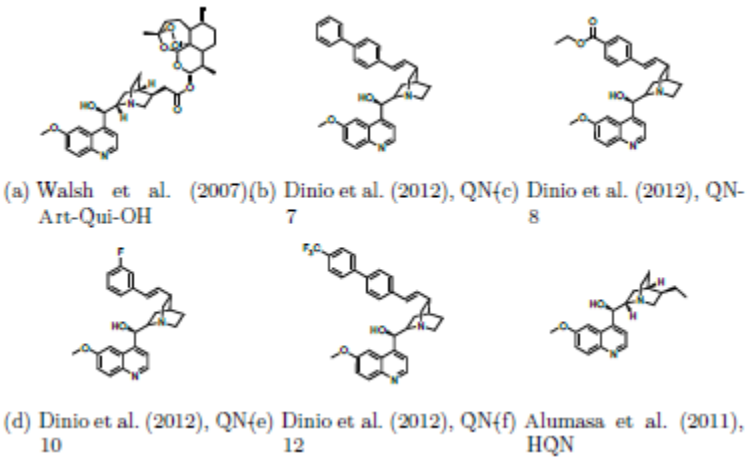

Figure 10: Structures of quinine analogs that demonstrate vinyl group modifications can exhibit a range of perturbations to antiplasmodial activity and beta-hematin formation inhibition.

Figure 10(a) Walsh and colleagues (2007) quinine and artemisinin drug conjugate. Figure 10(b) through Figure 10(e) Dinio and colleagues (2012) quinine analogs. Figure 10(f) Hydroquinine used in the work presented by Alumasa and colleagues (2011).

Unlike antiplasmodial activity, β-hematin formation inhibition by QN-8 and QN-12 (Figure 10(c) and Figure 10(e)) is similar to quinine at wild-type digestive vacuole pH (pH ~5.6), but are more potent than quinine at the *pfcrt* mutation induced pH (pH ~5.2). Alumasa and colleagues (2012) demonstrated that when the vinyl group is reduced to an alkane, as in hydroquinine (HQN, Figure 10(f)) then β-hematin formation inhibition was maintained comparable to quinine at both wild-type pH and *pfcrt* mutation pH. Furthermore, shifts in potency of quinine against HB3, Dd2, GC03, and 7G8 HQN were similar to the shifts in potency of HQN against those same strains. And while HQN exhibits comparable antiplasmodial activity to quinine against D-6, it however is not as potent against W-2. Taken together, the following work suggests that the vinyl group does not play an essential role in β-hematin formation inhibition, but it does play a minor role in antiplasmodial activity.

Substitutions at hydroxyl

The alcohol at the C9 position of quinine was used as a chemical handle in several antimalarial discovery campaigns. Panda and coworkers (2012) demonstrated that quinine-fluoroquinolone antibiotic conjugates through amino acid linkers at the C9 alcohol maintained activity against the 3D7 strain of *P. falciparum*. Specifically, levofloxacin-quinine conjugates were of comparable activity to quinine when linked with glycine, alanine, and phenylalanine linkers, as seen in Figure 11(a). Similarly, oxolinic acid and nalidixic acid quinine conjugated with alanine or norfloxacin through a glycine linker also maintained similar activity to quinine, but not all combinations showed low nanomolar potency. Both the oxolinic-Val (Figure 11(c)) and the enrofloxacin-Ile (Figure 11(b)) quinine conjugates were significantly less potent than most in the series (IC_{50} against 3D7 strain = 183 nM and 207 nM, respectively). Later work by this group (2013) conjugated amino acids and peptides through the alcohol as carbonyls. However, the activity of these quinine analogs against 3D7 compared to quinine was either maintained as seen in Figure 11(d) IC_{50} = 17 nM, or greatly reduced, as seen in Figure 11(e) (IC_{50} = 550 nM).

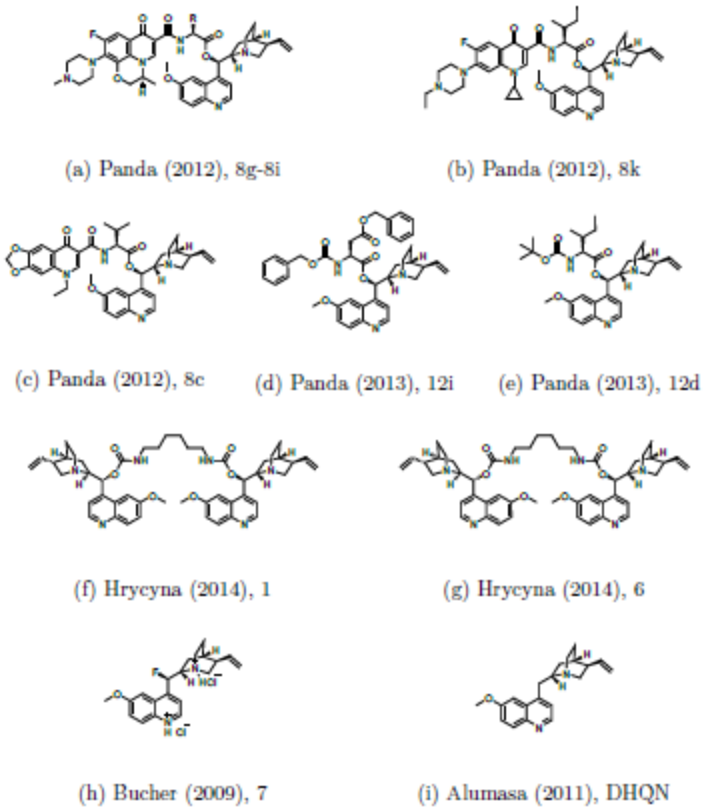

Figure 11: Structures of quinine analogs that demonstrate alcohol group modifications can exhibit a range of perturbations to antiplasmodial activity and beta-hematin formation inhibition.

Figure 11(a), Figure 11(b), Figure 11(c) Panda and colleagues (2012) quinine and fluoroquinolone drug conjugates through amino acid linkers; R = Ala, Gly, and Phe. Figure 11(d) and Figure 11(e) Panda and colleagues (2013) quinine amino acid analogs with varying activity. Figure 11(f) and Figure 11(g) Hrycyna and colleagues (2014) quinine dimers through the C9 position alcohol. Figure 11(h) Bucher et. al. (2009) demonstrate the change to antiplasmodial activity with fluorine substitution products of quinine. Figure 11(i) Alumasa and colleagues (2011) demonstrate how the loss of the alcohol changes antiplasmodial activity and β-hematin formation inhibition.

A set of quinine dimers joined through ester, amide, and carbamate bonds at the C9 position of quinine, containing different chemical linkers was synthesized by Hrycyna and colleagues. The compounds, Figure 11(f) and Figure 11(g), showed enhanced potency in the resistant strains FCB, P31, and Dd2, but reduced potency against the sensitive strain HB3, compared to quinine. A larger subset of compounds synthesized in that work showed comparable β-hematin formation inhibition to quinine. Work presented by Bucher and colleagues (2009) on cinchona alkaloids resulting in fluorine substitution of the C9 alcohol with the stereochemistry conserved, inverted, or a ring expansion from quinuclidine moiety to 1-azabicyclo [3.2.2]nonane can be used to further elucidate structure-activity trends. The potency of the fluorine-substituted stereochemical retention product of quinine, Figure 11(h), was reduced by over one hundred-fold compared to quinine against the drug-sensitive NF54 strain, quinine IC_{50} = 19 nM, Figure 11(h) IC_{50} = 3.0

μM. The authors note that this may be due to the adoption of a *gauche* configuration of the FCCN atoms, which may perturb the antiplasmodial activity, but for the sake of this discussion we can simply conclude that this substitution is not well tolerated. To further conclude the necessity of the C9 alcohol (or some other electron-donating oxygen-containing arrangement) for antiplasmodial activity, Alumasa et al. **2011** demonstrated that dihydro-quinine, Figure 11(i), exhibits complete loss of activity against HB3, Dd2, GC03, and 7G8 (IC_{50} > 10 μM) strains. Additionally, DHQN demonstrated decreased efficacy in the inhibition of β-hematin compared to quinine. Collectively, these findings suggest that the C9 alcohol is necessary for inhibition of β-hematin, but an electron-withdrawing group capable of hydrogen bonding is required for antimalarial activity. The analogs of quinine and their varying potency in sensitive strains could be attributed to perturbation of underlying antiplasmodial activity or decreased proton trapping leading to reduced drug concentration inside the digestive vacuole as different moieties were added to the C9 position. Differences in these analogs' potency between sensitive strains and resistant strains, as well as differences in potency from one resistant strain to another, may also be attributed to the propensity of the attached moiety for efflux rather than directly affecting antiplasmodial activity.

Variations to the quinoline

Modifying the substituent patterns of the quinoline ring has been widely employed as a means of diversifying quinine analogs. It has been demonstrated that the loss of the 6-position alcohol on the quinoline ring in quinine, which is the same structure as the alkaloid cinchonine (Figure 6(c)), reduces inhibition of β-hematin compared to quinine, at pH 5.6 β-hematin formation inhibition IC_{50} of cinchonine = 170 ± 36 μM compared to IC_{50} of quinine = 49 ± 0.4 μM. However, cinchonine exhibits enhanced potency against the drug-resistant strains HB3, Dd2, GCO3, and 7G8 of *P. falciparum* compared to quinine. More generally, the quinoline has been a starting point for many other successful antimalarials, Figure 12, such as primaquine, chloroquine, and mefloquine among others, and has proven to be integral to antimalarial activity.

Variations to the quinuclidine

Varying the quinuclidine ring of quinine has been demonstrated to perturb its antimalarial activity. Ring expansion of quinine by fluorination to 1-azabicyclo [3.2.2]nonane product results in an inactive antimalarial in drug-sensitive NF54 strain, IC_{50} = 8.2 μM. Furthermore the loss of quinuclidine to a bis-ethylamine product (DQQN Figure 12(f)) results in substantial loss in activity against HB3 (~2.6 μM), Dd2 (~2.1 μM), GC03 (~2.7 μM), and 7G8 (~1.6 μM), and the activity is further reduced against HB3 (IC_{50} = 9.6 μM), Dd2, GC03, and 7G8 (IC_{50} > 10 μM) if the amine is removed (DADQQN, Figure 12(g)). In *Pf*CRT mutant conditions (pH 5.2) the des-quinuclidine quinine analogs do not inhibit β-hematin formation, IC_{50} > 2000 μM, and are less potent at wild-type *Pf*CRT conditions (pH 5.6) IC_{50} DQQN = 210 ± 12 μM, IC_{50} DADQQN = 1900 ± 53 μM, than quinine, IC_{50} = 49 ± 0.4 μM. Given the suite of other active quinoline antimalarials, like primaquine, chloroquine, or mefloquine (seen in Figure 12), it is clear that the quinuclidine is not strictly required for quinoline antiplasmodial activity or inhibition of β-hematin formation. However, in the case of quinine, it is clear that the quinuclidine ring is absolutely necessary for quinine's antiplasmodial activity and inhibition of β-hematin formation.

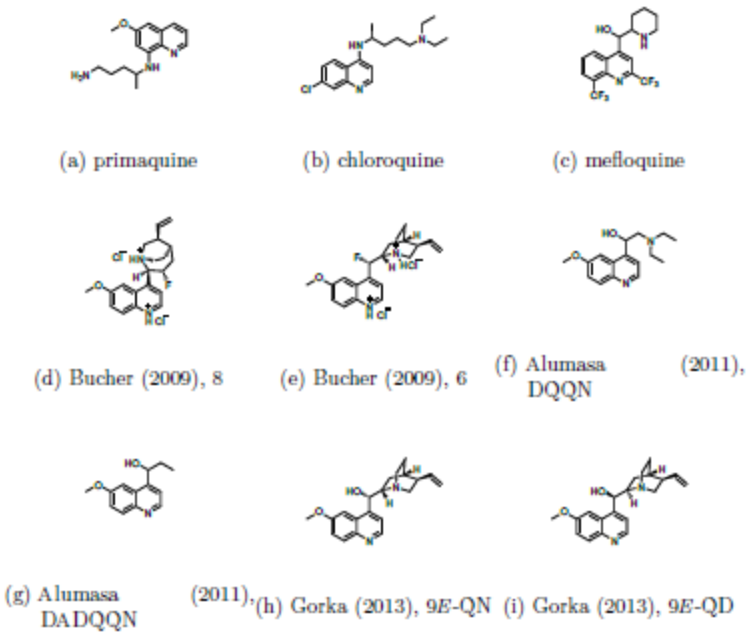

Figure 12: Structures of quinine analogs that demonstrate quinoline, quinuclidine, and stereochemical modifications can exhibit a range of perturbations to antiplasmodial activity and beta-hematin formation inhibition.

Figure 12(a), Figure 12(b), Figure 12(c) are examples of quinoline ring-containing antimalarials. Figure 12(d) - Figure 12(e) Bucher and colleagues (2009) fluorinated quinine products that resulted in quinuclidine ring expansion and C9 chiral inversion. Figure 12(f) and Figure 12(g) Alumasa and colleagues (2011) demonstrate that the loss of the quinuclidine changes antiplasmodial activity and β-hematin formation inhibition. Figure 12(h) and Figure 12(i) Gorka and colleagues (2013) demonstrated the effect of chirality in quinine and quinidine on antiplasmodial potency and inhibition of β-hematin formation using diastereomers of each cinchona alkaloid.

Changing stereochemistry

Inversion of the stereochemical centers of quinine has offered limited structure-activity relationship trends. The inverted stereochemical product of quinine via fluorination results in a *9S*-F product that is inactive against the drug sensitive NF54 strain, IC_{50} = 8.2 μM. When compared to the stereochemical retention product, Figure 11(h), we can observe a reduction in antiplasmodial activity from the inverted product compared to the retention product, IC_{50} = 3.0 μM. The diastereomers quinine (Figure 6(a), 9*R*) and quinidine (Figure 6(b), 9*S*) have been demonstrated to be active in drug sensitive HB3 and GC03 strains of *P. falciparum*, albeit differing in degree of potency, quinine IC_{50} v HB3 = 81 ± 8.4 nM, IC_{50} v GC03 = 99 ± 13 nM; and quinidine IC_{50} v HB3 = 18 ± 2.2 nM, IC_{50} v GC03 = 28 ± 7.6 nM. In addition, the inhibition of β-hematin formation between the two alkaloids indicates quinidine as the stronger inhibitor, at pH 5.6 (wild-type *Pf*CRT conditions) quinidine IC_{50} = 23 ± 2.3 μM; and in similar conditions quinine IC_{50} = 49 ± 0.4 μM. However, Gorka and colleagues (2013) showed that 9-*Epi*-quinine and 9-*Epi*-quinidine, (inverse stereochemistry at C9 and C8 of each) were virtually inactive compared to the parent alkaloid. A similar trend is observed when comparing β-hematin formation inhibition, demonstrated by a massive reduction in β-hematin IC_{50} of the each

diastereomers analog in both *Pf*CRT wild-type and mutant conditions 9-*Epi*-quinine and 9-*Epi*-quinidine IC_{50} at pH 5.2 > 1 mM at pH 5.6 > 3 mM..

As demonstrated above, the structure-activity relationships surrounding quinine have been studied in a circuitous manner, and these examples are only a small portion of the totality of work around this compound. And while it is still difficult to say without a structure-activity relationship study around quinine itself that the compound is the best balance of potency, efficacy, and safety, there is still much we can dissect from the collected work around quinine. Modifications to the vinyl group have been shown to largely affect antiplasmodial activity, but not so much inhibition of β-hematin formation, a representation of hemozoin inhibition. Conversely, changes to the hydroxyl moiety can greatly perturb the potency of β-hematin formation inhibition, while changes to antiplasmodial potency are largely dependent on the substrates amended to that position. Variation in the substitution pattern of the quinoline ring indicates that the ring itself contributes greatly to antiplasmodial activity, likely through inhibiting hemozoin inhibition, and different permutations of moieties connected to the ring in different arrangements led to antimalarials with different mechanisms of action. The quinuclidine ring contributes greatly to quinine's antiplasmodial activity and ability to inhibit β-hematin formation; without this ring, quinine is ineffective as an antimalarial. Lastly, the stereochemistry arrangement of carbon 8 and 9 remains incredibly important to antiplasmodial activity; upsetting this balance results in a virtual loss of antiplasmodial potency and β-hematin inhibition.

4.2.4. Uses

Early in its discovery, the bark was dried and ground to a fine powder and mixed commonly with wine or port, and was often mixed with cinnamon, cloves, and oranges to mask the bitter taste of the powder. Different species of the cinchona tree contained varied proportions of each of the four alkaloids, Figure 6, found in the bark. But after the four cinchona alkaloids had been extracted and characterized from the bark in 1820, each alkaloid was taken as a singular purified salt. However, it wasn't until 1866 that the efficacy of each alkaloid was evaluated in humans, during what is considered the first clinical trial ever performed. Despite the similar efficacy of each of the four alkaloids given as sulfate salts, quinine became the predominant extract from 1890 onwards, due to the increased quinine concentrations found from the predominant cinchona bark supply. As early as 1730s, a British Naval surgeon began to use spirts like brandy or whiskey, to administer quinine to troops. But as purified quinine became more regularly available, it was soon mixed with botanical extracts and sweeteners and offered as a "tonic". These tonics were incorporated into the British Army as a way to provide prophylaxis against malaria in endemic areas. And in 1870, "Indian Quinine Tonic" by Schweppes was created and was soon co-administered by the East India Trading Company and the British army with lime to prevent scurvy, and gin as a moral booster. A review by Simonetti and colleagues (2022) provides a deep look at the rise of the gin and tonic as a staple cocktail, a history that is inextricably linked to quinine, which happened to be quite the enjoyable read. Quinine remained the dominant antimalarial until the 1920s, but as the first synthetic antimalarials, such as mepacrine and later chloroquine, rose to prominence, our reliance on the natural product waned. As chloroquine-resistant malaria emerged and spread in the 1950s, quinine was yet again called upon and was increasingly prescribed. To this day, quinine remains a World Health Organization-recommended therapeutic option in selective intervention conditions.

Quinine salt formulation is predominantly a chloride ion (either hydrochloride dihydrate or dihydrochloride), but others such as mono sulfates, citrate, and phosphate salt formulations have been used.[m] Quinine has schizonticidal activity during the intra-erythrocytic stage of all human malaria parasites, but is gametocytocidal in only *P. malariae*, *P. ovale*, and *P. vivax*. Furthermore, quinine has no noted activity against the hepatic stage of infection, a fact which brings into question the wisdom of its use as a prophylactic. There are many adverse reactions to quinine use, and if improperly administered, the side effects can be severe. Commonly, there is a group of dose-related and reversible side effects observed with the use of cinchona alkaloids referred to as cinchonism, which include: tinnitus, headache, vomiting, visual disturbances, and dysphoria, among others. More severe side effects such as agranulocytosis, and massive hemolysis with hemoglobinuria have been observed. In patients with G6PD deficiency, quinine can induce hemolysis. Administration of 2-8 grams of quinine can be fatal in adults. As of 2024, the WHO Malaria Guidelines still recommend quinine as an alternative treatment option for uncomplicated malaria in the first trimester of pregnancy. Additionally, quinine is recommended as a second-line treatment for severe malaria in both children and adults, as well as a second-line pre-referral treatment for severe malaria.

4.2.5. Impact on Human History

Despite quinine's shortcomings in the light of modern antimalarials, its discovery and use have had a profound effect on our shared history, one that should not be understated. What began as a cure for intermittent fever soon shaped modern drug discovery and the world as we know it today. Quinine inspired natural product discovery and total synthesis, and later led to the design of analogs based on its structure—the central dogma of modern medicinal chemistry. Quinine supercharged imperialism and greatly influenced European expansion and sustained occupation in Africa, Asia, and South America, which led to the drug labeled as "…*a tool of empire*." Global quinine trade and the antimalarial efforts thereafter created the groundwork for international coordinated health initiatives, influencing global campaigns against polio, smallpox, and other communicable diseases. It was even a source of great influence on wartime decisions and logistics during the Second World War in the Pacific theater of operations. Quinine has made its mark on human history, and its discovery has greatly impacted our efforts toward creating antimalarials.

4.3. "Modern" Antimalarial Drugs

As I had mentioned previously, quinine laid the groundwork for modern drug discovery and the central dogma of medicinal chemistry. Through countless scientific advancements in the growing fields of chemistry and biology, we began to develop drug discovery programs; some of the first (and arguably the first) were borne out of the direct need for other antimalarials. Today, there are 25 unique drugs that are recommended by the World Health Organization and the Centers for Disease Control for the prevention and treatment of malaria.[n] There are many useful ways to classify these antimalarials, as well as others used in the past: treatment or prophylaxis, treating complicated or uncomplicated malaria, suggested treatment for children, adults, or while pregnant, etc. Perhaps based on which stage of the parasite they are active against gametocytes or hypnozoites, or which stage during the intra-erythrocytic lifecycle, or an extension of this type of thinking, which species of parasite the antimalarial is effective against. But the most useful way to classify these antimalarials for our intents and purposes is by their chemical structure

and/or activity. For which there are five classes of antimalarials: quinolines and quinoline-related, antifolates, anti-respiratory, antimicrobials, and artemisinin derivatives.

4.3.1. Quinolines and Quinoline-Related

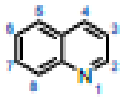

Figure 13: Structure of quinoline ring with numbering pattern.

Nearly a century of drug development rooted in the chemical structure of quinine has ultimately led to one of the largest classes of antimalarials: quinolines and quinoline-related compounds. The quinoline containing antimalarials can be further segregated into the following subclasses: 4-aminoquinolines, 8-aminoquinolines, 4-methanolquinolines, arylamino-alcohol, and acridine-related.

4-Aminoquinolines

The activity, resistance profiles, and mechanism of actions of the 4-aminoquinolines antimalarials chloroquine, amodiaquine, and piperaquine are central to this thesis and are therefore discussed in depth in a later in Chapter 5.

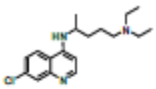

(a) chloroquine

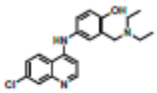

(b) amodiaquine

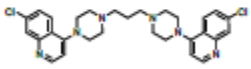

(c) piperaquine

Figure 14: Structures of 4-aminoquinolines derived from quinine.

Figure 14(a) Chloroquine, Figure 14(b) Amodiaquine, Figure 14(c) Piperaquine. Note the central 4-aminoquinoline ring that is maintained through each structure.

8-Aminoquinolines

Pamaquine, or plasmochin Figure 15(a), was the first 8-aminoquinoline discovered and was arguably the first widely successful synthetic antimalarial. Inspired by the discovery of synthetic textile dyes, the silk merchant Friedrich Bayer and a textile dyer named Friedrich Weskott formed Friedrich Bayer & Co. in 1863. Their purpose was to commercially develop and discover new textile dyes based on the synthesis of mauve, and eventually led them to discover and develop histological dyes, such as fucine and methylene blue.[9] Despite methylene blue's utility as an antimalarial, having proven its ability to cure an acute *P. vivax* infection in 1891, its use was limited due to toxicity.[9] It wasn't until almost 30 years after methylene blue was discovered and in the wake of the First World War that Bayer would begin a concerted effort to develop

synthetic antimalarials.[9] Taking heavy inspiration from both methylene blue and quinine, Bayer's Elberfeld laboratory, Interessengemeinschaft Farberwerke (IG Faber), discovered two powerful antimalarial scaffolds, the 4-aminoquinolines and 8-aminoquinolines. And in 1924, the 8-aminoquinoline pamaquine was first synthesized. The new antimalarial was quickly adopted as a radical cure against *P. vivax* and was widely used for many years. However, pamaquine exhibited severe hemotoxicity and neurotoxicity in some patients and hemolytic toxicity in patients of African descent. Due to the severe side effect profile of pamaquine and the loss of quinine through Japanese occupation of Indonesia, United States authorities initiated an antimalarial drug discovery program in 1941.[9] The Board for the Coordination of Malarial Studies emphasized its antimalarial drug campaign to discover safer 8-aminoquinolines. After the Allies in Africa confiscated experimental antimalarial drugs synthesized by IG Faber in 1943, the US government, through a pharmaceutical company. seized Bayer's intellectual property of two decades' worth of antimalarial drug discovery. Only several years later, Robert Elderfield at Columbia University synthesized primaquine, Figure 15(b), the 8-aminoquinoline that would effectively replace pamaquine.[9] Chemically, primaquine is an analog of pamaquine, as the only difference between the two is the loss of the two aliphatic side chains of the terminal amine. But that relatively small change led to a better safety profile and greater potency against malaria. It saw broad use for many years as a radical cure against latent *P. vivax* and *P. ovale* infections, as well as single dose gametocytocidal in *P. falciparum*. Though safer across a broader pool of patients, hemolytic toxicity was still apparent in some patients of African descent. It was around this same time that researchers observed that those same patients who were sensitive to primaquine were also sensitive to pamaquine. These observations eventually led to the discovery of G6PD deficiency, a hereditary disease found in populations of African and Mediterranean descent (more in Section 2.2). Tafenoquine is a recent addition to 8-aminoquinolines, first synthesized in 1979 as part of the U.S. Army Antimalarial Drug Research Programme performed at Walter Reed Army Research Institute, WRAIR. The additions to 2, 4, and 6 positions of the 8-aminoquinoline ring of the primaquine scaffold lend this compound enhanced metabolic stability and increased potency compared to its predecessor. Tafenoquine is tolerated in G6PD-normal and non-pregnant adults, and is an efficacious blood and hepatic schizonticide, as well as a weekly prophylactic against all malarias. Additionally, tafenoquine can be used as a single dose hypnozoitocidal against *P. vivax* and *P. ovale*. Unfortunately, 8-aminoquinolines are the only weapons we have against latent episodic malaria infections—recrudesces of *P. vivax* and *P. ovale* by hypnozoites. More troublesome, they all exhibit some level of hemolytic toxicity in G6PD-deficient subjects, severely crippling their universal utility.

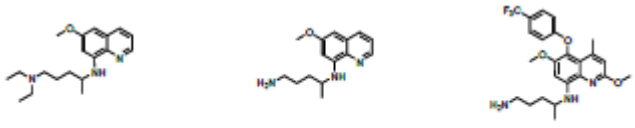

(a) pamaquine (b) primaquine (c) tafenoquine

Figure 15: Structures of 8-aminoquinolines.

Figure 15(a) Pamaquine, Figure 15(b) Primaquine, Figure 15(c) Tafenoquine. Note the central 8-aminoquinoline ring that is maintained through each structure.

4-Methanolquinolines

There are only two successful 4-methanolquinoline antimalarials available today, quinine and mefloquine.

Since quinine (Figure 16(a)) and the other cinchona alkaloids were discussed at length in Section 4.2, there is nothing of note that I would be willing to add here. Mefloquine was discovered sometime prior to its first publication in 1975 during the same large drug campaign conducted at the Walter Reed Army Research Institute that discovered tafenoquine. The drug was developed to combat the rising abundance of chloroquine-resistant malaria, and later it was developed as a prophylactic largely due to its impressive whole blood half-life ($t_{1/2}$) ≈ 2 weeks. It is a schizonticidal antimalarial, active against all 5 species of human-infecting malaria during the erythrocytic stage. However, mefloquine is ineffective at providing a radical cure against latent malaria caused by *P. vivax* and *P. ovale* dormant infections.

Like the cinchona alkaloids, mefloquine is a chiral compound and exists as a racemate, the two racemic forms (*42rythron* and *threo*) each consists of an optical pair, (-) and (+) isomers, Figure 16(b) and Figure 16(c) Only the *42rythron*-enantiomers are used clinically, but the pharmacokinetics and pharmacodynamics of each (±)-isomer can differ significantly. It has been demonstrated the (+)-isomer to be more potent than the (-)-isomer *in vitro* against drug sensitive and chloroquine resistant *P. falciparum*.[·] And pharmacokinetic analysis of the two (±)-isomers indicates the plasma concentration of the (-)-isomer is approximately 3-times as high as the (+)-isomer.[⁻]. Similar to quinine, mefloquine was long thought to disrupt heme digestion through increasing the pH of the digestive vacuole; other studies suggested that additional inhibition of proteins related to the heme digestion pathway contributes to its antimalarial activity. However, more recent studies suggest that mefloquine inhibits parasite protein synthesis. *P. falciparum* resistance to mefloquine has been attributed to amplification of the PFMDR1 gene in malaria endemic areas of Southeast Asia. Additionally, intrinsic resistance to mefloquine has been noted in some areas of Africa, but some suggest this was generated from parasites exhibiting cross-resistance to quinine, previously used in the area.[⁻] Quickly after mefloquine approval and widespread use, patients using it as a prophylactic reported neurotoxicity. Despite the high incidence of neurotoxicity, mefloquine is still actively prescribed, but as an artemisinin-combination therapy with artesunate.

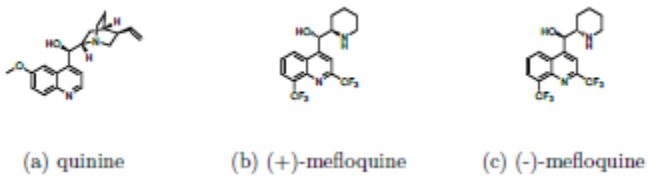

Figure 16: Chemical structures of 4-methanolquinoline antimalarials.

Figure 16(a) quinine and mefloquine, Figure 16(b) and Figure 16(c). Note the central 4-methanol quinoline ring that is maintained through each structure.

Arylamino-alcohols

Halofantrine and lumefantrine are both examples of the arylamino-alcohol class of antimalarials Figure 17, named so for the presence of the amine and alcohol containing aliphatic chain side chain protruding from the aromatic ring system. Halofantrine, Figure 17(a), was discovered sometime between 1963 and 1976 in the same WRAIR program as tafenoquine and mefloquine, but wasn't published until 1985.[9] Given as a racemic mixture, halofantrine is a blood schizonticide that can be used against *P. falciparum*, *P. vivax*, *P. ovale*, and *P. malariae*, but was primarily used to treat acute *P. falciparum* and *P. vivax* infections. Like many of the other quinoline and quinoline-like antimalarials, halofantrine has been demonstrated to inhibit hemozoin formation, but the full mechanism of action is still not fully understood. Unfortunately, after the drug was released for public use, troubling reports of severe cardiac arrest caused by ventricular arrhythmias during treatment with halofantrine began to appear. The drug is no longer listed as a treatment for malaria in the World Health Organization's Guidelines for malaria.

In contrast, lumefantrine Figure 17(b), also known as benflumetol, is still heavily prescribed as a part of a combination therapy with artemether (for more information see Section 4.3.5 and Table 1) for uncomplicated *P. falciparum* infection in pregnant women, children, and adults. It was discovered as part of the People's Republic of China's Project 523, similar to the U.S. Army Antimalarial Drug Research Programme, sometime in the 1970s, but wasn't published until 1981.[9] Similar to halofantrine, lumefantrine is given as a racemic mixture with no significant *in vitro* stereoselectivity; however enantioselective pharmacokinetic differences have been observed.[9] It is a blood schizonticide effective against all human infecting *Plasmodium*, previously thought to act through hemozoin formation inhibition, but recent studies suggest that is only a byproduct of its true mechanism of action.[–] Lumefantrine resistance can be generated *in vitro* and in animal models, and has been demonstrated to present as copy number variances and single nucleotide polymorphism in the *pfmdr1* gene.[9] The general consensus is that resistance in patient populations is driven by resistance to artemether, reducing the efficacy of the drug combination, leading to a rising desensitization to lumefantrine.

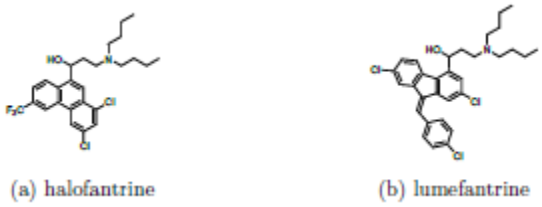

Figure 17: Chemical structures of the arylamino-alcohol antimalarials.

Figure 17(a) halofantrine and Figure 17(b) lumefantrine. Note the arylamino-alcohol group present in both structures.

Acridine-related

Mepacrine (Figure 18(a)), also known as quinacrine or atabrine, was discovered by the same antimalarial research program at Bayer that discovered pamaquine and chloroquine. The drug was a blood schizonticide used heavily by the United States in World War II as both a prophylaxis and treatment for *P. falciparum* and *P. vivax* infections. However, mounting

evidence of adverse side effects that were heightened in combination with pamaquine, along with skin developing a yellow pigmentation after sustained use, led it to be cast aside as a viable treatment for malaria. In contrast, pyronaridine (Figure 18(b)), mepacrine's successor, has been widely successful. First published in 1979 as part of Project 523, pyronaridine is an aza-acridine-based antimalarial.[›]. The drug was used as monotherapy in China after its initial discovery against *P. vivax.* and chloroquine-sensitive and chloroquine-resistant *P. falciparum* for many years. Effective against *P. ovale* and *P. malariae* in combination with artesunate Pyronaridine is a blood schizonticide in *P. falciparum* and *P. vivax* shown to inhibit hemozoin formation, and some additional studies have indicated activity against gametocytes of *P. falciparum in vitro* and in human clinical trials.[–] Though resistance to this drug was first noted in Thailand while in use as a monotherapy, its molecular underpinnings are unknown. And luckily, as a combination therapy, there have been no cases reported of pyronaridine-induced resistance.
It is recommended in children and adults with uncomplicated *P. falciparum* infections.

(a) mepacrine (b) pyronaridine

Figure 18: Chemical structures of the acridine-related antimalarials.

Figure 18(a) mepacrine and Figure 18(b) pyronaridine. Note the acridine, a fused nitrogen-containing aromatic ring system, backbone present in both structures.

4.3.2. Antifolates

Examples of antimalarial antifolates, Figure 19, are the sulfa drugs: sulfadoxine and sulfalene, in addition to proguanil and pyrimethamine. Antimalarial antifolates act by inhibiting the folate synthesis pathway of the parasite, often targeting either the dihydrofolate reductase or dihydropteroate synthase enzymes. Unfortunately, antifolate resistance is pervasive throughout malaria-endemic areas and has severely limited the effectiveness of these antimalarials. A mixture of sulfadoxine-pyrimethamine is still recommended in combination with an artemisinin-based derivative against uncomplicated *P. falciparum*, and is also widely used as a prophylactic. Similarly, proguanil is often taken together with atovaquone, see Section 4.3.3, as a prophylaxis by travelers visiting endemic areas.

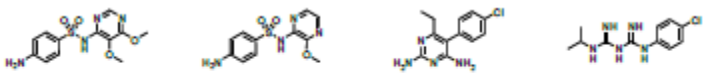

(a) sulfadoxine (b) sulfalene (c) pyrimethamine (d) proguanil

Figure 19: Structures of antifolate antimalarials.

Figure 19(a) sulfadoxine, Figure 19(b) sulfalene, Figure 19(c) pyrimethamine, and Figure 19(d) proguanil. Sulfadoxine and sulfalene are examples of sulfa-drugs, so called for the presence of the sulfonamide moiety in each compound. The chemical composition of both pyrimethamine and proguanil share an aryl chloride that contains a highly nitrogen rich moiety para to the chlorine, a biguanide in proguanil and a pyrimidine diamine in pyrimethamine.

4.3.3. Quinones and Quinolones

Atovaquone Figure 20(a) is currently the only approved antimalarial that targets the parasite's electron transport chain. As a mimetic of ubiquinone Figure 20(c), an important cofactor involved in cellular respiration, atovaquone acts by inhibiting the active site of ubiquinol oxidation in cytochrome bc_1 complex in parasite mitochondria. Inhibition of the bc_1 complex causes loss of mitochondrial function, which is responsible for providing essential intermediates for the pyrimidine biosynthesis pathway, necessary for parasite growth. It is effective against all human malaria causing *Plasmodium spp.*, and in combination with proguanil it has been demonstrated to effectively eliminate *P. falciparum* and *P. vivax* liver stage schizonts, but not hypnozoites. Resistance to atovaquone is often consistent with mutations in the parasites bc_1 complex in the Q_o site, where ubiquinone is oxidized to ubiquinol. This drawback, coupled with the high cost of the drug due to poor chemical yields, makes its widespread use in endemic areas impractical.

Endochin-like Quinolones (ELQs), especially ELQ-300, are in preclinical development by the Medicines for Malaria Venture as potential prophylactic agents. It, like atovaquone, targets the cytochrome bc_1 complex in *P. falciparum*; however, unlike atovaquone it targets the site of ubiquinol reduction to ubiquinone, the Q_i site. It has been found to be active against liver, blood, and sexual life cycles of *P. falciparum* and *P. vivax* and their respective malaria models. Preclinical evaluation is ongoing on this pharmacophore, with ever-evolving analogs being discovered and added to the pipeline.[,]

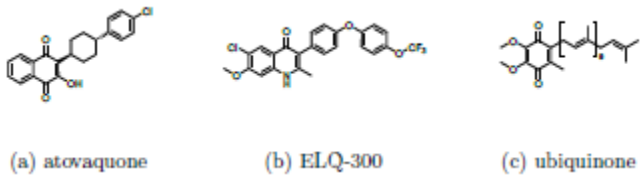

Figure 20: Structures of the some naphthoquinone antimalarials.

Figure 20(a) atovaquone and Figure 20(b) ELQ-300, and the quinone cofactor Figure 20(c) ubiquinone. Comparing the structures of the drugs to the co-factor, one can immediately see the quinone pharmacophore present in both. Although ELQ-300 contains a quinolone instead of a quinone, its potential to participate in redox reactions similar to ubiquinone are easy to imagine.

4.3.4. Antibiotics

A number of antibiotics that don't fall under the sulfa drug umbrella are recognized by the World Health Organization as antimalarials. Namely, doxycycline, tetracycline, and clindamycin are maintained as possible treatments under special circumstances in combination with quinine, but their use is no longer recommended by the World Health Organization. Additionally, other existing antibiotics, like fosmidomycin, have been repurposed and demonstrated to be an effective and safe antimalarial.

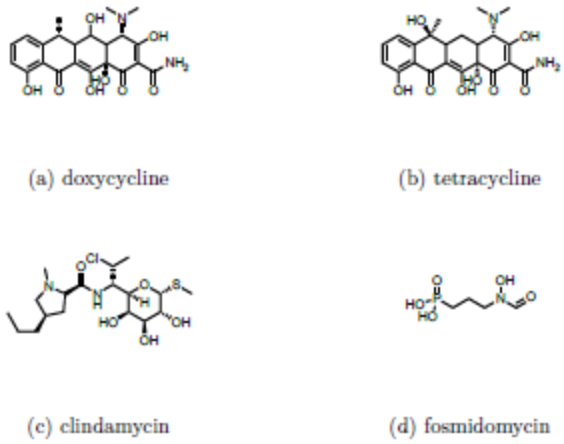

Figure 21: Structures of the antibiotic antimalarials recognized by the World Health Organization.

Figure 21(a) doxycycline, Figure 21(b) tetracycline, and Figure 21(c) clindamycin. Structure of the existing antibiotic Figure 21(d) fosmidomycin, which has been demonstrated to have antimalarial activity. Tetracycline and doxycycline belong to the class of tetracycline antibiotics, compounds that share the four fused-rings backbone. Clindamycin belongs to the lincosamide class of antibiotics, with a pyrrolidine ring fused through an amide bond to a pyranose sugar moiety. Fosmidomycin is an example of a phosphonic acid antibiotic, all of which contain the phosphonic acid moiety.

4.3.5. Artemisinin Derivatives

Artemisinin's discovery profoundly changed the antimalarial landscape over the last 20 years. Originally discovered by Professor Youyou Tu as a part of Project 523, artemisinin is a natural product that was extracted from the "*Artemisia annua*" plant, a long-standing natural medicine that was prescribed to people suffering recurring fevers. Artemisinin is a sesquiterpene lactone with a 1,2,4-trioxane ring "backbone" adorned with a unique endoperoxide bridge. However, the natural product exhibited poor ADME properties, and to overcome artemisinin's poor solubility and bioavailability, several semi-synthetic derivatives were developed. Reducing the lactone with sodium borohydride results in dihydroartemisinin; next, with the reduced product in hand, the hydroxyl group was methylated to form artemether. The reduced ketone was again used as a chemical handle and reacted with succinic anhydride in anhydrous conditions to yield the water-soluble product artesunate. It has been demonstrated that the endoperoxide is necessary for its antimalarial activity, as analogs without this moiety are inactive. Activation of the endoperoxide has been shown to generate carbon-centered radicals that have the potential to alkylate proteins and metabolites as well as produce reactive oxygen species (ROS), which together lead to parasite death.[7] In recent years, artemisinin analogs have been given in tandem with another antimalarial such as piperaquine or sulfadoxine-pyrimethamine; see Table 1 for a full list of combinations. These artemisinin combination therapies (ACTs) are the recommended for many types of interventions, including treating children and adults with uncomplicated *P. falciparum*. Although ACTs have played a major role in the millions of lives saved since 2000, resistance to ACTs in Southeast Asia and Sub-Saharan Africa has begun to weaken their utility.

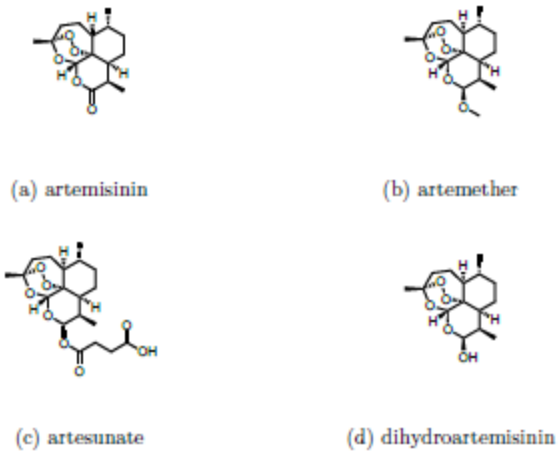

(a) artemisinin (b) artemether

(c) artesunate (d) dihydroartemisinin

Figure 22: Structures of the antimalarial artemisinin and artemisinin derivatives currently used in artemisinin combination therapies.

Notice the 1,2,4-trioxane ring system containing the peroxide bridge that is shared in each compound.

4.3.6. Clinical Trials

The Medicines for Malaria Venture has been instrumental in global initiatives to combat malaria since 1999. As such, they have harnessed global efforts to discover and develop new antimalarials. Seen above in Figure 23, there are a number of antimalarials that have been a part of their developmental pipeline. Tafenoquine, Figure 15(c) in Section 4.3.1, was a product of MMV's pipeline and is an approved antimalarial. Some are in clinical trials, such as cipargamin, ferroquine and sutidiazine, ganaplacide, and cabamiquine and pyronaridine, and others like MMV-533 or MMV-048 are in different stages of preclinical development. Also pictured above is artefenomel, Figure 23(h), an artemisinin-inspired antimalarial. This highly active and exciting compound was unfortunately removed from MMV's pipeline after conclusion of Phase IIb clinical trials, highlighting the challenging nature of drug development. Providing new antimalarials that can be developed in MMV's pipeline is instrumental to global initiatives of curing this disease.

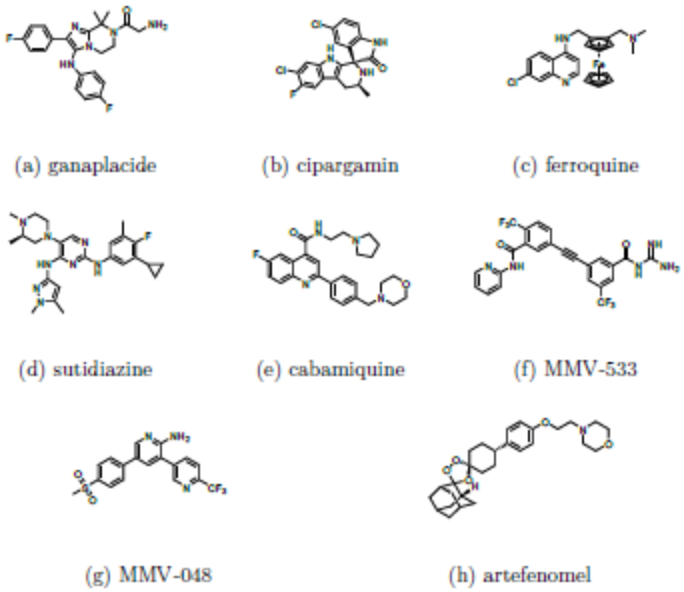

Figure 23: Structures of antimalarials that are in or have been in Medicines for Malaria Venture's pipeline.

5. 4-Aminoquinolines - Successes, Failings, and Potentials

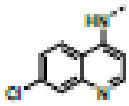

Figure 24: 4-Aminoquinoline Core.

As discussed in Chapter 4, there have been many small molecules that have provided humanity relief from this parasite and hope for one day eradicating the disease. No class of antimalarial embodies this more than 4-aminoquinolines. There are three 4-aminoquinolines that are still in clinical use today: chloroquine, amodiaquine, and piperaquine. These compounds are dogmatic to this thesis, so in addition to discussing their discovery and uses, a historical recollection of structure-activity relationships of amodiaquine and piperaquine analogs will be examined.

5.1. Historical Discovery

Aminoquinolines represent some of the first purely synthetic antimalarials discovered. The high demand for quinine at the turn of the 20th century ignited the flame that became the pharmaceutical industry we see today. Discussed below is the history that led to the discovery of chloroquine, amodiaquine, and piperaquine.

5.1.1. Chloroquine

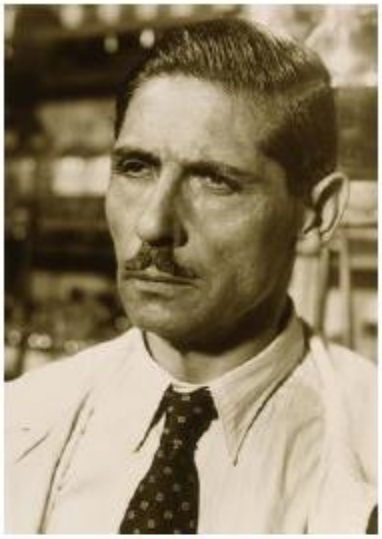

(a) Johann (Hans) Andersag

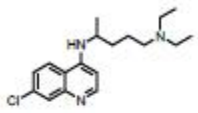

(b) Chloroquine

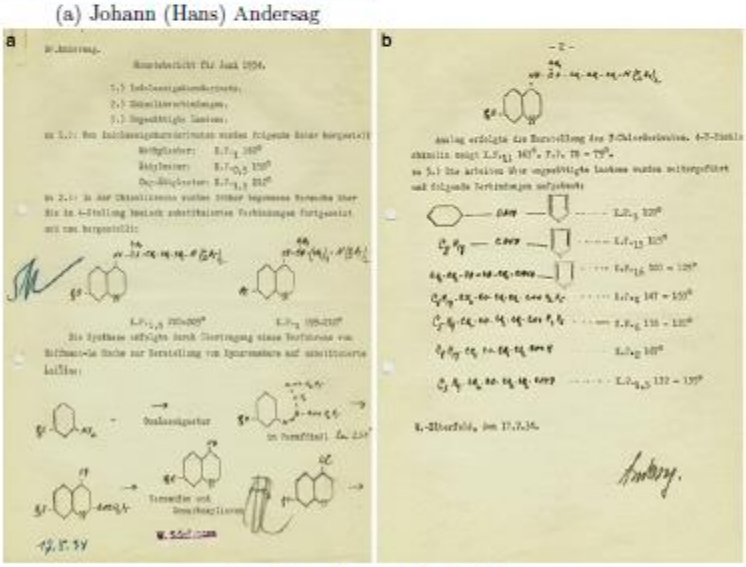

(c) Andersag's Resochin Synthesis

Figure 25: A portrait of German chemist John (Hans) Andersag (1902–1955).

Credited with discovering the 4-aminoquinolines Resochin (chloroquine) and Plasmochin. Excerpt from Andersag's laboratory notebook detailing his method for the synthesis of chloroquine dated July 17, 1934.

As mentioned before, the catalyst that led to today's pharmaceutical industry was the work that was performed at Bayer's laboratory IG Faber starting sometime in the 1920s. Considered one of the first drug discovery campaigns ever performed, the pioneering work of this group has vastly changed our relationship with disease. Early work proved to be challenging and often produced compounds that were less potent than quinine; additionally, success was confounded by the lack of a reliable and reproducible malaria model. After the avian model using *Plasmodium praecox*

(also referred to as *P. relictum*) was discovered and implemented, the program soon saw a number of early successes, namely pamaquine (plasmochin, see Section 4.3.1) in 1924 and mepacrine (atabrine, see Section 4.3.1) shortly thereafter. But the group's discovery of Resochin, later named chloroquine, in 1934 by the chemist Johann (Hans) Andersag (Figure 25) would become instrumental to malarial treatment and eradication in the 1950s, and many consider it to be the most important antimalarial ever developed. Early evaluation of its antimalarial activity in the avian model and shortly thereafter in *P. vivax* positive patients, led it to be set aside in favor of the safer methylated analog sontochin. Though resochin's efficacy was comparable to mepacrine, there were concerns with toxicity in the malaria model and in humans, though records of the human trials have never been discovered. Just over a decade later, despite initial discovery and rejection, and then later re-discovery and evaluation, resochin, now named chloroquine, was accepted as a viable treatment for Malaria by US Armed Forces in 1946.

Chloroquine quickly became a global treatment option for malaria, not only for US forces. Considered a well-tolerated drug with proven effectiveness and exhibiting a long half-life, it became a benchmark for malaria treatment and prophylaxis. So much so that mass administration of chloroquine was a major component of the World Health Organization's Malaria Eradication Program that started in 1955. The program initiated a number of directives that focused on disease monitoring, vector control, and mass treatment, among others. Due to its success, in 1982, the WHO was able to declare 24 countries to be endemically malaria-free preventing millions of deaths. But the success of chloroquine is not without its failings, as reports of chloroquine treatment of *P. falciparum* failing began in 1957 in both Columbia and the Cambodia-Thailand border. Today, chloroquine resistant *P. falciparum* is found in all major endemic areas including South America, Southeast Asia, and Africa. Despite widespread resistant *P. falciparum*, chloroquine remains a reliable and viable option against *P. vivax*, *P. ovale*, *P. malariae*, and *P. knowlesi*.

5.1.2. Amodiaquine

Chloroquine's success was used to springboard further development of other 4-aminoquinoline antimalarials that were synthesized as part of the United States discovery program that produced chloroquine. Early synthetic efforts of that program led to identifying 4-*t*-butyl-α-diethylamino-6-phenyl-*o*-cresol, Figure 26(a), as a antimalarial candidate. That work led J.H. Burkhalter and colleagues to evaluate analogs of this compound containing heterocycle nuclei. And in 1948, they published their findings, including the synthesis and evaluation of Camoquin, the compound that would later be called amodiaquine, Figure 26. Key structural components of amodiaquine that differ it from chloroquine are the aniline ring and its *para* hydroxyl substituent. Both the 7-chloro-4-aminoquinoline core and the tertiary amine of chloroquine are maintained in amodiaquine, though the amine is present as a Mannich base. Since its discovery, amodiaquine has seen moderate use worldwide. Benefiting from activity against chloroquine resistant strains of *P. falciparum*, it has been used in those endemic areas. However, due to reports of toxicity observed in patients using amodiaquine, its use has been limited.[–] Despite issues with toxicity, it is still used in an artemisinin combination therapy alongside artesunate, and has been effectively deployed in Africa since 2007.[,]

(a) 4-*t*-butyl- -diethylamino-6-phenyl-*o*-cresol

(b) amodiaquine

Figure 26: Structure of the cresol pharmacophore that exhibited antiplasmodial activity described in Burckhalter et al., (1946).

This compound was the inspiration that later led to the discovery of amodiaquine, Figure 4.2.

5.1.3. Piperaquine

Initiates in the late 1950's to overcome chloroquine resist *P. falciparum* led to the synthesis of piperaquine, at the time 13228-RP, by the French chemical and pharmaceutical manufacturer Rhône-Poulenc. It was field tested as prophylaxis in West Africa in the mid 1960's, but further development was halted for undisclosed reasons. However, as a part of Project 533, piperaquine was independently rediscovered and synthesized in China in 1966. It was field tested in malaria-endemic areas of Hainan Island in Southeast China and was found to be effective at curing ongoing infections and preventing recrudescence. Piperaquine was quickly adopted and used throughout Southeast Asia as a monotherapy for treatment and prophylaxis, and in 1978 replaced chloroquine as the recommended treatment for malaria by the Chinese National Malaria Control Programme. Its success as a monotherapy was short lived as some chloroquine-resistant *P. falciparum* field isolates were reported to be less sensitive to piperaquine than other chloroquine-sensitive *P. falciparum*. To combat this emerging resistance, piperaquine treatment was offered in combination with sulfadoxine as early as 1969. However, by the late 1980's *P. falciparum* resistance to chloroquine, amodiaquine, and piperaquine was widespread, and alternatives were actively pursued.

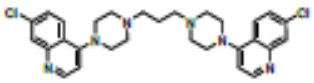

(a) piperaquine

Figure 27: Structure of piperaquine created by Rhône-Poulenc and rediscovered during Project 533.

But as they say, "the prodigal son returns," and yet again piperaquine was rediscovered in the 1990's, but this time as a candidate for the artemisinin combination therapies under development at the time. Piperaquine in combination with dihydroartemisinin was found to be an effective treatment for both chloroquine sensitive and resistant *P. falciparum* Unfortunately, resistance to dihydroartemisinin + piperaquine has been emerging in Asia, originating from the Cambodia-Thailand border.[,] And though reports of dihydroartemisinin + piperaquine treatment failures in Africa are minimal, concerns of widespread emergence threaten the progress that ACTs have made towards eradication.

Taken together, the 4-aminoquinoline scaffold has provided three incredibly effective proven antimalarials. Despite the history of resistance, each one is still used to this day to varying degrees. Therefore, I, like many others before me, claim that there are still 4-aminoquinolines yet to be discovered that may hold the key to eradicating this disease.

5.2. Targets, Troubling Resistance and Toxicology

The 4-aminoquinolines chloroquine, amodiaquine, and piperaquine are shown to be active against the erythrocytic stage of *P. falciparum* lifecycle. Though additionally chloroquine has been demonstrated to be active against gametocytes of *P. vivax*, *P. ovale* and *P. malariae*, it is ineffective against the pre-erythrocytic stage and hypnozoites. The mechanism of action of 4-aminoquinolines is complex and difficult to study, in part due to the nature of the disease, but in large part owing to its canonical mechanism of action. The putative mechanism of action of chloroquine, amodiaquine, and piperaquine has been strongly supported to be hemozoin formation inhibition. There has been evidence that demonstrates that 4-aminoquinolines, like chloroquine, can target amino acid synthesis, protein synthesis, digestive vacuole phospholipases, aspartic proteinases, and DNA and RNA synthesis.[–] However, some have argue that those mechanisms are unlikely due to the disparity between the concentration of drug required and what is achievable *in vivo*.[,]

As previously discussed in Section 3.2, hemozoin formation acts to protect the parasite from the liberated toxic heme byproduct of hemoglobin metabolism.
The severely auxotrophic parasite, lacking most of the molecular machinery to synthesize amino acids for protein synthesis, metabolizes host hemoglobin in the digestive vacuole, an acidic lysosomal-like organelle, to acquire essential amino acids through a catabolic pathway.

5.2.1. Hemoglobin Digestion in *P. falciparum*

Hemoglobin degradation occurs exclusively during the erythrocytic stage of the parasite's lifecycle. During the intraerythrocytic cycle, approximately 70% of the cytosolic contents of the host cell are taken up by the parasite, a large percentage being hemoglobin. Interestingly, *in vitro* studies have shown that only 1/5 of amino acids liberated during hemoglobin digestion are used by the parasite for protein synthesis, and furthermore, the amount of hemoglobin digestion the parasite exhibits have been shown to be both species and strain-dependent. The amount of hemoglobin acquired by the parasite during the intra-erythrocytic lifecycle is stage-dependent and occurs through four different pathways. During early ring-stage development, the parasite, including the parasitophorous vacuole, will flatten into a disc-like shape; it will then cup and fill with the host cell cytosol. The distal ends of the cup will converge, effectively enclosing the contents within; this "big gulp" is estimated to sequester 40% of the host's total hemoglobin. During the trophozoite and schizont stages, the parasite utilizes small hemoglobin vacuoles, cytostomal tubes, and phagotrophs to maintain and increase hemoglobin levels within the parasite. The hemoglobin-laden vacuole that is generated from the "Big Gulp" is thought to be the precursor to the digestive vacuole that develops later in the parasite life cycle. Through these different processes, hemoglobin finds its way to the digestive vacuole of the parasite, where it is broken down.

Hemoglobin catabolism in the digestive vacuole is mediated by a number of proteases. These include aspartic proteases (Plasmempsin-1, -2, -4, and histoaspartic protease (HAP)), cysteine proteases (Falcipain-2, -2', and 3), metaloprotease (Falcilysin), and several exopeptidases.

Evidence indicates that no single protease is essential to the pathway, but rather they act in concert as redundant processes. The process has been shown to proceed in a size-ordered fashion, beginning with plasmempsin-mediated degradation of hemoglobin into large peptide chains, and it is at this step that the co-factor heme is liberated. The large peptides are further cleaved into medium peptides (falcipain- and plasmempsin-mediated), small peptides (falcilysin-mediated), and finally into amino acids and dipeptides (exopeptidase-mediated). Amino acid and small peptidic products are transported from the digestive vacuole to the parasite's cytoplasm to be used for parasite protein synthesis or used for energy production through glycogenesis. The digestive vacuole-membrane bound chloroquine resistant transporter (CRT, *Pf*CRT in *P. falciparum*) likely plays a major role in this transportation. In addition, the predicted amino acid transporter (*Pf*AAT1) has also been shown to incorporate in the digestive vacuole membrane and is thought to mediate amino acid and small peptide transport to the cytosol, though that has yet to be properly demonstrated.[,] Interestingly, the majority of catabolism products liberated through this pathway are, in fact, not incorporated into the parasite's protein synthesis pathways and are instead transported out into the host cytoplasm. It has been hypothesized that the disparity between the amount of hemoglobin degradation and amino acid incorporation acts as a mechanism to generate space in host cytosol to enable parasite growth or correct cytosolic osmotic pressure to prevent premature lysis.[,]

In the hemoglobin-bound state, the iron oxidation state in ferriprotoporphyrin is ferrous iron (Fe^{2+}), however, when liberated, ferrous iron is oxidized to ferric iron (Fe^{3+}), (the ferriprotoporphyrin containing the ferric iron will henceforth be referred to only as heme). Ferric iron has been shown to generate reactive oxygen species (ROS), and when cellular concentrations of ROS outpace antioxidant capabilities, accumulation of oxidative stress, such as alkylation of proteins and the peroxidation of lipids, can lead to cell death. Other eukaryotes possess a heme detoxification enzyme, heme-oxygenase, to handle heme generated from endogenous hemoglobin catabolism. However, *Plasmodium spp.* genome does not, and only codes for a heme-oxygenase-divergent protein that lacks the critical catalytic residues found within the protein super-family. To detoxify the heme and therefore protect itself from oxidative stress, the parasite has developed a poorly understood capacity to sequester heme as hemozoin.

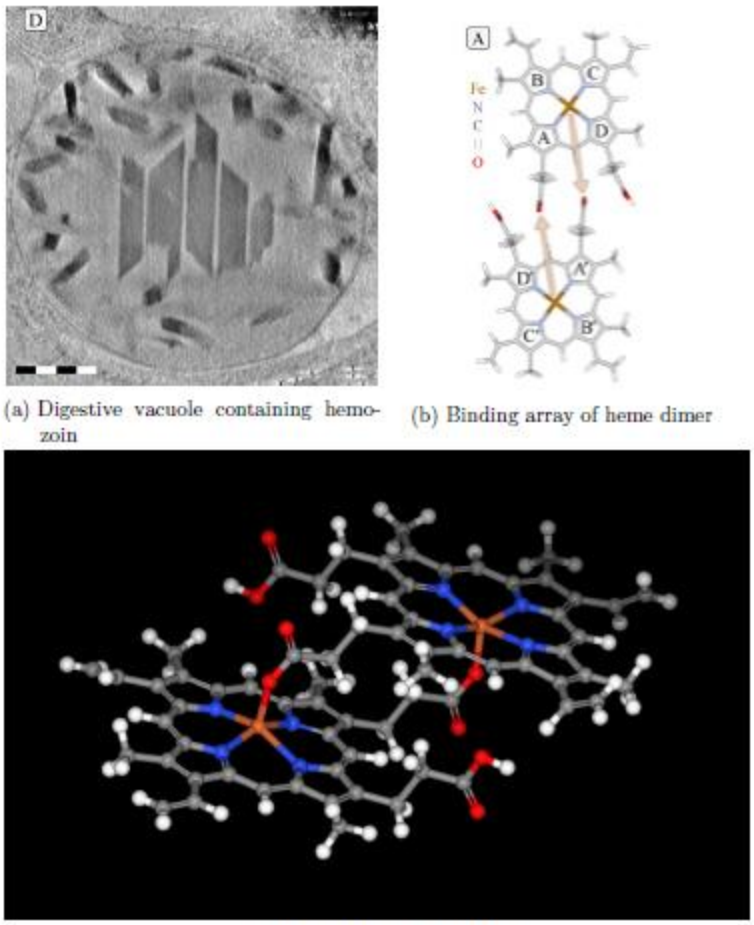

(a) Digestive vacuole containing hemozoin

(b) Binding array of heme dimer

(c) Hemozoin crystalline unit

Figure 28: Hemozoin: the crystalline structure and arrangement of heme monomers in hematin and hemozoin.

Figure 28(a) Hemozoin crystal morphology from a tomographic reconstruction of an intact digestive vacuole. Scale bar 500 nm. Figure 28(b) After liberation from hemoglobin, two heme monomers will complex to form hematin dimers through coordination of each central Fe atom to one of the two propionic acid groups. Pyrrole ring labeled A-D. Figure 28(c) Single solved unit cell of endogenous hemozoin in P. falciparum. Figure 28(a) and Figure 28(b) from Klar et al. (2024). Figure 28(c) from Cambridge Crystallographic Data Centre (CCDC), 3D viewing software of crystal deposition number: 2344281 from Klar et al. (2024).

The exact mechanism of hemozoin formation is not well understood, but there is evidence that in addition to the acidic nature of the vacuole (pH = 5.0–5.4), the digestive vacuole membrane and lipids are essential for the process.[–] There is some evidence that hemozoin biogenesis is protein-mediated, including a parasite lipocalin-like protein, as well as the heme-oxygenase-divergent protein and histidine-rich proteins.[–] As in the case of the parasite lipocalin-like protein, decreased expression was associated with reduced hemozoin production and enhanced ROS production.[,] But some cite localization of the heme-oxygenase-divergent protein and histidine-rich proteins occurring outside of the digestive vacuole as grounds for questioning their involvement in this process. The structure of hemozoin has been determined to be composed of heme (ferriprotoporphyrin IX) dimers that are linked through Fe-O atom coordination of the iron

core and propionate group of another heme. The structure of hemozoin was first described as a polymer, a continuous complex of Fe-O coordination of one heme molecule to the next. Though the nomenclature has stuck around, i.e., "hemozoin is a polymer", the structure was later determined to be a crystalline lattice of centrosymmetric dimers linked through hydrogen bonds.

5.2.2. 4-Aminoquinoline Mechanism of Action

Due to the confounding effect of not fully understanding the mechanism by which *Plasmodium* manages hemozoin formation, the exact mechanism of action of 4-aminoquinolines is difficult to fully discern. As the prominent 4-aminoquinoline, chloroquine's activity has been extensively studied. Proposed mechanisms of action have varied, including inhibition of protein synthesis, digestive vacuole phospholipases, aspartic proteinase, and effects on DNA and RNA synthesis.[–] However, these proposals should be viewed with skepticism, as they require the intracellular concentration of chloroquine to be much higher than what has been shown to be achieved *in vivo*. Despite these theories, the putative erythrocytic stage mechanism of action of 4-aminoquinolines antiplasmodial activity is the inhibition of hemozoin formation. It has been demonstrated that quinoline drugs like chloroquine and amodiaquine will inhibit spontaneous heme crystallization *in vitro*. Evidence that chloroquine will complex with heme as well as heme dimers supports this claim, but how these chloroquine-heme/heme dimer complexes contribute to cell death remains up for debate.[–] Some studies have found that these chloroquine-heme complexes are incorporated in the growing hemozoin crystal and thus terminate further growth, suggesting that inhibition of continued heme detoxification leads to membrane dysfunction.[,] Containing the same 4-aminoquinoline core, amodiaquine and piperaquine have been shown to share this mechanism of action.[,] Evidence for an alternative mechanism of action of amodiaquine indicated that it inhibits heme detoxification by glutathione, leading to membrane dysfunction.

The success of these antimalarials' mode of action is speculated to be heavily dependent on their ability to accumulate in the digestive vacuole. Early studies suggested that chloroquine accumulation was explained through ion-trapping or weak-base mechanisms.[,] As a diprotic weak base (pK_{a1} = 8.1, pK_{a2} = 10.2), at physiological pH (~7.4) a small portion of chloroquine is in a neutral state and can diffuse across erythrocyte and parasite membranes. Once it enters the digestive vacuole (pH = 5-5.4), both of chloroquine's nitrogens (quinoline ring and tertiary amine nitrogens) will become protonated. As a diprotonated species, chloroquine is effectively membrane impermeable and is therefore trapped inside the digestive vacuole. Modern studies have suggested that chloroquine accumulation is not solely dependent on ion-trapping, and that active transport or a carrier-mediated mechanism plays a role.[–] Amodiaquine and piperaquine are also weakly basic, both having ionizable nitrogen atoms at similar ranges to chloroquine, and have been demonstrated to accumulate in the digestive vacuole.[,]

5.2.3. Resistance to Chloroquine and other 4-Aminoquinolines

Since the putative mechanism of action of chloroquine was determined to be a nonprotein target, understanding the molecular drivers of chloroquine resistance was difficult to understand. Early indications of the mechanism of resistance in parasites were demonstrated to be associated with reduced accumulation. This was hypothesized to be a result of either enhanced efflux, reduced uptake, or an increased acidity in the digestive vacuole pH.[–] Just before the 21st century, resistance to chloroquine was identified to be associated with the *Plasmodium falciparum* chloroquine resistance transporter (PFCRT) gene.[,] And over the following twenty years the

mechanistic role of *pfcrt* in chloroquine drug resistance was defined, as well as its endogenous function.[–] Allelic exchange experiments using the a chloroquine sensitive strain (HB3) crossed with a chloroquine resistant strain (Dd2), demonstrated that the 8 different point mutations in Dd2 *Pf*CRT loci offer chloroquine resistance to progeny, namely through elevated *in vitro* IC_{50} values, chemosensitization by verapamil, and reduced accumulation of chloroquine. To date geographical variants of *pfcrt* alleles have been shown to harbor 4–10 non-synonymous mutations, additionally more than 30 variant residues in chloroquine resistant *pfcrt* have been identified.[,] In most chloroquine-resistant parasite lines, either a K76T (from clinical isolates) or K76N/I (from laboratory-adapted lines under chloroquine pressure) point mutation was found. Indeed, genetic studies have demonstrated that the K76T mutation is necessary, but is not solely responsible for chloroquine transport. Mutant *Pf*CRT has been shown to reduce chloroquine accumulation in the digestive vacuole; and therefore the current model suggests that reduced drug accumulation is due to *pfcrt*-mediated efflux of chloroquine from the digestive vacuole.[,] However, some studies challenge the current model and question the degree to which reduced chloroquine accumulation contributes to the reduced efficacy of chloroquine to kill resistant parasites.[,]

P. falciparum resistance to amodiaquine and piperaquine have been determined to be consistent with mutations in the *pfcrt* gene. Additional mutations in the multidrug resistance transporter *Pf*MDR1 gene have been found to confer resistance against amodiachin. Along with mutations in *Pf*CRT gene, copy number variance in *plasmempsin-2* and *plasmempsin-3*, aspartic proteases involved in hemoglobin digestion, have been associated with piperaquine resistance.

5.2.4. Amodiaquine Toxicity

As mentioned previously in Section 5.1.2, amodiaquine use has been severely limited by reports of harmful side effects. Reports of hepatotoxicity, agranulocytosis, and death informed the WHO's decision to remove monotherapy amodiaquine from its Essential Drug List in 1988.[,,,] Evidence suggests that the 4'-hydroxyl group of amodiaquine undergoes oxidation, forming a reactive quinone imine or semiquinoneimine intermediate, Figure 29. These toxic metabolites undergo further bioconjugation with glutathione, which should be viewed as a product of the detoxification pathway for the metabolites. However, the active detoxification of toxic metabolites does not explain the toxicity associated with amodiaquine use. It has been demonstrated that after a single dose in rats, amodiaquine induced covalent modifications of hepatic proteins.. Amodiaquine quinoneimine has been demonstrated to be extremely immunogenic in animal models. And more seriously, amodiaquine metabolite antibodies were present in a group of patients with serious adverse drug reactions, suggesting a similar mechanism that caused type II hypersensitivity reactions to penicillin and aminopyrine in humans.[,] Overcoming the metabolic instability of amodiaquine will go a long way towards unlocking this pharmacophore for robust and widespread use in efforts to eradicate malaria.

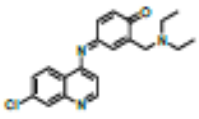

Figure 29: Structure of possible amodiaquine oxidation product, a reactive quinone imine.

5.3. Diversification over Abandonment

The argument for continued optimization of amodiaquine, rather than scaffold abandonment, is the combination of the following 5 facts. Generally, 4-aminoquinolines are relatively safe if properly prescribed. All three 4-aminoquinoline antimalarials are cheap to make on a large-scale, chloroquine has been reported to be $0.10 per treatment, while amodiaquine is slightly more expensive at $0.50 per treatment. Chloroquine is regarded as the single most effective antimalarial ever produced. Unlike chloroquine, the chemical space around amodiaquine remains open to exploration since most of the attention has been focused on chloroquine analogs. Lastly, amodiaquine and piperaquine have been shown to overcome chloroquine resistance.
In short, the main theme of this thesis is the continuation of optimizing the amodiaquine scaffold. Why, and more importantly, how I aimed to accomplish this is discussed in the following section.

5.3.1. SAR of Amodiaquine

Numbering of amodiaquine core for use during SAR analysis and discussion

One proven method to develop new drugs is to diversify the original chemotype through medicinal chemistry techniques. Due to the longevity of these antimalarials and their redeeming qualities, there have been many attempts to generate new 4-aminoquinolines. Cumulatively, that work can be viewed as a robust and informative structure-activity relationship (SAR) study that can be leveraged in continued 4-aminoquinoline development. To that end, amodiaquine offers a problem that most modern drug discovery and development pipelines routinely tackle. How do we reduce metabolic instability and toxicity? Utilizing the cumulative findings of SAR studies from developmental 4-aminoquinoline analogs, we can easily begin to form ideas for eliminating the toxic liability. As such, the cumulative SAR studies surrounding amodiaquine can be separated into three main alterations: the quinoline ring, the Mannich base, and the hydroxyl group. Comparing these studies to one another should be done sparingly, as throughout antimalarial drug discovery history the experimental landscape has changed many times. Early studies were all performed *in vivo*. First in ducks and chickens, then later canaries and lizards; some were performed in primates, but soon most were performed in mice with *P. berghei* and *P. yoelii*. The next big milestone was when Trager and Jensen (1976) developed a method for continuous cultivation of *P. falciparum*. Afterward, a myriad of different techniques were developed to investigate the effect that newly discovery compounds had on antimalarial activity. Therefore, we can only discuss the SAR of compounds within a defined set with relative accuracy, but we can only use broad strokes and generalizations when examining compounds from different publications and across 70 decades since the original discovery of amodiaquine. Herein, I present key findings and takeaways for each of the three changes.

Quinoline

As discussed earlier, the putative mechanism of action of the 4-aminoquinolines is understood to be disruption of hemozoin formation through heme-drug complexation. Early NMR studies confirmed that *ex vivo* heme-chloroquine complexation is facilitated through π-π stacking of the quinoline core and the porphyrin ring.[9] Therefore, most augmentation of the quinoline core, either by substitution or scaffold hopping, often resulted in diminished antimalarial activity.

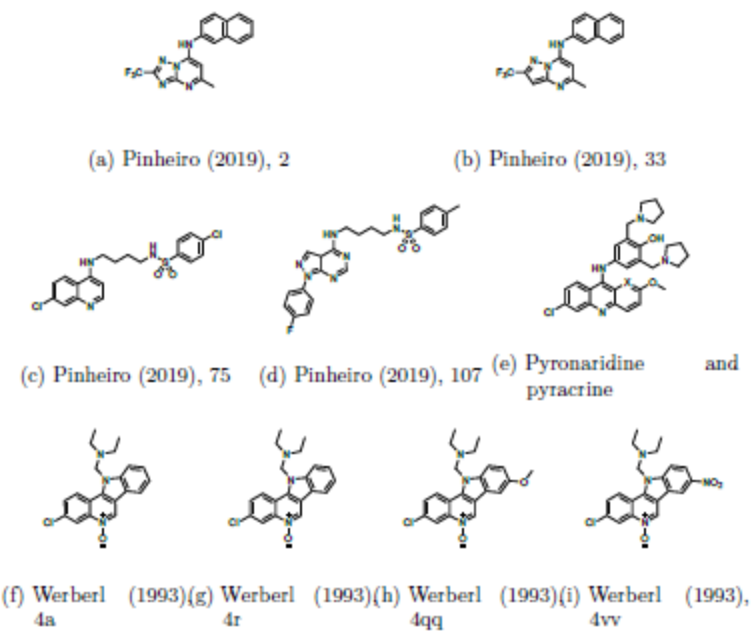

Figure 30: Compounds that illustrate SAR studies of the quinoline core scaffold hopping of 4-aminoquinoline and amodiaquine-analog antimalarials.

Figure 30(a), Figure 30(b), Figure 30(c), Figure 30(d) Structures of scaffold-hopping ring isosterism inspired by 4-aminoquinoline antimalarials amodiaquine and chloroquine. Figure 30(e) structures of the successful amodiaquine inspired aza-acridine, pyronaridine (X = N), and amodiaquine inspired acridine, pyracrine (X = C). Figure 30(f), Figure 30(g), Figure 30(h), Figure 30(i) Structures of scaffold-hopping ring-fusion inspired by 4-aminoquinoline antimalarials, resulting in N-oxide indoloquinolines.

Limited success of scaffold-hopping has been reported but often coincides with the molecule no longer targeting the hemozoin formation pathway. Triazolpyridines and pyrazolopyridines antimalarials generated from rational ring isosterism substitution inspired by amodiaquine were shown to exhibit reduced antimalarial activity (compared to amodiaquine) through dihydroorotate dehydrogenase inhibition (*Pf*DHODH). Fused ring systems similar to 4-aminoquinolines have been explored with varying degrees of success. Compounds featuring tricyclic rings as in aza-acridine, like pyronaridine, and other acridine analogs, like pyracrine, have been historically shown to maintain antiplasmodial activity.[–] But fusion of amodiaquine's quinoline and aryl amino rings, as in the case of indoloquinoline, was shown to lead to a loss of *in vivo* activity. *In vivo* activity of resulting indoloquinoline products was recovered when the 5-position nitrogen of the indoloquinoline ring (1-position of quinoline ring) was oxidized to form an N-oxide. Indoloquinoline compounds with the highest *in vivo* efficacy contained either a bromine or chlorine at the 3-position (7-position of quinoline) Figure 30(f), Figure 30(g), Figure 30(h), Figure 30(i).

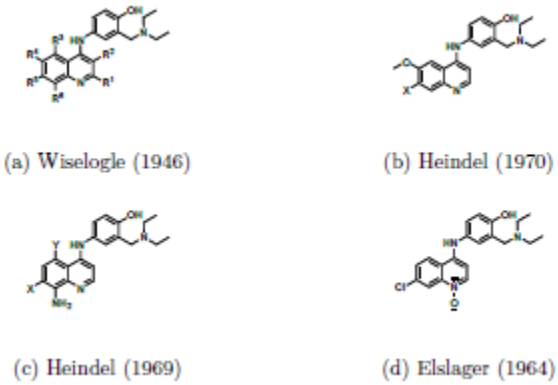

(a) Wiselogle (1946) (b) Heindel (1970)

(c) Heindel (1969) (d) Elslager (1964)

Figure 31: Structures of compounds that illustrate SAR studies of 4-aminoquinoline substituent pattern of amodiaquine and amodiaquine-analog antimalarials.

Figure 31(a) Derivatives featured the following substitutions: R^1 = -Ph, -Cl, -Me ; R^2 = -Ph, -Me, -CO_2Et ; R^3 = -Me , -Cl; R^4 = -OMe, -Me, -OH, -Cl, -NMe_2, -NHPh; R^5 = -OMe, -OEt, -OHx, -Me, -Br, -Cl; R^6 = -OMe, -Me, -NH_2, -Cl. Figure 31(b) Derivatives featured X = Cl, F, or CF_3. Figure 31(c) Derivatives featured X = H or Cl and Y = H or Cl.

There are many examples of SAR studies that have focused on quinoline substituent arrangements and the effect on antimalarial activity. The early work by the United States that eventually led to chloroquine and amodiaquine has been condensed into *A Survey of Antimalarial Drugs* (1946). Thomas and Werbel (1972) go on to describe the SAR of amodiaquine that was presented in *A Survey of Antimalarial Drugs* (1946), and they note the full 150 compound library and the effect of substitution on antimalarial activity, Figure 31(a). In short, a single chloro group at R^5 was by far the most active, but 7 (R^5) -methoxy, -ethoxy, -methyl, -bromo as well as 5,7-dimethyl and 6-methoxy derivatives maintained moderate activity, but all other quinoline substitutions in the series (R^1, R^2, R^3, R^4, R^6,) resulted in loss of activity. Much later, work performed by Heindel et al. (1970) evaluated the effect of 7-position substitution (X = Cl, F, CF_3) on the antiplasmodial activity of 6-methoxy-amodiaquine. The compounds that maintained a 7-position halogen (X = Cl or F) group maintained activity against the *P. berghei* malaria model, whereas the trifluoromethyl derivative (X = CF_3) loses activity. An earlier series by the same group assessed amodiaquine analogs bearing an 8-position amine and halogen substitution at the 7 and 5 positions. The 8-amino-amodiaquine derivatives exhibited reduced *in vivo* efficacy in a *P. berghei* model as the number of halogens was increased, as the des-halogen derivative (X = Y = H) was the most active followed by the derivative containing a single chloro group (X = Cl, Y = H). Likewise, the 5,7-dichloro containing analog (X = Y = Cl) was inactive in a *P. gallinaceum* mosquito infection assay. Similar to the of Werbel et al. (1993) preparation of a N-oxide amodiaquine by Elslager et al. (1964), Figure 31(d), demonstrated enhanced potency in a *P. berghei* model, relative to the parent compound.

As the quinoline core of amodiaquine is hypothesized to complex with heme, leading to inhibition of hemozoin formation, perturbations to that structure are not well tolerated. Amodiaquine-inspired scaffold hopping has resulted in some interesting leads, but often at the cost of potency or altering the putative mechanism of action. The substitution pattern of the

quinoline ring is not well tolerated, though N-oxides have been shown to enhance *in vivo* activity.

Mannich Base

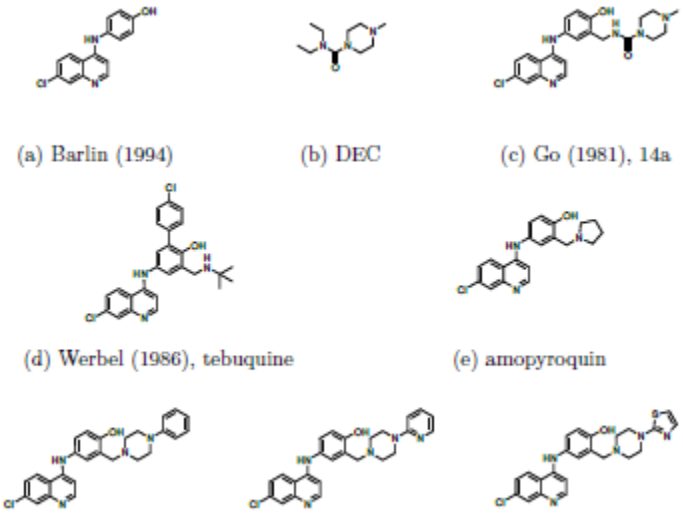

Figure 32: Structures of compounds that illustrate SAR studies of the Mannich base of amodiaquine and amodiaquine-analog antimalarials.

Figure 32(a) demonstrates that the Mannich base in amodiaquine is necessary for antimalarial activity.. Figure 32(b), Figure 32(c) and Figure 32(d) demonstrate the effectiveness of hybridizing amodiaquine with another antiplasmodial compound.' Figure 32(e), Figure 32(f), Figure 32(g), Figure 32(h) all demonstrate amodiaquine analogs that substitute the diethylamino Mannich base, with other Mannich bases.'

The *N*,*N*-diethyl amino Mannich base has been evaluated extensively, and has been often used as a chemical handle. It has been shown that a des-Mannich base of amodiaquine, results in near-complete loss of activity. In other studies, the Mannich base was substituted through an effort to hybridize amodiaquine with the antiparasitic drug diethylcarbamazine (DEC). The most active compound from that series was highly effective at reducing *P. berghei* in mice, exhibiting 2 times the efficacy of amodiaquine at reducing parasitemia. Another hybridization effort sought to improve amodiaquine through the addition of a more active an optimized α-(dialkyl amino)-*o*-cresol from amodiaquine's initial discovery, Figure 26(a). The addition of a *para*-chlorophenyl group to the meta position of amodiaquine along with substituting the *N*,*N*-diethyl Mannich base with a *tert*-butyl amine, resulted in a highly active antimalarial. This compound, known as tebuquine, revealed enhanced potency *in vivo*, activity against resistant *P. falciparum* strains, and improved metabolic stability when compared to the parent drug. However, development of tebuquine was halted due to preclinical toxicology reports of white blood cell cytotoxicity. An early amodiaquine analog with a pyrrolidino group instead of the *N*,*N*-diethyl amine, called amopyroquin, was demonstrated to be effective *in vivo* in rats and rabbit models, and later against *P. falciparum* and *P. vivax* infections in humans." Later amopyroquin was demonstrated to be more effective than chloroquine in some chloroquine resistant strains of *P. falciparum*. Guglielmo et al. (2009) explored amodiaquine analogs through expansion of Mannich base substitutions. Their most active compounds replaced amodiaquine's *N*,*N*-diethyl Mannich base

with a *N*-substituted piperazine ring featuring either a phenyl (Figure 32(f)), 2-pyridyl group (Figure 32(g)) or 2-thiazolyl (Figure 32(h)), the last exhibiting sub-nanomolar potency, IC_{50} = 0.67 nM and 0.42 nM against 3D7 and K1, respectively. Despite the three compounds demonstrating enhanced activity in drug sensitive and chloroquine resistant strains of *P. falciparum* compared to amodiaquine, that apparent increase in activity coincided with increased cytotoxicity in mammalian cell lines. Bis-Mannich quinoline compounds have been extensively explored by Gordon Barlin and colleagues.[–] Most of the standout compounds contained a 7-trifluoromethyl-quinoline; however, several 7-chloro quinoline bis-Mannich compounds were highly active and efficacious *in vivo*. Highly active amodiaquine analogs contained piperidyl bis-Mannich bases, some with the *para* hydroxyl (the 12 position in Figure 4.6), Figure 33(a) and Figure 33(e), and the rest with the hydroxyl group at the *ortho* position (10 or 14 position in Figure 4.6), Figure 33(b), Figure 33(c), Figure 33(d).

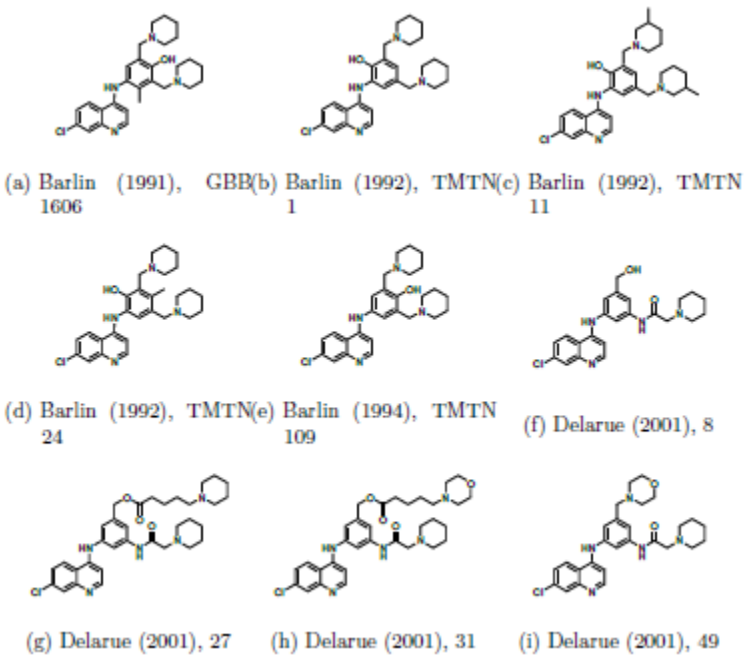

Figure 33: Structures of compounds that illustrate SAR studies of the Mannich base of amodiaquine and amodiaquine-analog antimalarials, continued.

Figure 33(a), Figure 33(b), Figure 33(c), Figure 33(d), Figure 33(e) Amodiaquine derivatives featuring a bis-Mannich base arrangement that led to highly active and efficacious antimalarials. , Figure 33(f), Figure 33(g), Figure 33(h), Figure 33(i) amodiaquine derivatives that replace the Mannich base with groups that contain hydrogen bond acceptors.

Delarue et al. (2001), hypothesized that replacing the Mannich base with hydrogen bond acceptors at both *meta* positions would result in elevated heme binding by aiding in complexation through the carboxylate side chains of heme. Structure-activity relationship of compounds included in the study indicates the Mannich base substitution is moderately tolerated at varying alkyl-length linkers between the amide coupling. Activity was reliant on nitrogen-based steric hindrance, and there is an obvious balancing between lipophilicity and flexibility.

Many late-stage compounds exhibited promising *in vitro* activity but demonstrated toxicity issues, The most promising compound cured *P. berghei* infection at 40 mg/kg/d.

In short, the Mannich base is essential to the antiplasmodial activity of amodiaquine. And if augmented, the new group can result in increased cytotoxicity and reduced *in vivo* efficacy. However, alkyl chain lengths and pKa of the nitrogens in the new group can heavily influence this outcome and have the possibility of creating a safe and highly active compound.

Para-hydroxyl

As stated in Section 5.2.4, patients treated with amodiaquine have been reported to develop hepatotoxicity and agranulocytosis. Elucidation of oxidative products led to the understanding that the *para*-hydroxyl is likely oxidized and forms a toxic intermediate, Figure 29. Therefore, much work has been performed to discover compounds that have eliminated or reduced the capacity for *para*-hydroxyl oxidation.

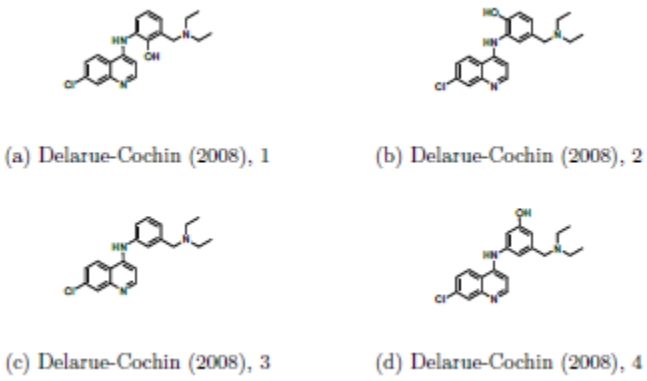

(a) Delarue-Cochin (2008), 1 (b) Delarue-Cochin (2008), 2

(c) Delarue-Cochin (2008), 3 (d) Delarue-Cochin (2008), 4

Figure 34: Compounds that illustrate SAR studies of the para-hydroxyl group of amodiaquine and amodiaquine-analog antimalarials.

Figure 34(a), Figure 34(b), Figure 34(c), Figure 34(d) Structures of amodiaquine derivatives that demonstrate the effect of the hydroxyl group on antimalarial activity.

A study conducted by Delarue-Cochin et al. (2008) evaluated the placement of amodiaquine's *para*-hydroxyl group, placing it at either ortho positions Figure 34(a) and Figure 34(b), the meta position Figure 34(d), or removing it completely, as in desoxy-amodiaquine Figure 34(c). Placement of the hydroxyl group at the ortho position adjacent to the Mannich base severely reduced activity against all *Plasmodium falciparum* strains tested, but activity was only moderately reduced when the hydroxyl group was at the other ortho position, when compared to amodiaquine. The *meta*-position hydroxyl analog still maintained activity but was less active than the latter ortho hydroxyl analog. Desoxy-amodiaquine was shown to maintain comparable activity against drug-sensitive and chloroquine-resistant *P. falciparum* strains. All compounds mentioned exhibited a slight reduction in MRC-5 cell cytotoxicity, but no compounds were selected for heme binding or *in vivo* efficacy studies.

Paul O'Neill and colleagues have contributed greatly to the advancement of modern amodiaquine-like compounds, and more importantly amodiaquine analogs, that exhibit an improved safety profile.[7–] In 1994, the group examined the contribution of fluorine substitution along the 4-aminophenyl ring Figure 35(a), Figure 35(b), Figure 35(c), Figure 35(d),

Figure 35(e) to antimalarial activity and metabolism of amodiaquine analogs. Mono, di, and tri substituted analogs were synthesized and evaluated, with most compounds exhibiting no significant reduction in antiplasmodial activity compared to amodiaquine in chloroquine sensitive and resistant *P. falciparum* strains. Interestingly, the 4-deoxy-4-fluoro amodiaquine also maintained antimalarial activity and exhibited no measurable oxidation potential, highlighting a possible solution to improving amodiaquine's safety profile.

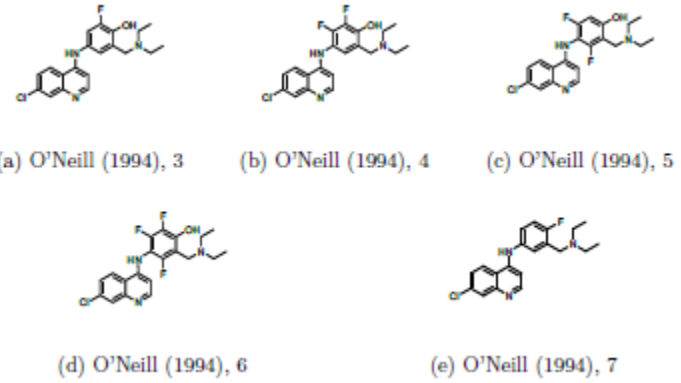

(a) O'Neill (1994), 3 (b) O'Neill (1994), 4 (c) O'Neill (1994), 5

(d) O'Neill (1994), 6 (e) O'Neill (1994), 7

Figure 35: Compounds that illustrate SAR studies of the para-hydroxyl group of amodiaquine and amodiaquine-analog antimalarials.

Figure 35(a), Figure 35(b), Figure 35(c), Figure 35(d), Figure 35(e) Structures of fluorine amodiaquine analogs aimed at reducing amodiaquine toxicity.

Later work with the same aim demonstrated that the position of amodiaquine's Mannich base and hydroxyl group could be interchanged Figure 36(a), resulting in amodiaquine regioisomers. As the oxidation of the para-hydroxyl group was suggested to form a toxic quinone imine, by exchanging the position of the two substituents, the resulting analog would be unable to undergo an oxidation event to form the toxic intermediate, due to an unfavorable electronic distribution. The meta-hydroxyl amodiaquine derivative containing the same diethylamino Mannich base as amodiaquine, dubbed isoquine Figure 36(b), was favored as the superior compound. Isoquine was demonstrated to maintain *in vitro* potency against chloroquine resistant and sensitive strains of *P. falciparum*, compared to amodiaquine, and was found to exhibit improved *in vivo* efficacy and evade bioactivation to a glutathione containing metabolite in rats. Further optimization of isoquine resulted in favor of the tert-butylamino compound, 4a Figure 36(c) (GSK369796). When compared to isoquine, the *N-tert*-butyl isoquine demonstrated improved *in vivo* efficacy in *P. berghei* and *P. yoelii* models, and pharmacokinetic properties. *N-tert*-butyl isoquine exhibited reduced blood clearance (CL) and improved bioavailability (%F) compared to isoquine.

Despite *N-tert* butyl isoquine demonstrating a superior pharmacokinetic profile to amodiaquine and chloroquine in mice, rats, dogs, and monkeys, development was halted due to exposure limitations and not demonstrating an improved safety window compared to amodiaquine and chloroquine.

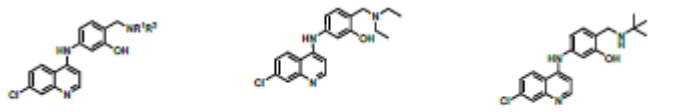

(a) O'Neill (2003) (b) O'Neill (2003), isoquine (c) O'Neill (2003), 4a

Figure 36: Compounds that illustrate SAR studies of the para-hydroxyl group of amodiaquine and amodiaquine-analog antimalarials.

Figure 36(a) Markush structure of compounds from O'Neill et al. (2003) that aim to reduce amodiaquine toxicity by swapping arrangement of para-hydroxyl and meta-Mannich base, resulting compounds isoquine and 4a (Figure 36(b), Figure 36(c)) were highly active, efficacious, with a safer toxicology profile.

It is clear that the hydroxyl group can be removed with little effect on antiplasmodial activity. Furthermore, moving it or replacing it with another electronegative moiety that resists oxidation has the potential to create a compound that overcomes amodiaquine's shortcomings. Examples like isoquine and GSK369796 highlight the importance of balancing lipophilicity and solubility for *in vivo* efficacy.

5.3.2. Rationale for Amodiachins

Taken together, previous structure-activity relationship studies provide actionable directions for continued amodiaquine analog diversification. The primary goal of amodiaquine analogs has been and continues to be maintaining antiplasmodial activity against drug-resistant *P. falciparum*, reducing toxicity, while improving *in vivo* efficacy in hopes of an improved pharmacokinetic profile. The compounds reported in Chapter 6 highlight the work towards these goals.

5.4. Bisquinolines

Another option to further develop amodiaquine analogs is to blend the chemotype with another 4-aminoquinoline. As piperaquine has proven to be a successful bisquinoline antimalarial, it was thought that successful amodiaquine analogs could be used to inspire the design of next-generation bisquinolines. Structure-activity relationship studies based around a bisquinoline core have yet to yield any approved antimalarials, besides piperaquine, but have produced extremely active antimalarials.

5.4.1. SAR of Bisquinolines

Most of the bisquinoline SAR studies are based on chloroquine and center on examining the effect of different bisquinoline linkages on antiplasmodial activity. One of the most successful campaigns was demonstrated early on by Vennerstrom et al. (1992), where the effect of the chain length and branching of N,N-alkylamine linkers was examined, as seen in Figure 37(a),

Figure 37(b), Figure 37(c). Notable relationships include the dependency of linker length Figure 37(c), as shifting from a 1,3-diaminopropane linker (X = CH_2) to a 1,4-diaminobutane linker (X = CH_2CH_2) reduced activity, but was restored when linked with a 1,5-diaminopentane (X = $CH_2CH_2CH_2$). Additionally, the branched propyl linker, 1,2-diaminopropane Figure 37(a), showed enhanced activity compared to the unbranched 3-diaminopropane. The bisquinoline with a 1,2-diaminocyclohexane linker, Figure 37(b), was demonstrated to be the most active compound from the series, suggesting the induced rigidity might contribute to its enhanced activity. Further studies on the 1,2-diaminocyclohexane-containing bisquinoline demonstrated that the S,S enantiomer, Ro 47-7737, was the superior antimalarial. The compound exhibited higher activity in both chloroquine resistant and sensitive strains of *P. falciparum* compared to the other enantiomers. Despite activity in *P. vivax* and enhanced *in vivo* efficacy in *P. berghei* compared to chloroquine, further development of Ro 47-7737 was halted due to observed phototoxicity during dose toxicity evaluation.

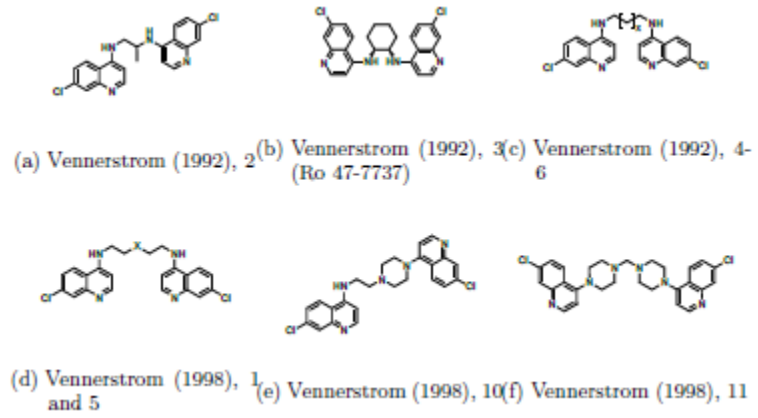

Figure 37: Compounds that illustrate SAR studies of bisquinoline antimalarials.

Figure 37(a), Figure 37(b), Figure 37(c) Structures of compounds that examined the effects of linker length and branching of bisquinolines on antimalarial activity. Figure 37(c) Derivatives feature X = CH_2, CH_2CH_2, $CH_2CH_2CH_2$. Figure 37(d) Structures of bisquinoline compounds (X = N or O), used to evaluate the influence of heteroatom substitution on antimalarial activity. , Figure 37(e), Figure 37(f) Structures of bisquinoline compounds used to further elucidate the contribution of heteroatom-containing linkers on antimalarial activity.

Following the previous work, Vennerstrom et al. (1998) examined the effect of incorporating nitrogen and oxygen atoms into the alkane linker of the bisquinolines on activity and heme binding, Figure 37(d). Many of the compounds from this series maintained nanomolar activity in both sensitive and chloroquine resistant (1.2 nM to 89 nM), only a small subset were efficacious *in vivo*. Interestingly, replacing the 1,5-diaminopentane linker with either a bis(2-aminoethyl)amine, Figure 37(d) (X = N), or bis(2-aminoethyl)ether, Figure 37(d) (X = O), did not improve *in vitro* activity, but the ether analog performed better *in vivo* than the parent, Figure 37(c) (X = $CH_2CH_2CH_2$). Two compounds with piperazine containing linkers, aminoethylpiperazine (Figure 37(f)) and di(piperazin-1-yl)methane (Figure 37(e)), provided a curative dose at 160 and 640 mg/kg to *P. berghei* infected mice. While the aminoethylpiperazine analog exhibited nanomolar activity in both strains of *P. falciparum*, the di(piperazin-1-yl)methane was inactive (>1000 nM).

In 2012, van Heerden et al. reported a series of polyamine-bridged bisquinolines that were aimed at capitalizing on the ion-trapping nature of 4-aminoquinolines by increasing the number of protonatable amines. They demonstrated that the negative effects of lengthening the chain of polyamines outweighed the positive effect of additional ionizable amines and increased solubility. The bisquinolines analogs with either a triethylenetetramine, Figure 38(a), or N^1,$N^{1'}$-(ethane-1,2-diyl)bis(propane-1,3-diamine), Figure 38(b), linkers demonstrated the highest activity, but they were significantly less active than piperaquine in both sensitive and chloroquine resistant *P. falciparum* strains.

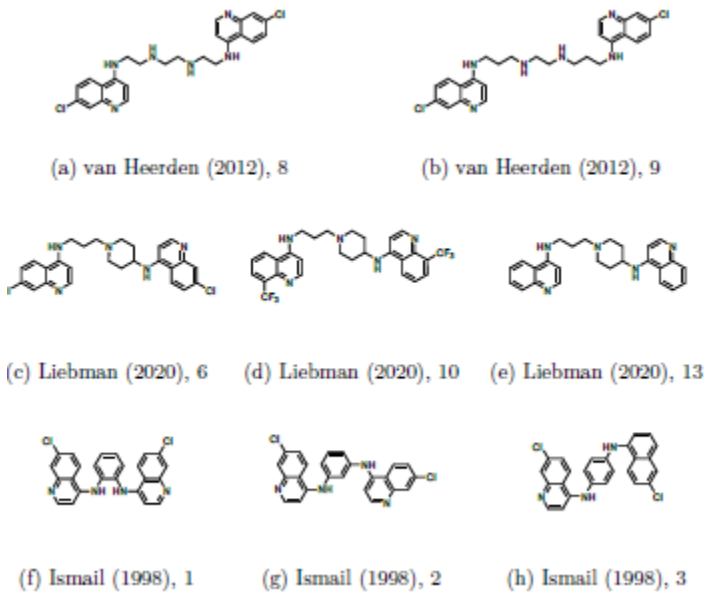

(a) van Heerden (2012), 8 (b) van Heerden (2012), 9

(c) Liebman (2020), 6 (d) Liebman (2020), 10 (e) Liebman (2020), 13

(f) Ismail (1998), 1 (g) Ismail (1998), 2 (h) Ismail (1998), 3

Figure 38: Compounds that illustrate SAR studies of bisquinoline antimalarials, continued.

Figure 38(a), Figure 38(b) Structures of bisquinoline compounds that were created to examine the extent that polyamine linkers influenced antimalarial activity. , Figure 38(c), Figure 38(d), Figure 38(e) A few examples of bisquinoline compounds that examined the influence that quinoline substitution had on antimalarial activity. , Figure 38(f), Figure 38(g), Figure 38(h) Highlighted structures of bisquinoline compounds that examined the influence that phenylenediamine linkers had on antimalarial activity.

Liebman et al. (2020) demonstrated similar findings in a series of bisquinolines designed taking inspiration from chloroquine and piperaquine, with varying alkylamine linkages between quinolines where the substituent pattern is unsymmetrical. The rationale for the series was that the tertiary amine in piperaquine reduces the compound's antiplasmodial activity, as the bisquinoline compound containing a 1-(3-aminopropyl)piperidin-4-amine linker was nearly an order of magnitude more active than piperaquine in chloroquine-sensitive and chloroquine-resistant *P. falciparum*. Unfortunately, the cytotoxicity of this compound was elevated compared to chloroquine when assessed in mouse spleen lymphocytes.

The compounds from a series discovered by Ismail et. al (1998) are some of the only bisquinolines that are remotely similar to amodiaquine. Instead of an alkyl linker, these bisquinolines were bridged through *ortho*-, *meta*-, or *para*-amino aniline. The three compounds were assessed only for antimalarial activity in the *P. berghei* mouse model. The *ortho* and *para*

products exhibited minimal activity at experimental doses; however, the *meta*-amino aniline was more active than chloroquine in the same conditions.

5.4.2. Rationale for Amodiaquine-inspired bisquinolines

Despite the intrigue in bisquinolines in the late 90's and their prolonged investigation thereafter, there remains a paucity of amodiaquine-inspired bisquinoline compounds. By taking an early-stage antimalarial compound that exhibits a real potential to be a therapeutic option, such as the compounds in Chapter 6, and blending it with a historically active chemotype, the resulting pharmacophore has the capacity to become a strong antimalarial candidate. Chapter 7 details the work toward this goal.

Part II. Results

6. Discovery of Amodiachins, a Novel Class of 4-Aminoquinoline Antimalarials Active Against Multidrug-Resistant Plasmodium falciparum.

The text, figures, schemes, and tables are previously published in the *Journal of Medicinal Chemistry* under the same title and are reprinted with permission. Terry Riscoe assisted the author in determining the antiplasmodial activity of each compound. *In vivo* efficacy experiments were performed by Dr. Yuexin Li. *In vitro* metabolic stability and pharmacokinetic experiments were performed by a contract research organization (CRO).

6.1. Introduction

Malaria is a devastating disease caused by the parasitic infection of *Plasmodium spp*., and is spread from host to host through infected female Anopheles mosquitoes.[1–5] Compared to pre-pandemic estimates in 2019, malaria cases have risen from 229 million to a staggering 263 million cases worldwide in 2023, while deaths have increased from 409,000 individuals in 2019 to an estimated 567,000 people in 2023.[1,3] The emergence and spread of resistant strains of the deadliest species, *P. falciparum* (*Pf*), threaten global prevention, treatment, and eradication efforts. Therefore, the discovery and development of novel therapies that overcome existing resistance mechanisms of *P. falciparum* are desperately needed.

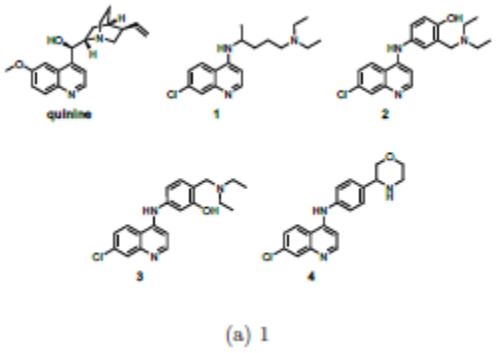

(a) 1

Figure 39: Chemical structures of the antimalarials quinine and select 4-aminoquinolines.

*Chloroquine (**1**), amodiaquine (**2**), and isoquine (**3**). Representative structure (**4**) of initial rationale for the amodiachin SAR study described henceforth.*

The discovery of the natural product quinine and its use to treat malaria inspired research programs that ultimately led to the discovery of successful 4-aminoquinoline antimalarials: chloroquine, amodiaquine, and piperaquine in particular (Figure 39). Unfortunately, chloroquine was deployed as a monotherapy in worldwide efforts to prevent and cure malaria, and now chloroquine resistance in *Plasmodium falciparum* has spread to virtually all disease-endemic areas around the globe. Further development of the 4-aminoquinoline scaffold gave rise to amodiaquine (**2**), which was shown to overcome chloroquine-resistant strains of *Pf*.[,] Despite decades of use, amodiaquine's clinical use has been restricted due to its connection with hepatotoxicity and agranulocytosis. The observed toxicity appears to be associated with the P-450-catalyzed oxidation of the *para*-hydroxyl moiety of amodiaquine.[,] Work to eliminate this metabolic liability resulted in an amodiaquine regioisomer, isoquine (**3**). When the *para*-hydroxyl and *meta*-Mannich base were interchanged, isoquine exhibited an improved toxicological profile and increased activity *in vitro* and *in vivo* compared to amodiaquine; however, during preclinical evaluation, isoquine underwent a high rate of first-pass metabolism, posing a significant challenge to further development and compromising isoquine activity in chloroquine-resistant (CQR) *Plasmodium* parasites. While the advancement of isoquine for clinical trials was halted, this work highlights exploitable chemical space that overcomes drug resistance to previous 4-aminoquinoline analogs. In our group's previous work of 4-aminoquinolines, structure activity relationship (SAR) studies focusing on the 3-methyl position of the quinoline in the sontochin-like series named "pharmachins" indicated improved activity against CQR strains when replaced by a trifluoromethoxy phenyl. This result suggested that increasing rigidity at the 3-position by adding aromatic rings and/or heterocycles improves potency against CQR and multidrug-resistant (MDR) strains. We decided to adopt the same strategy to rigidify the 4-position side chain of amodiaquine to overcome drug resistance and to address the toxicity issue by eliminating conversion to a toxic quinoneimine metabolite. Focusing on the aryl substitution pattern of amodiaquine we sought to replace the labile hydroxy group and diethylaminomethyl feature with basic substituted heterocycles (**4**, Figure 39) as a countermeasure to chloroquine resistance and to increase metabolic stability. Herein, we introduce a new series termed "amodiachins" (ADCs) by describing the associated structure activity profile against MDR *P. falciparum* parasites, and for select molecules we provide the results from testing for metabolic stability, cytotoxicity, pharmacokinetics, and efficacy in a murine model of malaria infection.

6.2. Chemistry

The initial compound design was focused on creating an amodiaquine-like structure with a *para*-substituted heterocycle, while incorporating a trifluoromethoxy phenyl at the 3-position of the quinoline ring, similar to the pharmachins. Compounds **7**-**21** were synthesized using the procedures outlined in Scheme [schm-adc1], Scheme [schm-adc2], and Scheme [schm-adc3]. Starting materials **5** and **6a** were commercially available, however **6b** was synthesized in-house using previously described methods. Respective 4-aminoquinolines were prepared using either, (i) ethanol and catalytic 12 M hydrochloric acid at reflux, or (ii) 2-ethoxyethanol and phenol at 150 °C.

Compounds **12**-**17** were prepared from the respective para-substituted bromobenzene (**9a-c**) and either alkylated with iodoethane or benzyl bromide (**10a**-**10d**). **11a**-**11d** were prepared through amination of the para-substituted bromobenzene intermediates using a Buchwald-Hartwig cross-coupling reaction to afford the para-substituted anilines. Final compounds **12**-**17** were prepared through previously described reaction conditions (ii).

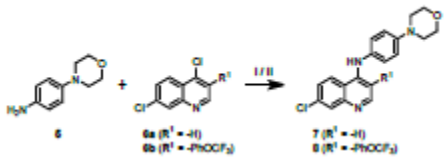

Figure 40: Synthesis of initially designed amodiachins. Reagents and conditions.

(i) aniline, 4-chloroquinoline, EtOH, fuming HCl, reflux 16 h. (ii): aniline, 4-chloroquinoline, phenol, EGEE, 150 °C, 12 h.

Scheme [schm-adc3] depicts the chemical synthesis of compounds **20**-**26** using methods (i) and (vi) to examine the contribution of the quinoline ring substituents to antiplasmodial activity. Commercially available **18a** and **18b** were used in the preparation of compounds **20**-**26** using a previously described method (i) or an alternative method (vi) where the appropriate 4-chloro containing quinoline was mixed with the appropriate aniline in the presence of phenol in DMF and heated to 150 °C for 45 min in a microwave reactor.

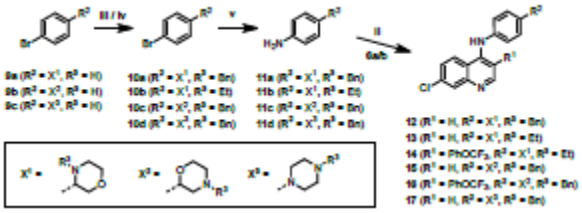

Figure 41: Synthesis of initially designed amodiachins. Reagents and conditions.

(i) aniline, 4-chloroquinoline, EtOH, fuming HCl, reflux 16 h. (ii): aniline, 4-chloroquinoline, phenol, EGEE, 150 °C, 12 h. (iii): substituted bromobenzene, 2M K2CO3, bromobenzene, DMF, 50 °C, 12 h. (iv): substituted bromobenzene, iodoethane, DIPEA, DMF, rt, 48 h. (v): substituted bromobenzene, Pd(t-Bu3P)2, Pd(dba)2, LiHMDS, toluene, 70 °C, 18 h, HCl.

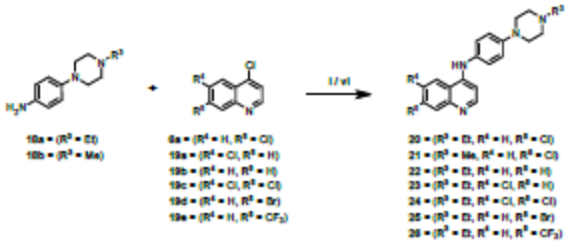

Figure 42: Synthesis of compounds to explore the contribution of substituents around benzenoid ring of the quinoline core.

Reagents and conditions: (i) aniline, 4-chloroquinoline, EtOH, fuming HCl, reflux 16 h. (vi) aniline, 4-chloroquinoline, phenol, DMF, 150 °C, 2 h.

Target compounds **31**-**45** were prepared by the synthesis outlined in Scheme [schm-adc4] to assess the contribution of the heterocycle to antiplasmodial activity and later the contribution of the tertiary amine's alkyl substituent (Scheme [schm-adc4], R^6, R^7) to *in vivo* antimalarial efficacy. Compounds **31** and **32** were synthesized from commercially available alkyl piperazines (**28a** and **28b**) and **27** with trimethylamine in DMSO at 120 °C for 16 h (vii). The resulting intermediates were reduced to the appropriate aniline and then used in the previously described procedure (i) with **6a** to afford the final product. Commercially available **30c**-**30e** and **6a** were used in previously described procedures (vi) to produce compounds **33**-**35**. Compounds **36** and **37** were synthesized from **30f** and **30g** in the presence of **6a** in THF at 120 °C for 20 minutes (ix). To afford compounds **40**-**45**, **36** and **37** were deprotected in the presence of trifluoroacetic acid in dichloromethane (x) and then reacted with the appropriate alkyl halide and either (xi) DIPEA in DMF at room temperature for 16 h or (xii) potassium carbonate in DMF at 85 °C for 16 h.

6.3. Results and Discussion

Compounds were assessed for antiplasmodial activity against drug-sensitive (D6) and multidrug-resistant (Dd2) strains of *Plasmodium falciparum* in a fluorescence-based antiplasmodial assay and are reported in Table 2, Table 3, Figures 46 and 47, and Table 6.·. The *P. falciparum* strain Dd2 is reported to be resistant to mefloquine, cycloguanil, pyrimethamine, and chloroquine.· Morpholine-containing compounds **7, 8,** and **12**-**16** had limited activity (*Pf*D6 and *Pf*Dd2 $IC_{50} \geq$ 250 nM, Table 2), with compounds **13** and **15** exhibiting minimal antiplasmodial activity against *Pf*D6, $IC_{50} = 69 \pm 28$ nM and 101 ± 15 nM, respectively.

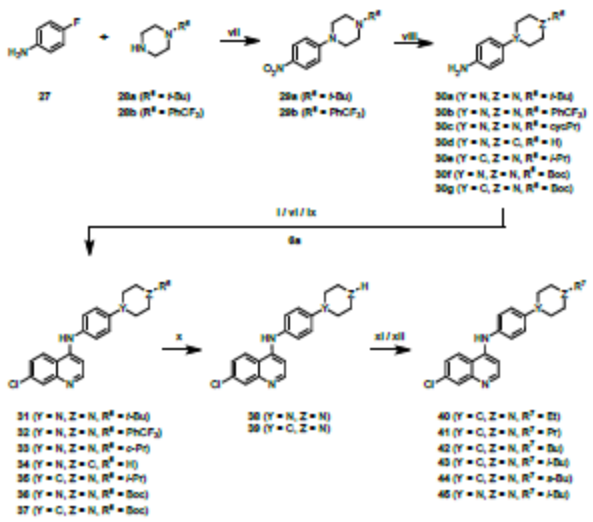

Figure 43: Synthesis of amodiachins that explored the contribution of the heterocycle.

Reagents and conditions: (vii) 27, substituted piperazine, TEA, DMSO, 120°C, 16 h. (viii) substituted nitrobenzene, Pd/C, MeOH,12 h. (i) aniline, 4-chloroquinoline, EtOH, fuming HCl, reflux 16 h. (vi) aniline, 4-chloroquinoline, phenol, DMF, 150 °C, 2 h. (ix) aniline, 4-chloroquinoline, THF, 120 °C, 20 m. (x): 4-analinoquinoline, TFA, DCM, 2 h. (xi): 4-analinoquinoline, iodoethane, DIPEA, DMF, rt, 16 h. (xii): 4-analinoquinoline, alkyl halide (1.2 equiv.), K2CO3, DMF, 85 °C, 16 h.

However, this level of activity was not maintained against the *Pf*Dd2 strain (Table 2). Moving away from the morpholine heterocycle, a piperazine ring was next implemented as in **17**. Promising activity against drug- sensitive *Pf*D6 IC_{50} = 20 ± 3 nM and drug-resistant *Pf*Dd2 IC_{50} = 26 ± 9 nM, was observed with this compound. Concerned that this molecule might be unstable to microsomal metabolism it was decided to replace the terminal aromatic ring with an ethyl (**20**) and methyl (**21**) group.

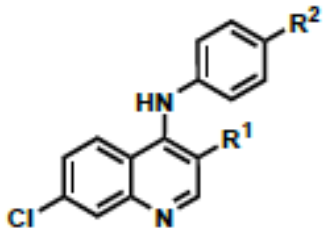

Figure 44: Markush structure (above) of select analogs and associated antiplasmodial activity against PfD6 and PfDd2 and cytotoxicity in HepG2 mammalian cells.

Antiplasmodial activity (IC_{50}) values and standard deviations (SD) were derived from the average of at least three independent experiments, each performed in quadruplicate. Cytotoxicity (CC_{50}) assay was performed using human hepatoma derived HepG2 cells across an initial

concentration of 200 µM to 10 nM in triplicate. ClogP values calculated using ChemDraw software (version 22). Details of assays performed can be found in Chapter 10.

The structure activity profile was further investigated by varying the substituents at the 6- and 7-positions of the quinoline ring Table 3. Interestingly, loss of the 7-position chlorine in **22** reduces potency in combination with decreased susceptibility against *Pf*Dd2. However, introducing a chlorine atom at the 6-position (**23**) returns activity across both strains, but a reduction in potency is still observed. It was not until the 7-position chlorine was reintroduced, as in **24**, that we observed the potency return to the low nanomolar (≤ 20 nM) range. Clearly, the 7-position chlorine was essential for potent activity and therefore substitutions were varied at the critical 7-position to include bromine **(25)**, as well as trifluoromethyl **(26)**. The importance of the 7-position chlorine to the antimalarial activity of some 4-aminoquinolines is well established across drug discovery campaigns and is suggested to play a vital role in the 4-aminoquinoline mechanism of action. Herein, we can see that although activity against *Pf*D6 and *Pf*Dd2 is maintained with both derivatives, **25** was more toxic to mammalian cells (CC_{50} = 48) than its progenitor **20**. Furthermore, the trifluoromethyl derivative, **26**, exhibited a slight decrease in antiplasmodial activity against the drug-sensitive *Pf*D6 strain.

Compound ID	**R1 Group**	**R2 Group**	**IC50 vs D6 ± SD (nM)**	**IC50 vs Dd2 ± SD (nM)**	**CC50 vs HepG2 (µM)**	**CLogP**
1	-	-	9.6 ± 2.0	106 ± 10.0	38	5.06
7	H	morpholine	≥ 250	≥ 250	> 200	4.6
8	4-methoxyphenyl	morpholine	≥ 250	≥ 250	> 200	7.61
12	H	benzyl morpholine	≥ 250	≥ 250	> 200	6.59
13	H	ethyl morpholine	69.0 ± 28.0	≥ 250	> 200	5.25
14	4-methoxyphenyl	ethyl morpholine	≥ 250	≥ 250	> 200	8.26
15	H	benzyl morpholine	101.0 ± 15.0	≥ 250	38	6.45
16	4-methoxyphenyl	benzyl morpholine	≥ 250	≥ 250	> 200	9.46
17	H	benzyl piperazine	20.0 ± 3.0	26 ± 9.0	> 200	6.88
20	H	ethyl piperazine	10.0 ± 3.0	26 ± 12.0	> 200	5.69
21	H	substituted piperazine	14.0 ± 5.0	23 ± 9.0	185	5.16
38	H	methyl piperazine	51.0 ± 66.0	30 ± 33.0	54	4.58

Table 2: Antimalarial activity, cytotoxicity, and physicochemical properties of selected quinoline-based compounds.

Compound ID	R³ Group	IC_{50} vs. D6 ± SD (nM)	IC_{50} vs. Dd2 ± SD (nM)	CC_{50} vs. HepG2 (μM)	CLogP
20	Substituted quinoline group	10 ± 3	27 ± 12	> 200	5.69
22	Substituted quinoline group	44 ± 27	90 ± 38	106	4.88
23	Substituted quinoline group	48 ± 30	53 ± 19	> 200	5.69
24	Disubstituted quinoline group	18 ± 10	26 ± 9	> 200	6.31
25	Bromo-substituted quinoline group	9 ± 4	14 ± 8	48	5.84
26	Trifluoromethyl-substituted quinoline group	15 ± 4	29 ± 10	> 200	5.93

Table 3: Markush structure and biological activity of select analogs

Having established that the 7-position chlorine atom was an essential element for antiplasmodial activity in this 4-aminoquinoline SAR campaign, we returned our focus to the 4-position sidechain. Indeed, from the results presented in Table 2, the attachment of a piperazine ring to the aromatic phenyl group greatly improves antiparasitic activity. We therefore decided to explore the effect of structural variation of the N-terminal group on antiplasmodial activity; results are reported in Figures 46 and 47. The *N*-Boc protected analog (**36**) exhibited diminished antiplasmodial activity, which may relate to the weakened basicity of the carbamate nitrogen. This is consistent with the poor activity of **38**, where the same nitrogen atom carries only a hydrogen atom. Use of a large aromatic trifluoromethylphenyl group (**38**) also diminished the activity relative to **20**. In hopes of enhancing basicity and metabolic stability at the outermost ring nitrogen, we introduced cyclopropyl (**33**) and *tert*-butyl (**31**) groups. While the results for **33** showed relatively modest antiplasmodial activity, we found that the potency of **31** was in the low nanomolar range (≤ 20 nM) against both *Pf*D6 and *Pf*Dd2. Following these results, we explored the contribution of the individual piperazine nitrogen atoms to antiplasmodial activity. This led to the design and synthesis of two novel piperidine derivatives – one with a nitrogen atom attached directly to the aromatic ring (**34**) and another with a nitrogen atom at the outermost position (**39**) as a secondary amine. The activity of **34** was severely reduced in both strains of *Pf*, but when the piperidine nitrogen was presented as a secondary amine (**39)** activity in *Pf*D6 was maintained compared to **20**, but susceptibility of *Pf*Dd2 was decreased to 71 ± 15 nM. This same effect was observed in the similar compound **38** (Table 2). Next, we decided to explore the impact of converting the outer secondary amine of **39** to a tertiary amine by addition of an ethyl group. That strategy proved effective; when adorned with an ethyl substituent, compound **40** provided impressively low nM IC_{50} values with an increase in activity against multidrug-resistant *Pf*Dd2. It is noteworthy that **40** exhibits a modest level of cytotoxicity against mammalian cells in culture (CC_{50} = 111 μM). We therefore decided to explore the impact of increasing the length and branching of the terminal alkyl group, as the addition of the ethyl substituent in **40** appeared to decrease the cytotoxicity compared to **39** (CC_{50} = 58 μM). Excitingly, the addition of an *N*-isopropyl group in **35** further decreased cell cytotoxicity (CC_{50} > 200 μM) while exhibiting

equipotency against *Pf*D6 and *Pf*Dd2. In summary, these results demonstrate that amodiachin derivatives containing either a 4-aminophenyl piperazine bridge or a 4-aminophenyl piperidine bridge exhibit excellent potency against both sensitive and multidrug-resistant strains of *Pf*. Furthermore, the presence, length, and degree of branching of the *N*-alkyl substituent can significantly influence potency against drug-sensitive and drug-resistant strains of *Pf*, and the degree of cytotoxicity.

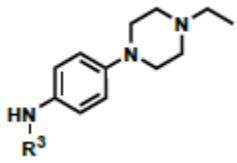

Figure 45: Markush structure (above) of select analogs and associated antiplasmodial activity against Pf D6 and Pf Dd2 and cytotoxicity.

Compound ID	**R³ Group**	**IC₅₀ vs. D6 ± SD (nM)**	**IC₅₀ vs. Dd2 ± SD (nM)**	**CC₅₀ vs. HepG2 (µM)**	**CLogP**
20	Substituted quinoline group	10 ± 3	27 ± 12	> 200	5.69
22	Substituted quinoline group	44 ± 27	90 ± 38	106	4.88
23	Substituted quinoline group	48 ± 30	53 ± 19	> 200	5.69
24	Disubstituted quinoline group	18 ± 10	26 ± 9	> 200	6.31
25	Bromo-substituted quinoline group	9 ± 4	14 ± 8	48	5.84
26	Trifluoromethyl-substituted quinoline group	15 ± 4	29 ± 10	> 200	5.93

Table 4: Markush structure and biological activity of select analogs.

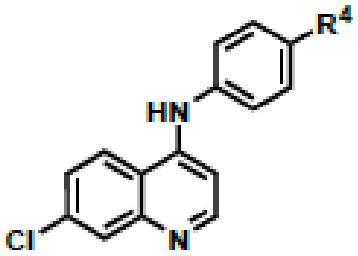

Figure 46: Markush Structure of Selected Antiplasmodial Analogs.

Compound ID	**r4**	**IC_{50} vs. D6 ± SD (nM)**	**IC_{50} vs. Dd2 ± SD (nM)**	**CC_{50} vs. HepG2 (µM)**	**CLogP**
36	Chemical structure for compound 36 was not available in the uploaded source image.	69 ± 34	217 ± 57	> 200	6.57
32	Chemical structure for compound 32 was not available in the uploaded source image.	54 ± 27	95 ± 41	> 200	7.7
33	Chemical structure for compound 33 was not available in the uploaded source image.	27 ± 22	68 ± 54	> 200	5.53
31	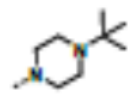	11 ± 13	11 ± 8	> 200	6.39
34		197 ± 75	200 ± 71	> 200	5.98
39	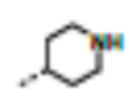	9 ± 2	71 ± 15	58	5.34

Compound ID	r4	IC_{50} vs. D6 ± SD (nM)	IC_{50} vs. Dd2 ± SD (nM)	CC_{50} vs. HepG2 (µM)	CLogP
40		5 ± 2	11 ± 3	111	6.32
35	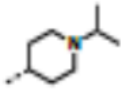	4 ± 2	10 ± 6	> 200	6.63

Figure 47: Compound activity and physicochemical properties.

At this point, amodiachins were selected for use in further studies based on antiplasmodial activity (*Pf*D6 IC_{50} < 20 nM), susceptibility in the drug-resistant strain (*Pf*D6 IC_{50} / *Pf*Dd2 IC_{50} < 2.5), and cytotoxicity (CC_{50} > 100 µM). Compounds were next evaluated for metabolic stability in pooled liver murine microsomes (Table 5), from which intrinsic metabolic stability ($t_{1/2}$) was calculated.

Compound	$t_{1/2}$ (min), CL_{int} (mL/min/kg)	% *Py* Suppression (2.5 mg/kg/d)	ED_{50} v *Py* (mg/kg/d)	ED_{90} v *Py* (mg/kg/d)	NRD (mg/kg/d)
17	, 391.9	%	-	-	-
20	, 2930	%			ND (10)
21	, 3784	-	-	-	-
31	∞ , 0.00	%			ND (20)
40	, 496.7	%			ND (10)
35	, 123.6	%			ND (10)

Table 5: Microsomal stability, parasite burden suppression, and in vivo efficacy of select amodiachins.

The values $t_{1/2}$ and CL_{int} determined from HPLC UV traces from pooled murine liver microsomes incubated with drug. All animal studies used group sizes of n = 4 per dose regimen. (-) = not performed. ND() = not detected at corresponding dosage. Full procedure for microsomal stability and in vivo assays can be found in Chapter 2.

The difference between methyl and ethyl in the *N*-alkyl substituent (**21** and **20**) at the outermost nitrogen of piperazine did not enhance metabolic stability ($t_{1/2}$ = 1.44 and 1.86 min, respectively). However, when capped with a benzyl moiety as in **17**, stability was noticeably increased ($t_{1/2}$ = 13.9 min). Interestingly, when adorned with a heavily branched *tert*-butyl group found in **31**, no detectable amount of compound was metabolized over the course of the experiment. Evaluating piperidine-containing analogs led to a similar observation, increasing the *N*-alkyl branching by a single carbon in **40** increases stability ($t_{1/2}$ = 11.0 to 44.1 min) as seen in **35**. All compounds except **21** were down-selected for *in vivo* assessment of antiplasmodial

activity in a modified Peter's 4-day murine malaria model against *P. yoelii*. Each analog was tested at a fixed dose of 2.5 mg/kg/d, and parasitemia on the fifth day was determined from direct microscopic analysis of Giemsa-stained blood smears. Percent parasite suppression (Table 5) was calculated from the average parasitemia of experimental groups compared to the average parasitemia of the vehicle-only control group. All compounds except **17** exhibited modest suppression at this dose and were selected as candidates for further evaluation to establish the effective dose to reduce parasitemia by 50% (ED_{50}) and 90% (ED_{90}), as well as attempts to determine a non-recrudescence dose (NRD). Compounds **20** and **40** exhibited a relatively large gap between ED_{50} and ED_{90}, suggesting rapid metabolism, as previously indicated by the results of the microsomal stability assay, or possibly due to poor absorption. The most effective antimalarial from this screen was **35,** with an ED_{50} and ED_{90} of 1.1 and 4.1 mg/kg/d, respectively. Since **35** exhibited a high degree of antiplasmodial activity in addition to superior *in vivo* efficacy and metabolic stability, we thought to investigate the interplay of the piperidyl *N*-alkyl substituent and the resulting pharmacodynamic and pharmacokinetic profile.

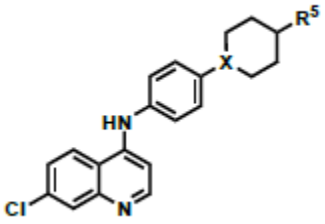

Figure 48: Markush Structure of R^5-Substituted Antiplasmodial Analogs.

Compound ID	**R^5 substituent**	**IC_{50} vs. Pf D6 ± SD (nM)**	**IC_{50} vs. Pf Dd2 ± SD (nM)**	**CC_{50} vs. HepG2 (µM)**	**CLogP**
40	R^5 structure for compound 40 was not available in the uploaded source file.	5.0 ± 2.0	11 ± 3	111	6.32
35	R^5 structure for compound 35 was not available in the uploaded source file.	4.0 ± 2.0	10 ± 6	> 200	6.63
41		8.0 ± 3.0	15 ± 6	> 200	6.85
42	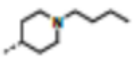	4.0 ± 4.0	11 ± 13	> 200	7.37

Compound ID	R^5 substituent	IC_{50} vs. Pf D6 ± SD (nM)	IC_{50} vs. Pf Dd2 ± SD (nM)	CC_{50} vs. HepG2 (µM)	CLogP
43	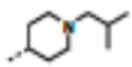	7.0 ± 7.0	10 ± 11	> 200	7.25
44	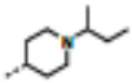	2.6 ± 1.7	9 ± 9	> 200	7.15
45		8.0 ± 2.0	12 ± 6	> 200	6.62

Table 6: R^5 analogs and associated activity against Pf D6 and Pf Dd2, cytotoxicity in HepG2 cells, and calculated CLogP values.

Markush structure of selected analogs and associated antiplasmodial activity against Pf D6 and Pf Dd2 and cytotoxicity in HepG2 mammalian cells.

Antiplasmodial activity (IC_{50}) values and standard deviations (SD) were derived from the average of at least three independent experiments, each performed in quadruplicate.

The cytotoxicity (CC_{50}) assay used human hepatoma-derived HepG2 cells across concentrations from 200 µM to 10 nM and was performed in triplicate.

CLogP values were calculated using ChemDraw software, version 22. Details of the assays are provided in Chapter 10.

Abbreviations: IC_{50}, half-maximal inhibitory concentration; CC_{50}, half-maximal cytotoxic concentration; SD, standard deviation; nM, nanomolar; µM, micromolar; Pf, Plasmodium falciparum.

Compound	$t_{1/2}$ (min); CLint (mL/min/kg)	% Py suppression (2.5 mg/kg/day)	ED_{50} vs. Py (mg/kg/day)	ED_{90} vs. Py (mg/kg/day)	NRD (mg/kg/day)	SDC (mg/kg)
35	44.1; 123.6	48%	Not performed	Not performed	Not performed	Not performed
41	70.0; 78.0	39%	Not performed	Not performed	Not performed	Not performed
42	42.1; 129.7	53%	Not performed	Not performed	Not performed	Not performed
43	48.2; 113.3	91%	2.2	2.7	16	50
44	55.5; 98.3	71%	Not performed	Not performed	Not performed	Not performed
45	6.47; 842.9	30%	Not performed	Not performed	Not performed	Not performed

Table 7: Microsomal stability, parasite burden suppression, and in vivo efficacy of select amodiachins.

The $t_{1/2}$ and CLint values were determined from HPLC UV traces from pooled murine liver microsomes incubated with the drug.

All animal studies used group sizes of n = 4 per dose regimen.

A dash in the source table indicates that the test was not performed. In this accessible table, each dash has been replaced with "Not performed."

The full procedure for microsomal stability and in vivo assays is provided in Chapter 10.

Abbreviations: $t_{1/2}$, half-life; CLint, intrinsic clearance; Py, Plasmodium yoelii; ED_{50} and ED_{90}, effective doses producing 50% and 90% effects; NRD and SDC are reproduced from the source table because the full terms were not provided in the supplied image; HPLC, high-performance liquid chromatography; UV, ultraviolet.

Compounds **41**-**44** were synthesized to explore the effect of piperidyl N-alkyl substituents on *in vitro* activity and *in vivo* efficacy by including structural isomers of 3- and 4-carbon alkyl chains. All compounds exhibited similar *in vitro* activities against *Pf*D6 and *Pf*Dd2 (Table 6) and sustained minimal cytotoxicity (CC_{50} > 200 μM). When examined for murine microsomal stability (Table 7), **41** demonstrated superior stability ($t_{1/2}$ = 70 minutes) compared to compounds **42**, **43**, and **44**, which displayed similar stability to **35**. Given the excellent *in vitro* profile of **41**-**44**, all compounds were selected for *Py* parasite suppression (Table 7). Surprisingly, **41** produced the lowest degree of parasitemia suppression among the tested analogs, with 39% suppression compared to control, whereas **43** reduced parasitemia by 91% compared to control. Although **41**-**44** met the selection thresholds, *in vivo* efficacy was assessed for **43** alone, due to the high degree of *Py* suppression (Table 7). Compound **43** revealed an impressive *in vivo* efficacy profile, albeit with a higher ED_{50} (2.2 mg/kg/d) than compounds **20**, **40**, and **35** (ED_{50} = 1.5, 1.8, and 1.1 mg/kg/d, respectively), but an ED_{90} = 2.7 mg/kg/d was the lowest compared to all previously tested compounds (Table 5). When given at 16 mg/kg/d, **43** eliminated the parasite burden by Day 5, and recrudescence was prevented for the remainder of the experiment (Day 30). It should be noted that 3 out of 4 mice were cured at the end of the 30-day experiment when dosed at 8 mg/kg/d. Due to its excellent *in vivo* efficacy, **43** was tested in a single-dose cure experiment at 50 mg/kg. At this dose, parasites remained undetectable throughout the 30-day experiment, demonstrating a single-dose cure.

Microsomal stability, parasite burden suppression, and in vivo efficacy of select amodiachins. The values, $t_{1/2}$ and CL_{int}, were determined from HPLC UV traces from pooled murine liver microsomes incubated with drug. All animal studies used group sizes of n = 4 per dose regimen. (-) = not performed. Full procedure for microsomal stability and in vivo assays can found in Chapter 2.

Compound	$t_{1/2}$ (min), CL_{int} (mL/min/kg)	% *Py* Suppression (2.5 mg/kg/d)	ED_{50} v *Py* (mg/kg/d)	ED_{90} v *Py* (mg/kg/d)	NRD (mg/kg/d)	SDC (mg/kg)
Compound	$t_{1/2}$ (min), CL_{int} (mL/min/kg)	% *Py* Suppression (2.5 mg/kg/d)	ED_{50} v *Py* (mg/kg/d)	ED_{90} v *Py* (mg/kg/d)	NRD (mg/kg/d)	SDC (mg/kg)

Compound	$t_{1/2}$ (min), CL_{int} (mL/min/kg)	% *Py* Suppression (2.5 mg/kg/d)	ED_{50} v *Py* (mg/kg/d)	ED_{90} v *Py* (mg/kg/d)	NRD (mg/kg/d)	SDC (mg/kg)
35	, 123.6	%	-	-	-	-
41	, 78.0	%	-	-	-	-
42	, 129.7	%	-	-	-	-
43	, 113.3	%				
44	, 98.3	%	-	-	-	-
45	, 842.9	%	-	-	-	-

Having demonstrated that the *iso*-butyl group unlocks superior *in vivo* efficacy in the amodiachin series, we prepared a piperazine mimetic of **43** for the purpose of direct comparison (**45**). Although **45** exhibited similar antiplasmodial activity *in vitro* against cultured parasites (*Pf*D6 and *Pf*Dd2 IC_{50} = 8 ± 3 and 12 ± 6 nM), the compound displayed relatively poor metabolic stability ($t_{1/2}$ = 6.47 min), which was observed for the other piperazine-containing amodiachins in the series. When evaluated for parasitemia suppression at 2.5 mg/kg, parasite burden was only reduced by 30% compared to control. This result compares poorly to the 91% parasite suppression observed in piperidine analog **43**. Taken together, our data suggest that **43** has superior *in vivo* efficacy compared to all other compounds in this series. To further explore the developmental potential of **43**, we investigated its pharmacokinetic profile in mice following a single oral dose of 10.0 mg/kg and an IV injection of 0.5 mg/kg in PEG-400 (Figure 49 and Table 8).

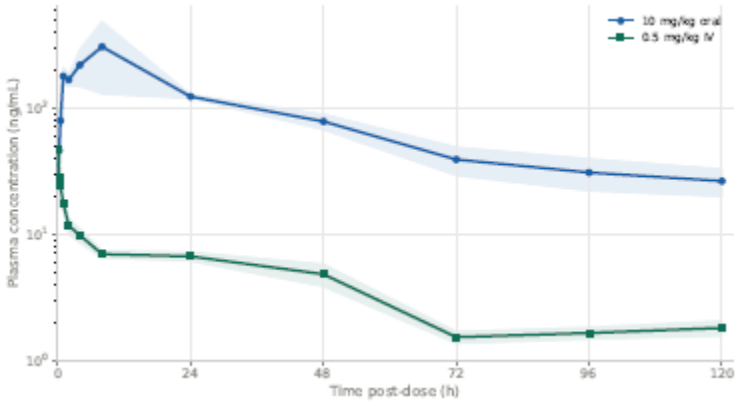

Figure 49: Mean plasma concentration-time profiles of 43 after IV dose at 0.5 mg/kg and PO dose at 10 mg/kg in male CD1 mice(n=3).

*Compound **43** was prepared in PEG-400 to yield clear solutions at 0.1 mg/mL for IV via tail vein and 10 mg/mL for PO dosing via oral gavage. No abnormal clinical symptoms were observed during the entire in-life study.*

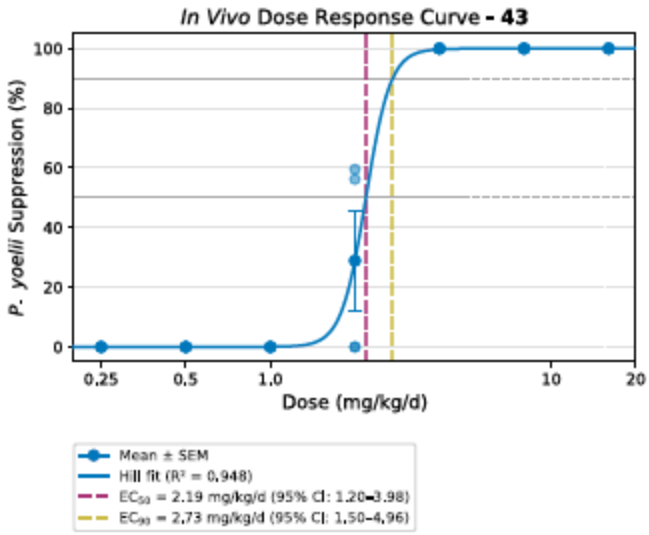

Figure 50: 43 versus P. yoelii growth suppression mouse malaria model described in Table 1.6.

*The in vivo efficacy of **43** was measured using a modified 4-day Peters test. Dose-response pairs were fit to a three-parameter Hill equation (with suppression constrained between 0–100%) to estimate the compound's potency, yielding EC_{50} and EC_{90} values with 95% confidence intervals. Full procedure for in vivo assays can found in Chapter 2.*

Administration route and dose	**Parameter**	**Calculated value**
Intravenous, 0.5 mg/kg	CL	9.78 mL/min/kg
Intravenous, 0.5 mg/kg	Vss	62.4 L/kg
Intravenous, 0.5 mg/kg	$t_{1/2}$	74 h
Intravenous, 0.5 mg/kg	AUCINF	851 h·ng/mL
Intravenous, 0.5 mg/kg	MRTINF	100 h
Oral, 10.0 mg/kg	Tmax	8.0 h
Oral, 10.0 mg/kg	Cmax	304 ng/mL
Oral, 10.0 mg/kg	$t_{1/2}$	85 h
Oral, 10.0 mg/kg	AUCINF	13,603 h·ng/mL
Oral, 10.0 mg/kg	MRTINF	82.8 h
Oral, 10.0 mg/kg	F	76%

Table 8: Pharmacokinetic properties of compound 43 in male CD1 mice (n = 3) after an oral dose of 10 mg/kg and an intravenous dose of 0.5 mg/kg.

The final three sampling times in the intravenous experiment, at 72, 96, and 120 hours, were below the lower limit of quantification (LLOQ = 1 ng/mL) and were excluded from the pharmacokinetic analysis.

Abbreviations: CL, clearance; Vss, volume of distribution at steady state; $t_{1/2}$, half-life; AUCINF, area under the concentration-time curve extrapolated to infinity; MRTINF, mean residence time extrapolated to infinity; Tmax, time to maximum plasma concentration; Cmax, maximum plasma concentration; F, bioavailability; PO, oral administration; IV, intravenous administration.

It is noteworthy that **43** appeared to be well absorbed, with an absolute bioavailability of 76% (F) and a maximum blood-stream concentration reached in 8 hours (T_{max}), achieving a maximum concentration of 304 ng/mL (C_{max}). The half-life of **43** given through IV administration compared to PO administration agreed well across the two experiments ($T_{1/2}$ = 74 h and 85 h, respectively). These results, taken together with the ability of **43** to overcome multidrug-resistance mechanisms present in the Dd2 strain of *Pf*, its relatively long metabolic stability in murine microsomes, and its ability to completely cure an infection in this challenging *P. yoelii* murine malaria model, highlight **43** as a potent compound with potential as a novel antimalarial against multidrug-resistant *Plasmodium falciparum* parasites.

6.4. Summary and Concluding Remarks

Our interest in revisiting amodiaquine stems from its rapid schizonticidal activity and the relatively unexplored chemical space surrounding its 4-aminophenyl side chain. In this study, we synthesized analogs bearing diverse nitrogen-containing heterocycles linked through this side chain and found that introducing a piperazine ring at this position unlocked potent antiplasmodial activity. Further exploration into the quinoline ring confirmed the superiority of a 7-position chlorine atom, as it contributed to excellent low nanomolar potency against both drug-sensitive and multidrug-resistant strains of *P. falciparum*, with limited cytotoxicity. The superior qualities of the piperazine-containing amodiachins led us to expand the structure-activity profiling to replace it with the structurally related piperidine. When assessed for metabolic stability and parasite suppression *in vivo*, the piperidine-containing derivative **35** hinted at the improved potential of this new subseries. Structural isomers of **35** were prepared containing linear and branched 3- and 4-carbon alkyl chains. *In vitro* and *in vivo* assessment of these derivatives revealed that compound **43** possessed impressive *in vitro* antiplasmodial IC_{50} values and superior efficacy *in vivo* compared to the other members of this series. *In vivo* efficacy of **43** was remarkable, with a very sharp action curve against murine malaria, as evidenced by ED_{50} and ED_{90} values of 2.2 and 2.7 mg/kg/day, respectively, following 4 days of oral dosing, seen in Figure 50. An NRD of 16 mg/kg/day for **43** over the same time interval was also a distinguishing positive attribute over other derivatives in this series, along with the single-dose cure of 50 mg/kg. Pharmacokinetic analysis of **43** revealed rapid oral absorption and extended pharmacokinetics. It's interesting to note that the lead-likeness of the series was not improved as a result of the SAR study optimization effort.[,] Structural modifications that improved *in vitro* activity often reduced lead-likeness properties, while efforts to enhance lead-likeness tended to diminish *in vitro* potency. Ultimately, compounds that were effective *in vivo* also demonstrated strong *in vitro* activity, despite lacking conventional lead-like characteristics. Collectively, these findings highlight the potential of amodiachins, such as **43,** as viable 4-aminoquinoline replacement candidates.

The persistent global burden of malaria and the evolving landscape of antimalarial drug resistance compel efforts to discover new therapeutics that address gaps in the treatment of acute and severe infections. The compounds described here, particularly **43** (ADC-028), represent

promising candidates to overcome these challenges and offer the potential to advance global malaria eradication initiatives.

7. Designing Novel Bisquinoline Antimalarials from Historical 4-Aminoquinolines to Combat Drug-Resistant Malaria

The text, figures, schemes, and tables were previously published in the *Antimicrobial Agents and Chemotherapy* under the same title and are reprinted with permission. The author and Terry Riscoe contributed equally to determining the antiplasmodial activity of each compound. *In vivo* efficacy experiments were performed by Dr. Yuexin Li. *In vitro* metabolic stability and pharmacokinetic experiments were performed by a CRO.

7.1. Introduction

Plasmodium falciparum (*Pf*) causes the most severe form of malaria, causing approximately 597,000 deaths in 2023, mostly among children aged 5 and under. The parasite's complex life cycle aids in its evasion of global-eradication initiatives and consequently has produced strains of parasites that carry resistance to multiple antimalarials. During the blood stage of infection, *Plasmodium spp.* lack the machinery to synthesize essential amino acids and thus acquire them by protease-mediated digestion of host hemoglobin in acidified digestive vacuoles, lysosomal-like organelles. Cytotoxic heme is released during this process, but is detoxified via aggregation into an inert biomolecule, hemozoin.[9] Inhibition of this protective pathway is part of the mechanism of action of 4-aminoquinoline antimalarials (Figure 51) such as chloroquine (**CQ**), amodiaquine (**AQ**), and piperaquine (**PPQ**).[9] Resistance to 4-aminoquinolines results primarily from the accumulation of mutations in the *P. falciparum* chloroquine resistance transporter (*pfcrt*), which promote 4-aminoquinoline efflux from the digestive vacuole, vastly reducing their antiplasmodial activity. Chloroquine-resistant *P. falciparum* strains were first identified in 1957 in Cambodia and quickly spread throughout Asia and into Africa by the 1970's. Chloroquine was integral to early eradication and treatment efforts, and as chloroquine-resistant strains emerged, successful 4-aminoquinoline chloroquine analogs like amodiaquine and piperaquine were developed to be effective against those strains. Sadly, resistance to those antimalarials and cytotoxicity issues have put their continued effectiveness at risk. Development of 4-aminoquinoline analogs continues today, aiming to discover antimalarials active against not only chloroquine-resistant parasites, but also multidrug-resistant *P. falciparum*.

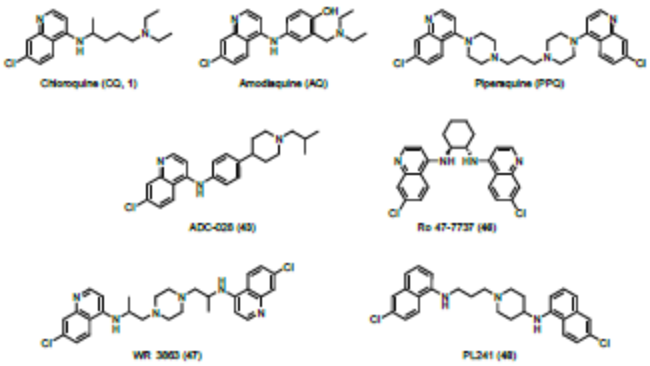

Figure 51: Structural representations of 4-aminoquinoline antimalarials.

*Chloroquine (**CQ**), amodiaquine (**AQ**), piperaquine (PPQ) and amodiachin-028 (ADC-028, **43**). Survey representation of symmetrical and unsymmetrical 4-aminoquinoline compounds from other antimalarial drug discovery programs, including Ro 47-7737 (**46**), WR 3863 (**47**), and PL241 (**48**).*

Our recent work on 4-aminoquinoline-based analogs led to the development of ADC-028 (**43**), illustrated in Figure 51. This compound was designed to overcome the toxicity of amodiaquine and the pharmacokinetic shortcomings of isoquine.[7] Compound **43** exhibited nanomolar activity against multidrug-resistant strains of *P. falciparum* (IC_{50} v *Pf*Dd2 = 17 nM), was non-cytotoxic (CC_{50} vs HepG2 > 20 µM), and was moderately stable *in vitro* (intrinsic metabolic stability, $t_{1/2}$ = 48.2 min). The compound was effective in a mouse malaria model (ED_{90} = 2.5 mg/kg/d) and provided complete cures of infected animals at 16 mg/kg/day in the standard modified Peters 4-Day test and a single-dose cure at 50 mg/kg. Its pharmacokinetic profile exhibited a extended bloodstream half-life ($T_{1/2}$ = 84 h) and excellent oral bioavailability (%F = 74). Taking these characteristics together, **43** was identified as the frontrunner of that set of compounds. In addition, the structure activity relationship (SAR) study from that series highlighted several key structural moieties that could expand SAR profiling into unexplored chemical space. Motivated by both the high therapeutic potential of **43** and the existing precedent for both symmetrical and unsymmetrical bis-4-aminoquinolines (**46**-**48**) antimalarials, we decided to investigate a bis-quinoline pharmacophore incorporating components of the aminophenyl piperidine core found in **43**.[7] The results of this investigation are presented below.

7.2. Results and Discussion

7.2.1. Rationale and Chemistry

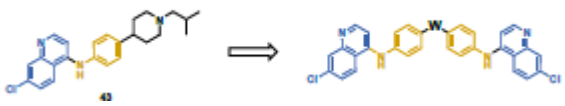

Figure 52: Structure of 43 (ADC-028) with structural variations of interest and Markush structure of bisquinoline designs.

*Compound **43** with the 7-chloro-N-phenylquinolin-4-amine core (highlighted in blue) the aniline moiety (highlighted in yellow) that is directly connected to the quinoline core and the Markush structure of desired symmetrical bisquinolines that utilize these structural components.*

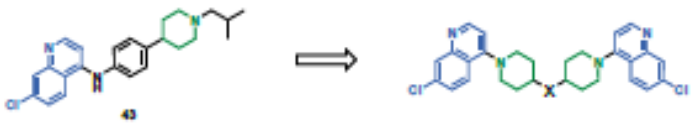

Figure 53: Structure of 43 (ADC-028) with structural variations of interest and Markush structure of bisquinoline designs.

*Compound **43** with the 7-chloro-N-phenylquinolin-4-amine core (blue) in addition to the piperidine moiety (green) and the Markush structure of desired symmetrical bisquinolines that utilize these structural components.*

Our initial design was based on the intrinsic antiplasmodial activity of the 7-chloro-N-phenylquinolin-4-amine core, highlighted in blue (7-chloroquinoline) and gold (aniline) in Figure 52, which is shared between **43** and other antiplasmodial compounds. We sought to vary the atom **W** between two symmetrical cores (Figure 52) utilizing a variety of commercially available bis-anilines, **49a**-**h**. The conditions used in the synthesis of compounds **51**-**58** are summarized in Scheme [schm-apq-1]. Starting material **50** was prepared from commercially available 4-hydroxy-7-chloroquine using previously published methods. Compounds **51**-**58** were afforded from **50** when reacted with the appropriate bis-aniline and phenol in DMF at 150° C for 2 hours in a microwave reactor. Again, we sought to diversify the bisquinoline structure by varying the connecting atom **X** between the two symmetrical bisquinoline cores by utilizing a bis-piperidine moiety in lieu of a bis-aniline, as seen in Figure 53. The reaction scheme that illustrates the synthesis of compounds **60** and **61** can be found in Scheme [schm-apq-2], utilizing identical reaction conditions as described in Scheme [schm-apq-1].

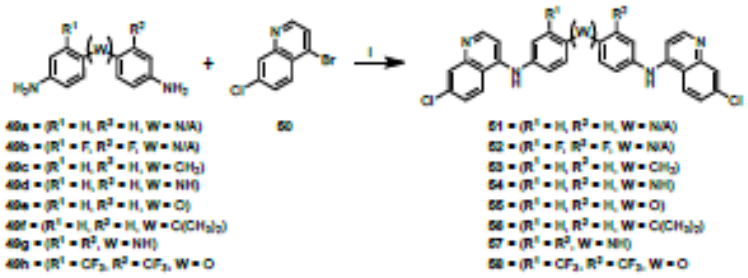

Figure 54: Scheme 6. Synthetic scheme used to generate compounds 51-58.

*Reagents and conditions: (i) linker, 4-bromo-7-chloroquinoline, phenol, DMF, 2 h, 150 °C.**

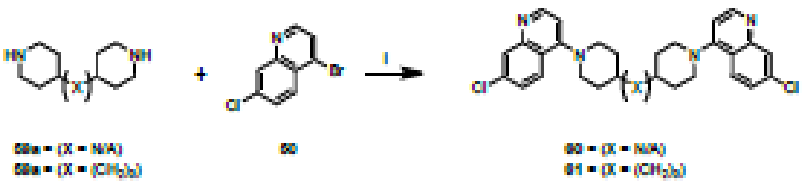

Figure 55: Scheme 7: Synthetic scheme used to generate compounds 60-61.

*Reagents and conditions: (i) linker, 4-bromo-7-chloroquinoline, phenol, DMF, 2 h, 150 °C.**

We next returned to the original inspiration for this compound series, and sought to utilize the original structure of **43**, but retain both the aniline and piperidine elements and include a second quinoline onto the terminal nitrogen of the piperidine ring, as illustrated in Figure 56.

Figure 56: Compound 43 with the 7-chloro-N-phenylquinolin-4-amine core highlighted in blue.

In addition to the aniline moiety in yellow and the piperidine in blue followed by the Markush structure of possible unsymmetrical bisquinolines that utilize those structural constituents.

Compounds **67-72** were afforded using the reaction conditions outlined in Scheme [schm-apq-3]. In short, the initial quinoline with or without the 7-position chlorine atom (**50** or **62**), was reacted together with a boc-protected 4-(4-aminophenyl)piperidine or 4-(4-aminophenyl)piperazine in THF at 120° C for 20 minutes (**63a,b**). The solid boc-containing products (**64a-c**) were filtered and washed with excess THF and subjected to a short aqueous workup before deprotection in TFA in DCM. The resulting intermediates (**65a-c**) were used in reactions with either 2-chloro-4-fluoropyridine (**66**), and diisopropylethylamine in N-methyl-2-pyrillidone at 150° C for 2 hours to produce **67,** or 4-bromo-quinoline with or without a 7-position chlorine atom (**50** and **61**, respectively) using similar conditions as previously described conditions to produce compounds **68-72**.

7.2.2. In vitro activity of bisquinolines vs *P. falciparum* and their relative cytotoxicity

Table 1 and Table 10 contain compound cytotoxicity (CC_{50}) against HepG2 mammalian cells and the mean and standard deviations of antiplasmodial activity (IC_{50}) determined from a fluorescence-based antiplasmodial activity assay. Proven efficacious antimalarials chloroquine (**CQ**) and piperaquine (**PPQ**) were used as controls to illustrate benchmark cytotoxicity, and the activity of other 4-aminoquinolines against the drug-sensitive *P. falciparum* D6 (*Pf*D6) strain, as well as to highlight the resistance profile against the multidrug-resistant *P. falciparum* Dd2 (*Pf*Dd2) strain. In Table 1, all compounds used in this assay, except for **52** and **61**, exhibit IC_{50} values lower than 50 nM against both *Pf*D6 and *Pf*Dd2, indicating an elevated level of intrinsic antiplasmodial potency, while simultaneously highlighting the capacity to overcome the resistance mechanisms of the *Pf*Dd2 strain.

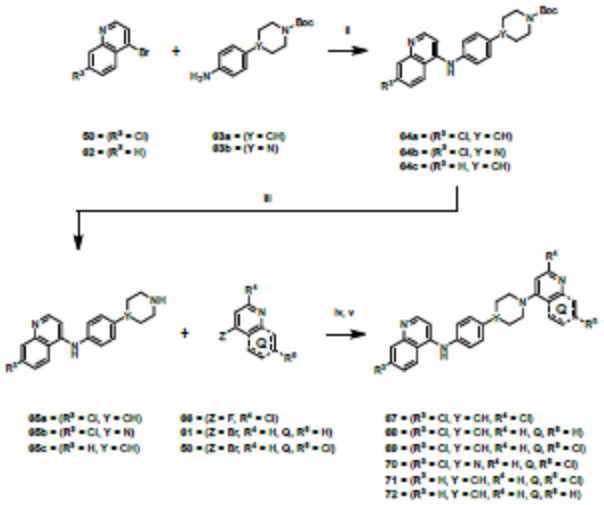

Figure 57: Scheme 8: Synthetic scheme used to generate compounds 67-72.

Compound ID	***Z group***	***IC_{50} vs. Pf D6 ± SD (nM)***	***IC_{50} vs. Pf Dd2 ± SD (nM)***	***CC_{50} vs. HepG2 (μM)***	***Log selectivity index (pSI)***
CQ	*Not applicable*	*10.0 ± 2.0*	*106.0 ± 10.0*	*37.8*	*3.6*
PPQ	*Chemical structure shown in source table*	*3.8 ± 1.6*	*5.8 ± 1.8*	*≥ 120*	*≥ 4.5*
51	*Chemical structure shown in source table*	*14.6 ± 1.3*	*10.0 ± 2.0*	*> 200*	*≥ 4.1*
52	*Chemical structure shown in source table*	*≥ 250*	*111.0 ± 13.0*	*> 200*	*< 2.9*
53	*Chemical structure shown in source table*	*11.0 ± 4.0*	*7.0 ± 5.0*	*> 200*	*≥ 4.3*
54	*Chemical structure shown in source table*	*9.0 ± 6.0*	*6.8 ± 1.8*	*100.0*	*4.0*
55	*Chemical structure shown in source table*	*10.4 ± 1.9*	*7.0 ± 7.0*	*> 200*	*≥ 4.3*
56	*Chemical structure shown in source table*	*19.0 ± 10.0*	*15.0 ± 9.0*	*96.4*	*3.7*
57	*Chemical structure shown in source table*	*6.0 ± 2.0*	*6.0 ± 6.0*	*24.5*	*3.6*
58	*Chemical structure shown in source table*	*45.0 ± 16.0*	*38.0 ± 8.0*	*> 200*	*≥ 3.6*
60	*Chemical structure shown in source table*	*16.0 ± 4.0*	*28.0 ± 4.0*	*58.0*	*> 3.5*
61	*Chemical structure shown in source table*	*170.0 ± 60.0*	*140.0 ± 20.0*	*> 200*	*> 3.1*

Table 9: Activity of bisquinolines against drug-sensitive Pf D6 and multidrug-resistant Pf Dd2 strains, cytotoxicity in HepG2 cells, and selectivity index.

Structure activity relationship profiling of bisquinolines vs. drug-sensitive (D6) and multidrug-resistant (Dd2) strains of Plasmodium falciparum, and the impact of the bisquinoline linker on antimalarial activity and cytotoxicity. Markush structure of compounds in the table (top), followed by the activity of each compound against a drug-sensitive strain of P. falciparum (PfD6), a multidrug-resistant strain of P. falciparum (PfDd2), cytotoxicity against HepG2 mammalian cells, and selectivity index metrics. Antiplasmodial activity (IC_{50}) values and standard deviations (SD) were derived from the average of at least three independent

experiments, each performed in quadruplicate. The cytotoxicity (CC_{50}) assay was performed using human hepatoma-derived HepG2 cells across an initial concentration range of 200 µM to 10 nM in triplicate. Log of Selectivity Index (pSI) was calculated using Equation 1; pSI classification: (< 1) = potentially cytotoxic/nonselective, (1-2) = low selectivity, (2-3) = moderate selectivity, (3-4) = high selectivity, > 4 = very high selectivity. Cytotoxicity of ***CQ*** *and* ***PPQ*** *was reported from published sources.[·] Details of the assays performed are found in Chapter 2.*

Compounds **67-72** in Table 10, exhibit similar antiplasmodial activity against both strains of *P. falciparum* with a range of IC_{50} values from 14 nM to 5 nM against *Pf*D6 and 20 nM to 7.4 nM against *Pf*Dd2, regardless of the piperazine vs piperidine containing 4-aminoquinolines. The majority of compounds described in Table 1 and Table 10 demonstrate promising cytotoxicity profiles, with CC_{50} values exceeding 50 µM. Therefore, to further evaluate this series of compounds for future development, we implemented the selectivity index on a log scale (pSI), to quantify the margin between a compound's potency and cytotoxicity. Indeed, most of the compounds in Table 1 and Table 10, are either highly selective (pSI = 3 – 4) or very highly selective (pSI > 4), indicating a low probability of cytotoxicity at a therapeutic dose. However, compound **52** has the lowest pSI (< 2.9), and due to activity against the PfD6 strain ($IC_{50} \geq 250$ nM) lying outside of our testing range, it is difficult to say how cytotoxic the compound might be. When comparing the CC_{50} values of compounds found in Table 10, that differ only at the 7-position of the 4-aminophenyl quinoline—such as compounds **68** (CC_{50} > 200 µM) and **72** (CC_{50} = 12.8 µM) or compounds **69** (CC_{50} > 200 µM) and **71** (CC_{50} = 11.8 µM)—it is apparent that the 7-position chlorine atom of the 4-aminophenyl quinoline is key to low cytotoxicity.

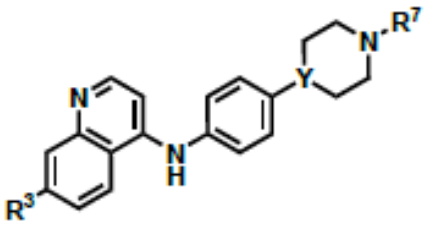

Figure 58: Markush Structure of R⁶- and R⁷-Substituted Analogs.

Compound	***Structural variables***	***IC_{50}, Pf D6 ± SD (nM)***	***IC_{50}, Pf Dd2 ± SD (nM)***	***CC_{50}, HepG2 (µM)***	***Log pSI***
43	*R^3: Cl; Y: C; R^7: branched alkyl group*	*7.0 ± 7.0*	*10.0 ± 11.0*	*> 200*	*≥ 4.6*
67	*R^3: Cl; Y: C; R^7: chloro-substituted pyridyl group*	*86.0 ± 23.0*	*82.0 ± 15.0*	*> 200*	*≥ 3.4*
68	*R^3: Cl; Y: C; R^7: quinolinyl group*	*5.0 ± 2.0*	*10.1 ± 0.5*	*> 200*	*≥ 4.6*

69	*R^3: Cl; Y: C; R^7: chloro-substituted quinolinyl group*	*14.0 ± 3.0*	*7.9 ± 1.0*	*> 200*	*≥ 4.2*
70	*R^3: Cl; Y: N; R^7: chloro-substituted quinolinyl group*	*8.1 ± 1.9*	*7.4 ± 1.4*	*> 200*	*≥ 4.4*
71	*R^3: H; Y: C; R^7: chloro-substituted quinolinyl group*	*8.5 ± 0.2*	*10.0 ± 2.0*	*12.2*	*3.2*
72	*R^3: H; Y: C; R^7: quinolinyl group*	*5.0 ± 3.0*	*20.0 ± 23.0*	*11.8*	*3.4*

Table 10: Activity against Pf D6 and Pf Dd2, cytotoxicity in HepG2 cells, and log selectivity index. Portrait format.

*Structure activity relationship profiling of bisquinolines vs. drug-sensitive (D6) and multidrug-resistant (Dd2) strains of Plasmodium falciparum, and the impact of the bisquinoline linker on antimalarial activity and cytotoxicity. Markush structure of compounds in the table (top), followed by the activity of each compound against a drug-sensitive strain of P. falciparum (PfD6), a multidrug-resistant strain of P. falciparum (PfDd2), cytotoxicity against HepG2 mammalian cells, and selectivity index metrics. Antiplasmodial activity (IC_{50}) values and standard deviations (SD) were derived from the average of at least three independent experiments, each performed in quadruplicate. The cytotoxicity (CC_{50}) assay was performed using human hepatoma-derived HepG2 cells across an initial concentration range of 200 µM to 10 nM in triplicate. Log of Selectivity Index (pSI) was calculated using Equation 1; pSI classification: (< 1) = potentially cytotoxic/nonselective, (1-2) = low selectivity, (2-3) = moderate selectivity, (3-4) = high selectivity, > 4 = very high selectivity. Cytotoxicity of **CQ** and **PPQ** was reported from published sources.[7] Details of the assays performed are found in Chapter 2.*

In our pipeline, a $CC_{50} \leq 20$ µM serves as a heuristic threshold for identifying toxic analogs in early-stage discovery. Although the cytotoxicity of **57** is near that threshold and **71** and **72** are below it, they are still within an order of magnitude of that of chloroquine, an FDA-approved antimalarial, in the same assay (CC_{50} = 38 µM). Additionally, each compound's selectivity index indicates an effective concentration *in vitro* against *Pf*D6 that id more than three orders of magnitude smaller than its potentially cytotoxic dose *in vitro* (CC_{50}). Based on this context, we chose to continue evaluating the therapeutic potential of **57**, **71**, and **72**. We interpret these results as support for our initial hypothesis of highly active and non-cytotoxic antimalarials within this chemical space, which in turn stimulated us to further evaluate these compounds for metabolic stability and *in vivo* efficacy.

7.2.3. Metabolic stability and *in vivo* efficacy of selected bisquinolines

Compounds from Table 1 and Table 10 that exhibited both excellent therapeutic potential (*Pf*D6 and *Pf*Dd2 IC_{50} < 20 nM) and demonstrated a high selectivity index value (pSI > 3), were chosen for evaluation for *in vivo* efficacy experiments. Prior to *in vivo* experiments, the intrinsic metabolic stability ($t_{1/2}$) of each selected compound was measured in pooled murine liver microsomes; values are shown in Table 11 and Table 12. A predicted ratio of compound that would remain in circulation after first-pass metabolism, predicted hepatic extraction ratio (E_H), was calculated from each $t_{1/2}$. Both $t_{1/2}$ and E_H were used to aid in the down-selection and interpretation of *in vivo* experiments moving forward. The results of these experiments on compounds presented in Table 1 are reported in Table 11, and the results of compounds from Table 10 are found within Table 12.

Compound	**IC_{50} vs. Pf D6 ± SD (nM)**	**Py suppression at 5 mg/kg/day (%)**	**$t_{1/2}$ (min)**	**E_h**
51	14.6 ± 1.3	0	398	0.13
53	11 ± 4	100	58.5	0.51
54	91 ± 6	48	247	0.20
55	10.4 ± 1.9	63	55.8	0.52
56	19 ± 10	Not performed	16.4	0.79
57	6 ± 2	78	3.06	0.95
60	16 ± 4	0	23.4	0.72

Table 11: Intrinsic Metabolic Stability and In Vivo Efficacy Against P. Yoelii Murine Malaria Model of Bisquinolines from Table 2.1.

Activity of selected compounds against drug-sensitive P. falciparum (IC_{50} v PfD6) and their efficacy in a murine malaria infection challenge at 5 mg/kg/d (Py suppression). Compounds were evaluated for intrinsic metabolic stability ($t_{1/2}$) in pooled liver murine microsomes and their predicted in vivo hepatic extraction ratio calculated (E_H). In vitro half-life ($t_{1/2}$) determined from HPLC UV traces of drug after incubation with pooled murine liver microsomes. In vivo efficacy (% Py suppression) was the percent suppression of parasitemia of a treated group compared to the control group. Predicted hepatic extraction ratio (E_H) calculated from $t_{1/2}$ using Equation 2, E_H classification range: (< 0.3) = low, (0.3 – 0.7) = intermediate, (0.7 – 0.95) = high, (> 0.95) = very high. (-) = not performed. All animal studies used group sizes of n = 4 per dose regimen. Full procedure for microsomal stability and in vivo assays can be found in Chapter 2.

Notice that **51** and **54** possess excellent intrinsic metabolic stability in murine microsomes ($t_{1/2}$ = 399 min. and 247 min., respectively). We had hypothesized that reducing rotational freedom of the diphenyl amine linker may enhance metabolic stability, but compared to **54**, the carbazole linker in **57** introduced a metabolic liability, substantially reducing *in vitro* half-life to 3.06 minutes. From the series presented in Table 10, compound **69** possesses enhanced intrinsic metabolic stability ($t_{1/2}$ = 121 min) compared to the corresponding piperazine analog **70** ($t_{1/2}$ = 34.38 min). A clear trend of metabolic stability emerged among the piperidine-containing compounds **68**, **69**, **71**, and **72**. If the presence of two 7-position chlorine atoms (**69**) is reduced to include only one chlorine atom on either quinoline (**68** and **71**), the *in vitro* metabolic stability is substantially reduced, $t_{1/2}$ = 42.3 min. and 38.6 min, respectively. This is further illustrated by

the complete absence of 7-position chlorine atoms in **72** and its *in vitro* half-life of 14.33 minutes, near an order of magnitude shorter than **69**.

Select compounds were then evaluated for *in vivo* efficacy of parasite clearance in a murine malaria challenge model at 5 mg/kg/d in PEG-400 using a modified Peter's 4-Day test. Despite the similar *in vitro* activity across compounds in Table 11, only **53** was able to completely clear the infection by Day 5 of the challenge at this dose. This was an unexpected result considering that **51** and **54** exhibit the two longest *in vitro* half-lives reported in Table 11 or Table 12. Despite the increased metabolic liability of **57** compared to its bioisostere **54**, it was more efficacious *in vivo* (*Py* suppression of: **57** = 78%, **54** = 48%). Of the compounds represented in Table 12, **68**-**70** exhibit excellent *in vivo* efficacy and completely cleared *P. yoelii* infection by Day 5 of the study, despite their relative differences in *in vitro* metabolic stability. Compound **72** exhibited respectable efficacy *in vivo* (*Py* suppression = 85%), but not to the same degree of **68**-**70**. Therefore, **69** was selected for further *in vivo* studies to more fully assess its efficacy in this malaria infection model.

Compound	**IC_{50} vs. Pf D6 ± SD (nM)**	**Py suppression at 5 mg/kg/day (%)**	**ED_{50} vs. Py (mg/kg/day)**	**ED_{90} vs. Py (mg/kg/day)**	**NRD (mg/kg/day)**	**$t_{1/2}$ (min)**	**E_h**
68	5 ± 2	100	Not performed	Not performed	Not performed	42.3	0.59
69	14 ± 3	100	0.32	0.51	10	121	0.33
70	8.1 ± 1.9	100	0.28	0.98	Not detected at 10 mg/kg/day	34.4	0.64
71	8.5 ± 0.2	Not performed	Not performed	Not performed	Not performed	38.6	0.61
72	5 ± 3	85	Not performed	Not performed	Not performed	14.3	0.81

Table 12: In vitro half-life (t1/2) determined from HPLC UV traces of drug after incubation with pooled murine liver microsomes.

In vivo efficacy (% Py suppression) was the percent suppression of parasitemia of a treated group compared to the control group. Predicted hepatic extraction ratio (E_H) calculated from $t_{1/2}$ using Equation 2 (Chapter 2), E_H classification range: (< 0.3) = low, (0.3 – 0.7) = intermediate, (0.7 – 0.95) = high, (> 0.95) = very high. Full procedure for microsomal stability and in vivo assays can be found in the Materials and Methods section. (-) = not performed. ND() = not detected at corresponding dosage. All animal studies used group sizes of n = 4 per dose regimen.

Excitingly, **69** demonstrated a high level of *in vivo* efficacy, with a 90% reduction in parasitemia compared to the control (PEG-400 only) at 0.51 mg/kg/d. Perhaps an even more exciting result was that **69** completely cleared the infection and protected the animals against parasite recrudescence (NRD) at 10 mg/kg/d. Given the superior *in vivo* performance of **69**, we decided to further assess the *in vivo* efficacy of its bioisostere **70**. The compound exhibited similar efficacy (ED_{50} = 0.32 mg/kg/d, ED_{90} = 0.51 mg/kg/d) to **69**; however, a non-recrudescence dose

was not achieved across the entire tested dose range. With these results in hand, we moved to further evaluate the clinical potential of **69** as the frontrunner compound.

7.2.4. Single dose pharmacokinetics of compound *69*

To evaluate the *in vivo* performance of **69**, a dual-arm (oral and IV) pharmacokinetic (PK) experiment was performed. Plasma concentration versus time of **69** following single-dose oral gavage (PO) of 10 mg/kg and intravenous injection (IV) of 0.5 mg/kg administration of **69** in mice are shown in Figure 59, and the resulting pharmacokinetic parameters are summarized below in Table 13. It is noteworthy that **69** appears to be moderately well absorbed, with an absolute oral bioavailability of 43% (F) and a maximum blood-stream concentration reached in 8 hours (T_{max}), achieving a maximum concentration of 1162 ng/mL (C_{max}). The bloodstream half-life of **69** given through IV administration compared to PO administration agreed well across the two arms of the experiment, $T_{1/2}$ = 30.9 hours and 27.2 hours, respectively.

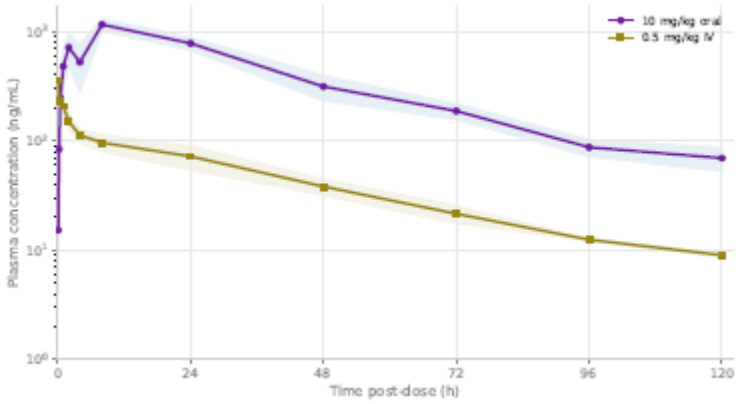

Figure 59: Mean plasma concentration-time profiles of 69 after IV dose at 0.5 mg/kg and PO dose at 10 mg/kg in male CD1 mice(n=3).

*Compound **69** was prepared in PEG-400 to yield clear solutions at 0.1 mg/mL for IV via tail vein and 10 mg/mL for PO dosing via oral gavage. No abnormal clinical symptoms were observed during the entire in-life study.*

Administration	**Parameter**	**Calculated value**
0.5 mg/kg, IV	CL	1.49 mL/min/kg
0.5 mg/kg, IV	V_{ss}	3.76 L/kg
0.5 mg/kg, IV	$T_{1/2}$	30.9 hr
0.5 mg/kg, IV	AUC_{INF}	5580 hr*ng/mL
0.5 mg/kg, IV	MRT_{INF}	41.9 hr
10.0 mg/kg, PO	T_{max}	8.0 hr
10.0 mg/kg, PO	C_{max}	1162 ng/mL
10.0 mg/kg, PO	$T_{1/2}$	27.2 hr

Administration	Parameter	Calculated value
10.0 mg/kg, PO	AUC_{INF}	48126 hr*ng/mL
10.0 mg/kg, PO	MRT_{INF}	39.5 hr
10.0 mg/kg, PO	F	43%

Table 13: Pharmacokinetic properties of 69 in male CD1 mice (n = 3) after PO dose of 10 mg/kg and IV dose of 0.5 mg/kg.

Pharmacokinetic parameters were estimated by non-compartmental model using WinNonLin version 8.2.

7.2.5. Structure-activity profiling of bisquinolines

Initial designs of bisquinolines focused on combinations of key structural features, namely the quinoline core, aniline, and piperazine moiety. First, we sought to use the simplest bis-aniline linker, benzidine, passing over *p*-phenylenediamine as a starting point due to the work described in Ismail et al. (1998), to create compound **51**. We next sought to disrupt coplanarity in the aromatic rings found in the linker of **51** by adding opposing fluorine atoms, as seen in **52**. This change, however, had a great cost to activity against both strains of *P. falciparum* (*Pf*D6 $IC_{50} \geq$ 250 nM, *Pf*Dd2 IC_{50} = 111 nM) compared to the parent compound **51**, so this design strategy was abandoned. We next introduced complexity and flexibility by introducing a carbon, nitrogen, and oxygen atom between the two aromatic rings, resulting in methylene (**53**), amine (**54**), and ether (**55**) bi-aryls. Notice that all three compounds exhibit similar antiplasmodial activity, and the only difference of note is that **54** exhibited cytotoxicity against HepG2 cells (CC_{50} = 100 μM). To further increase chemical diversity of each of these three compounds from one another, we introduced a dimethyl to the methylene linker (**56**), changed the diphenylamine linker to a carbazole (**57**), and introduced trifluoromethyl groups to the biaryl ether (**58**). These changes to the chemical structure showed a slight reduction in the antiplasmodial activity across both strains of **56** (*Pf*D6 IC_{50} = 19 nM, *Pf*Dd2 IC_{50} = 15 nM) and in **58** (*Pf*D6 IC_{50} = 45 nM, *Pf*Dd2 IC_{50} = 38 nM) when compared to the parent compounds. Both **56** and **57** showed an increase in cytotoxicity, CC_{50} = 96 μM and 25 μM, respectively, compared to the corresponding parent compound. We incorporated the piperidine moiety, as outlined in Figure 2B, in **60** as a bridged bi-piperidine, and in **61** as a piperidine-based analog of piperaquine by including a *n*-propyl alkane between the two rings. Compound **60** showed excellent antiplasmodial activity, *Pf*D6 IC_{50} = 17 nM, *Pf*Dd2 IC_{50} = 28 nM; however, **61,** which we expected to be similarly active to piperaquine, exhibited over an order of magnitude reduction in potency against drug-sensitive (*Pf*D6 IC_{50} = 170 nM) and a substantial reduction in potency against multidrug-resistant *P. falciparum* (*Pf*Dd2 IC_{50} = 140 nM), when compared to **60**.

The next series of compounds contained all three structural components - the quinoline cores, the aniline, and the piperidine. Compound **67** was prepared to probe whether the piperidinyl quinoline ring feature is required for antiplasmodial activity, or whether an alternative nitrogen-containing aromatic constituent could maintain potency. Although **67** retains activity (*Pf*D6 IC_{50} = 86 ± 23 nM, *Pf*Dd2 IC_{50} = 82 ± 15 nM), it was notably less potent than most analogs in Table 1. Compounds **68**-**72** were made to evaluate the role of the 7-position chlorine found in the quinoline rings, but we found that the chlorine can be removed from either quinoline ring or both without a noticeable change in potency (IC_{50}s vs: *Pf*D6 = 5 – 14 nM; *Pf*Dd2 = 7 – 20 nM).

However, the 4-anilinoquinoline chlorine is clearly important for maintaining low cytotoxicity, as bioisosteres **71** and **72** ($CC_{50} \approx 12$ μM) were markedly more cytotoxic than **68** ($CC_{50} > 200$ μM), despite the latter being a positional isomer of **71**.

Despite some compounds exhibiting measurable cytotoxicity, all but compound **52** demonstrate strong selectivity for *P. falciparum* over the reference mammalian cell line, with selectivity indices (pSI) ≥ 3, many demonstrating pSI ≥ 4—highlighting their potential as promising antimalarial candidates. And while antiplasmodial potency was broadly conserved across the entire series, as 11 of 16 compounds exhibit *Pf*D6 and *Pf*Dd2 IC_{50}s ≤ 20 nM, differences in metabolic stability and parasite suppression revealed some key structure-property relationships.

7.2.6. DMPK-efficacy profiling of bisquinolines

Table 11 indicates no clear relationships between *in vitro* potency and *in vivo* efficacy of the compounds from Table 1. Despite their high potency (*Pf*D6 and *Pf*Dd2 IC_{50}s ≤ 20 nM) and low predicted hepatic extraction ratio ($E_H < 0.3$), compounds **51** and **53** were less effective at suppressing parasitemia in the murine malaria model than other compounds with similar potency but higher predicted hepatic extraction. For example, compound **53** completely suppressed infection notwithstanding a predicted intermediate level of hepatic extraction during first-pass metabolism ($E_H = 0.51$). Similarly, compound **57** suppressed parasite burden by 78%, despite very high predicted hepatic extraction ($E_H = 0.95$). These results suggest the formation of active metabolites of **53** and **57** with enhanced *in vivo* efficacy, or insufficient absorption and distribution of compounds **51** and **54**, which reduces their ability to suppress parasitemia burden.

A similar observation can be made for **55**, in that the degree of *in vitro* potency and predicted hepatic extraction ratio ($E_H = 0.52$) should lead to robust *in vivo* efficacy; however, parasitemia was suppressed by only 63% on Day 5. Again, this could be attributed to partial or insufficient absorption and distribution, which in turn reduces efficacy.

Compounds reported in Table 12 do not suffer from the same disparity between potency, metabolic stability, and *in vivo* efficacy as seen in the compounds listed in Table 11. Clearly, **68**, **69**, **70**, and **72** demonstrate impressive *in vivo* efficacy, which matches in kind with their reduced metabolic stability. In essence, **72** is as potent *in vitro* as **68**, but the decreased metabolic stability of **72** predicts a high level of hepatic extraction ($E_H = 0.81$), which is reflected by a diminished *in vivo* efficacy compared to **68**; *Py* suppression = 85% and 100%, respectively. Furthermore, we can observe this agreement when **69** and **70** are compared. Compound **70** is marginally more potent than **71** *in vitro*, which likely contributes to a lower ED_{50} than **69**. However, one possible explanation for why the ED_{90} of **69** is lower than the ED_{90} of **70** is that a higher fraction of **69** is predicted to remain in circulation after first-pass metabolism ($E_H = 0.33$ and 0.64, respectively), allowing an effective therapeutic concentration to be reached and maintained for a longer duration. This reasoning could ultimately explain the recrudescence of *P. yoelii* observed when mice were treated with **70** at a similar dose to **69**, whereas **69** cured the infection and provided full protection against parasite recrudescence (NRD = 10 mg/kg/d).

7.3. Summary and Discussion

We have previously used historical antiparasitic drugs as potential starting points for new chemical leads for the development of novel antimalarials, e.g. using endochin to develop endochin-like quinolones (ELQs).[77] Our first foray into 4-aminoquinolines led to the

development of the pharmachins, a series of sontochin-based analogs that ultimately led to highly active and efficacious antimalarials. Our second campaign into this chemical space originated from a desire to improve the metabolic instability and cytotoxicity observed in the use of amodiaquine. This work resulted in the amodiachin series, which produced a metabolically stable ($T_{1/2}$ = 84 hr) and efficacious antimalarial, ADC-028 (**43**). Our initial rationale for the work described here set out to expand the SAR around that scaffold by incorporating key structural elements of **43** into a bisquinoline arrangement similar to piperaquine.

We hoped to find compounds with enhanced antiplasmodial activity, safety, metabolic stability, and *in vivo* efficacy in that chemical space. To this end, compound **69** exhibits enhanced antiplasmodial activity against both drug-sensitive (D6) and multidrug-resistant (Dd2) strains of *P. falciparum* compared to compound **43**. The two compounds have similar safety profiles against HepG2, but **69** exhibits increased intrinsic metabolic stability, $t_{1/2}$ = 121 minutes. The efficacy of **69** *in vivo* is far superior to its parent compound, with a seven-fold increase in potency, ED_{90} = 0.51 mg/kg/d and 2.5 mg/kg/d, respectively, in addition to protecting animals from recrudescence at two-thirds of the dose, NRD of **43** = 16 mg/kg/d and an NRD of **69** = 10 mg/kg/d. Pharmacokinetic analysis of **69** found that the half-life of an oral dose was 27.2 hours in the mouse model, effectively a third of the half-life of **43** using the same route of administration, but still incredibly stable and long-lasting in this model. Unfortunately, the oral bioavailability (F = 43%) of **69** is nearly half of compound **43** (F = 76%). Though **69** does not outperform **43** at every benchmark, it still succeeds at providing an excellent starting point for continued exploration and development within this chemical space.

Part III. Conclusion

8. Conclusion

8.1. Summary

Malaria, a disease that quite possibly affected dinosaurs—the prehistoric kind—still ravages humans today. Not only does it infect hundreds of millions each year, but it also kills hundreds of thousands of children and women. It wasn't until a few hundred years ago, with the discovery of quinine, that we began to be able to fight back against this disease. Since that time, we have made considerable progress towards eliminating malaria, but in the last several years we have begun to lose ground. The emergence of multidrug-resistant strains of malaria harboring resistance to frontline treatments has become a significant hurdle to eradication efforts. Therefore, one path to eliminating Malaria is discovering and developing novel antimalarials that overcome these resistant strains.

Targeting the deadliest form of malaria, *P. falciparum*, we sought to improve on the historic 4-aminoquinoline scaffold, primarily amodiaquine. Compared to chloroquine or piperaquine, malaria resistance to this drug is not nearly as pervasive as the other two. Suffering from issues relating to metabolic stability, amodiaquine offered a fantastic starting point to develop derivatives that are active against multidrug-resistant strains and are metabolically stable.

In pursuit of this goal, I have created two related but distinct amodiaquine-related antimalarial series. The initial foray into the chemical space was met with compounds that were nearly inactive; however, after some relatively small chemical modifications, I fell into a rich activity

well. Later changes to the structure were aimed at improving *in vivo* efficacy and maintaining metabolic activity. The top-performing compound in the series, identified as ADC-028, is a strong candidate for further studies. It offers nanomolar activity in drug-sensitive and drug-resistant strains, low cytotoxicity, and excellent projected hepatic clearance. Demonstrating a non-recrudescence dose of 16 mg/kg/d is an incredible feat, not to mention exhibiting an impressive bloodstream half-life of 84 hours and favorable bioavailability (76%). The potential that ADC-028 has as an antimalarial in pre-lead optimization stands out as a testament to what our approach to drug discovery and optimization can produce.

The second series of 4-aminoquinolines was inspired by the success of ADC-028. By defining three structural motifs present in the compound, we expanded the scope of the series to investigate how each one contributes to overall antiplasmodial activity. But it soon became its own project, pursuing a bisquinoline scaffold to be offered as a backup to another 4-aminoquinoline antimalarial, piperaquine—and thus named amodiapiperaquine (APQ). It became apparent that a bisquinoline that heavily relied on the original scaffold, APQ-002, offered superior antiplasmodial activity against both sensitive and resistant strains, low cytotoxicity, and exceptional projected hepatic clearance. The compound provided a non-recrudescence dose of 10 mg/kg/d, an even greater feat compared to its parent molecule. Despite demonstrating greater efficacy *in vivo* than ADC-028, APQ-002 was not as stable ($t_{1/2}$ = 27.2 hours) nor as bioavailable (%F = 43) as its predecessor. It wasn't until the pharmacokinetic experiments were performed on this compound that we found that it and several others were inactive against piperaquine-resistant strains of *P. falciparum*; see Appendix D for full account. The consequence of these results is that this series will probably be abandoned, which is unfortunate because I believe derivatives of APQ-002 would be excellent candidates for continued optimization studies.

8.2. Contemplation

Despite the relative success of this work, given what I know now, today I might approach this problem differently.

Designing compounds based on a compromised pharmacophore has inherent risks. In this specific case, *P. falciparum* has developed widespread resistance to the other 4-aminoquinoline antimalarials. Without any evidence to support the claim, there has always been a small part of me that has wondered if this is inherent to the pharmacophore rather than the parasite. I think given the number of antimalarials that *Plasmodium* currently has shown to be resistant to, the evidence that demonstrates the problem lies with the parasite outweighs the other worry. Be that as it may, the ultimate goal with this work was developing a possible new antimalarial that could be used in the future. If a 4-aminoquinoline-resistant background is persistent throughout endemic areas, are we not adding fuel to the fire, rather than suffocating it? To prove my point, for the last decade, much of the resistance profiling of new antimalarials during development is performed on the *P. falciparum* Dd2 strain background. If we consider each time a new antimalarial was discovered - a purely novel pharmacophore, like chloroquine or artemisinin - and its success and the impact it had on curing the disease, I think you might arrive at a similar idea. You would need to ignore the multitude of confounding issues that prevent us from curing the disease now, like distribution, vector population control, education, etc. But underneath that bramble, you would find the path to eradication is arguably a cheap, stable, highly potent, safe, and completely novel antimalarial.

I would argue that derivatization projects result in a compound that is shoehorned into solving some limitation of the parent drug; better safety profile, longer half-life, overcoming resistance, etc. Rarely does it arrive at a derivative so completely transformative that it overshadows the parent compound, and though the proverbial *silver bullet* antimalarial has yet to be found, one could argue that it may yet happen. But this is only a limitation of a project like this; it is a risk that is acknowledged and understood, not evidence for never taking on this kind of challenge.

A final chink in the proverbial armor of this project would be the *in vitro* testing. A small but maybe fatal flaw is that these compounds have only been tested against the D6 and Dd2 strains of *P. falciparum*; I have selectively designed antimalarials for these strains and have ignored perhaps more pertinent ones. Clinical isolates harboring resistance to other 4-aminoquinolines (especially piperaquine and amodiaquine), in combination with lab-generated strains, would have perhaps been a better option. It is true that in Appendix D, the results of this kind of study are reported, but unfortunately they occurred at the end of the SAR studies and could not be used to guide further optimization studies. The argument is that strains harboring resistance to amodiaquine or piperaquine would have been a better starting point given the rationale of the initial studies, i.e., analogs of amodiaquine and piperaquine. These strains would have provided a resistance profile that would have better mimicked the strains these compounds might be used against clinically. This opinion does not negate the advantage that the Dd2 strain provides, as resistance to chloroquine is widespread, it is necessary to assess compounds against this genetic background. It does however, suggest that utilizing different drug-resistant strains at an earlier point in the project would have been beneficial.

And lastly, the acronym ADC that was used to describe the amodiachins has been a stain on my conscience since it was pointed out to me 6 years ago. Despite all the things I could do to benefit humanity if I had a time machine, changing the acronym would make the list as well.

8.3. Future Work

As this is a doctoral project at an academic institution, expecting to deliver a fully fleshed-out drug discovery project, from hit to clinical studies or lead optimization, is unrealistic. To get this project to that point would take much, *much* more time, the work of many hands, lots of money, and an insane amount of luck. Be that as it may, these compounds have real potential to provide relief to those who are afflicted with this terrible disease. We have a moral obligation as scientists to pursue leads such as these to find out if they do indeed hold the power to be useful to people living in resource-poor malaria-endemic regions of the world. Despite the near-insurmountable goal of getting these compounds to market, it is necessary for us to pursue this project to the fullest extent, to fill knowledge gaps, and to open doors for future therapeutic exploration.

To complement the work that has already been performed, the following is a brief summary of some of the future work that was described in Section 6.4 and Section 7.3, in addition to other experiments that should be performed in short order.

8.3.1. Mechanistic Studies

There are, of course, a myriad of ways one could approach studying the mechanism of action of these compounds. As previously discussed in Section 5.2.2, the putative mechanism of action of 4-aminoquinolines is the inhibition of hemozoin formation. As noted in both Section 6.4 and

Section 7.3, *ex vivo* beta-hematin inhibition studies and *in vitro* hemozoin formation inhibition studies have been discussed as a way to demonstrate if antiplasmodial activity may be exhibited through heme binding. Performing these experiments will aid in future compound optimization decision-making while providing tangible support for the current mechanism of action hypothesis.

8.3.2. Toxicology and Safety Studies

Now, none of the mice that were administered these compounds displayed any physical signs of toxicity, but that does not preclude any further assessment of toxicity of these compounds, namely **43** (ADC-028) and (**69**) APQ-002. As a class, 4-aminoquinolines have been shown to inhibit the human ether-a-go-go (hERG) related channel. Proper function of this potassium-gated channel is essential for cardiac repolarization; inhibition of this channel can cause long QT syndrome and potentially fatal arrhythmia. As such, moving forward, all prospective 4-aminoquinoline antimalarials will need to be evaluated for hERG inhibition in single-cell patch-clamp electrophysiology experiments. In general, compounds that are hERG inhibitors are often lipophilic, polyaromatic basic amines, which *basically* describes every compound that I ever synthesized. Because hERG inhibition has been a persistent and widespread issue for medicinal chemists, there are many guides on how one can implement structural changes to reduce hERG inhibition. Further compound optimization to reduce probable cardiotoxicity through hERG channel inhibition would focus on reducing either the basicity of amines or the lipophilicity of the aromatic rings, among several other structural modifications that have been shown to reduce hERG channel inhibition. Moreover, hERG channel inhibition should be assessed frequently and included as a down-selection metric in further analog optimization efforts of these molecules, especially during lead optimization.

8.3.3. ADME Optimization

The early success of these two pharmacophores has left many questions and too few answers in terms of how the structure influences activity, and by extension, efficacy. Therefore, there is a strong case to continue further structure-activity relationship studies for both series to better understand how structure influences absorption, distribution, metabolism, and excretion (ADME). In the case of the amodiachins, the final alkyl scan demonstrated drastic differences in efficacy while activity remained relatively unchanged. The subtle differences in computationally derived measurements such as lipophilicity, basicity, total polar surface area,…etc. between each compound do not reflect, nor begin to describe, the difference in efficacy. A lipophilic scan of the alkyl side chain would begin to offer insight into its effect on the pharmacophore's *in vivo* efficacy. As for the bisquinoline series, there were several compounds from the initial screen that had excellent *in vitro* activity but performed poorly in the mouse model. Anecdotally, the solubility of these compounds was poor, and I struggled to get them into solution in common vehicles. Structure activity relationship studies should be conducted to determine if the activity of these compounds can translate into *in vivo* efficacy. Beyond structural variation to improve ADME properties, one can also employ improving ADME properties through salt formulation and particle size reduction optimization experiments.

8.4. Implications of Findings

The work that has been shared in this thesis is a testament to not only the utility of 4-aminoquinolines, but more importantly as an example that compromised drugs can be used to

find new potential leads. Drugs like chloroquine have a lauded history and have made a substantial impact on our ability to treat this disease for nearly a century. The rise of resistance to it, other 4-aminoquinolines, and other antimalarials alike threatens the vast amount of human power that has been poured into this problem.

This work showcases a possible escape from the slowly tightening jaws of resistant malaria. Continued work like this will benefit those who are less fortunate than many of those reading this thesis. This is not an expose of how newer methods of drug discovery are unable to deliver the same outcome, but rather a reminder that this method should not be set aside in lieu of newer methods. Because the goalposts haven't moved. And I like to think that all of us engaged in this type of work are all motivated by the chance that one day we will provide the world with an effective, inexpressive, and safe antimalarial that is active against current multidrug-resistant strains, which would relieve the pain, suffering, and loss caused by this disease each year. In other words, I hope someone, and hopefully soon, discovers better antimalarials than the ones that I did.

References

(1)

Poinar, G. Plasmodium Dominicana n. Sp. (Plasmodiidae: Haemospororida) from Tertiary Dominican Amber. *Systematic Parasitology* **2005**, *61* (1), 47–52. https://doi.org/10.1007/s11230-004-6354-6.

(2)

Escalante, A. A.; Ayala, F. J. Evolutionary Origin of Plasmodium and Other Apicomplexa Based on rRNA Genes. *Proceedings of the National Academy of Sciences of the United States of America* **1995**, *92* (13), 5793–5797.

(3)

Benton, M. J. The Triassic. *Current Biology* **2016**, *26* (23), R1214–R1218. https://doi.org/10.1016/j.cub.2016.10.060.

(4)

Carter, R.; Mendis, K. N. Evolutionary and Historical Aspects of the Burden of Malaria. *Clinical Microbiology Reviews* **2002**, *15* (4), 564–594. https://doi.org/10.1128/CMR.15.4.564-594.2002.

(5)

Gelabert, P.; Olalde, I.; de-Dios, T.; Civit, S.; Lalueza-Fox, C. Malaria Was a Weak Selective Force in Ancient Europeans. *Scientific Reports* **2017**, *7*, 1377. https://doi.org/10.1038/s41598-017-01534-5.

(6)

Angel, J. L. Porotic Hyperostosis, Anemias, Malarias, and Marshes in the Prehistoric Eastern Mediterranean. *Science* **1966**, *153* (3737), 760–763. https://doi.org/10.1126/science.153.3737.760.

(7)

Wang, T.; McFadden, C.; Buckley, H.; Domett, K.; Willis, A.; Trinh, H. H.; Matsumura, H.; Vlok, M.; Oxenham, M. F. Paleoepidemiology of Cribra Orbitalia: Insights from Early Seventh Millennium BP Con Co Ngua, Vietnam. *American Journal of Biological Anthropology* **2023**, *181* (2), 250–261. https://doi.org/10.1002/ajpa.24738.

(8)

Michel, M.; Skourtanioti, E.; Pierini, F.; Guevara, E. K.; Mötsch, A.; Kocher, A.; Barquera, R.; Bianco, R. A.; Carlhoff, S.; Coppola Bove, L.; Freilich, S.; Giffin, K.; Hermes, T.; Hiß, A.; Knolle, F.; Nelson, E. A.; Neumann, G. U.; Papac, L.; Penske, S.; Rohrlach, A. B.; Salem, N.; Semerau, L.; Villalba-Mouco, V.; Abadie, I.; Aldenderfer, M.; Beckett, J. F.; Brown, M.; Campus, F. G. R.; Chenghwa, T.; Cruz Berrocal, M.; Damašek, L.; Duffett Carlson, K. S.; Durand, R.; Ernée, M.; Fântăneanu, C.; Frenzel, H.; García Atiénzar, G.; Guillén, S.; Hsieh, E.; Karwowski, M.; Kelvin, D.; Kelvin, N.; Khokhlov, A.; Kinaston, R. L.; Korolev, A.; Krettek, K.-L.; Küßner, M.; Lai, L.; Look, C.; Majander, K.; Mandl, K.; Mazzarello, V.; McCormick, M.; de Miguel Ibáñez, P.; Murphy, R.; Németh, R. E.; Nordqvist, K.; Novotny, F.; Obenaus, M.; Olmo-Enciso, L.; Onkamo, P.; Orschiedt, J.; Patrushev, V.; Peltola, S.; Romero, A.; Rubino, S.; Sajantila, A.; Salazar-García, D. C.; Serrano, E.; Shaydullaev, S.; Sias, E.; Šlaus, M.; Stančo, L.; Swanston, T.; Teschler-Nicola, M.; Valentin, F.; Van de Vijver, K.; Varney, T. L.; Vigil-Escalera Guirado, A.; Waters, C. K.; Weiss-Krejci, E.; Winter, E.; Lamnidis, T. C.; Prüfer, K.; Nägele, K.; Spyrou, M.; Schiffels, S.; Stockhammer, P. W.; Haak, W.; Posth, C.; Warinner, C.; Bos, K. I.; Herbig, A.; Krause, J. Ancient Plasmodium Genomes Shed Light on the History of Human Malaria. *Nature* **2024**, *631* (8019), 125–133. https://doi.org/10.1038/s41586-024-07546-2.

(9)

Luzzatto, L. Sickle Cell Anaemia and Malaria. *Mediterranean Journal of Hematology and Infectious Diseases* **2012**, *4* (1), e2012065. https://doi.org/10.4084/MJHID.2012.065.

(10)

Kariuki, S. N.; Williams, T. N. Human Genetics and Malaria Resistance. *Human Genetics* **2020**, *139* (6), 801–811. https://doi.org/10.1007/s00439-020-02142-6.

(11)

WHO. *World Malaria Report 2025*; World Health Organization: Geneva, 2025.

(12)

Arrow, K. J.; Panosian, C.; Gelband, H. A Brief History of Malaria. In *Saving Lives, Buying Time: Economics of Malaria Drugs in an Age of Resistance*; National Academies Press (US), 2004.

(13)

Laveran, C. L. Classics in Infectious Diseases: A Newly Discovered Parasite in the Blood of Patients Suffering from Malaria. Parasitic Etiology of Attacks of Malaria: Charles Louis Alphonse Laveran (1845-1922). *Reviews of Infectious Diseases* **1982**, *4* (4), 908–911. https://doi.org/10.1093/4.4.908.

(14)

Ronald Ross; Patrick Manson. The Beast in the Mosquito: The Correspondence of Ronald Ross and Patrick Manson. *Clio Medica* **1998**, *51*, II–XXXV, 1–528.

(15)

Cook, G. C. Ronald Ross (1857-1932): 100 Years Since the Demonstration of Mosquito Transmission of Plasmodium Spp–on 20 August 1897. *Transactions of the Royal Society of Tropical Medicine and Hygiene* **1997**, *91* (4), 487–488. https://doi.org/10.1016/s0035-9203(97)90295-9.

(16)

Aly, A. S. I.; Vaughan, A. M.; Kappe, S. H. I. Malaria Parasite Development in the Mosquito and Infection of the Mammalian Host. *Annual review of microbiology* **2009**, *63*, 195–221. https://doi.org/10.1146/annurev.micro.091208.073403.

(17)

Graumans, W.; Jacobs, E.; Bousema, T.; Sinnis, P. When Is a Plasmodium-infected Mosquito an Infectious Mosquito? *Trends in parasitology* **2020**, *36* (8), 705–716. https://doi.org/10.1016/j.pt.2020.05.011.

(18)

Tavares, J.; Formaglio, P.; Thiberge, S.; Mordelet, E.; Van Rooijen, N.; Medvinsky, A.; Ménard, R.; Amino, R. Role of Host Cell Traversal by the Malaria Sporozoite During Liver Infection. *The Journal of Experimental Medicine* **2013**, *210* (5), 905–915. https://doi.org/10.1084/jem.20121130.

(19)

Meis, J. F. G. M.; Verhave, J. P.; Jap, P. H. K.; Sinden, R. E.; Meuwissen, J. H. E. T. Malaria Parasites—Discovery of the Early Liver Form. *Nature* **1983**, *302* (5907), 424–426. https://doi.org/10.1038/302424a0.

(20)

Hulden, L.; Hulden, L. Activation of the Hypnozoite: A Part of Plasmodium Vivax Life Cycle and Survival. *Malaria Journal* **2011**, *10*, 90. https://doi.org/10.1186/1475-2875-10-90.

(21)

Shortt, H. E.; Garnham, P. C. C. The Pre-Erythrocytic Development of Plasmodium Cynomolgi and Plasmodium Vivax. *Transactions of the Royal Society of Tropical Medicine and Hygiene* **1948**, *41* (6), 785–795. https://doi.org/10.1016/s0035-9203(48)80006-4.

(22)

Frevert, U. Sneaking in Through the Back Entrance: The Biology of Malaria Liver Stages. *Trends in Parasitology* **2004**, *20* (9), 417–424. https://doi.org/10.1016/j.pt.2004.07.007.

(23)

Garnham, P. C. C.; Bird, R. G.; Baker, J. R.; Killick-Kendrick, R. Electron Microscope Studies on the Motile Stages of Malaria Parasites VII. The Fine Structure of the Merozoites of Exoerythrocytic Schizonts of Plasmodium Berghei Yoelii. *Transactions of The Royal Society of Tropical Medicine and Hygiene* **1969**, *63* (3), 328–332. https://doi.org/10.1016/0035-9203(69)90005-4.

(24)

Sturm, A.; Amino, R.; van de Sand, C.; Regen, T.; Retzlaff, S.; Rennenberg, A.; Krueger, A.; Pollok, J.-M.; Menard, R.; Heussler, V. T. Manipulation of Host Hepatocytes by the Malaria Parasite for Delivery into Liver Sinusoids. *Science* **2006**, *313* (5791), 1287–1290. https://doi.org/10.1126/science.1129720.

(25)

Antinori, S.; Galimberti, L.; Milazzo, L.; Corbellino, M. Biology of Human Malaria Plasmodia Including Plasmodium Knowlesi. *Mediterranean Journal of Hematology and Infectious Diseases* **2012**, *4* (1), e2012013. https://doi.org/10.4084/MJHID.2012.013.

(26)

Dvorak, J. A.; Miller, L. H.; Whitehouse, W. C.; Shiroishi, T. Invasion of Erythrocytes by Malaria Merozoites. *Science* **1975**, *187* (4178), 748–750. https://doi.org/10.1126/science.803712.

(27)

Trager, W.; Jensen, J. B. Human Malaria Parasites in Continuous Culture. *Science* **1976**, *193* (4254), 673–675. https://doi.org/10.1126/science.781840.

(28)

Simoiu, M.; Codreanu, R.; Corlatescu, A.-D.; Pauna, A. M.; Cilievici, S. E. Camillo Golgi's Impact on Malaria Studies. *Cells* **2023**, *12* (17), 2156. https://doi.org/10.3390/cells12172156.

(29)

Hadley, T. J. Invasion of Erythrocytes by Malaria Parasites: A Cellular and Molecular Overview. *Annual Review of Microbiology* **1986**, *40*, 451–477. https://doi.org/10.1146/annurev.mi.40.100186.002315.

(30)

Billker, O.; Shaw, M. K.; Margos, G.; Sinden, R. E. The Roles of Temperature, pH and Mosquito Factors as Triggers of Male and Female Gametogenesis of Plasmodium Berghei in Vitro. *Parasitology* **1997**, *115 (Pt 1)*, 1–7. https://doi.org/10.1017/s0031182097008895.

(31)

Billker, O.; Lindo, V.; Panico, M.; Etienne, A. E.; Paxton, T.; Dell, A.; Rogers, M.; Sinden, R. E.; Morris, H. R. Identification of Xanthurenic Acid as the Putative Inducer of Malaria Development in the Mosquito. *Nature* **1998**, *392* (6673), 289–292. https://doi.org/10.1038/32667.

(32)

Sinden, R. E.; Strong, K. An Ultrastructural Study of the Sporogonic Development of Plasmodium Falciparum in Anopheles Gambiae. *Transactions of the Royal Society of Tropical Medicine and Hygiene* **1978**, *72* (5), 477–491. https://doi.org/10.1016/0035-9203(78)90167-0.

(33)

Vanderberg, J. P. Studies on the Motility of Plasmodium Sporozoites. *The Journal of Protozoology* **1974**, *21* (4), 527–537. https://doi.org/10.1111/j.1550-7408.1974.tb03693.x.

(34)

Vanderberg, J. P. Development of Infectivity by the Plasmodium Berghei Sporozoite. *The Journal of Parasitology* **1975**, *61* (1), 43–50.

(35)

Plewes, K.; Leopold, S. J.; Kingston, H. W. F.; Dondorp, A. M. Malaria: What's New in the Management of Malaria? *Infectious Disease Clinics of North America* **2019**, *33* (1), 39–60. https://doi.org/10.1016/j.idc.2018.10.002.

(36)

Wassmer, S. C.; Taylor, T. E.; Rathod, P. K.; Mishra, S. K.; Mohanty, S.; Arevalo-Herrera, M.; Duraisingh, M. T.; Smith, J. D. Investigating the Pathogenesis of Severe Malaria: A Multidisciplinary and Cross-Geographical Approach. *The American Journal of Tropical Medicine and Hygiene* **2015**, *93* (3 Suppl), 42–56. https://doi.org/10.4269/ajtmh.14-0841.

(37)

Beeson, J. G.; Brown, G. V. Pathogenesis of Plasmodium Falciparum Malaria: The Roles of Parasite Adhesion and Antigenic Variation. *Cellular and molecular life sciences: CMLS* **2002**, *59* (2), 258–271. https://doi.org/10.1007/s00018-002-8421-y.

(38)

John, C. C.; Bangirana, P.; Byarugaba, J.; Opoka, R. O.; Idro, R.; Jurek, A. M.; Wu, B.; Boivin, M. J. Cerebral Malaria in Children Is Associated With Long-term Cognitive Impairment. *Pediatrics* **2008**, *122* (1), e92–e99. https://doi.org/10.1542/peds.2007-3709.

(39)

Desai, M.; ter Kuile, F. O.; Nosten, F.; McGready, R.; Asamoa, K.; Brabin, B.; Newman, R. D. Epidemiology and Burden of Malaria in Pregnancy. *The Lancet. Infectious Diseases* **2007**, *7* (2), 93–104. https://doi.org/10.1016/S1473-3099(07)70021-X.

(40)

Milner, D. A. Malaria Pathogenesis. *Cold Spring Harbor Perspectives in Medicine* **2018**, *8* (1), a025569. https://doi.org/10.1101/cshperspect.a025569.

(41)

Mueller, I.; Galinski, M. R.; Baird, J. K.; Carlton, J. M.; Kochar, D. K.; Alonso, P. L.; del Portillo, H. A. Key Gaps in the Knowledge of Plasmodium Vivax, a Neglected Human Malaria Parasite. *The Lancet. Infectious Diseases* **2009**, *9* (9), 555–566. https://doi.org/10.1016/S1473-3099(09)70177-X.

(42)

Mueller, I.; Zimmerman, P. A.; Reeder, J. C. Plasmodium Malariae and Plasmodium Ovale – the "Bashful" Malaria Parasites. *Trends in parasitology* **2007**, *23* (6), 278–283. https://doi.org/10.1016/j.pt.2007.04.009.

(43)

WHO. *WHO Guidelines for Malaria*; World Health Organization, 2024.

(44)

Poser, C. M.; Bruyn, G. W. Treatment of Malaria. In *An Illustrated History of Malaria*; The Parthenon Publishing Group Limited, 1999; pp 75–95.

(45)

Rodrigues, P. T.; Valdivia, H. O.; de Oliveira, T. C.; Alves, J. M. P.; Duarte, A. M. R. C.; Cerutti-Junior, C.; Buery, J. C.; Brito, C. F. A.; de Souza, J. C.; Hirano, Z. M. B.; Bueno, M. G.; Catão-Dias, J. L.; Malafronte, R. S.; Ladeia-Andrade, S.; Mita, T.; Santamaria, A. M.; Calzada, J. E.; Tantular, I. S.; Kawamoto, F.; Raijmakers, L. R. J.; Mueller, I.; Pacheco, M. A.; Escalante, A. A.; Felger, I.; Ferreira, M. U. Human Migration and the Spread of Malaria Parasites to the New World. *Scientific Reports* **2018**, *8*, 1993. https://doi.org/10.1038/s41598-018-19554-0.

(46)

Zhu, L. Products of the Empire: Cinchona: A Short History, 2018.

(47)

Simonetti, O.; Contini, C.; Martini, M. The History of Gin and Tonic; the Infectious Disease Specialist Long Drink. When Gin and Tonic Was Not Ordered but Prescribed. *Le Infezioni in Medicina* **2022**, *30* (4), 619–626. https://doi.org/10.53854/liim-3004-18.

(48)

Miller, L. H.; Rojas-Jaimes, J.; Low, L. M.; Corbellini, G. What Historical Records Teach Us about the Discovery of Quinine. *The American Journal of Tropical Medicine and Hygiene* **2022**, *108* (1), 7–11. https://doi.org/10.4269/ajtmh.22-0404.

(49)

Jarcho, S. *Quinine's Predecessor : Francesco Torti and the Early History of Cinchona*; Baltimore : Johns Hopkins University Press, 1993.

(50)

Achan, J.; Talisuna, A. O.; Erhart, A.; Yeka, A.; Tibenderana, J. K.; Baliraine, F. N.; Rosenthal, P. J.; D'Alessandro, U. Quinine, an Old Anti-Malarial Drug in a Modern World: Role in the Treatment of Malaria. *Malaria Journal* **2011**, *10* (1), 144. https://doi.org/10.1186/1475-2875-10-144.

(51)

Quinine. *Drugbank*.

(52)

Urban Hellgren; Orjan Ericsson; Lars L. Gustafsson. Quinine. In *Handbook of Drugs for Tropical Parasitic Infections*; Taylor & Francis Group, 1995; p 265.

(53)

Maryadele J. O'Neil. Quinine. In *The Merck Index*; An Encyclopedia of Chemicals, Drugs, and Biologicals.; Royal Society of Chemistry: Cambridge, UK, 2013; p 1494.

(54)

Alumasa, J. N.; Gorka, A. P.; Casabianca, L. B.; Comstock, E.; de Dios, A. C.; Roepe, P. D. The Hydroxyl Functionality and a Rigid Proximal N Are Required for Forming a Novel Non-Covalent Quinine-Heme Complex. *Journal of inorganic biochemistry* **2011**, *105* (3), 467–475. https://doi.org/10.1016/j.jinorgbio.2010.08.011.

(55)

Warhurst, D. C. The Quinine-Haemin Interaction and Its Relationship to Antimalarial Activity. *Biochemical Pharmacology* **1981**, *30* (24), 3323–3327. https://doi.org/10.1016/0006-2952(81)90606-7.

(56)

Polet, H.; Barr, C. F. Chloroquine and Dihydroquinine. In Vitro Studies of Their Antimalarial Effect Upon Plasmodium Knowlesi. *The Journal of Pharmacology and Experimental Therapeutics* **1968**, *164* (2), 380–386. https://doi.org/10.1016/S0022-3565(25)28142-3.

(57)

Ziegler, J.; Schuerle, T.; Pasierb, L.; Kelly, C.; Elamin, A.; Cole, K. A.; Wright, D. W. The Propionate of Heme Binds N4O2 Schiff Base Antimalarial Drug Complexes. *Inorganic Chemistry* **2000**, *39* (16), 3731–3733. https://doi.org/10.1021/ic000295h.

(58)

Conklin, K. A.; Chou, S. C. Antimalarials: Effects on in Vivo and in Vitro Protein Synthesis. *Science* **1970**, *170* (3963), 1213–1214. https://doi.org/10.1126/science.170.3963.1213.

(59)

Punihaole, D.; Workman, R. J.; Upadhyay, S.; Bruggen, C. V.; Schmitz, A. J.; Reineke, T. M.; Frontiera, R. R. New Insights into Quinine–DNA Binding Using Raman Spectroscopy and Molecular Dynamics Simulations. *The journal of physical chemistry. B* **2018**, *122* (43), 9840. https://doi.org/10.1021/acs.jpcb.8b05795.

(60)

Clements R. Markham. *Travels in Peru and India*; William Clowes and Sons, 1862.

(61)

Kaufman, T. S.; Rúveda, E. A. The Quest for Quinine: Those Who Won the Battles and Those Who Won the War. *Angewandte Chemie International Edition* **2005**, *44* (6), 854–885. https://doi.org/10.1002/anie.200400663.

(62)

Cova, T. F. G. G.; Pais, A. A. C. C.; Seixas de Melo, J. S. Reconstructing the Historical Synthesis of Mauveine from Perkin and Caro: Procedure and Details. *Scientific Reports* **2017**, *7* (1), 6806. https://doi.org/10.1038/s41598-017-07239-z.

(63)

Woodward, R. B.; Doering, W. E. The Total Synthesis of Quinine. *Journal of the American Chemical Society* **1945**, *67* (5), 860–874. https://doi.org/10.1021/ja01221a051.

(64)

Rabe, P.; Kindler, K. Über die partielle Synthese des Chinins. Zur Kenntnis der China-Alkaloide XIX. *Berichte der deutschen chemischen Gesellschaft* **1918**, *51* (1), 466–467. https://doi.org/10.1002/cber.19180510153.

(65)

Seeman, J. I. The Woodward–Doering/Rabe–Kindler Total Synthesis of Quinine: Setting the Record Straight. *Angewandte Chemie International Edition* **2007**, *46* (9), 1378–1413. https://doi.org/10.1002/anie.200601551.

(66)

Stork, G.; Niu, D.; Fujimoto, A.; Koft, E. R.; Balkovec, J. M.; Tata, J. R.; Dake, G. R. The First Stereoselective Total Synthesis of Quinine. *Journal of the American Chemical Society* **2001**, *123* (14), 3239–3242. https://doi.org/10.1021/ja004325r.

(67)

Jones, R. A.; Panda, S. S.; Hall, C. D. Quinine Conjugates and Quinine Analogues as Potential Antimalarial Agents. *European Journal of Medicinal Chemistry* **2015**, *97*, 335–355. https://doi.org/10.1016/j.ejmech.2015.02.002.

(68)

Walsh, J. J.; Coughlan, D.; Heneghan, N.; Gaynor, C.; Bell, A. A Novel Artemisinin–Quinine Hybrid with Potent Antimalarial Activity. *Bioorganic & Medicinal Chemistry Letters* **2007**, *17* (13), 3599–3602. https://doi.org/10.1016/j.bmcl.2007.04.054.

(69)

Dinio, T.; Gorka, A. P.; McGinniss, A.; Roepe, P. D.; Morgan, J. B. Investigating the Activity of Quinine Analogues Vs. Chloroquine Resistant Plasmodium Falciparum. *Bioorganic & medicinal chemistry* **2012**, *20* (10), 3292–3297. https://doi.org/10.1016/j.bmc.2012.03.042.

(70)

Karle, J. M.; Karle, I. L.; Gerena, L.; Milhous, W. K. Stereochemical Evaluation of the Relative Activities of the Cinchona Alkaloids Against Plasmodium Falciparum. *Antimicrobial Agents and Chemotherapy* **1992**, *36* (7), 1538–1544. https://doi.org/10.1128/AAC.36.7.1538.

(71)

Panda, S. S.; Bajaj, K.; Meyers, M. J.; Sverdrup, F. M.; Katritzky, A. R. Quinine Bis-Conjugates with Quinolone Antibiotics and Peptides: Synthesis and Antimalarial Bioassay. *Organic & Biomolecular Chemistry* **2012**, *10* (45), 8985. https://doi.org/10.1039/c2ob26439k.

(72)

Panda, S. S.; Ibrahim, M. A.; Küçükbay, H.; Meyers, M. J.; Sverdrup, F. M.; El-Feky, S. A.; Katritzky, A. R. Synthesis and Antimalarial Bioassay of Quinine – Peptide Conjugates. *Chemical Biology & Drug Design* **2013**, *82* (4), 361–366. https://doi.org/10.1111/cbdd.12134.

(73)

Hrycyna, C. A.; Summers, R. L.; Lehane, A. M.; Pires, M. M.; Namanja, H.; Bohn, K.; Kuriakose, J.; Ferdig, M.; Henrich, P. P.; Fidock, D. A.; Kirk, K.; Chmielewski, J.; Martin, R. E. Quinine Dimers Are Potent Inhibitors of the Plasmodium Falciparum Chloroquine Resistance Transporter and Are Active Against Quinoline-Resistant P. Falciparum. *ACS Chemical Biology* **2014**, *9* (3), 722–730. https://doi.org/10.1021/cb4008953.

(74)

Bucher, C.; Sparr, C.; Schweizer, W. B.; Gilmour, R. Fluorinated Quinine Alkaloids: Synthesis, X-ray Structure Analysis and Antimalarial Parasite Chemotherapy. *Chemistry – A European Journal* **2009**, *15* (31), 7637–7647. https://doi.org/10.1002/chem.200900505.

(75)

Gorka, A. P.; Sherlach, K. S.; De Dios, A. C.; Roepea, P. D. Relative to Quinine and Quinidine, Their 9-Epimers Exhibit Decreased Cytostatic Activity and Altered Heme Binding but Similar Cytocidal Activity Versus Plasmodium Falciparum. *Antimicrobial Agents and Chemotherapy* **2013**, *57* (1), 365–374. https://doi.org/10.1128/AAC.01234-12.

(76)

Neghina, R.; Iacobiciu, I.; Neghina, A. M.; Marincu, I. Malaria, a Journey in Time: In Search of the Lost Myths and Forgotten Stories. *The American Journal of the Medical Sciences* **2010**, *340* (6), 492–498. https://doi.org/10.1097/MAJ.0b013e3181e7fe6c.

(77)

Bombay (Presidency); Madras (India : Presidency); India; Great Britain. East India (Chinchona Cultivation): Return to an Address of the Honourable the House of Commons, Dated ... For Copy of All Correspondence Between the Secretary of State for India and the Governor General, and the Governors of Madras and Bombay, Relating to the Cultivation of Chinchona Plants, from ... *Correspondence relating to chinchona cultivation in India1870/1875* **1870**, v.

(78)

Schlagenhauf, P. Malaria: From Prehistory to Present. *Infectious Disease Clinics of North America* **2004**, *18* (2), 189–205. https://doi.org/10.1016/j.idc.2004.01.002.

(79)

Stanley, S. L. Chapter 950 - Antiparasitic Agents. In *Infectious Diseases (Third Edition)*; Cohen, J., Opal, S. M., Powderly, W. G., Eds.; Mosby: London, 2010; pp 1490–1507. https://doi.org/10.1016/B978-0-323-04579-7.00150-7.

(80)

Daniel R. Headrick. *The Tools of Empire: Technology and European Imperialism in the Nineteenth Century*, 1st ed.; Oxford University Press, 1981.

(81)

Edwin G. Tse; Marat Korsik; Matthew H. Todd. The Past, Present, and Future of Antimalarial Medicines. *Malaria Journal* **2019**, *18*. https://doi.org/10.1186/s12936-019-2724-z.

(82)

David Greenwood. Conflicts of Interest: The Genesis of Synthetic Antimalarial Agents in Peace and War. *Journal of Antimicrobial Chemotherapy* **1995**, *36*, 857–872.

(83)

Ambruster, H. W. *Treason's Peace - German Dyes and American Dupes*; The Bechhurst Press,: New York, N.Y., 1947.

(84)

Baird, J. K. 8-Aminoquinoline Therapy for Latent Malaria. *Clinical Microbiology Reviews* **2019**. https://doi.org/10.1128/cmr.00011-19.

(85)

da Silva, A. F. C.; Benchimol, J. L. Malaria and Quinine Resistance: A Medical and Scientific Issue Between Brazil and Germany (1907-19). *Medical History* **2014**, *58* (1), 1–26. https://doi.org/10.1017/mdh.2013.69.

(86)

Lu, G.; Nagbanshi, M.; Goldau, N.; Mendes Jorge, M.; Meissner, P.; Jahn, A.; Mockenhaupt, F. P.; Müller, O. Efficacy and Safety of Methylene Blue in the Treatment of Malaria: A Systematic Review. *BMC Medicine* **2018**, *16*, 59. https://doi.org/10.1186/s12916-018-1045-3.

(87)

Slater, L. B. *War and Disease: Biomedical Research on Malaria in the Twentieth Century*; Rutgers University Press, 2009.

(88)

Dascombe, M. J.; B. Drew, M. G.; Evans, P. G.; D. Ismail, F. M. Rational Design Strategies for the Development of Synthetic Quinoline and Acridine Based Antimalarials. *Frontiers in Drug Design & Discovery: Structure-Based Drug Design in the 21st Century* **2007**, 559–609. https://doi.org/10.2174/000000007780960634.

(89)

Von Wilhelm Roehl. *The Effect of Plasmochin on Bird Malaria*; Johann Ambrosius Barth, 1926.

(90)

Shannon, J. A. Chemotherapy in Malaria. *Bulletin of the New York Academy of Medicine* **1946**, *22* (7), 345–357.

(91)

Coatney, G. R. Pitfalls in a Discovery: The Chronicle of Chloroquine. *The American Journal of Tropical Medicine and Hygiene* **1963**, *12* (2), 121–128. https://doi.org/10.4269/ajtmh.1963.12.121.

(92)

Elderfield, R. C.; Craig, L. C. A Study of Plasmochin and the Occurrence of Rearrangements in the Preparation of Certain Plasmo Chin Analogs. *Journal of the American Chemical Society* **1946**, *68*, 1516–1523. https://doi.org/10.1021/ja01212a039.

(93)

Edgcomb, J. H.; Arnold, J.; Yount, E. H.; Alving, A. S.; Eichelberger, L.; Jeffery, G. M.; Eyles, D.; Young, M. D. Primaquine, SN 13272, a New Curative Agent in Vivax Malaria; a Preliminary Report. *Journal. National Malaria Society* **1950**, *9* (4), 285–292.

(94)

Hockwald, R. S.; Arnold, J.; Clayman, C. B.; Alving, A. S. Toxicity of Primaquine in Negroes. *Journal of the American Medical Association* **1952**, *149* (17), 1568–1570. https://doi.org/10.1001/jama.1952.72930340027010c.

(95)

Jiang, J.-B.; Guo, X.-B.; Li, G.-Q.; Cheung Kong, Y.; Arnold, K. ANTIMALARIAL ACTIVITY OF MEFLOQUINE AND QINGHAOSU. *The Lancet* **1982**, *320* (8293), 285–288. https://doi.org/10.1016/S0140-6736(82)90268-9.

(96)

Trenholme, C. M.; Williams, R. L.; Desjardins, R. E.; Frischer, H.; Carson, P. E.; Rieckmann, K. H.; Canfield, C. J. Mefloquine (WR 142,490) in the Treatment of Human Malaria. *Science (New York, N.Y.)* **1975**, *190* (4216), 792–794. https://doi.org/10.1126/science.1105787.

(97)

Croft, A. M. A Lesson Learnt: The Rise and Fall of Lariam and Halfan. *Journal of the Royal Society of Medicine* **2007**, *100* (4), 170–174. https://doi.org/10.1258/jrsm.100.4.170.

(98)

Sweeney, T. R. The Present Status of Malaria Chemotherapy: Mefloquine, a Novel Antimalarial. *Medicinal Research Reviews* **1981**, *1* (3), 281–301. https://doi.org/10.1002/med.2610010304.

(99)

Karle, J. M.; Olmeda, R.; Gerena, L.; Milhous, W. K. *Plasmodium Falciparum*: Role of Absolute Stereochemistry in the Antimalarial Activity of Synthetic Amino Alcohol Antimalarial Agents. *Experimental Parasitology* **1993**, *76* (4), 345–351. https://doi.org/10.1006/expr.1993.1042.

(100)

Brocks, D. R.; Mehvar, R. Stereoselectivity in the Pharmacodynamics and Pharmacokinetics of the Chiral Antimalarial Drugs. *Clinical Pharmacokinetics* **2003**, *42* (15), 1359–1382. https://doi.org/10.2165/00003088-200342150-00004.

(101)

Gimenez, F.; Farinotti, R.; Pennie, R. A.; Koren, G.; Crevoisier, C.; Wainer, I. W. Stereoselective Pharmacokinetics of Mefloquine in Healthy Caucasians After Multiple Doses. *Journal of Pharmaceutical Sciences* **1994**, *83* (6), 824–827. https://doi.org/10.1002/jps.2600830613.

(102)

Simpson, J. A.; Price, R.; ter Kuile, F.; Teja-Isavatharm, P.; Nosten, F.; Chongsuphajaisiddhi, T.; Looareesuwan, S.; Aarons, L.; White, N. J. Population Pharmacokinetics of Mefloquine in Patients with Acute Falciparum Malaria. *Clinical Pharmacology & Therapeutics* **1999**, *66* (5), 472–484. https://doi.org/10.1016/S0009-9236(99)70010-X.

(103)

Kerb, R.; Fux, R.; Mörike, K.; Kremsner, P. G.; Gil, J. P.; Gleiter, C. H.; Schwab, M. Pharmacogenetics of Antimalarial Drugs: Effect on Metabolism and Transport. *The Lancet Infectious Diseases* **2009**, *9* (12), 760–774. https://doi.org/10.1016/S1473-3099(09)70320-2.

(104)

Foley, M.; Tilley, L. Quinoline Antimalarials: Mechanisms of Action and Resistance. *International Journal for Parasitology* **1997**, *27* (2), 231–240. https://doi.org/10.1016/S0020-7519(96)00152-X.

(105)

Wong, W.; Bai, X.-C.; Sleebs, B. E.; Triglia, T.; Brown, A.; Thompson, J. K.; Jackson, K. E.; Hanssen, E.; Marapana, D. S.; Fernandez, I. S.; Ralph, S. A.; Cowman, A. F.; Scheres, S. H. W.; Baum, J. Mefloquine Targets the Plasmodium Falciparum 80S Ribosome to Inhibit Protein Synthesis. *Nature Microbiology* **2017**, *2* (6), 1–9. https://doi.org/10.1038/nmicrobiol.2017.31.

(106)

Price, R. N.; Uhlemann, A.-C.; Brockman, A.; McGready, R.; Ashley, E.; Phaipun, L.; Patel, R.; Laing, K.; Looareesuwan, S.; White, N. J.; Nosten, F.; Krishna, S. Mefloquine Resistance in Plasmodium Falciparum and Increased Pfmdr1 Gene Copy Number. *Lancet* **2004**, *364* (9432), 438–447. https://doi.org/10.1016/S0140-6736(04)16767-6.

(107)

White, N. J. Mefloquine. *BMJ : British Medical Journal* **1994**, *308* (6924), 286–287. https://doi.org/10.1136/bmj.308.6924.286.

(108)

Schlagenhauf, P.; Adamcova, M.; Regep, L.; Schaerer, M. T.; Rhein, H.-G. The Position of Mefloquine as a 21st Century Malaria Chemoprophylaxis. *Malaria Journal* **2010**, *9*, 357. https://doi.org/10.1186/1475-2875-9-357.

(109)

Mockenhaupt, F. P. Mefloquine Resistance in *Plasmodium Falciparum*. *Parasitology Today* **1995**, *11* (7), 248–253. https://doi.org/10.1016/0169-4758(95)80201-0.

(110)

Cosgriff, T. M.; Boudreau, E. F.; Pamplin, C. L.; Doberstyn, E. B.; Desjardins, R. E.; Canfield, C. J. Evaluation of the Antimalarial Activity of the Phenanthrenemethanol Halofantrine (WR 171,669). *The American Journal of Tropical Medicine and Hygiene* **1982**, *31* (6), 1075–1079. https://doi.org/10.4269/ajtmh.1982.31.1075.

(111)

Bryson, H. M.; Goa, K. L. Halofantrine. A Review of Its Antimalarial Activity, Pharmacokinetic Properties and Therapeutic Potential. *Drugs* **1992**, *43* (2), 236–258. https://doi.org/10.2165/00003495-199243020-00009.

(112)

Su, X.; Miller, L. H. The Discovery of Artemisinin and Nobel Prize in Physiology or Medicine. *Science China. Life sciences* **2015**, *58* (11), 1175–1179. https://doi.org/10.1007/s11427-015-4948-7.

(113)

Deng, R. X.; Yu, L. B.; Zhang, H. B.; Geng, R. L.; Ye, K. L.; Zhang, D. F. [Studies on antimalarial agents–alpha-(alkylaminomethyl)-halogenated-4-fluorenemethanols (author's transl)]. *Yao Xue Xue Bao = Acta Pharmaceutica Sinica* **1981**, *16* (12), 920–924.

(114)

Wernsdorfer, W. H.; Landgraf, B.; Kilimali, V. A. E. B.; Wernsdorfer, G. Activity of Benflumetol and Its Enantiomers in Fresh Isolates of *Plasmodium Falciparum* from East Africa. *Acta Tropica* **1998**, *70* (1), 9–15. https://doi.org/10.1016/S0001-706X(97)00141-1.

(115)

Gabani, B. B.; Dixit, A.; Kiran, V.; Bestha, R. M.; Narayanan, B.; Srinivas, N. R.; Mullangi, R. Enantioselective in Vitro ADME, Absolute Oral Bioavailability, and Pharmacokinetics of (-)-Lumefantrine and (+)-Lumefantrine in Mice. *Xenobiotica; the Fate of Foreign Compounds in Biological Systems* **2021**, *51* (2), 202–209. https://doi.org/10.1080/00498254.2020.1823523.

(116)

Ezzet, F.; van Vugt, M.; Nosten, F.; Looareesuwan, S.; White, N. J. Pharmacokinetics and Pharmacodynamics of Lumefantrine (Benflumetol) in Acute Falciparum Malaria. *Antimicrobial Agents and Chemotherapy* **2000**, *44* (3), 697–704. https://doi.org/10.1128/aac.44.3.697-704.2000.

(117)

Combrinck, J. M.; Mabotha, T. E.; Ncokazi, K. K.; Ambele, M. A.; Taylor, D.; Smith, P. J.; Hoppe, H. C.; Egan, T. J. Insights into the Role of Heme in the Mechanism of Action of Antimalarials. *ACS chemical biology* **2013**, *8* (1), 133–137. https://doi.org/10.1021/cb300454t.

(118)

de Villiers, K. A.; Egan, T. J. Heme Detoxification in the Malaria Parasite: A Target for Antimalarial Drug Development. *Accounts of chemical research* **2021**, *54* (11), 2649–2659. https://doi.org/10.1021/acs.accounts.1c00154.

(119)

Fançony, C.; Fortes-Gabriel, E.; Zage, F.; Alexiou, E.; Broumou, I.; Pernaute-Lau, L.; Panzo, J.; António, E. J.; Cristovão, M. S.; Domingos, J. M.; Sassoma, E.; Kuatoko, F.; Rosario, E. V. N.; Martins, A.; Färnert, A.; Bernardino, L.; de Sousa, T. N.; Gil, J. P. Artemether-Lumefantrine Treatment Selects Plasmodium Falciparum Multidrug Resistance 1 (Pfmdr1) Increased Copy Number Among African Malaria Infections. *The Journal of Infectious Diseases* **2025**, *231* (6), e1119–e1128. https://doi.org/10.1093/infdis/jiaf155.

(120)

Anderson, T. J. C.; Nair, S.; Qin, H.; Singlam, S.; Brockman, A.; Paiphun, L.; Nosten, F. Are Transporter Genes Other Than the Chloroquine Resistance Locus (Pfcrt) and Multidrug Resistance Gene (Pfmdr) Associated with Antimalarial Drug Resistance? *Antimicrobial Agents and Chemotherapy* **2005**, *49* (6), 2180–2188. https://doi.org/10.1128/AAC.49.6.2180-2188.2005.

(121)

Treatment and Prevention of Malaria, 1st ed.; Milestones in Drug Therapy; Springer Basel, 2012. https://doi.org/10.1007/978-3-0346-0480-2.

(122)

KYLE, R. A.; BARTHOLOMEW, L. G. Variations in Pigmentation from Quinacrine: Report of Case Mimicking Chronic Hepatic Disease. *Archives of Internal Medicine* **1962**, *109* (4), 458–462. https://doi.org/10.1001/archinte.1962.03620160084011.

(123)

Zheng, X. Y.; Xia, Y.; Gao, F. H.; Chen, C. [Synthesis of 7351, a new antimalarial drug (author's transl)]. *Yao Xue Xue Bao = Acta Pharmaceutica Sinica* **1979**, *14* (12), 736–737.

(124)

Cui, L.; Su, X. Discovery, Mechanisms of Action and Combination Therapy of Artemisinin. *Expert review of anti-infective therapy* **2009**, *7* (8), 999–1013. https://doi.org/10.1586/eri.09.68.

(125)

Croft, S. L.; Duparc, S.; Arbe-Barnes, S. J.; Craft, J. C.; Shin, C.-S.; Fleckenstein, L.; Borghini-Fuhrer, I.; Rim, H.-J. Review of Pyronaridine Anti-Malarial Properties and Product Characteristics. *Malaria Journal* **2012**, *11*, 270. https://doi.org/10.1186/1475-2875-11-270.

(126)

Groger, M.; Tona Lutete, G.; Mombo-Ngoma, G.; Ntamabyaliro, N. Y.; Kahunu Mesia, G.; Muena Mujobu, T. B.; Dimessa Mbadinga, L. B.; Zoleko Manego, R.; Egger-Adam, D.; Borghini-Fuhrer, I.; Shin, J.; Miller, R.; Arbe-Barnes, S.; Duparc, S.; Ramharter, M.

Effectiveness of Pyronaridine-Artesunate Against Plasmodium Malariae, Plasmodium Ovale Spp, and Mixed-Plasmodium Infections: A Post-Hoc Analysis of the CANTAM-Pyramax Trial. *The Lancet. Microbe* **2022**, *3* (8), e598–e605. https://doi.org/10.1016/S2666-5247(22)00092-1.

(127)

Bailly, C. Pyronaridine: An Update of Its Pharmacological Activities and Mechanisms of Action. *Biopolymers* **2021**, *112* (4), e23398. https://doi.org/10.1002/bip.23398.

(128)

Chavalitshewinkoon-Petmitr, P.; Pongvilairat, G.; Auparakkitanon, S.; Wilairat, P. Gametocytocidal Activity of Pyronaridine and DNA Topoisomerase II Inhibitors Against Multidrug-Resistant Plasmodium Falciparum in Vitro. *Parasitology International* **2000**, *48* (4), 275–280. https://doi.org/10.1016/s1383-5769(99)00028-8.

(129)

Roth, J. M.; Sawa, P.; Makio, N.; Omweri, G.; Osoti, V.; Okach, S.; Choy, F.; Schallig, H. D. F. H.; Mens, P. Pyronaridine–Artesunate and Artemether–Lumefantrine for the Treatment of Uncomplicated Plasmodium Falciparum Malaria in Kenyan Children: A Randomized Controlled Non-Inferiority Trial. *Malaria Journal* **2018**, *17* (1), 199. https://doi.org/10.1186/s12936-018-2340-3.

(130)

Walter, R. D.; Bergmann, B.; Kansy, M.; Wiese, M.; Seydel, J. K. Pyrimethamin-Resistant Plasmodium Falciparum Lack Cross-Resistance to Methotrexate and 2,4-Diamino-5-(substituted Benzyl) Pyrimidines. *Parasitology Research* **1991**, *77* (4), 346–350. https://doi.org/10.1007/BF00930913.

(131)

Zhang, Y.; Meshnick, S. R. Inhibition of Plasmodium Falciparum Dihydropteroate Synthetase and Growth in Vitro by Sulfa Drugs. *Antimicrobial Agents and Chemotherapy* **1991**, *35* (2), 267–271. https://doi.org/10.1128/aac.35.2.267.

(132)

Gregson, A.; Plowe, C. V. Mechanisms of Resistance of Malaria Parasites to Antifolates. *Pharmacological Reviews* **2005**, *57* (1), 117–145. https://doi.org/10.1124/pr.57.1.4.

(133)

National Academies of Sciences, E.; Division, H. and M.; Drugs, C. to R. L.-T. H. E. of A.; Practice, B. on P. H. and P. H.; Styka, A. N.; Savitz, D. A. Atovaquone/Proguanil. In *Assessment of Long-Term Health Effects of Antimalarial Drugs When Used for Prophylaxis*; National Academies Press (US), 2020.

(134)

Baggish, A. L.; Hill, D. R. Antiparasitic Agent Atovaquone. *Antimicrobial Agents and Chemotherapy* **2002**, *46* (5), 1163–1173. https://doi.org/10.1128/AAC.46.5.1163-1173.2002.

(135)

Nixon, G. L.; Moss, D. M.; Shone, A. E.; Lalloo, D. G.; Fisher, N.; O'Neill, P. M.; Ward, S. A.; Biagini, G. A. Antimalarial Pharmacology and Therapeutics of Atovaquone. *Journal of Antimicrobial Chemotherapy* **2013**, *68* (5), 977–985. https://doi.org/10.1093/jac/dks504.

(136)

Meltzer, E.; Rahav, G.; Schwartz, E. Vivax Malaria Chemoprophylaxis: The Role of Atovaquone-Proguanil Compared to Other Options. *Clinical Infectious Diseases* **2018**, *66* (11), 1751–1755. https://doi.org/10.1093/cid/cix1077.

(137)

Balta, V. A.; Stiffler, D.; Sayeed, A.; Tripathi, A. K.; Elahi, R.; Mlambo, G.; Bakshi, R. P.; Dziedzic, A. G.; Jedlicka, A. E.; Nenortas, E.; Romero-Rodriguez, K.; Canonizado, M. A.; Mann, A.; Owen, A.; Sullivan, D. J.; Prigge, S. T.; Sinnis, P.; Shapiro, T. A. Clinically Relevant Atovaquone-Resistant Human Malaria Parasites Fail to Transmit by Mosquito. *Nature Communications* **2023**, *14* (1), 6415. https://doi.org/10.1038/s41467-023-42030-x.

(138)

Nilsen, A.; Miley, G. P.; Forquer, I. P.; Mather, M. W.; Katneni, K.; Li, Y.; Pou, S.; Pershing, A. M.; Stickles, A. M.; Ryan, E.; Kelly, J. X.; Doggett, J. S.; White, K. L.; Hinrichs, D. J.; Winter, R. W.; Charman, S. A.; Zakharov, L. N.; Bathurst, I.; Burrows, J. N.; Vaidya, A. B.; Riscoe, M. K. Discovery, Synthesis, and Optimization of Antimalarial 4(1H)-Quinolone-3-Diarylethers. *Journal of Medicinal Chemistry* **2014**, *57* (9), 3818–3834. https://doi.org/10.1021/jm500147k.

(139)

Pou, S.; Winter, R. W.; Dodean, R. A.; Liebman, K.; Li, Y.; Mather, M. W.; Nepal, B.; Nilsen, A.; Handford, M. J.; Riscoe, T. M.; Laxson, S.; Kirtley, P. J.; Aleshnick, M.; Zakharov, L. N.; Kelly, J. X.; Smilkstein, M. J.; Wilder, B. K.; Kortagere, S.; Vaidya, A. B.; Alday, P. H.; Doggett, J. S.; Riscoe, M. K. 3-Position Biaryl Endochin-like Quinolones with Enhanced Antimalarial Performance. *ACS Infectious Diseases* **2024**, *10* (7), 2419–2442. https://doi.org/10.1021/acsinfecdis.4c00140.

(140)

Pou, S.; Liebman, K. M.; Winter, R. W.; Nilsen, A.; Li, Y.; Lyche, I. N.; Riscoe, T. M.; Montgomery, J.; Gramelspacher, M. J.; Dodean, R. A.; Zakharov, L. N.; Nepal, B.; Kelly, J. X.; Smilkstein, M. J.; Kortagere, S.; Vaidya, A. B.; Alday, P. H.; Doggett, J. S.; Kudyba, K.; Roncal, N.; Ashraf, K.; Leed, S.; Lee, P. J.; Madejczyk, M. S.; Roth, A.; Riscoe, M. K. Revisiting 2-Substituted-4(1H)-Quinolones for Targeting the Plasmodium Falciparum Cytochrome Bc1 Complex. *Journal of Medicinal Chemistry* **2026**. https://doi.org/10.1021/acs.jmedchem.5c03295.

(141)

Drugs, I. of M. (US). C. on the E. of A.; Arrow, K. J.; Panosian, C.; Gelband, H. Antimalarial Drugs and Drug Resistance. In *Saving Lives, Buying Time: Economics of Malaria Drugs in an Age of Resistance*; National Academies Press (US), 2004.

(142)

Missinou, M. A.; Borrmann, S.; Schindler, A.; Issifou, S.; Adegnika, A. A.; Matsiegui, P.-B.; Binder, R.; Lell, B.; Wiesner, J.; Baranek, T.; Jomaa, H.; Kremsner, P. G. Fosmidomycin for Malaria. *Lancet* **2002**, *360* (9349), 1941–1942. https://doi.org/10.1016/S0140-6736(02)11860-5.

(143)

Tu, Y. Artemisinin—A Gift from Traditional Chinese Medicine to the World (Nobel Lecture). *Angewandte Chemie International Edition* **2016**, *55* (35), 10210–10226. https://doi.org/10.1002/anie.201601967.

(144)

The Chemistry and Synthesis of Qinghaosu Derivatives. China Cooperative Research Group on Qinghaosu and Its Derivatives as Antimalarials. *Journal of Traditional Chinese Medicine = Chung I Tsa Chih Ying Wen Pan* **1982**, *2* (1), 9–16.

(145)

Jefford, C. W.; Vicente, M. G. H.; Jacquier, Y.; Favarger, F.; Mareda, J.; Millasson-Schmidt, P.; Brunner, G.; Burger, U. The Deoxygenation and Isomerization of Artemisinin and Artemether and Their Relevance to Antimalarial Action. *Helvetica Chimica Acta* **1996**, *79* (5), 1475–1487. https://doi.org/10.1002/hlca.19960790520.

(146)

Meshnick, S. R.; Thomas, A.; Ranz, A.; Xu, C.-M.; Pan, H.-Z. Artemisinin (Qinghaosu): The Role of Intracellular Hemin in Its Mechanism of Antimalarial Action. *Molecular and Biochemical Parasitology* **1991**, *49* (2), 181–189. https://doi.org/10.1016/0166-6851(91)90062-B.

(147)

Stocks, P. A.; Bray, P. G.; Barton, V. E.; Al-Helal, M.; Jones, M.; Araujo, N. C.; Gibbons, P.; Ward, S. A.; Hughes, R. H.; Biagini, G. A.; Davies, J.; Amewu, R.; Mercer, A. E.; Ellis, G.; O'Neill, P. M. Evidence for a Common Non-Heme Chelatable-Iron-Dependent Activation Mechanism for Semisynthetic and Synthetic Endoperoxide Antimalarial Drugs. *Angewandte Chemie* **2007**, *46* (33), 6278–6283. https://doi.org/10.1002/anie.200604697.

(148)

WHO. *World Malaria Report 2024*; World Health Organization: Geneva, 2024.

(149)

Ataba, E.; Dorkenoo, A. M.; Nguepou, C. T.; Bakai, T.; Tchadjobo, T.; Kadzahlo, K. D.; Yakpa, K.; Atcha-Oubou, T. Potential Emergence of Plasmodium Resistance to Artemisinin Induced by

the Use of Artemisia Annua for Malaria and COVID-19 Prevention in Sub-African Region. *Acta Parasitologica* **2022**, *67* (1), 55–60. https://doi.org/10.1007/s11686-021-00489-y.

(150)

Noedl, H.; Se, Y.; Schaecher, K.; Smith, B. L.; Socheat, D.; Fukuda, M. M.; Artemisinin Resistance in Cambodia 1 (ARC1) Study Consortium. Evidence of Artemisinin-Resistant Malaria in Western Cambodia. *The New England Journal of Medicine* **2008**, *359* (24), 2619–2620. https://doi.org/10.1056/NEJMc0805011.

(151)

Jensen, M.; Mehlhorn, H. Seventy-Five Years of Resochin® in the Fight Against Malaria. *Parasitology Research* **2009**, *105* (3), 609–627. https://doi.org/10.1007/s00436-009-1524-8.

(152)

Loeb, F.; Clark, W. M.; Coatney, G. R.; Coggeshall, L. T.; Dieuaide, F. R.; Dochez, A. R.; Hakansson, E. G.; Marshall, E. K., Jr.; Marvel, C. S.; McCoy, O. R.; Sapero, J. J.; Sebrell, W. H.; Shannon, J. A.; Carden, G. A., Jr. Activity of a New Antimalarial Agent, Chloroquine (SN 7618): Statement Approved by the Board for Coordination of Malarial Studies. *Journal of the American Medical Association* **1946**, *130* (16), 1069–1070. https://doi.org/10.1001/jama.1946.02870160015006.

(153)

Greenwood, B. M.; Fidock, D. A.; Kyle, D. E.; Kappe, S. H. I.; Alonso, P. L.; Collins, F. H.; Duffy, P. E. Malaria: Progress, Perils, and Prospects for Eradication. *The Journal of Clinical Investigation* **2008**, *118* (4), 1266–1276. https://doi.org/10.1172/JCI33996.

(154)

Talisuna, A. O.; Bloland, P.; D'Alessandro, U. History, Dynamics, and Public Health Importance of Malaria Parasite Resistance. *Clinical Microbiology Reviews* **2004**, *17* (1), 235–254. https://doi.org/10.1128/CMR.17.1.235-254.2004.

(155)

Burckhalter, J. H.; Tendick, F. H.; Jones, E. M.; Holcomb, W. F.; Rawlins, A. L. Aminoalkylphenols as Antimalarials. I. Simply Substituted α-Aminocresols1. *Journal of the American Chemical Society* **1946**, *68* (10), 1894–1901. https://doi.org/10.1021/ja01214a008.

(156)

Burckhalter, J. H.; Tendick, F. H.; Jones, E. M.; Jones, P. A.; Holcomb, W. F.; Rawlins, A. L. Aminoalkylphenols as Antimalarials. II.1 (Heterocyclic-amino)-α-Amino-o-Cresols. The Synthesis of Camoquin2. *Journal of the American Chemical Society* **1948**, *70* (4), 1363–1373. https://doi.org/10.1021/ja01184a023.

(157)

Watkins, W. M.; Spencer, H. C.; Kariuki, D. M.; Sixsmith, D. G.; Boriga, D. A.; Kipingor, T.; Koech, D. K. Effectiveness of Amodiaquine as Treatment for Chloroquine-Resistant Plasmodium Falciparum Infections in Kenya. *The Lancet* **1984**, *323* (8373), 357–359. https://doi.org/10.1016/S0140-6736(84)90410-0.

(158)

Neftel, K. A.; Woodtly, W.; Schmid, M.; Frick, P. G.; Fehr, J. Amodiaquine Induced Agranulocytosis and Liver Damage. *British Medical Journal (Clinical research ed.)* **1986**, *292* (6522), 721–723. https://doi.org/10.1136/bmj.292.6522.721.

(159)

Lind, D. E.; Levi, J. A.; Vincent, P. C. Amodiaquine-Induced Agranulocytosis: Toxic Effect of Amodiaquine in Bone Marrow Cultures In Vitro. *British Medical Journal* **1973**, *1* (5851), 458–460. https://doi.org/10.1136/bmj.1.5851.458.

(160)

Adjuik, M.; Agnamey, P.; Babiker, A.; Borrmann, S.; Brasseur, P.; Cisse, M.; Cobelens, F.; Diallo, S.; Faucher, J.; Garner, P.; Gikunda, S.; Kremsner, P.; Krishna, S.; Lell, B.; Loolpapit, M.; Matsiegui, P.-B.; Missinou, M.; Mwanza, J.; Ntoumi, F.; Olliaro, P.; Osimbo, P.; Rezbach, P.; Some, E.; Taylor, W. Amodiaquine-Artesunate Versus Amodiaquine for Uncomplicated Plasmodium Falciparum Malaria in African Children: A Randomised, Multicentre Trial. *The Lancet* **2002**, *359* (9315), 1365–1372. https://doi.org/10.1016/S0140-6736(02)08348-4.

(161)

Kuang, P. ASAQ DNDi, 2002.

(162)

Cisse, B.; Cairns, M.; Faye, E.; NDiaye, O.; Faye, B.; Cames, C.; Cheng, Y.; NDiaye, M.; Lô, A. C.; Simondon, K.; Trape, J.-F.; Faye, O.; NDiaye, J. L.; Gaye, O.; Greenwood, B.; Milligan, P. Randomized Trial of Piperaquine with Sulfadoxine-Pyrimethamine or Dihydroartemisinin for Malaria Intermittent Preventive Treatment in Children. *PLoS ONE* **2009**, *4* (9), e7164. https://doi.org/10.1371/journal.pone.0007164.

(163)

Huang, S. THE PRESENT STATUS OF MALARIA CONTROL IN THE PEOPLE'S REPUBLIC OF CHINA. *Japanese Journal of Tropical Medicine and Hygiene* **1980**, *8* (3-4), 159–172. https://doi.org/10.2149/tmh1973.8.159.

(164)

Davis, T. M. E.; Hung, T.-Y.; Sim, I.-K.; Karunajeewa, H. A.; Ilett, K. F. Piperaquine. *Drugs* **2005**, *65* (1), 75–87. https://doi.org/10.2165/00003495-200565010-00004.

(165)

Chen, L.; Qu, F. Y.; Zhou, Y. C. Field Observations on the Antimalarial Piperaquine. *Chinese Medical Journal* **1982**, *95* (4), 281–286.

(166)

Liu, D. Surveillance of Antimalarial Drug Resistance in China in the 1980s–1990s. *Infectious Diseases of Poverty* **2014**, *3*, 8. https://doi.org/10.1186/2049-9957-3-8.

(167)

Hien, T. T.; Dolecek, C.; Mai, P. P.; Dung, N. T.; Truong, N. T.; Thai, L. H.; Hoai An, D. T.; Thanh, T. T.; Stepniewska, K.; White, N. J.; Farrar, J. Dihydroartemisinin-Piperaquine Against Multidrug-Resistant *Plasmodium Falciparum* Malaria in Vietnam: Randomised Clinical Trial. *The Lancet* **2004**, *363* (9402), 18–22. https://doi.org/10.1016/S0140-6736(03)15163-X.

(168)

Leang, R.; Barrette, A.; Bouth, D. M.; Menard, D.; Abdur, R.; Duong, S.; Ringwald, P. Efficacy of Dihydroartemisinin-Piperaquine for Treatment of Uncomplicated Plasmodium Falciparum and Plasmodium Vivax in Cambodia, 2008 to 2010. *Antimicrobial Agents and Chemotherapy* **2013**, *57* (2), 818–826. https://doi.org/10.1128/AAC.00686-12.

(169)

Leang, R.; Taylor, W. R. J.; Bouth, D. M.; Song, L.; Tarning, J.; Char, M. C.; Kim, S.; Witkowski, B.; Duru, V.; Domergue, A.; Khim, N.; Ringwald, P.; Menard, D. Evidence of Plasmodium Falciparum Malaria Multidrug Resistance to Artemisinin and Piperaquine in Western Cambodia: Dihydroartemisinin-Piperaquine Open-Label Multicenter Clinical Assessment. *Antimicrobial Agents and Chemotherapy* **2015**, *59* (8), 4719–4726. https://doi.org/10.1128/AAC.00835-15.

(170)

Surolia, N.; Padmanaban, G. Chloroquine Inhibits Heme-Dependent Protein Synthesis in Plasmodium Falciparum. *Proceedings of the National Academy of Sciences* **1991**, *88* (11), 4786–4790. https://doi.org/10.1073/pnas.88.11.4786.

(171)

Ginsburg, H.; Geary, T. G. Current Concepts and New Ideas on the Mechanism of Action of Quinoline-Containing Antimalarials. *Biochemical Pharmacology* **1987**, *36* (10), 1567–1576. https://doi.org/10.1016/0006-2952(87)90038-4.

(172)

Vander Jagt, D. L.; Hunsaker, L. A.; Campos, N. M. Characterization of a Hemoglobin-Degrading, Low Molecular Weight Protease from Plasmodium Falciparum. *Molecular and Biochemical Parasitology* **1986**, *18* (3), 389–400. https://doi.org/10.1016/0166-6851(86)90095-2.

(173)

Cohen, S. N.; Yielding, K. L. Inhibition of DNA and RNA Polymerase Reactions by Chloroquine. *Proceedings of the National Academy of Sciences* **1965**, *54* (2), 521–527. https://doi.org/10.1073/pnas.54.2.521.

(174)

Meshnick, S. R. Chloroquine as Intercalator: A Hypothesis Revived. *Parasitology Today* **1990**, *6* (3), 77–79. https://doi.org/10.1016/0169-4758(90)90215-p.

(175)

Olliaro, P. Mode of Action and Mechanisms of Resistance for Antimalarial Drugs. *Pharmacology & Therapeutics* **2001**, *89* (2), 207–219. https://doi.org/10.1016/s0163-7258(00)00115-7.

(176)

O'Neill, P. M.; Victoria E. Barton; Stephan A. Ward; James Chadwick. 4-Aminoquinolines: Chloroquine, Amodiaquine and Next-Generation Analogues. In *Treatment and Prevention of Malaria*; Milestones in Drug Therapy; Springer Basel, 2012; pp 19–44.

(177)

Elliott, D. A.; McIntosh, M. T.; Hosgood, H. D.; Chen, S.; Zhang, G.; Baevova, P.; Joiner, K. A. Four Distinct Pathways of Hemoglobin Uptake in the Malaria Parasite Plasmodium Falciparum. *Proceedings of the National Academy of Sciences* **2008**, *105* (7), 2463–2468. https://doi.org/10.1073/pnas.0711067105.

(178)

Liu, J.; Istvan, E. S.; Gluzman, I. Y.; Gross, J.; Goldberg, D. E. Plasmodium Falciparum Ensures Its Amino Acid Supply with Multiple Acquisition Pathways and Redundant Proteolytic Enzyme Systems. *Proceedings of the National Academy of Sciences* **2006**, *103* (23), 8840–8845. https://doi.org/10.1073/pnas.0601876103.

(179)

Goldberg, D. E.; Slater, A. F.; Cerami, A.; Henderson, G. B. Hemoglobin Degradation in the Malaria Parasite Plasmodium Falciparum: An Ordered Process in a Unique Organelle. *Proceedings of the National Academy of Sciences* **1990**, *87* (8), 2931–2935. https://doi.org/10.1073/pnas.87.8.2931.

(180)

Wiser, M. F. The Digestive Vacuole of the Malaria Parasite: A Specialized Lysosome. *Pathogens* **2024**, *13* (3), 182. https://doi.org/10.3390/pathogens13030182.

(181)

Shafik, S. H.; Cobbold, S. A.; Barkat, K.; Richards, S. N.; Lancaster, N. S.; Llinás, M.; Hogg, S. J.; Summers, R. L.; McConville, M. J.; Martin, R. E. The Natural Function of the Malaria

Parasite's Chloroquine Resistance Transporter. *Nature Communications* **2020**, *11* (1), 3922. https://doi.org/10.1038/s41467-020-17781-6.

(182)

Cowell, A.; Winzeler, E. Exploration of the Plasmodium Falciparum Resistome and Druggable Genome Reveals New Mechanisms of Drug Resistance and Antimalarial Targets. *Microbiology Insights* **2018**, *11*, 1178636118808529. https://doi.org/10.1177/1178636118808529.

(183)

Krugliak, M.; Zhang, J.; Ginsburg, H. Intraerythrocytic Plasmodium Falciparum Utilizes Only a Fraction of the Amino Acids Derived from the Digestion of Host Cell Cytosol for the Biosynthesis of Its Proteins. *Molecular and Biochemical Parasitology* **2002**, *119* (2), 249–256. https://doi.org/10.1016/s0166-6851(01)00427-3.

(184)

Lew, V. L.; Tiffert, T.; Ginsburg, H. Excess Hemoglobin Digestion and the Osmotic Stability of Plasmodium Falciparum-Infected Red Blood Cells. *Blood* **2003**, *101* (10), 4189–4194. https://doi.org/10.1182/blood-2002-08-2654.

(185)

Hanssen, E.; Knoechel, C.; Dearnley, M.; Dixon, M. W. A.; Le Gros, M.; Larabell, C.; Tilley, L. Soft X-ray Microscopy Analysis of Cell Volume and Hemoglobin Content in Erythrocytes Infected with Asexual and Sexual Stages of Plasmodium Falciparum. *Journal of Structural Biology* **2012**, *177* (2), 224–232. https://doi.org/10.1016/j.jsb.2011.09.003.

(186)

Okada, K. The Novel Heme Oxygenase-Like Protein from Plasmodiumfalciparum Converts Heme to Bilirubin IXalpha in the Apicoplast. *FEBS letters* **2009**, *583* (2), 313–319. https://doi.org/10.1016/j.febslet.2008.12.015.

(187)

Klar, P. B.; Waterman, D. G.; Gruene, T.; Mullick, D.; Song, Y.; Gilchrist, J. B.; Owen, C. D.; Wen, W.; Biran, I.; Houben, L.; Regev-Rudzki, N.; Dzikowski, R.; Marom, N.; Palatinus, L.; Zhang, P.; Leiserowitz, L.; Elbaum, M. Cryo-Tomography and 3D Electron Diffraction Reveal the Polar Habit and Chiral Structure of the Malaria Pigment Crystal Hemozoin. *ACS Central Science* **2024**, *10* (8), 1504–1514. https://doi.org/10.1021/acscentsci.4c00162.

(188)

Fitch, C. D.; Cai, G. Z.; Chen, Y. F.; Shoemaker, J. D. Involvement of Lipids in Ferriprotoporphyrin IX Polymerization in Malaria. *Biochimica Et Biophysica Acta* **1999**, *1454* (1), 31–37. https://doi.org/10.1016/s0925-4439(99)00017-4.

(189)

Ambele, M. A.; Egan, T. J. Neutral Lipids Associated with Haemozoin Mediate Efficient and Rapid β-Haematin Formation at Physiological pH, Temperature and Ionic Composition. *Malaria Journal* **2012**, *11*, 337. https://doi.org/10.1186/1475-2875-11-337.

(190)

Hoang, A. N.; Ncokazi, K. K.; de Villiers, K. A.; Wright, D. W.; Egan, T. J. Crystallization of Synthetic Haemozoin (Beta-Haematin) Nucleated at the Surface of Lipid Particles. *Dalton Transactions* **2010**, *39* (5), 1235–1244. https://doi.org/10.1039/b914359a.

(191)

Kapishnikov, S.; Weiner, A.; Shimoni, E.; Guttmann, P.; Schneider, G.; Dahan-Pasternak, N.; Dzikowski, R.; Leiserowitz, L.; Elbaum, M. Oriented Nucleation of Hemozoin at the Digestive Vacuole Membrane in Plasmodium Falciparum. *Proceedings of the National Academy of Sciences of the United States of America* **2012**, *109* (28), 11188–11193. https://doi.org/10.1073/pnas.1118120109.

(192)

Pisciotta, J. M.; Coppens, I.; Tripathi, A. K.; Scholl, P. F.; Shuman, J.; Bajad, S.; Shulaev, V.; Sullivan, D. J. The Role of Neutral Lipid Nanospheres in Plasmodium Falciparum Haem Crystallization. *The Biochemical Journal* **2007**, *402* (1), 197–204. https://doi.org/10.1042/BJ20060986.

(193)

Burda, P.-C.; Crosskey, T.; Lauk, K.; Zurborg, A.; Söhnchen, C.; Liffner, B.; Wilcke, L.; Pietsch, E.; Strauss, J.; Jeffries, C. M.; Svergun, D. I.; Wilson, D. W.; Wilmanns, M.; Gilberger, T.-W. Structure-Based Identification and Functional Characterization of a Lipocalin in the Malaria Parasite Plasmodium Falciparum. *Cell Reports* **2020**, *31* (12), 107817. https://doi.org/10.1016/j.celrep.2020.107817.

(194)

Sullivan, D. J.; Gluzman, I. Y.; Goldberg, D. E. Plasmodium Hemozoin Formation Mediated by Histidine-Rich Proteins. *Science* **1996**, *271* (5246), 219–222. https://doi.org/10.1126/science.271.5246.219.

(195)

Jani, D.; Nagarkatti, R.; Beatty, W.; Angel, R.; Slebodnick, C.; Andersen, J.; Kumar, S.; Rathore, D. HDP-a Novel Heme Detoxification Protein from the Malaria Parasite. *PLoS pathogens* **2008**, *4* (4), e1000053. https://doi.org/10.1371/journal.ppat.1000053.

(196)

Matz, J. M.; Drepper, B.; Blum, T. B.; van Genderen, E.; Burrell, A.; Martin, P.; Stach, T.; Collinson, L. M.; Abrahams, J. P.; Matuschewski, K.; Blackman, M. J. A Lipocalin Mediates Unidirectional Heme Biomineralization in Malaria Parasites. *Proceedings of the National*

Academy of Sciences of the United States of America **2020**, *117* (28), 16546–16556. https://doi.org/10.1073/pnas.2001153117.

(197)

Slater, A. F.; Swiggard, W. J.; Orton, B. R.; Flitter, W. D.; Goldberg, D. E.; Cerami, A.; Henderson, G. B. An Iron-Carboxylate Bond Links the Heme Units of Malaria Pigment. *Proceedings of the National Academy of Sciences of the United States of America* **1991**, *88* (2), 325–329. https://doi.org/10.1073/pnas.88.2.325.

(198)

Fitch, C. D.; Kanjananggulpan, P. The State of Ferriprotoporphyrin IX in Malaria Pigment. *Journal of Biological Chemistry* **1987**, *262* (32), 15552–15555. https://doi.org/10.1016/S0021-9258(18)47761-7.

(199)

Egan, T. J.; Ross, D. C.; Adams, P. A. Quinoline Anti-Malarial Drugs Inhibit Spontaneous Formation of Beta-Haematin (Malaria Pigment). *FEBS letters* **1994**, *352* (1), 54–57. https://doi.org/10.1016/0014-5793(94)00921-x.

(200)

Adams, P. A.; Berman, P. A.; Egan, T. J.; Marsh, P. J.; Silver, J. The Iron Environment in Heme and Heme-Antimalarial Complexes of Pharmacological Interest. *Journal of Inorganic Biochemistry* **1996**, *63* (1), 69–77. https://doi.org/10.1016/0162-0134(95)00212-x.

(201)

Egan, T. J.; Mavuso, W. W.; Ross, D. C.; Marques, H. M. Thermodynamic Factors Controlling the Interaction of Quinoline Antimalarial Drugs with Ferriprotoporphyrin IX. *Journal of Inorganic Biochemistry* **1997**, *68* (2), 137–145. https://doi.org/10.1016/s0162-0134(97)00086-x.

(202)

Egan, T. J.; Marques, H. M. The Role of Haem in the Activity of Chloroquine and Related Antimalarial Drugs. *Coordination Chemistry Reviews* **1999**, *190–192*, 493–517. https://doi.org/10.1016/S0010-8545(99)00112-5.

(203)

Sullivan, D. J.; Gluzman, I. Y.; Russell, D. G.; Goldberg, D. E. On the Molecular Mechanism of Chloroquine's Antimalarial Action. *Proceedings of the National Academy of Sciences of the United States of America* **1996**, *93* (21), 11865–11870. https://doi.org/10.1073/pnas.93.21.11865.

(204)

Buller, R.; Peterson, M. L.; Almarsson, Ö.; Leiserowitz, L. Quinoline Binding Site on Malaria Pigment Crystal: A Rational Pathway for Antimalaria Drug Design. *Crystal Growth & Design* **2002**, *2* (6), 553–562. https://doi.org/10.1021/cg025550i.

(205)

Herraiz, T.; Guillén, H.; González-Peña, D.; Arán, V. J. Antimalarial Quinoline Drugs Inhibit β-Hematin and Increase Free Hemin Catalyzing Peroxidative Reactions and Inhibition of Cysteine Proteases. *Scientific Reports* **2019**, *9* (1), 15398. https://doi.org/10.1038/s41598-019-51604-z.

(206)

Warhurst, D. C.; Craig, J. C.; Adagu, I. S.; Guy, R. K.; Madrid, P. B.; Fivelman, Q. L. Activity of Piperaquine and Other 4-Aminoquinoline Antiplasmodial Drugs Against Chloroquine-Sensitive and Resistant Blood-Stages of Plasmodium Falciparum. Role of Beta-Haematin Inhibition and Drug Concentration in Vacuolar Water- and Lipid-Phases. *Biochemical Pharmacology* **2007**, *73* (12), 1910–1926. https://doi.org/10.1016/j.bcp.2007.03.011.

(207)

Ginsburg, H.; Famin, O.; Zhang, J.; Krugliak, M. Inhibition of Glutathione-Dependent Degradation of Heme by Chloroquine and Amodiaquine as a Possible Basis for Their Antimalarial Mode of Action. *Biochemical Pharmacology* **1998**, *56* (10), 1305–1313. https://doi.org/10.1016/s0006-2952(98)00184-1.

(208)

Hawley, S. R.; Bray, P. G.; Park, B. K.; Ward, S. A. Amodiaquine Accumulation in Plasmodium Falciparum as a Possible Explanation for Its Superior Antimalarial Activity over Chloroquine. *Molecular and Biochemical Parasitology* **1996**, *80* (1), 15–25. https://doi.org/10.1016/0166-6851(96)02655-2.

(209)

Geary, T. G.; Divo, A. D.; Jensen, J. B.; Zangwill, M.; Ginsburg, H. Kinetic Modelling of the Response of Plasmodium Falciparum to Chloroquine and Its Experimental Testing in Vitro. Implications for Mechanism of Action of and Resistance to the Drug. *Biochemical Pharmacology* **1990**, *40* (4), 685–691. https://doi.org/10.1016/0006-2952(90)90302-2.

(210)

Sanchez, C. P.; Wünsch, S.; Lanzer, M. Identification of a Chloroquine Importer in Plasmodium Falciparum. Differences in Import Kinetics Are Genetically Linked with the Chloroquine-Resistant Phenotype. *The Journal of Biological Chemistry* **1997**, *272* (5), 2652–2658. https://doi.org/10.1074/jbc.272.5.2652.

(211)

Ferrari, V.; Cutler, D. J. Kinetics and Thermodynamics of Chloroquine and Hydroxychloroquine Transport Across the Human Erythrocyte Membrane. *Biochemical Pharmacology* **1991**, *41* (1), 23–30. https://doi.org/10.1016/0006-2952(91)90006-q.

(212)

Shafik, S. H.; Richards, S. N.; Corry, B.; Martin, R. E. Mechanistic Basis for Multidrug Resistance and Collateral Drug Sensitivity Conferred to the Malaria Parasite by Polymorphisms

in PfMDR1 and PfCRT. *PLOS Biology* **2022**, *20* (5), e3001616. https://doi.org/10.1371/journal.pbio.3001616.

(213)

L'Episcopia, M.; Kelley, J.; Djeunang Dongho, B. G.; Patel, D.; Schmedes, S.; Ravishankar, S.; Perrotti, E.; Modiano, D.; Lucchi, N. W.; Russo, G.; Talundzic, E.; Severini, C. Targeted Deep Amplicon Sequencing of Antimalarial Resistance Markers in Plasmodium Falciparum Isolates from Cameroon. *International journal of infectious diseases: IJID: official publication of the International Society for Infectious Diseases* **2021**, *107*, 234–241. https://doi.org/10.1016/j.ijid.2021.04.081.

(214)

Fitch, C. D. Plasmodium Falciparum in Owl Monkeys: Drug Resistance and Chloroquine Binding Capacity. *Science* **1970**, *169* (3942), 289–290. https://doi.org/10.1126/science.169.3942.289.

(215)

Warhurst, D. New Developments: Chloroquine-Resistance in Plasmodium Falciparum. *Drug Resistance Updates: Reviews and Commentaries in Antimicrobial and Anticancer Chemotherapy* **2001**, *4* (3), 141–144. https://doi.org/10.1054/drup.2001.0194.

(216)

Jiang, H.; Joy, D. A.; Furuya, T.; Su, X. Current Understanding of the Molecular Basis of Chloroquine-Resistance in Plasmodium Falciparum. *Journal of Postgraduate Medicine* **2006**, *52* (4), 271–276.

(217)

Ridley, R. G. Malaria: Dissecting Chloroquine Resistance. *Current Biology* **1998**, *8* (10), R346–R349. https://doi.org/10.1016/S0960-9822(98)70218-0.

(218)

Su, X.; Kirkman, L. A.; Fujioka, H.; Wellems, T. E. Complex Polymorphisms in an Approximately 330 kDa Protein Are Linked to Chloroquine-Resistant P. Falciparum in Southeast Asia and Africa. *Cell* **1997**, *91* (5), 593–603. https://doi.org/10.1016/s0092-8674(00)80447-x.

(219)

Wellems, T. E.; Walker-Jonah, A.; Panton, L. J. Genetic Mapping of the Chloroquine-Resistance Locus on Plasmodium Falciparum Chromosome 7. *Proceedings of the National Academy of Sciences of the United States of America* **1991**, *88* (8), 3382–3386. https://doi.org/10.1073/pnas.88.8.3382.

(220)

Fidock, D. A.; Nomura, T.; Talley, A. K.; Cooper, R. A.; Dzekunov, S. M.; Ferdig, M. T.; Ursos, L. M.; Sidhu, A. B.; Naudé, B.; Deitsch, K. W.; Su, X. Z.; Wootton, J. C.; Roepe, P. D.;

Wellems, T. E. Mutations in the P. Falciparum Digestive Vacuole Transmembrane Protein PfCRT and Evidence for Their Role in Chloroquine Resistance. *Molecular Cell* **2000**, *6* (4), 861–871. https://doi.org/10.1016/s1097-2765(05)00077-8.

(221)

Sidhu, A. B. S.; Verdier-Pinard, D.; Fidock, D. A. Chloroquine Resistance in Plasmodium Falciparum Malaria Parasites Conferred by Pfcrt Mutations. *Science (New York, N.Y.)* **2002**, *298* (5591), 210–213. https://doi.org/10.1126/science.1074045.

(222)

Ecker, A.; Lehane, A. M.; Clain, J.; Fidock, D. A. PfCRT and Its Role in Antimalarial Drug Resistance. *Trends in Parasitology* **2012**, *28* (11), 504–514. https://doi.org/10.1016/j.pt.2012.08.002.

(223)

Ecker, A.; Adele M. Lehane; David A. Fidock. Molecular Markers of Plasmodium Resistance to Antimalarials. In *Treatment and Prevention of Malaria*; Milestones in Drug Therapy; Springer Basel, 2012; pp 249–280.

(224)

Summers, R. L.; Nash, M. N.; Martin, R. E. Know Your Enemy: Understanding the Role of PfCRT in Drug Resistance Could Lead to New Antimalarial Tactics. *Cellular and Molecular Life Sciences* **2012**, *69* (12), 1967–1995. https://doi.org/10.1007/s00018-011-0906-0.

(225)

Martin, R. E.; Marchetti, R. V.; Cowan, A. I.; Howitt, S. M.; Bröer, S.; Kirk, K. Chloroquine Transport via the Malaria Parasite's Chloroquine Resistance Transporter. *Science* **2009**, *325* (5948), 1680–1682. https://doi.org/10.1126/science.1175667.

(226)

Bray, P. G.; Martin, R. E.; Tilley, L.; Ward, S. A.; Kirk, K.; Fidock, D. A. Defining the Role of PfCRT in Plasmodium Falciparum Chloroquine Resistance. *Molecular Microbiology* **2005**, *56* (2), 323–333. https://doi.org/10.1111/j.1365-2958.2005.04556.x.

(227)

Sanchez, C. P.; Dave, A.; Stein, W. D.; Lanzer, M. Transporters as Mediators of Drug Resistance in *Plasmodium Falciparum*. *International Journal for Parasitology* **2010**, *40* (10), 1109–1118. https://doi.org/10.1016/j.ijpara.2010.04.001.

(228)

Gligorijevic, B.; Purdy, K.; Elliott, D. A.; Cooper, R. A.; Roepe, P. D. Stage Independent Chloroquine Resistance and Chloroquine Toxicity Revealed via Spinning Disk Confocal Microscopy. *Molecular and Biochemical Parasitology* **2008**, *159* (1), 7–23. https://doi.org/10.1016/j.molbiopara.2007.12.014.

(229)

Cabrera, M.; Paguio, M. F.; Xie, C.; Roepe, P. D. Reduced Digestive Vacuolar Accumulation of Chloroquine Is Not Linked to Resistance to Chloroquine Toxicity. *Biochemistry* **2009**, *48* (47), 11152–11154. https://doi.org/10.1021/bi901765v.

(230)

Hatton, C. S.; Peto, T. E.; Bunch, C.; Pasvol, G.; Russell, S. J.; Singer, C. R.; Edwards, G.; Winstanley, P. Frequency of Severe Neutropenia Associated with Amodiaquine Prophylaxis Against Malaria. *Lancet* **1986**, *1* (8478), 411–414. https://doi.org/10.1016/s0140-6736(86)92371-8.

(231)

Olliaro, P. L.; Mussano, P. Amodiaquine for Treating Malaria. *The Cochrane Database of Systematic Reviews* **2003**, *2003* (2), CD000016. https://doi.org/10.1002/14651858.CD000016.

(232)

O'Neill, P. M.; Mukhtar, A.; Stocks, P. A.; Randle, L. E.; Hindley, S.; Ward, S. A.; Storr, R. C.; Bickley, J. F.; O'Neil, I. A.; Maggs, J. L.; Hughes, R. H.; Winstanley, P. A.; Bray, P. G.; Park, B. K. Isoquine and Related Amodiaquine Analogues: A New Generation of Improved 4-Aminoquinoline Antimalarials. *Journal of Medicinal Chemistry* **2003**, *46* (23), 4933–4945. https://doi.org/10.1021/jm030796n.

(233)

Harrison, A. C.; Kitteringham, N. R.; Clarke, J. B.; Park, B. K. The Mechanism of Bioactivation and Antigen Formation of Amodiaquine in the Rat. *Biochemical Pharmacology* **1992**, *43* (7), 1421–1430. https://doi.org/10.1016/0006-2952(92)90198-R.

(234)

Clarke, J. B.; Neftel, K.; Kitteringham, N. R.; Park, B. K. Detection of Antidrug IgG Antibodies in Patients with Adverse Drug Reactions to Amodiaquine. *International Archives of Allergy and Immunology* **1991**, *95* (4), 369–375. https://doi.org/10.1159/000235475.

(235)

Sinha, S.; Sarma, P.; Sehgal, R.; Medhi, B. Development in Assay Methods for in Vitro Antimalarial Drug Efficacy Testing: A Systematic Review. *Frontiers in Pharmacology* **2017**, *8*. https://doi.org/10.3389/fphar.2017.00754.

(236)

Moreau, S.; Perly, B.; Chachaty, C.; Deleuze, C. A Nuclear Magnetic Resonance Study of the Interactions of Antimalarial Drugs with Porphyrins. *Biochimica Et Biophysica Acta* **1985**, *840* (1), 107–116. https://doi.org/10.1016/0304-4165(85)90167-9.

(237)

Constantinidis, I.; Satterlee, J. D. UV-visible and Carbon NMR Studies of Chloroquine Binding to Urohemin I Chloride and Uroporphyrin I in Aqueous Solutions. *Journal of the American Chemical Society* **1988**, *110* (13), 4391–4395. https://doi.org/10.1021/ja00221a045.

(238)

Pinheiro, L. C. S.; Feitosa, L. M.; Gandi, M. O.; Silveira, F. F.; Boechat, N. The Development of Novel Compounds Against Malaria: Quinolines, Triazolpyridines, Pyrazolopyridines and Pyrazolopyrimidines. *Molecules* **2019**, *24* (22), 4095. https://doi.org/10.3390/molecules24224095.

(239)

Werbel, L.; Kesten, S.; Turner, W. Structure-Activity Relationships of Antimalarial Indolo[3,2-*c*]quinolines [1, 2]. *European Journal of Medicinal Chemistry* **1993**, *28* (11), 837–852. https://doi.org/10.1016/0223-5234(93)90036-E.

(240)

Ringwald, P.; Bickii, J.; Basco, L. K. Efficacy of Oral Pyronaridine for the Treatment of Acute Uncomplicated Falciparum Malaria in African Children. *Clinical Infectious Diseases* **1998**, *26* (4), 946–953. https://doi.org/10.1086/513942.

(241)

Sereekhajornjaru, N.; Somboon, C.; Rattanajak, R.; Denny, W. A.; Wilairat, P.; Auparakkitanon, S. Comparison of Hematin-Targeting Properties of Pynacrine, an Acridine Analog of the Benzonaphthyridine Antimalarial Pyronaridine. *Acta Tropica* **2014**, *140*, 181–183. https://doi.org/10.1016/j.actatropica.2014.09.002.

(242)

Peters, W.; Robinson, B. L. The Chemotherapy of Rodent Malaria. XLVII. Studies on Pyronaridine and Other Mannich Base Antimalarials. *Annals of Tropical Medicine and Parasitology* **1992**, *86* (5), 455–465. https://doi.org/10.1080/00034983.1992.11812694.

(243)

Wiselogle, F. Y. *A Survey of Antimalarial Drugs, 1941-1945 ...*; Edwards, 1946.

(244)

Thompson, P. E.; Werbel, L. M. *Antimalarial Agents: Chemistry and Pharmacology*; Elsevier Science, 1972.

(245)

Heindel, N. D.; Molnar, J. Synthesis and Antimalarial Activity of Amodiaquine Analogs. *Journal of Medicinal Chemistry* **1970**, *13* (1), 156–157. https://doi.org/10.1021/jm00295a051.

(246)

Heindel, N. D.; Bechara, I. S.; Ohnmacht, C. J.; Molnar, J.; Lemke, T. F.; Kennewell, P. D. Diaminoquinoline Antimalarials. *Journal of Medicinal Chemistry* **1969**, *12* (5), 797–801. https://doi.org/10.1021/jm00305a017.

(247)

Edward F. Elslager; Eva H. Gold; Frank H. Tendick; Leslie M. Werbel; Donald F. Worth. Amodiaquine N-Oxides and Other 7-Chloro-4-Aminoquinoline N-Oxides. *Journal of Heterocyclic Chemistry* **Febuary 1964**, *1* (1), 6–12. https://doi.org/10.1002/jhet.5570010102.

(248)

Barlin, G.; Ireland, S.; Nguyen, T.; Kotecka, B.; Rieckmann, K. Potential Antimalarials. XXI. Mannich Base Derivatives of 4-[7-Chloro(and 7-Trifluoromethyl)quinolin-4-Ylamino]phenols. *Australian Journal of Chemistry* **1994**, *47*, 1553–1560. https://doi.org/10.1071/CH9941553.

(249)

Go, M.; Ngiam, T.; Wan, A. S. C. Synthesis of Some Novel Amodiaquine Analogs as Potential Antimalarial and Antifilarial Compounds. *Journal of Medicinal Chemistry* **1981**, *24* (12), 1471–1475. https://doi.org/10.1021/jm00144a020.

(250)

Werbel, L. M.; Cook, P. D.; Elslager, E. F.; Hung, J. H.; Johnson, J. L.; Kesten, S. J.; McNamara, D. J.; Ortwine, D. F.; Worth, D. F. Antimalarial Drugs. 60. Synthesis, Antimalarial Activity, and Quantitative Structure-Activity Relationships of Tebuquine and a Series of Related 5-[(7-Chloro-4-Quinolinyl)amino]-3-[(alkylamino)methyl][1,1'-Biphenyl]-2-Ols and N.omega.-Oxides. *Journal of Medicinal Chemistry* **1986**, *29* (6), 924–939. https://doi.org/10.1021/jm00156a009.

(251)

Thompson, P. E.; K. Weston; A. J. Glazko; R. A. Fisken; T. A. Reutner; A. Bayles; J. K. Weston. Laboratory Studies on Amopyroquin (Propaquin): An Antimalarial Compound. *Antibiotic Chemotherapy* **1958**, *8*, 450–460.

(252)

Guglielmo, S.; Bertinaria, M.; Rolando, B.; Crosetti, M.; Fruttero, R.; Yardley, V.; Croft, S. L.; Gasco, A. A New Series of Amodiaquine Analogues Modified in the Basic Side Chain with in Vitro Antileishmanial and Antiplasmodial Activity. *European Journal of Medicinal Chemistry* **2009**, *44* (12), 5071–5079. https://doi.org/10.1016/j.ejmech.2009.09.012.

(253)

Verdier, F.; Pussard, E.; Clavier, F.; Le Bras, J.; Gaudebout, C. Pharmacokinetics of Intramuscular Amopyroquin in Healthy Subjects and Determination of a Therapeutic Regimen for Plasmodium Falciparum Malaria. *Antimicrobial Agents and Chemotherapy* **1989**, *33* (3), 316–321. https://doi.org/10.1128/aac.33.3.316.

(254)

Pussard, E.; Verdier, F.; Faurisson, F.; Clavier, F.; Simon, F.; Gaudebout, C. Disposition of Amopyroquin in Rats and Rabbits and in Vitro Activity Against Plasmodium Falciparum. *Antimicrobial Agents and Chemotherapy* **1988**, *32* (4), 568–572. https://doi.org/10.1128/aac.32.4.568.

(255)

L. H. Schmidt; Dennis Vaughan; Donna Mueller; Ruth Crosby; Rebecca Hamilton. Activities of Various 4-Aminoquinolines Against Infections with Chloroquine-Resistant Strains of Plasmodium Falciparum. *Antimicrobial Agents and Chemotherapy* **1977**, *11* (5), 826–843.

(256)

Barlin, G. B.; Jiravinyu, C.; Butcher, G. A.; Kotecka, B.; Rieckmann, K. The in Vitro and in Vivo Antimalarial Activity of Some Mannich Bases Derived from 4-(7'-Trifluoromethyl-1',5'-Naphthyridin-4'-Ylamino)phenol, 2-(7'-Trifluoromethyl-Quinolin-4'-Ylamino)phenol, and 4'-Chloro-5-(7"-Trifluoromethylquinolin-4"-Ylamino)biphenyl -2-Ols. *Annals of Tropical Medicine and Parasitology* **1992**, *86* (4), 323–331. https://doi.org/10.1080/00034983.1992.11812674.

(257)

Barlin, G.; Nguyen, T.; Kotecka, B.; Rieckmann, K. Potential Antimalarials. XV. Di-Mannich Bases of 2-(7'-Chloroquinolin-4'-Ylamino)phenol and 2-[7'-Bromo(and Trifluoromethyl)-1',5'-Naphthyridin-4'-Ylamino]phenol. *Australian Journal of Chemistry - AUST J CHEM* **1992**, *45*. https://doi.org/10.1071/CH9921651.

(258)

Barlin, G.; Nguyen, T.; Kotecka, B.; Rieckmann, K. Potential Antimalarials. XVII. Di- and Mono-Mannich Bases of 2(and 4)-[2(and 8)-Trifluoromethylquinolin-4-ylamino]phenol. *Australian Journal of Chemistry* **1993**, *46*, 21–29. https://doi.org/10.1071/CH9930021.

(259)

Kotecka, B.; Barlin, G.; Edstein, M.; Rieckmann, K. New Quinoline Di-Mannich Base Compounds with Greater Antimalarial Activity Than Chloroquine, Amodiaquine, or Pyronaridine. *Antimicrobial agents and chemotherapy* **1997**, *41*, 1369–1374. https://doi.org/10.1128/AAC.41.6.1369.

(260)

Delarue, S.; Girault, S.; Maes, L.; Debreu-Fontaine, M. A.; Labaeïd, M.; Grellier, P.; Sergheraert, C. Synthesis and in Vitro and in Vivo Antimalarial Activity of New 4-Anilinoquinolines. *Journal of Medicinal Chemistry* **2001**, *44* (17), 2827–2833. https://doi.org/10.1021/jm010842o.

(261)

Delarue-Cochin, S.; Paunescu, E.; Maes, L.; Mouray, E.; Sergheraert, C.; Grellier, P.; Melnyk, P. Synthesis and Antimalarial Activity of New Analogues of Amodiaquine. *European Journal of Medicinal Chemistry* **2008**, *43* (2), 252–260. https://doi.org/10.1016/j.ejmech.2007.03.008.

(262)

O'Neill, P. M.; Harrison, A. C.; Storr, R. C.; Hawley, S. R.; Ward, S. A.; Park, B. K. The Effect of Fluorine Substitution on the Metabolism and Antimalarial Activity of Amodiaquine. *Journal of Medicinal Chemistry* **1994**, *37* (9), 1362–1370. https://doi.org/10.1021/jm00035a017.

(263)

O'Neill, P. M.; Willock, D. J.; Hawley, S. R.; Bray, P. G.; Storr, R. C.; Ward, S. A.; Park, B. K. Synthesis, Antimalarial Activity, and Molecular Modeling of Tebuquine Analogues. *Journal of Medicinal Chemistry* **1997**, *40* (4), 437–448. https://doi.org/10.1021/jm960370r.

(264)

O'Neill, P. M.; Shone, A. E.; Stanford, D.; Nixon, G.; Asadollahy, E.; Park, B. K.; Maggs, J. L.; Roberts, P.; Stocks, P. A.; Biagini, G.; Bray, P. G.; Davies, J.; Berry, N.; Hall, C.; Rimmer, K.; Winstanley, P. A.; Hindley, S.; Bambal, R. B.; Davis, C. B.; Bates, M.; Gresham, S. L.; Brigandi, R. A.; Gomez-de-las-Heras, F. M.; Gargallo, D. V.; Parapini, S.; Vivas, L.; Lander, H.; Taramelli, D.; Ward, S. A. Synthesis, Antimalarial Activity, and Preclinical Pharmacology of a Novel Series of 4′-Fluoro and 4′-Chloro Analogues of Amodiaquine. Identification of a Suitable "Back-Up" Compound for N-tert-Butyl Isoquine. *Journal of Medicinal Chemistry* **2009**, *52* (7), 1828–1844. https://doi.org/10.1021/jm8012757.

(265)

O'Neill, P. M.; Park, B. K.; Shone, A. E.; Maggs, J. L.; Roberts, P.; Stocks, P. A.; Biagini, G. A.; Bray, P. G.; Gibbons, P.; Berry, N.; Winstanley, P. A.; Mukhtar, A.; Bonar-Law, R.; Hindley, S.; Bambal, R. B.; Davis, C. B.; Bates, M.; Hart, T. K.; Gresham, S. L.; Lawrence, R. M.; Brigandi, R. A.; Gomez-delas-Heras, F. M.; Gargallo, D. V.; Ward, S. A. Candidate Selection and Preclinical Evaluation of *N* - *Tert* -Butyl Isoquine (GSK369796), An Affordable and Effective 4-Aminoquinoline Antimalarial for the 21st Century. *Journal of Medicinal Chemistry* **2009**, *52* (5), 1408–1415. https://doi.org/10.1021/jm8012618.

(266)

Vennerstrom, J. L.; Ellis, W. Y.; Ager, A. L.; Andersen, S. L.; Gerena, L.; Milhous, W. K. Bisquinolines. 1. N,N-Bis(7-Chloroquinolin-4-Yl)alkanediamines with Potential Against Chloroquine-Resistant Malaria. *Journal of Medicinal Chemistry* **1992**, *35* (11), 2129–2134. https://doi.org/10.1021/jm00089a025.

(267)

Ridley, R. G.; Matile, H.; Jaquet, C.; Dorn, A.; Hofheinz, W.; Leupin, W.; Masciadri, R.; Theil, F. P.; Richter, W. F.; Girometta, M. A.; Guenzi, A.; Urwyler, H.; Gocke, E.; Potthast, J. M.; Csato, M.; Thomas, A.; Peters, W. Antimalarial Activity of the Bisquinoline Trans-N1,N2-Bis (7-Chloroquinolin-4-Yl)cyclohexane-1,2-Diamine: Comparison of Two Stereoisomers and

Detailed Evaluation of the S,S Enantiomer, Ro 47-7737. *Antimicrobial Agents and Chemotherapy* **1997**, *41* (3), 677–686. https://doi.org/10.1128/AAC.41.3.677.

(268)

Vennerstrom, J. L.; Ager, A. L.; Dorn, A.; Andersen, S. L.; Gerena, L.; Ridley, R. G.; Milhous, W. K. Bisquinolines. 2. Antimalarial N,N-Bis(7-Chloroquinolin-4-Yl)heteroalkanediamines. *Journal of Medicinal Chemistry* **1998**, *41* (22), 4360–4364. https://doi.org/10.1021/jm9803828.

(269)

van Heerden, L.; Cloete, T. T.; Breytenbach, J. W.; de Kock, C.; Smith, P. J.; Breytenbach, J. C.; N'Da, D. D. Synthesis and *in Vitro* Antimalarial Activity of a Series of Bisquinoline and Bispyrrolo[1,2a]quinoxaline Compounds. *European Journal of Medicinal Chemistry* **2012**, *55*, 335–345. https://doi.org/10.1016/j.ejmech.2012.07.037.

(270)

Ismail, F. M.; Dascombe, M. J.; Carr, P.; Mérette, S. A.; Rouault, P. Novel Aryl-Bis-Quinolines with Antimalarial Activity in-Vivo. *The Journal of Pharmacy and Pharmacology* **1998**, *50* (5), 483–492. https://doi.org/10.1111/j.2042-7158.1998.tb06189.x.

(271)

Liebman, K. M.; Burgess, S. J.; Gunsaru, B.; Kelly, J. X.; Li, Y.; Morrill, W.; Liebman, M. C.; Peyton, D. H. Unsymmetrical Bisquinolines with High Potency Against P. Falciparum Malaria. *Molecules* **2020**, *25* (9), 2251. https://doi.org/10.3390/molecules25092251.

(272)

Handford, M. J.; Li, Y.; Riscoe, T.; Liebman, K. M.; Kelly, J. X.; Riscoe, M. K. Discovery of Amodiachins, a Novel Class of 4-Aminoquinoline Antimalarials Active Against Multidrug-Resistant Plasmodium Falciparum. *Journal of medicinal chemistry* **2025**, *68* (20), 21156–21171. https://doi.org/10.1021/acs.jmedchem.5c00936.

(273)

Mita, T.; Tanabe, K. Evolution of Plasmodium Falciparum Drug Resistance: Implications for the Development and Containment of Artemisinin Resistance. *Japanese Journal of Infectious Diseases* **2012**, *65* (6), 465–475. https://doi.org/10.7883/yoken.65.465.

(274)

Chawira, A. N.; Warhurst, D. C.; Robinson, B. L.; Peters, W. The Effect of Combinations of Qinghaosu (Artemisinin) with Standard Antimalarial Drugs in the Suppressive Treatment of Malaria in Mice. *Transactions of The Royal Society of Tropical Medicine and Hygiene* **1987**, *81* (4), 554–558. https://doi.org/10.1016/0035-9203(87)90404-4.

(275)

Uwimana, A.; Legrand, E.; Stokes, B. H.; Ndikumana, J.-L. M.; Warsame, M.; Umulisa, N.; Ngamije, D.; Munyaneza, T.; Mazarati, J.-B.; Munguti, K.; Campagne, P.; Criscuolo, A.; Ariey,

F.; Murindahabi, M.; Ringwald, P.; Fidock, D. A.; Mbituyumuremyi, A.; Menard, D. Emergence and Clonal Expansion of in Vitro Artemisinin-Resistant Plasmodium Falciparum Kelch13 R561H Mutant Parasites in Rwanda. *Nature Medicine* **2020**, *26* (10), 1602–1608. https://doi.org/10.1038/s41591-020-1005-2.

(276)

Asua, V.; Conrad, M. D.; Aydemir, O.; Duvalsaint, M.; Legac, J.; Duarte, E.; Tumwebaze, P.; Chin, D. M.; Cooper, R. A.; Yeka, A.; Kamya, M. R.; Dorsey, G.; Nsobya, S. L.; Bailey, J.; Rosenthal, P. J. Changing Prevalence of Potential Mediators of Aminoquinoline, Antifolate, and Artemisinin Resistance Across Uganda. *The Journal of Infectious Diseases* **2021**, *223* (6), 985–994. https://doi.org/10.1093/infdis/jiaa687.

(277)

WHO. *World Malaria Report 2020*; World Health Organization: Geneva, 2020.

(278)

O'Neill, P. M.; Bray, P. G.; Hawley, S. R.; Ward, S. A.; Park, B. K. 4-Aminoquinolines–past, Present, and Future: A Chemical Perspective. *Pharmacology & Therapeutics* **1998**, *77* (1), 29–58. https://doi.org/10.1016/s0163-7258(97)00084-3.

(279)

Pou, S.; Winter, R. W.; Nilsen, A.; Kelly, J. X.; Li, Y.; Doggett, J. S.; Riscoe, E. W.; Wegmann, K. W.; Hinrichs, D. J.; Riscoe, M. K. Sontochin as a Guide to the Development of Drugs Against Chloroquine-Resistant Malaria. *Antimicrobial Agents and Chemotherapy* **2012**, *56* (7), 3475–3480. https://doi.org/10.1128/AAC.00100-12.

(280)

Liebman, K. *New 4-Aminoquinoline Compounds to Reverse Drug Resistance in P. Falciparum Malaria, and a Survey of Early European Antimalarial Treatments*; 2000. https://doi.org/10.15760/etd.2112.

(281)

Lee, S.; Jørgensen, M.; Hartwig, J. F. Palladium-Catalyzed Synthesis of Arylamines from Aryl Halides and Lithium Bis(trimethylsilyl)amide as an Ammonia Equivalent. *Organic Letters* **2001**, *3* (17), 2729–2732. https://doi.org/10.1021/ol016333y.

(282)

Smilkstein, M.; Sriwilaijaroen, N.; Kelly, J. X.; Wilairat, P.; Riscoe, M. Simple and Inexpensive Fluorescence-Based Technique for High-Throughput Antimalarial Drug Screening. *Antimicrobial Agents and Chemotherapy* **2004**, *48* (5), 1803–1806. https://doi.org/10.1128/AAC.48.5.1803-1806.2004.

(283)

Bennett, T. N.; Paguio, M.; Gligorijevic, B.; Seudieu, C.; Kosar, A. D.; Davidson, E.; Roepe, P. D. Novel, Rapid, and Inexpensive Cell-Based Quantification of Antimalarial Drug Efficacy. *Antimicrobial Agents and Chemotherapy* **2004**, *48* (5), 1807–1810. https://doi.org/10.1128/AAC.48.5.1807-1810.2004.

(284)

Baniecki, M. L.; Wirth, D. F.; Clardy, J. High-Throughput Plasmodium Falciparum Growth Assay for Malaria Drug Discovery. *Antimicrobial Agents and Chemotherapy* **2007**, *51* (2), 716–723. https://doi.org/10.1128/aac.01144-06.

(285)

Sun, W.; Tanaka, T. Q.; Magle, C. T.; Huang, W.; Southall, N.; Huang, R.; Dehdashti, S. J.; McKew, J. C.; Williamson, K. C.; Zheng, W. Chemical Signatures and New Drug Targets for Gametocytocidal Drug Development. *Scientific Reports* **2014**, *4* (1), 3743. https://doi.org/10.1038/srep03743.

(286)

Rossi, N. R. D. L. P.; Fialho, S. N.; Gouveia, A. de J.; Ferreira, A. S.; da Silva, M. A.; Martinez, L. D. N.; Paula do Nascimento, W. da S.; Gonzaga Jr, A.; de Medeiros, D. S. S.; de Barros, N. B.; de Cássia Alves, R.; Gonçalves, G. M.; Teles, C. G. B. Quinine and Chloroquine: Potential Preclinical Candidates for the Treatment of Tegumentary *Leishmania*sis. *Acta Tropica* **2024**, *252*, 107143. https://doi.org/10.1016/j.actatropica.2024.107143.

(287)

Ravindar, L.; Hasbullah, S. A.; Rakesh, K. P.; Hassan, N. I. Recent Developments in Antimalarial Activities of 4-Aminoquinoline Derivatives. *European Journal of Medicinal Chemistry* **2023**, *256*, 115458. https://doi.org/10.1016/j.ejmech.2023.115458.

(288)

Ager, A. L. Rodent Malaria Models. In *Antimalarial Drugs I: Biological Background, Experimental Methods, and Drug Resistance*; Peters, W., Richards, W. H. G., Eds.; Handbook of Experimental Pharmacology; Springer: Berlin, Heidelberg, 1984; pp 225–264. https://doi.org/10.1007/978-3-662-35326-4_8.

(289)

Teague, S. J.; Davis, A. M.; Leeson, P. D.; Oprea, T. The Design of Leadlike Combinatorial Libraries. *Angewandte Chemie International Edition* **1999**, *38* (24), 3743–3748. https://doi.org/10.1002/(SICI)1521-3773(19991216)38:24%3C3743::AID-ANIE3743%3E3.0.CO;2-U.

(290)

Hann, M. M.; Oprea, T. I. Pursuing the Leadlikeness Concept in Pharmaceutical Research. *Current Opinion in Chemical Biology* **2004**, *8* (3), 255–263. https://doi.org/10.1016/j.cbpa.2004.04.003.

(291)

Handford, M. J.; Li, Y.; Riscoe, T.; Zhang, X.; Kelly, J. X.; Riscoe, M. K. Designing Novel Bisquinoline Antimalarials from Historical 4-Aminoquinolines to Combat Drug-Resistant Malaria. *Antimicrobial Agents and Chemotherapy* **2026**, e0130025. https://doi.org/10.1128/aac.01300-25.

(292)

Istvan, E. S.; Dharia, N. V.; Bopp, S. E.; Gluzman, I.; Winzeler, E. A.; Goldberg, D. E. Validation of Isoleucine Utilization Targets in Plasmodium Falciparum. *Proceedings of the National Academy of Sciences of the United States of America* **2011**, *108* (4), 1627–1632. https://doi.org/10.1073/pnas.1011560108.

(293)

Chugh, M.; Sundararaman, V.; Kumar, S.; Reddy, V. S.; Siddiqui, W. A.; Stuart, K. D.; Malhotra, P. Protein Complex Directs Hemoglobin-to-Hemozoin Formation in Plasmodium Falciparum. *Proceedings of the National Academy of Sciences* **2013**, *110* (14), 5392–5397. https://doi.org/10.1073/pnas.1218412110.

(294)

Sigala, P. A.; Goldberg, D. E. The Peculiarities and Paradoxes of Plasmodium Heme Metabolism. *Annual Review of Microbiology* **2014**, *68*, 259–278. https://doi.org/10.1146/annurev-micro-091313-103537.

(295)

Mungthin, M.; Bray, P. G.; Ridley, R. G.; Ward, S. A. Central Role of Hemoglobin Degradation in Mechanisms of Action of 4-Aminoquinolines, Quinoline Methanols, and Phenanthrene Methanols. *Antimicrobial Agents and Chemotherapy* **1998**, *42* (11), 2973–2977.

(296)

Bray, P. G.; Janneh, O.; Raynes, K. J.; Mungthin, M.; Ginsburg, H.; Ward, S. A. Cellular Uptake of Chloroquine Is Dependent on Binding to Ferriprotoporphyrin IX and Is Independent of NHE Activity in Plasmodium Falciparum. *Journal of Cell Biology* **1999**, *145* (2), 363–376. https://doi.org/10.1083/jcb.145.2.363.

(297)

Benazet, F. Resistance of Plasmodium berghei to chloroquine and 4-aminoquinolines. *Annales des Sociétés belges de Médecine tropicale* **1965**, *45* (4), 455–458.

(298)

Margolis, B. J.; Long, K. A.; Laird, D. L. T.; Ruble, J. C.; Pulley, S. R. Assembly of 4-Aminoquinolines via Palladium Catalysis: A Mild and Convenient Alternative to S_N Ar Methodology. *The Journal of Organic Chemistry* **2007**, *72* (6), 2232–2235. https://doi.org/10.1021/jo062168u.

(299)

Birrell, G. W.; Chavchich, M.; Ager, A. L.; Shieh, H.-M.; Heffernan, G. D.; Zhao, W.; Krasucki, P. E.; Saionz, K. W.; Terpinski, J.; Schiehser, G. A.; Jacobus, L. R.; Shanks, G. D.; Jacobus, D. P.; Edstein, M. D. JPC-2997, a New Aminomethylphenol with High in Vitro and in Vivo Antimalarial Activities Against Blood Stages of Plasmodium. *Antimicrobial Agents and Chemotherapy* **2015**, *59* (1), 170–177. https://doi.org/10.1128/AAC.03762-14.

(300)

Obach, R. S. Prediction of Human Clearance of Twenty-Nine Drugs from Hepatic Microsomal Intrinsic Clearance Data: An Examination of In Vitro Half-Life Approach and Nonspecific Binding to Microsomes. *Drug Metabolism and Disposition* **1999**, *27* (11), 1350–1359. https://doi.org/10.1016/S0090-9556(24)14938-0.

(301)

Nilsen, A.; LaCrue, A. N.; White, K. L.; Forquer, I. P.; Cross, R. M.; Marfurt, J.; Mather, M. W.; Delves, M. J.; Shackleford, D. M.; Saenz, F. E.; Morrisey, J. M.; Steuten, J.; Mutka, T.; Li, Y.; Wirjanata, G.; Ryan, E.; Duffy, S.; Kelly, J. X.; Sebayang, B. F.; Zeeman, A.-M.; Noviyanti, R.; Sinden, R. E.; Kocken, C. H. M.; Price, R. N.; Avery, V. M.; Angulo-Barturen, I.; Jiménez-Díaz, M. B.; Ferrer, S.; Herreros, E.; Sanz, L. M.; Gamo, F.-J.; Bathurst, I.; Burrows, J. N.; Siegl, P.; Guy, R. K.; Winter, R. W.; Vaidya, A. B.; Charman, S. A.; Kyle, D. E.; Manetsch, R.; Riscoe, M. K. Quinolone-3-Diarylethers: A New Class of Drugs for a New Era of Malaria Eradication. *Science translational medicine* **2013**, *5* (177), 177ra37. https://doi.org/10.1126/scitranslmed.3005029.

(302)

Smilkstein, M. J.; Pou, S.; Krollenbrock, A.; Bleyle, L. A.; Dodean, R. A.; Frueh, L.; Hinrichs, D. J.; Li, Y.; Martinson, T.; Munar, M. Y.; Winter, R. W.; Bruzual, I.; Whiteside, S.; Nilsen, A.; Koop, D. R.; Kelly, J. X.; Kappe, S. H. I.; Wilder, B. K.; Riscoe, M. K. ELQ-331 as a Prototype for Extremely Durable Chemoprotection Against Malaria. *Malaria Journal* **2019**, *18* (1), 291. https://doi.org/10.1186/s12936-019-2921-9.

(303)

Zhi-Jun, Y.; Sriranganathan, N.; Vaught, T.; Arastu, S. K.; Ansar Ahmed, S. A Dye-Based Lymphocyte Proliferation Assay That Permits Multiple Immunological Analyses: mRNA, Cytogenetic, Apoptosis, and Immunophenotyping Studies. *Journal of Immunological Methods* **1997**, *210* (1), 25–39. https://doi.org/10.1016/S0022-1759(97)00171-3.

(304)

Coatney, G. R. *The Primate Malarias*; U.S. National Institute of Allergy and Infectious Diseases, 1971.

(305)

Huff, C. G. Studies on the Evolution of Some Disease-Producing Organism. *The Quarterly Review of Biology* **1938**, *13*, 196–206.

(306)

Huff, C. G. A Consideration of the Problem of Evolution of Malaria Parasites. *Revista Del Instituto De Salubridad Y Enfermedades Tropicales* **1945**, *6* (4), 253–258.

(307)

Christophers, R. Malaria from a Zoological Point of View. *Proceedings of the Royal Society of Medicine* **1934**, *27* (8), 991–1000.

(308)

Bruce-Chwatt, L. J. Paleogenesis and Paleo-Epidemiology of Primate Malaria. *Bulletin of the World Health Organization* **1965**, *32* (3), 363–387.

(309)

Ball, G. H. Some Considerations Regarding the Sporozoa. *The Journal of Protozoology* **1960**, *7* (1), 1–6. https://doi.org/10.1111/j.1550-7408.1960.tb00699.x.

(310)

Manwell, R. D. Some Evolutionary Possibilites in the History of the Malraia Parasites. *Indian Journal of Malariology* **1955**, *9* (4), 247–253.

(311)

Bray, R. S. *Studies on the Exo-Erythrocyctic Cycle of the Genus Plasmodium.*; London School of Hygiene and Tropical Medicine Memoir; Robert Maclamore and Co. Ltd., 1957.

(312)

Bray, R. S. The Exoerythrocytic Phase of Malaria Parasites. *International Review of Tropical Medicine* **1963**, *2*, 41–74.

(313)

Garnham, P. C. C. Classification and Evolution. In *Malaria parasites and other haemosoridia*; Blackwell Scientific Publications, 1966; pp 60–84.

(314)

Cockburn, T. A. The Evolution and Eradication of Infectious Diseases. *John Hopkins University Press* **1964**, *7* (4), 498–499. https://doi.org/10.1353/pbm.1964.0020.

(315)

Ricklefs, Robert. E.; Outlaw, D. C. A Molecular Clock for Malaria Parasites Science. *Science* **2010**, *329* (5988), 226–229. https://doi.org/10.1126/science.1188954.

(316)

Silva, J. C.; Egan, A.; Arze, C.; Spouge, J. L.; Harris, D. G. A New Method for Estimating Species Age Supports the Coexistence of Malaria Parasites and Their Mammalian Hosts.

Molecular Biology and Evolution **2015**, *32* (5), 1354–1364. https://doi.org/10.1093/molbev/msv005.

(317)

Liu, W.; Li, Y.; Learn, G. H.; Rudicell, R. S.; Robertson, J. D.; Keele, B. F.; Ndjango, J.-B. N.; Sanz, C. M.; Morgan, D. B.; Locatelli, S.; Gonder, M. K.; Kranzusch, P. J.; Walsh, P. D.; Delaporte, E.; Mpoudi-Ngole, E.; Georgiev, A. V.; Muller, M. N.; Shaw, G. M.; Peeters, M.; Sharp, P. M.; Rayner, J. C.; Hahn, B. H. Origin of the Human Malaria Parasite Plasmodium Falciparum in Gorillas. *Nature* **2010**, *467* (7314), 420–425. https://doi.org/10.1038/nature09442.

(318)

Pacheco, M. A.; Battistuzzi, F. U.; Junge, R. E.; Cornejo, O. E.; Williams, C. V.; Landau, I.; Rabetafika, L.; Snounou, G.; Jones-Engel, L.; Escalante, A. Timing the Origin of Human Malarias: The Lemur Puzzle BMC. *BMC Evolutionary Biology* **2011**, *11* (299). https://doi.org/10.1186/1471-2148-11-299.

(319)

Pacheco, M. A.; Reid, M. J. C.; Schillaci, M. A.; Lowenberger, C. A.; Galdikas, B. M. F.; Jones-Engel, L.; Escalante, A. A. The Origin of Malarial Parasites in Orangutans. *PLOS ONE* **2012**, *7* (4), e34990. https://doi.org/10.1371/journal.pone.0034990.

(320)

Faust, C.; Dobson, A. P. Primate Malarias: Diversity, Distribution and Insights for Zoonotic *Plasmodium*. *One Health* **2015**, *1*, 66–75. https://doi.org/10.1016/j.onehlt.2015.10.001.

(321)

Escalante, A. A.; Cornejo, O. E.; Freeland, D. E.; Poe, A. C.; Durrego, E.; Collins, W. E.; Lal, A. A. A Monkey's Tale: The Origin of Plasmodium Vivax as a Human Malaria Parasite. *Proceedings of the National Academy of Sciences of the United States of America* **2005**, *102* (6), 1980–1985. https://doi.org/10.1073/pnas.0409652102.

(322)

Escalante, A. A.; Freeland, D. E.; Collins, W. E.; Lal, A. A. The Evolution of Primate Malaria Parasites Based on the Gene Encoding Cytochrome b from the Linear Mitochondrial Genome. *Proceedings of the National Academy of Sciences of the United States of America* **1998**, *95* (14), 8124–8129.

(323)

Perkins, S. L.; Schall, J. A Molecular Phylogeny of Malarial Parasites Recovered from Cytochrome b Gene Sequences. *Journal of Parasitology* **2002**, *88* (5), 972–978. https://doi.org/10.1645/0022-3395(2002)088%5B0972:AMPOMP%5D2.0.CO;2.

(324)

Hayakawa, T.; Culleton, R.; Otani, H.; Horii, T.; Tanabe, K. Big Bang in the Evolution of Extant Malaria Parasites. *Molecular Biology and Evolution* **2008**, *25* (10), 2233–2239. https://doi.org/10.1093/molbev/msn171.

(325)

Escalante, A. A.; Ayala, F. J. Phylogeny of the Malarial Genus Plasmodium, Derived from rRNA Gene Sequences. *Proceedings of the National Academy of Sciences* **1994**, *91* (24), 11373–11377. https://doi.org/10.1073/pnas.91.24.11373.

(326)

Ollomo, B.; Durand, P.; Prugnolle, F.; Douzery, E.; Arnathau, C.; Nkoghe, D.; Leroy, E.; Renaud, F. A New Malaria Agent in African Hominids. *PLoS Pathogens* **2009**, *5* (5), e1000446. https://doi.org/10.1371/journal.ppat.1000446.

(327)

Rich, S. M.; Leendertz, F. H.; Xu, G.; LeBreton, M.; Djoko, C. F.; Aminake, M. N.; Takang, E. E.; Diffo, J. L. D.; Pike, B. L.; Rosenthal, B. M.; Formenty, P.; Boesch, C.; Ayala, F. J.; Wolfe, N. D. The Origin of Malignant Malaria. *Proceedings of the National Academy of Sciences of the United States of America* **2009**, *106* (35), 14902–14907. https://doi.org/10.1073/pnas.0907740106.

(328)

Krief, S.; Escalante, A. A.; Pacheco, M. A.; Mugisha, L.; André, C.; Halbwax, M.; Fischer, A.; Krief, J.-M.; Kasenene, J. M.; Crandfield, M.; Cornejo, O. E.; Chavatte, J.-M.; Lin, C.; Letourneur, F.; Grüner, A. C.; McCutchan, T. F.; Rénia, L.; Snounou, G. On the Diversity of Malaria Parasites in African Apes and the Origin of Plasmodium Falciparum from Bonobos. *PLoS Pathogens* **2010**, *6* (2), e1000765. https://doi.org/10.1371/journal.ppat.1000765.

(329)

Prugnolle, F.; Durand, P.; Neel, C.; Ollomo, B.; Ayala, F. J.; Arnathau, C.; Etienne, L.; Mpoudi-Ngole, E.; Nkoghe, D.; Leroy, E.; Delaporte, E.; Peeters, M.; Renaud, F. African Great Apes Are Natural Hosts of Multiple Related Malaria Species, Including Plasmodium Falciparum. *Proceedings of the National Academy of Sciences of the United States of America* **2010**, *107* (4), 1458–1463. https://doi.org/10.1073/pnas.0914440107.

(330)

Waters, A. P.; Higgins, D. G.; McCutchan, T. F. Plasmodium Falciparum Appears to Have Arisen as a Result of Lateral Transfer Between Avian and Human Hosts. *Proceedings of the National Academy of Sciences of the United States of America* **1991**, *88*, 3140–3144. https://doi.org/10.1073/pnas.88.8.3140.

(331)

Waters, A. P.; Higgins, D. G.; McCutchan, T. F. Evolutionary Relatedness of Some Primate Models of Plasmodium. *Molecular Biology and Evolution* **1993**, *10* (4), 914–923. https://doi.org/10.1093/oxfordjournals.molbev.a040038.

(332)

Livingstone, F. Anthropological Implications of Sickle Cell Gene Distribution in West Africa. *American Anthropologist* **1958**, *60* (3), 533–562.

(333)

Jeffares, D. C.; Pain, A.; Berry, A.; Cox, A. V.; Stalker, J.; Ingle, C. E.; Thomas, A.; Quail, M. A.; Siebenthall, K.; Uhlemann, A.-C.; Kyes, S.; Krishna, S.; Newbold, C.; Dermitzakis, E. T.; Berriman, M. Genome Variation and Evolution of the Malaria Parasite Plasmodium Falciparum. *Nature Genetics* **2007**, *39* (1), 120–125. https://doi.org/10.1038/ng1931.

(334)

Su, X.-Z.; Mu, J.; Joy, D. A. The "Malaria's Eve" Hypothesis and the Debate Concerning the Origin of the Human Malaria Parasite *Plasmodium Falciparum*. *Microbes and Infection* **2003**, *5* (10), 891–896. https://doi.org/10.1016/S1286-4579(03)00173-4.

(335)

Rich, S. M.; Licht, M. C.; Hudson, R. R.; Ayala, F. J. Malaria's Eve: Evidence of a Recent Population Bottleneck Throughout the World Populations of *Plasmodium Falciparum*. *Proceedings of the National Academy of Sciences* **1998**, *95* (8), 4425–4430. https://doi.org/10.1073/pnas.95.8.4425.

(336)

Coluzzi, M. The Clay Feet of the Malaria Giant and Its African Roots: Hypotheses and Inferences about Origin, Spread and Control of Plasmodium Falciparum. *Parassitologia* **1999**, *41* (1-3), 277–283.

(337)

Okombo, J.; Mok, S.; Qahash, T.; Yeo, T.; Bath, J.; Orchard, L. M.; Owens, E.; Koo, I.; Albert, I.; Llinás, M.; Fidock, D. A. Piperaquine-Resistant PfCRT Mutations Differentially Impact Drug Transport, Hemoglobin Catabolism and Parasite Physiology in Plasmodium Falciparum Asexual Blood Stages. *PLoS pathogens* **2022**, *18* (10), e1010926. https://doi.org/10.1371/journal.ppat.1010926.

(338)

Ross, L. S.; Dhingra, S. K.; Mok, S.; Yeo, T.; Wicht, K. J.; Kümpornsin, K.; Takala-Harrison, S.; Witkowski, B.; Fairhurst, R. M.; Ariey, F.; Menard, D.; Fidock, D. A. Emerging Southeast Asian PfCRT Mutations Confer Plasmodium Falciparum Resistance to the First-Line Antimalarial Piperaquine. *Nature Communications* **2018**, *9* (1), 3314. https://doi.org/10.1038/s41467-018-05652-0.

(339)

Dhingra, S. K.; Small-Saunders, J. L.; Ménard, D.; Fidock, D. A. Plasmodium Falciparum Resistance to Piperaquine Driven by PfCRT. *The Lancet. Infectious diseases* **2019**, *19* (11), 1168–1169. https://doi.org/10.1016/S1473-3099(19)30543-2.

(340)

Hagenah, L. M.; Dhingra, S. K.; Small-Saunders, J. L.; Qahash, T.; Willems, A.; Schindler, K. A.; Rangel, G. W.; Gil-Iturbe, E.; Kim, J.; Akhundova, E.; Yeo, T.; Okombo, J.; Mancia, F.; Quick, M.; Roepe, P. D.; Llinás, M.; Fidock, D. A. Additional PfCRT Mutations Driven by Selective Pressure for Improved Fitness Can Result in the Loss of Piperaquine Resistance and Altered Plasmodium Falciparum Physiology. *mBio* **2024**, *15* (1), e0183223. https://doi.org/10.1128/mbio.01832-23.

Glossary

Definitions of key terms and acronyms used in this dissertation.

acetonitrile

area under the curve from last time point

A historical medical term for malaria or a similar illness, characterized by violent, paroxysmal fits of shivering, alternating with high fever and sweating.

A naturally occurring organic compound containing nitrogen, typically basic in nature, derived from plants, and possessing potent physiological effects on humans.

A large phylum of parasitic alveolates possessing a unique, specialized structure called an apical complex, which is utilized to attach to and penetrate host cells.

The quality, state, or characteristic of a microorganism that renders it completely incapable of causing disease or harm inside a host organism.

An expansive phylum of invertebrate animals characterized by an exoskeleton, segmented bodies, and jointed appendages, frequently serving as vectors that transmit parasites between vertebrate hosts.

tert-butyloxycarbonyl

intrinsic clearance

A genus of evergreen shrubs and trees native to the Andes, renowned for producing bark rich in quinine, which historically served as the primary therapeutic treatment for malaria.

A subclass of microscopic, spore-forming, obligate intracellular parasites belonging to the phylum Apicomplexa that primarily infect the epithelial lining of animal intestinal tracts.

Porosities in the orbital roof of crania.

dichloromethane

N,N-diisopropylethylamine

dimethylformamide

dimethyl sulfoxide

An order of insects commonly known as true flies, characterized by possessing a single pair of flight wings and a pair of sensory halteres, serving as primary biological vectors for various apicomplexan parasites.

A profound state of unease, dissatisfaction, anxiety, or general unhappiness, serving as the emotional polar opposite of euphoria.

gas chromatography-mass spectroscopy

Possessing the specific capacity to destroy gametocytes, the sexual stages of malarial parasites present in the bloodstream, thereby preventing transmission from the vertebrate host to the insect vector.

The sexual phase of an apicomplexan life cycle where merozoites differentiate into male and female germ cells, known as microgametocytes and macrogametocytes.

hydrochloric acid

high performance liquid chromatography

High resolution accurate mass mass spectroscopy

An abnormal condition where an excess of free hemoglobin is excreted in the urine, often turning it dark or black following severe intravascular hemolysis.

The premature rupture, destruction, or lysis of red blood cells, resulting in the release of hemoglobin into the surrounding blood plasma.

dipotassium ethylenediaminetetraacetic acid

lower limit of quantification

The movement or exchange of genetic material between distinct, non-parental organisms rather than through vertical transmission from parent to offspring.

multidrug-resistant

mean residence time extrapolated to infinity

methanol

not determined

N-Methyl-2-pyrrolidone

nuclear magnetic resonance

non-recrudescence dose

polyethylene glycol - 400

Plasmodium falciparum

Plasmodium falciparum D6 strain.

Plasmodium falciparum Dd2 strain.

A genus of unicellular, obligate intracellular protozoan parasites that replicate within vertebrate and mosquito hosts, famously known as the causative agents of malaria.

A genus of unicellular, obligate intracellular protozoan parasites that replicate within vertebrate and mosquito hosts, famously known as the causative agents of malaria.

Plasmodium yoelii

Plasmodium falciparum chloroquine resistant transport

pharmacokinetic

per os (by mouth)

The specific three-dimensional arrangement of atoms or chemical features within a molecule that is directly responsible for its biological and pharmacological activity.

perforations on the surface of cranial bones.

Historical categorization of persistent fever, largely though to be caused by malaria, that increased in severity every 4rd day.

room temperature

structure activity relationship

standard deviation

A form of asexual reproduction consisting of multiple fission, during which the nucleus divides several times before the cytoplasm splits to produce multiple daughter cells called merozoites.

Relating to or acting against the schizont stage of a parasite, particularly referring to antimalarial drugs that target asexual parasites in blood or tissue.

The final, spore-forming reproductive phase of the parasite lifecycle that occurs externally or within an invertebrate vector, involving asexual division of a zygote to yield infectious sporozoites.

tetrahydrofuran

tetramethylsilane

Historical categorization of persistent fever, largely though to be caused by malaria, that increased in severity every 3rd day.

A historical surgical intervention involving the drilling or scraping of a hole into the human skull to treat intracranial diseases or release evil spirits.

intrinsic metabolic stability

time to peak drug concentration

ultra performance liquid chromatography

apparent volume of distribution at steady state

Part IV. Experimental Methods

9. Chemistry Methods

9.1. Materials and Methods of Chapter 6

9.1.1. Materials

All solvents, starting materials, and reagents were acquired from commercial sources, including (but not limited to): Fisher Scientific, TCI Chemicals, Combi Blocks, Enamine, Sigma Aldrich. Reaction progress was monitored by TLC, GCMS, or HPLC when permitted. Microware reactions were performed with a Biotage Initiator+. Both reverse phase and normal phase flash chromatography was performed using Biotage Isolera and columns including Sfär Silica, Sfär Silica HC, Sfär Silica-Duo, Sfär Silica-KP Amino, and Sfär C18-Duo. ^{1}H NMR spectra were taken on a Bruker 400 MHz instrument, and chemical shifts are reported relative to TMS (0.0 ppm) and NMR Solvent ($CDCl_3$, DMSO-d_6, or CD_3OD). Final compounds were measured to be >95% pure by high performance liquid chromatography (HPLC) using an Agilent Technologies 1260 Infinity II system (unless otherwise noted). High-resolution mass spectrometry (HRMS) using electrospray ionization was performed by the Portland State University BioAnalytical Mass Spectrometry Facility and by Oregon Health & Science University's Bioanalytical Shared Resource/Pharmacokinetics (BSR/PK) Core Facility for additional structure verification.

9.1.2. General Synthetic Methods

General Procedure (i)**:** To a round bottom flask a mixture of aniline (1.1 equiv.) and 4-chloroquinoline (1 equiv.) was dissolved in ethanol (0.1 M) and catalytic fuming HCl (0.05 equiv.) added. The resulting mixture was refluxed for 16 h, where upon the resulting 4-anilinoquinoline precipitates as an HCl salt. The reaction mixture was condensed *in vacuo* and the resulting 4-anilinoquinoline was resuspended in methylene chloride and aqueous 2 M sodium hydroxide. The resulting organic layer was extracted with water, brine, dried with magnesium sulfate, concentrated in vacuo, and purified by flash chromatography.

General Procedure (ii)*:* To a Carius tube a mixture of aniline (3 equiv.), 4-chloroquinoline (1 equiv.), and phenol (0.05 equiv.) was dissolved in 2-ethoxyethanol (0.1 M). The resulting mixture was heated to 150 °C for 12 hours. The reaction mixture was condensed *in vacuo* and was resuspended in methylene chloride and aqueous 2 M sodium hydroxide. The resulting organic layer was extracted with water, brine, dried with magnesium sulfate, concentrated in vacuo, and purified by flash chromatography.

General Procedure (iii): To a round bottom flask equipped with a stir bar para substituted bromobenzene (1 equiv.) was dissolved in DMF followed by the addition of 2M potassium

carbonate (2 equiv.) and bromobenzene (1.1 equiv.). The flask was fixed with a septa and stirred at 50 °C for 12 h. Reaction mixture was diluted with water and extracted with ethyl acetate. Organic layers were combined, treated with aqueous 2M sodium hydroxide, and washed with water and a saturated sodium chloride solution. Organic layer was separated, dried with magnesium sulfate, and gravity filtered. Filtrate was condensed in vacuo and purified by flash chromatography.

General Procedure (iv): To a round bottom flask equipped with a stir bar para substituted bromobenzene (1 equiv.) was dissolved in DMF (0.5 M) followed by the addition of iodoethane (1.1 equiv.) and N,N-diisopropylethylamine. The flask was fixed with a septa and stirred at room temperature for 48 h. Reaction mixture was diluted with water and extracted with ethyl acetate. Organic layers were combined and washed with 2M sodium hydroxide, water, and saturated sodium chloride solution. The organic layer was dried with magnesium sulfate and gravity filtered. Filtrate was condensed in vacuo and purified by flash chromatography.

General Procedure (v): To a dry round bottom flask equipped with a stir bar under inert conditions toluene (0.4 M) was added and degassed with argon for 10 m. bis(tri-tert-butylphosphine)palladium(0) (2.5% molar equiv.) and bis(dibenzylideneacetone)palladium(0) (2.5% molar equiv.) was added to the flask and stirred for 5 m. The substituted aryl halide (1 equiv.) was added, and the reaction vessel was capped with reflux condenser and septa and placed under inert atmosphere. 1M lithium bis(trimethylsilyl)amide in toluene (1.5 equiv.) was added under inert conditions and the reaction was heated to 70 °C for 18 h. Upon consumption of substituted aryl halide, the crude reaction mixture was diluted in ethyl acetate and the newly formed silylamide was deprotected with 1 drop of 1 M hydrochloric acid. The mixture was washed with 2 M sodium hydroxide, water, and brine, and dried with magnesium sulfate. The dried organic layer was filtered and condensed in vacuo and purified by flash chromatography.

General Procedure (vi): To a microwave reactor flask a mixture of aniline (1 equiv.), 4-chloroquinoline (1.2 equiv.) and phenol (2.0 equiv.) were dissolved in DMF (1.0 M). The flask was sealed and heated to 150 °C for 2 h on high adsorption. The reaction mixture was condensed in vacuo and resuspended in methylene chloride and aqueous 2 M sodium hydroxide. The organic layer was extracted with water, brine, dried with magnesium sulfate, concentrated in vacuo, and purified via flash chromatography to afford desired 4-anilinoquinoline.

General Procedure (vii): To a round bottom flask equipped with magnetic stir bar was charged with 4-fluoronitrobenzene (1 equiv.), substituted piperazine (1.1 equiv.). Solids were dissolved in dimethyl sulfoxide (1.0 M) and trimethylamine (3.5 equiv.) was added the reaction vessel was heated at 120 °C for 16 hours. The resulting mixture was allowed to cool to room temperature and filtered over vacuum filtration using minimal amounts of DMSO to transfer. Resulting solid was recrystallized using ethanol and ethyl acetate, filtered over vacuum filtration, and then air dried.

General Procedure (viii): A mixture of piperazine substituted nitrobenzene (1.0 equiv.) and wet palladium on carbon (0.1 equiv.) were dissolved in methanol (0.025 M) in a shaker flask. Shaker flask sparged with hydrogen at 45 psi and shaken for 12 hours in Parr Hydrogenator. Pd/C filtered over celite with excess methanol and resulting filtrate condensed in vacuo. Solid resuspended in ethyl acetate and basified with 2 M sodium hydroxide. The organic layer was washed with water and saturated sodium chloride solution and dried with magnesium sulfate.

The mixture was condensed in vacuo and purified via flash chromatography to afford piperazine substituted aniline.

General Procedure (ix): To a microwave reactor flask a mixture of aniline (1 equiv.) and 4-chloroquinoline (1.2 equiv.) were dissolved in THF (1.0 M). The flask was sealed and heated to 120 °C for 20 min on high adsorption. The reaction mixture was condensed in vacuo and resuspended in methylene chloride and aqueous 2 M sodium hydroxide. The resulting organic layer was extracted with water, brine, dried with magnesium sulfate, concentrated in vacuo, and purified via flash chromatography to afford desired 4-anilinoquinoline.

General Procedure (x): Boc-protected 4-anilinoquinoline (1 equiv.) dissolved in methylene chloride (1.0 M) and trifluoroacetic acid added (20 equiv.), reaction stirred at room temperature for 2 hours. Reaction mixture diluted in methylene chloride and aqueous 2 M sodium hydroxide. Resulting precipitate filtered over vacuum filtration and washed with additional methylene chloride and water. Solid air dried to yield desired 4-anilinoquinoline, no further purification needed.

General Procedure (xi): A solution of 4-anilinoquinoline (1.0 equiv.), iodoethane (1.1 equiv.), and N,N-diisopropylethylamine (2.0 equiv.) in dimethylformamide (0.2 M) was stirred at room temperature for 16 h. Upon completion, reaction mixture was poured over ice and resulting solid separated by vacuum filtration. Solid was dissolved in methylene chloride, dried with magnesium sulfate, condensed in vacuo, and purified using flash chromatography to afford alkylated 4-anilinoquinoline.

General Procedure (xii): A stirred solution of 4-anilinoquinoline (1.0 equiv.), alkyl halide (1.2 equiv.), and potassium carbonate (5.0 equiv.) in dimethylformamide (0.2 M) was heated to 85 °C for 16 h. Upon completion, reaction mixture condensed in vacuo. Resulting solid dissolved in methylene chloride and filtered using vacuum filtration. Filtrate extracted with 2 M sodium hydroxide and brine, condensed in vacuo, dry loaded onto celite and purified via flash chromatography. Fractions containing desired product were condensed in vacuo, and resulting solid upon the addition of aqueous 2 M sodium hydroxide was filtered via vacuum filtration and dried in a vacuum oven to afford alkylated 4-anilinoquinoline.

9.2. Materials and Methods of Chapter 7

Materials and Instruments. All solvents, starting materials, and reagents were acquired from commercial sources, including (but not limited to): Fisher Scientific, TCI Chemicals, Combi Blocks, Enamine, Sigma Aldrich. Reaction progress was monitored by TLC, GCMS, or HPLC when permitted. Both reverse phase and normal phase flash chromatography was performed using a Biotage Isolera with the following column types: Sfär Silica HC and Sfär C18-Duo. ^{1}H NMR spectra were acquired on a Bruker 400 MHz instrument, and chemical shifts are reported relative to TMS (0.0 ppm) or NMR Solvent ($CDCl_3$, DMSO-d_6, or CD_3OD). Final compounds are reported as > 95% pure determined via NMR as many compounds produced did not exhibit necessary solubility in HPLC mobile phase solvents. High-resolution accurate mass mass spectrometry (HRAM/MS) using electrospray ionization was performed by the Oregon Health & Science University's Bioanalytical Shared Resource/Pharmacokinetics Core for additional structure verification.

General Procedure (i): A microwave reactor flask equipped with a magnetic stir bar was charged with bis-aniline (1 equiv.), 4-bromo-7-chloroquinoline (3 equiv.), phenol (3.0 equiv.), and DMF (1.0 M). The flask was sealed and heated at 150 °C for 2 hours under high absorption. Upon completion, the reaction mixture was transferred to an appropriately sized round-bottom flask and concentrated *in vacuo*. The resulting solids were resuspended in dichloromethane. The organic solution was subjected to an aqueous workup in a separatory funnel. The solution was sequentially treated with 2 M sodium hydroxide (to pH > 10), then washed with water, and finally with saturated sodium chloride. The organic layer was separated, dried over magnesium sulfate, and gravity filtered. The filtrate was concentrated *in vacuo* and purified by automated flash chromatography. Fractions containing the desired bis-quinoline were combined and concentrated *in vacuo*.

General Procedure (ii): A microwave reactor flask equipped with a magnetic stir bar was charged with aniline (1 equiv.), 4-chloroquinoline (1.2 equiv.), and THF (1.0 M). The flask was sealed and heated at 120 °C for 20 minutes under high absorption. Upon completion, the reaction mixture was filtered and washed with excess THF. The resulting solids were resuspended and triturated with methanol. While suspended in methanol the purified solids were treated with 2 M sodium hydroxide (to pH > 10) and stirred for 1.5 hr. The solution was then concentrated *in vacuo* until only water remained. The resulting suspension was separated by vacuum filtration, and the residue washed with water. The remaining solids were dried for 24 hr to afford the desired product and used without further purification.

The title compound was prepared using *General Procedure (iii)*. In short, 0.6493 g (1.61 mmol) of **64c intermediate** were charged to a 100 mL Erlenmeyer flask equipped with a magnetic stir bar and suspended in 30 mL dichloromethane. Slowly 3.0 mL (39.2 mmol, 25 equiv.) trifluoroacetic acid was added drop-wise while stirring using a glass dropper. As TFA was added initial turgid suspension went fully into solution. After 4 h, remaining TFA was neutralized with 50 mL of 2M sodium hydroxide solution and until pH > 10. Resulting white precipitate was filtered, and washed with water (3 x 5 mL), ethyl acetate (3 x 5 mL), and DCM (3 x 10 mL). Solid was dried overnight in vacuum oven.

General procedure (v): A microwave reactor flask equipped with a magnetic stir bar was charged with the appropriate free-amine heterocycle-linked anilinoquinoline (1 equiv.), 4-bromo-7-chloroquinoline (2 equiv.), phenol (2.0 equiv.), and DMF (1.0 M). The flask was sealed and heated at 150 °C for 2 hours under high absorption. Upon completion, the reaction mixture was transferred to an appropriately sized round-bottom flask and concentrated *in vacuo*. The resulting solids were resuspended in dichloromethane. The organic solution was subjected to an aqueous workup in a separatory funnel. The solution was sequentially treated with 2 M sodium hydroxide (to pH > 10), then washed with water, and finally with saturated sodium chloride. The organic layer was separated, dried over magnesium sulfate, and gravity filtered. The filtrate was concentrated *in vacuo* and purified by automated flash chromatography. Fractions containing the desired bis-quinoline were combined and concentrated *in vacuo*.

10. Biological Methods

10.0.1. Plasmodium falciparum Drug Sensitivity:

See Appendix C for complete list.

10.1. Methods used in Chapter 6

10.1.1. Parasite Culture:

P. falciparum parasites were thawed from frozen stock and cultured in suspended human erythrocytes (Lampire Biological Laboratories, Pipersville, PA) not more than 28 days old at 2% hematocrit. The culture medium used: RPMI-1640 supplemented with 25 mM HEPES buffer, 25 mg/L gentamicin sulfate, 45 mg/L hypoxanthine, 10 mM glucose, 2 mM glutamine, and 0.5% Albumax II (complete medium).[29] Cultures were maintained in a standard low oxygen atmosphere (5% O_2, 5% CO_2, 90% N_2) in a Forma Series II 3110 environmental chamber and incubated at 37 °C. Cultures were subpassaged every 3–4 days into a fresh culture flask containing complete media and erythrocytes.

10.1.2. In vitro antiplasmodial activity (IC_{50}) against *P. falciparum*:

Final compounds were assessed for *in vitro* antiplasmodial activity against D6 and Dd2 strains of *P. falciparum* using the previously described fluorescence-based SYBR Green assay.[20] In short, compounds were prepared as 10 mM stocks in DMSO. Compounds were evaluated in quadruplicate in flat-bottomed clear 96-well plates and plated at a 2-fold serial dilution with the final column left untreated to span a range of 0.25-250 nM. Asynchronous *P. falciparum* infected erythrocytes in growth media were added to each well for a total volume of 100 µL, final hematocrit of 2%, and initial parasitemia of 0.2%. Controls included non-infected red blood cells, 10 mM chloroquine and amodiaquine. Plates were incubated in controlled low oxygen atmosphere (5% O_2, 5% CO_2, 90% N_2) at 37 °C. 72 h post inoculation, all wells are simultaneously lysed and dyed using 100 µL of a SYBR Green I dye-detergent solution. Plates were incubated at ambient temperature and atmosphere in the dark for at least 1 h. Fluorescence was read at 497 nm excitation and 520 nm emission bands with a Spectramax iD3 plate reader. Fluorescence values were normalized with respect to the untreated control wells representing normal parasite growth and plotted against the logarithm of drug concentration. An IC_{50} was determined for each compound by fitting this data to a variable slope nonlinear regression curve using Graphpad Prism software (v. 9).

10.1.3. HepG2 Cytotoxicity Assay:

Final compounds were assessed for mammalian cytotoxicity using an immortalized human liver carcinoma cell line (HepG2) using previously described methods.[30] In short, final compounds were prepared in DMSO as 10 mM stock solutions. Human hepatocarcinoma (HepG2) cells were cultured in RPMI-1640 medium containing 10% fetal bovine serum at 37 °C in a humidified 5% CO_2 atmosphere. To 96-well flat-bottomed tissue culture plates, HepG2 cells were added at 2 x 10^4 density with an additional 160 µL of complete culture media per well and were incubated overnight at 37 °C to allow for adherence. Compound stocks aliquots were applied as 40 µL solutions in complete media to each well in a serial dilution series that ranged from 200-0.2 µL as duplicates. A 10 mM DMSO stock of mefloquine was used as a positive control and prepared as previously described. After drug-treated plates were incubated in 5% CO_2 atmosphere at 37 °C for 24 h, they were aspirated and 200 µL of complete media was added to each well for an additional 24 h incubation in same conditions as previously mentioned. 20 µL of resazurin (Alamar Blue) in PBS buffer was added to each well to a final concentration of 10 µM, and the plates were incubated for 3 h. Fluorescence was measured at 560 nm excitation and 590 nm emission bands using a Spectramax iD3 plate reader. Fluorescence output values were

normalized to the untreated control wells and plotted against the logarithm of drug concentration. Cytotoxicity (CC_{50}) was determined for each compound by fitting this data to a variable slope nonlinear regression curve using Graphpad Prism software (v. 9).

10.1.4. In Vivo Parasite Suppression against murine *Plasmodium yoelii*:

The parasite suppression of select compounds at a fixed dose was measured using a modified 4-day Peters test. Female CF1 mice from Charles River Laboratories were inoculated intravenously with approximately 2.5–5.0 × 10^4 parasitized erythrocytes (murine malaria *Plasmodium yoelii*, lethal Kenya strain MR4 MRA-428) from a donor mouse (experiment day zero). On the following 4 days (Days 1-4), solutions of the test compounds in PEG-400 (PEG-400 only for control mice) were administered by oral gavage once daily. Parasitemia of each mouse was determined by microscopic examination of Giemsa-stained blood smears on Day 5. Percent parasite suppression assessed by comparing parasitemia of treated mice relative to untreated controls using Graphpad Prism (v. 9).

10.1.5. In Vivo Efficacy (ED_{50}, ED_{90}, and NRD) against murine *Plasmodium yoelii*:

The *in vivo* efficacy of select compounds was measured using a modified 4-day Peters test. Female CF1 mice from Charles River Laboratories were inoculated intravenously with approximately 2.5–5.0 × 10^4 parasitized erythrocytes (murine malaria *Plasmodium yoelii*, lethal Kenya strain MR4 MRA-428) from a donor mouse (experiment day zero). On the following 4 days (Day 1–4), solutions of the test compounds in PEG-400 (PEG-400 only for control mice) were administered by oral gavage once daily. Select compounds were assessed at 1.0, 2.5, 5.0, and 10 mg/kg/d, additional experiments outside of the previous range were added if necessary to obtain an interpolated ED_{50} and ED_{90} value. Parasitemia of each mouse was determined by microscopic examination of Giemsa-stained blood smears on Day 5. Mice with no observable parasitemia by microscopic analysis on Day 5 were monitored twice weekly for parasitemia until parasites were observed, or until Day 30. *In vivo* efficacy against infection (ED_{50} and ED_{90}) assessed by generating dose–response curves of parasitemia of treated mice relative to untreated controls using Graphpad Prism (v. 9). Non-recrudescence dose was identified as minimum dose required to maintain a 0% parasitemia by microscopic analysis until Day 30.

10.1.6. Efficacy of a Single Dose Cure (SDC) of 43 against murine *Plasmodium yoelii*:

The efficacy of a single dose of **43** was measured using a modified 4-day Peters test. Female CF1 mice from Charles River Laboratories were inoculated intravenously with approximately 2.5–5.0 × 10^4 parasitized erythrocytes (murine malaria *Plasmodium yoelii*, lethal Kenya strain MR4 MRA-428) from a donor mouse (Day 0). On the following day (Day 1), a solution of **43** at 50 mg/kg in PEG-400 (PEG-400 only for control mice) was administered by oral gavage. Parasitemia of each mouse was determined by microscopic examination of Giemsa-stained blood smears on Day 5. Mice with no observable parasitemia by microscopic analysis on Day 5 were monitored twice weekly for parasitemia until parasites were observed, or until Day 30. The single dose cure was identified as a dose required to maintain 0% parasitemia by microscopic analysis until Day 30.

10.1.7. Murine Microsomal Stability :

Select compounds were assessed for murine microsomal stability in pooled liver microsomes performed at ChemPartner, Shanghai, China. Compounds were incubated at 37 °C and 1 μM concentration in murine liver microsomes (Corning) for 1 h at a protein concentration of 0.5 mg/mL in potassium phosphate buffer at pH 7.4 containing 1.0 mM EDTA. The metabolic reaction was initiated by NADPH and quenched with ice-cold acetonitrile at 15 min increments up to 1 h. The progress of compound metabolism was followed by LC-MS/MS (ESI positive ion, LC-MS/MS-034(API-6500+) using a C18 stationary phase (ACQUITY UPLC BEH C18 (2.1 × 50 mm, 1.7 μm)) and a MeOH/water mobile phase containing 0.25% FA and 1 mM NH_4OAc. Imipramine or Osalmid were used as internal standards, ketanserin was used as a metabolically unstable control compound. Concentration versus time data for each compound were fitted to an exponential decay function to determine the first-order rate constant for substrate depletion, which was then used to calculate the degradation half-life ($t_{1/2}$) and predicted intrinsic clearance value (Cl_{int}) from an assumed murine hepatic blood flow of 90 mL/min/kg.

10.1.8. Pharmacokinetic Study of 43 in Mice.

The title compound was selected for pharmacokinetic analysis in mice at a PO dose of 10 mg/kg and IV dose of 0.5 mg/kg performed at ChemPartner in Shanghai, China. Three groups of three male CF1 mice (JH Laboratory Animal) were used in each arm of the study and were administer the drug in PEG-400 at 1 mg/mL by oral gavage and in PEG-400 at 0.1 mg/mL by tail vein. At the following time points: 0.083 h, 0.25 h, 0.5 h, 1 h, 2 h, 4 h, 8 h, 24 h, 48 h, 72 h, 96 h, and 120 h post dose administration a single group of mice were manually restrained and approximately 93 μL of blood were taken from the animals via facial vein for semi-serial bleeding into K_2EDTA tubes. Samples were put on ice and centrifuged (2000 G, 5 min at under 4 °C) within 15 minutes of collection. An aliquot of 10 μL sample was added to 20 μL 10mM NH_4OAc and 3 μL internal standard (Diclofenac, 200 ng/mL) in ACN. The mixture was vortexed for 1 m, then added to 800 μL MTBE and continued to vortex for an additional 10 min followed by centrifugation at 14000 rpm for 5 min. A 700 μL aliquot of the supernatant was condensed under nitrogen steam. Samples were reconstituted with 200 μL of 1:1 methanol/water and vortexed for 2 min. 1 μL of solution was injected into LC-MS/MS-21 (Triple Quad 6500) and ran on a Waters ACQUITY UPLC HSS T3 (2.1 x 50 mm, 1.8 μm) column. Pharmacokinetic analysis as a best-fit curve was prepared from drug concentration in plasma as a function of time using non-compartmental analysis as implemented in WinNonlin software (Pharsight – Mountain View, CA). The exposure (AUC_{last}), half-life ($T_{1/2}$), maximum concentration (C_{max}) and time of maximum concentration (T_{max}) were determined from the data. Goodness-of-fit was assessed by the r^2 (linear regression coefficient) of the drug concentration on the terminal phase. Bioavailability (F) was calculated using the following equation, where AUC is area under the curve for oral (po) and tail vein (iv) and D is dose for oral (po) and tail vein (iv):

$$F = 100 \bullet \frac{AUC_{po} \bullet D_{iv}}{AUC_{iv} \bullet D_{po}}$$

Ethical Use of Animals Statement. The procedures involved, together with all matters relating to the care, handling, and housing of the animals used in this study, were approved by the Portland VA Medical Center Institutional Animal Care and Use Committee. Protocol and approval IRBNet #: 1635615-8.

10.2. Methods used in Chapter 7

10.2.1. Parasite Culture:

P. falciparum parasites were thawed from frozen stock and cultured in suspended human erythrocytes (Lampire Biological Laboratories, Pipersville, PA) not more than 28 days old at 2% hematocrit. The culture medium used: RPMI-1640 supplemented with 25 mM HEPES buffer, 25 mg/L gentamicin sulfate, 45 mg/L hypoxanthine, 10 mM glucose, 2 mM glutamine, and 0.5% Albumax II (complete medium). Cultures were maintained in a standard low oxygen atmosphere (5% O2, 5% CO2, 90% N2) in a Forma Series II 3110 environmental chamber and incubated at 37 °C. Cultures were subpassaged every 3–4 days into a fresh culture flask containing complete media and erythrocytes.

10.2.2. In vitro Antiplasmodial Activity (IC_{50}) against *P. falciparum*:

Final compounds were assessed for in vitro antiplasmodial activity against D6 and Dd2 strains of *P. falciparum* using the previously described fluorescence-based SYBR Green assay. In short, compounds were prepared as 10 mM stocks in DMSO. Compounds were evaluated in quadruplicate in flat-bottomed clear 96-well plates and plated at a 2-fold serial dilution with the final column left untreated to span a range of 0.25-250 nM. Asynchronous *P. falciparum* infected erythrocytes in growth media were added to each well for a total volume of 100 µL, final hematocrit of 2%, and initial parasitemia of 0.2%. Controls included non-infected red blood cells, 10 mM chloroquine and amodiaquine. Plates were incubated in controlled low oxygen atmosphere (5% O_2, 5% CO_2, 90% N_2) at 37 °C. 72 h post inoculation, all wells are simultaneously lysed and dyed using 100 µL of a SYBR Green I dye-detergent solution. Plates were incubated at ambient temperature and atmosphere in the dark for at least 1 h. Fluorescence was read at 497 nm excitation and 520 nm emission bands with a Spectramax iD3 plate reader. Fluorescence values were normalized with respect to the untreated control wells representing normal parasite growth and plotted against the logarithm of drug concentration. An IC_{50} was determined for each compound by fitting this data to a variable slope nonlinear regression curve using Graphpad Prism software (v. 9).

10.2.3. HepG2 Cytotoxicity Assay:

Final compounds were assessed for mammalian cytotoxicity using an immortalized human liver carcinoma cell line (HepG2) using previously described methods. In short, final compounds were prepared in DMSO as 10 mM stock solutions. Human hepatocarcinoma (HepG2) cells were cultured in RPMI-1640 medium containing 10% fetal bovine serum at 37 °C in a humidified 5% CO_2 atmosphere. To 96-well flat-bottomed tissue culture plates, HepG2 cells were added at 2 x 10^4 density with an additional 160 µL of complete culture media per well and were incubated overnight at 37 °C to allow for adherence. Compound stocks aliquots were applied as 40 µL solutions in complete media to each well in a serial dilution series that ranged from 200-0.2 µL as duplicates. A 10 mM DMSO stock of mefloquine was used as a positive control and prepared as previously described. After drug-treated plates were incubated in 5% CO_2 atmosphere at 37 °C for 24 h, they were aspirated and 200 µL of complete media was added to each well for an additional 24 h incubation in same conditions as previously mentioned. 20 µL of resazurin (Alamar Blue) in PBS buffer was added to each well to a final concentration of 10 µM, and the plates were incubated for 3 h. Fluorescence was measured at 560 nm excitation and 590 nm emission bands using a Spectramax iD3 plate reader. Fluorescence output values were

normalized to the untreated control wells and plotted against the logarithm of drug concentration. Cytotoxicity (CC_{50}) was determined for each compound by fitting this data to a variable slope nonlinear regression curve using Graphpad Prism software (v. 9).

10.2.4. In Vivo Parasite Suppression against Murine *Plasmodium yoelii*:

The parasite suppression of select compounds at a fixed dose was measured using a modified 4-day Peters test. Female CF1 mice from Charles River Laboratories were inoculated intravenously with approximately 2.5–5.0 × 10^4 parasitized erythrocytes (murine malaria *Plasmodium yoelii*, lethal Kenya strain MR4 MRA-428) from a donor mouse (experiment day zero). On the following 4 days (Days 1-4), solutions of the test compounds in PEG-400 (PEG-400 only for control mice) were administered by oral gavage once daily. Parasitemia of each mouse was determined by microscopic examination of Giemsa-stained blood smears on Day 5. Percent parasite suppression assessed by comparing parasitemia of treated mice relative to untreated controls using Graphpad Prism (v. 9). The procedures involved, together with all matters relating to the care, handling, and housing of the animals used in this study, were approved by the Portland VA Medical Center Institutional Animal Care and Use Committee.

10.2.5. In Vivo Efficacy (ED_{50}, ED_{90}, and NRD) against Murine *Plasmodium yoelii*:

The in vivo efficacy of select compounds was measured using a modified 4-day Peters test. Female CF1 mice from Charles River Laboratories were inoculated intravenously with approximately 2.5–5.0 × 104 parasitized erythrocytes (murine malaria *Plasmodium yoelii*, lethal Kenya strain MR4 MRA-428) from a donor mouse (experiment day zero). On the following 4 days (Day 1–4), solutions of the test compounds in PEG-400 (PEG-400 only for control mice) were administered by oral gavage once daily. Select compounds were assessed at 1.0, 2.5, 5.0, and 10 mg/kg/d, additional experiments outside of the previous range were added if necessary to obtain an interpolated ED_{50} and ED_{90} value. Parasitemia of each mouse was determined by microscopic examination of Giemsa-stained blood smears on Day 5. Mice with no observable parasitemia by microscopic analysis on Day 5 were monitored twice weekly for parasitemia until parasites were observed, or until Day 30. *In vivo* efficacy against infection (ED_{50} and ED_{90}) assessed by generating dose–response curves of parasitemia of treated mice relative to untreated controls using Graphpad Prism (v. 9). Non-recrudescence dose was identified as minimum dose required to maintain a 0% parasitemia by microscopic analysis until Day 30. The procedures involved, together with all matters relating to the care, handling, and housing of the animals used in this study, were approved by the Portland VA Medical Center Institutional Animal Care and Use Committee.

10.2.6. Murine Microsomal Stability:

Select compounds were assessed for murine microsomal stability in pooled liver microsomes performed at ChemPartner, Shanghai, China. Compounds were incubated at 37 °C and 1 μM concentration in murine liver microsomes (Corning) for 1 h at a protein concentration of 0.5 mg/mL in potassium phosphate buffer at pH 7.4 containing 1.0 mM EDTA. The metabolic reaction was initiated by NADPH and quenched with ice-cold acetonitrile at 15 min increments up to 1 h. The progress of compound metabolism was followed by LC-MS/MS (ESI positive ion, LC-MS/MS-034(API-6500+)) using a C18 stationary phase (ACQUITY UPLC BEH C18 (2.1 × 50 mm, 1.7 μm)) and a MeOH/water mobile phase containing 0.25% FA and 1 mM NH_4OAc. Imipramine or Osalmid were used as internal standards, ketanserin was used as a metabolically

unstable control compound. Concentration versus time data for each compound were fitted to an exponential decay function to determine the first-order rate constant for substrate depletion, which was then used to calculate the degradation half-life ($t_{1/2}$) and predicted intrinsic clearance value (Cl_{int}) from an assumed murine hepatic blood flow of 90 mL/min/kg.

10.2.7. Pharmacokinetic Study of 69 in Mice:

Select compounds were used in a pharmacokinetic analysis in mice at a PO dose of 10 mg/kg and IV dose of 0.5 mg/kg performed at ChemPartner in Shanghai, China. Three groups of three male CF1 mice (JH Laboratory Animal) were used in each arm of the study and were administer the drug in PEG-400 at 1 mg/mL by oral gavage and in PEG-400 at 0.1 mg/mL by tail vein. At the following time points: 0.083 h, 0.25 h, 0.5 h, 1 h, 2 h, 4 h, 8 h, 24 h, 48 h, 72 h, 96 h, and 120 h post dose administration a single group of mice were manually restrained and approximately 93 µL of blood were taken from the animals via facial vein for semi-serial bleeding into K_2EDTA tubes. Samples were put on ice and centrifuged (2000 G, 5 min at under 4 °C) within 15 minutes of collection. An aliquot of 10 µL sample was added to 20 µL 10mM NH_4OAc and 3 µL internal standard (Diclofenac, 200 ng/mL) in ACN. The mixture was vortexed for 1 m, then added to 800 µL MTBE and continued to vortex for additional 10 min followed by centrifugation at 14000 rpm for 5 min. A 700 µL aliquot of the supernatant was condensed under nitrogen steam. Samples were reconstituted with 200 µL of 1:1 methanol/water and vortexed for 2 min. 1 µL of solution was injected into LC-MS/MS-21 (Triple Quad 6500) and ran on a Waters ACQUITY UPLC HSS T3 (2.1 x 50 mm, 1.8 µm) column. Pharmacokinetic analysis as a best-fit curve was prepared from drug concentration in plasma as a function of time using non-compartmental analysis as implemented in WinNonlin software (Pharsight – Mountain View, CA). The exposure (AUC_{last}), half-life ($T_{1/2}$), maximum concentration (C_{max}) and time of maximum concentration (T_{max}) will be determined form data. Goodness-of-fit was assessed by the r^2 (linear regression coefficient) of the drug concentration on the terminal phase. Bioavailability (F) was calculated using Equation [eq-bioavailability], where AUC is area under the curve for oral (po) and tail vein (iv) and D is dose for oral (po) and tail vein (iv):

$$\begin{equation} \phantomsection\label{eq-bioavailability}{ F=100*((AUC~po~*D~iv~)/(AUC~iv~*D~po~)) } \end{equation}$$

Equations

1. Log of Selectivity Index (pSI)

$$pSI = \log_{10}\left(\frac{HepG2\ CC_{50}(nM)}{PfD6\ IC_{50}\ (nM)}\right)$$

2. Predicted Hepatic Extraction Ratio (E_H)

Each degradation half-life ($t_{1/2}$) was used to calculate [2a] a predicted *in vivo* hepatic clearance value (CL_{int}) before [2b] a predicted *in vivo* hepatic extraction ratio (E_H).

[2a] $$CL_{int} = \left(\frac{\ln 2}{t_{1/2}}\right) \times \left(\frac{1}{(microsomal\ protien\ [conc]\ (mg/mL)}\right) \times (Scaling\ Factor)$$

[2b] $$E_H = \frac{CL_{blood}}{Q} = \frac{CL_{int}}{Q + CL_{int}}$$

Microsomal protein concentration = (0.5 mg/mL). Scaling Factor for mice = (microsomal protein per gram of liver = 45 mg/g) x (liver weight per gram of body weight = 87.5 g/kg) = 3937.5. Hepatic Blood Flow (Q) of mice = 90 (mL/min/kg).

E_H classifications are based on the following assumptions, outlined in Obach, (1999)[20]:

1. NADPH-dependent oxidative metabolism predominates other metabolic routes.
2. Rates of *in vitro* metabolism and enzymatic activity are reflective of those *in vivo*.

Calculations of CL_{int} are based on the "*in vitro* $t_{1/2}$ method" (Obach, 1999), which utilize the following assumptions:

1) Concentration of substrate used is well below apparent K_M for turnover.

2) There is no mechanism-based inactivation of enzyme, or significant product inhibition.

3. Bioavailability

$$F = 100 \bullet \frac{AUC_{po} \bullet D_{iv}}{AUC_{iv} \bullet D_{po}}$$

B. Malaria's many "chicken or the egg"

The staggering longevity of malaria and its microscopic size lends itself to an origin story that is difficult to capture. The very nature of how it came into existence leaves little in the way of a fossil record or molecular trail, making definitive conclusions elusive. As such the debate continues as to how malaria had evolved into a parasite that occupies both insects and vertebrate hosts.

1. From Invertebrates to Vertebrates

A theory provided by C. G. Huff, suggesting that the parasite first occupied insects and then migrated to vertebrate hosts.› Offering that this must be true since the group of invertebrate hosts (set of dipterans) that malaria occupies is much smaller compared to group of vertebrate hosts (birds, reptiles, and mammals). As the tree-dwelling nature of mammals such as monkeys and rats, and birds would co-habitat with the mosquito, and therefore proximity facilitates the acquisition of a new host. And secondly, that a high degree of pathogenicity in host-parasites relationships are traditionally thought be recent in origin, and therefore since malaria is relatively apathogenic in dipterans, compared to its vertebrate host–it is thought that they originate from the former. The main counter arguments to the first rationale is the group of dipterans that malaria inhabits can also be characterized a diverse and since reptiles are regarded as some of original vertebrate hosts, they too must have been tree-dwelling. The second is that associations drawn from pathogenicity and age of parasite-host system is far too simple. Though extended parasite-host association are often low-pathogenic in nature, there is no reason to conclude that is the rule.

2. From Vertebrates to Invertebrates

The second theory is that malaria originated from an intestinal parasite in vertebrate hosts that later moved to invertebrates. Arguing that malaria in birds and reptiles could have preceded blood-sucking diptera in evolution. Furthermore, the frequency of vertebrate intestinal-infecting Coccidia, an evolutionary similar apicomplexan thought to be the common ancestor of *Plasmodiidae*, to become tissue-inhabiting.[9] But the greatest challenge to the first theory when considering alternative explanations, is the mental gymnastics one must do when trying to construct an ancestral *plasmodium* without the intervention of a vertebrate host *if* the life cycle of modern *plasmodium* is similar to the one found in ancient diptera.[10] In essence, if the former opinion is true, then it suggests that schizogony and gametogony should be in the invertebrate and sporogony in the vertebrate host, very much contrary to modern malaria's lifecycle.[9] This theory is not without opposing viewpoints, namely that the parasite could have evolved after blood-sucking insects and the potential of Coccidia to become tissue-inhabiting does not mean that it must. Additionally, this theory does not explain why malaria is not found in other blood-sucking arthropods, *i.e.* fleas, ticks, mites, or lice, for if the parasite originated in vertebrates, then presumably there where millions of years for which it could have adapted to these other insects. Although, most of the evidence supporting one opinion or the other is largely subjective, the greatest weight of available evidence supports the origin of malaria as a vertebrate-borne intestinal-tissue parasite that evolved to invade to the blood of animal and then eventually jumped to dipteran hosts, but I digress. And, although much time has been spent discussing the to classical theories of malaria emergence, the focus of this dissertation is not a complete phylogenetic analysis of malaria divergence. Therefore we will skip ahead a few millions of years to malaria's jump to monkeys.

Early attempts in drafting a timeline of malaria's jump to primates, largely relied on microscopy morphological analysis of a small number of primate *Plasmodium. spp* and the ecological understanding of primate radiation.[11] However, as the use of molecular analysis became increasing prevalent, that timeline of lateral transfer to monkeys and apes was orginally placed at 13-78 mya.[9] Later the inclusion of great apes and lemurs move the timeline,
[10] found in

The question of timing in malaria's history further extends to the emergence of *Plasmodium falciparum*. Cumulative work in molecular phylogentic inference supports that human plasmodium parasites are derived from two distinct clades of non-human primate Plasmodium. One clade includes Plasmodium vivax, malarie, ovale and a large number of primate infecting plasmodium, including knowlesi, that are largely found in Southeast Asia.[9,10] The second includes P. falciparum and several linages of african ape malaria together.[11,10] Initally, molecular phylogenetic examination of small-subunit ribosomal RNA sequences of modern *Plasmodium* species, concluded that *P. falciparum* was strongly associated with two avian parasites.[9] Further supporting the notion put forth by Livingstone, that this lateral transfer from avians to humans is recent and likely coincides with onset of human populations moving to agrarian-like societies sometime from 5000 to 10,000 years ago. Soon after, Escalante and colleagues preformed a similar experiment, but included additional species of *Plasmodium* not included in the work by Waters *et. al.*
Concluding that *P. falciparum*'s is more closely related the chimpanzee-borne malaria *P. reiechenowi*, though still of avian decent.[9] Though more recently, Liu and colleagues show that the origin of the P. falciparum lineage is instead from the lateral transfer of gorilla-borne malaria. There have been a number of estimations of the origin of P. falciparum, but they have largely

based those estimations on P. reichenowi and P. falciparum diverging congruently with the divergence of chimps and humans.[–] Additionally, others in the past have cite the spread of agrarian-based societies in sub-Saharan Africa or the evolution and divergence of African Anopheles mosquitos species as evidence for more recent divergence of *P. falciparum*.[,] The lack of fossil records or first-hand accounts of *P. falciparum* divergence creates a particular difficult task of estimating *P. falciparum* divergence, and therefore one could consider the point in time of *P. falciparum* origin forevermore only speculative.

C. P. falciparum Antimalarial Resistance

The following parasite strains were used in this study and obtained through BEI Resources, NIAID, NIH. *Plasmodium falciparum*, Strain D6 (MRA-285, originally from Sierra Leone, has modest resistance to mefloquine). *Plasmodium falciparum*, Strain Dd2 (MRA-150, originated from Indochina; derived from W2-mef and is resistant to chloroquine, pyrimethamine, and mefloquine).

D. Piperaquine Survival Assay

Parasite survival characterization of the *Plasmodium falciparum* chloroquine resistance transporter (CRT) isogenic mutant and wild-type panel against bis-quinoline compounds.

D.1. Methods

Drug preparation**: Drug stocks were prepared at a 10 mM stock concentration in dimethyl sulfoxide (DMSO). From this stock, 1 mM aliquots were prepared as a working stock and stored at -20°C while the original stock put away for long-term storage at -20°C. Piperaquine (PPQ) stock was made to 100nM in 0.05% lactic acid and stored in -20°C.

D.1.1. Parasite culture

P. falciparum strains Dd2-B2, RF12, 3D7 Dd2_GC03 (WT), Dd2_PfCRT_F145I, Dd2_PfCRT_T93S, and Dd2_Dd2 were used for this study (Table 14). Dd2-B2 is a clone from the *Plasmodium falciparum* Dd2 line previously obtained from Thomas Wellems (NIAID, NIH). RF12 is a culture-adapted PPQ-resistant Cambodian isolate that encodes the PfCRT H97Y mutation added to the 8 mutations present in Dd2 as well as two copies of plasmepsins 2/3. This isolate, which was earlier called PH1263-C, also carries the K13 C3580Y mutation that confers artemisinin partial resistance. 3D7 is the canonical *P. falciparum* drug-sensitive parasite whose genome is the reference wild-type. Dd2_GC03 is an isogenic zinc-finger nuclease (ZFN) edited line expressing the CQ-sensitive 3D7 wildtype (WT) isoform. Dd2_PfCRT_F145I and Dd2_PfCRT_T93S are resistant mutants edited using customized zinc-finger nucleases that express the PPQ-resistant F145I and T93S mutations, respectively, on the Dd2 haplotype background of the *P. falciparum* chloroquine resistance transporter (Pf3D7_070900).[,] Dd2_Dd2 is a recombinant isogenic parasite strain expressing the Dd2 pfcrt allele, used as a recombinant control. Parasite strains and relative sensitivity or resistance to piperaquine and chloroquine are found in Table 14. Parasites were cultured in human red blood cells (RBCs) at 2% hematocrit in RPMI-1640 media, supplemented with 25 mM HEPES, 50 mg L-hypoxanthine, 2mM L-glutamine, 0.21% sodium bicarbonate, 0.5% (wt/vol) AlbuMAXII and 10 μg/mL gentamycin. Cultures were maintained at 37°C in modular incubator chambers at 5% O_2, 5% CO_2 and 90% N_2.

Parasite Strain	Edited (Y/N)	PPQ (sensitive/resistant)	CQ (sensitive/resistant)
Dd2-B2	N	sensitive	resistant
RF12	N	resistant	resistant
Dd2_ GC03 (WT)	Y	sensitive	sensitive
Dd2_PfCRT_F145I	Y	resistant	sensitive
Dd2_PfCRT_T93S	Y	resistant	resistant (low)
Dd2_Dd2	Y	sensitive	resistant
3D7	N	sensitive	sensitive

Table 14: Detailed list of parasites used in this study and resistant/sensitive profile.

Piperaquine survival assay: To assess parasite susceptibility to piperaquine (PPQ), lines described in Table 14 were examined using PPQ survival assays (PSAs). Schizont stage parasite cultures were collected using a 70% percoll gradient and incubated at 37°C in modular incubator for reinvasion into RBCs. Lysis of remaining schizonts was performed using 5% D-sorbitol, followed by a wash with complete medium, and 0-6 hours post invasion (hpi) ring-stage parasite cultures were isolated. Tightly synchronized ring parasites were incubated at 0.3% starting parasitemia and 1% hematocrit and exposed to a 10-point, 2-fold dilution series in duplicate of bis-quinoline compound in parallel with drug-free controls in complete medium. Parasites were incubated for 72 hours at 37°C. Parasite survival was assessed by flow cytometry using SYBR Green I and MitoTracker Deep Red FM (Life Technologies) as nuclear and mitochondrial stains, respectively.

D.2. Results

D.2.1. Chemosensitivity Profiling of Control Compound

Piperaquine (PPQ) acts by binding to heme and inhibiting heme detoxification via hemozoin formation. Resistance is mediated by several mutant isoforms of PfCRT that enable this drug-peptide transporter to transport PPQ out of the digestive vacuole, away from its heme target and site of action. PPQ was earlier reported to exhibit a mean IC_{50} value of 19.9 nM against Dd2_Dd2 parasites (Dd2 gene edited to express the Dd2 pfcrt allele). For the studies reported herein, PPQ exhibited a mean IC_{50} value of 20.0 nM in Dd2-B2. Parasite survival curves are shown in Figure 60 and the IC_{50} and IC_{90} data and fold shifts relative to the PPQ-sensitive Dd2-B2 line are shown in Table 15.

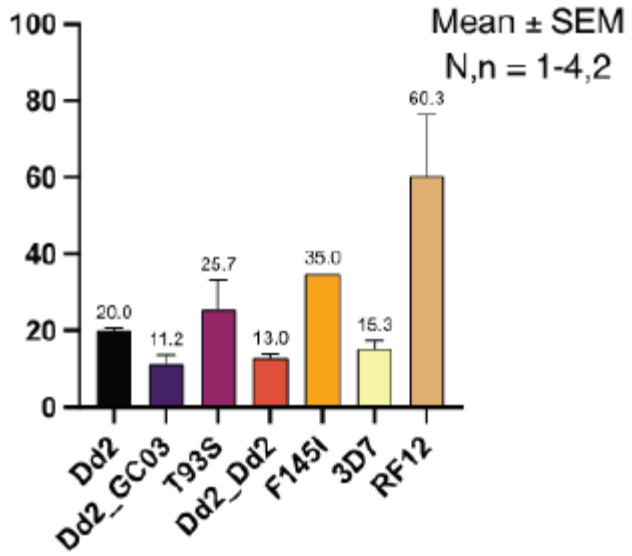

Figure 60: Comparative IC50 of piperaquine (PPQ) against Dd2-B2, RF12, 3D7 Dd2_GC03, Dd2_PfCRT_F145I, Dd2_PfCRT_T93S, and Dd2_Dd2. IC50s for each line are presented as means ± SEMs (N, n = 2-3,2).

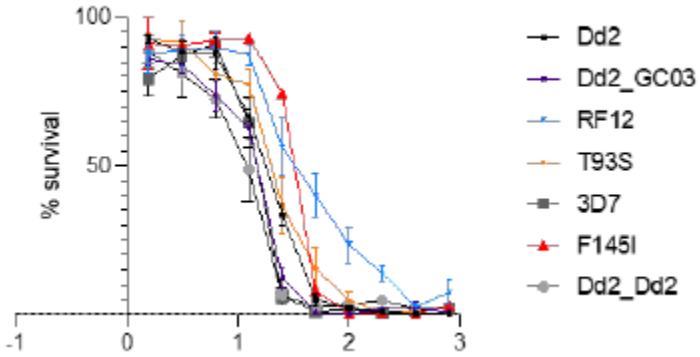

Figure 61: Combined average percent inhibition of Dd2-B2, RF12, 3D7, Dd2_GC03, Dd2_PfCRT_F145I, Dd2_PfCRT_T93S, and Dd2_Dd2 when treated with piperaquine (PPQ) on a log10 scale.

Error bars represent ± SEM (N,n = 2-4,2). A noticeable shift in inhibition was observed for RF12. A slight shift in inhibition was also observed in Dd2_PfCRT_F145I. PPQ sensitivity was observed in Dd2_GC03, Dd2_Dd2, and 3D7.

Measure	Dd2-B2	3D7	RF12	Dd2_GC03	Dd2_PfCRT_F145I	Dd2_PfCRT_T93S	Dd2_Dd2
IC50 (nM)	20	15.3	60.3	11.2	35	25.7	13
IC90 (nM)	45.8	23.9	NA	18.7	49.9	72.8	23.5
IC50 shift	Not reported	0.8	3.0	0.6	1.8	1.3	0.7

Measure	Dd2-B2	3D7	RF12	Dd2_GC03	Dd2_PfCRT_F145I	Dd2_PfCRT_T93S	Dd2_Dd2
IC90 shift	Not reported	0.5	NA	0.4	1.1	1.6	0.5
N	3	3	3	3	1	2	3

Table 15: IC50 and IC90 shift of PfCRT mutants against PPQ.

These data show a moderate increase in IC_{50} in Dd2 parasites expressing the pfcrt Dd2+F145I allele. That parasite harbors a single copy of plasmepsins 2/3. We recently reported that this line reverts its level of resistance due spontaneous emergence of mutants that have improved growth relative to the original Dd2+F145I mutant and that tend to become less PPQ-resistant. We suspect that this line had begun to revert during the course of these studies.

A greater increase in IC_{50} was observed with RF12, which expresses the PfCRT Dd2+FH97Y isoform as well as two copies of plasmepsins 2/3. We note that an IC_{90} increase was not observed due to the biphasic nature of the response curve.

D.2.2. Activity of Compounds 54, 69, and 70

The mean IC_{50} value of **54** in Dd2-B2 parasites was 16.4 nM (Figure 62). Based on the percent survival curve, the mutant PfCRT line expressing the PPQ-resistant mutation F145I can be considered resistant to **54** (Figure 63). RF12 and 3D7 can also be considered resistant to **54**. The parasite survival in all lines against **54** is more dispersed than in **69** or **70**. No evidence of biphasic survival is observed in F145I or T93S, and some biphasic survival is observed at the highest concentration in RF12. Some decrease in survival is observed in Dd2_Dd2. The IC_{50} and IC_{90} data and fold shifts relative to Dd2-B2 line are shown in Table 16.

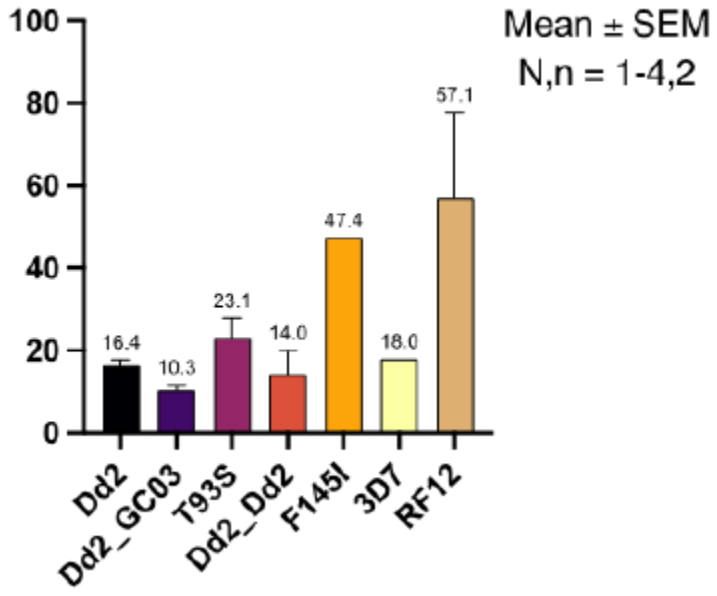

Figure 62: Comparative IC50 of 11 against Dd2-B2, RF12, 3D7 Dd2_GC03, Dd2_PfCRT_F145I, Dd2_PfCRT_T93S, and Dd2_Dd2. IC50s for each line are presented as means ± SEMs (N, n = 2-3,2).

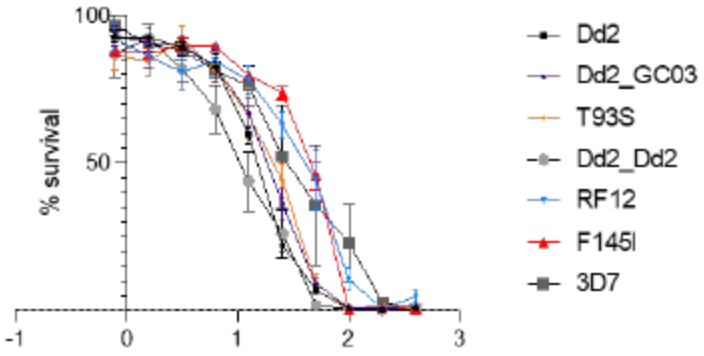

Figure 63: Percent parasite survival against 54 (N,n = 1-4,2).

*Evidence of increased parasite survival against **54** is seen in RF12, and Dd2_PfCRT_F145I, both piperaquine-resistant parasites. No biphasic parasite survival is seen in Dd2_PfCRT_F145I, or Dd2_PfCRT_T93S. Slight biphasic survival is observed in RF12 at the highest concentration. Increased survival in 3D7 is also observed, and some decrease in survival in Dd2_Dd2 can be observed.*

Measure	Dd2-B2	3D7	RF12	Dd2_GC03	Dd2_PfCRT_F145I	Dd2_PfCRT_T93S	Dd2_Dd2
IC50 (nM)	16.4	18.0	57.1	10.3	47.4	23.1	14.0
IC90 (nM)	47.3	39.8	NA	27.5	89.4	54.7	35.3
IC50 shift	Not reported	1.1	3.5	0.6	2.9	1.4	0.9
IC90 shift	Not reported	0.8	NA	0.6	1.9	1.2	0.7
N	4	1	2	4	1	3	3

Table 16: IC50 and IC90 shift of PfCRT mutants against 54.

The mean IC_{50} value of **69** in Dd2-B2 parasites was 15.2 nM (Figure 64). Based on the percent survival curve, the mutant PfCRT line expressing the PPQ-resistant mutation F145I can be considered resistant to **69** (Figure 65). RF12 can also be considered resistant to **69** at higher concentrations based on increased survival in the parasite survival curve. Evidence of biphasic survival is seen in the percent survival curve for RF12 and Dd2_PfCRT_F145I parasites, and some evidence of biphasic nature is seen in Dd2_PfCRT_T93S. The IC_{50} and IC_{90} data and fold shifts relative to Dd2-B2 line are shown in Table 17.

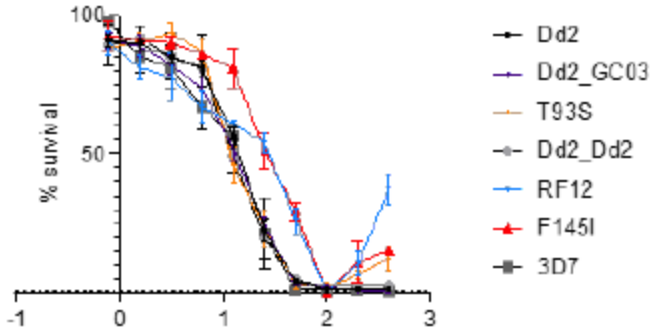

Figure 64: Comparative IC50 of 69 against Dd2-B2, RF12, 3D7 Dd2_GC03, Dd2_PfCRT_F145I, Dd2_PfCRT_T93S, and Dd2_Dd2. IC50s for each line are presented as means ± SEMs (N, n = 2-3,2).

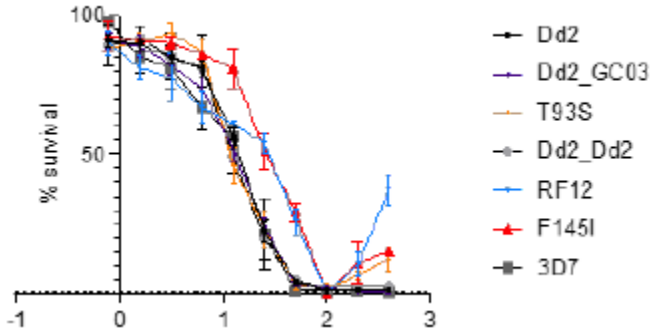

Figure 65: Percent parasite survival against 69 (N,n = 1-4,2). Evidence of increased parasite survival against 69 is seen in RF12 and Dd2_PfCRT_F145I, both piperaquine-resistant parasites.

Biphasic parasite survival is seen in RF12 and Dd2_PfCRT_F145I, and some evidence of biphasic survival is shown in Dd2_PfCRT_T93S.

Measure	**Dd2-B2**	**3D7**	**RF12**	**Dd2_GC03**	**Dd2_PfCRT_F145I**	**Dd2_PfCRT_T93S**	**Dd2_Dd2**
IC50 (nM)	15.2	16.1	43.1	7.1	33.6	14.7	12.5
IC90 (nM)	42.4	33.8	NA	20	95.3	39.6	32.0
IC50 shift	Not reported	1.1	2.8	0.5	2.2	1.0	0.8
IC90 shift	Not reported	0.8	NA	0.5	2.2	0.9	0.8
N	4	2	2	4	1	3	3

Table 17: IC50 and IC90 shifts of P. falciparum PfCRT mutants against 69.

The mean IC_{50} value of **70** in Dd2-B2 parasites was 17.4 nM (Figure 66). No IC_{90} values for **70** could be calculated for the RF12 due to the biphasic nature of the inhibition curve, indicating cross resistance. Therefore, mean IC_{50} values were used as the comparison. Based on the percent

survival curve, RF12 can be considered resistant to **70**. Also, the mutant PfCRT line expressing the PPQ-resistant mutation F145I also showed evidence of some cross resistance (Figure 66). This line is known to be unstable in vitro and the F145I phenotype is quickly reverted, as discussed above, therefore only one data point was achieved with two technical replicates. Evidence of biphasic survival is seen in the percent survival curve for RF12 and Dd2_PfCRT_F145I parasites, and some evidence of biphasic nature is seen in Dd2_PfCRT_T93S. Decreased parasite survival compared to Dd2-B2 is seen in 3D7, a PPQ-sensitive line. The IC_{50} and IC90 data and fold shifts relative to Dd2-B2 line are shown in Table 18.

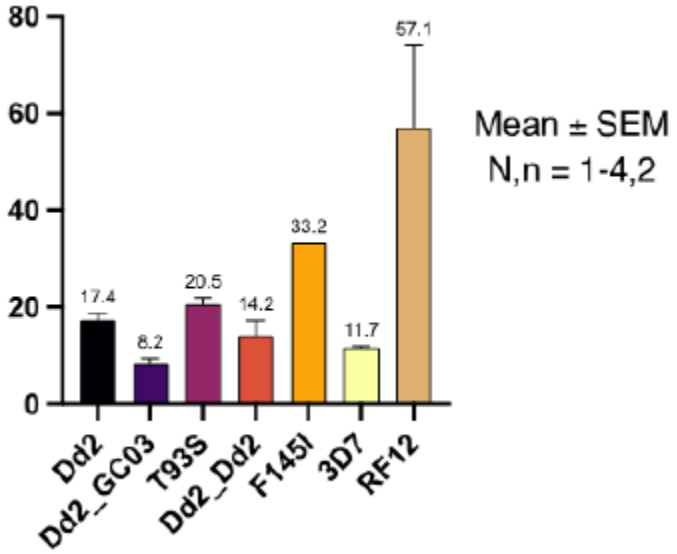

Figure 66: Comparative IC50 of 70 against Dd2-B2, RF12, 3D7 Dd2_GC03, Dd2_PfCRT_F145I, Dd2_PfCRT_T93S, and Dd2_Dd2.

IC_{50}s for each line are presented as means ± SEMs (N, n = 2-3,2).

*Percent parasite survival against **70** (N,n = 1-4,2). Evidence of increased parasite survival against **70** is seen in RF12 and Dd2_PfCRT_F145I, both piperaquine-resistant parasites. Biphasic parasite survival is seen in RF12 and Dd2_PfCRT_F145I, and some evidence of biphasic survival is shown in Dd2_PfCRT_T93S.*

Measure	Dd2-B2	3D7	RF12	Dd2_GC03	Dd2_PfCRT_F145I	Dd2_PfCRT_T93S	Dd2_Dd2
IC50 (nM)	16.4	18.0	57.1	10.3	47.4	23.1	14.0
IC90 (nM)	47.3	39.8	NA	27.5	89.4	54.7	35.3
IC50 shift	Not reported	1.1	3.5	0.6	2.9	1.4	0.9
IC90 shift	Not reported	0.8	NA	0.6	1.9	1.2	0.7
N	4	1	2	4	1	3	3

Table 18: IC50 and IC90 values and shifts for P. falciparum PfCRT mutants against 70.

D.3. Discussion

This report demonstrates increased parasite survival compared to Dd2-B2 in piperaquine (PPQ)-resistant parasite lines (RF12, Dd2_PfCRT_F145I, and Dd2_PfCRT_T93S) and PPQ-sensitive 3D7 against all **54**, **69**, and **70**. Similar fold-shifts in IC_{50} and IC_{90} are observed in **54**, **69**, and **70** as in PPQ. Biphasic parasite survival is seen in **69**, and **70** in RF12 and Dd2_PfCRT_F145I; however, no evidence of biphasic survival is seen in Dd2_PfCRT_F145I with **54**, and some evidence of biphasic survival is seen in RF12 at the highest concentrations of **54**.

3D7 shows some increase in survival against **54** despite PPQ-sensitivity. In contrast, 3D7 shows a decrease in survival against **70** compared to Dd2-B2. This in combination with the biphasic survival of RF12 and Dd2_PfCRT_F145I may indicate that **70** functions most similarly to PPQ.

In summary, increased parasite survival is evident in RF12 and Dd2_PfCRT_F145I for all compounds tested in this experiment. There is some increase in parasite survival in **54** for 3D7 and a decrease in 3D7 parasite survival against **70**. There are biphasic survival curves against **70** and **69** in RF12, Dd2_PfCRT_F145I, and Dd2_PfCRT_T93S, which are all PPQ-resistant.

E. Synthetic Details of Presented Compounds

A full list of General Synthetic Procedures can be found in Chapter 9

E.1. Synthetic details of Compounds presented in Chapter 6

7-chloro-N-(4-morpholinophenyl)quinolin-4-amine (7). Prepared using general procedure (i) with 7.22 mmol **5**, and 21.6 mmol **6a**. Yield = 80% (2.452 g). ^{1}H NMR (METHANOL-d_4, 400 MHz) δ 8.56 (d, 1H, *J*=9.1 Hz), 8.35 (d, 1H, *J*=7.1 Hz), 7.95 (d, 1H, *J*=1.8 Hz), 7.80 (dd, 1H, *J*=2.1, 9.1 Hz), 7.4-7.4 (m, 2H), 7.2-7.3 (m, 2H), 6.83 (d, 1H, *J*=7.1 Hz), 3.9-3.9 (m, 4H), 3.3-3.3 (m, 4H). HRMS (ESI) - *m/z* of [$C_{19}H_{19}ClN_3O^+$]: 340.1216, actual: 340.1207.

7-chloro-N-(4-morpholinophenyl)-3-(4-(trifluoromethoxy)-phenyl)quinolin-4-amine (8). Prepared using General Procedure (ii) with 3.00 mmol **5**, 1.02 mmol **6b**. Yield = 38% (0.195 g). ^{1}H NMR (CHLOROFORM-d, 400 MHz) δ 8.69 (s, 1H), 8.06 (d, 1H, *J*=2.1 Hz), 7.70 (d, 1H, *J*=9.1 Hz), 7.45 (d, 2H, *J*=7.4 Hz), 7.3-7.3 (m, 3H), 7.2-7.3 (m, 1H), 6.79 (s, 4H), 6.00 (s, 1H), 3.8-3.9 (m, 4H, *J*=3.9, 5.6 Hz), 3.1-3.1 (m, 4H). HRMS (ESI) - *m/z* of [$C_{26}H_{22}ClF_3N_3O_2^+$]: 500.1354, actual: 500.1347.

4-benzyl-3-(4-bromophenyl)morpholine (10a). Prepared using General Procedure (iii) with 9.89 mmol **9a**. Yield = 85% (2.780 g). ^{1}H-NMR (DMSO-d_6, 400 MHz): δ 7.53-7.50 (m, 2H), 7.35-7.26 (m, 7H), 4.50 (dd, *J* = 10.2, 2.3 Hz, 1H), 3.94-3.90 (m, 1H), 3.66 (td, *J* = 11.4, 2.4 Hz, 1H), 3.55-3.47 (m, 2H), 2.85-2.82 (m, 1H), 2.70-2.67 (m, 1H), 2.15 (td, *J* = 11.5, 3.3 Hz, 1H), 1.94 (dd, *J* = 11.3, 10.3 Hz, 1H).

3-(4-bromophenyl)-4-ethylmorpholine (10b). Prepared using General Procedure (iv) with 20.6 mmol **9a**. Yield = 60% (4.123 g). ^{1}H-NMR (CHLOROFORM-d, 400 MHz): δ 7.47 (d, *J* = 8.6 Hz, 2H), 7.27 (d, *J* = 8.1 Hz, 2H), 3.98-3.94 (m, 1H), 3.80-3.74 (m, 1H), 3.69 (ddd, *J* = 10.7, 2.8, 1.1 Hz, 1H), 3.38-3.28 (m, 2H), 3.00 (d, *J* = 11.8 Hz, 1H), 2.60-2.51 (m, 1H), 2.37 (td, *J* = 11.7, 3.4 Hz, 1H), 2.03 (dq, *J* = 13.0, 6.6 Hz, 1H), 0.97 (t, *J* = 7.2 Hz, 3H).

4-benzyl-2-(4-bromophenyl)morpholine (10c). Prepared using General Procedure (iii) with 3.99 mmol **9b**. Yield = 70% (2.809 g). ^{1}H-NMR (DMSO-d_6, 400 MHz): δ 7.59 (d, *J* = 8.6 Hz, 2H), 7.48 (d, *J* = 8.3 Hz, 2H), 7.33-7.21 (m, 5H), 3.78 (dt, *J* = 11.3, 1.5 Hz, 1H), 3.68-3.64 (m, 1H), 3.60 (d, *J* = 13.4 Hz, 1H), 3.53 (td, *J* = 11.5, 2.3 Hz, 1H), 3.40 (dd, *J* = 10.1, 3.3 Hz, 1H), 3.27 (d, *J* = 11.0 Hz, 1H), 2.93 (d, *J* = 13.4 Hz, 1H), 2.64 (d, *J* = 11.8 Hz, 1H), 2.20 (td, *J* = 11.8, 3.3 Hz, 1H).

1-benzyl-4-(4-bromophenyl)piperazine (10d). Prepared using General Procedure (iii) with 4.00 mmol **9c**. Yield = 35% (0.461 g). ^{1}H-NMR (DMSO-d_6, 400 MHz): δ 7.35-7.31 (m, 6H), 7.29-7.25 (m, 1H), 6.90-6.86 (m, 2H), 3.52 (s, 2H), 3.14-3.11 (m, 4H), 2.51-2.48 (m, 4H).

4-(4-benzylmorpholin-3-yl)aniline (11a). Prepared using General Procedure (v) with 7.75 mmol **10a**. Yield = 81% (1.638 g). ^{1}H-NMR (DMSO-d_6, 400 MHz): δ 7.33-7.30 (m, 4H), 7.27-7.23 (m, 1H), 6.95 (d, *J* = 8.3 Hz, 2H), 6.48 (d, *J* = 8.5 Hz, 2H), 4.99 (s, 2H), 4.26 (dd, *J* = 10.2, 2.1 Hz, 1H), 3.87-3.84 (m, 1H), 3.61 (td, *J* = 11.4, 2.3 Hz, 1H), 3.49 (s, 2H), 2.70-2.65 (m, 2H), 2.12 (td, *J* = 11.5, 3.3 Hz, 1H), 1.96 (dd, *J* = 11.2, 10.5 Hz, 1H).

4-(4-ethylmorpholin-3-yl)aniline (11b). Prepared using General Procedure (v) with 9.30 mmol **10b**. Yield = 76% (1.467 g). ^{1}H-NMR (DMSO-d_6, 400 MHz): δ 6.97 (d, *J* = 8.3 Hz, 2H), 6.51 (d, *J* = 8.5 Hz, 2H), 4.97 (s, 2H), 3.82 (dt, *J* = 11.1, 1.6 Hz, 1H), 3.56 (td, *J* = 11.4, 2.3 Hz, 1H), 3.50-3.46 (m, 1H), 3.17 (t, *J* = 10.6 Hz, 1H), 3.02 (dd, *J* = 10.2, 3.4 Hz, 1H), 2.91-2.87 (m, 1H), 2.49-2.45 (m, 1H), 2.17 (td, *J* = 11.7, 3.4 Hz, 1H), 1.90 (dq, *J* = 12.9, 6.6 Hz, 1H), 0.86 (t, *J* = 7.2 Hz, 3H).

4-(4-benzylmorpholin-2-yl)aniline (11c). Prepared using General Procedure (v) with 2.72 mmol **10c**. Yield = 86% (0.625 g). ^{1}H-NMR (CHLOROFORM-d, 400 MHz): δ 8.51 (d, *J* = 5.3 Hz, 1H), 8.03 (d, *J* = 2.1 Hz, 1H), 7.85 (d, *J* = 8.9 Hz, 1H), 7.46 (dd, *J* = 8.9, 2.2 Hz, 1H), 7.23-7.20 (m, 2H), 7.03-6.99 (m, 2H), 6.72 (d, *J* = 5.3 Hz, 1H), 6.52 (s, 1H), 3.25 (t, *J* = 5.1 Hz, 4H), 2.60 (t, *J* = 5.0 Hz, 4H), 2.18 (d, *J* = 7.4 Hz, 2H), 1.91-1.81 (m, 1H), 0.96 (d, *J* = 6.6 Hz, 6H).

4-(4-benzylpiperazin-1-yl)aniline (11d). Prepared using General Procedure (v) with 1.50 mmol **10d**. Yield = 69% (0.278 g). ^{1}H-NMR (METHANOL-d_4, 400 MHz): δ 7.40-7.33 (m, 4H), 7.30 (dd, *J* = 5.4, 3.5 Hz, 1H), 6.89-6.79 (m, 4H), 3.61 (s, 2H), 3.15 (t, *J* = 5.0 Hz, 4H), 2.66 (t, *J* = 5.0 Hz, 4H).

N-(4-(4-benzylmorpholin-3-yl)phenyl)-7-chloroquinolin-4-amine (12). Prepared using General Procedure (ii) with 0.930 **11a** and 0.606 mmol **6a**. Yield = 24% (0.062 g). ^{1}H NMR (CHLOROFORM-d, 400 MHz) δ 8.56 (d, 1H, *J*=5.3 Hz), 8.03 (d, 1H, *J*=2.1 Hz), 7.85 (d, 1H, *J*=9.0 Hz), 7.5-7.6 (m, 2H), 7.46 (dd, 1H, *J*=2.2, 8.9 Hz), 7.3-7.3 (m, 6H), 7.2-7.3 (m, 1H), 6.98 (d, 1H, *J*=5.3 Hz), 6.61 (s, 1H), 3.8-3.9 (m, 2H), 3.81 (d, 1H, *J*=8.6 Hz), 3.7-3.8 (m, 1H), 3.48 (s, 2H), 2.94 (d, 1H, *J*=13.4 Hz), 2.8-2.8 (m, 1H, *J*=11.9 Hz), 2.31 (dt, 1H, *J*=3.4, 11.8 Hz). HRMS (ESI) - *m/z* of [$C_{26}H_{25}ClN_3O^+$]: 430.1687, actual: 430.1679.

7-chloro-N-(4-(4-ethylmorpholin-3-yl)phenyl)quinolin-4-amine (13). Prepared using General Procedure (ii) with 0.507 mmol **11b** and 1.52 mmol **6a**. Yield = 18% (0.062 g). ^{1}H NMR (CHLOROFORM-d, 400 MHz) δ 8.57 (d, 1H, *J*=5.4 Hz), 8.03 (d, 1H, *J*=2.1 Hz), 7.85 (d, 1H, *J*=9.0 Hz), 7.45 (dd, 1H, *J*=2.2, 8.9 Hz), 7.41 (d, 2H, *J*=8.3 Hz), 7.27 (s, 1H), 7.24 (s, 1H), 6.98 (d, 1H, *J*=5.3 Hz), 6.63 (br s, 1H), 3.9-4.0 (m, 1H), 3.76 (dq, 2H, *J*=2.3, 11.3 Hz), 3.4-3.4 (m, 1H, *J*=10.9, 10.9 Hz), 3.3-3.4 (m, 1H), 3.00 (br d, 1H, *J*=11.6 Hz), 2.62 (qd, 1H, *J*=7.4, 12.7 Hz),

2.37 (dt, 1H, *J*=3.4, 11.7 Hz), 2.06 (s, 1H), 0.99 (t, 3H, *J*=7.2 Hz). HRMS (ESI) - *m/z* of [$C_{21}H_{23}ClN_3O^+$]: 368.1529, actual: 368.1522.

7-chloro-N-(4-(4-ethylmorpholin-3-yl)phenyl)-3-(4-(trifluoromethoxy)phenyl)quinolin-4-amine (14). Prepared using General Procedure (ii) with 0.946 **11b** and 0.605 mmol **6b**. Yield = 18% (0.057 g). ^{1}H NMR (CHLOROFORM-d, 400 MHz) δ 8.75 (s, 1H), 8.10 (s, 1H), 7.76 (d, 1H, *J*=9.0 Hz), 7.4-7.4 (m, 2H), 7.35 (br d, 1H, *J*=9.0 Hz), 7.3-7.3 (m, 1H), 7.2-7.3 (m, 1H), 7.15 (br d, 2H, *J*=7.8 Hz), 6.71 (br d, 2H, *J*=8.1 Hz), 6.08 (s, 1H), 3.93 (br d, 1H, *J*=11.0 Hz), 3.7-3.8 (m, 1H), 3.6-3.7 (m, 1H), 3.32 (br t, 1H, *J*=10.8 Hz), 3.2-3.2 (m, 1H), 2.96 (br d, 1H, *J*=11.9 Hz), 2.5-2.6 (m, 1H), 2.3-2.4 (m, 1H), 1.9-2.0 (m, 1H), 0.95 (br t, 3H, *J*=7.1 Hz). HRMS (ESI) - *m/z* of [$C_{28}H_{26}ClF_3N_3O_2^+$]: 528.1667, actual: 528.1662.

N-(4-(4-benzylmorpholin-2-yl)phenyl)-7-chloroquinolin-4-amine (15). Prepared using General Procedure (ii) with 0.904 **11c** and 0.602 mmol **6a**. Yield = 21% (0.054 g). ^{1}H NMR (CHLOROFORM-d, 400 MHz) δ 8.54 (d, 1H, *J*=5.3 Hz), 8.03 (d, 1H, *J*=2.1 Hz), 7.85 (d, 1H, *J*=9.0 Hz), 7.4-7.5 (m, 3H), 7.3-7.4 (m, 5H), 7.26 (s, 2H), 7.2-7.3 (m, 2H), 6.92 (d, 1H, *J*=5.4 Hz), 6.59 (s, 1H), 4.60 (dd, 1H, *J*=2.3, 10.2 Hz), 4.0-4.1 (m, 1H), 3.86 (dt, 1H, *J*=2.4, 11.4 Hz), 3.57 (s, 2H), 2.94 (td, 1H, *J*=1.9, 11.4 Hz), 2.7-2.8 (m, 1H), 2.31 (dt, 1H, *J*=3.4, 11.5 Hz), 2.1-2.2 (m, 1H). HRMS (ESI) - *m/z* of [$C_{26}H_{25}ClN_3O^+$]: 430.1687, actual: 430.1682.

N-(4-(4-benzylmorpholin-2-yl)phenyl)-7-chloro-3-(4-(trifluoromethoxy)phenyl)quinolin-4-amine (16). Prepared using General Procedure (ii) with 0.933 mmol **11c** and 0.602 mmol **6b**. Yield = 33% (0.117 g). ^{1}H NMR (DMSO-d_6, 400 MHz) δ 8.75 (s, 1H), 8.71 (s, 1H), 8.23 (d, 1H, *J*=9.1 Hz), 8.04 (d, 1H, *J*=2.1 Hz), 7.61 (dd, 1H, *J*=2.3, 9.0 Hz), 7.4-7.5 (m, 2H), 7.2-7.4 (m, 7H), 6.92 (d, 2H, *J*=8.4 Hz), 6.6-6.6 (m, 2H, *J*=8.6 Hz), 4.27 (dd, 1H, *J*=1.8, 10.1 Hz), 3.85 (dd, 1H, *J*=1.9, 11.3 Hz), 3.59 (dt, 1H, *J*=2.1, 11.4 Hz), 3.4-3.5 (m, 2H), 2.65 (br d, 2H, *J*=11.6 Hz), 2.09 (dt, 1H, *J*=3.2, 11.5 Hz), 1.84 (t, 1H, *J*=10.9 Hz). HRMS (ESI) - *m/z* of [$C_{33}H_{28}ClF_3N_3O_2^+$]: 590.1825, actual: 590.1816.

N-(4-(4-benzylpiperazin-1-yl)phenyl)-7-chloroquinolin-4-amine (17). Prepared using General Procedure (ii) with 0.904 mmol **11d** and 0.642 mmol **6a**. Yield = 46% (0.125 g). ^{1}H NMR (CHLOROFORM-d, 400 MHz) δ 8.48 (d, 1H, *J*=5.3 Hz), 8.01 (d, 1H, *J*=2.1 Hz), 7.82 (d, 1H, *J*=9.0 Hz), 7.43 (dd, 1H, *J*=2.2, 8.9 Hz), 7.3-7.4 (m, 5H), 7.1-7.2 (m, 2H), 6.9-7.0 (m, 2H), 6.69 (d, 1H, *J*=5.4 Hz), 6.48 (s, 1H), 3.59 (s, 2H), 3.2-3.3 (m, 4H), 2.6-2.7 (m, 4H). HRMS (ESI) – *m/z* of [$C_{26}H_{26}ClN_4^+$]: 429.1840, actual: 429.1840.

7-chloro-N-(4-(4-ethylpiperazin-1-yl)phenyl)quinolin-4-amine (20). Prepared using General Procedure (i) with 1.50 mmol **18a** and 1.68 mmol **6a**. Yield = 42% (0.287 g). ^{1}H NMR (CHLOROFORM-d, 400 MHz) δ 8.48 (d, 1H, *J*=5.3 Hz), 8.00 (d, 1H, *J*=2.1 Hz), 7.83 (d, 1H, *J*=9.0 Hz), 7.43 (dd, 1H, *J*=2.2, 8.9 Hz), 7.2-7.2 (m, 2H), 6.9-7.0 (m, 2H), 6.70 (d, 1H, *J*=5.4 Hz), 6.50 (s, 1H), 3.2-3.3 (m, 4H), 2.6-2.7 (m, 4H), 2.50 (q, 2H, *J*=7.2 Hz), 1.15 (t, 3H, *J*=7.2 Hz). HRMS (ESI) - *m/z* of [$C_{21}H_{24}ClN_4^+$]: 367.1689, actual: 367.1687.

7-chloro-N-(4-(4-methylpiperazin-1-yl)phenyl)quinolin-4-amine (21). Prepared using General Procedure (i) with 1.50 mmol **18b** and 1.65 mmol **6a**. Yield = 57% (0.300 g). ^{1}H NMR (CHLOROFORM-d, 400 MHz) δ 8.48 (d, 1H, *J*=5.3 Hz), 8.00 (d, 1H, *J*=2.0 Hz), 7.83 (d, 1H, *J*=9.0 Hz), 7.43 (dd, 1H, *J*=2.2, 8.9 Hz), 7.2-7.2 (m, 2H), 6.9-7.0 (m, 2H), 6.70 (d, 1H, *J*=5.4 Hz), 6.53 (s, 1H), 3.2-3.3 (m, 4H), 2.6-2.6 (m, 4H), 2.37 (s, 3H). HRMS (ESI) - *m/z* of [$C_{20}H_{22}ClN_4^+$]: 353.1533, actual: 353.1526.

6-chloro-N-(4-(4-ethylpiperazin-1-yl)phenyl)quinolin-4-amine (22). Prepared using General Procedure (vi) with 1.01 mmol **18a** and 1.21 mmol **19a**. Yield = 62% (0.232 g). ^{1}H NMR (METHANOL-d_4, 400 MHz) δ 8.32 (d, 1H, *J*=5.5 Hz), 8.28 (dd, 1H, *J*=0.8, 8.4 Hz), 7.8-7.9 (m, 1H), 7.71 (ddd, 1H, *J*=1.3, 6.9, 8.4 Hz), 7.53 (ddd, 1H, *J*=1.3, 7.0, 8.4 Hz), 7.3-7.3 (m, 2H), 7.1-7.1 (m, 2H), 6.72 (d, 1H, *J*=5.5 Hz), 3.3-3.3 (m, 3H), 2.7-2.7 (m, 4H), 2.54 (q, 2H, *J*=7.3 Hz), 1.19 (t, 3H, *J*=7.3 Hz). HRMS (ESI) - *m/z* of [$C_{21}H_{25}N_4^+$]: 333.2079, actual: 333.2074.

N-(4-(4-ethylpiperazin-1-yl)phenyl)quinolin-4-amine (23). Prepared using General Procedure (i) with 1.01 mmol **18a** and 1.21 mmol **19b**. Yield = 11% (0.036 g). ^{1}H NMR (CHLOROFORM-d, 400 MHz) δ 8.48 (d, 1H, *J*=5.3 Hz), 7.96 (d, 1H, *J*=9.0 Hz), 7.89 (d, 1H, *J*=2.3 Hz), 7.60 (dd, 1H, *J*=2.2, 8.9 Hz), 7.2-7.2 (m, 2H), 7.0-7.0 (m, 2H), 6.73 (d, 1H, *J*=5.3 Hz), 6.40 (s, 1H), 3.2-3.3 (m, 4H), 2.6-2.7 (m, 4H), 2.50 (q, 2H, *J*=7.2 Hz), 1.15 (t, 3H, *J*=7.2 Hz). HRMS (ESI) - *m/z* of [$C_{21}H_{24}ClN_4^+$]: 367.1689, actual: 367.1686. HRMS (ESI) – *m/z* of [$C_{21}H_{23}Cl_2N_4^+$]: 401.1294, actual: 401.1294.

6,7-dichloro-N-(4-(4-ethylpiperazin-1-yl)phenyl)quinolin-4-amine (24). Prepared using General Procedure (i) with 1.01 mmol **18a** and 1.02 mmol **19c**. Yield = 6.9% (0.028 g). ^{1}H NMR (DMSO-d_6, 400 MHz) δ 8.99 (s, 1H), 8.75 (s, 1H), 8.40 (d, 1H, *J*=5.4 Hz), 8.07 (s, 1H), 7.2-7.2 (m, 2H, *J*=8.0 Hz), 7.0-7.1 (m, 2H, *J*=8.1 Hz), 6.66 (d, 1H, *J*=5.4 Hz), 3.1-3.2 (m, 4H), 2.4-2.4 (m, 2H), 1.05 (t, 3H, *J*=7.2 Hz)

7-bromo-N-(4-(4-ethylpiperazin-1-yl)phenyl)quinolin-4-amine (25). Prepared using General Procedure (vi) with 1.00 mmol **18a** and 1.30 mmol **19d**. Yield = 22% (0.093 g). ^{1}H NMR (DMSO-d_6, 400 MHz) δ 8.93 (s, 1H), 8.3-8.4 (m, 2H), 8.01 (d, 1H, *J*=2.1 Hz), 7.64 (dd, 1H, *J*=2.1, 9.0 Hz), 7.20 (d, 2H, *J*=8.9 Hz), 7.01 (d, 2H, *J*=9.0 Hz), 6.64 (d, 1H, *J*=5.4 Hz), 3.1-3.2 (m, 4H), 2.5-2.6 (m, 4H), 2.38 (d, 2H, *J*=7.3 Hz), 1.04 (t, 3H, *J*=7.2 Hz). HRMS (ESI) - *m/z* of [$C_{21}H_{24}BrN_4^+$]: 413.1160, actual: 413.1160.

N-(4-(4-ethylpiperazin-1-yl)phenyl)-7-(trifluoromethyl)-quinolin-4-amine (26). Prepared using General Procedure (vi) with 0.63 mmol **18a** and 0.64 mmol **19e**. Yield = 46% (0.141 g). ^{1}H NMR (DMSO-d_6, 400 MHz) δ 9.0-9.1 (m, 1H), 8.6-8.7 (m, 1H), 8.4-8.5 (m, 1H), 8.1-8.2 (m, 1H), 7.76 (dd, 1H, *J*=1.8, 8.9 Hz), 7.2-7.2 (m, 2H), 7.0-7.1 (m, 2H), 6.7-6.8 (m, 1H), 3.1-3.2 (m, 4H), 2.5-2.5 (m, 4H), 2.3-2.5 (m, 2H), 1.05 (t, 3H, *J*=7.2 Hz). HRMS (ESI) - *m/z* of [$C_{22}H_{24}F_3N_4^+$]: 401.1953, actual: 401.1948.

1-(tert-butyl)-4-(4-nitrophenyl)piperazine (29a). Prepared using General Procedure (vii) with 5.5 mmol **27** and 6.0 mmol **28a**. Yield = 53% (0.773 g). ^{1}H-NMR (CHLOROFORM-d, 400 MHz): δ 8.14-8.10 (m, 2H), 6.83-6.79 (m, 2H), 3.42-3.40 (m, 4H), 2.73-2.70 (m, 4H), 1.11 (s, 9H).

1-(4-nitrophenyl)-4-(4-(trifluoromethyl)phenyl)piperazine (29b). Prepared using General Procedure (vii) with 18.0 mmol **27** and 19.8 mmol **28b**. Yield = 20% (1.254 g). ^{1}H-NMR (CHLOROFORM-d, 400 MHz): δ 8.21-8.17 (m, 2H), 7.55 (d, *J* = 8.6 Hz, 2H), 6.97 (d, *J* = 8.7 Hz, 2H), 6.91-6.87 (m, 2H), 3.64 (dd, *J* = 6.5, 4.1 Hz, 4H), 3.51 (dd, *J* = 6.5, 4.1 Hz, 4H).

4-(4-(tert-butyl)piperazin-1-yl)aniline (30a). Prepared using General Procedure (viii) with 2.62 mmol **29a.** Yield = 56%. ^{1}H-NMR (CHLOROFORM-d, 400 MHz): δ 6.82 (d, *J* = 8.8 Hz, 2H), 6.65 (d, *J* = 8.8 Hz, 2H), 3.41 (s, 1H), 3.06 (t, *J* = 4.9 Hz, 4H), 2.74 (t, *J* = 4.9 Hz, 4H), 1.11 (s, 9H).

4-(4-(4-(trifluoromethyl)phenyl)piperazin-1-yl)aniline (30b). Prepared using General Procedure (viii) with 3.57 mmol **29b**. Yield = 53% (0.773 g). ^{1}H-NMR (CHLOROFORM-d, 400 MHz): δ 7.54-7.51 (m, 2H), 7.02-6.98 (m, 2H), 6.90-6.87 (m, 2H), 6.72-6.69 (m, 2H), 3.50 (s, 1H), 3.46-3.43 (m, 4H), 3.22-3.19 (m, 4H).

N-(4-(4-(tert-butyl)piperazin-1-yl)phenyl)-7-chloroquinolin-4-amine (31). Prepared using General Procedure (vi) with 0.88 mmol **30a** and 1.01 mmol **6a**. Yield = 18% (0.072 g). ^{1}H NMR (CHLOROFORM-d, 400 MHz) δ 8.48 (d, 1H, *J*=5.4 Hz), 8.01 (d, 1H, *J*=2.1 Hz), 7.83 (d, 1H, *J*=9.0 Hz), 7.43 (dd, 1H, *J*=2.2, 8.9 Hz), 7.1-7.2 (m, 2H), 6.9-7.0 (m, 2H), 6.70 (d, 1H, *J*=5.4 Hz), 6.50 (s, 1H), 3.2-3.3 (m, 4H), 2.7-2.8 (m, 4H), 1.14 (s, 9H). HRMS (ESI) - *m/z* of [$C_{23}H_{28}ClN_4^+$]: 395.2003, actual: 395.2000.

7-chloro-N-(4-(4-(4-(trifluoromethyl)phenyl)piperazin-1-yl)phenyl)quinolin-4-amine (32). Prepared using General Procedure (vi) with 0.63 mmol **30b** and 0.64 mmol **6a**. Yield = 46% (0.141 g). ^{1}H NMR (CHLOROFORM-d, 400 MHz) δ 8.50 (d, 1H, *J*=5.3 Hz), 8.02 (d, 1H, *J*=2.1 Hz), 7.84 (d, 1H, *J*=9.0 Hz), 7.53 (d, 2H, *J*=8.6 Hz), 7.44 (dd, 1H, *J*=2.1, 8.9 Hz), 7.2-7.3 (m, 2H), 7.0-7.1 (m, 2H), 7.00 (d, 2H, *J*=8.6 Hz), 6.72 (d, 1H, *J*=5.4 Hz), 6.53 (s, 1H), 3.4-3.5 (m, 4H), 3.3-3.4 (m, 4H). HRMS (ESI) - *m/z* of [$C_{26}H_{23}ClF_3N_4^+$]: 483.1564, actual: 483.1562.

7-chloro-N-(4-(4-cyclopropylpiperazin-1-yl)phenyl)quinolin-4-amine (33). Prepared using General Procedure (i) with 1.50 mmol **30c** and 0.78 mmol **6a**. Yield = 6% (0.019 g). ^{1}H-NMR (DMSO-d_6, 400 MHz): δ 8.91 (s, 1H), 8.41 (d, *J* = 9.1 Hz, 1H), 8.37 (d, *J* = 5.4 Hz, 1H), 7.85 (d, *J* = 2.2 Hz, 1H), 7.53 (dd, *J* = 9.0, 2.3 Hz, 1H), 7.22-7.18 (m, 2H), 7.03-6.99 (m, 2H), 6.63 (d, *J* = 5.4 Hz, 1H), 3.11 (t, *J* = 5.0 Hz, 4H), 2.69 (t, *J* = 5.0 Hz, 4H), 1.67 (tt, *J* = 6.7, 3.4 Hz, 1H), 0.48-0.43 (m, 2H), 0.37-0.34 (m, 2H). HRMS (ESI) - *m/z* of [$C_{22}H_{24}ClN_4^+$]: 379.1690, actual: 379.1685.

7-chloro-N-(4-(piperidin-1-yl)phenyl)quinolin-4-amine (34). Prepared using General Procedure (i) with 1.00 mmol **30d** and 1.14 mmol **6a**. Yield = 15% (0.052 g). ^{1}H NMR (DMSO-d_6, 400 MHz) δ 8.91 (s, 1H), 8.42 (d, 1H, *J*=9.0 Hz), 8.3-8.4 (m, 1H), 7.85 (d, 1H, *J*=2.3 Hz), 7.53 (dd, 1H, *J*=2.3, 9.0 Hz), 7.1-7.2 (m, 2H), 7.0-7.1 (m, 2H), 6.62 (d, 1H, *J*=5.4 Hz), 3.1-3.2 (m, 4H), 1.64 (br d, 4H, *J*=5.1 Hz), 1.5-1.6 (m, 2H). HRMS (ESI) - *m/z* of [$C_{20}H_{21}ClN_3^+$]: 338.1424, actual: 338.1419.

7-chloro-N-(4-(1-isopropylpiperidin-4-yl)phenyl)quinolin-4-amine (35). Prepared using General Procedure (i) with 1.10 mmol **30e** and 1.0 mmol **6a**. Yield = 29% (0.111 g). ^{1}H NMR (METHANOL-d_4, 400 MHz) δ 8.35 (d, 1H, *J*=5.6 Hz), 8.29 (d, 1H, *J*=9.0 Hz), 7.85 (d, 1H, *J*=2.0 Hz), 7.49 (dd, 1H, *J*=2.1, 9.0 Hz), 7.3-7.4 (m, 4H), 6.86 (d, 1H, *J*=5.6 Hz), 3.1-3.1 (m, 2H), 2.8-2.9 (m, 1H), 2.62 (tt, 1H, *J*=3.9, 12.1 Hz), 2.4-2.5 (m, 2H), 1.9-2.0 (m, 2H), 1.8-1.9 (m, 2H), 1.16 (d, 6H, *J*=6.6 Hz). HRMS (ESI) - *m/z* of [$C_{23}H_{27}ClN_3^+$]: 380.1894, actual: 380.1890.

tert-butyl 4-(4-((7-chloroquinolin-4-yl)amino)phenyl)-piperazine-1-carboxylate (36). Prepared using General Procedure (ix) with 5.52 mmol **30f** and 5.53 mmol **6a**. Yield = 69% (1.672 g). ^{1}H NMR (CHLOROFORM-d, 400 MHz) δ 8.49 (d, 1H, *J*=5.3 Hz), 8.01 (d, 1H, *J*=2.1 Hz), 7.84 (d, 1H, *J*=9.0 Hz), 7.44 (dd, 1H, *J*=2.1, 9.0 Hz), 7.2-7.2 (m, 2H), 7.0-7.0 (m, 2H), 6.71 (d, 1H, *J*=5.3 Hz), 6.51 (s, 1H), 3.6-3.7 (m, 4H), 3.1-3.2 (m, 5H), 1.5-1.5 (m, 9H). HRMS (ESI) - *m/z* of [$C_{24}H_{28}ClN_4O_2^+$]: 439.1901, actual: 439.1899.

tert-butyl 4-(4-((7-chloroquinolin-4-yl)amino)phenyl)-piperidine-1-carboxylate (37). Prepared using General Procedure (ix) with 5.80 mmol **30f** and 5.81 mmol **6a**. Yield = 87% (2.210 g). ^{1}H-NMR (DMSO-d_6, 400 MHz): δ 9.04 (s, 1H), 8.45-8.41 (m, 2H), 7.89 (d, *J* = 2.2 Hz, 1H), 7.57 (dd, *J* = 9.0, 2.3 Hz, 1H), 7.33-7.28 (m, 4H), 6.87 (d, *J* = 5.4 Hz, 1H), 4.09 (d, *J* = 11.7 Hz, 2H), 2.83-2.67 (m, 3H), 1.79 (d, *J* = 13.2 Hz, 2H), 1.56-1.45 (m, 2H), 1.43 (s, 9H).

7-chloro-N-(4-(piperazin-1-yl)phenyl)quinolin-4-amine (38). Prepared using general procedure (x) with 3.42 mmol **36**. Yield = 40% (0.464 g) ^{1}H-NMR (CHLOROFORM-d, 400 MHz): δ 8.54 (d, *J* = 5.3 Hz, 1H), 8.03 (d, *J* = 2.1 Hz, 1H), 7.85 (d, *J* = 9.0 Hz, 1H), 7.46 (dd, *J* = 9.0, 2.2 Hz, 1H), 7.30-7.27 (m, 2H), 7.25-7.22 (m, 2H), 6.91 (d, *J* = 5.3 Hz, 1H), 6.55 (dd, *J* = 2.6, 0.3 Hz, 1H), 3.24-3.20 (m, 2H), 2.80-2.74 (m, 2H), 2.66-2.63 (m, 1H), 1.89-1.84 (m, 2H), 1.72-1.62 (m, 2H). HRMS (ESI) - *m/z* of [$C_{19}H_{20}ClN_4^+$]: 339.1376, actual: 339.1372.

7-chloro-N-(4-(piperidin-4-yl)phenyl)quinolin-4-amine (39). Prepared using general procedure (x) with 3.51 mmol **37**. Yield = 69%. ^{1}H NMR (CHLOROFORM-d, 400 MHz) δ 8.54 (d, 1H, *J*=5.3 Hz), 8.03 (d, 1H, *J*=2.1 Hz), 7.85 (d, 1H, *J*=9.0 Hz), 7.45 (dd, 1H, *J*=2.2, 8.9 Hz), 7.3-7.3 (m, 2H), 7.2-7.3 (m, 2H), 6.91 (d, 1H, *J*=5.3 Hz), 6.58 (s, 1H), 3.22 (br d, 2H, *J*=11.8 Hz), 2.77 (dt, 2H, *J*=2.3, 12.1 Hz), 2.65 (s, 1H), 1.8-1.9 (m, 2H), 1.7-1.7 (m, 2H). HRMS (ESI) - *m/z* of [$C_{20}H_{21}ClN_3^+$]: 338.1424, actual: 338.1419.

7-chloro-N-(4-(1-ethylpiperidin-4-yl)phenyl)quinolin-4-amine (40). Title compound prepared using General Procedure (xi) with 1.00 mmol **39** and 1.12 mmol iodoethane. Yield =: 30% (0.108 g). ^{1}H NMR (METHANOL-d_4, 400 MHz) δ 8.37 (d, 1H, *J*=5.5 Hz), 8.30 (d, 1H, *J*=9.0 Hz), 7.87 (d, 1H, *J*=2.1 Hz), 7.51 (dd, 1H, *J*=2.3, 9.0 Hz), 7.3-7.4 (m, 4H), 6.88 (d, 1H, *J*=5.5 Hz), 3.15 (br d, 2H, *J*=11.8 Hz), 2.64 (tt, 1H, *J*=4.0, 11.9 Hz), 2.54 (q, 2H, *J*=7.3 Hz), 2.17 (dt, 2H, *J*=2.6, 11.9 Hz), 1.9-2.0 (m, 2H), 1.8-1.9 (m, 2H), 1.18 (t, 3H, *J*=7.3 Hz). HRMS (ESI) - *m/z* of [$C_{22}H_{25}ClN_3^+$]: 366.1737, actual: 366.1732.

7-chloro-N-(4-(1-propylpiperidin-4-yl)phenyl)quinolin-4-amine (41). Title compound was prepared using General Procedure (xii) with 1.00 mmol **39** and 1.2 mmol iodopropane. Yield =: 26% (0.099 g). ^{1}H NMR (DMSO-d_6, 400 MHz) δ 9.04 (s, 1H), 8.4-8.5 (m, 2H), 7.88 (d, 1H, *J*=2.1 Hz), 7.56 (dd, 1H, *J*=2.2, 9.1 Hz), 7.3-7.3 (m, 4H), 6.86 (d, 1H, *J*=5.4 Hz), 2.9-3.0 (m, 2H), 2.5-2.5 (m, 1H), 0.00 (t, 2H, *J*=7.4 Hz), 1.9-2.0 (m, 2H), 1.7-1.8 (m, 2H), 1.6-1.7 (m, 2H), 1.46 (sxt, 2H, *J*=7.4 Hz), 0.00 (t, 3H, *J*=7.3 Hz). HRMS (ESI) - *m/z* of [$C_{24}H_{29}ClN_3^+$]: 394.2051, actual: 394.2046

N-(4-(1-butylpiperidin-4-yl)phenyl)-7-chloroquinolin-4-amine (42). Title compound was prepared using General Procedure (xii) with 1.00 mmol **39** and 1.2 mmol iodobutane. Yield =: 63% (0.249 g). ^{1}H NMR (DMSO-d_6, 400 MHz) δ 9.04 (s, 1H), 8.4-8.5 (m, 2H), 7.88 (d, 1H, *J*=2.3 Hz), 7.56 (dd, 1H, *J*=2.2, 9.1 Hz), 7.3-7.3 (m, 4H), 6.86 (d, 1H, *J*=5.4 Hz), 2.96 (br d, 2H, *J*=11.4 Hz), 2.4-2.5 (m, 1H), 2.28 (br t, 2H, *J*=7.1 Hz), 1.9-2.0 (m, 2H, *J*=2.0, 2.0, 2.0, 9.9, 9.9 Hz), 1.7-1.8 (m, 2H), 1.6-1.7 (m, 2H, *J*=3.5, 3.5, 3.5, 3.5, 8.6, 8.6, 8.6 Hz), 1.4-1.5 (m, 2H), 1.30 (sxtd, 2H, *J*=7.2, 14.8 Hz), 0.90 (t, 3H, *J*=7.3 Hz). HRMS (ESI) - *m/z* of [$C_{24}H_{29}ClN_3^+$]: 394.2051, actual: 394.2046.

7-chloro-N-(4-(1-isobutylpiperidin-4-yl)phenyl)quinolin-4-amine (43). Title compound was prepared using General Procedure (xii) with 1.00 mmol **39** and 2.03 mmol 1-iodo-2-methylpropane. Yield =: 43% (0.168 g). ^{1}H NMR (DMSO-d_6, 400 MHz) δ 9.04 (s, 1H), 8.4-8.5 (m, 2H), 7.88 (d, 1H, *J*=2.1 Hz), 7.56 (dd, 1H, *J*=2.3, 9.0 Hz), 7.3-7.3 (m, 4H), 6.86 (d, 1H,

J=5.4 Hz), 2.93 (br d, 2H, *J*=11.4 Hz), 2.4-2.5 (m, 1H), 2.06 (d, 2H, *J*=7.4 Hz), 1.9-2.0 (m, 2H), 1.7-1.8 (m, 3H), 1.6-1.7 (m, 2H), 0.88 (d, 6H, *J*=6.5 Hz). HRMS (ESI) - *m/z* of [$C_{24}H_{29}ClN_3^+$]: 394.2051, actual: 394.2045.

N-(4-(1-(sec-butyl)piperidin-4-yl)phenyl)-7-chloroquinolin-4-amine (44). Title compound was prepared using General Procedure (xii) with 1.01 mmol **39** and 1.2 mmol 2-iodobutane. Yield =: 50% (0.201 g). ^{1}H NMR (DMSO-d_6, 400 MHz) δ 9.04 (s, 1H), 8.4-8.4 (m, 2H), 7.88 (d, 1H, *J*=2.3 Hz), 7.56 (dd, 1H, *J*=2.3, 9.0 Hz), 7.2-7.3 (m, 4H), 6.85 (d, 1H, *J*=5.4 Hz), 2.7-2.9 (m, 2H), 2.4-2.5 (m, 2H), 2.39 (dt, 1H, *J*=2.3, 11.6 Hz), 2.1-2.3 (m, 1H), 1.77 (br d, 2H, *J*=12.9 Hz), 1.6-1.7 (m, 2H), 1.5-1.6 (m, 1H), 1.27 (dsxt, 1H, *J*=6.4, 7.4 Hz), 0.93 (d, 3H, *J*=6.5 Hz), 0.87 (t, 3H, *J*=7.4 Hz). HRMS (ESI) - *m/z* of [$C_{24}H_{29}ClN_3^+$]: 394.2051, actual: 394.2046.

7-chloro-N-(4-(4-isobutylpiperazin-1-yl)phenyl)quinolin-4-amine (45). Title compound was prepared using General Procedure (xii) with 0.50 mmol **38** and 1.20 mmol 1-iodo-2-methylpropane. Yield = 19% (0.037 g). ^{1}H NMR (CHLOROFORM-d, 400 MHz) δ 8.48 (d, 1H, *J*=5.3 Hz), 8.00 (d, 1H, *J*=2.1 Hz), 7.83 (d, 1H, *J*=9.0 Hz), 7.43 (dd, 1H, *J*=2.1, 8.9 Hz), 7.2-7.2 (m, 2H), 6.9-7.0 (m, 2H), 6.69 (d, 1H, *J*=5.4 Hz), 6.50 (s, 1H), 3.2-3.3 (m, 4H), 2.6-2.6 (m, 4H), 2.16 (d, 2H, *J*=7.4 Hz), 1.83 (quind, 1H, *J*=6.9, 13.6 Hz), 0.94 (d, 6H, *J*=6.6 Hz). HRMS (ESI) - *m/z* of [$C_{23}H_{28}ClN_4^+$]: 395.2003, actual: 395.1992.

E.2. Synthetic details of Compounds presented in Chapter 7

General Procedures can be found in

4-bromo-7-chloroquinoline (50). The title compound was prepared as described. In short, 20.20 g (112 mmol) of 7-chloro-4-hydroxyquinoline was charged to a 500 mL round bottom flask containing 250 mL DMF (0.45 M). Flask was equipped with a stir bar and placed in an ice bath, followed by the slow addition of phosphorus tribromide (12 mL, 1.1 equivalence) using an addition funnel and stirred overnight. Reaction mixture was decanted onto ice and saturated sodium bicarbonate was added until pH > 10. Crude product was extracted in a separatory funnel with 3 x 100 mL washes of ethyl acetate. Organic layers were combined and washed in a separatory funnel with water (2 x 200 mL), followed by aqueous saturated sodium chloride (2 x 100 mL). Resulting organic layer dried with magnesium sulfate and gravity filtered, the filtrate was then condensed in rotary evaporator. Crude material was recrystallized in hot ethyl acetate to form final product as white needle-like crystals. Yield = 80% (21.76 grams, 89.7 mmol). ^{1}H NMR (DMSO-d_6, 400 MHz) ppm: δ 8.78 (d, *J* = 4.7 Hz, 1H), 8.19 (d, *J* = 7.2 Hz, 1H), 8.18 (s, 1H), 8.00 (d, *J* = 4.7 Hz, 1H), 7.82 (dd, *J* = 8.9, 2.3 Hz, 1H).

N*^{4},*N*$^{4'}$-bis(7-chloroquinolin-4-yl)-[1,1'-biphenyl]-4,4'-diamine (51)**. The title compound was prepared using ***General Procedure (i) in the following proportions: 0.185 g (1.0 mmol) benzidine (**49a**), 0. 728 g (3.0 mmol, 3.0 equiv.) **50**, 0.189 g (1.95 mmol, 1.9 equiv.) phenol, and 10 mL dimethylformamide (0.1 M). Final product isolated as golden powder. Yield = 91%, 0.464 g (0.91 mmol).
^{1}H NMR (DMSO-d_6, 400 MHz) ppm: δ 9.26 (s, 1H), 8.57 (d, 1H, *J* = 5.4 Hz), 8.52 (d, 1H, *J* = 9.1 Hz), 7.98 (d, 1H, *J* = 2 3 Hz), 7.83 (d, 3H, *J* = 8.5 Hz), 7.66 (dd, 2H, *J* = 2.3, 9.0 Hz), 7.53 (d, 3H, *J* = 8.6 Hz), 7.11 (d, 1H, *J* = 5.3 Hz). HRAM/MS (ESI positive): $[M+H]^+$ of $[C_{30}H_{20}Cl_2N_4]$ = 507.11377; observed = 507.11375.

N*⁴,*N*⁴'-bis(7-chloroquinolin-4-yl)-2,2'-difluoro-[1,1'-biphenyl]-4,4'-diamine (52).** The title compound was prepared using ***General Procedure (i) in the following proportions: 0.225 g (1.0 mmol) 2,2'-difluoro-[1,1'-biphenyl]-4,4'-diamine (**49b**), 0.487 g (2.0 mmol, 2.0 equiv.) **50**, 0.177 g (1.88 mmol, 1.8 equiv.) phenol, and 5 mL dimethylformamide (0.2 M). Final product isolated as yellow solid. Yield = 90%, 0.488 g (0.90 mmol). ^{1}H NMR (DMSO-d_6, 400 MHz) δ ppm: 10.96 (br s, 2H), 8.74 (d, 2H, *J* = 9.1 Hz), 8.67 (d, 2H, *J* = 6.9 Hz), 8.09 (d, 2H, *J* = 2.0 Hz), 7.97 (dd, 2H, *J* = 2.0, 9.1 Hz), 7.74 (td, 2H, *J* = 4.4, 8.4 Hz), 7.6-7.6 (m, 2H), 7.52 (dd, 2H, *J* = 2.0, 8.3 Hz), 7.15 (d, 2H, *J* = 6.9 Hz). HRAM/MS (ESI positive): $[M+H]^+$ of $[C_{30}H_{18}Cl_2F_2N_4]$ = 543.09493; observed = 543.09516.

N*,*N*'-(methylenebis(4,1-phenylene))bis(7-chloroquinolin-4-amine) (53)**. The title compound was prepared using ***General Procedure (i) in the following proportions: 0.199 g (1.0 mmol) 4,4'-methylenedianiline (**49c**), 0.537 g (2.2 mmol, 2.2 equiv.) **50**, 0.281 g (3.00 mmol, 3 equiv.) phenol, and 3 mL dimethylformamide (0.33 M). Final product isolated as yellow-tan powder. Yield = 91%, 0.475 g (0.91 mmol). ^{1}H NMR (DMSO-d_6, 400 MHz) δ ppm: 9.95 (br s, 2H), 8.56 (d, 2H, *J* = 9.1 Hz), 8.48 (d, 2H, *J* = 6.1 Hz), 7.95 (d, 2H, *J* = 2.1 Hz), 7.74 (dd, 2H, *J* = 9.0, 1.9 Hz), 7.40 (q, 8H, *J* =8.9), 6.85 (d, 2H, *J* = 6.3 Hz), 4.06 (s, 2H). HRAM/MS (ESI positive): $[M+H]^+$ of $[C_{31}H_{22}Cl_2N_4]$ = 521.12942; observed = 521.12947.

N*¹-(7-chloroquinolin-4-yl)-*N*⁴-(4-((7-chloroquinolin-4-yl)amino)phenyl)benzene-1,4-diamine (54)**. The title compound was prepared using ***General Procedure (i) in the following proportions: 0.399 g (2.0 mmol) *N*¹-(4-aminophenyl)benzene-1,4-diamine (**49d**), 0.638 g (6.8 mmol, 3.4 equiv.) **50**, 1.170 g (4.8 mmol, 2.4 equiv.) phenol, and 10 mL dimethylformamide (0.2 M). Final product isolated as tan-brown solid. Yield = 46%, 0.486 g (0.93 mmol). ^{1}H NMR (DMSO-d_6, 400 MHz) δ ppm: 8.98 (s, 2H), 8.4-8.5 (m, 4H), 8.30 (s, 1H), 7.87 (d, 2H, *J* = 2.1 Hz), 7.55 (dd, 2H, *J* = 2.3, 9.0 Hz), 7.2-7.3 (m, 4H), 7.2-7.2 (m, 4H), 6.70 (d, 2H, *J* = 5.4 Hz). HRAM/MS (ESI positive): $[M+H]^+$ of $[C_{30}H_{21}Cl_2N_5]$ = 522.12467; observed = 522.12476.

N*,*N*'-(oxybis(4,1-phenylene))bis(7-chloroquinolin-4-amine) (55)**. The title compound was prepared using ***General Procedure (i) in the following proportions: 0.200 g (1.0 mmol) 4,4'-oxydianiline (**49e**), 0.5148 g (2.1 mmol, 2.1 equiv.) **50**, 0.308 g (3.3 mmol, 3.3 equiv.) phenol, and 3 mL dimethylformamide (0.33 M). Final product isolated as white powder. Yield = 91%, 0.477 g (0.91 mmol). ^{1}H NMR (DMSO-d_6, 400 MHz) δ ppm: 9.09 (s, 1H), 8.4-8.5 (m, 2H), 7.89 (d, 1H, *J* = 2.3 Hz), 7.58 (dd, 1H, *J* = 2.2, 9.1 Hz), 7.4-7.4 (m, 2H), 7.1-7.2 (m, 2H), 6.84 (d, 1H, *J* = 5.4 Hz). HRAM/MS (ESI negative): $[M-H]^-$ of $[C_{30}H_{20}Cl_2N_4O]$ = 521.09304; observed = 521.09434.

N*,*N*'-(propane-2,2-diylbis(4,1-phenylene))bis(7-chloroquinolin-4-amine) (56)**. The title compound was prepared using ***General Procedure (i) in the following proportions: 0.229 g (1.0 mmol) 4,4'-(propane-2,2-diyl)dianiline (**49f**), 0.539 g (2.2 mmol, 2.2 equiv.) **50**, 0.291 g (3.1 mmol, 3 equiv.) phenol, and 4 mL dimethylformamide (0.25 M). Final product isolated as gold-hued solid. Yield = 41%, 0.225 g (0.41 mmol). ^{1}H NMR (DMSO-d_6, 400 MHz) δ ppm: 9.05 (s, 2H), 8.4-8.5 (m, 4H), 7.89 (d, 2H, *J* = 2.1 Hz), 7.57 (dd, 2H, *J* = 2.3, 9.0 Hz), 7.3-7.4 (m, 8H), 6.91 (d, 2H, *J* = 5.4 Hz), 1.71 (s, 6H). HRAM/MS (ESI negative): $[M-H]^-$ of $[C_{33}H_{26}Cl_2N_4]$ = 547.14507; observed = 547.14650.

N*³,*N*⁶-bis(7-chloroquinolin-4-yl)-9H-carbazole-3,6-diamine (57)**. The title compound was prepared using ***General Procedure (i) in the following proportions: 0.205 g (1.0 mmol) 9*H*-

carbazole-3,6-diamine (**49g**), 0.538 g (2.2 mmol, 2.2 equiv.) **50**, 0.288 g (3.0 mmol, 3 equiv.) phenol, and 3 mL dimethylformamide (0.33 M). Final product isolated as brown solid. Yield = 37%, 0.201 g (0.39 mmol). ^{1}H-NMR (DMSO-d_6, 400 MHz) δ ppm: 11.44 (s, 1H), 9.17 (s, 2H), 8.50 (d, 2H, *J* = 9.1 Hz), 8.36 (d, 2H, *J* = 5.4 Hz), 8.13 (d, 2H, *J* = 1.9 Hz), 7.86 (d, 2H, *J* = 2.3 Hz), 7.60 (d, 2H, *J* = 8.5 Hz), 7.55 -7.58 (m, 2H), 7.36 – 7.44 (m, 2H), 6.64 (d, 2H, *J* = 5.4 Hz). HRAM/MS (ESI positive): $[M+H]^+$ of $[C_{30}H_{19}Cl_2N_5]$ = 520.10907; observed = 520.10907.

N*,*N*'-(oxybis(3-(trifluoromethyl)-4,1-phenylene))bis(7-chloroquinolin-4-amine) (58)**. The title compound was prepared using ***General Procedure (i) in the following proportions: 0.338 g (1.0 mmol) 4,4'-oxybis(3-(trifluoromethyl)aniline) (**49h**), 0.536 g (2.2 mmol, 2.2 equiv.) **50**, 0.291 g (3.00 mmol, 3 equiv.) phenol, and 3 mL dimethylformamide (0.33 M). Final product isolated as white solid. Yield = 48%, 0.319 g (0.48 mmol). ^{1}H-NMR (DMSO-d_6, 400 MHz) δ ppm: 9.30 (s, 2H), 8.53 (d, 2H, *J* = 5.3 Hz), 8.40 (d, 2H, *J* = 9.1 Hz), 7.93 (d, 2H, *J* = 2.0 Hz), 7.76 (d, 2H, *J* = 2.3 Hz), 7.7-7.7 (m, 2H), 7.63 (dd, 2H, *J* = 9.0, 2.1 Hz), 7.23 (d, 2H, *J* = 8.8 Hz), 7.01 (b d, 2H *J* = 5.0 Hz). HRAM/MS (ESI positive): $[M+H]^+$ of $[C_{32}H_{18}Cl_2F_6N_4O]$ = 659.08375; observed = 659.08375.

1,1'-bis(7-chloroquinolin-4-yl)-4,4'-bipiperidine (60). The title compound was prepared using ***General Procedure (i)*** in the following proportions: 0.563 g (2.1 mmol) tert-butyl [4,4'-bipiperidine]-1-carboxylate (**59b**), 1.663 g (6.7 mmol, 3.2 equiv.) **50**, 0.371 g (3.9 mmol, 3 equiv.) phenol, and 3 mL dimethylformamide (0.33 M). Final product isolated as tan powder. Yield = 42%, 0.432 g (0.88 mmol). ^{1}H NMR (DMSO-d_6, 400 MHz) δ ppm: 8.69 (d, 2H, *J* = 5.0 Hz), 8.02 (d, 2H, *J* = 9.0 Hz), 7.97 (d, 2H, *J* = 2.0 Hz), 7.57 (dd, 2H, *J* = 1.9, 8.9 Hz), 7.02 (d, 2H, *J* = 5.1 Hz), 3.63 (br d, 5H, *J* = 12.1 Hz), 2.85 (br t, 5H, *J* = 11.6 Hz), 1.94 (br d, 4H, *J* = 12.1 Hz), 1.5-1.7 (m, 4H), 1.47 (br d, 2H, *J* = 8.6 Hz). HRAM/MS (ESI): $[M+H]^+$ of $[C_{28}H_{28}Cl_2N_4]$ = 491.17637; observed = 491.17673.

1,3-bis(1-(7-chloroquinolin-4-yl)piperidin-4-yl)propane (61). The title compound was prepared using ***General Procedure (i)*** in the following proportions: 0.176 g (0.83 mmol) of 1,3-di(piperidin-4-yl)propane (**59b**), 0.628 g (2.6 mmol, 3 equiv.) of **50**, 0.191 g (2.0 mmol, 2.4 equiv.) of phenol, and 3 mL dimethylformamide (0.28 M). Final product isolated as clear solid. Yield = 26%, 0.115 g (0.21 mmol). ^{1}H NMR (DMSO-d_6, 400 MHz) δ ppm: 8.68 (d, 2H, *J* = 5.0 Hz), 7.9-8.0 (m, 4H), 7.55 (dd, 2H, *J* = 2.3, 9.0 Hz), 6.98 (d, 2H, *J* = 5.0 Hz), 3.53 (br d, 4H, *J* = 12.1 Hz), 2.81 (br t, 4H, *J* = 11.3 Hz), 1.85 (br d, 4H, *J* = 9.5 Hz), 1.3-1.6 (m, 12H). HRAM/MS (ESI positive): $[M+H]^+$ of $[C_{31}H_{34}Cl_2N_4]$ = 533.22332; observed = 533.22325.

tert-butyl 4-(4-((7-chloroquinolin-4-yl)amino)phenyl)-piperidine-1-carboxylate (64a). The title compound was prepared using ***General Procedure (ii)*** in the following propotions: 1.150 g (5.80 mmol) **50**, 1.603 g (5.80 mmol, 1 equiv.) 4-(aminophenyl)-piperadine-1-Boc (**63a**), and 10 mL tertrohydrofuran (0.58 M). Final product isolated as a white solid. Yield = 87%, 1.924 g (4.40 mmol). ^{1}H NMR (DMSO-d_6, 400 MHz) δ ppm: 9.03 (s, 1H), 8.44 (d, 1H, *J* = 5.4 Hz), 8.42 (d, 1H, *J* = 9.3 Hz), 7.88 (d, 1H, *J* = 2.3 Hz), 7.56 (dd, 1H, *J* = 2.3, 9.0 Hz), 7.30 (s, 4H), 6.86 (d, 1H, *J* = 5.4 Hz), 4.09 (br d, 2H, *J* = 11.8 Hz), 2.82 (br s, 1H), 2.6-2.8 (m, 1H), 1.79 (br d, 2H, *J* = 12.5 Hz), 1.4-1.6 (m, 3H), 1.42 (s, 9H)

tert-butyl 4-(4-((7-chloroquinolin-4-yl)amino)phenyl)-piperazine-1-carboxylate (64b). The title compound was prepared using ***General Procedure (ii)*** in the following propotions: 1.096 g (5.52 mmol) 4,7-chloroquinoline (**5**), 1.533 g (5.52 mmol) 4-(aminophenyl)-piperizine-1-Boc

(**63b**), and 10 mL tertrohydrofuran (0.44 M). Final product isolated as a white solid. Yield = 69%, 1.681 g (3.83 mmol). ^{1}H NMR (400 MHz, CHLOROFORM-*d*) δ ppm: 8.49 (d, *J* = 5.25 Hz, 1H) 8.01 (d, *J* = 2.13 Hz, 1H) 7.84 (d, *J* = 9.01 Hz, 1H) 7.44 (dd, *J* = 9.01, 2.13 Hz, 1H) 7.18 - 7.24 (m, 2H) 6.96 - 7.02 (m, 2H) 6.71 (d, *J* = 5.25 Hz, 1H) 6.51 (s, 1H) 3.56 - 3.67 (m, 4H) 3.12 - 3.21 (m, 5H) 1.46 - 1.52 (m, 9H).

tert-butyl 4-(4-(quinolin-4-ylamino)phenyl)piperidine-1-carboxylate (64c). The title compound was prepared using ***General Procedure (ii)*** in the following proportions: 0.523 g (2.20 mmol) 4-bromoquinoline (**62**), 0.691 g (2.50 mmol) 4-(aminophenyl)-piperadine-1-Boc (*63c*), and 5 mL tertrohydrofuran (0.44 M). Final product isolated as a white solid. Yield = 80%, 0.714 g (1.77 mmol). ^{1}H NMR (DMSO-d_6, 400 MHz) δ ppm: 8.88 (s, 1H), 8.43 (d, 1H, *J* = 5.3 Hz), 8.37 (d, 1H, *J* = 8.5 Hz), 7.86 (d, 1H, *J* = 8.0 Hz), 7.68 (t, 1H, *J* = 7.3 Hz), 7.52 (t, 1H, *J* = 7.3 Hz), 7.29 (s, 4H), 6.87 (d, 1H, *J* = 5.3 Hz), 4.0-4.2 (m, 2H), 3.17 (d, 1H, *J* = 5.1 Hz), 2.82 (br s, 1H), 2.70 (tt, 1H, *J* = 3.2, 11.9 Hz), 1.79 (br d, 2H, *J* = 12.3 Hz), 1.4-1.6 (m, 2H), 1.43 (s, 9H).

7-chloro-N-(4-(piperidin-4-yl)phenyl)quinolin-4-amine (65a). The title compound was prepared using ***General Procedure (iii)*** using the following proportions: 4.440 g (10.1 mmol) **64a intermediate**, 100 mL dichloromethane, and 23 mL (303 mmol, 30 equiv.) trifluoroacetic acid. Final product isolated as a white solid. Yield = 97%, 3.310 g (9.80 mmol). ^{1}H NMR (CHLOROFORM-*d*, 400 MHz) δ ppm: 8.54 (d, 1H, *J* = 5.3 Hz), 8.03 (d, 1H, *J* = 2.1 Hz), 7.85 (d, 1H, *J* = 9.0 Hz), 7.45 (dd, 1H, *J* = 2.2, 8.9 Hz), 7.3-7.3 (m, 2H), 7.2-7.3 (m, 2H), 6.91 (d, 1H, *J* = 5.3 Hz), 6.58 (s, 1H), 3.22 (br d, 2H, *J* = 11.8 Hz), 2.77 (dt, 2H, *J* = 2.3, 12.1 Hz), 2.65 (s, 1H), 1.8-1.9 (m, 2H), 1.7-1.7 (m, 2H).

7-chloro-N-(4-(piperazin-1-yl)phenyl)quinolin-4-amine (65b). The title compound was prepared using ***General Procedure (iii)*** using the following proportions: 1.501 g (3.42 mmol) **64b intermediate**, 10 mL dichloromethane, and 4 mL (52.6 mmol, 15 equiv.) trifluoroacetic acid. Final product isolated as a yellow solid. Yield = 40%, 0.464 g (1.37 mmol). ^{1}H NMR (400 MHz, DMSO-d_6) δ ppm: 8.91 (s, 1 H) 8.87 - 8.96 (m, 1 H) 8.41 (d, *J* = 9.01 Hz, 1 H) 8.37 (d, *J* = 5.38 Hz, 1 H) 7.84 (d, *J* = 2.25 Hz, 1 H) 7.52 (dd, *J* = 9.01, 2.25 Hz, 1 H) 7.19 (d, *J* = 8.88 Hz, 2 H) 6.94 - 7.07 (m, 2 H) 6.62 (d, *J* = 5.38 Hz, 1 H) 2.99 - 3.13 (m, 4 H) 2.77 - 2.91 (m, 4 H).

N-(4-(piperidin-4-yl)phenyl)quinolin-4-amine (65c). The title compound was prepared using ***General Procedure (iii)*** in the following propprtions: 0.6493 g (1.61 mmol) **64c intermediate**, 30 mL dichloromethane, and 3.0 mL (39.2 mmol, 25 equiv.) trifluoroacetic acid. Final product isolated as a yellow/straw-colored solid. Yield = 81%, 0.396 g (1.31 mmol). ^{1}H NMR (DMSO-d_6, 400 MHz) δ ppm: 8.89 (br s, 1H), 8.43 (d, 1H, *J* = 5.3 Hz), 8.38 (d, 1H, *J* = 8.4 Hz), 7.86 (d, 1H, *J* = 8.4 Hz), 7.69 (t, 1H, *J* = 7.6 Hz), 7.52 (t, 1H, *J* = 7.6 Hz), 7.29 (q, 4H, *J* = 8.6 Hz), 6.87 (d, 1H, *J* = 5.3 Hz), 3.1-3.2 (m, 3H), 2.6-2.8 (m, 2H), 2.0-2.1 (m, 1H), 1.8-1.9 (m, 2H), 1.5-1.7 (m, 2H).

7-chloro-*N*-(4-(1-(2-chloropyridin-4-yl)piperidin-4-yl)phenyl)quinolin-4-amine (67). The title compound was prepared using ***General Procedure (iv)*** in the following proportions: 0.340 g (1.0 mmol) of **65a**, 0.218 g (2.2 mmol, 2.2 equiv.) 2-chloro-4-fluoropyridine (**66**), and 0.25 mL (1.4 mmol., 1.4 equiv.) *N*,*N*-diisopropylethylamine, and 2 mL (0.5 M) N-methyl-2-pyrillidone. Final product isolated as white powder. Yield = 30%, 0.130 g (0.30 mmol). ^{1}H NMR (DMSO-d_6, 400 MHz) δ ppm: 9.04 (s, 1H), 8.4-8.5 (m, 2H), 7.94 (d, 1H, *J* = 5.7 Hz), 7.88 (d, 1H, *J* = 2.3 Hz), 7.56 (dd, 1H, *J* = 2.3, 9.0 Hz), 7.3-7.3 (m, 4H), 6.9-6.9 (m, 3H), 4.11 (br d, 2H, *J* = 13.4

Hz), 2.9-3.0 (m, 2H), 2.85 (tt, 1H, *J* = 3.4, 12.0 Hz), 1.88 (br d, 2H, *J* = 11.9 Hz), 1.64 (dq, 2H, *J* = 3.6, 12.5 Hz). HRAM/MS (ESI positive): $[M+H]^+$ of $[C_{25}H_{22}Cl_2N_4]$ = 449.12942; observed = 449.12952.

7-chloro-*N*-(4-(1-(quinolin-4-yl)piperidin-4-yl)phenyl)-quinolin-4-amine (68). The title compound was prepared using ***General Procedure (v)*** in the following proportions: 0.334 g (0.99 mmol) of **65a**, 0.417 g (2.00 mmol, 2.0 equiv.) of **62**, 0.201 g (2.1 mmol, 2.1 equiv.) phenol, and 3 mL dimethylformamide (0.33 M). Final product isolated as white powder. Yield = 53%, 0.246 g (0.53 mmol). ^{1}H NMR (DMSO-d_6, 400 MHz) δ ppm: 9.07 (s, 1H), 8.70 (d, 1H, *J* = 5.0 Hz), 8.4-8.5 (m, 2H), 8.09 (d, 1H, *J* = 8.5 Hz), 7.96 (dd, 1H, *J* = 0.8, 8.4 Hz), 7.89 (d, 1H, *J* = 2.3 Hz), 7.70 (ddd, 1H, *J* = 1.3, 6.9, 8.3 Hz), 7.5-7.6 (m, 2H), 7.4-7.5 (m, 2H), 7.3-7.4 (m, 2H), 7.03 (d, 1H, *J* = 5.0 Hz), 6.90 (d, 1H, *J* = 5.4 Hz), 3.69 (br d, 2H, *J* = 12.1 Hz), 2.9-3.0 (m, 2H), 2.8-2.9 (m, 1H), 2.0-2.1 (m, 4H). HRAM/MS (ESI positive): $[M+H]^+$ of $[C_{29}H_{25}ClN_4]$ = 465.18405; observed = 465.18392.

7-chloro-*N*-(4-(1-(7-chloroquinolin-4-yl)piperidin-4-yl)phenyl)quinolin-4-amine (**69**). The title compound was prepared using ***General Procedure (v)*** in the following proportions: 0.335 g (1.0 mmol) of **65a**, 0.484 g (2.0 mmol, 2 equiv.) of **50**, 0.207 g (2.2 mmol, 2.2 equiv.) phenol, and 5 mL dimethylformamide (0.33 M). Final product isolated as tan powder. Yield = 86%, 0.432 g (0.86 mmol). ^{1}H NMR (CHLOROFORM-*d*, 400 MHz) δ ppm: 8.74 (d, 1H, *J* = 5.0 Hz), 8.57 (d, 1H, *J* = 5.3 Hz), 8.05 (t, 2H, *J* = 2.3 Hz), 8.00 (d, 1H, *J* = 9.0 Hz), 7.87 (d, 1H, *J* = 9.0 Hz), 7.46 (t, 2H, *J* = 9.2 Hz), 7.4-7.4 (m, 2H), 7.3-7.3 (m, 2H), 6.96 (d, 1H, *J* = 5.3 Hz), 6.89 (d, 1H, *J* = 5.0 Hz), 6.61 (br s, 1H), 3.74 (br d, 2H, *J* = 12.1 Hz), 2.9-3.1 (m, 2H), 2.7-2.9 (m, 1H),2.0-2.2 (m, 4H). HRAM/MS (ESI negative): $[M-H]^-$ of $[C_{29}H_{24}Cl_2N_4]$ = 497.12942; observed = 497.13077.

7-chloro-*N*-(4-(4-(7-chloroquinolin-4-yl)piperazin-1-yl)phenyl)quinolin-4-amine (**70**). The title compound was prepared using ***General Procedure (v)*** in the following proportions: 0.058 g (0.17 mmol) of **65b**, 0.083 g (0.34 mmol, 2 equiv.) **50**, 0.032 g (0.34 mmol, 2 equiv.) phenol, and 2 mL dimethylformamide (0.1 M). Final product isolated as yellow solid. Yield = 31%, 0.026 g (0.052 mmol). ^{1}H NMR (CHLOROFORM-*d*, 400 MHz) δ ppm: 8.77 (d, 1H, *J* = 4.9 Hz), 8.52 (d, 1H, *J* = 5.3 Hz), 8.08 (d, 1H, *J* = 2.1 Hz), 8.02 (dd, 2H, *J* = 3.4, 5.6 Hz), 7.85 (d, 1H, *J* = 9.0 Hz), 7.46 (ddd, 2H, *J* = 2.3, 7.0, 9.0 Hz), 7.3-7.3 (m, 1H), 7.2-7.3 (m, 1H), 7.1-7.1 (m, 2H), 6.92 (d, 1H, *J* = 5.1 Hz), 6.75 (d, 1H, *J* = 5.4 Hz), 6.54 (s, 1H), 3.5-3.5 (m, 4H), 3.4-3.4 (m, 4H). HRAM/MS (ESI positive): $[M+H]^+$ of $[C_{28}H_{23}Cl_2N_5]$ = 500.14032; observed = 500.14042.

N*-(4-(1-(7-chloroquinolin-4-yl)piperidin-4-yl)phenyl)-quinolin-4-amine (71)**. The title compound was prepared using ***General Procedure (v) in the following proportions: 0.164 g (0.54 mmol) of **65c**,1 0.207 g (0.85 mmol, 1.6 equiv.) of **50**, 0.102 g (1.1 mmol, 2.0 equiv.) phenol, and 3 mL dimethylformamide (0.2 M). Final product isolated as tan powder. Yield = 22%, 0.055 g (0.12 mmol). ^{1}H NMR (DMSO-d_6, 400 MHz) δ ppm: 8.92 (s, 1H), 8.72 (d, 1H, *J* = 5.0 Hz), 8.45 (d, 1H, *J* = 5.4 Hz), 8.39 (d, 1H, *J* = 8.0 Hz), 8.10 (d, 1H, *J* = 9.0 Hz), 7.99 (d, 1H, *J* = 2.1 Hz), 7.87 (d, 1H, *J* = 7.6 Hz), 7.70 (t, 1H, *J* = 7.1 Hz), 7.58 (dd, 1H, *J* = 2.1, 9.0 Hz), 7.53 (t, 1H, *J* = 7.2 Hz), 7.4-7.4 (m, 2H), 7.3-7.4 (m, 2H), 7.06 (d, 1H, *J* = 5.0 Hz), 6.91 (d, 1H, *J* = 5.3 Hz), 3.68 (br d, 2H, *J* = 12.0 Hz), 2.9-3.1 (m, 2H), 2.7-2.9 (m, 1H), 2.0-2.1 (m, 4H). HRAM/MS (ESI positive): $[M+H]^+$ of $[C_{29}H_{25}ClN_4]$ = 465.18405; observed = 465.18410.

N*-(4-(1-(quinolin-4-yl)piperidin-4-yl)phenyl)quinolin-4-amine (72)**. The title compound was prepared using ***General Procedure (v) in the following proportions: 0.203 g (0.67 mmol) of **65c**, 0.196 g (0.94 mmol, 1.4 equiv.) of **62**, 0.119 g (1.3 mmol, 1.9 equiv.) phenol, and 3 mL dimethylformamide (0.22 M). Final product isolated as straw-colored powder. Yield = 61%, 0.177 g (0.41 mmol). ^{1}H NMR (DMSO-d_6, 400 MHz) δ ppm: 8.93 (s, 1H), 8.70 (d, 1H, J = 4.9 Hz), 8.45 (d, 1H, J = 5.3 Hz), 8.40 (d, 1H, J = 8.4 Hz), 8.09 (d, 1H, J = 8.4 Hz), 7.96 (d, 1H, J = 8.4 Hz), 7.88 (d, 1H, J = 8.3 Hz), 7.70 (br t, 2H, J = 6.3 Hz), 7.55 (tt, 2H, J = 7.0, 7.9 Hz), 7.42 (d, 2H, J = 8.3 Hz), 7.35 (d, 2H, J = 8.3 Hz), 7.04 (d, 1H, J = 5.0 Hz), 6.9-7.0 (m, 1H), 3.69 (br d, 2H, J = 11.9 Hz), 2.97 (br t, 2H, J = 10.4 Hz), 2.7-2.9 (m, 1H), 2.0-2.1 (m, 4H). HRAM/MS (ESI positive): $[M+H]^+$ of $[C_{29}H_{26}N_4]$ = 431.22302; observed = 431.22282.

F. Chemical Characterization of Select Compounds

F.1. ^{1} *H NMR of compounds presented in Chapter 6*

-1in-1in

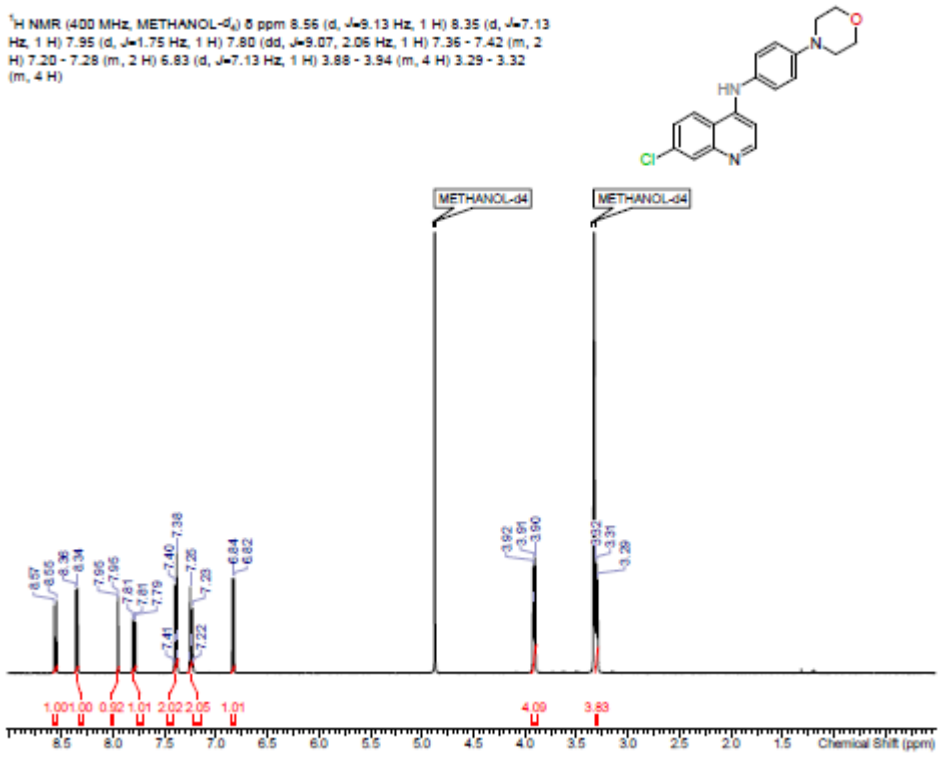

Figure 67: 1H NMR spectra of 7.

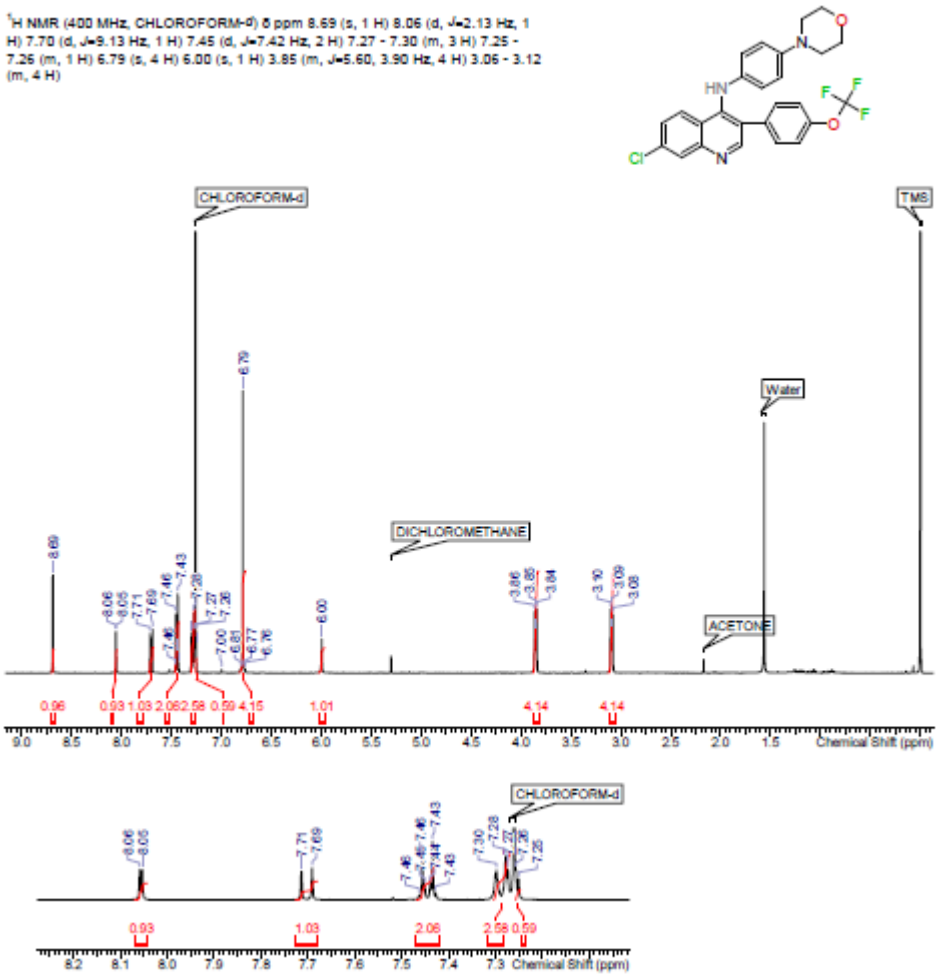

Figure 68: 1H NMR spectra of 8.

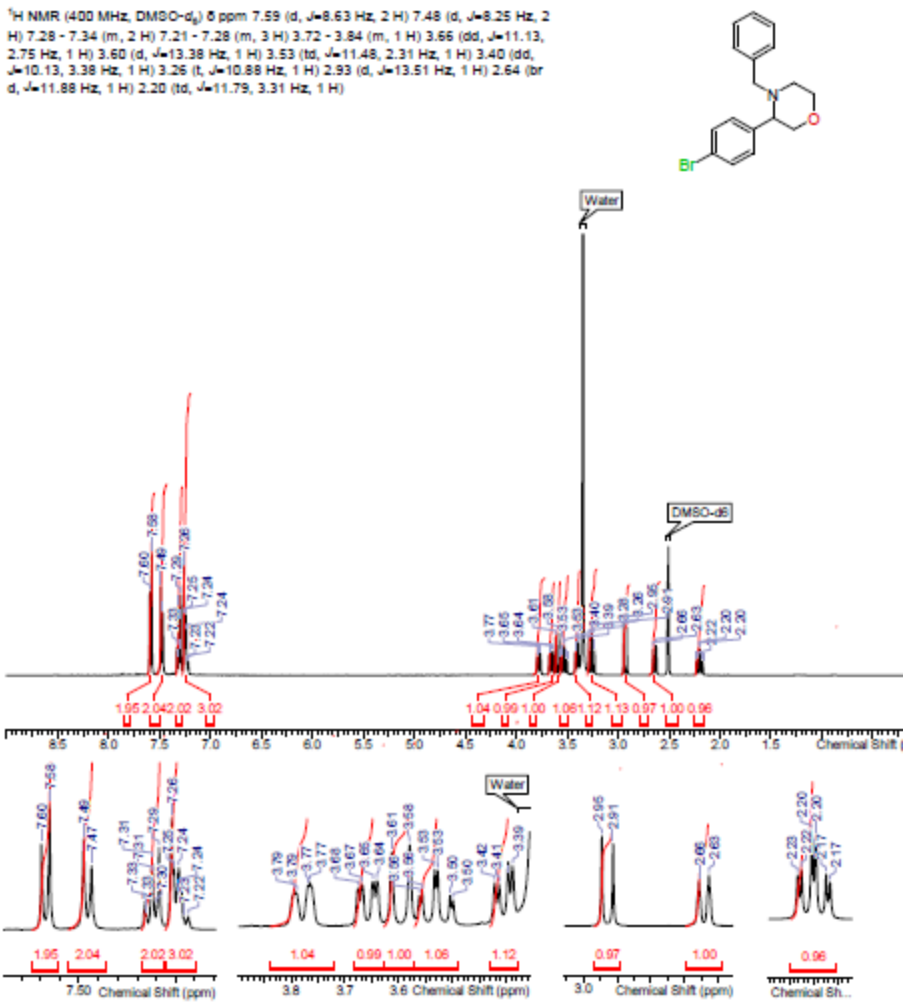

Figure 69: ^{1}H NMR spectra of 10a.

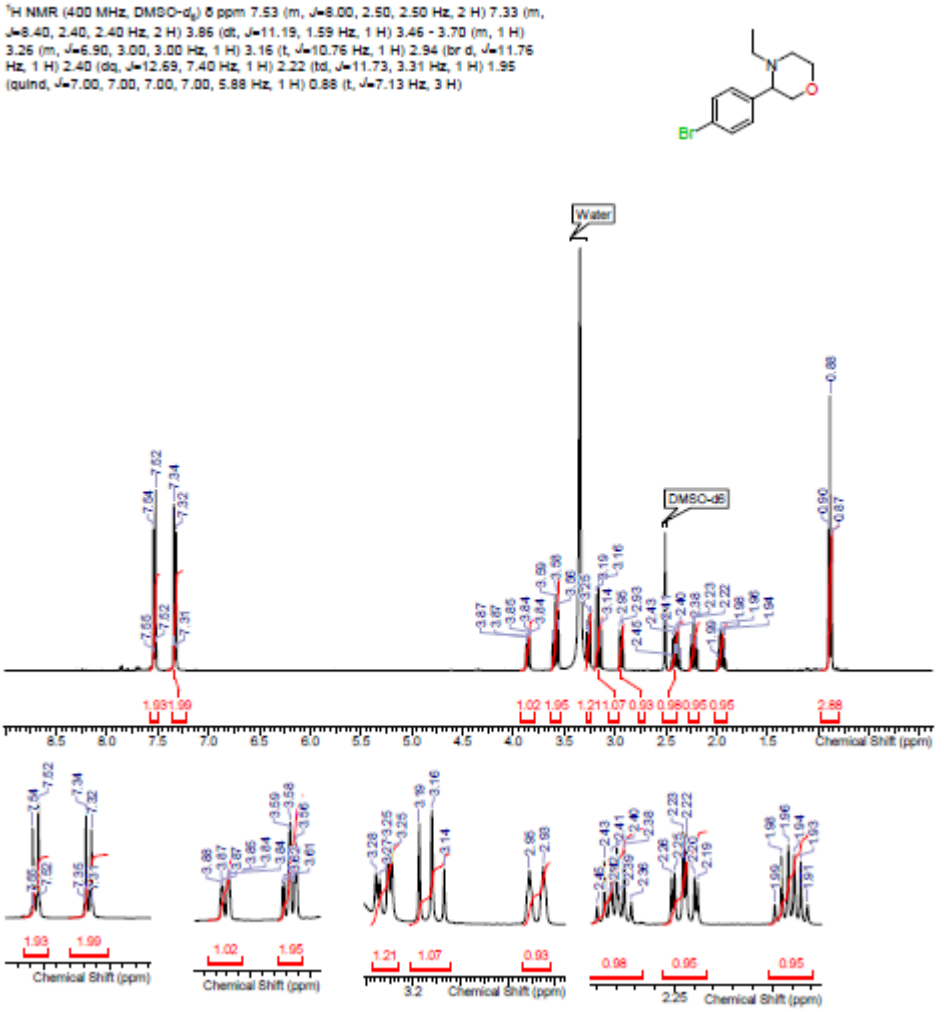

Figure 70: ^{1}H NMR spectra of 10b.

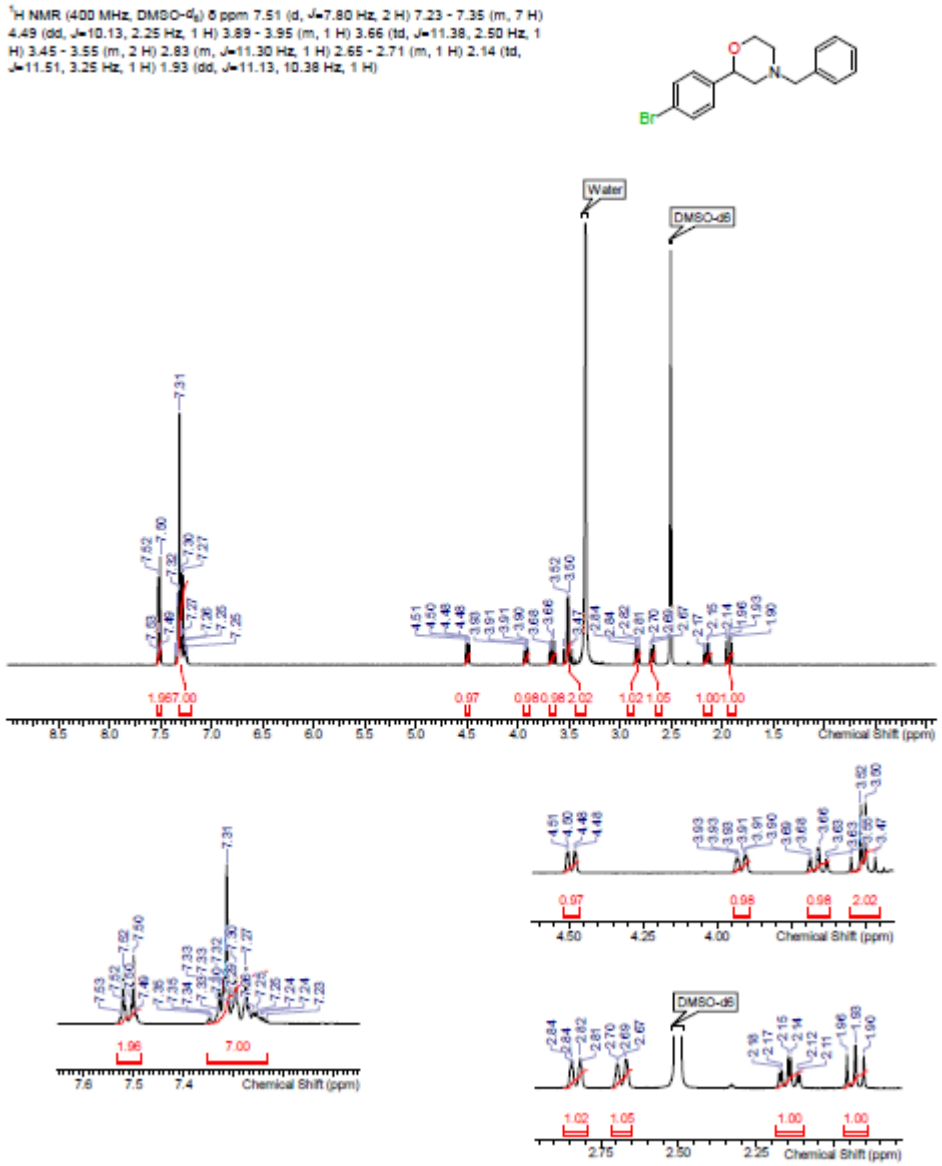

Figure 71: [1]H NMR spectra of 10c.

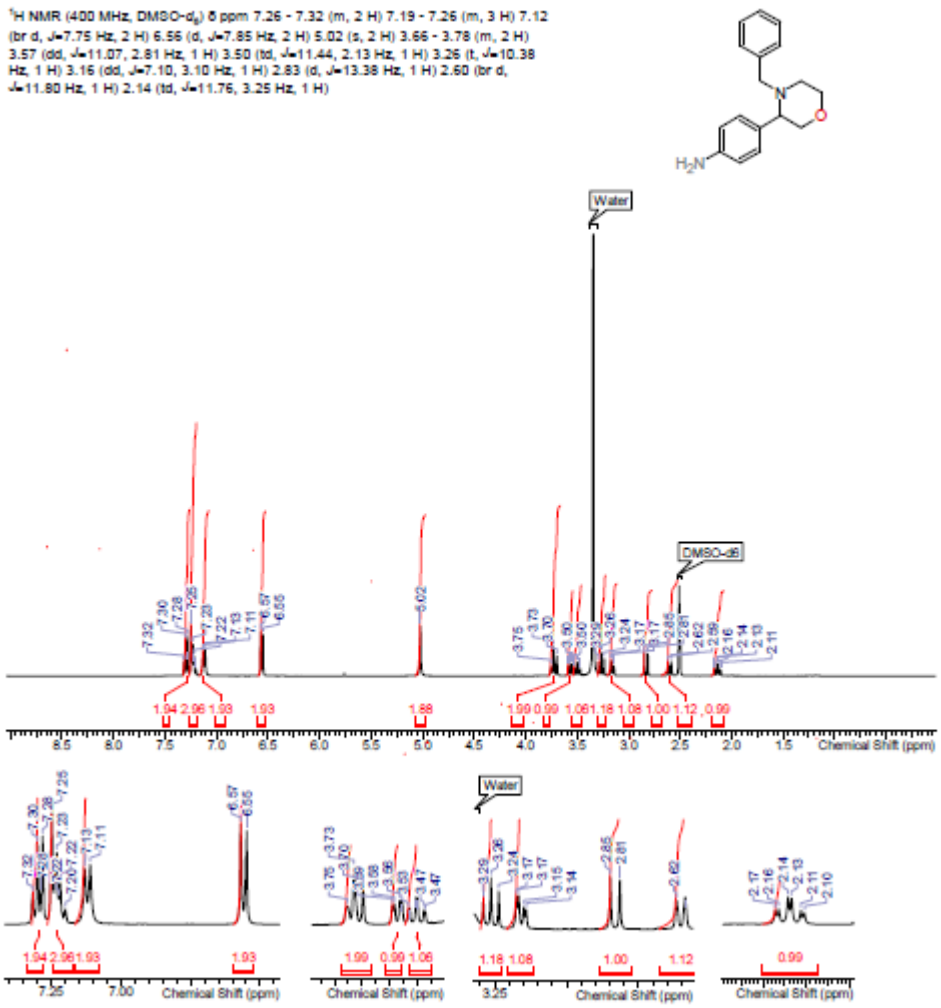

Figure 72: [1]H NMR spectra of 11a.

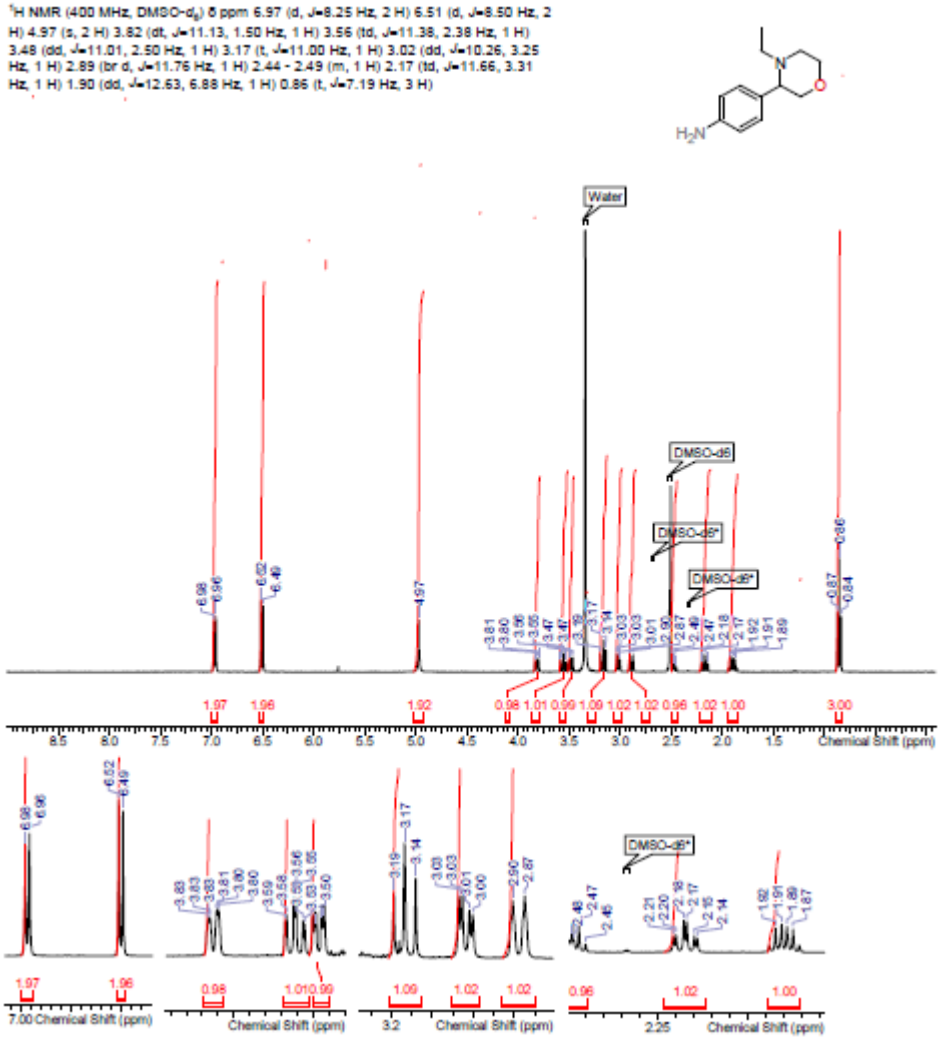

Figure 73: ^{1}H NMR spectra of 11b.

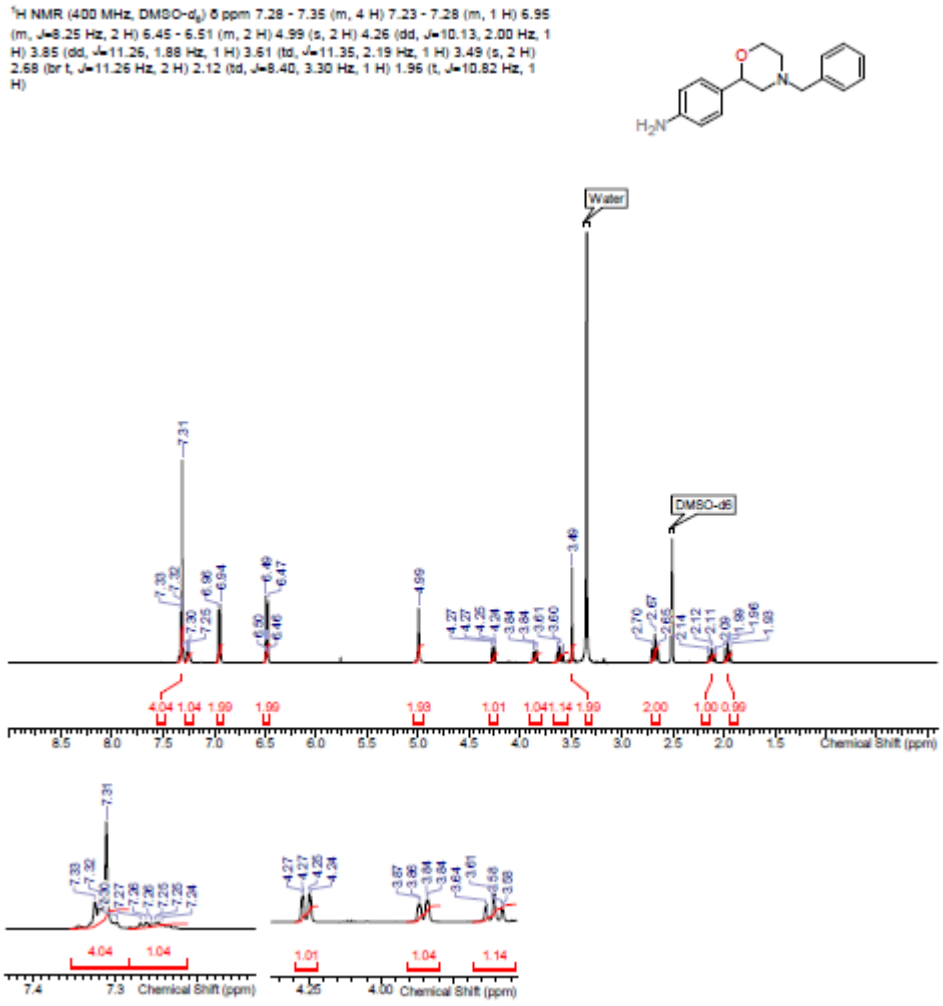

Figure 74: [1]H NMR spectra of 11c.

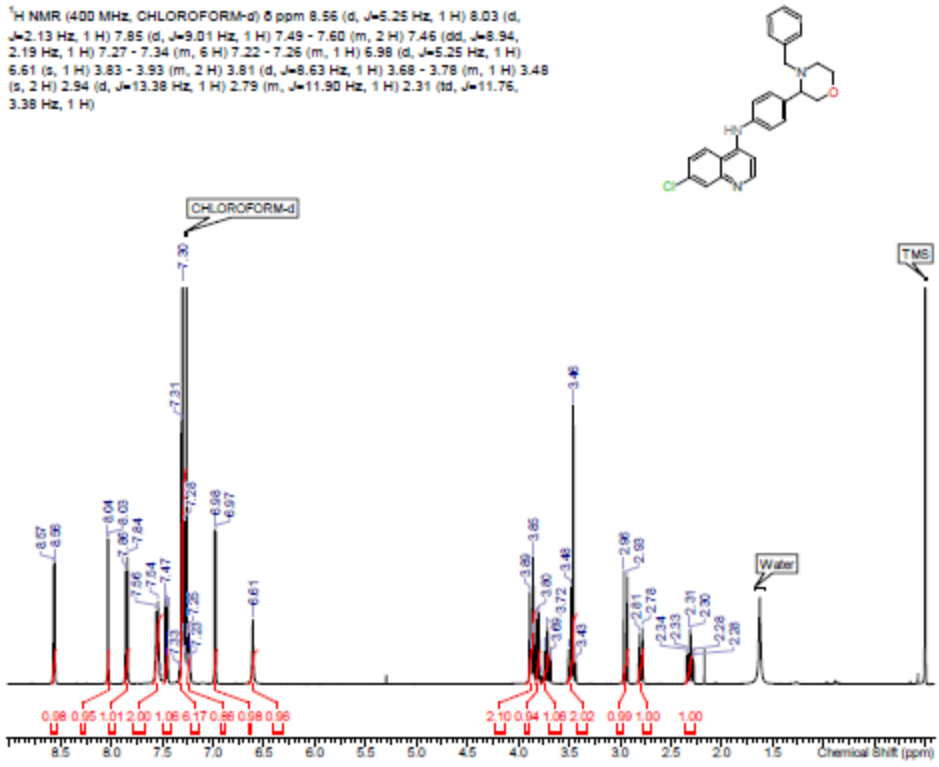

Figure 75: [1]H NMR spectra of 12.

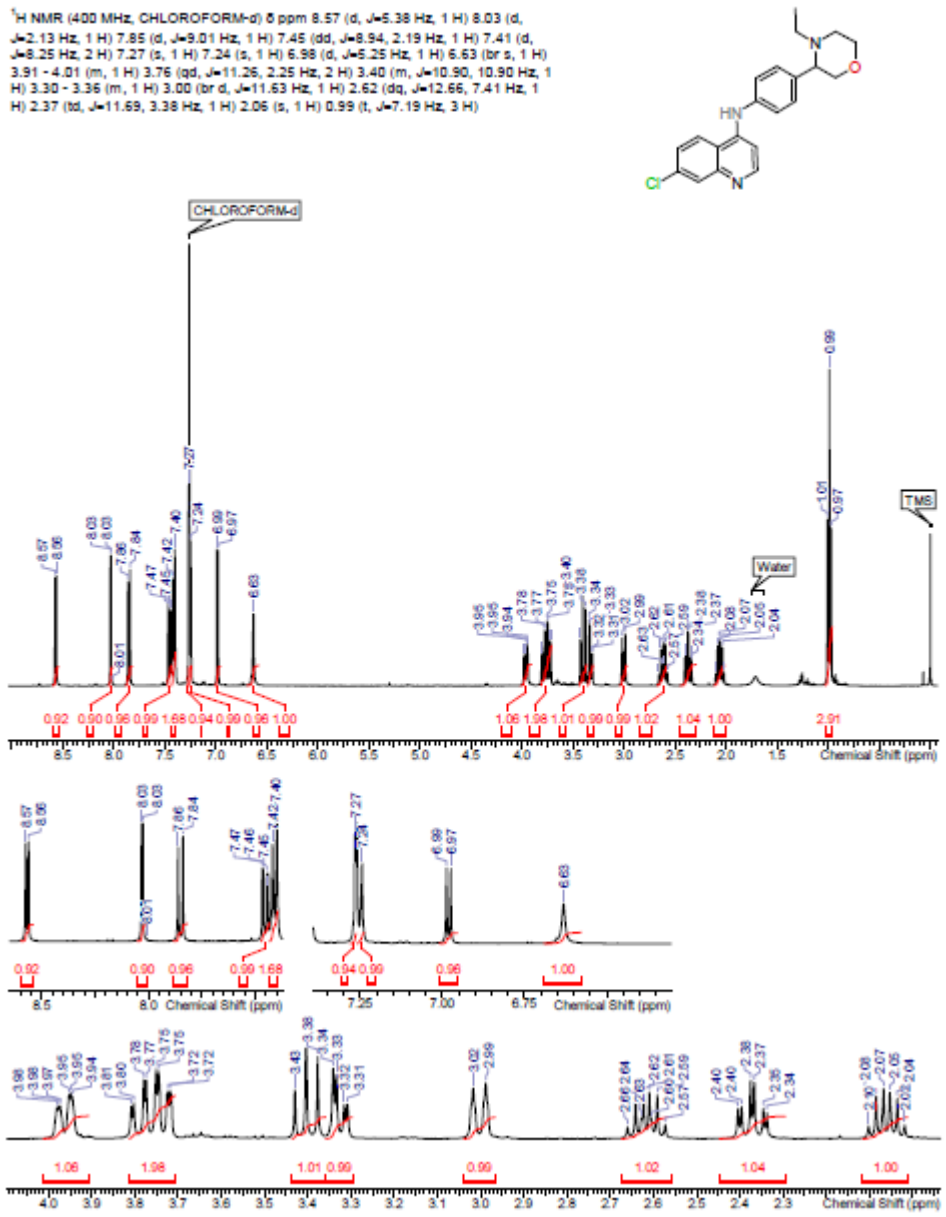

Figure 76: [1]H NMR spectra of 13.

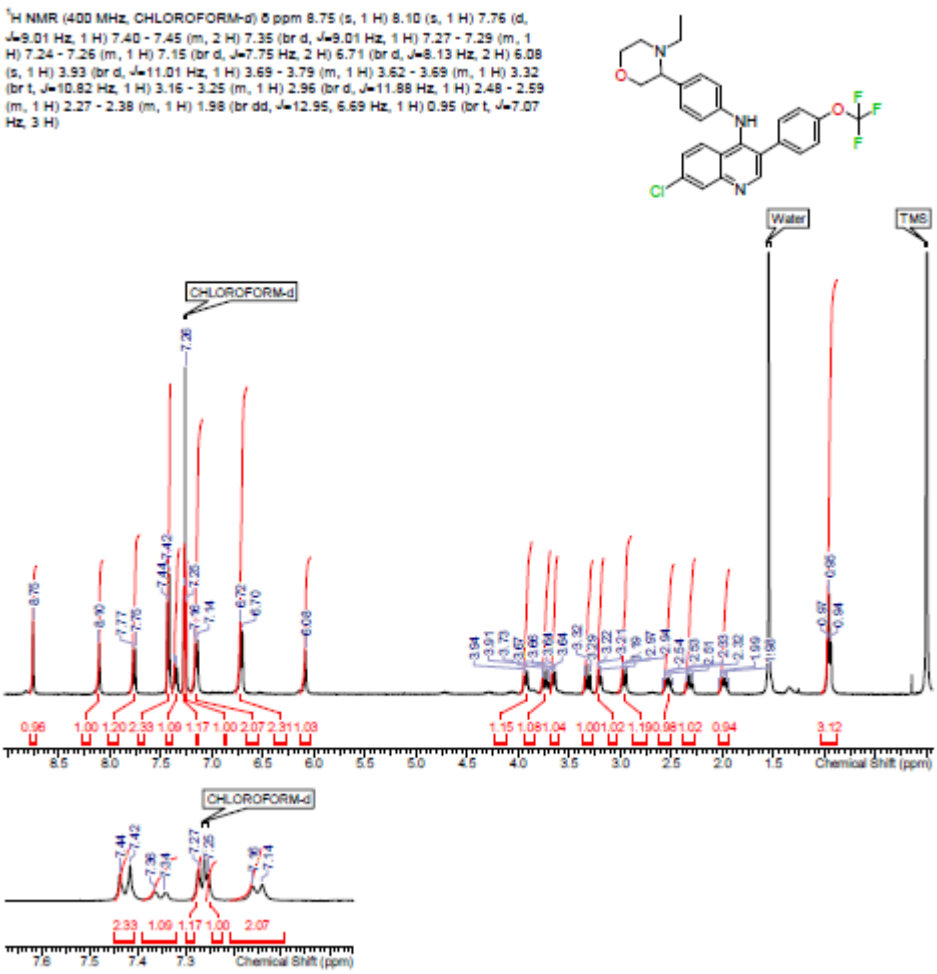

Figure 77: ^{1}H NMR spectra of 14.

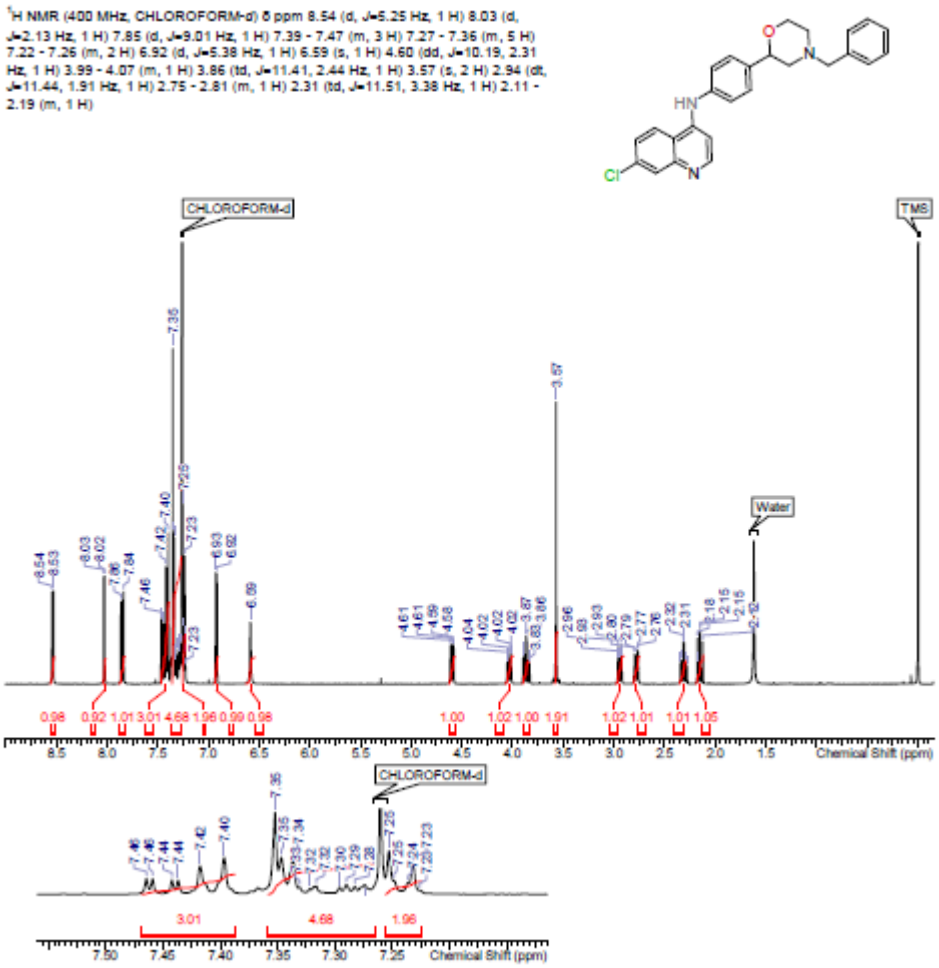

Figure 78: [1]H NMR spectra of 15.

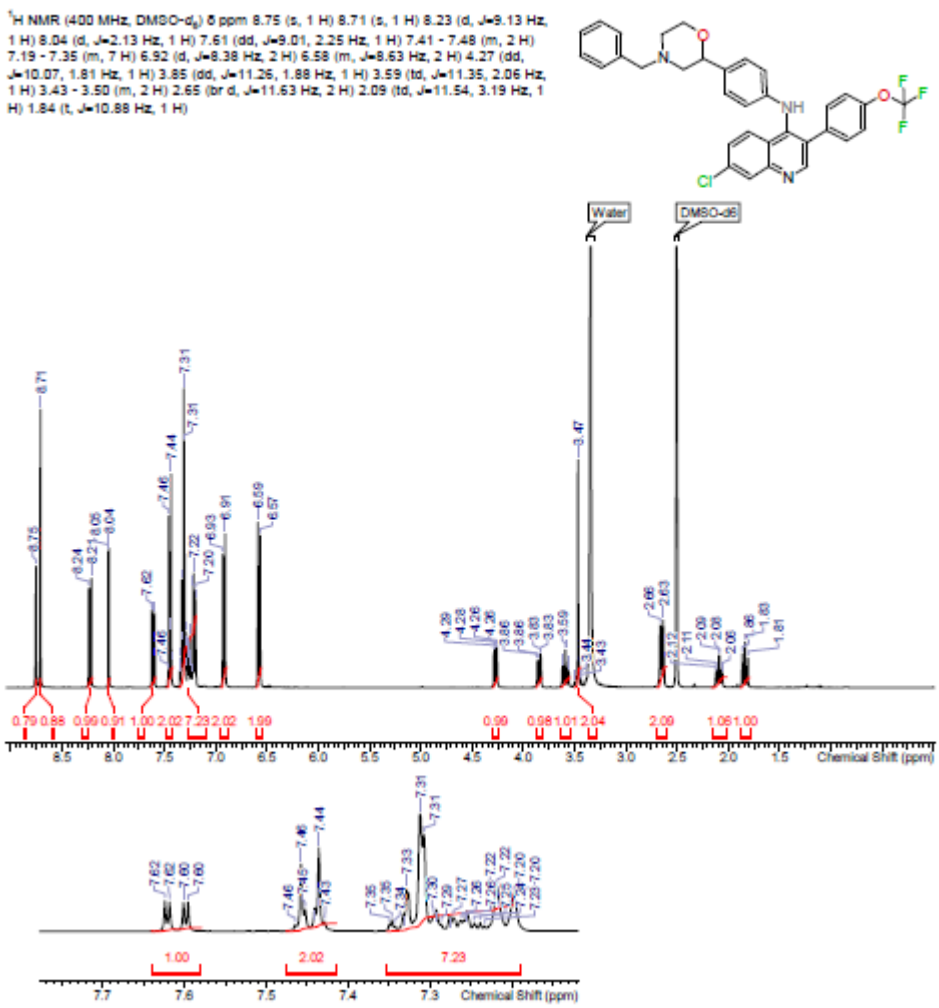

Figure 79: ^{1}H NMR spectra of 16.

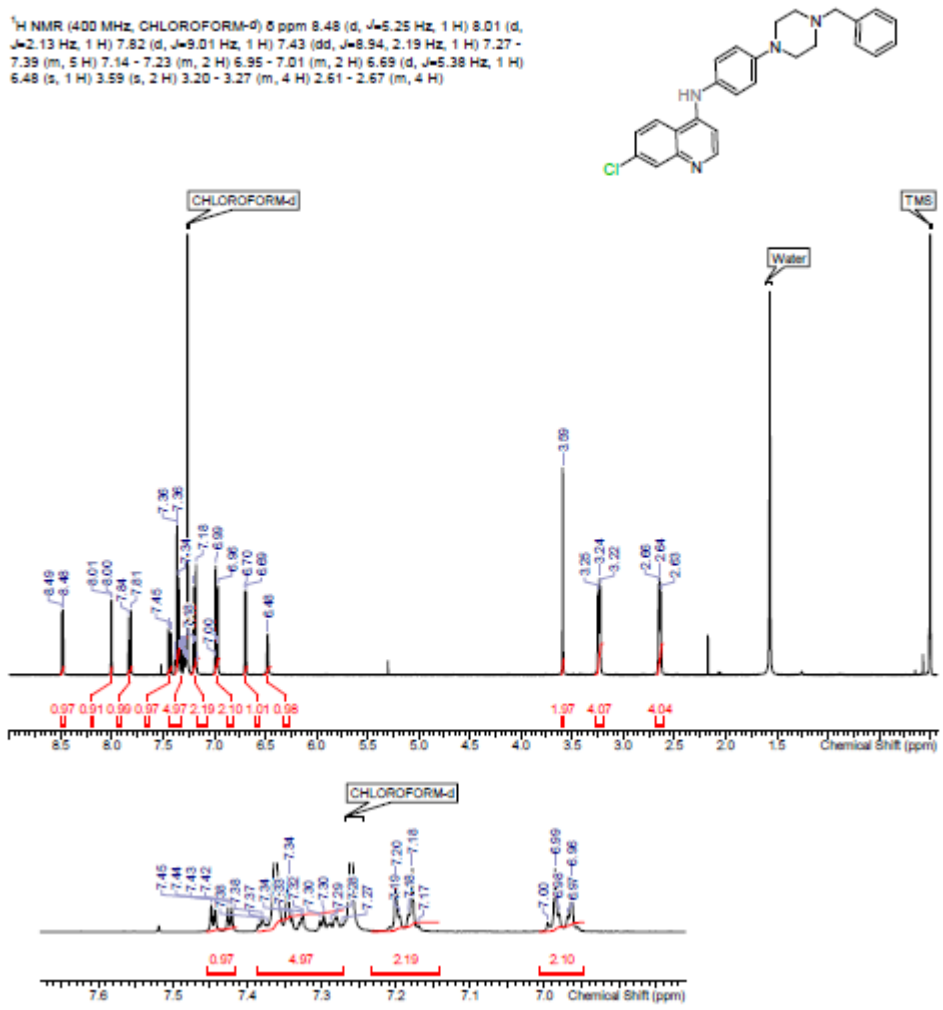

Figure 80: [1]H NMR spectra of 17.

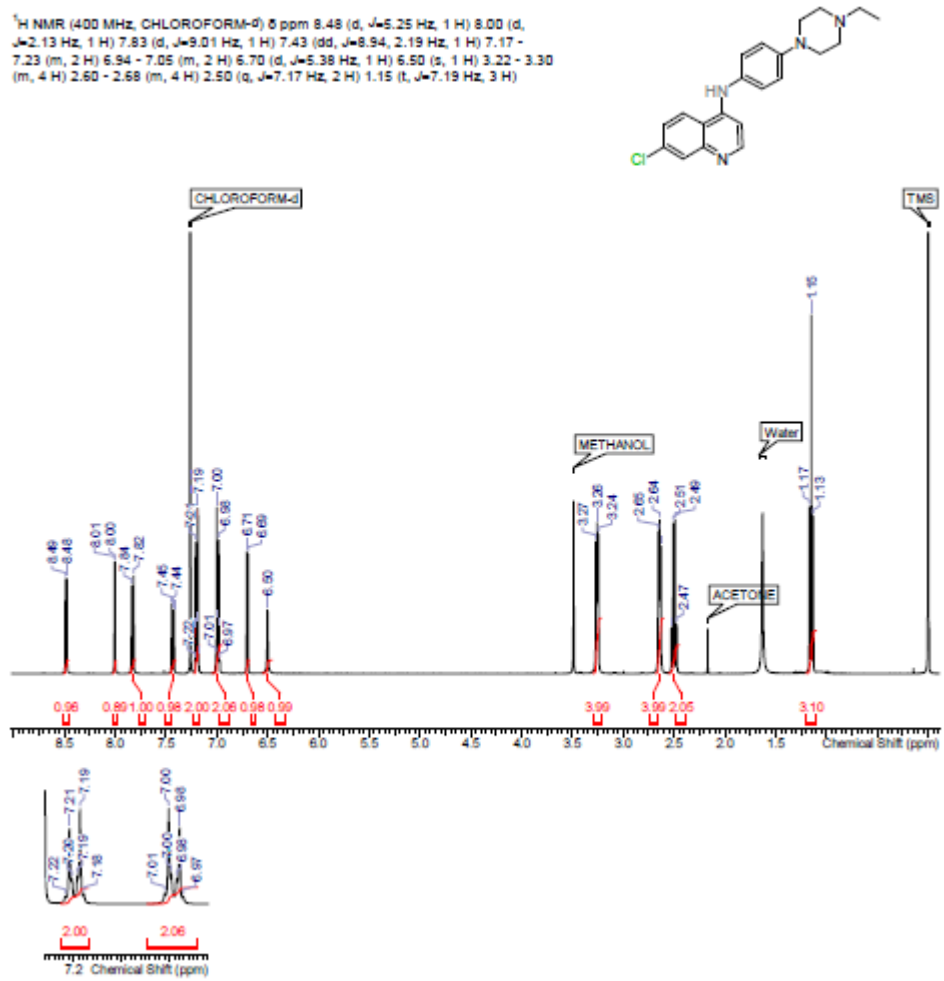

Figure 81: [1]H NMR spectra of 20.

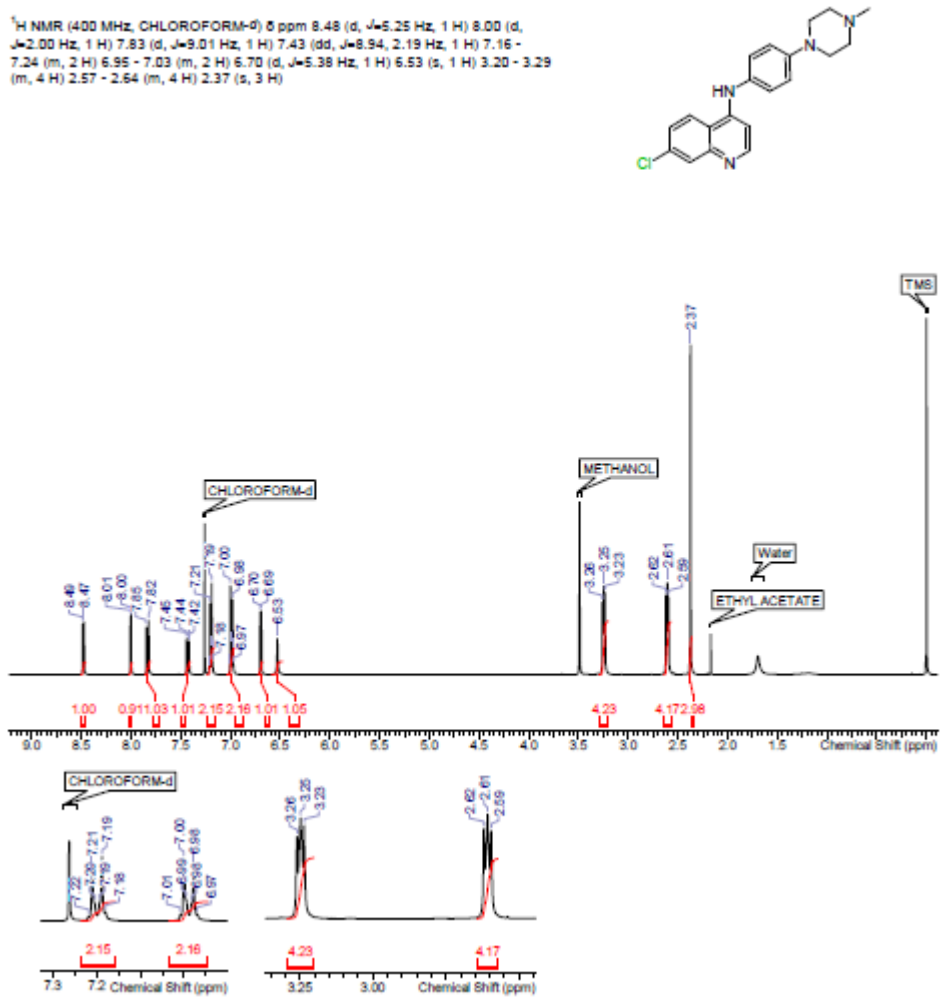

Figure 82: [1]H NMR spectra of 21.

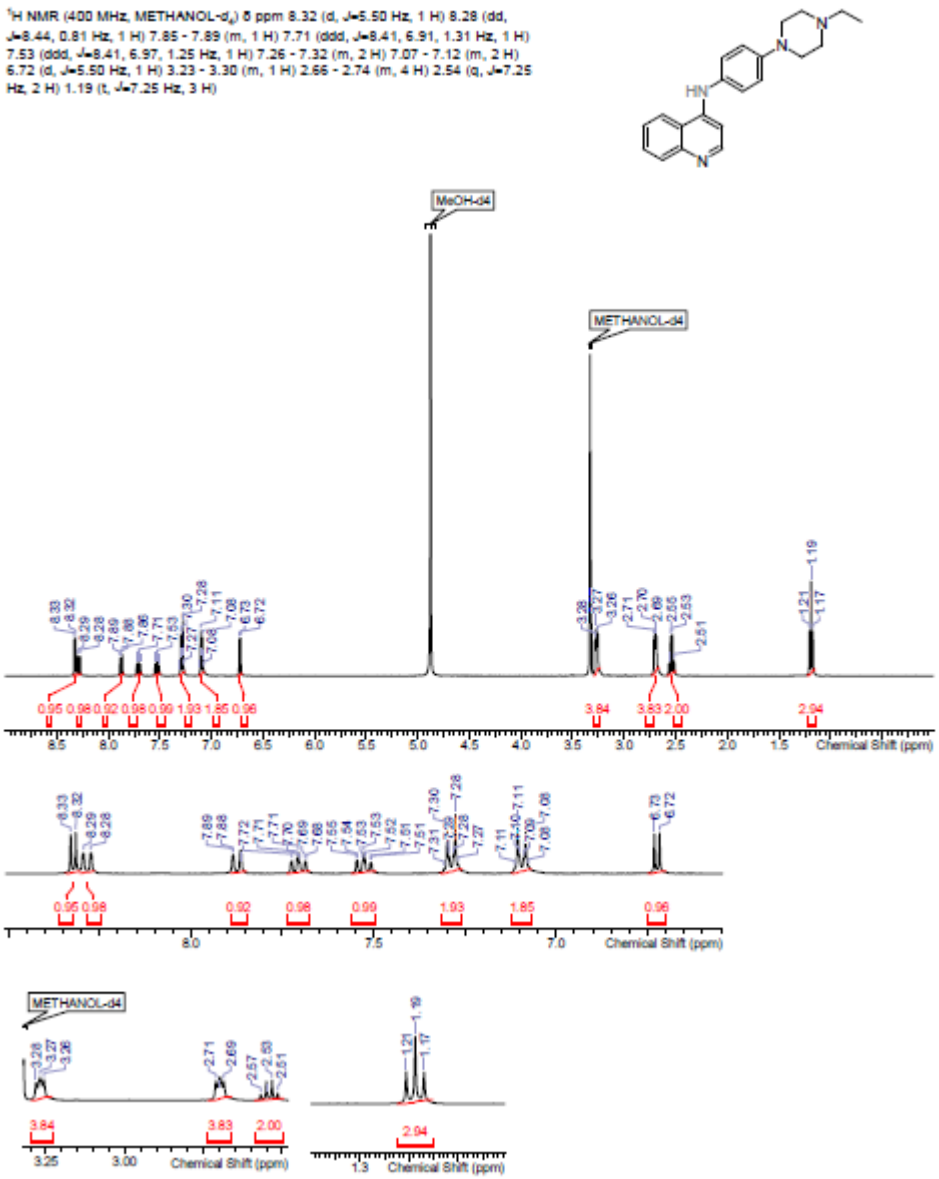

Figure 83: ^{1}H NMR spectra of 22.

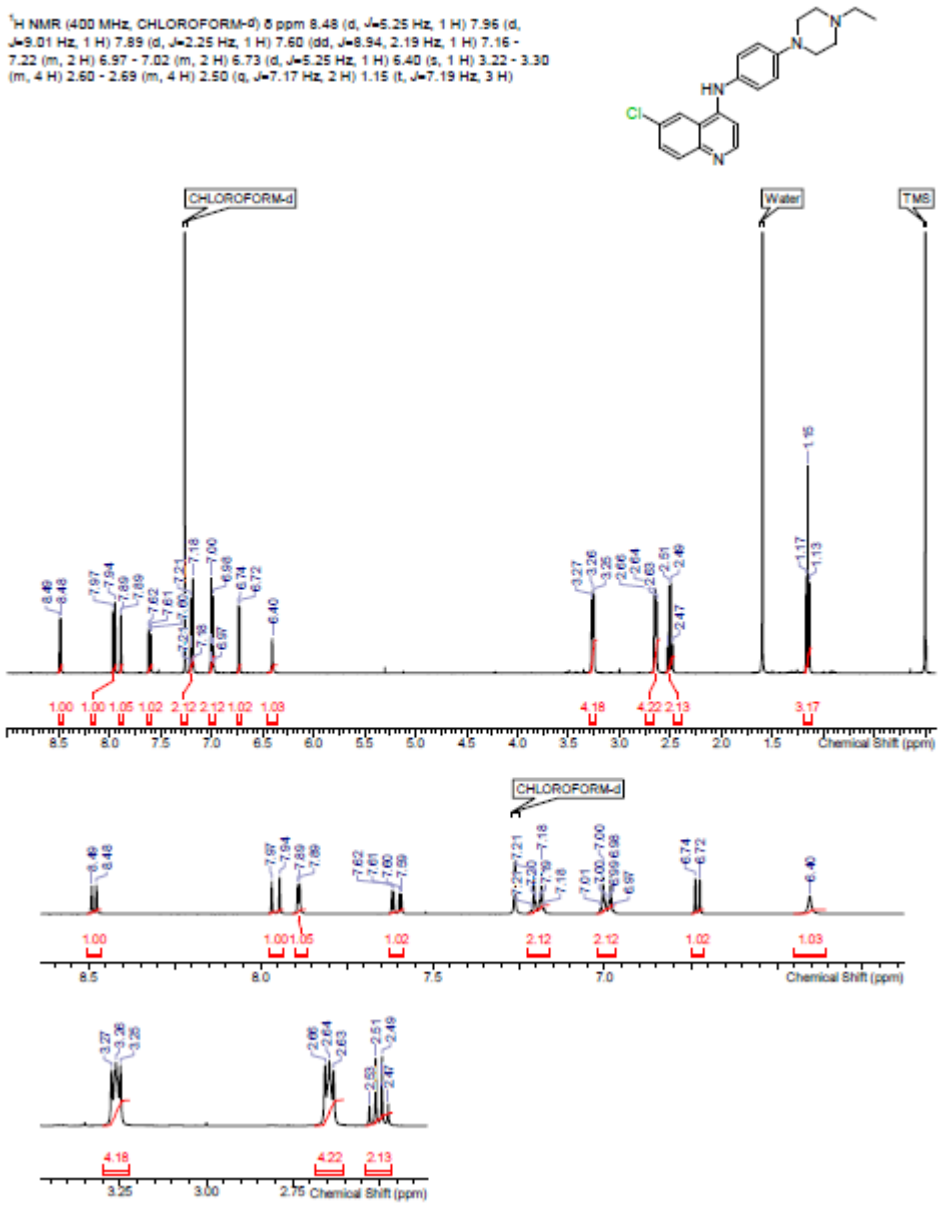

Figure 84: ^{1}H NMR spectra of 23.

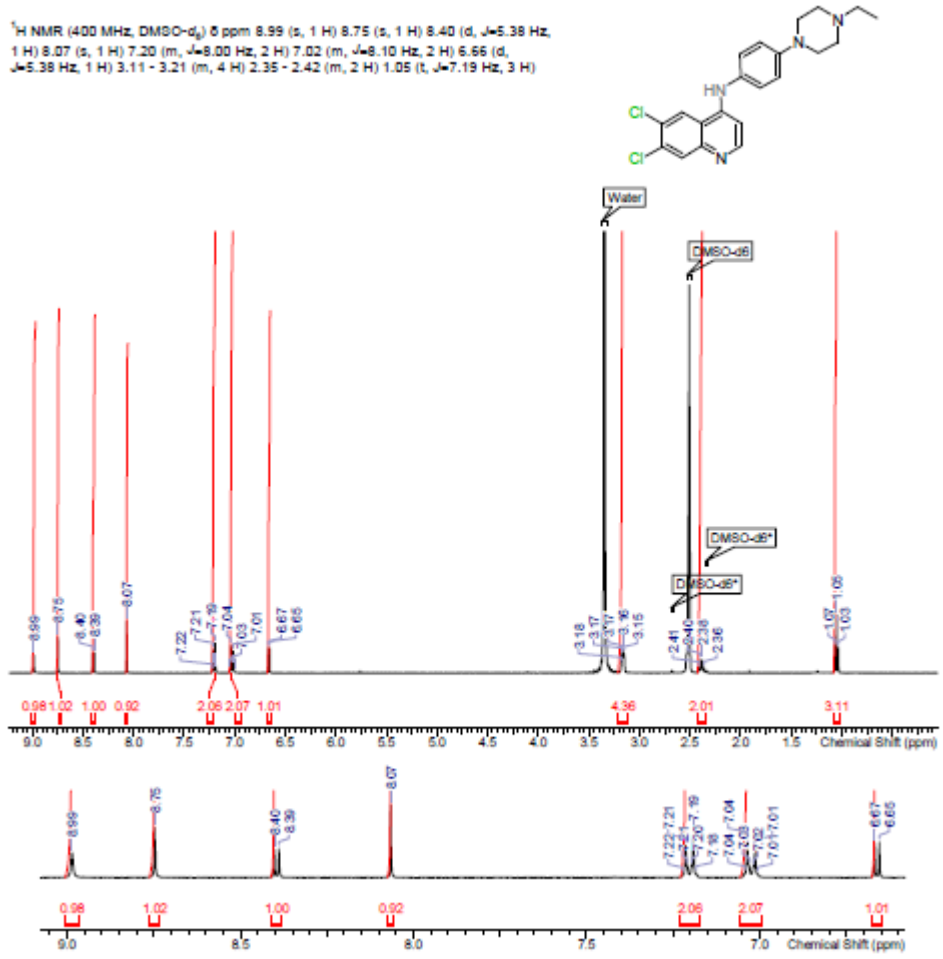

Figure 85: [1]H NMR spectra of 24.

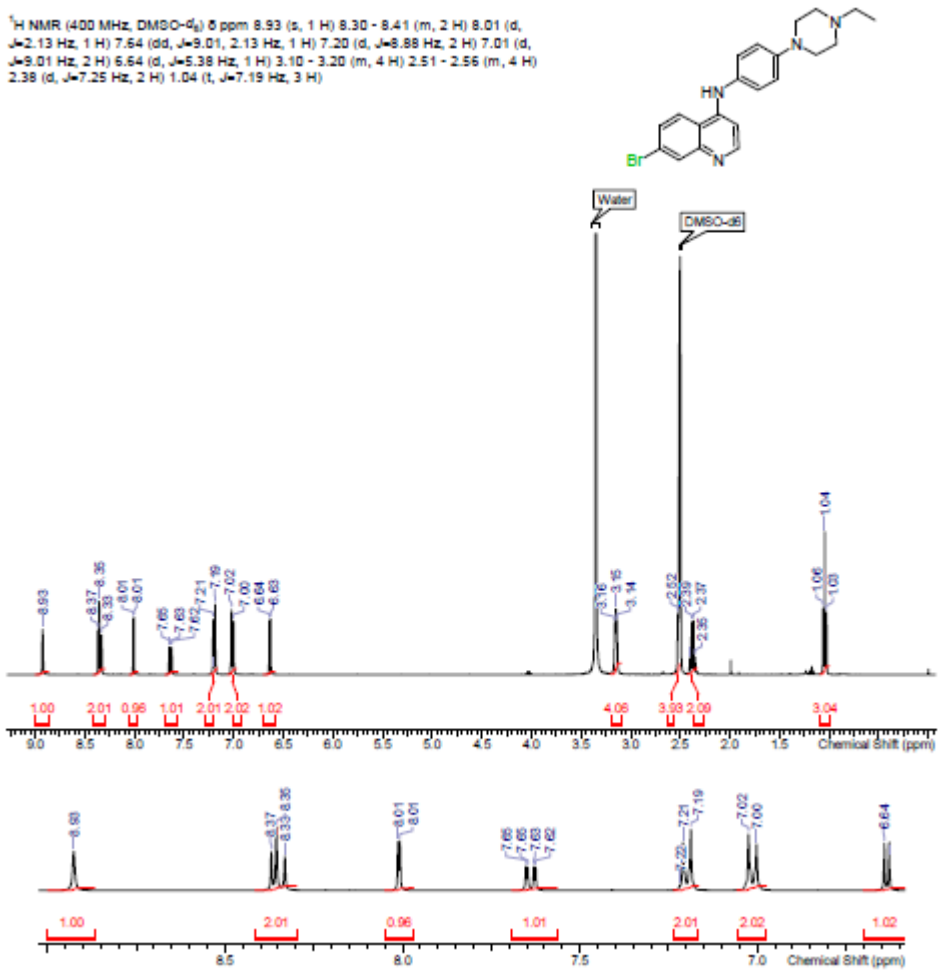

Figure 86: [1]H NMR spectra of 25.

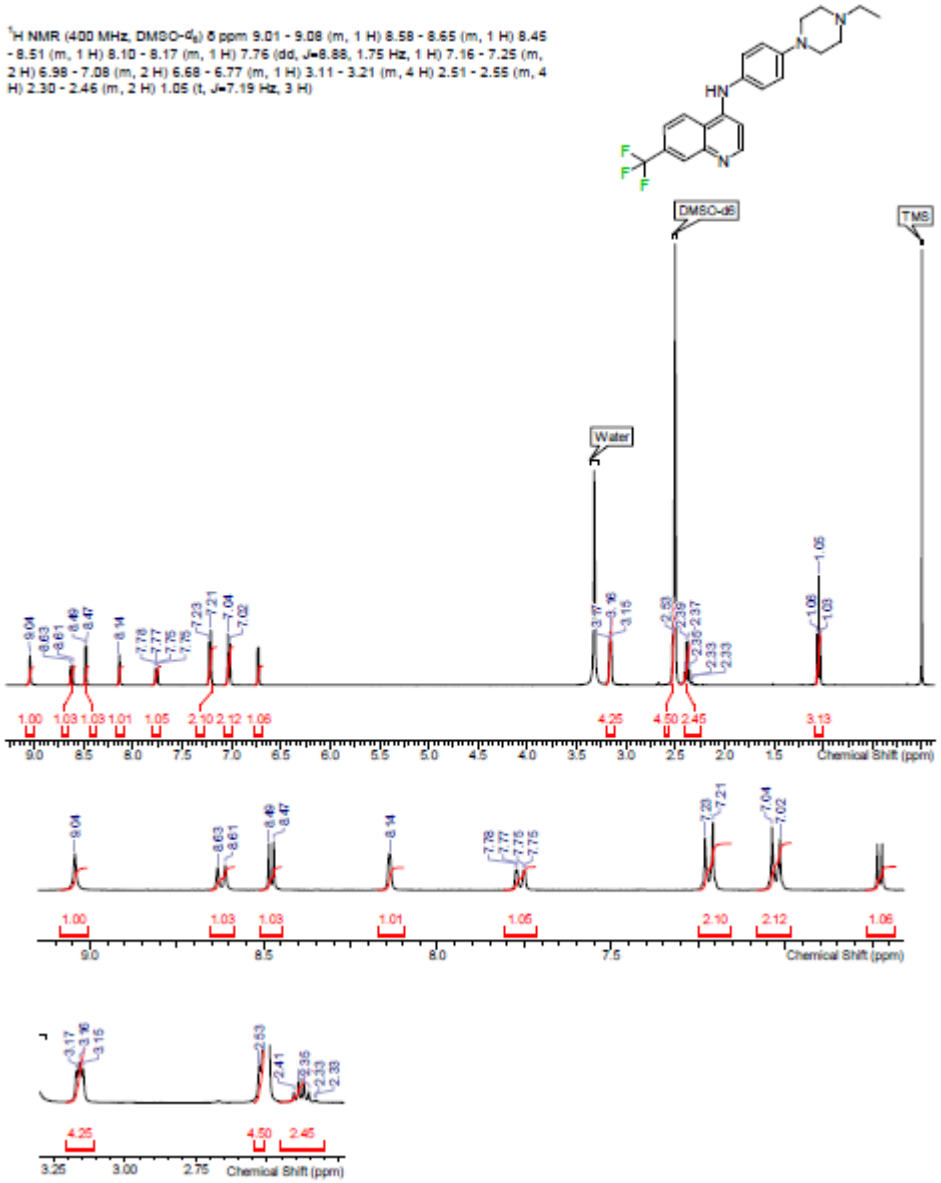

Figure 87: ^{1}H NMR spectra of 26.

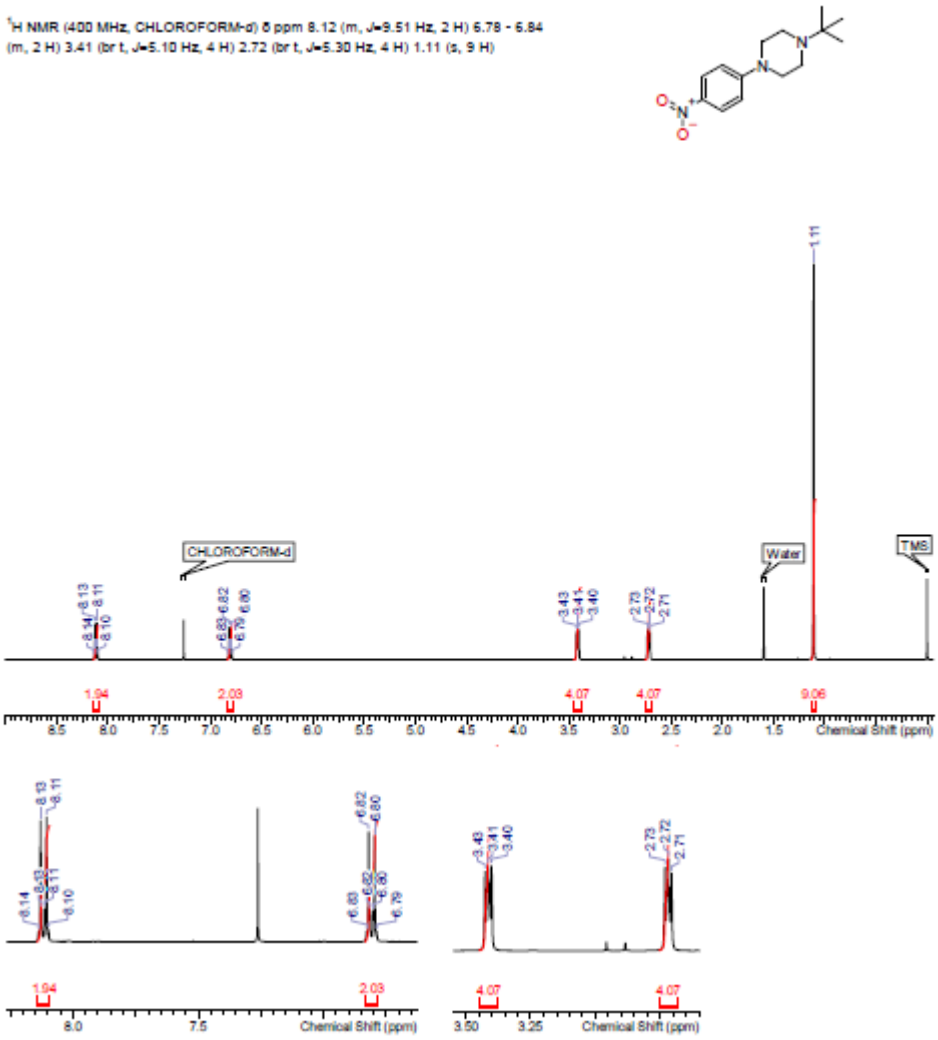

Figure 88: [1]H NMR spectra of 29a.

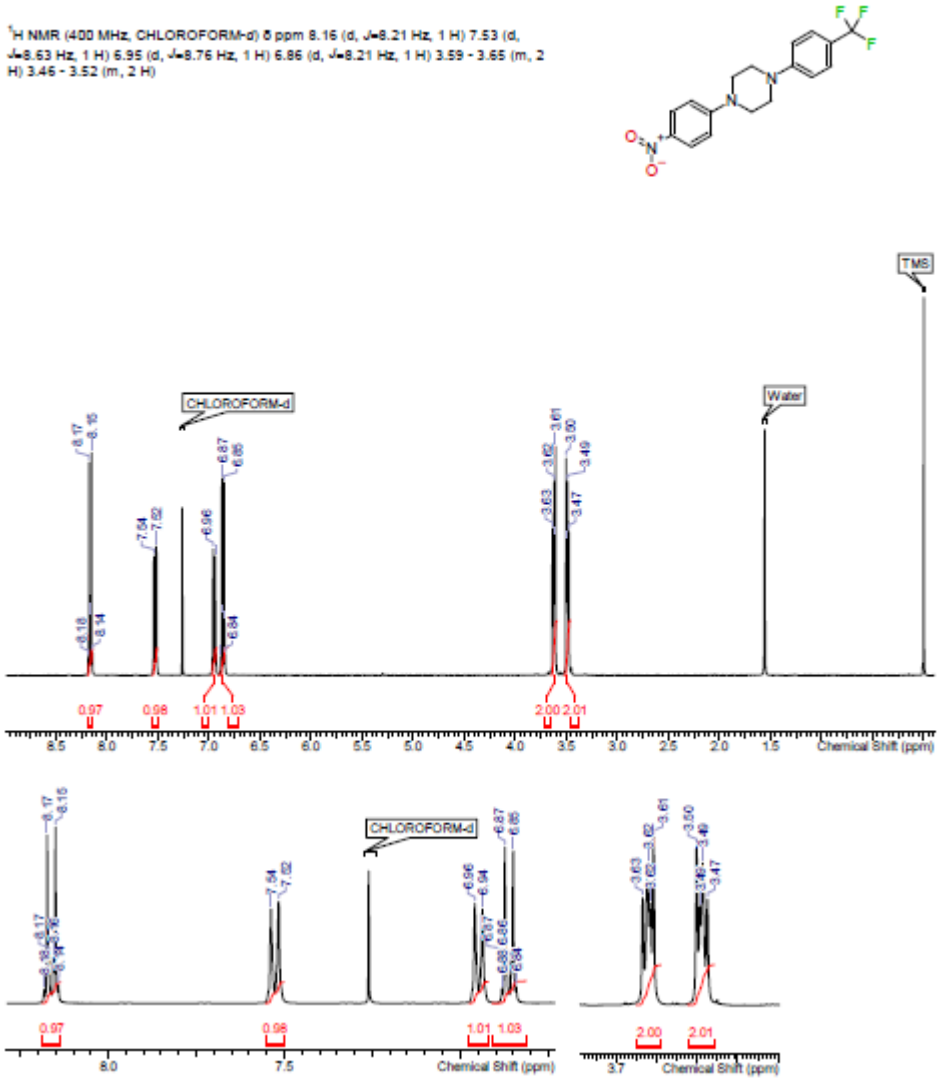

Figure 89: [1]H NMR spectra of 29b.

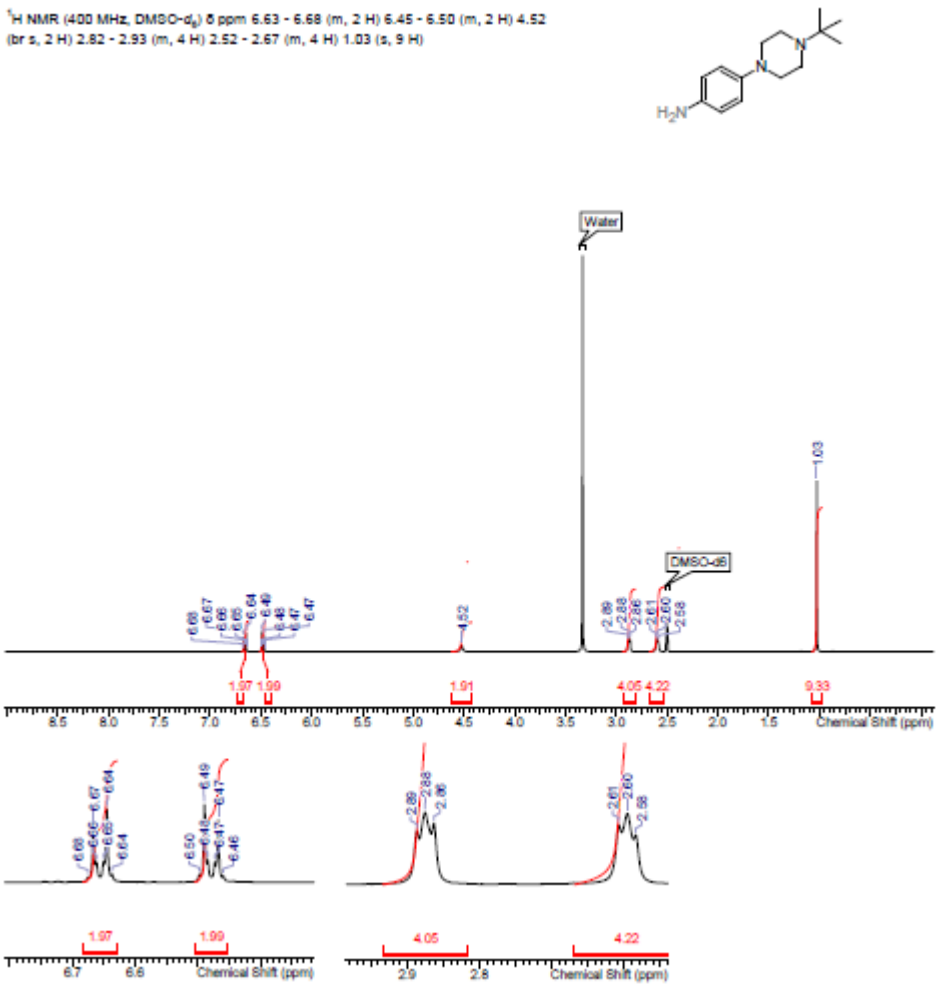

Figure 90: [1]H NMR spectra of 30a.

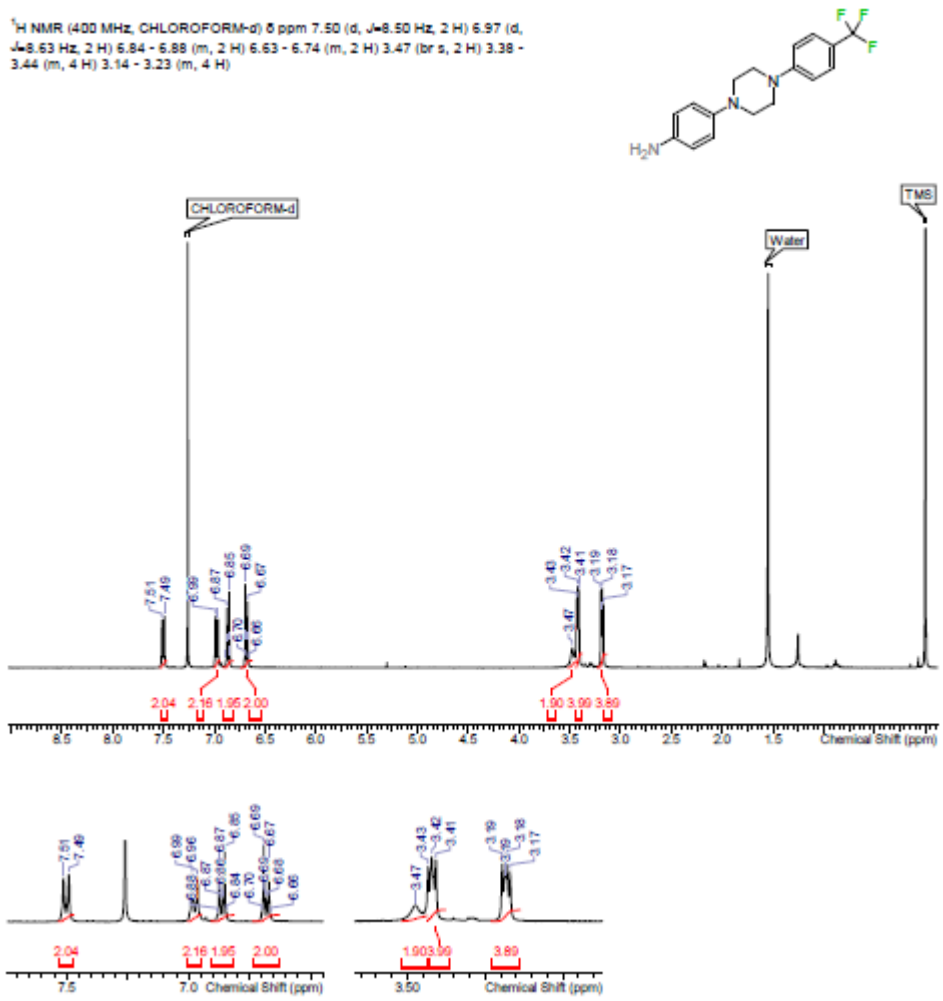

Figure 91: ^{1}H NMR spectra of 30b.

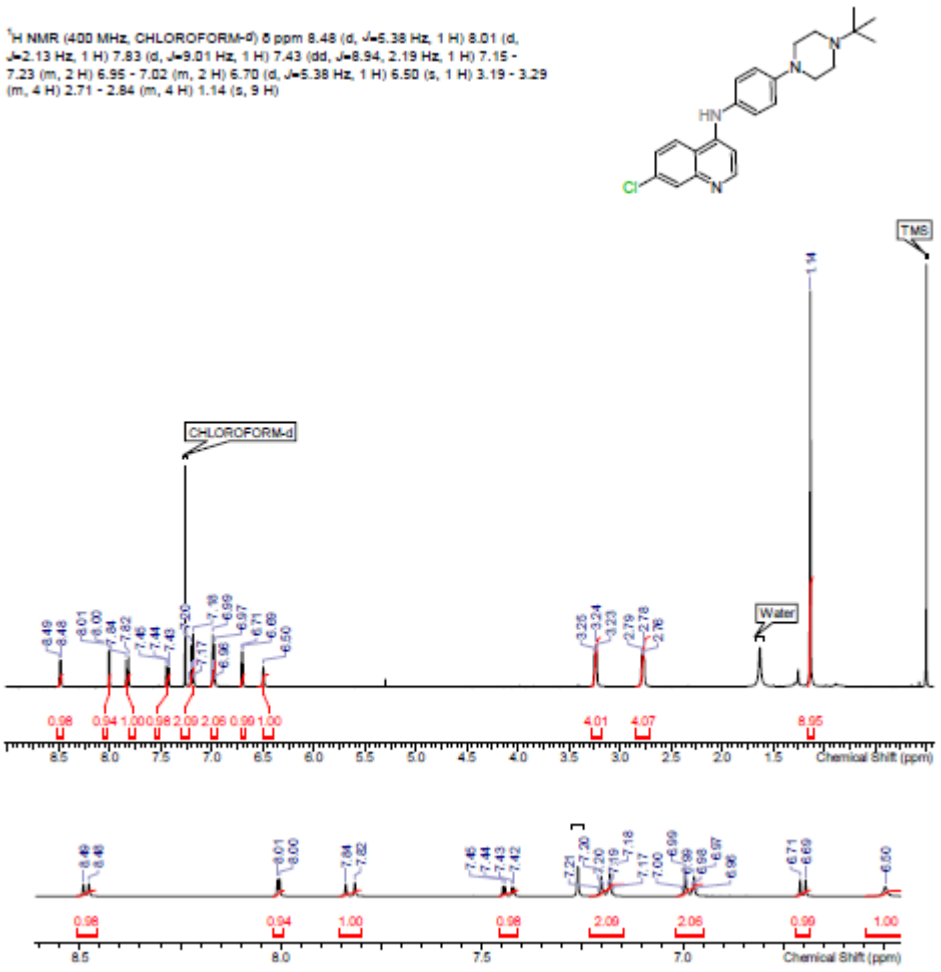

Figure 92: [1]H NMR spectra of 31.

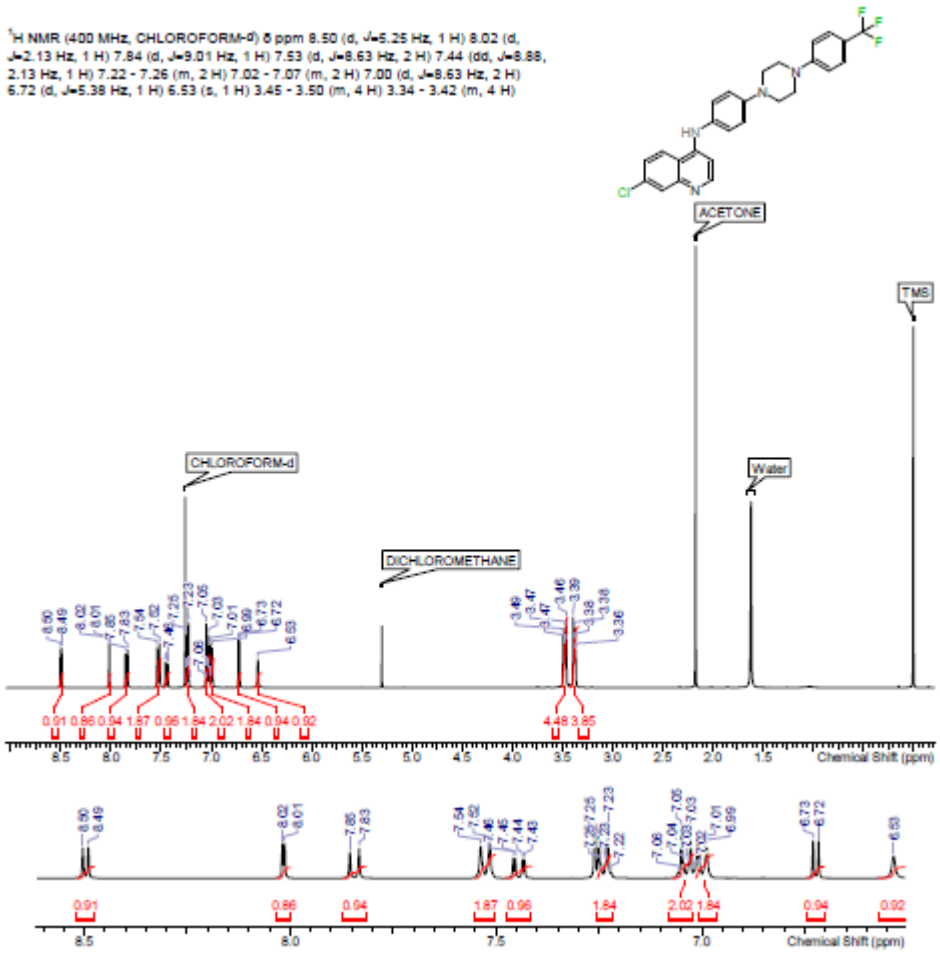

Figure 93: ^{1}H NMR spectra of 32.

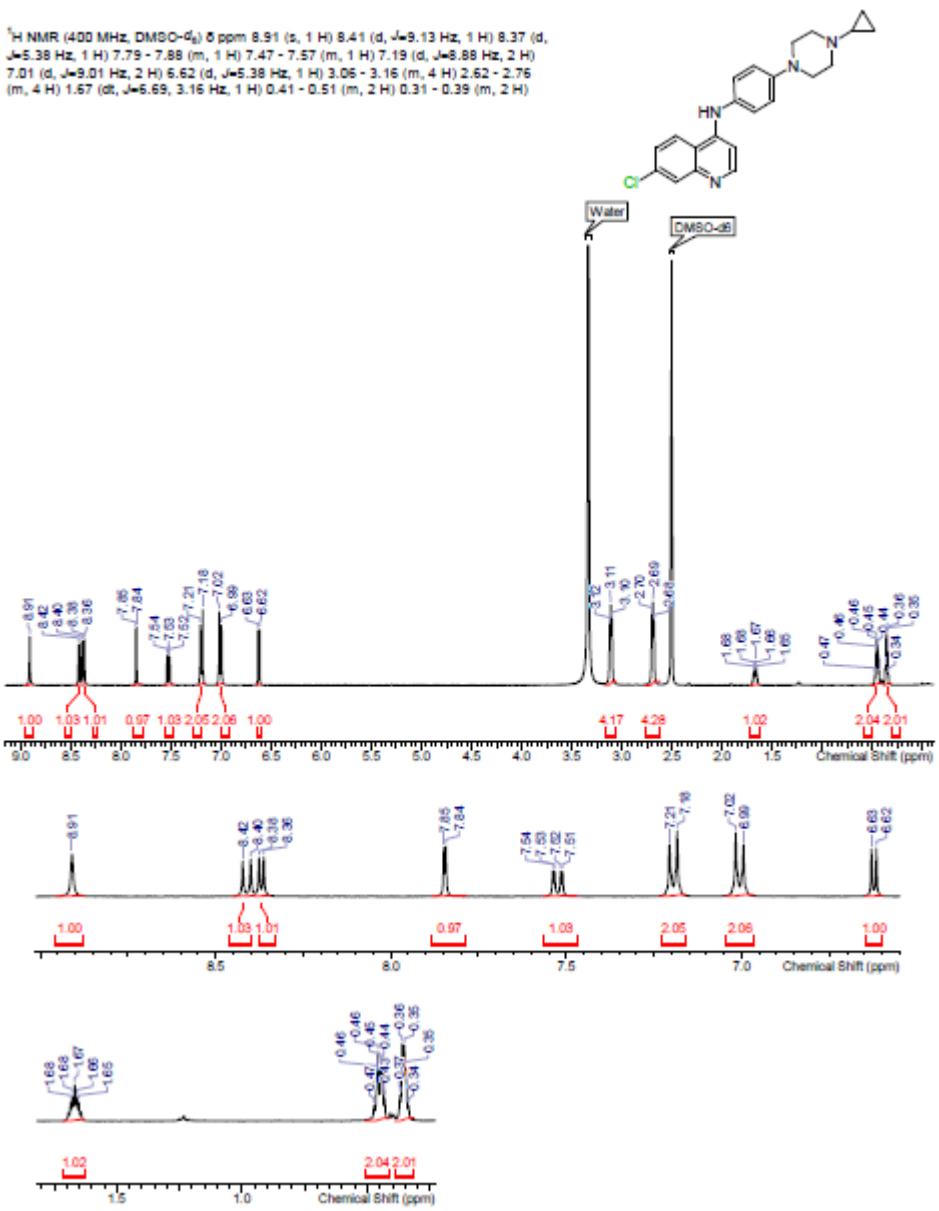

Figure 94: ^{1}H NMR spectra of 33.

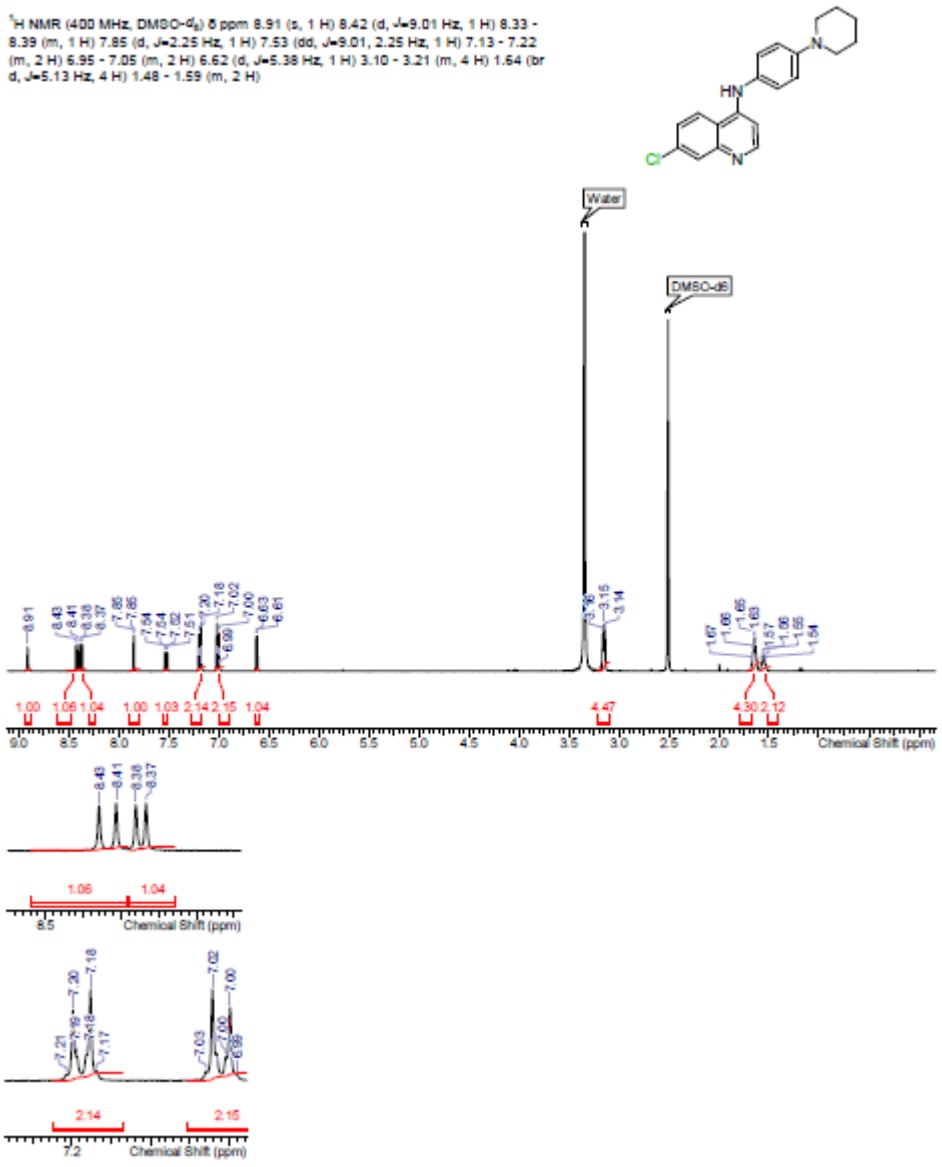

Figure 95: ^{1}H NMR spectra of 34.

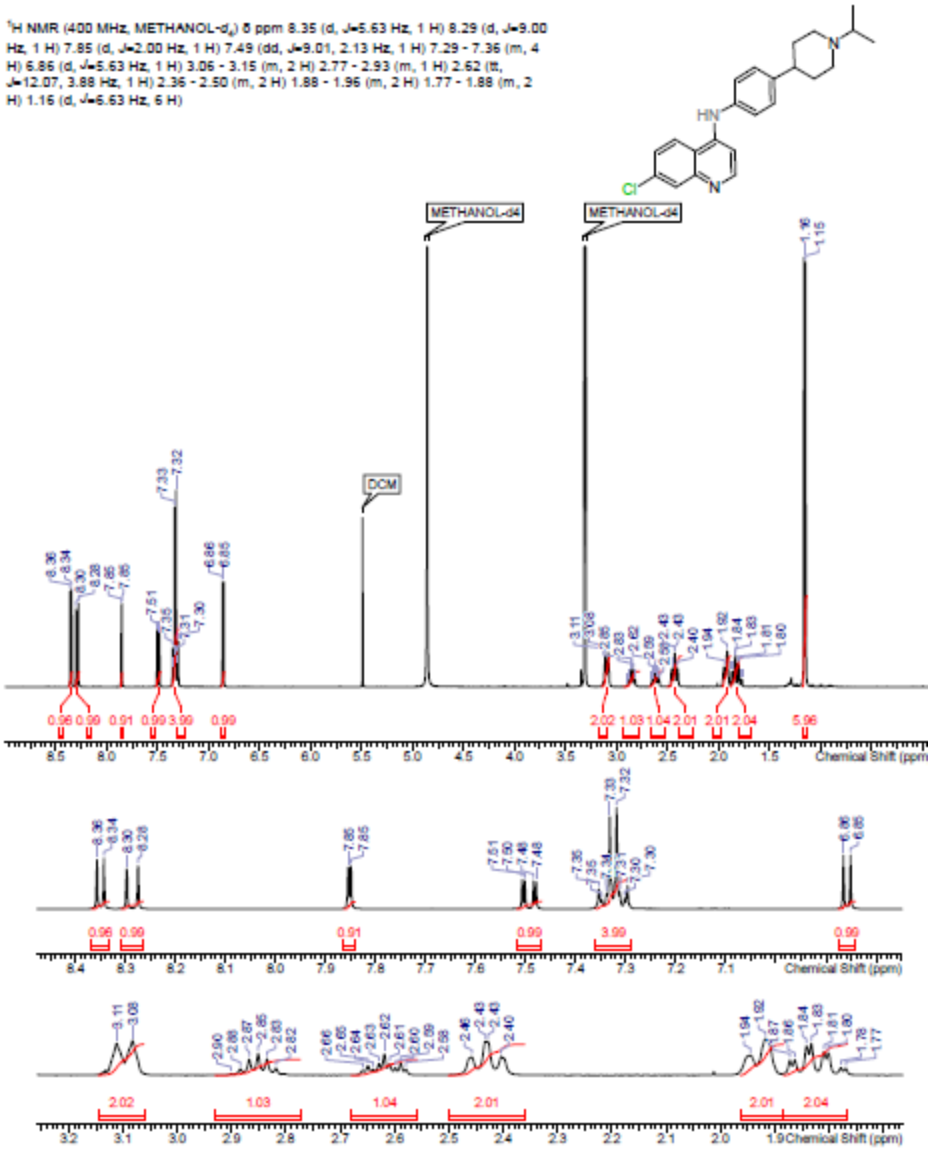

Figure 96: [1]H NMR spectra of 35.

^{1}H NMR spectra of **36**.

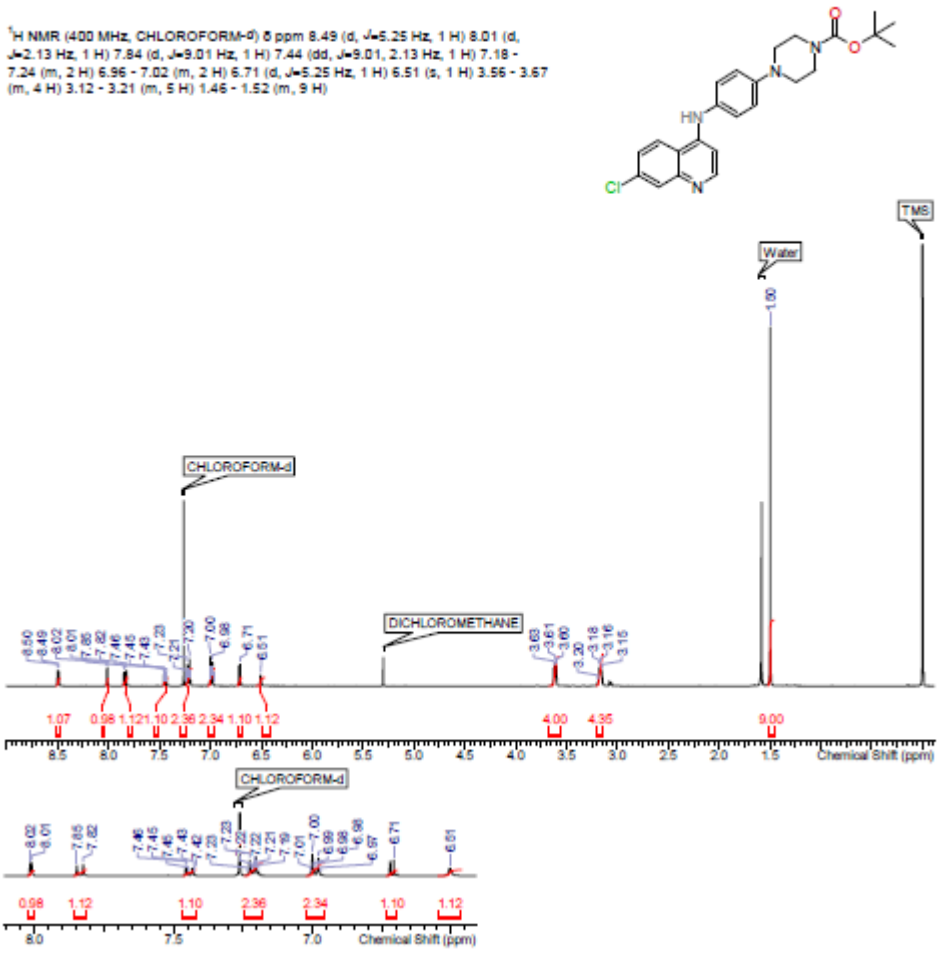

Figure 97: ^{1}H NMR spectra of 36.

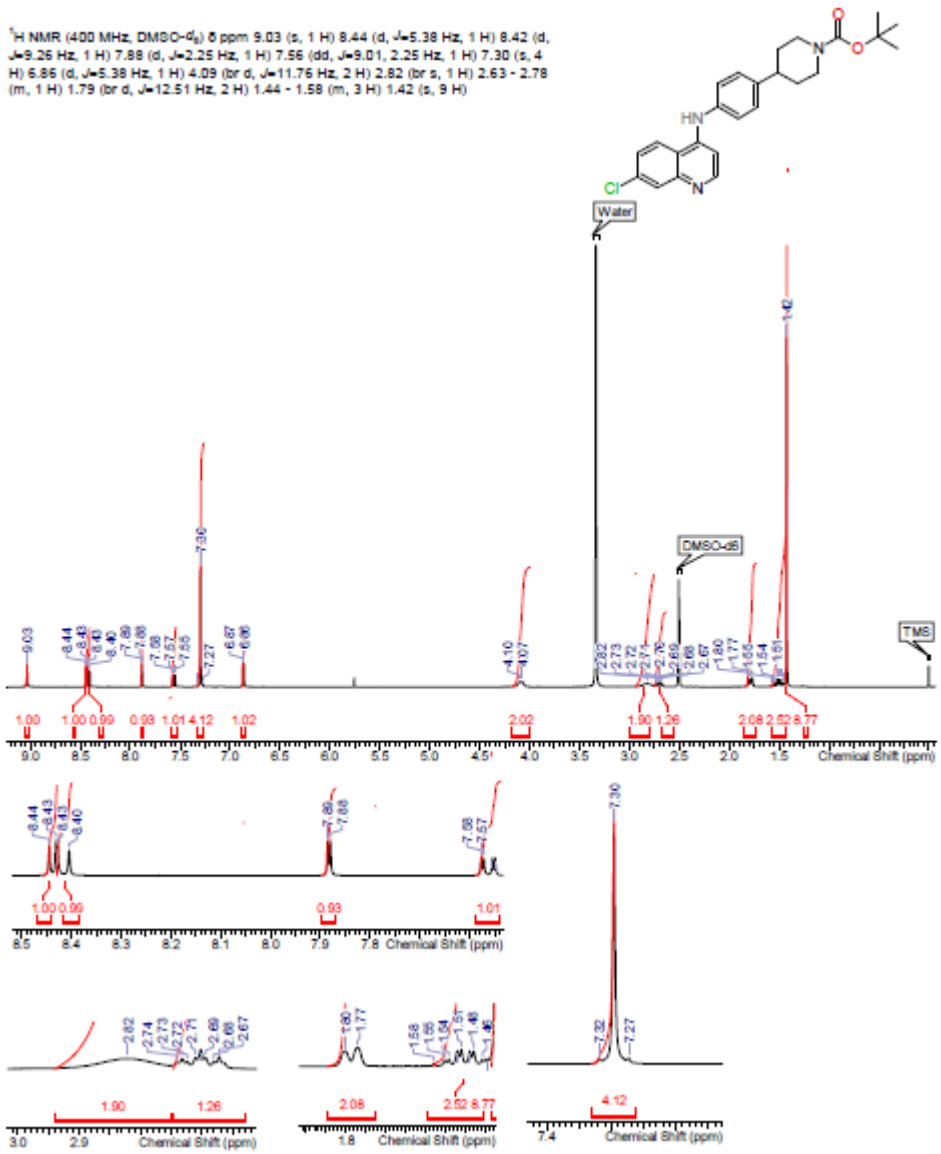

Figure 98: [1]H NMR spectra of 37.

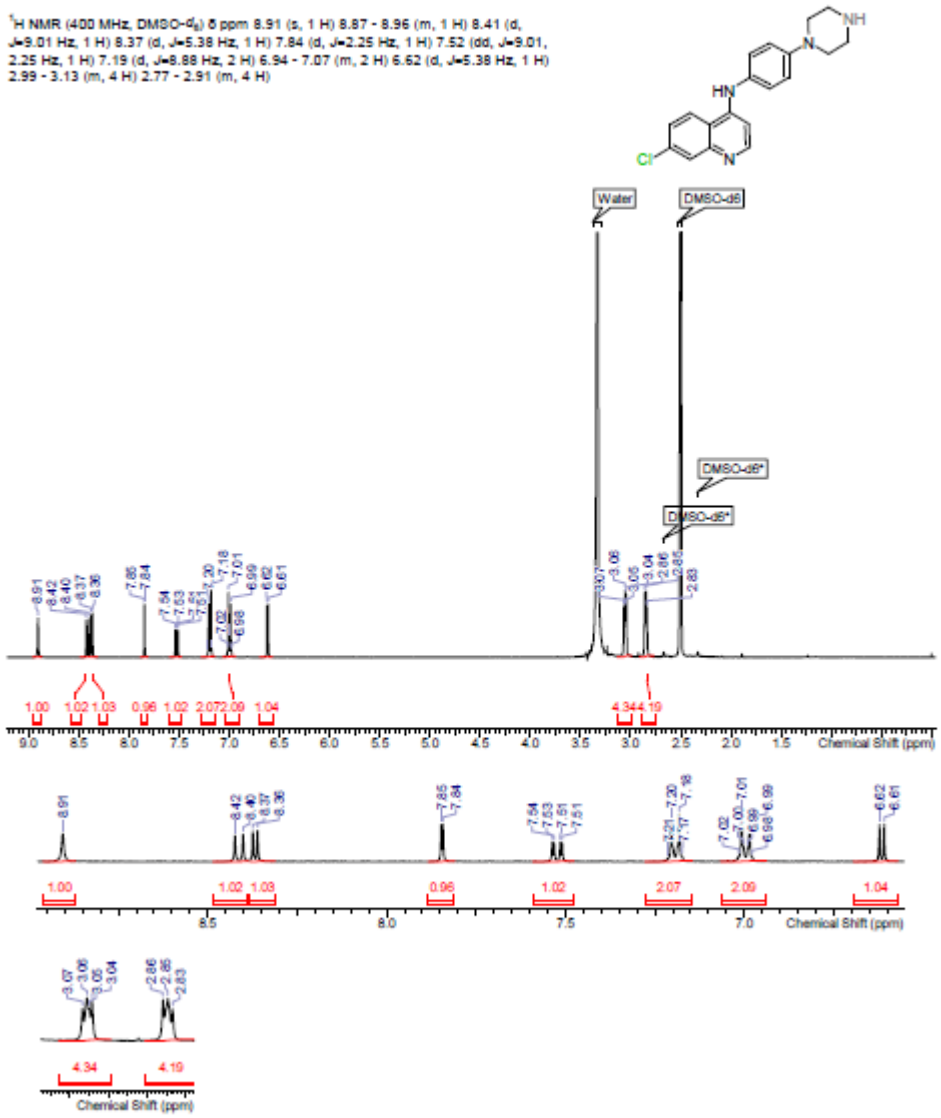

Figure 99: ^{1}H NMR spectra of 38.

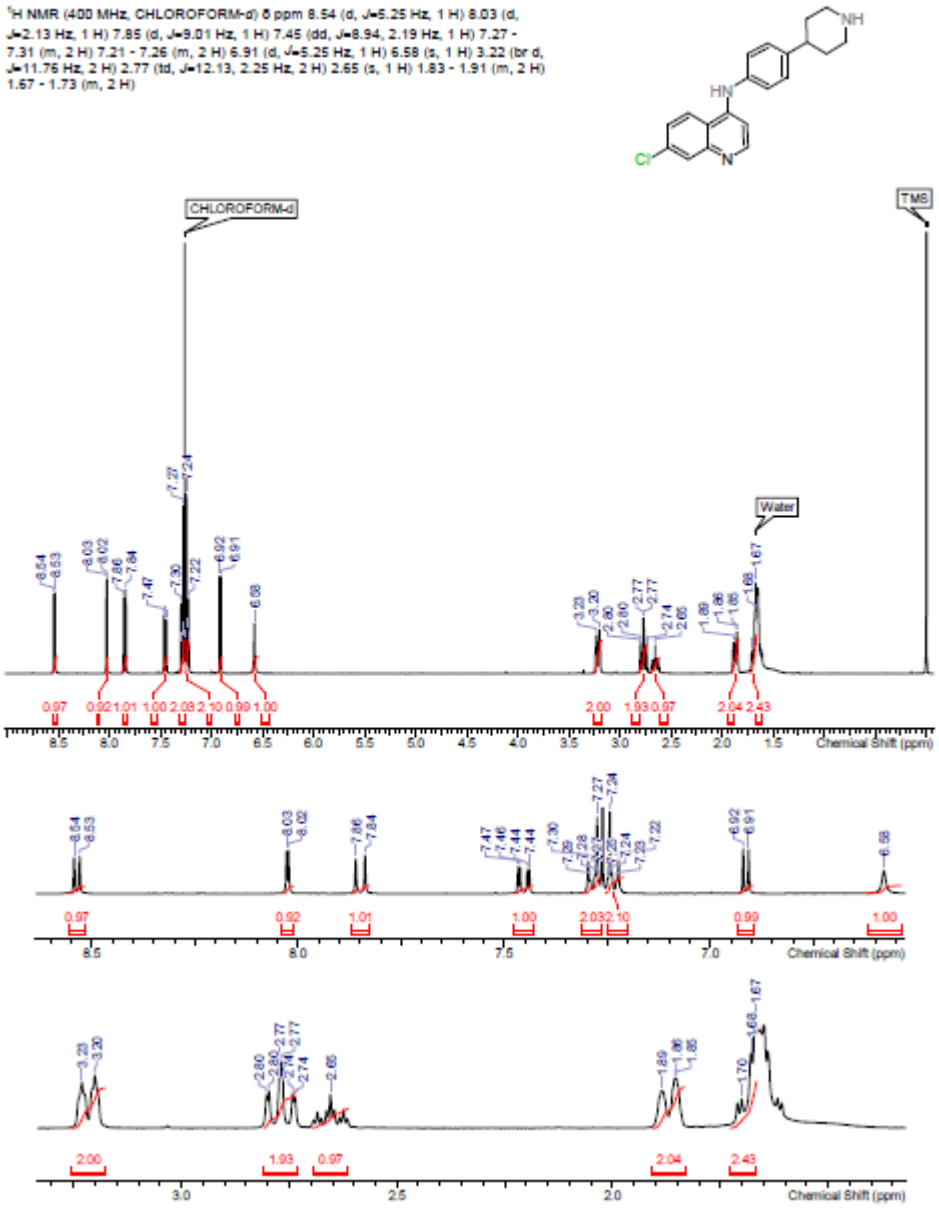

Figure 100: [1]H NMR spectra of 39.

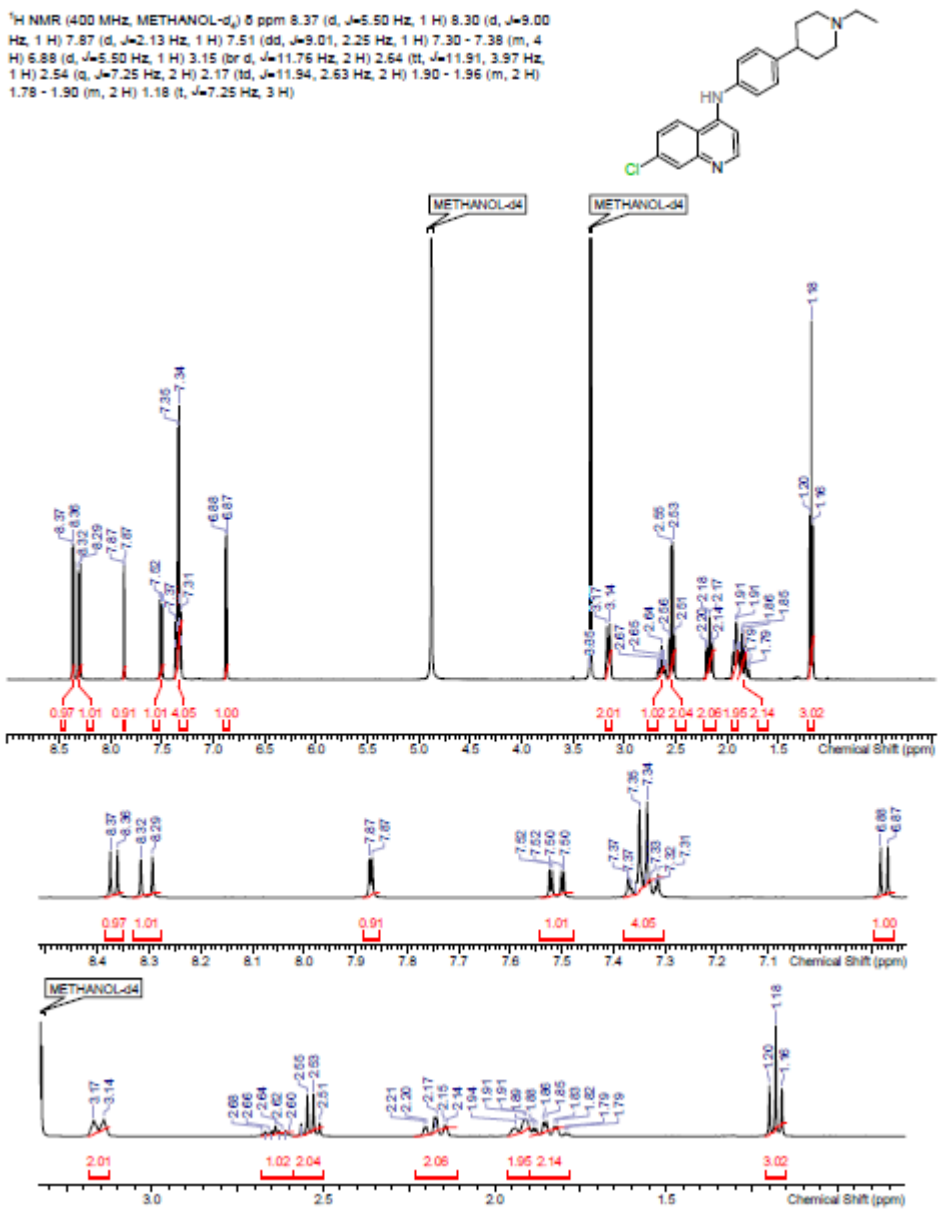

Figure 101: [1]H NMR spectra of 40.

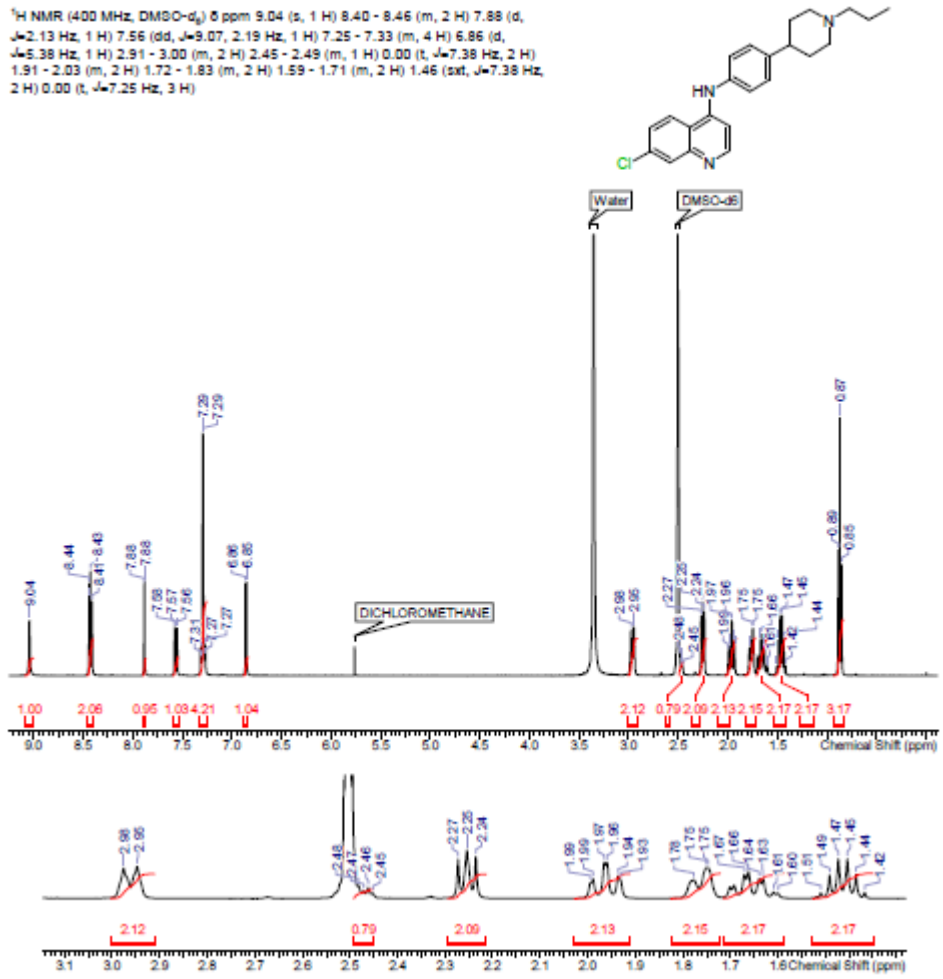

Figure 102: [1]H NMR spectra of 41.

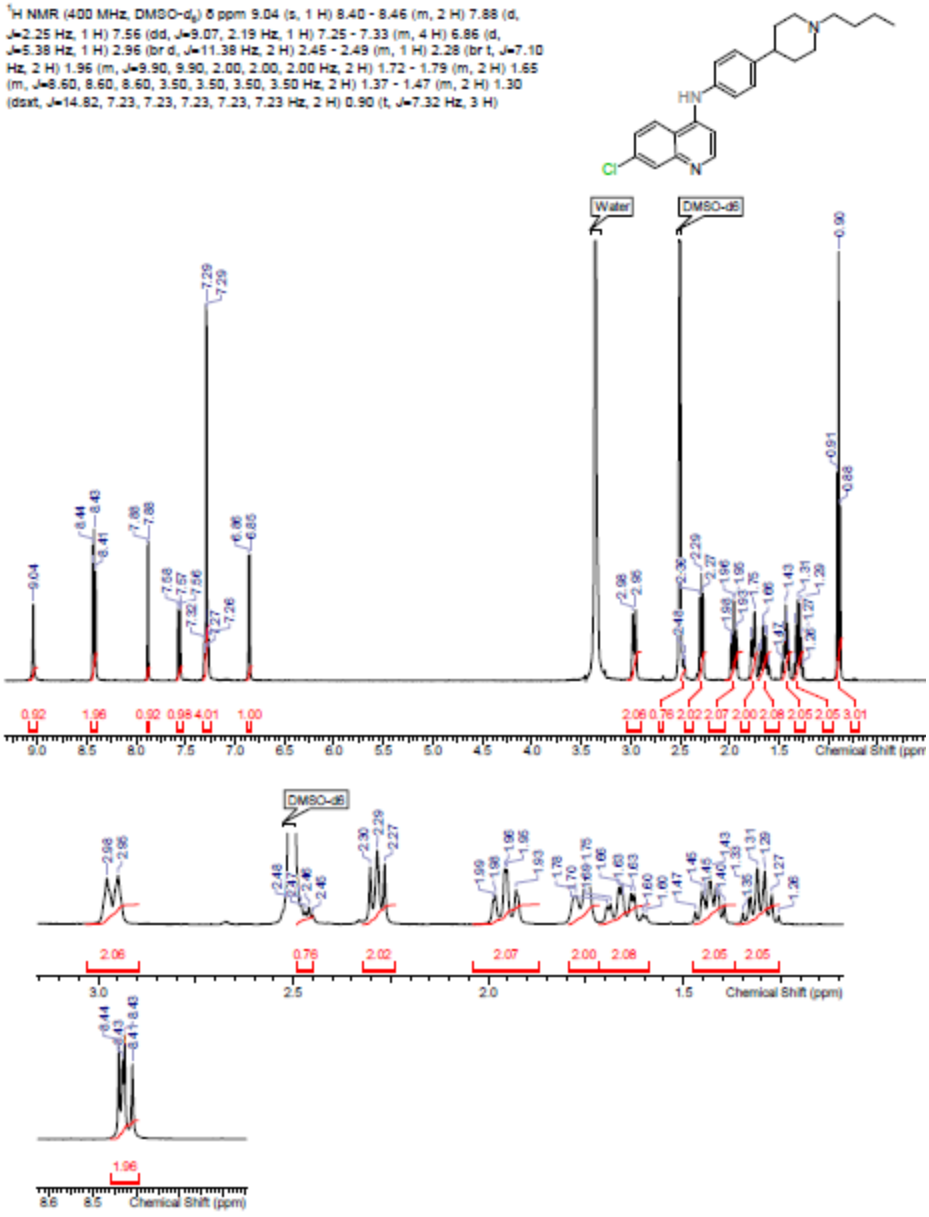

Figure 103: ^{1}H NMR spectra of 42.

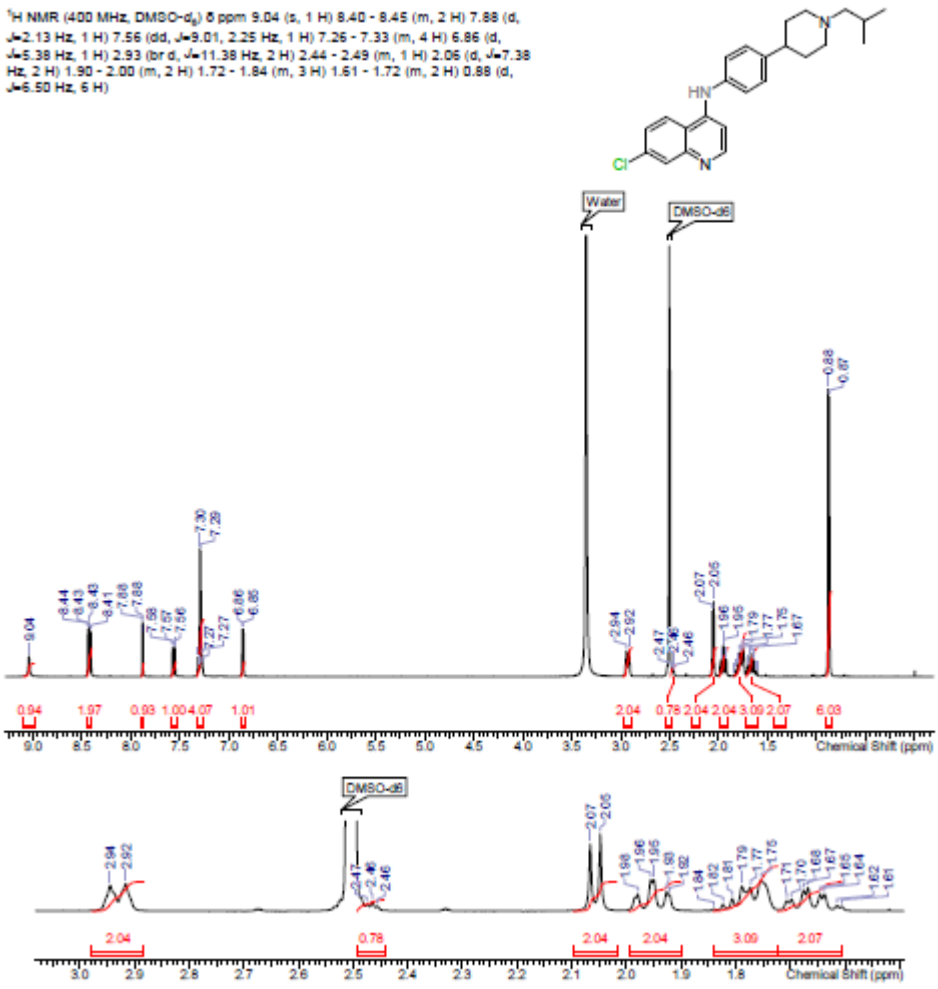

Figure 104: [1]H NMR spectra of 43.

^{1}H NMR spectra of **44**.

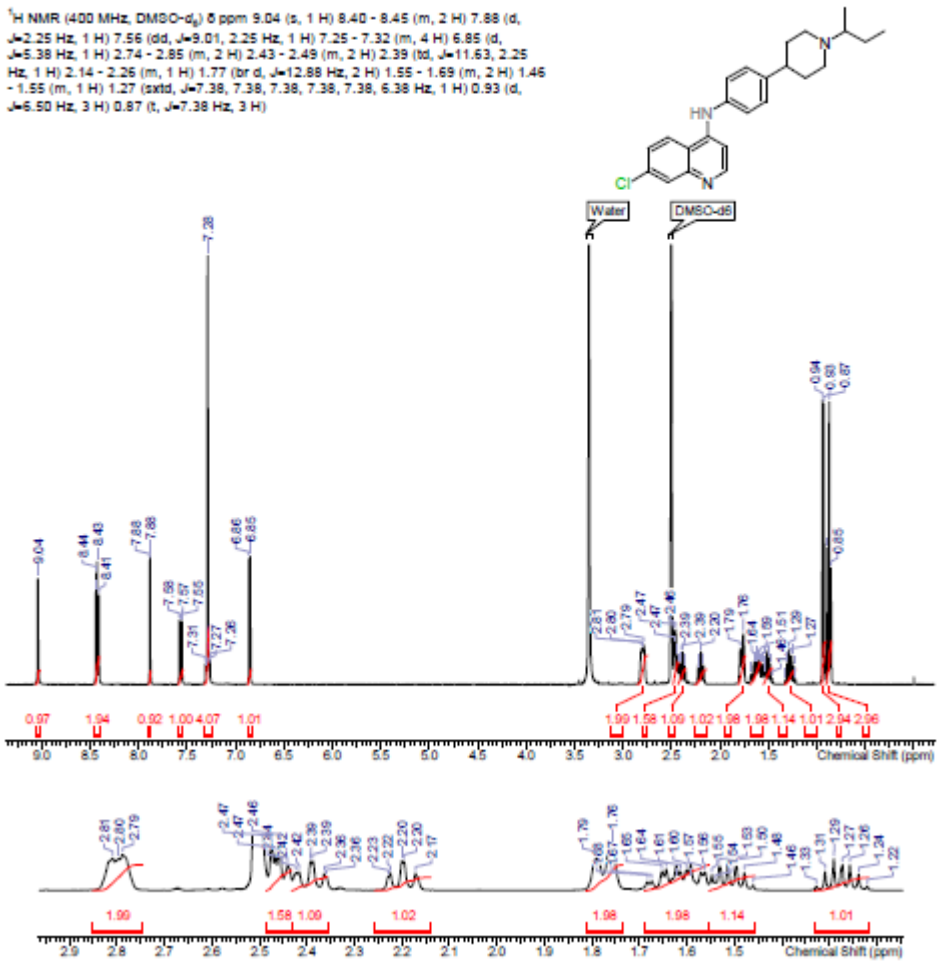

Figure 105: ^{1}H NMR spectra of 44.

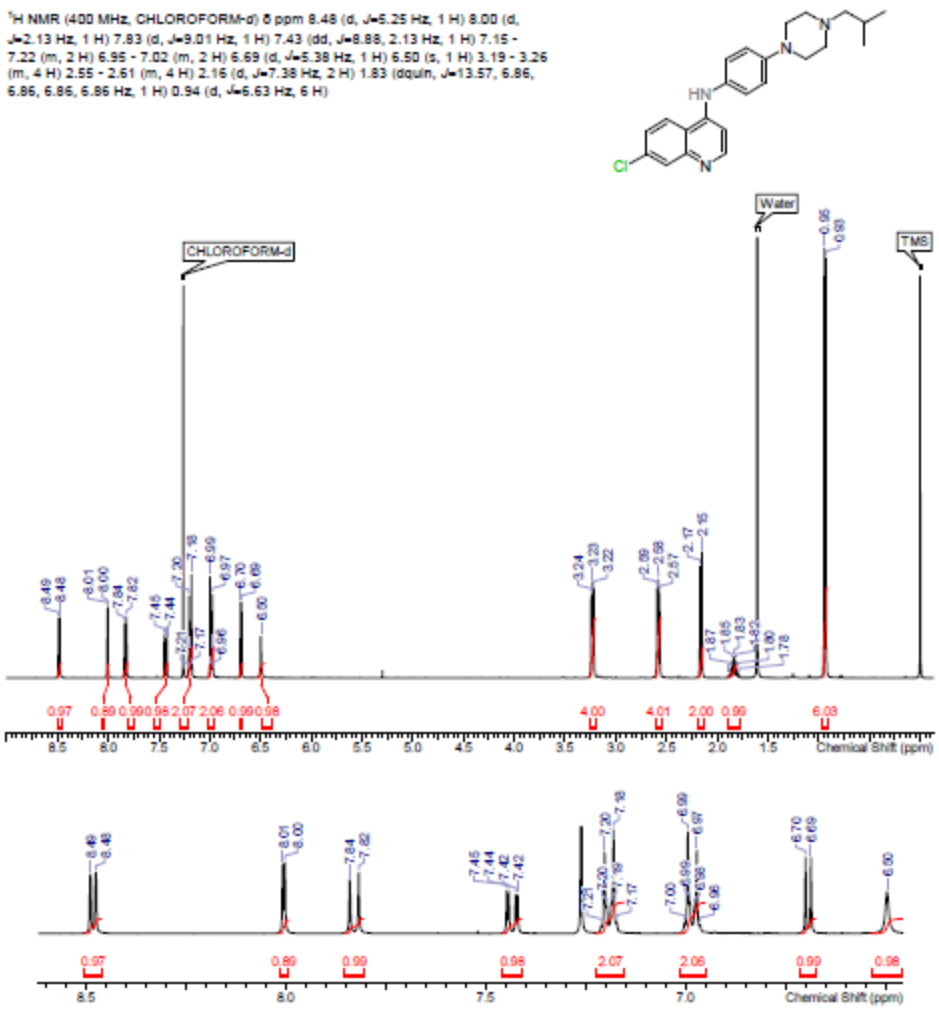

Figure 106: [1]H NMR spectra of 45.

F.2. ^{1} NMR of Compounds presented in Chapter 7

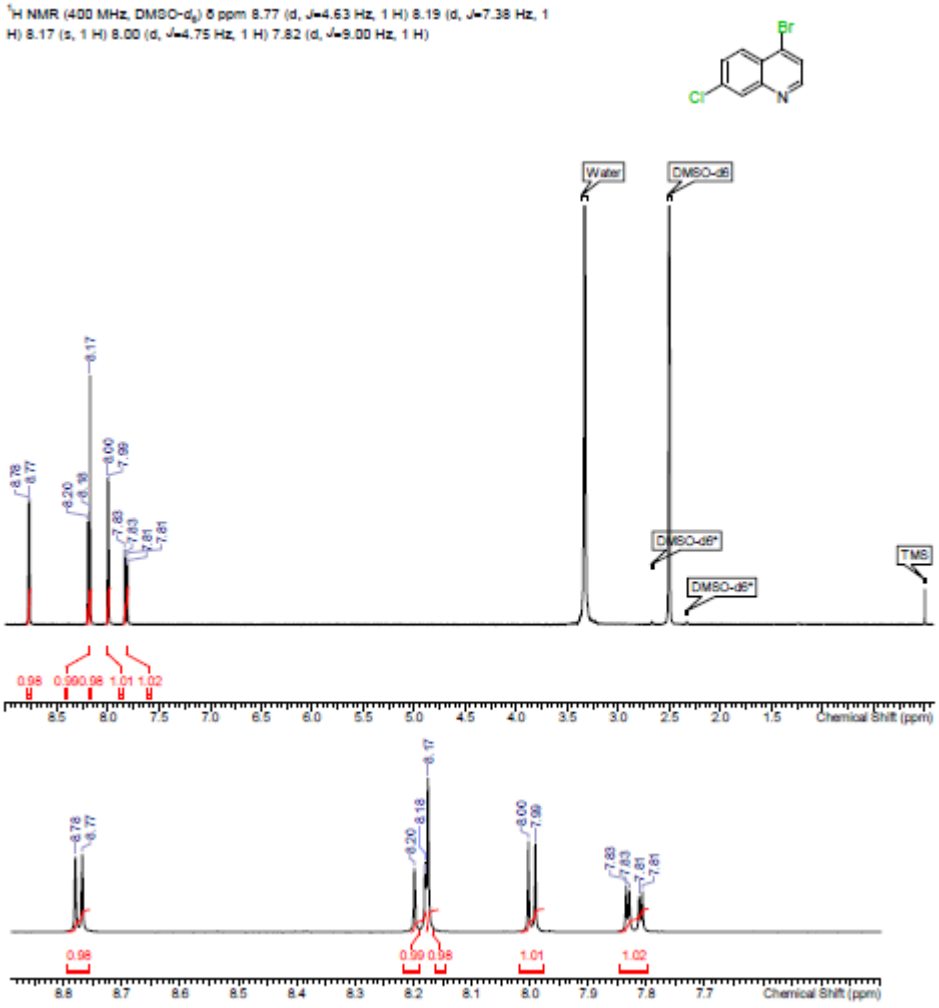

Figure 107: ^{1}H NMR spectra of 50.

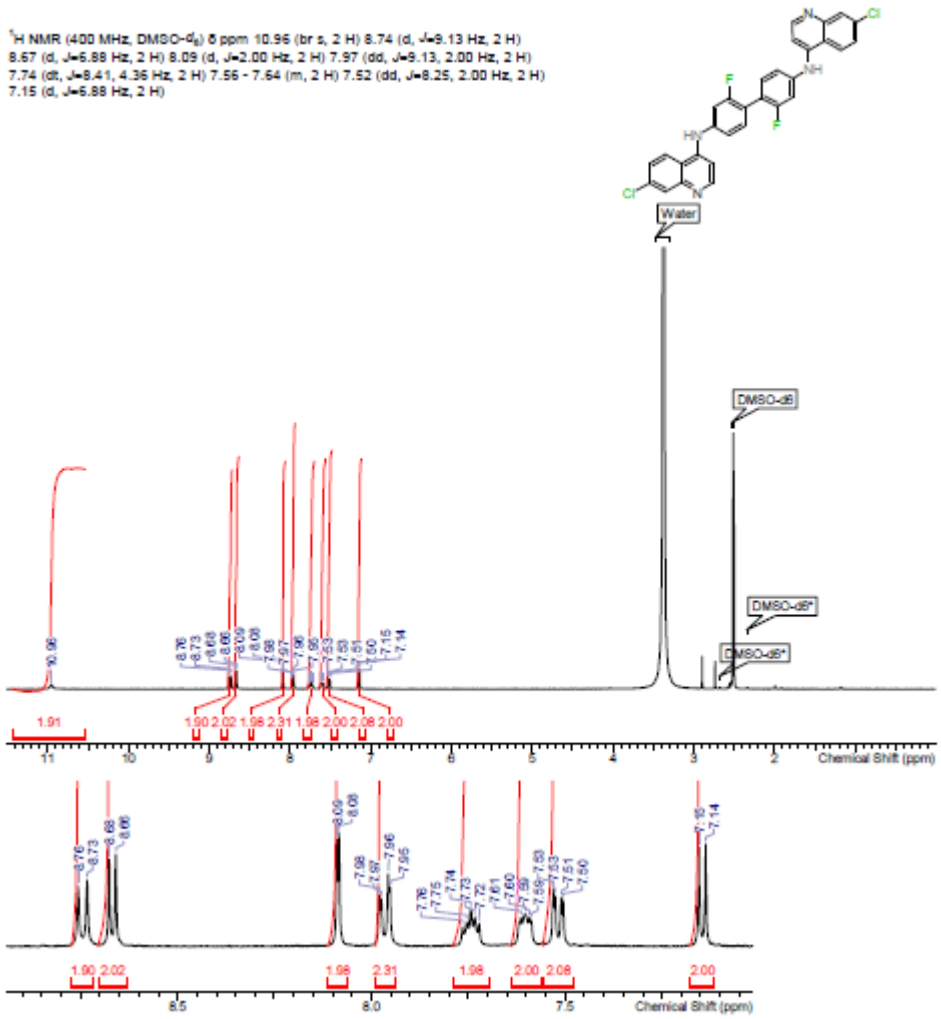

Figure 108: ^{1}H NMR spectra of 51.

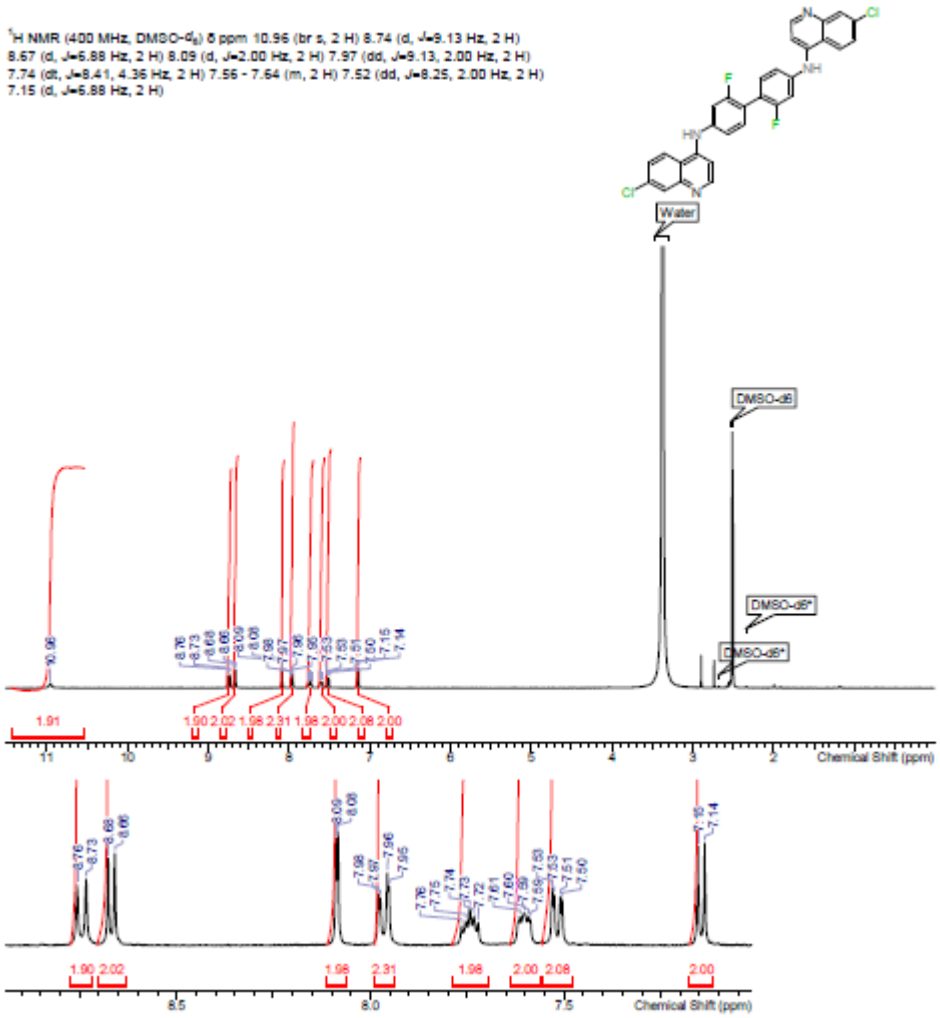

Figure 109: ^{1}H NMR spectra of 52.

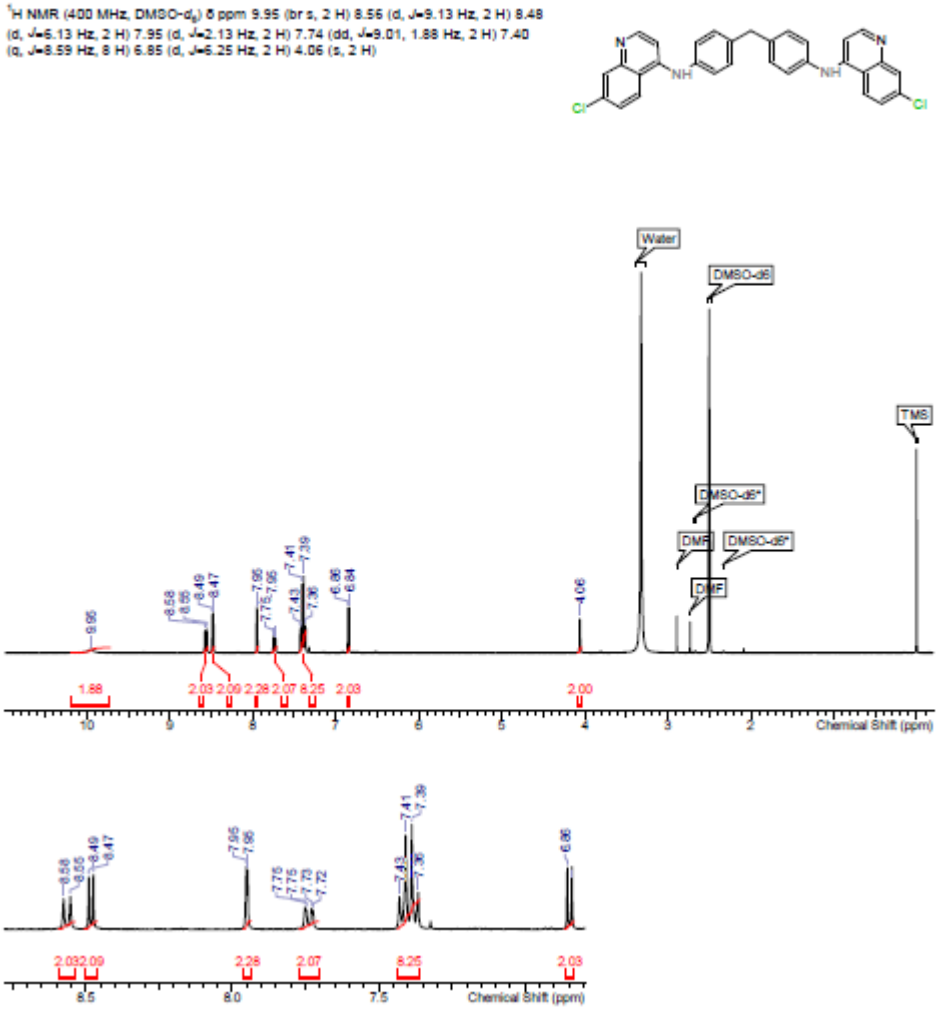

Figure 110: [1]H NMR spectra of 53.

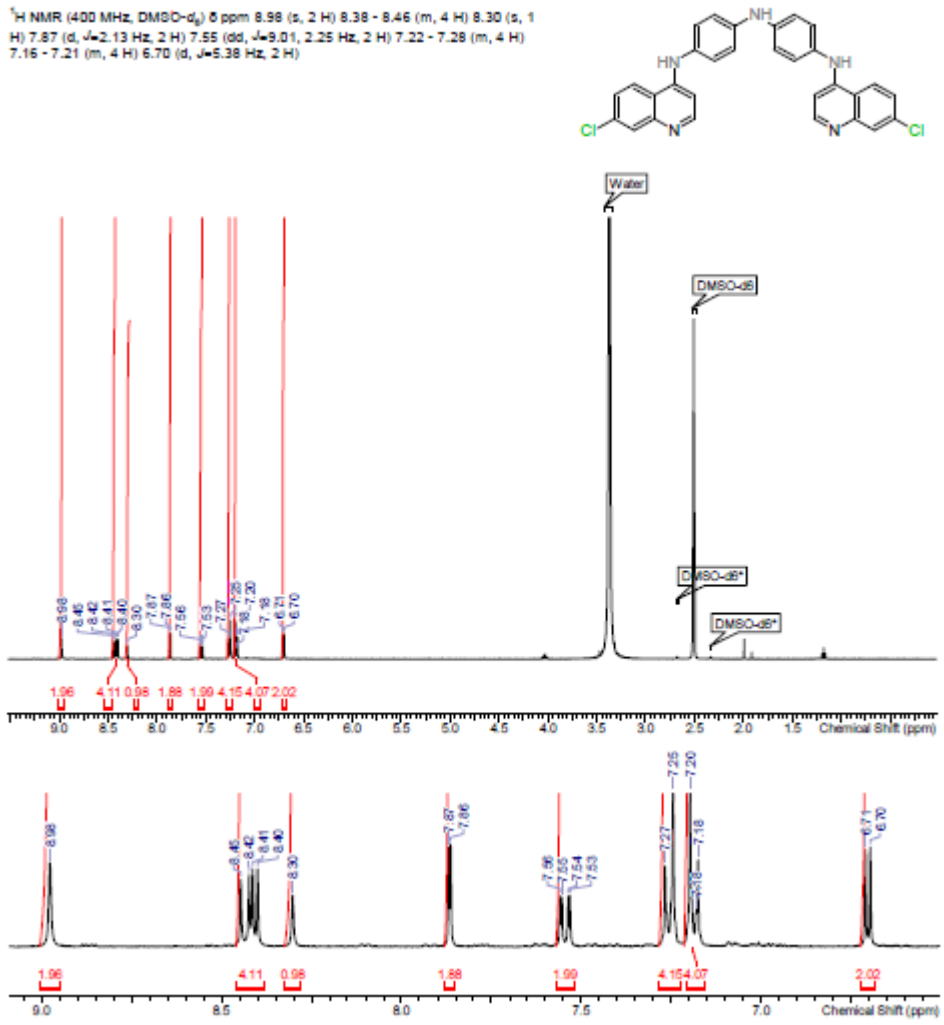

Figure 111: [1]H NMR spectra of 54.

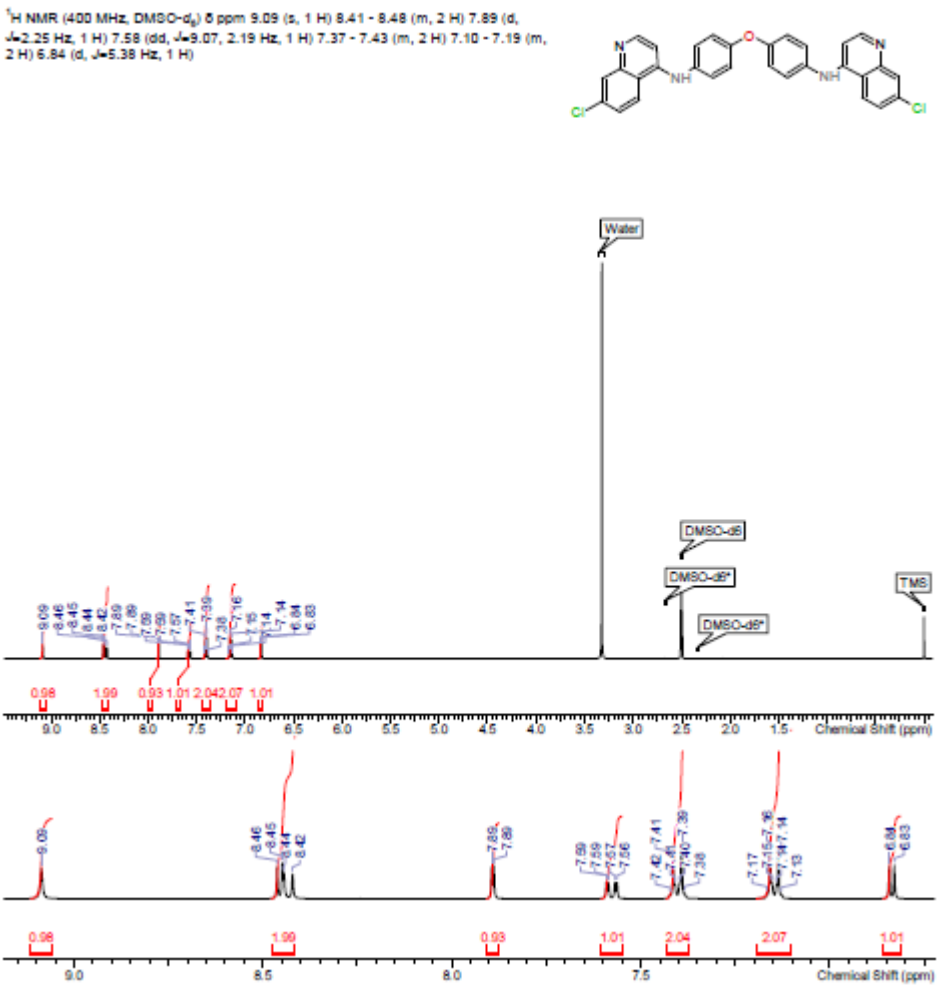

Figure 112: [1]H NMR spectra of 55.

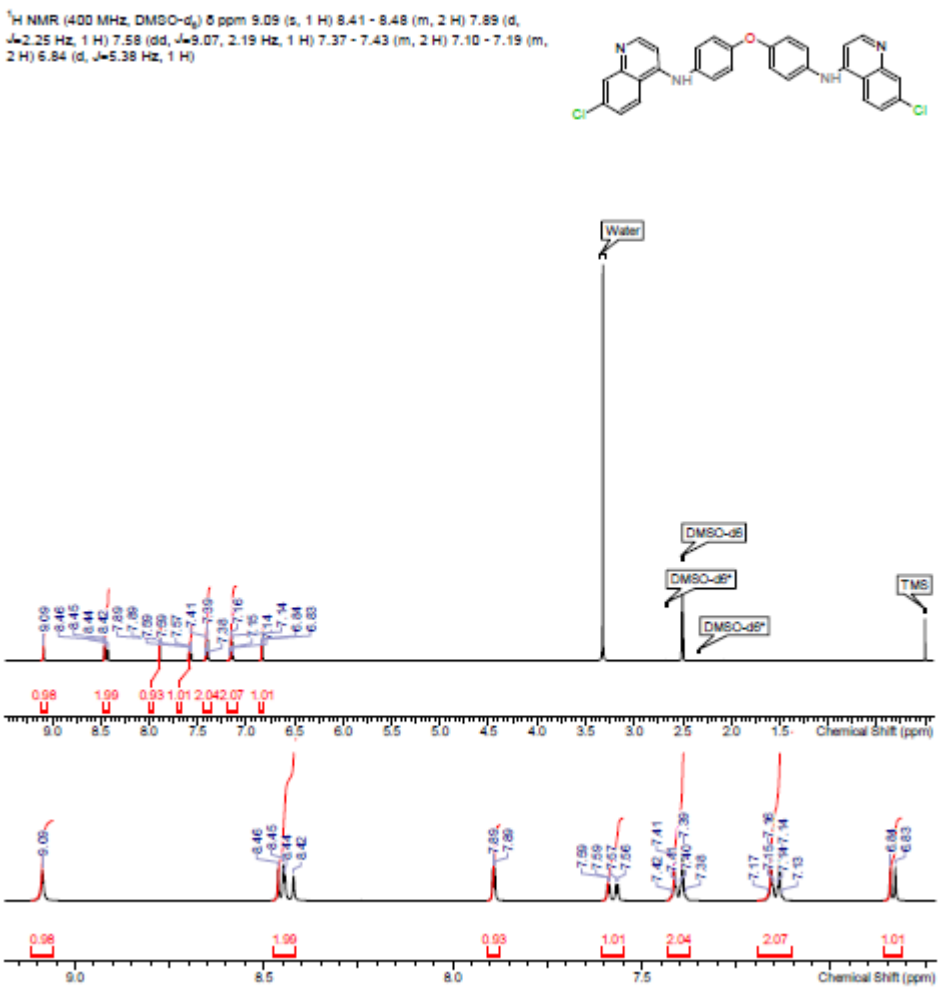

Figure 113: [1]H NMR spectra of 56.

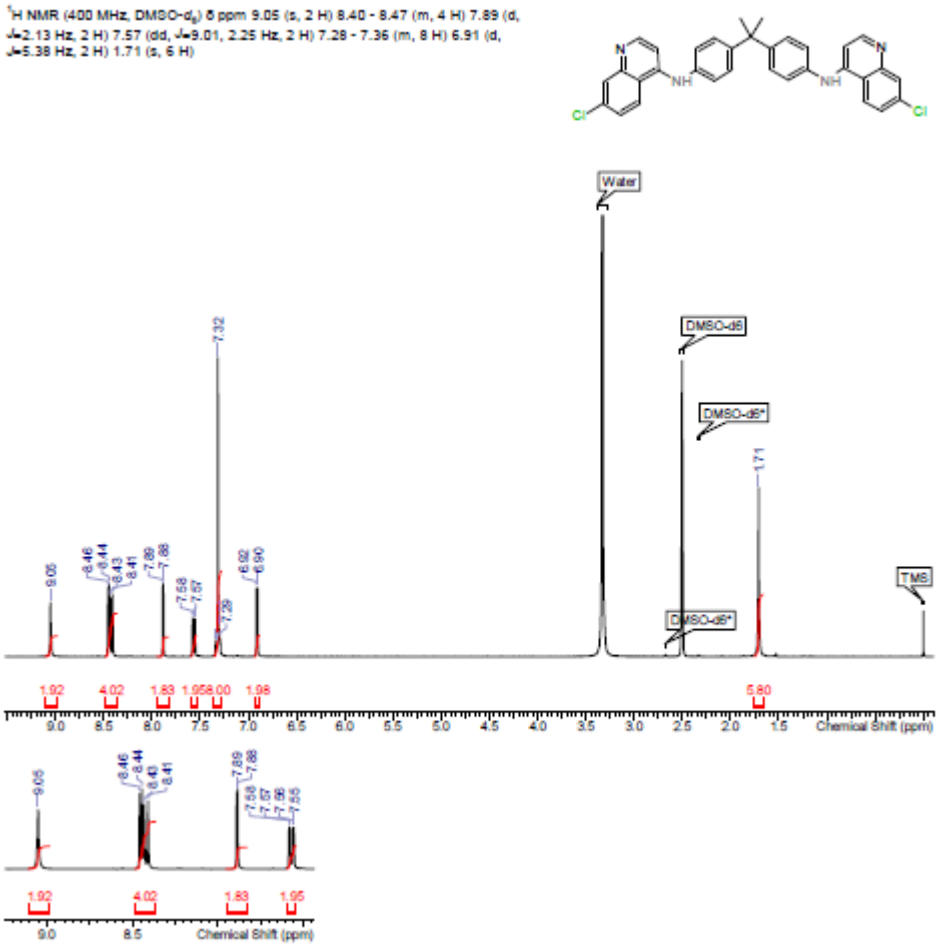

Figure 114: ^{1}H NMR spectra of 57.

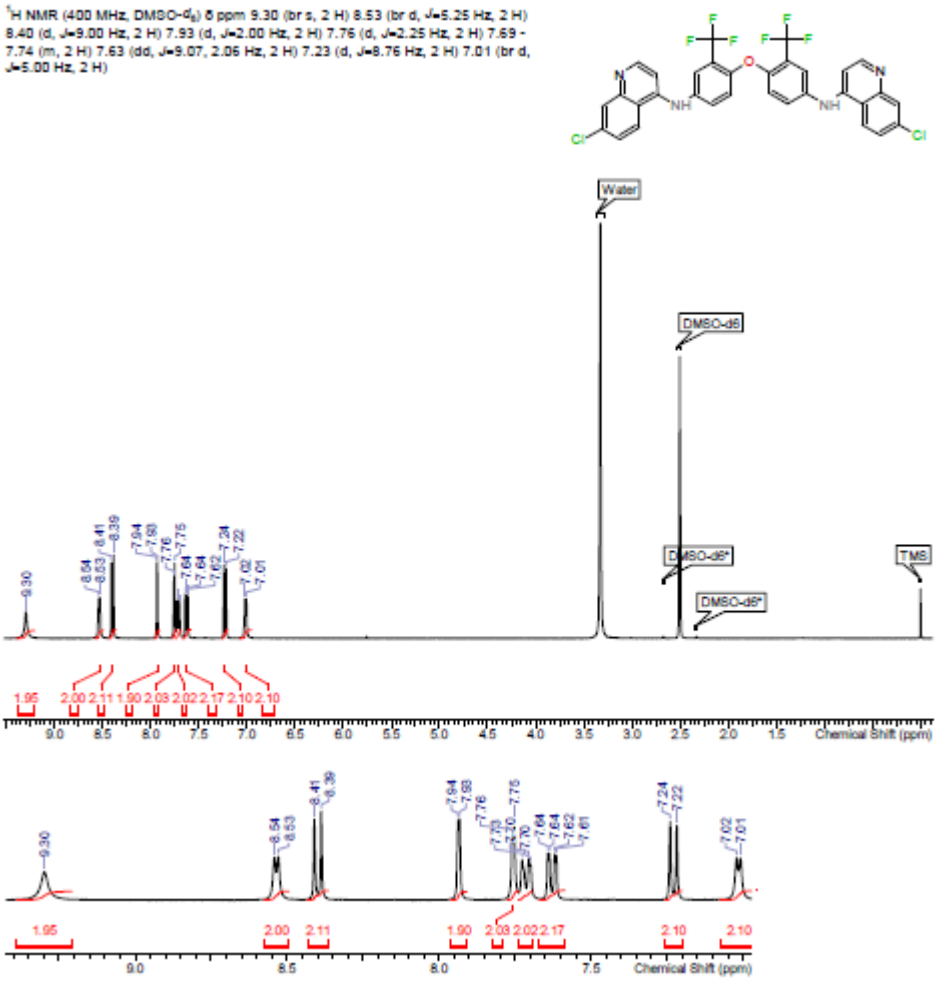

Figure 115: ^{1}H NMR spectra of 58.

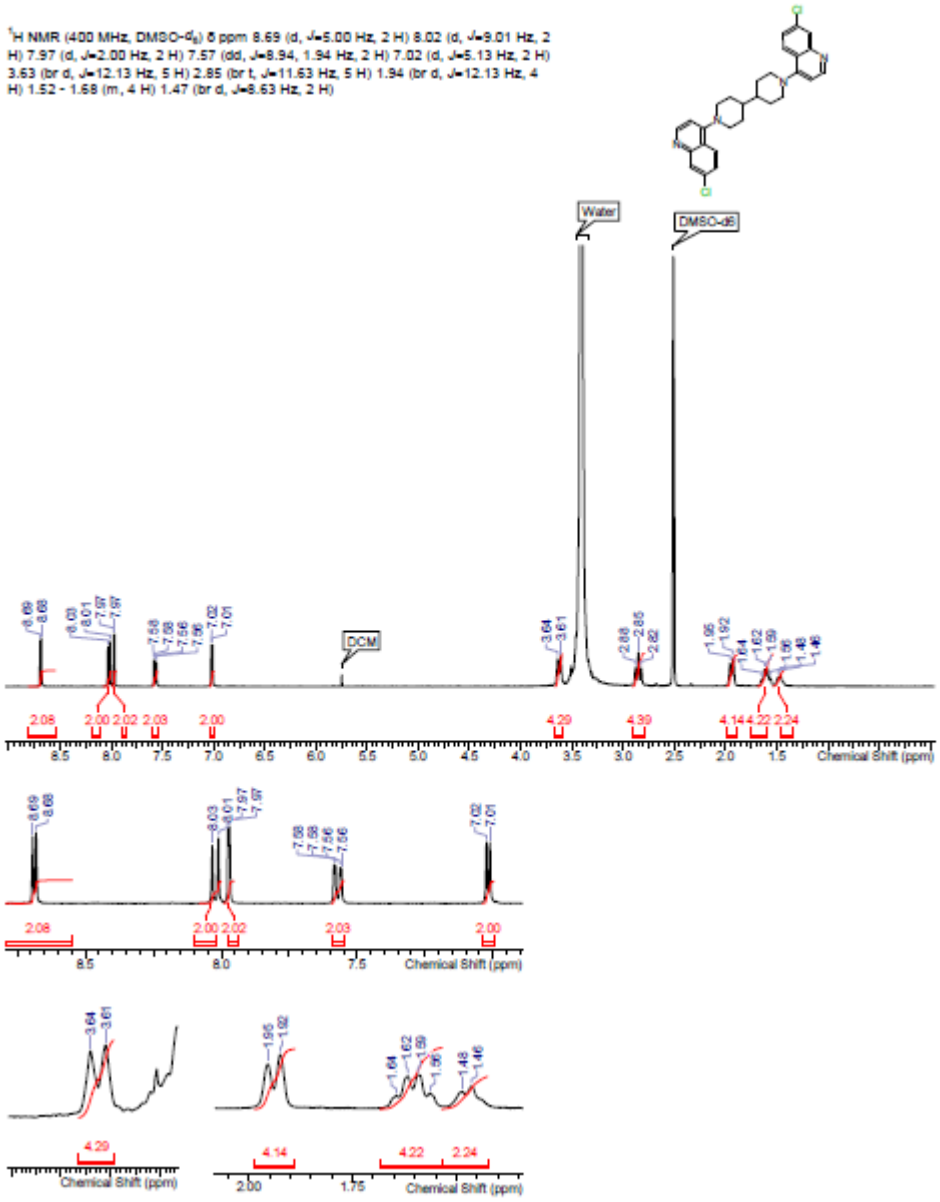

Figure 116: [1]H NMR spectra of 60.

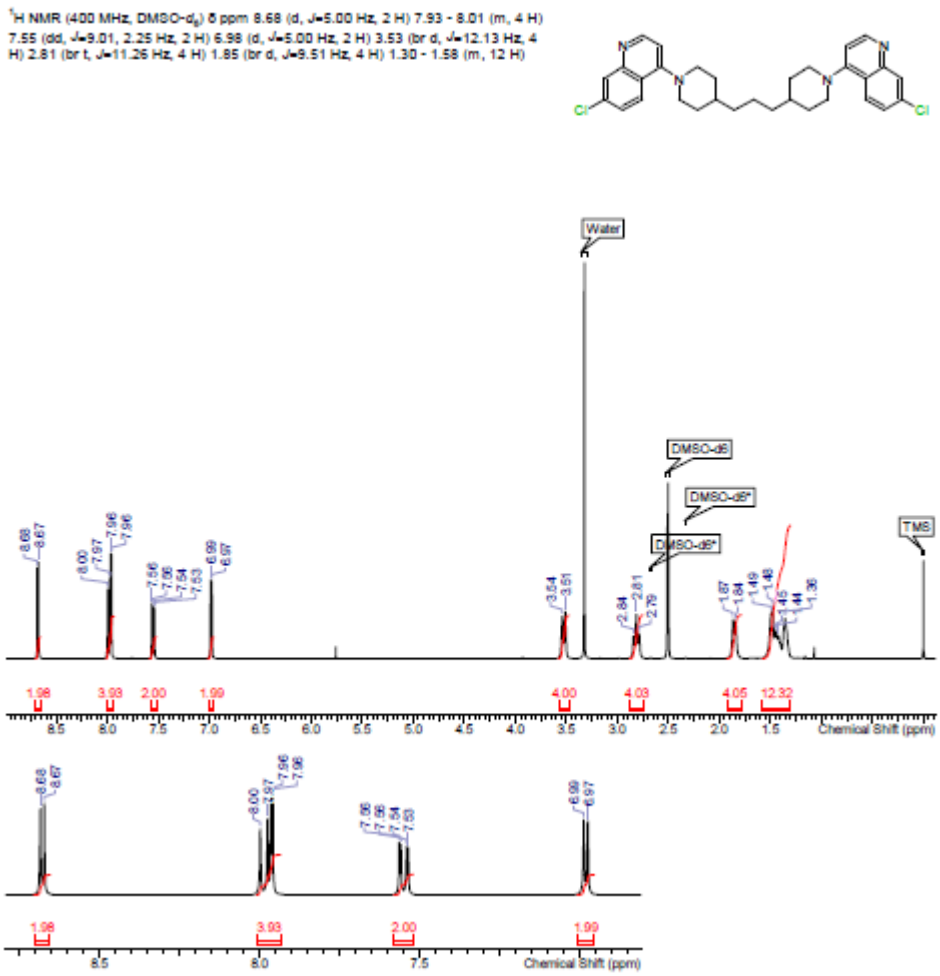

Figure 117: [1]H NMR spectra of 61.

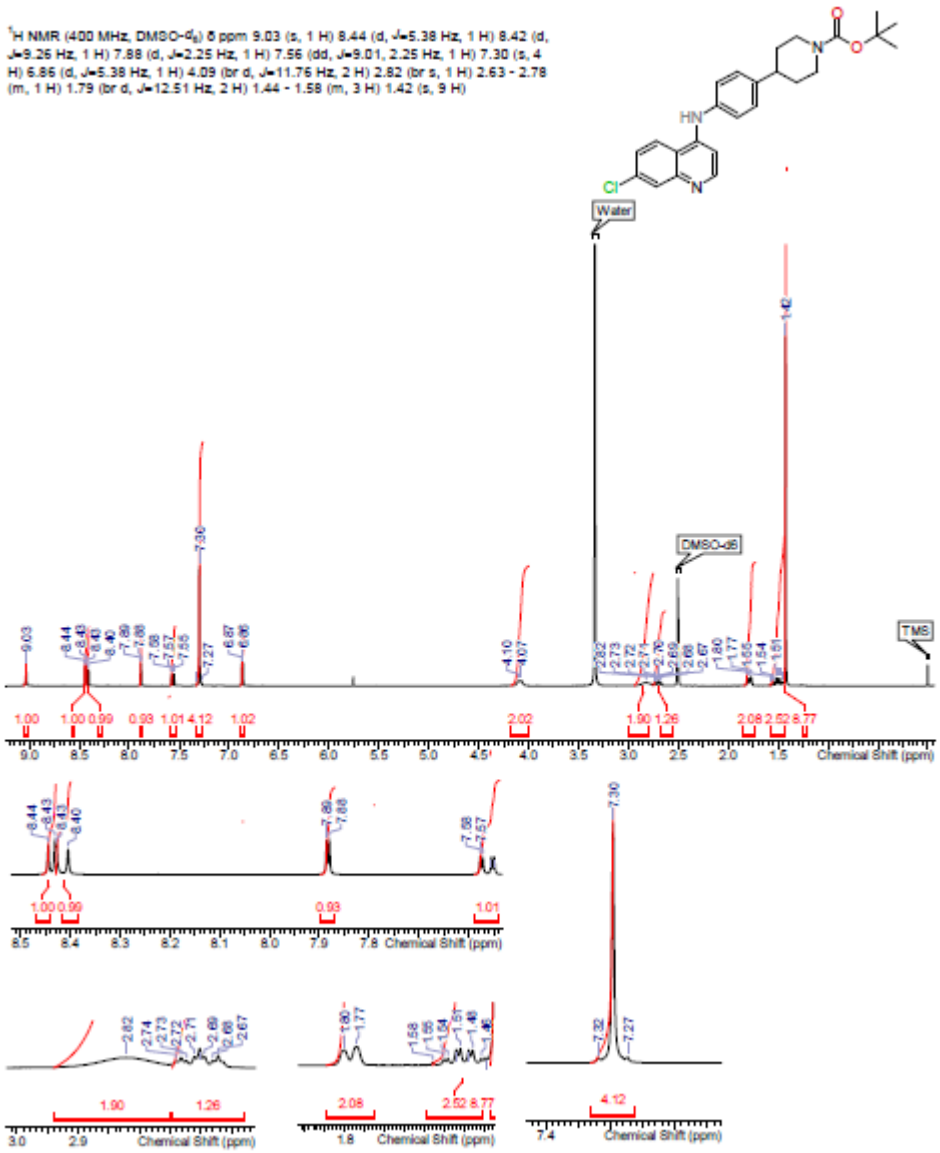

Figure 118: [1]H NMR spectra of 64a.

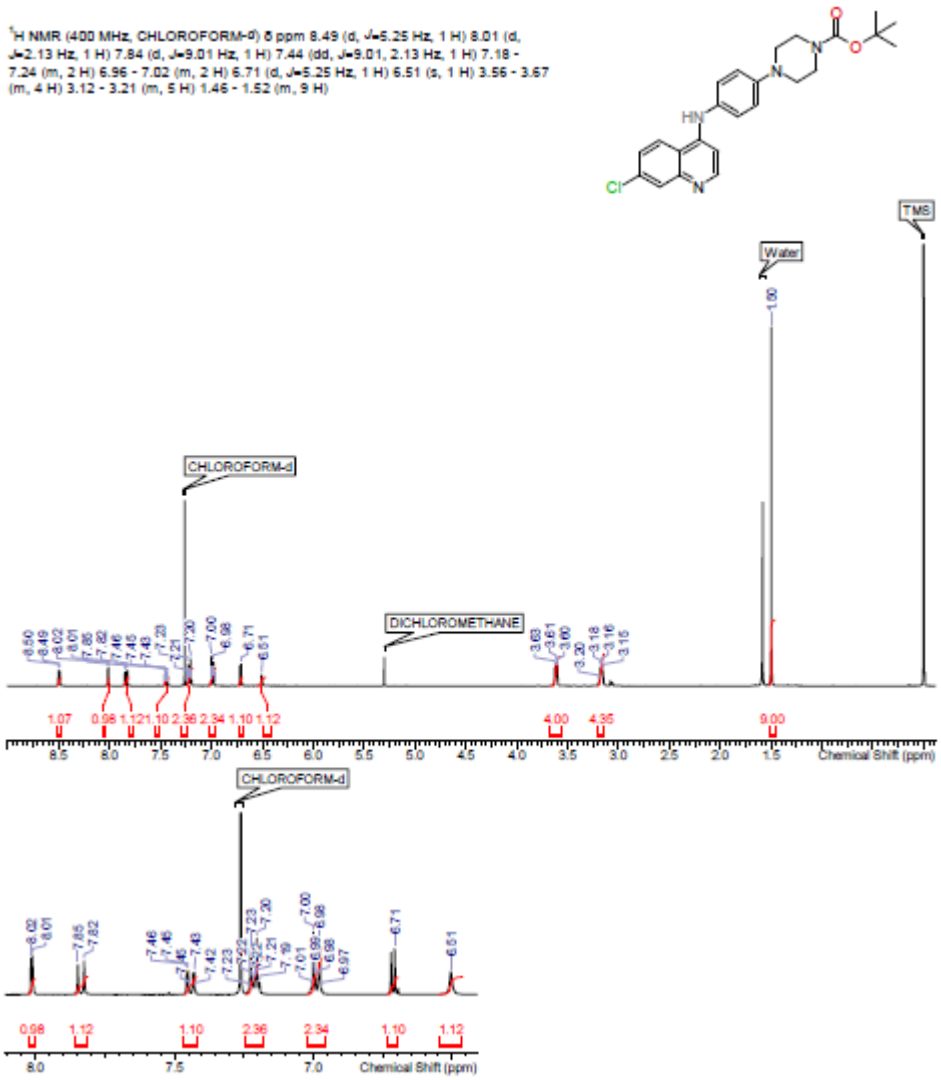

Figure 119: [1]H NMR spectra of 64b.

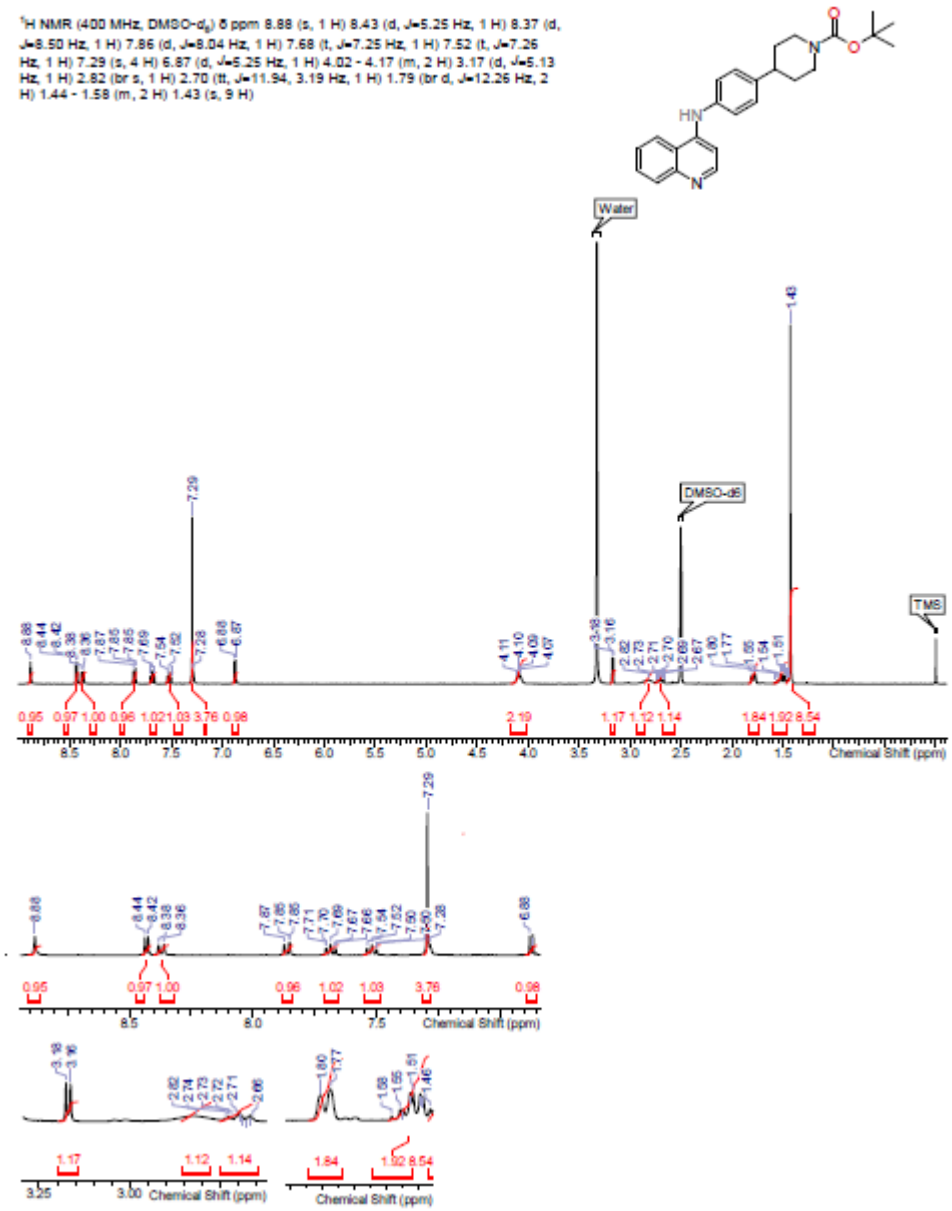

Figure 120: ^{1}H NMR spectra of 64c.

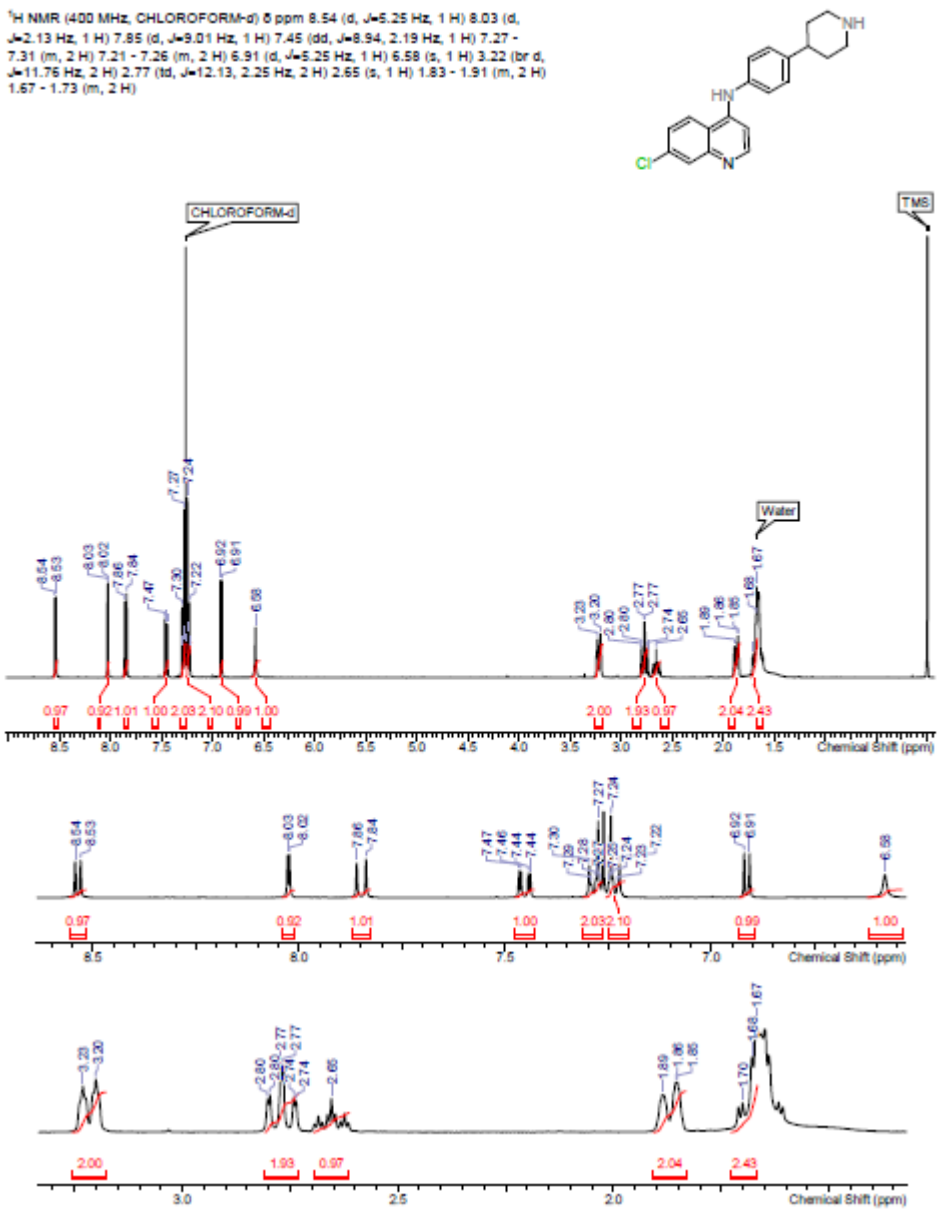

Figure 121: [1]H NMR spectra of 65a.

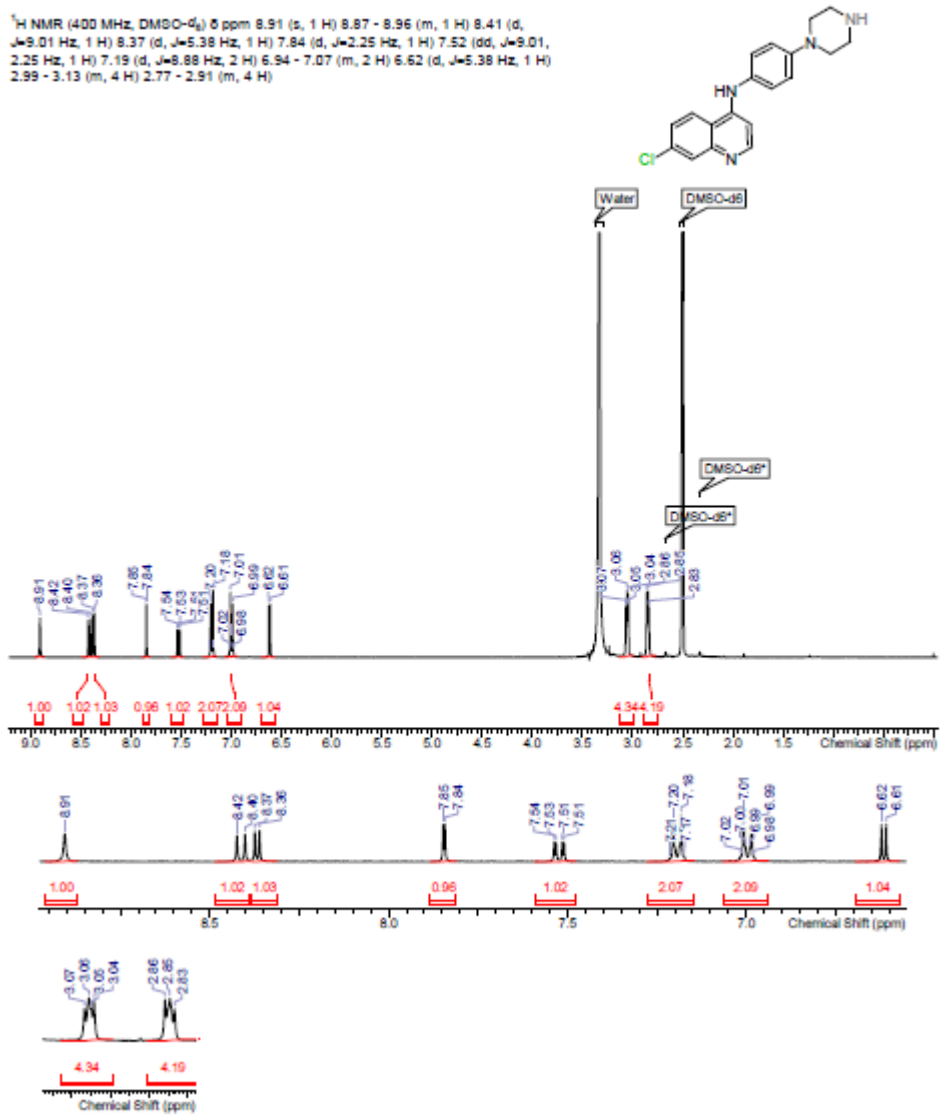

Figure 122: [1]H NMR spectra of 65b.

^{1}H NMR (400 MHz, DMSO-d_6) δ ppm 8.89 (br s, 1 H) 8.43 (d, J=5.25 Hz, 1 H) 8.38 (d, J=8.38 Hz, 1 H) 7.86 (d, J=8.38 Hz, 1 H) 7.69 (t, J=7.63 Hz, 1 H) 7.52 (t, J=7.63 Hz, 1 H) 7.29 (q, J=8.63 Hz, 4 H) 6.87 (d, J=5.25 Hz, 1 H) 3.12 - 3.21 (m, 3 H) 2.65 - 2.83 (m, 2 H) 2.00 - 2.09 (m, 1 H) 1.77 - 1.85 (m, 2 H) 1.55 - 1.75 (m, 2 H)

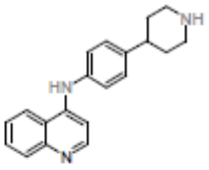

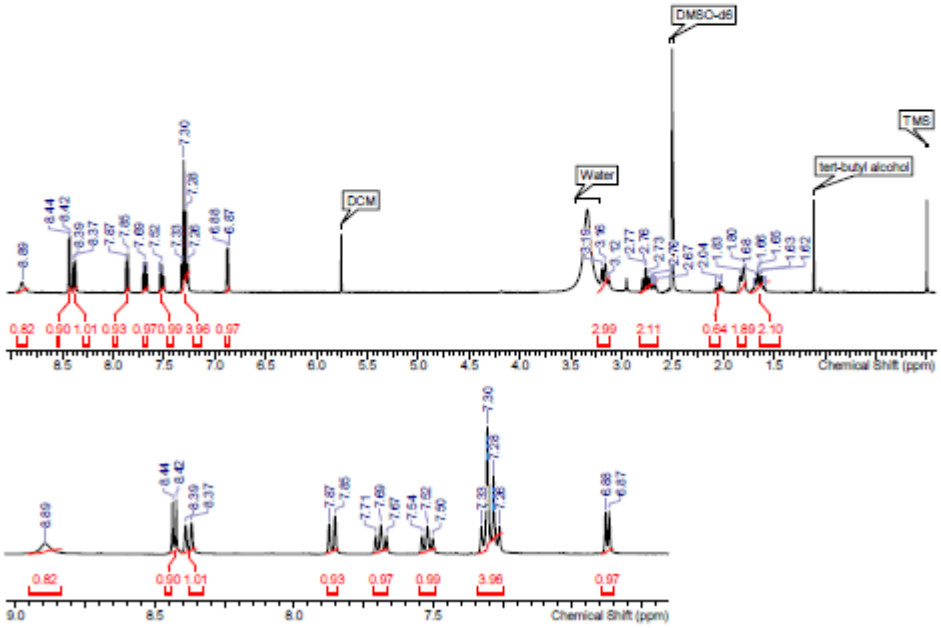

Figure 123: ^{1}H NMR spectra of 65c.

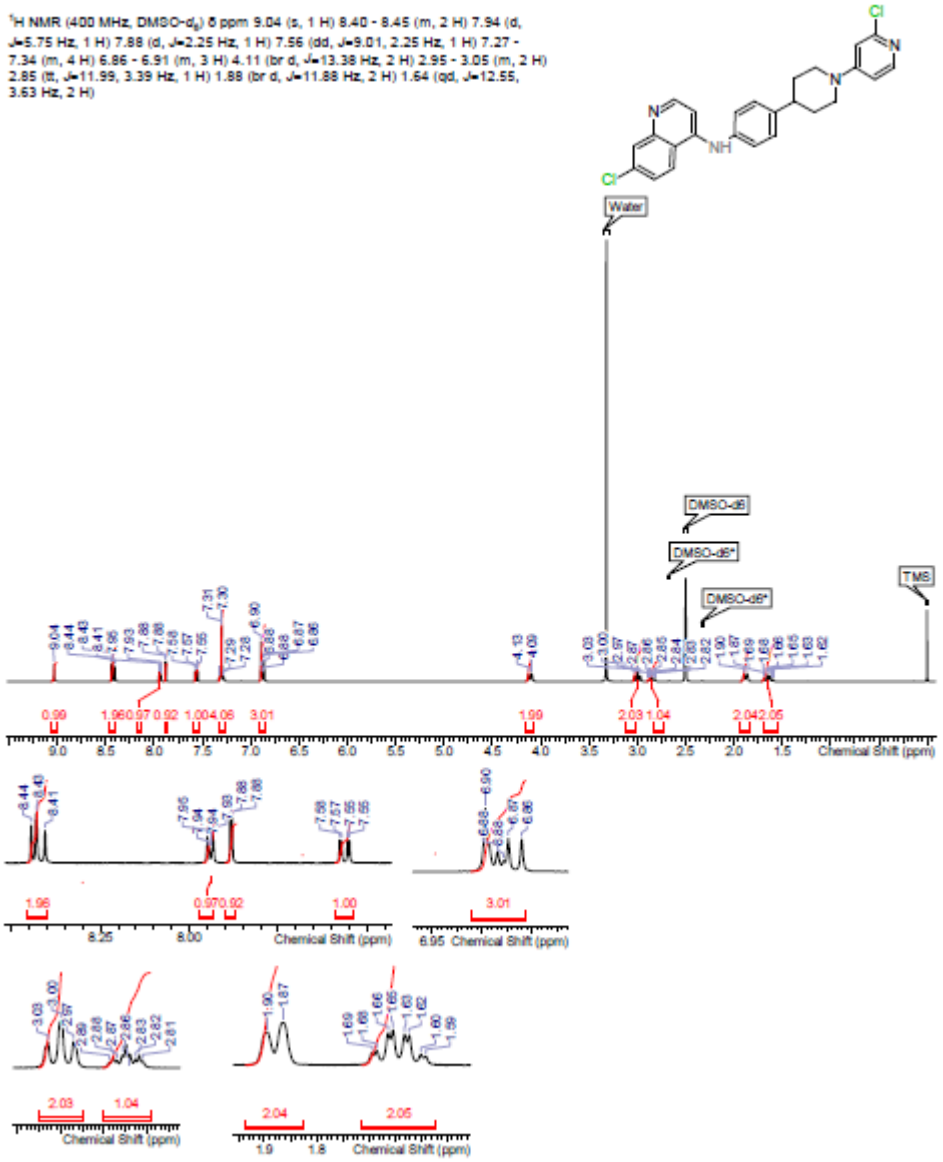

Figure 124: [1]H NMR spectra of 67.

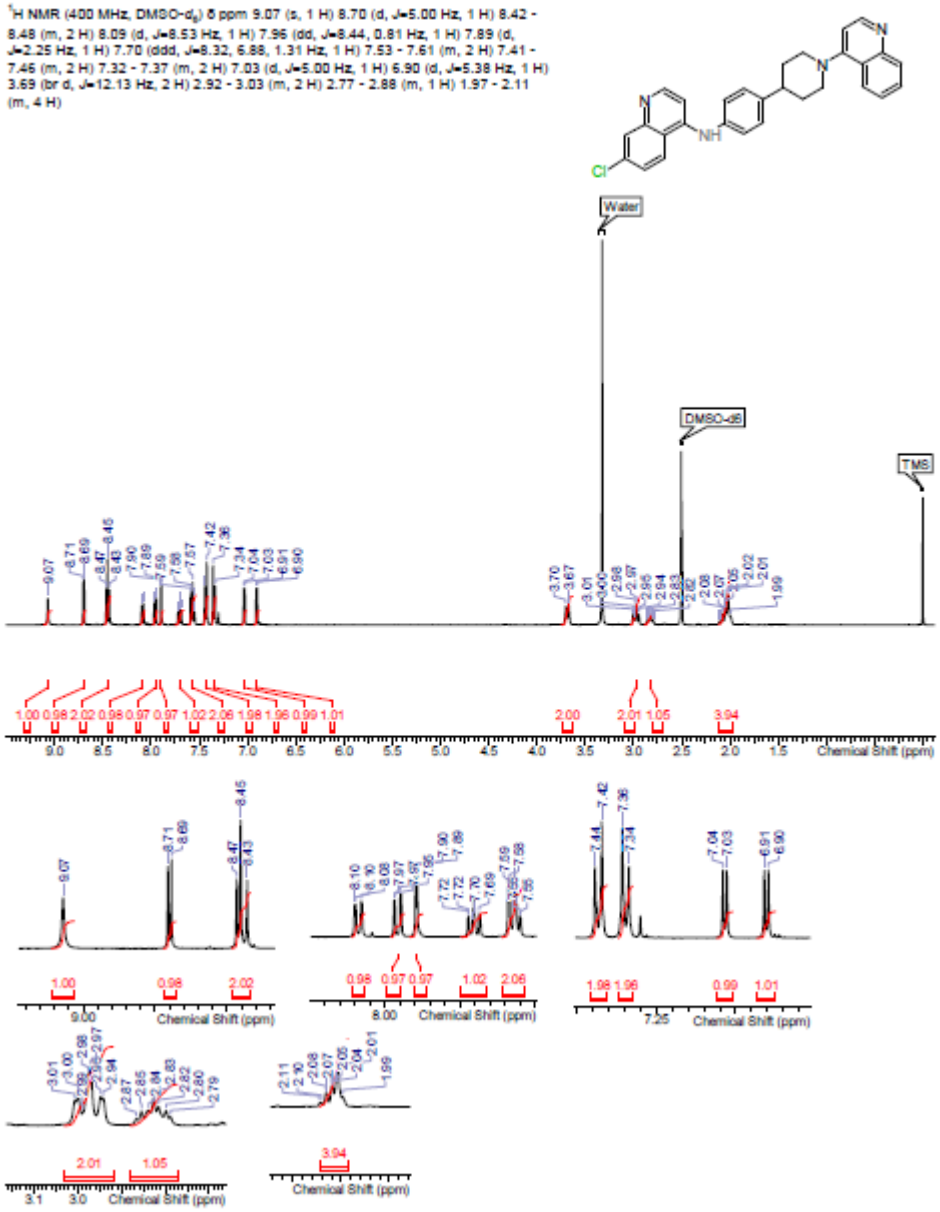

Figure 125: ^{1}H NMR spectra of 68.

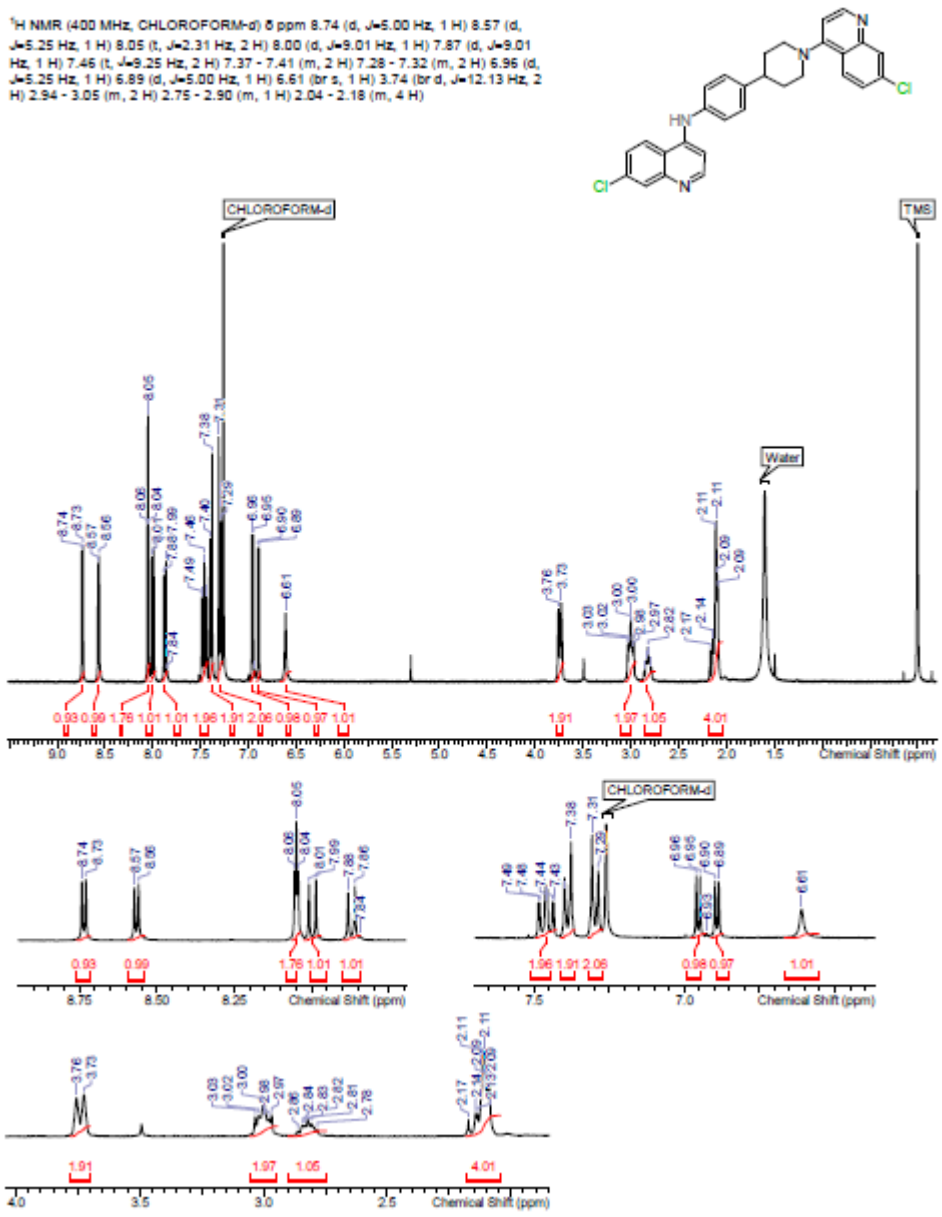

Figure 126: [1]H NMR spectra of 69.

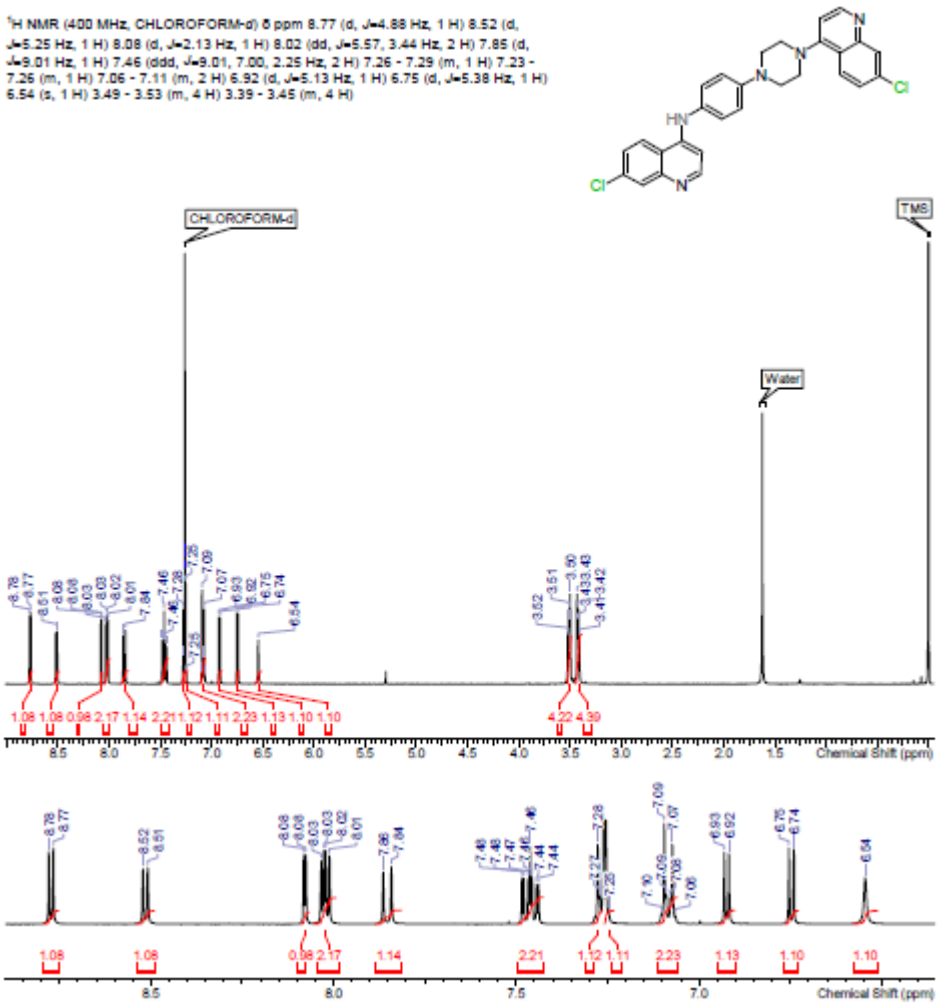

Figure 127: [1]H NMR spectra of 70.

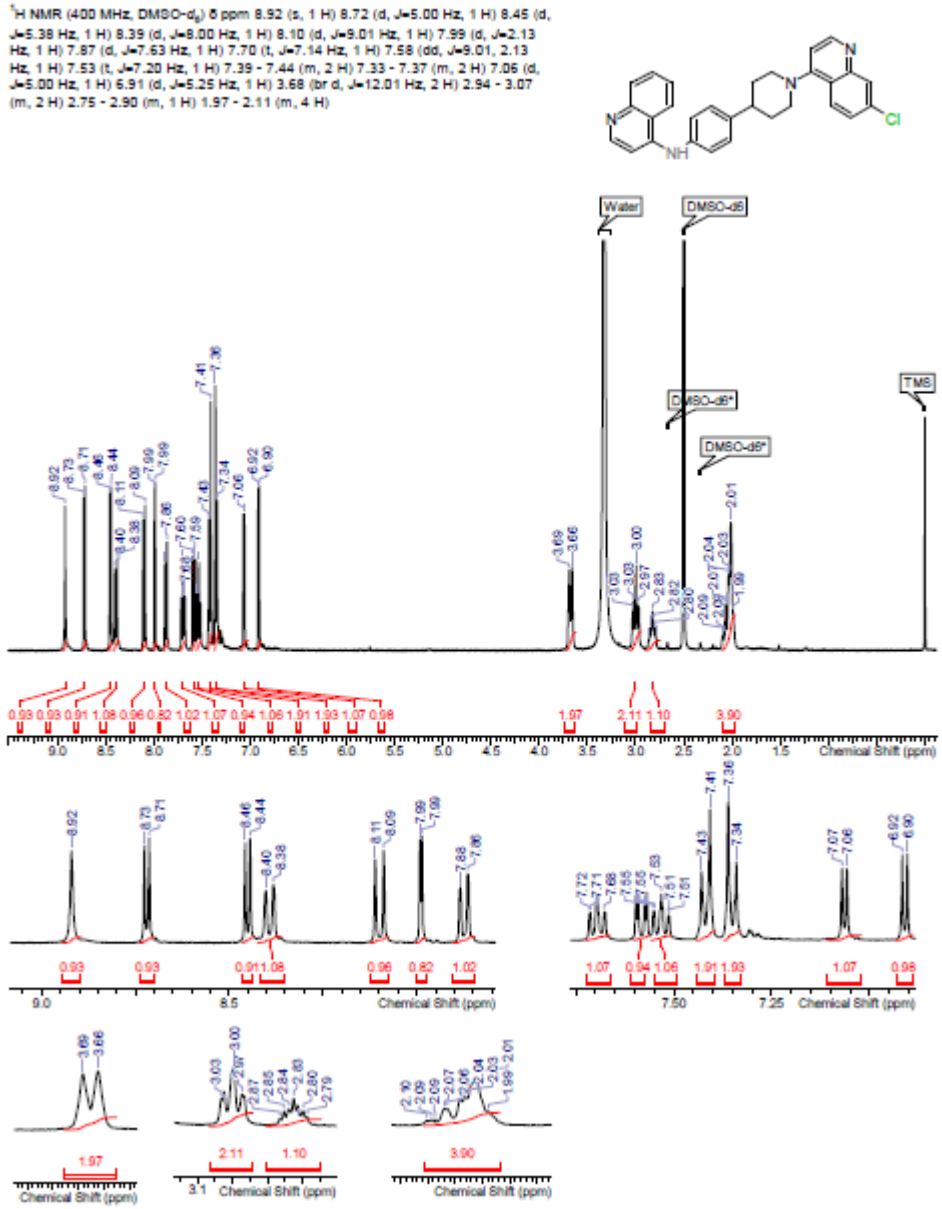

Figure 128: [1]H NMR spectra of 71.

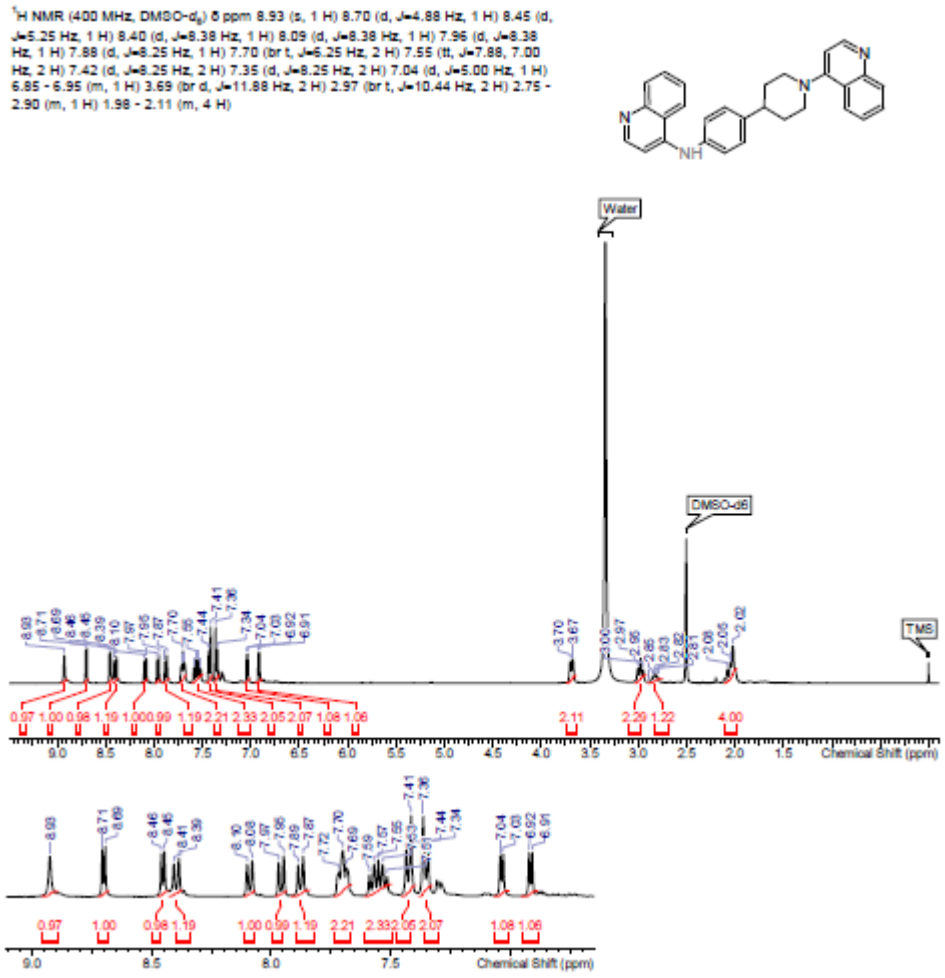

Figure 129:[1]H NMR spectra of 72.

F.3. High Resolution Mass Spectrometry of Compounds presented in Chapter 6

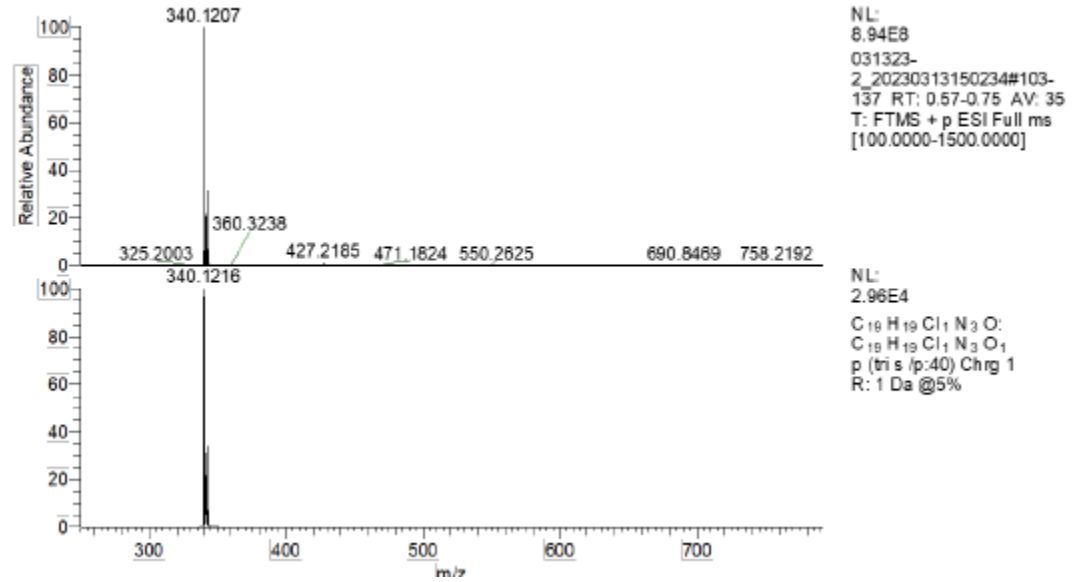

Figure 130: HRMS trace of 7. High Resolution Mass Spectrometry using (ESI): actual m/z M + H (top) over expected m/z M + H (bottom).

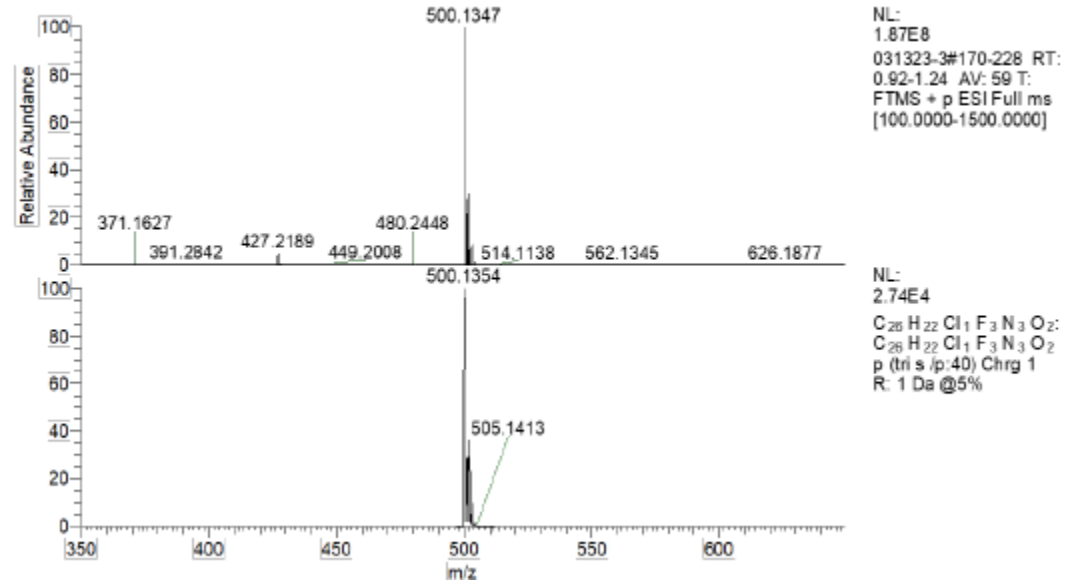

Figure 131: HRMS trace of 8. High Resolution Mass Spectrometry using (ESI): actual m/z M + H (top) over expected m/z M + H (bottom).

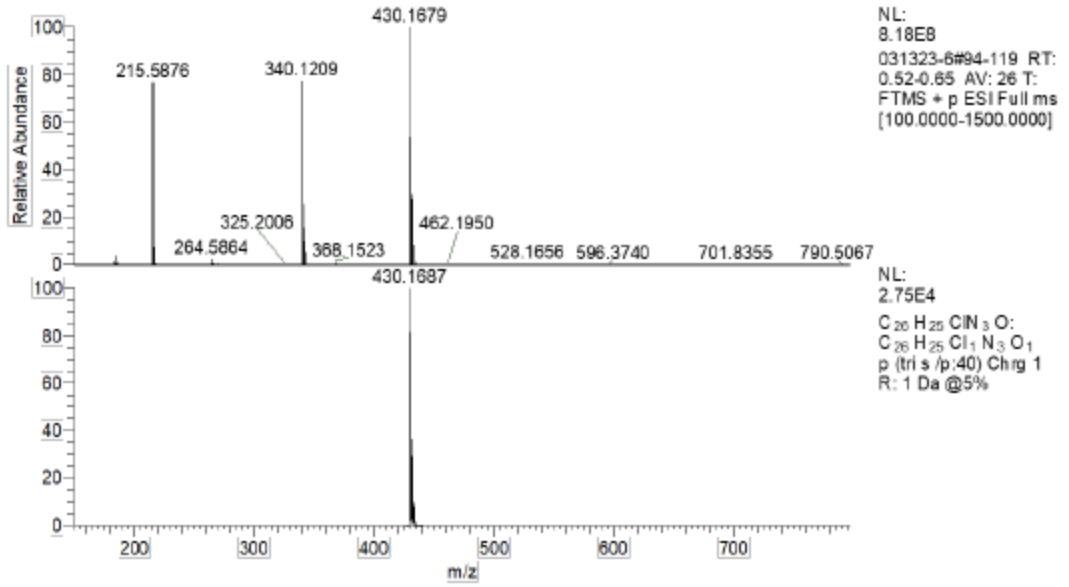

Figure 132: HRMS trace of 12. High Resolution Mass Spectrometry using (ESI): actual m/z M + H (top) over expected m/z M + H (bottom).

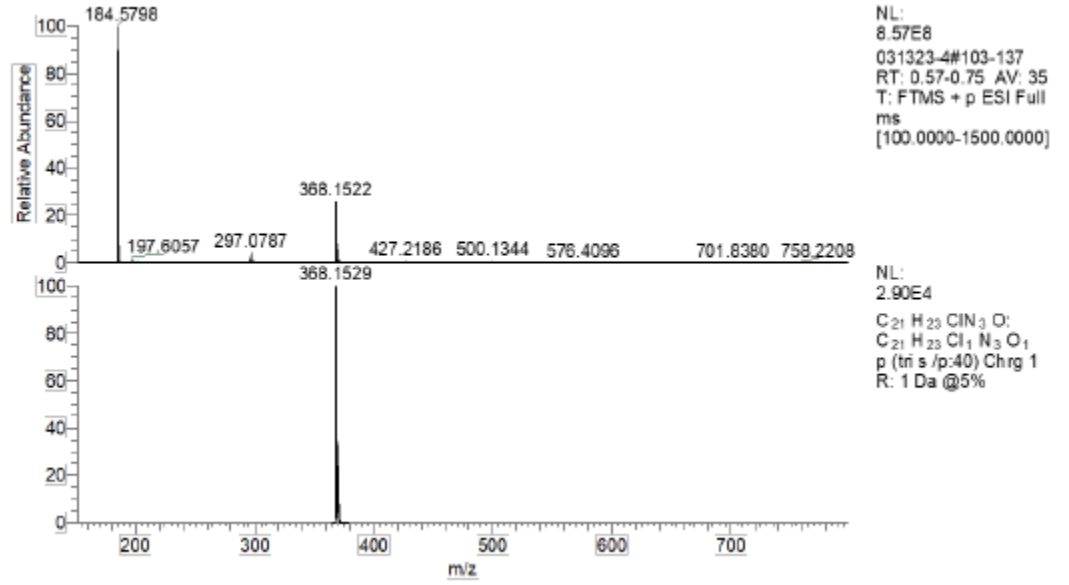

Figure 133: HRMS trace of 13. High Resolution Mass Spectrometry using (ESI): actual m/z M + H (top) over expected m/z M + H (bottom).

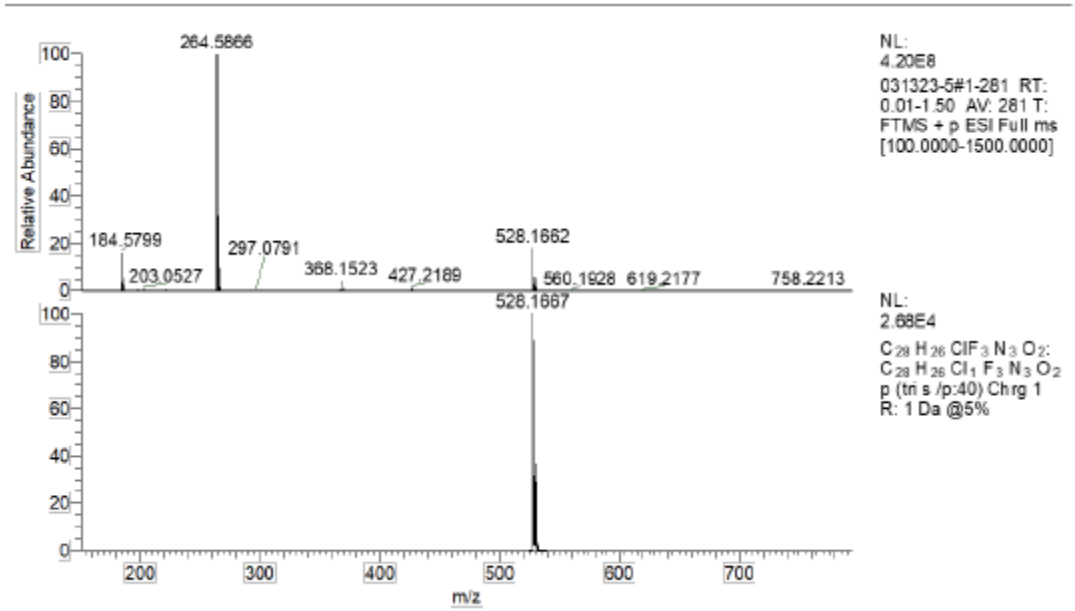

Figure 134: HRMS trace of 14. High Resolution Mass Spectrometry using (ESI): actual m/z M + H (top) over expected m/z M + H (bottom).

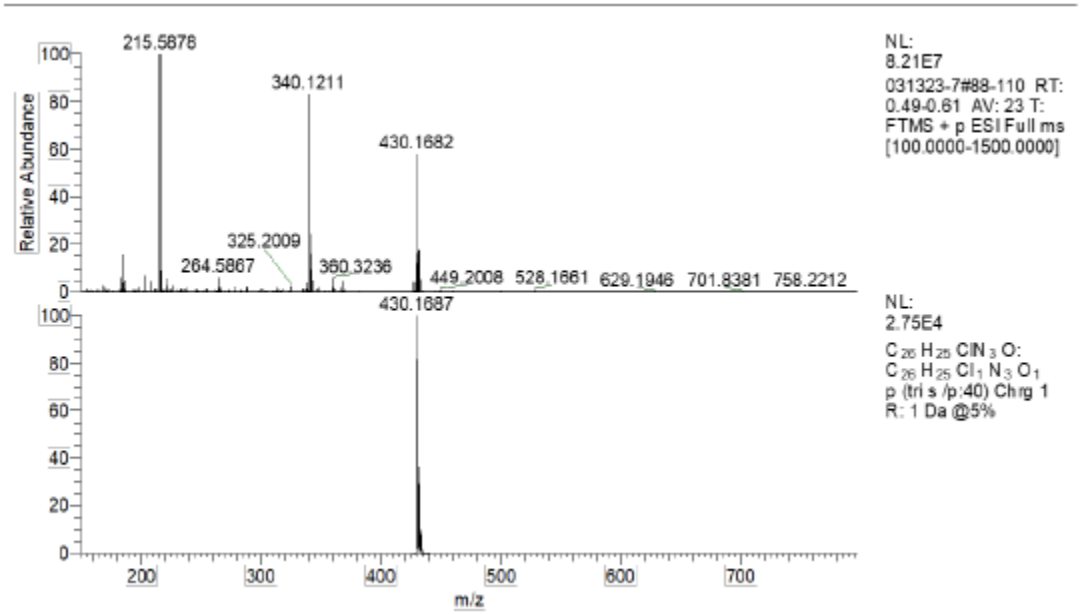

Figure 135: HRMS trace of 15. High Resolution Mass Spectrometry using (ESI): actual m/z M + H (top) over expected m/z M + H (bottom).

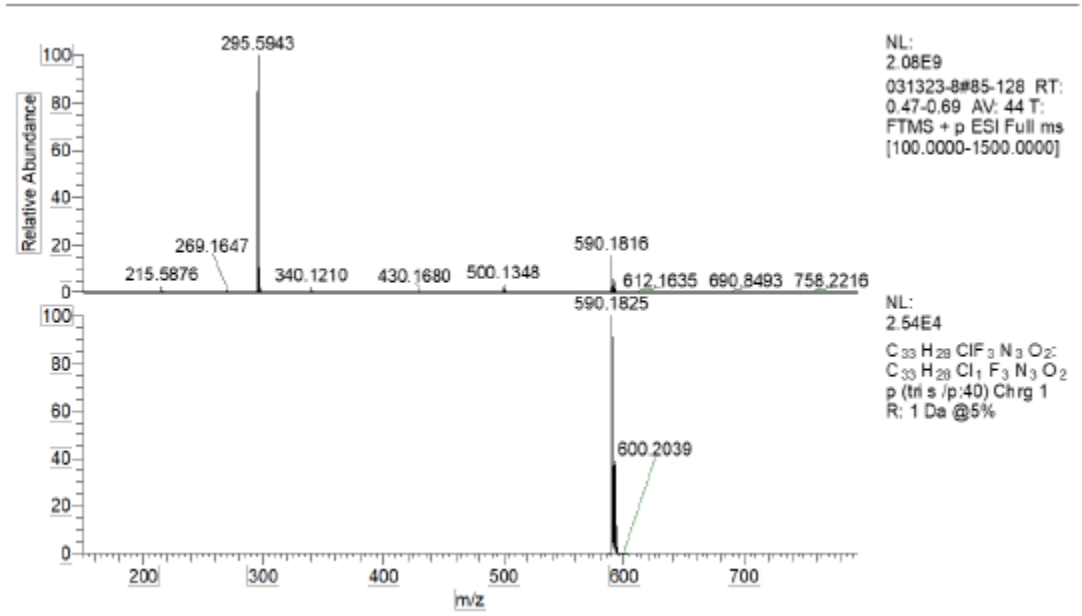

Figure 136: HRMS trace of 16. High Resolution Mass Spectrometry using (ESI): actual m/z M + H (top) over expected m/z M + H (bottom).

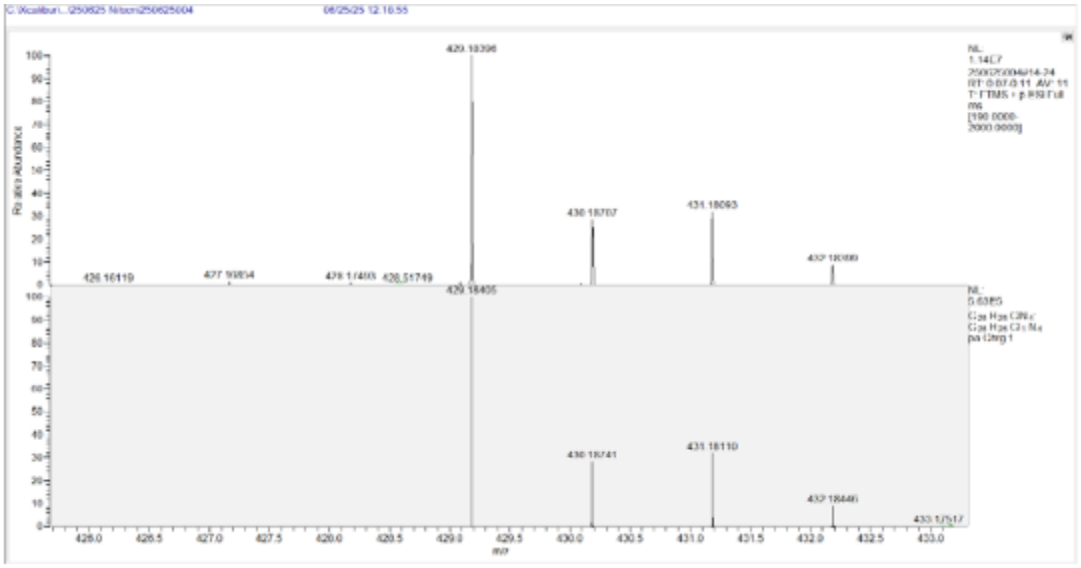

Figure 137: HRMS trace of 17. High Resolution Mass Spectrometry using (ESI): actual m/z M + H (top) over expected m/z M + H (bottom).

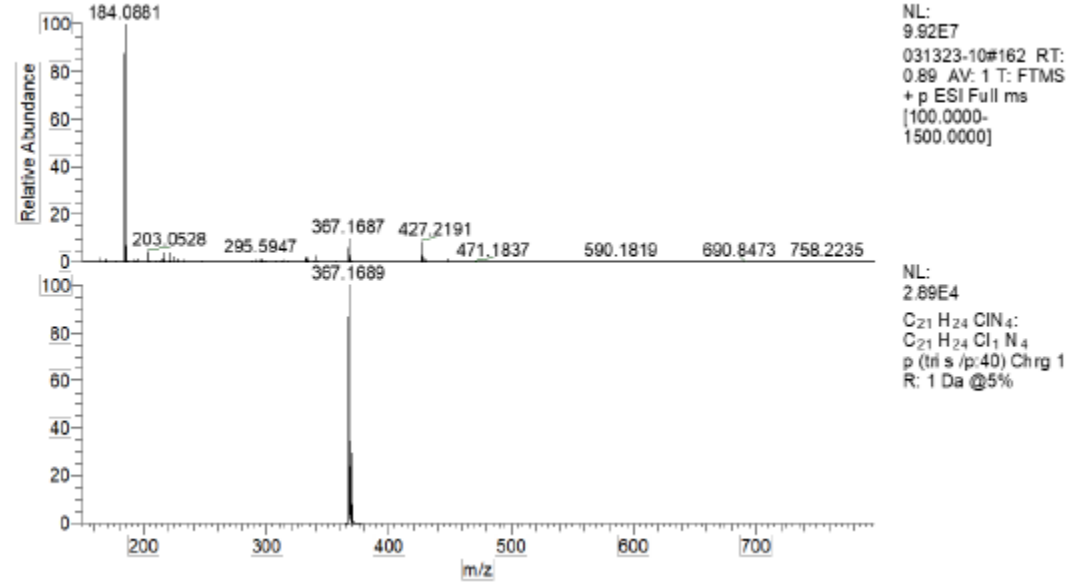

Figure 138: HRMS trace of 20. High Resolution Mass Spectrometry using (ESI): actual m/z M + H (top) over expected m/z M + H (bottom).

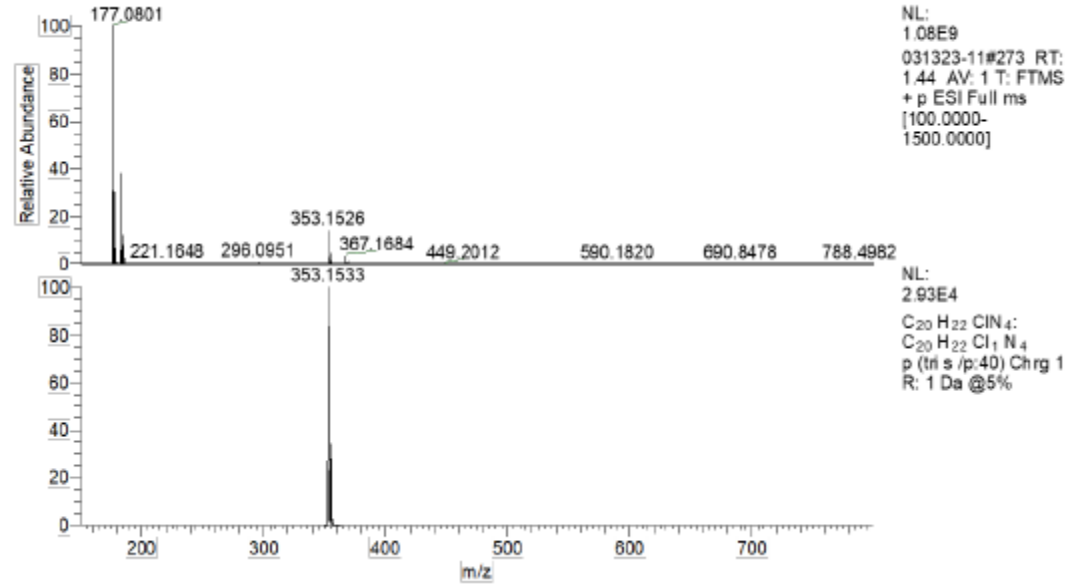

Figure 139: HRMS trace of 21. High Resolution Mass Spectrometry using (ESI): actual m/z M + H (top) over expected m/z M + H (bottom).

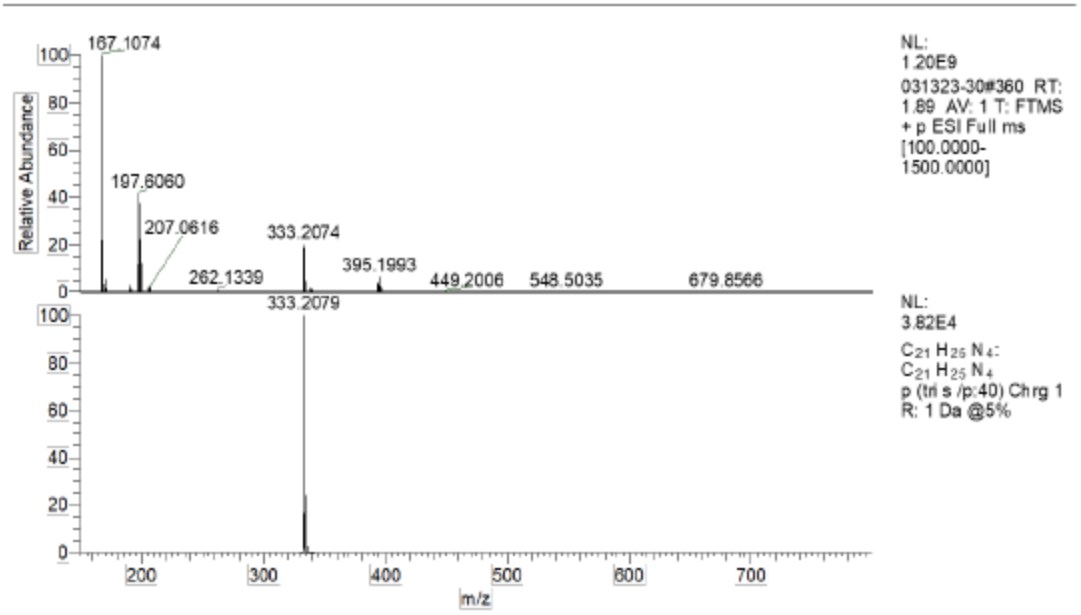

Figure 140: HRMS trace of 22. High Resolution Mass Spectrometry using (ESI): actual m/z M + H (top) over expected m/z M + H (bottom).

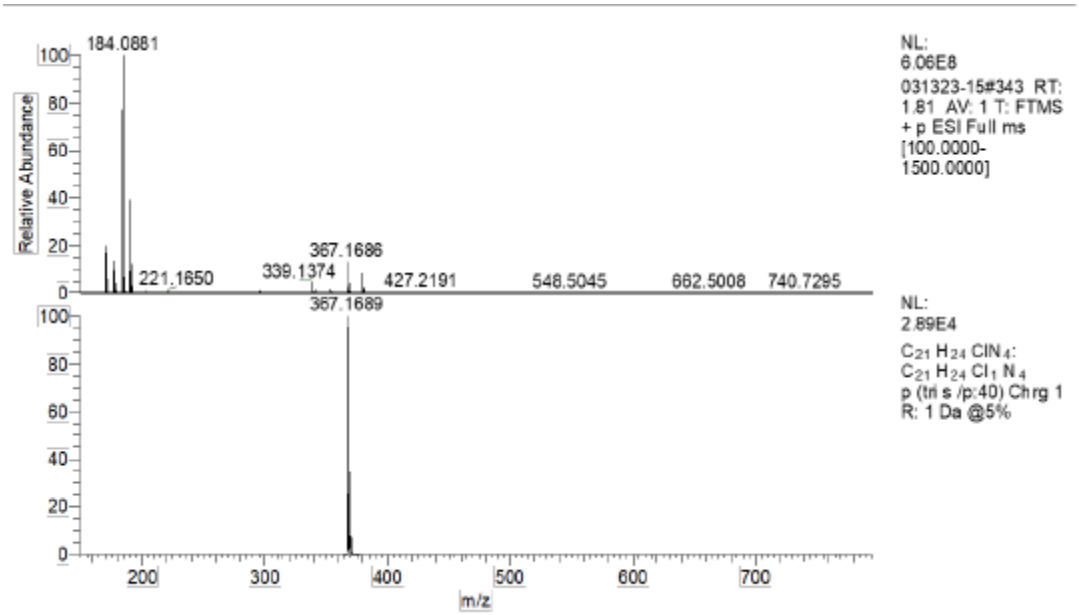

Figure 141: HRMS trace of 23. High Resolution Mass Spectrometry using (ESI): actual m/z M + H (top) over expected m/z M + H (bottom).

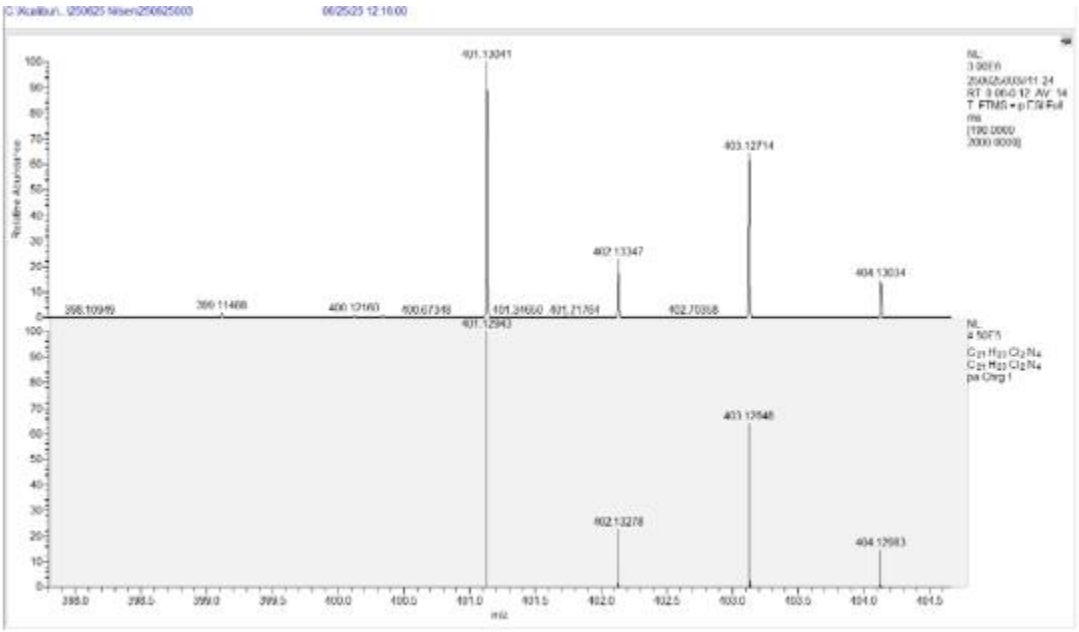

Figure 142: HRMS trace of 24. High Resolution Mass Spectrometry using (ESI): actual m/z M + H (top) over expected m/z M + H (bottom).

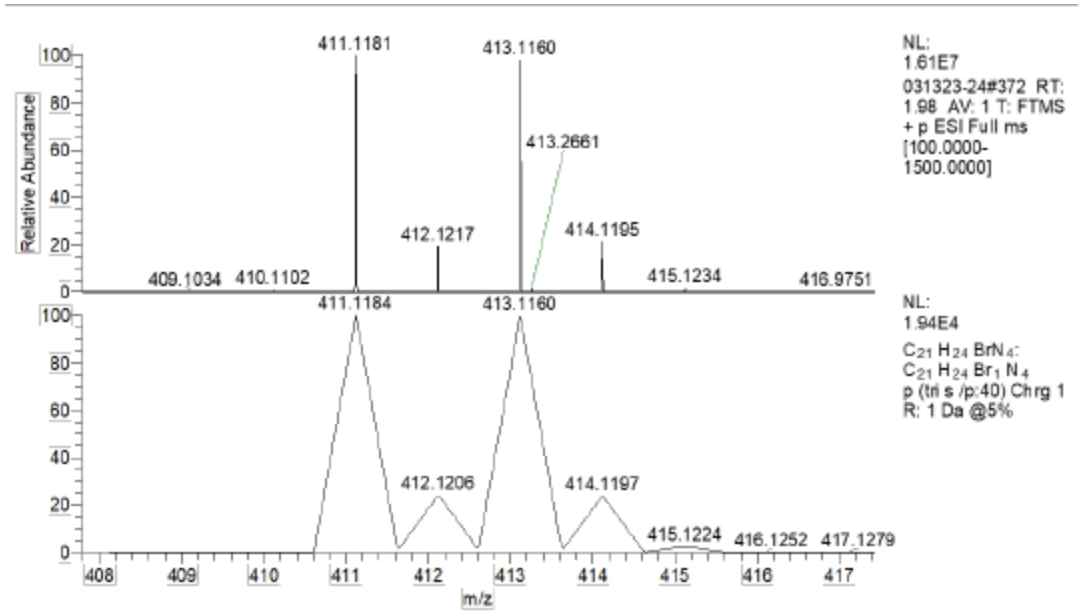

Figure 143: HRMS trace of 25. High Resolution Mass Spectrometry using (ESI): actual m/z M + H (top) over expected m/z M + H (bottom).

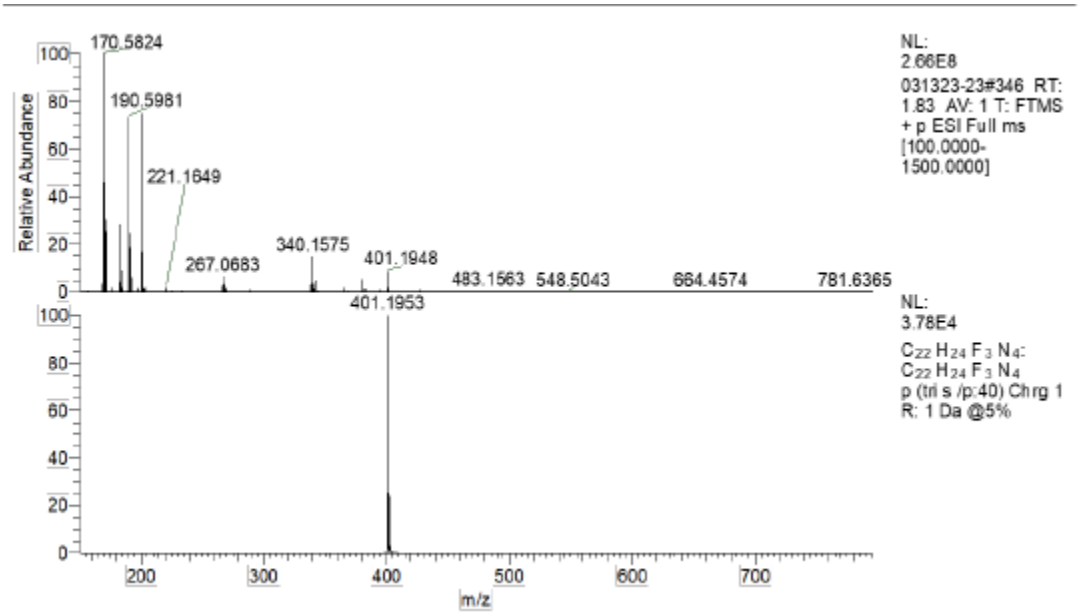

Figure 144: HRMS trace of 26. High Resolution Mass Spectrometry using (ESI): actual m/z M + H (top) over expected m/z M + H (bottom).

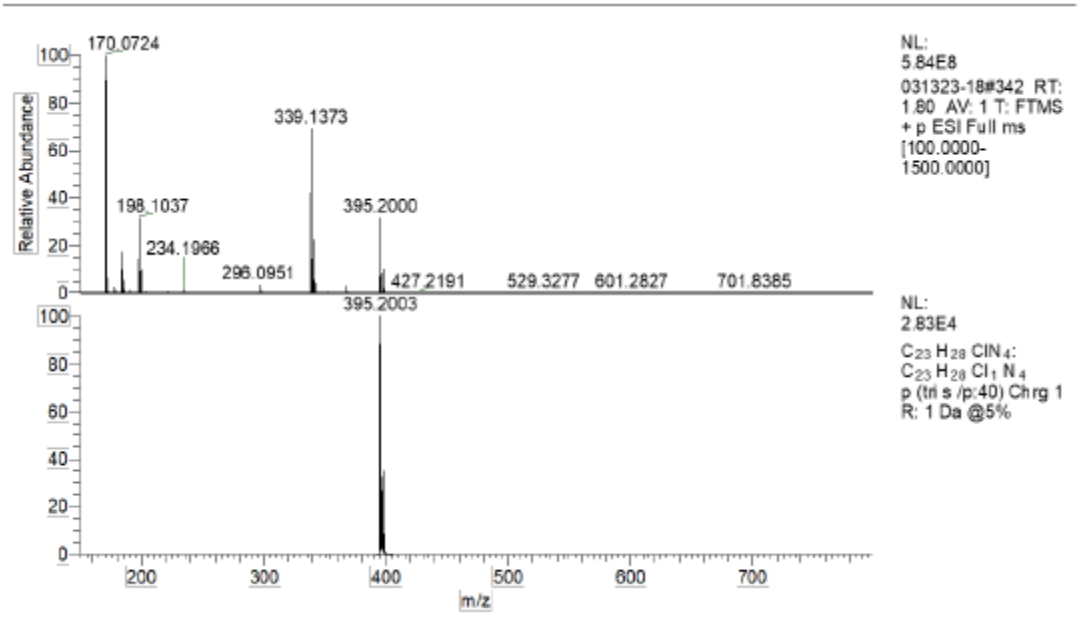

Figure 145: HRMS trace of 31. High Resolution Mass Spectrometry using (ESI): actual m/z M + H (top) over expected m/z M + H (bottom).

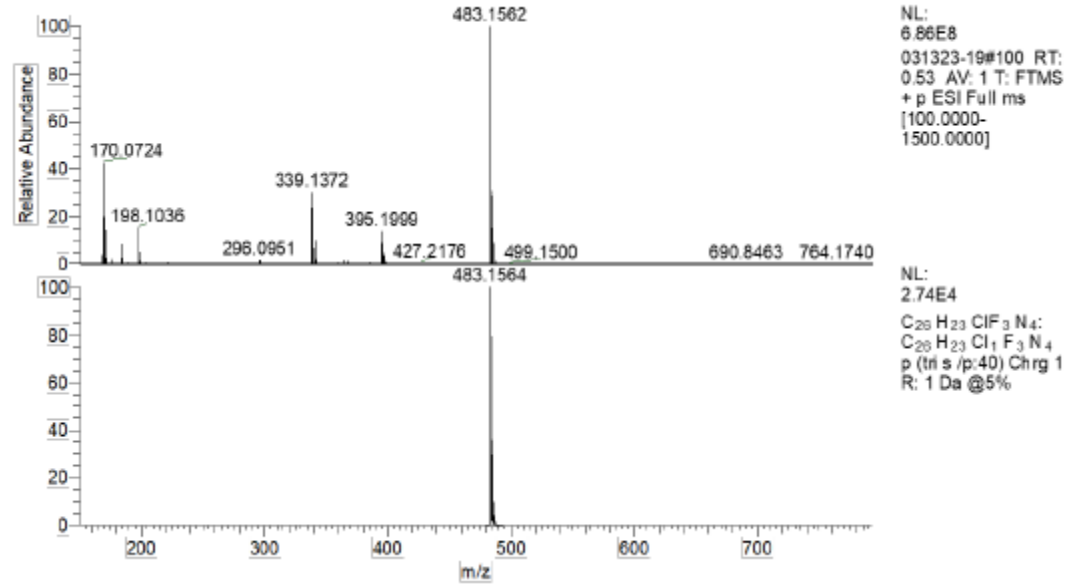

Figure 146: HRMS trace of 32. High Resolution Mass Spectrometry using (ESI): actual m/z M + H (top) over expected m/z M + H (bottom).

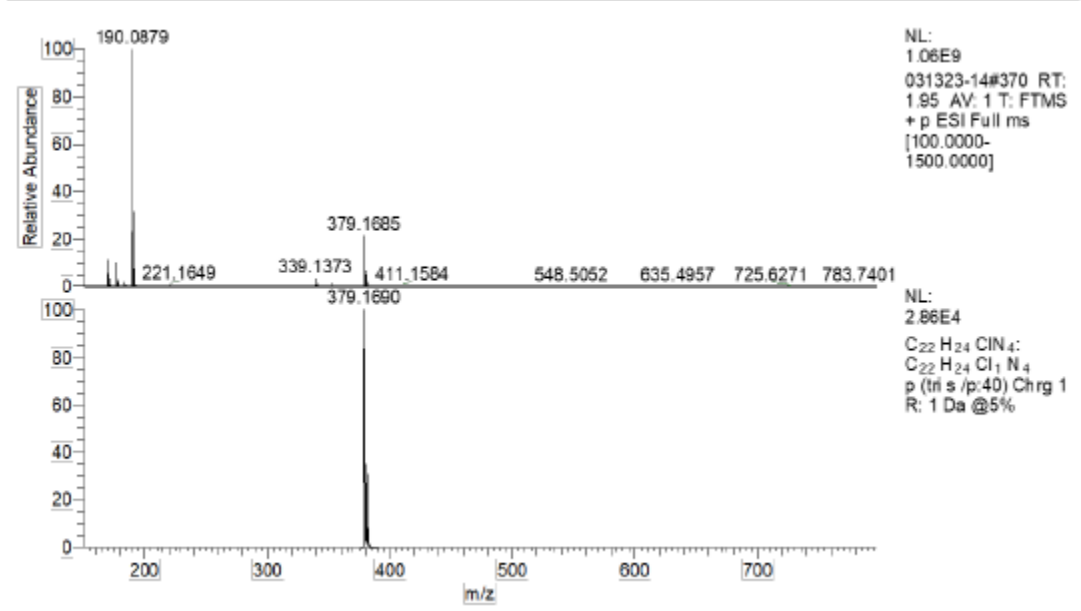

Figure 147: HRMS trace of 33. High Resolution Mass Spectrometry using (ESI): actual m/z M + H (top) over expected m/z M + H (bottom).

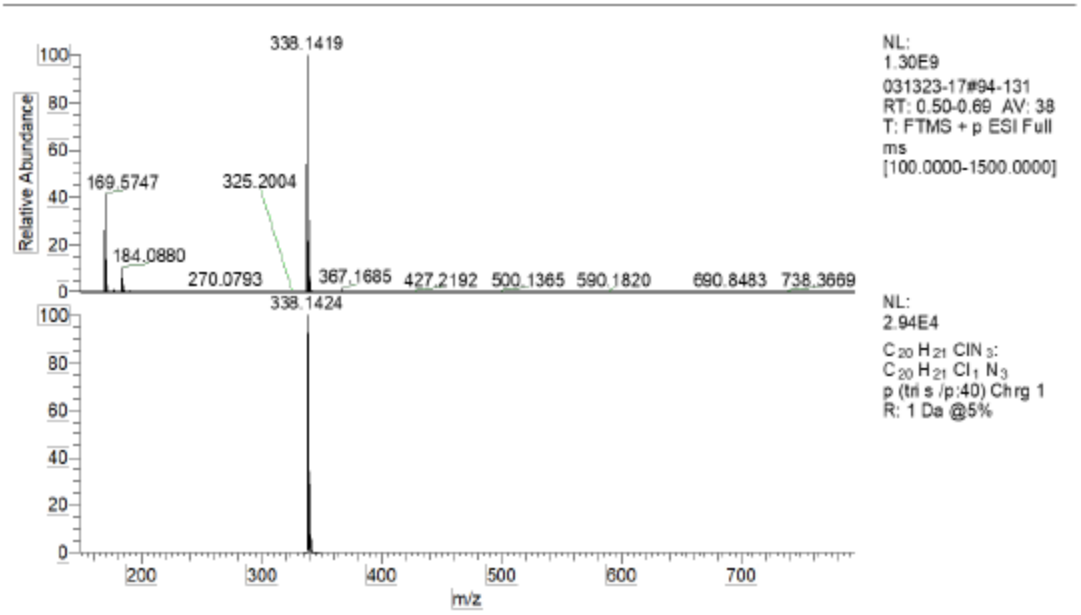

Figure 148: HRMS trace of 34. High Resolution Mass Spectrometry using (ESI): actual m/z M + H (top) over expected m/z M + H (bottom).

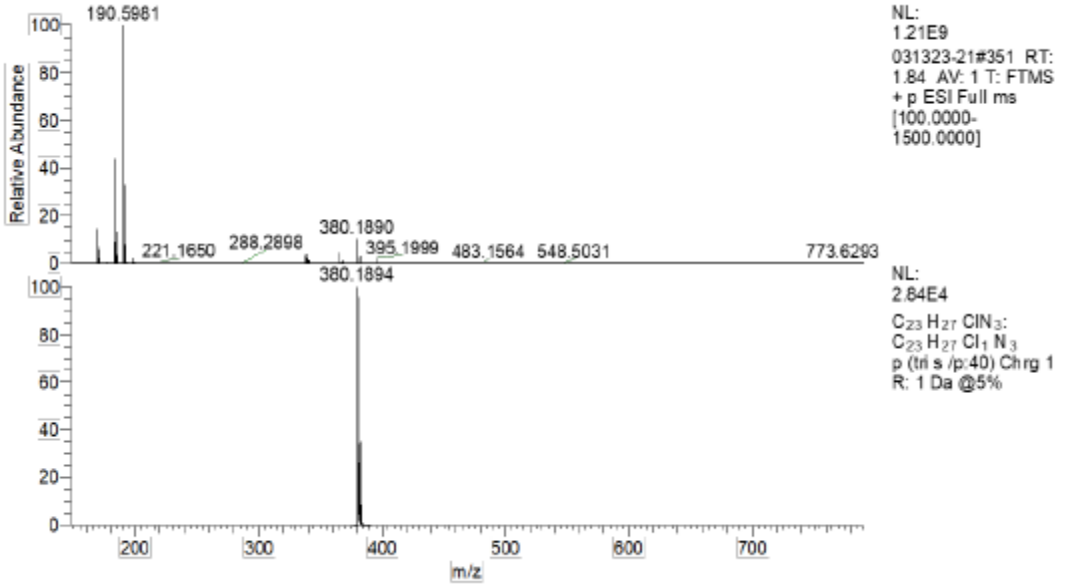

Figure 149: HRMS trace of 35. High Resolution Mass Spectrometry using (ESI): actual m/z M + H (top) over expected m/z M + H (bottom).

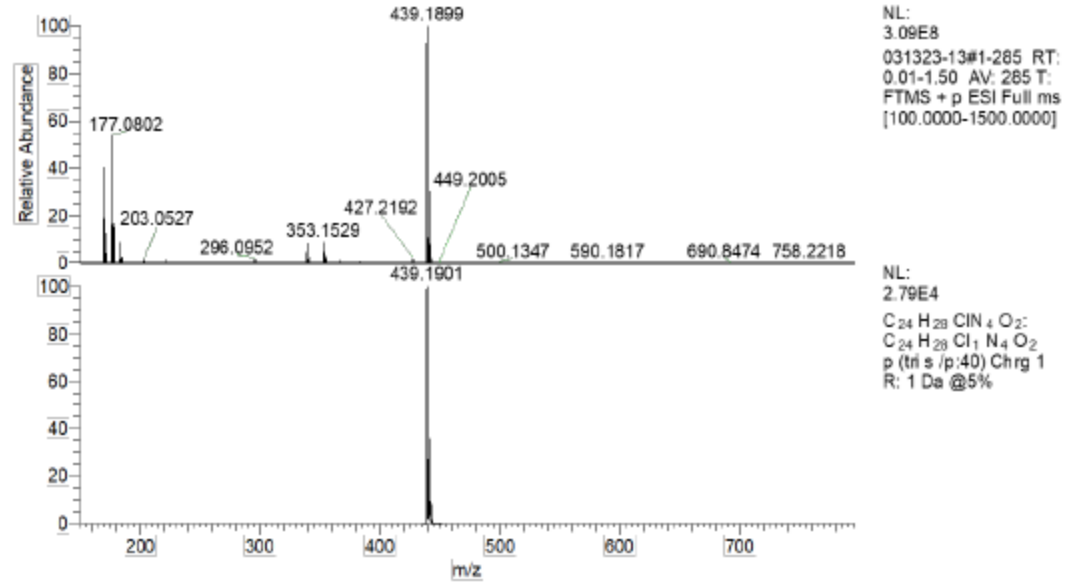

Figure 150: HRMS trace of 36. High Resolution Mass Spectrometry using (ESI): actual m/z M + H (top) over expected m/z M + H (bottom).

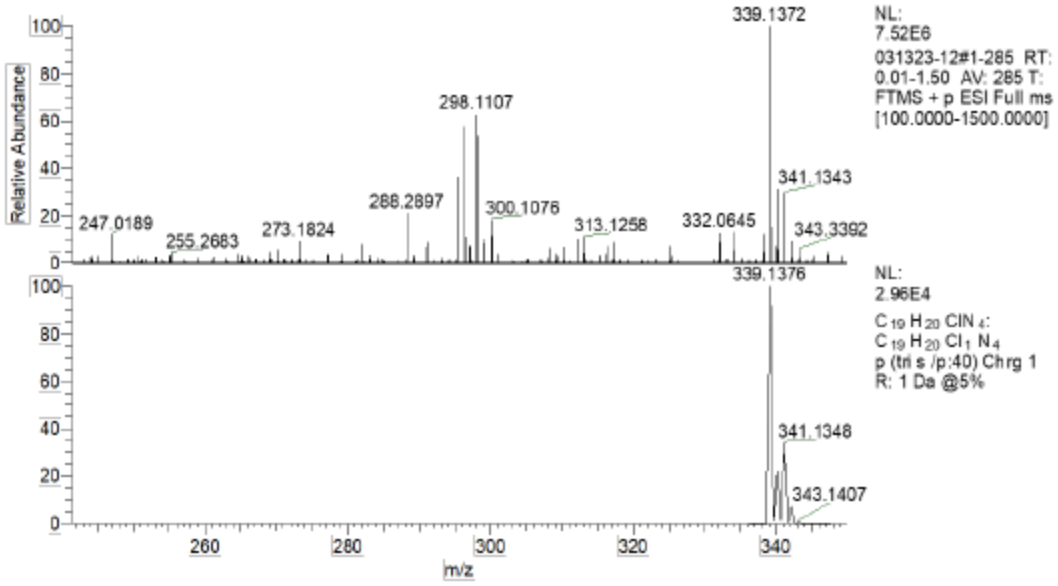

Figure 151: HRMS trace of 38. High Resolution Mass Spectrometry using (ESI): actual m/z M + H (top) over expected m/z M + H (bottom).

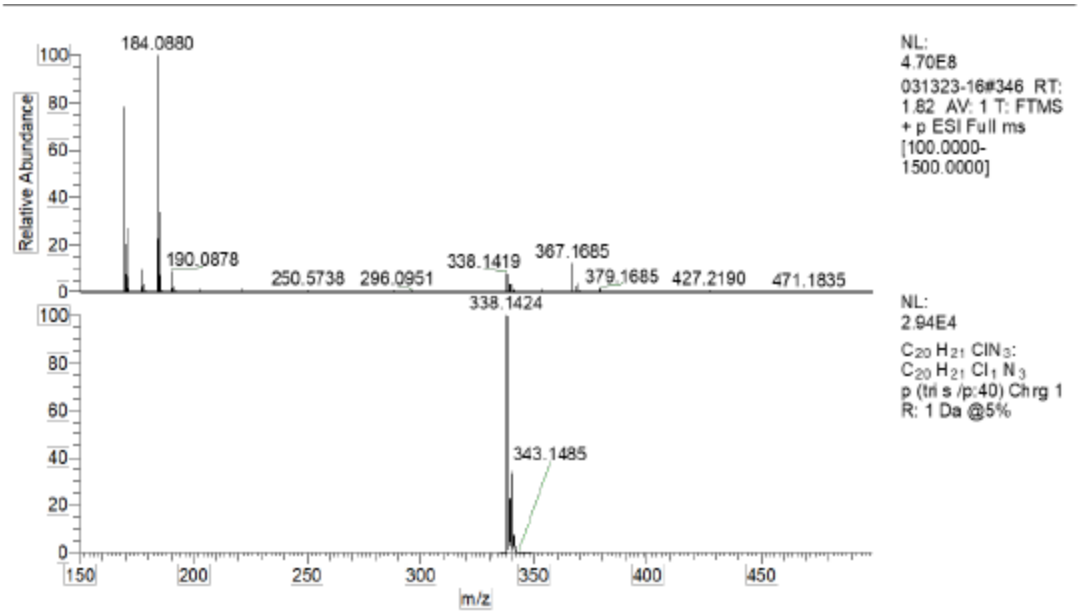

Figure 152: HRMS trace of 39. High Resolution Mass Spectrometry using (ESI): actual m/z M + H (top) over expected m/z M + H (bottom).

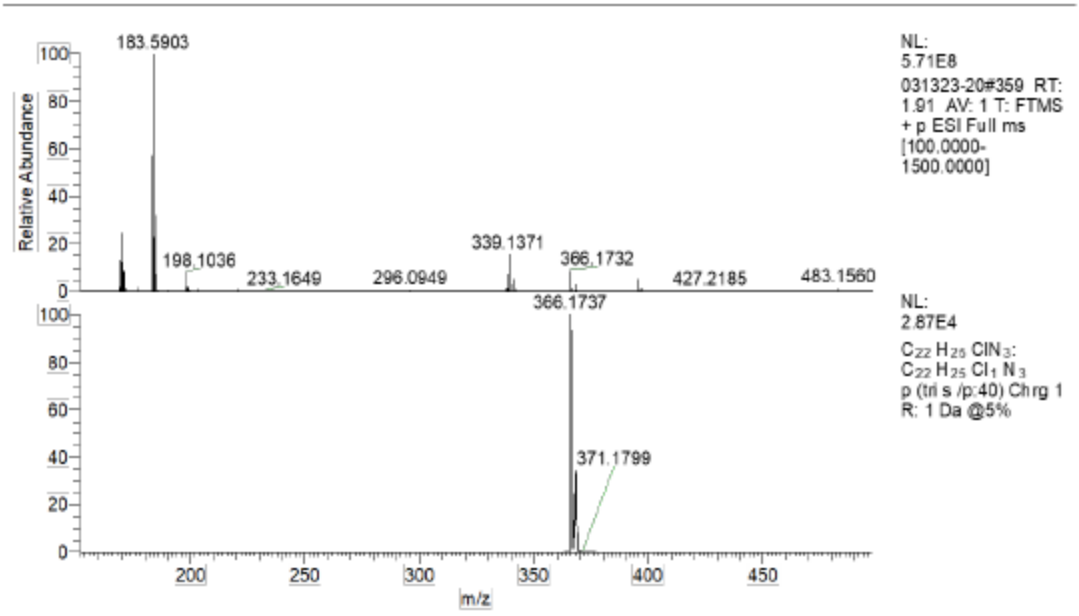

Figure 153: HRMS trace of 40. High Resolution Mass Spectrometry using (ESI): actual m/z M + H (top) over expected m/z M + H (bottom).

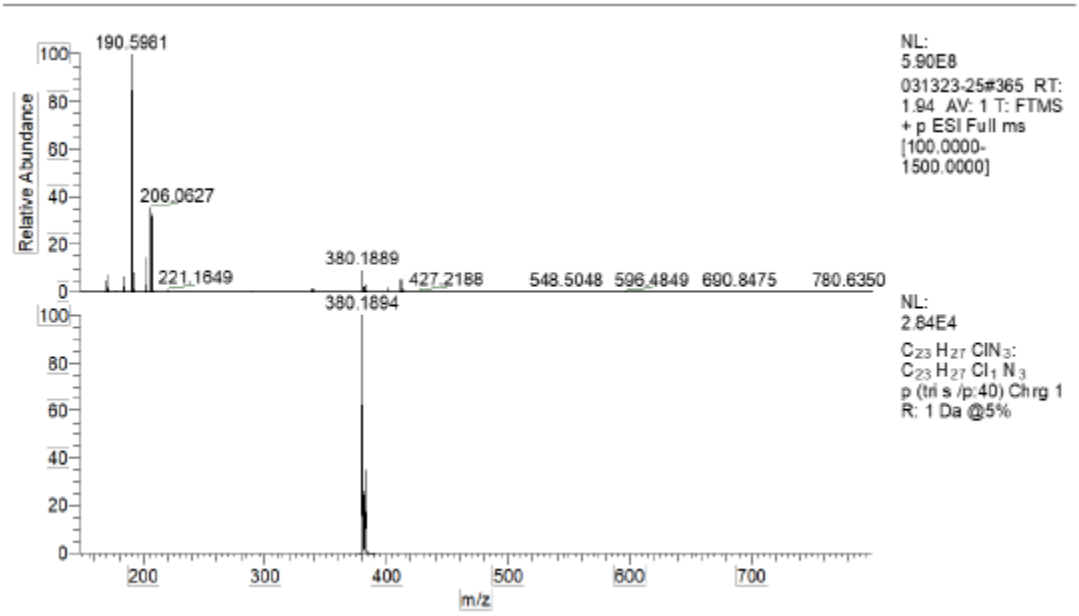

Figure 154: HRMS trace of 41. High Resolution Mass Spectrometry using (ESI): actual m/z M + H (top) over expected m/z M + H (bottom).

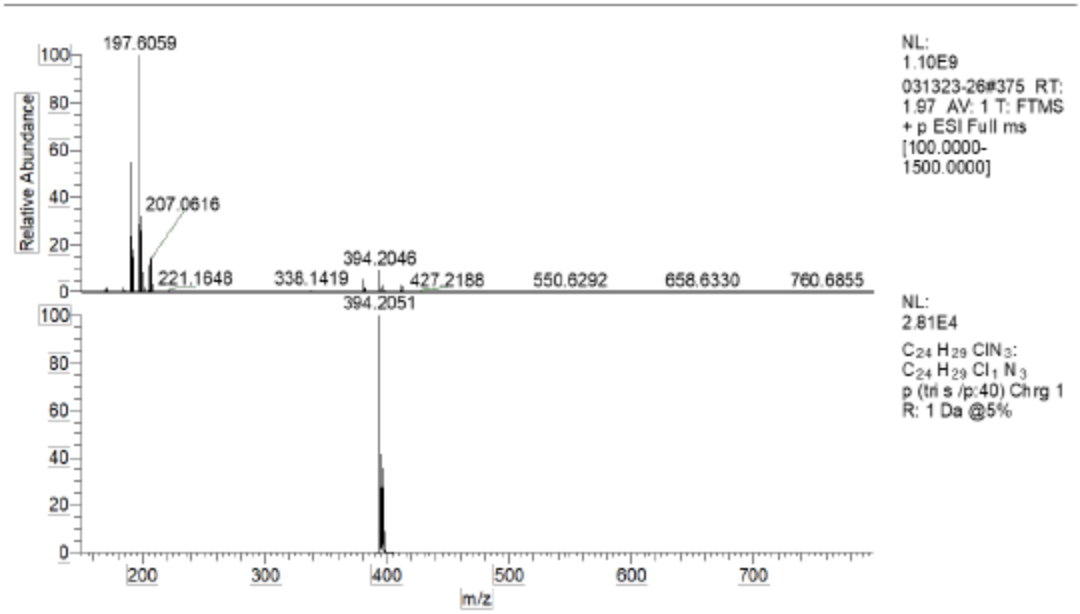

Figure 155: HRMS trace of 42. High Resolution Mass Spectrometry using (ESI): actual m/z M + H (top) over expected m/z M + H (bottom).

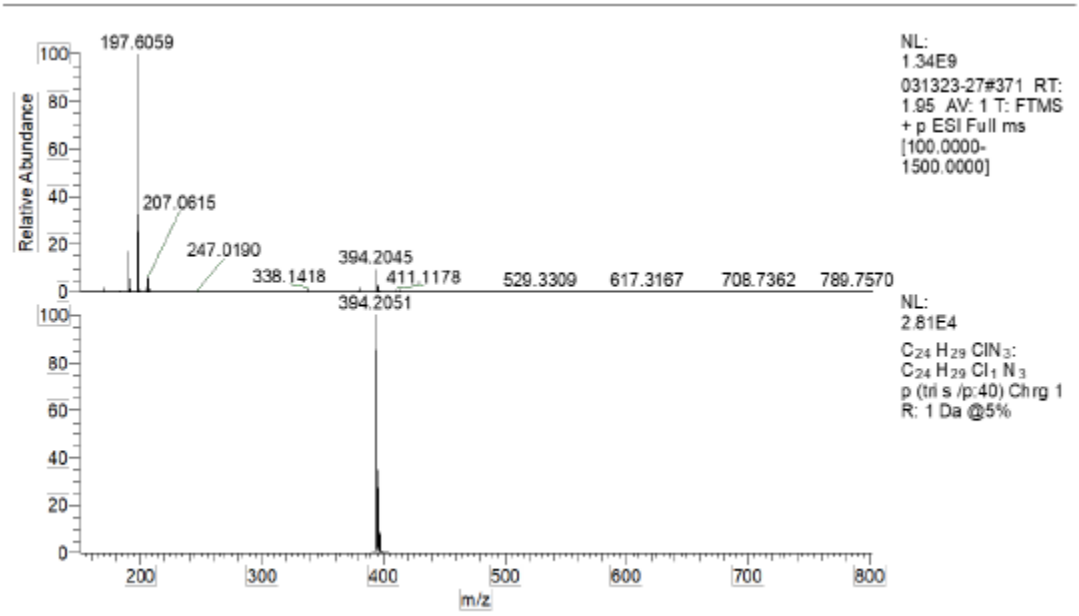

Figure 156: HRMS trace of 43. High Resolution Mass Spectrometry using (ESI): actual m/z M + H (top) over expected m/z M + H (bottom).

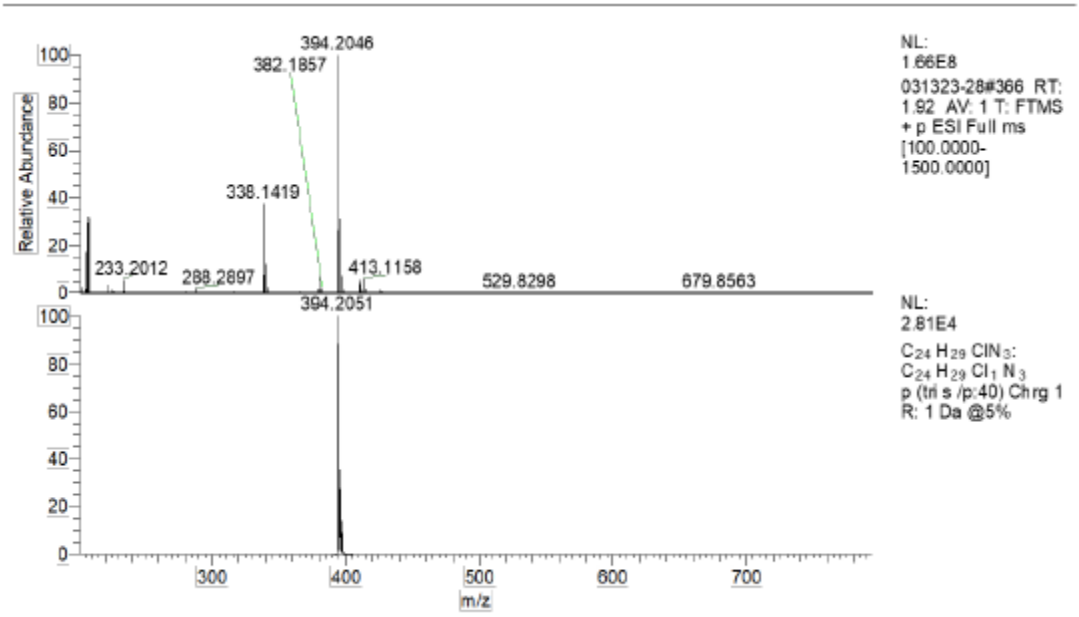

Figure 157: HRMS trace of 44. High Resolution Mass Spectrometry using (ESI): actual m/z M + H (top) over expected m/z M + H (bottom).

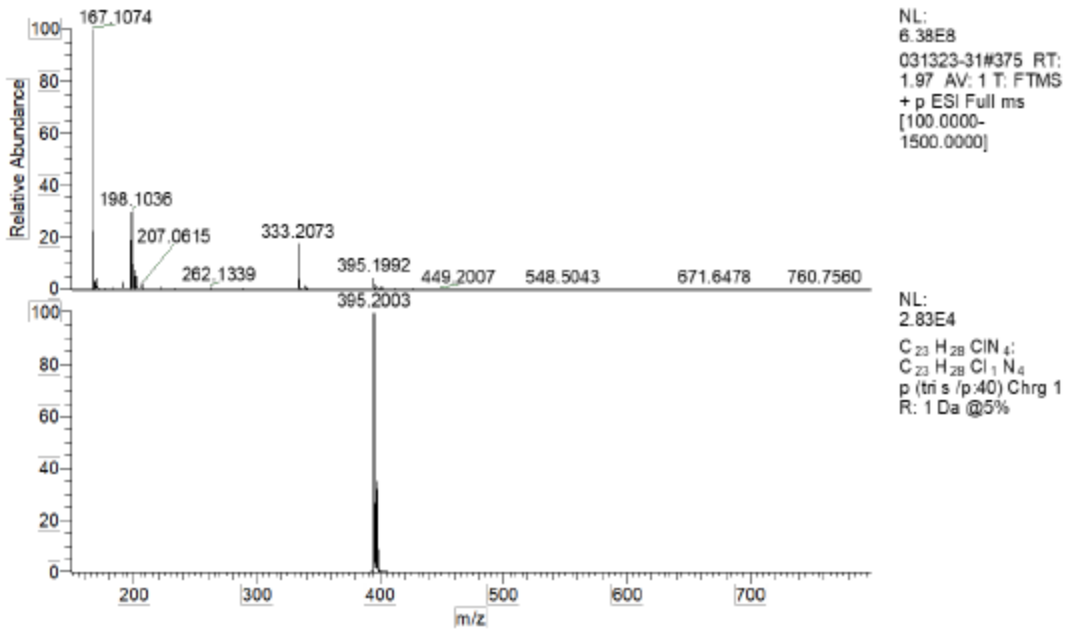

Figure 158: HRMS trace of 45. High Resolution Mass Spectrometry using (ESI): actual m/z M + H (top) over expected m/z M + H (bottom).

F.4. High Resolution Mass Spectrometry of Compounds presented in Chapter 7

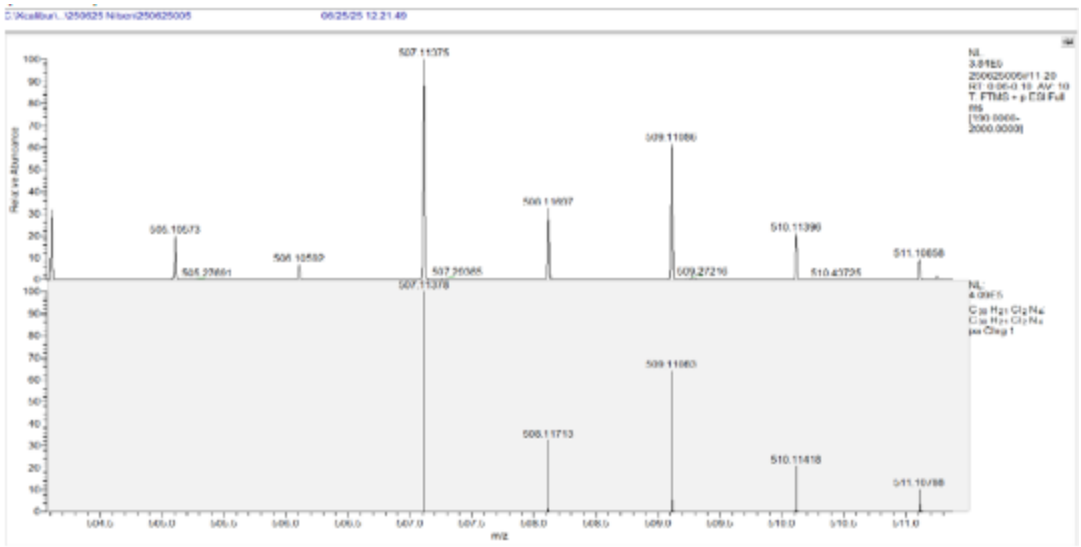

Figure 159: HRAM/MS Chromatogram of 51. High Resolution Accurate Mass/Mass Spectrometry using positive mode ESI: [M+H]+ of [C30H20Cl2N4] = 507.11377 amu (top); observed = 507.11375 amu (bottom).

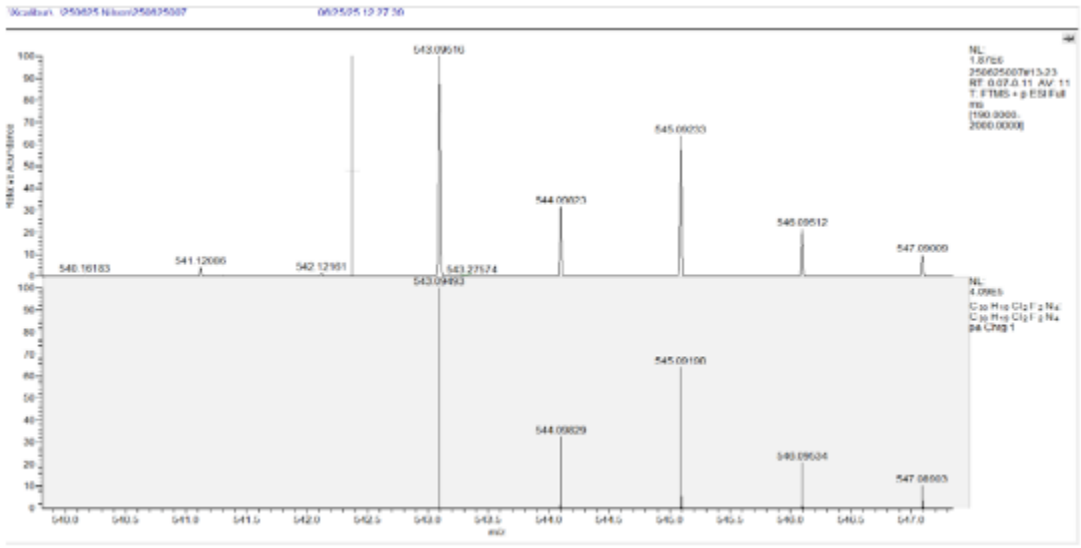

*Figure 160: HRAM/MS Chromatogram of *52**. High Resolution Accurate Mass/Mass Spectrometry using positive mode ESI: [M+H]+ of [C30H18Cl2F2N4] = 543.09493 amu (top); observed = 543.09516 (bottom).*

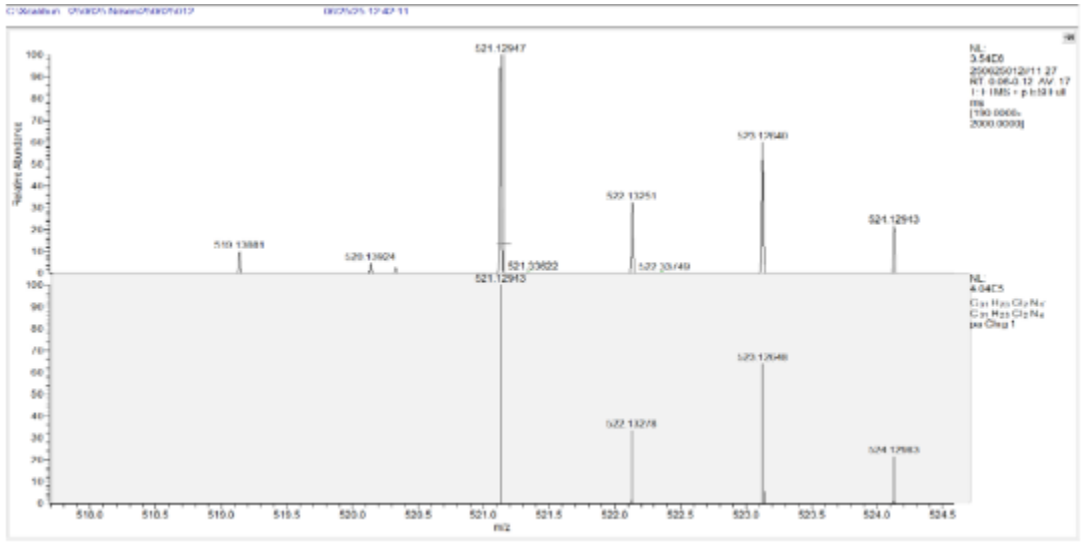

Figure 161: HRAM/MS Chromatogram of 53. High Resolution Accurate Mass/Mass Spectrometry using positive mode ESI: [M+H]+ of [C31H22Cl2N4] = 521.12942 amu (top); observed = 521.12947 (bottom).

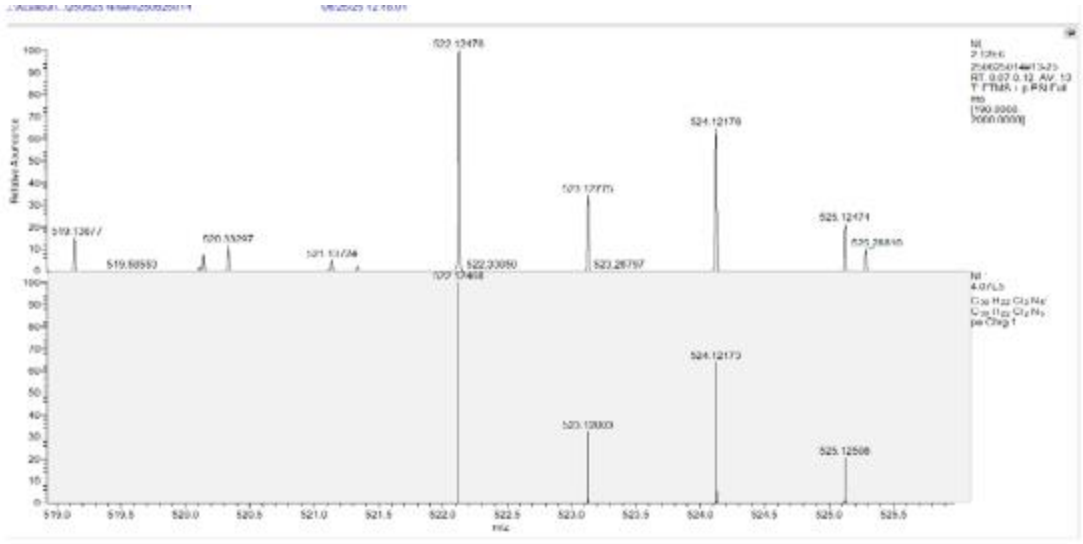

Figure 162: HRAM/MS Chromatogram of 54. High Resolution Accurate Mass/Mass Spectrometry using positive mode ESI: [M+H]+ of [C30H21Cl2N5] = 522.12467 amu (top); observed = 522.12476 (bottom).

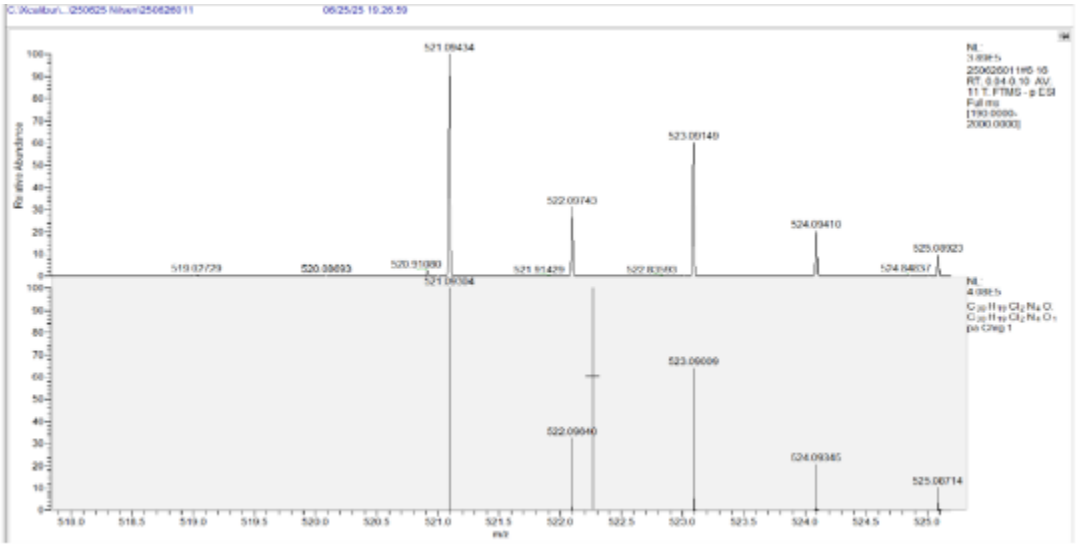

Figure 163: HRAM/MS Chromatogram of 55. High Resolution Accurate Mass/Mass Spectrometry using negative mode ESI: [M-H]- of [C30H20Cl2N4O] = 521.09304 amu (top); observed = 521.09434 amu (bottom).

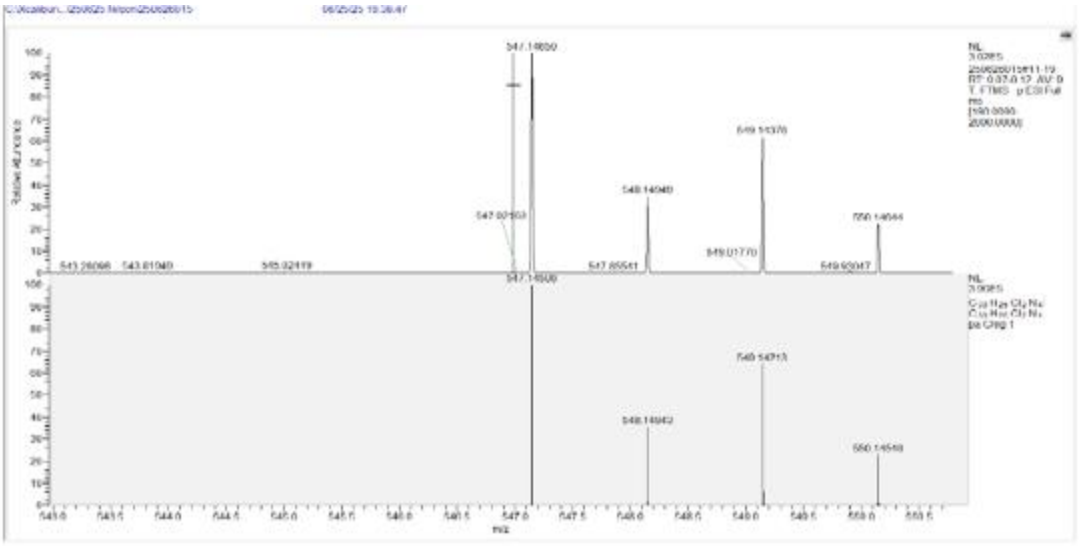

Figure 164: HRAM/MS Chromatogram of 56. High Resolution Accurate Mass/Mass Spectrometry using negaitive mode ESI: [M-H]- of [C33H26Cl2N4] = 547.14507 amu (top); observed = 547.14650 (bottom).

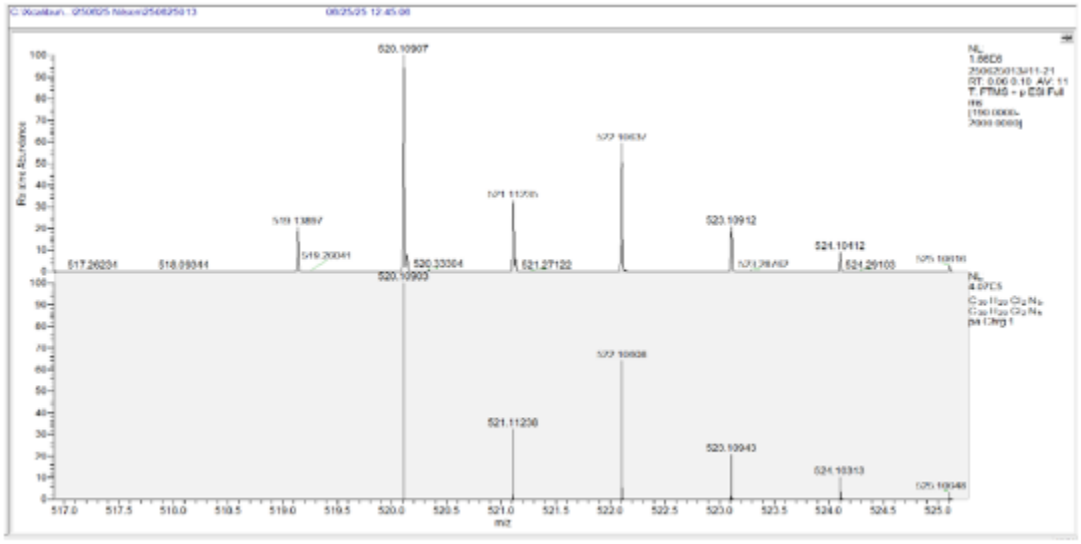

Figure 165: HRAM/MS Chromatogram of 57. High Resolution Accurate Mass/Mass Spectrometry using positive mode ESI: [M+H]+ of [C30H19Cl2N5] = 520.10907 amu (top); observed = 520.10907 amu (bottom).

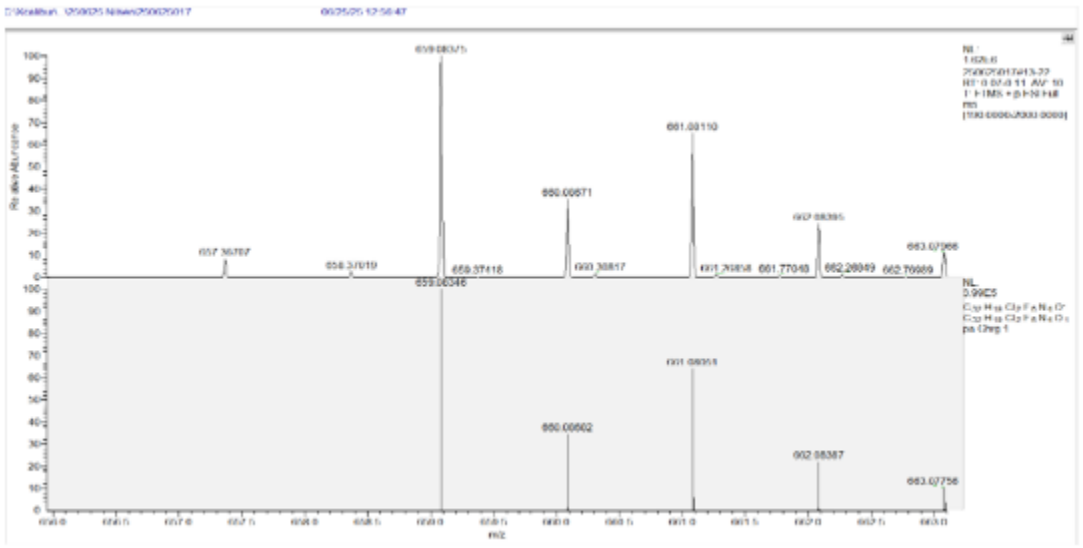

Figure 166: HRAM/MS Chromatogram of 58. High Resolution Accurate Mass/Mass Spectrometry using positive mode ESI: [M+H]+ of [C32H18Cl2F6N4O] = 659.08375 amu (top); observed = 659.08375 amu (bottom).

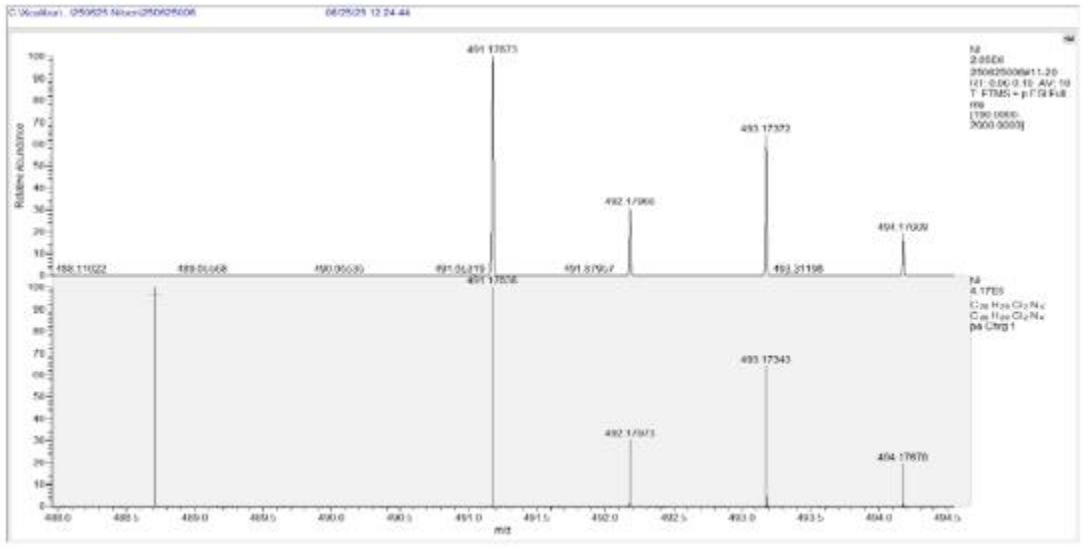

Figure 167: HRAM/MS Chromatogram of 60. High Resolution Accurate Mass/Mass Spectrometry using positive mode ESI: [M+H]+ of [C28H28Cl2N4] = 491.17637 amu (top); observed = 491.17673 amu (bottom).

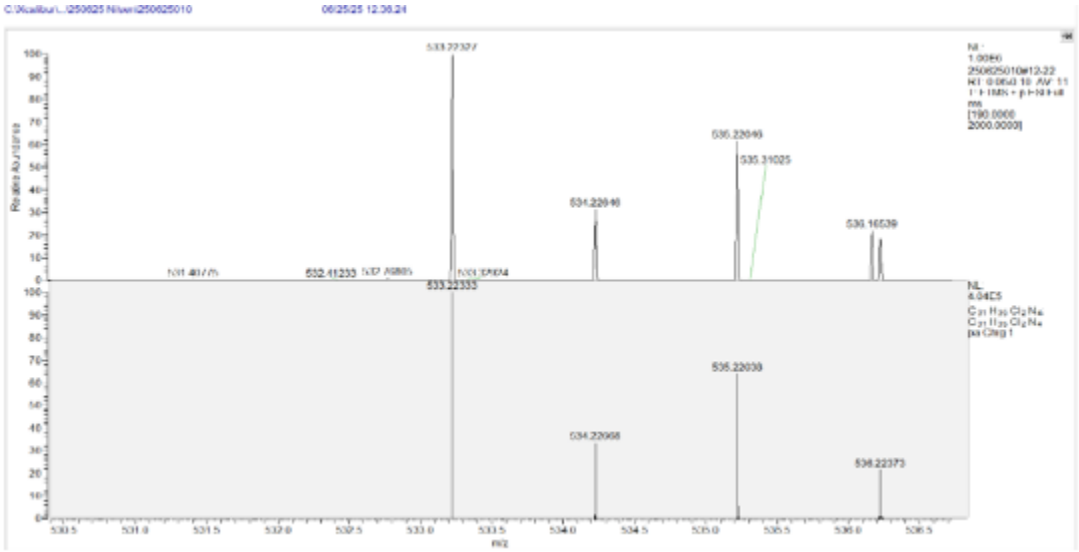

Figure 168: HRAM/MS Chromatogram of 61. High Resolution Accurate Mass/Mass Spectrometry using positive mode ESI: [M+H]+ of [C31H34Cl2N4] = 533.22332 amu (top); observed = 533.22325 amu (bottom).

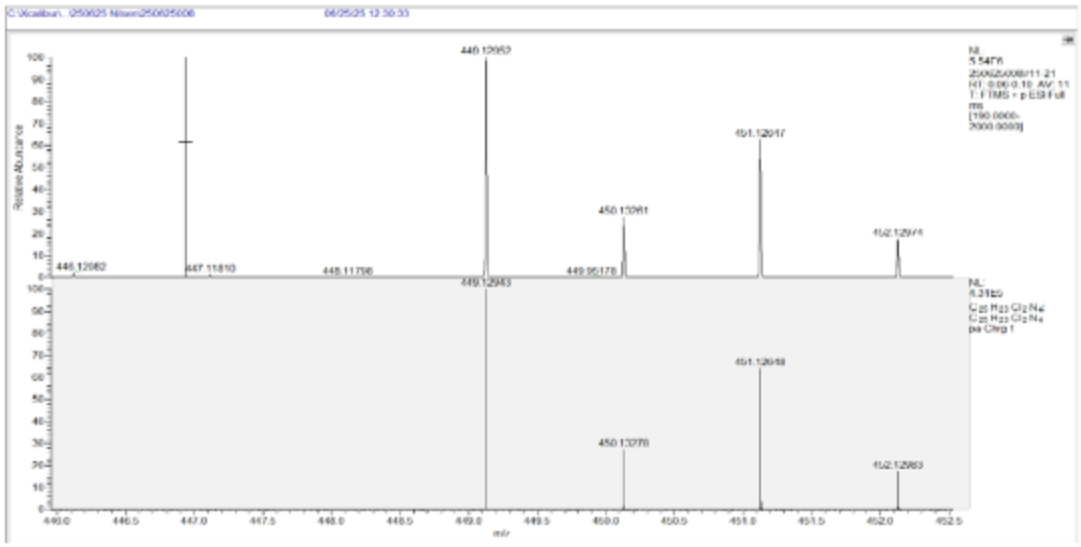

Figure 169: HRAM/MS Chromatogram of 67. High Resolution Accurate Mass/Mass Spectrometry using positive mode ESI: [M+H]+ of [C25H22Cl2N4] = 449.12942 amu (top); observed = 449.12952 amu (bottom).

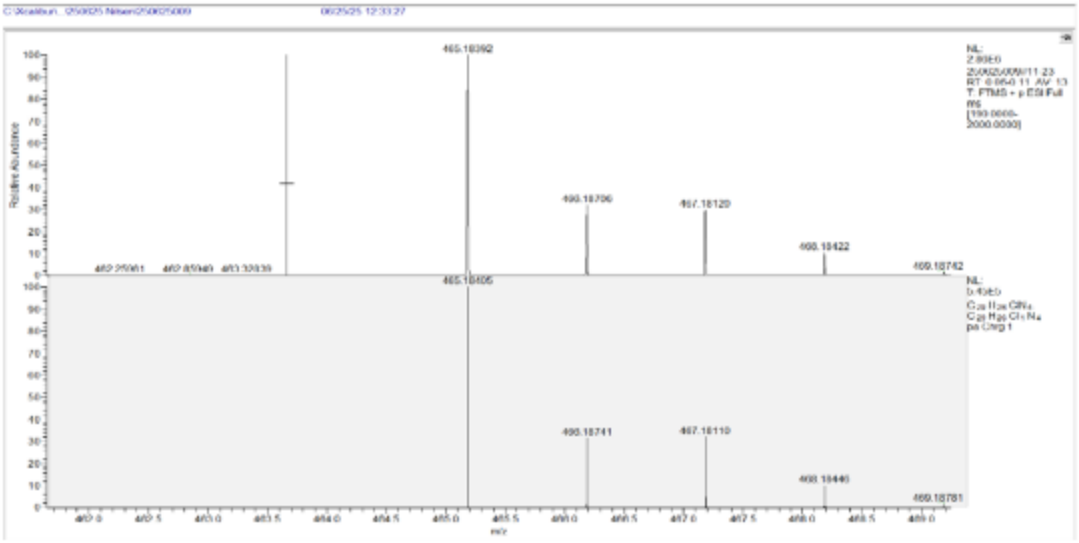

Figure 170: HRAM/MS Chromatogram of 68. High Resolution Accurate Mass/Mass Spectrometry using positive mode ESI: [M+H]+ of [C29H25ClN4] = 465.18405 amu (top); observed = 465.18392 amu (bottom).

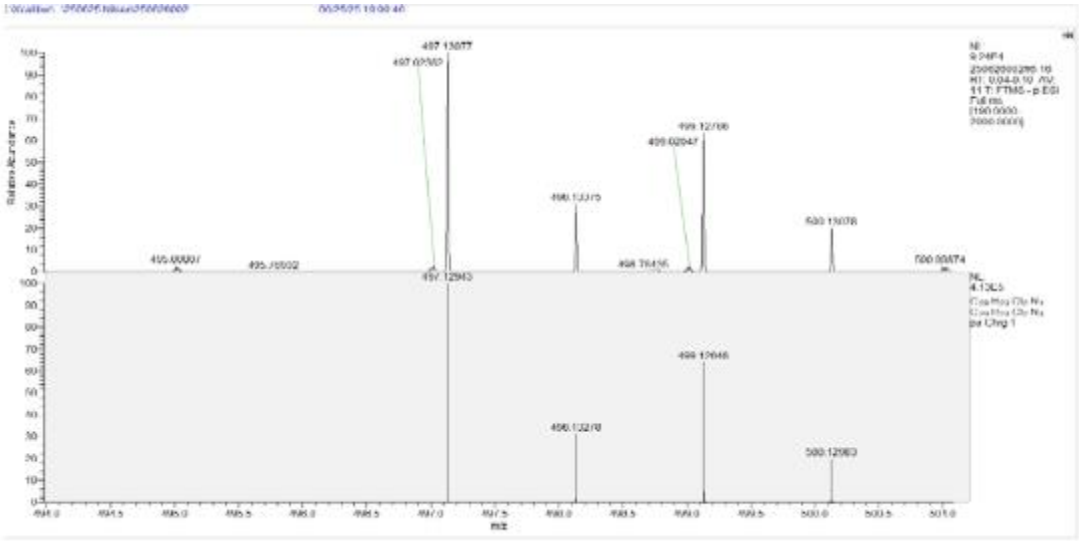

Figure 171: HRAM/MS Chromatogram of 69. High Resolution Accurate Mass/Mass Spectrometry using negative mode ESI: [M-H]- of [C29H24Cl2N4] = 497.12942 amu (top); observed = 497.13077 amu (bottom).

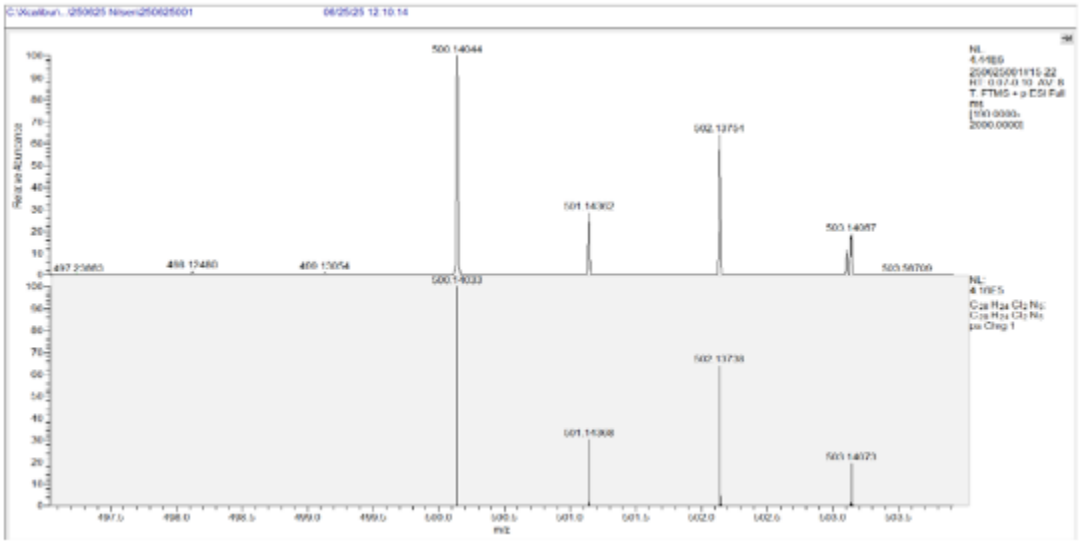

Figure 172: HRAM/MS Chromatogram of 70. High Resolution Accurate Mass/Mass Spectrometry using positive mode ESI: [M+H]+ of [C28H23Cl2N5] = 500.14032 amu (top); observed = 500.14042 amu (bottom).

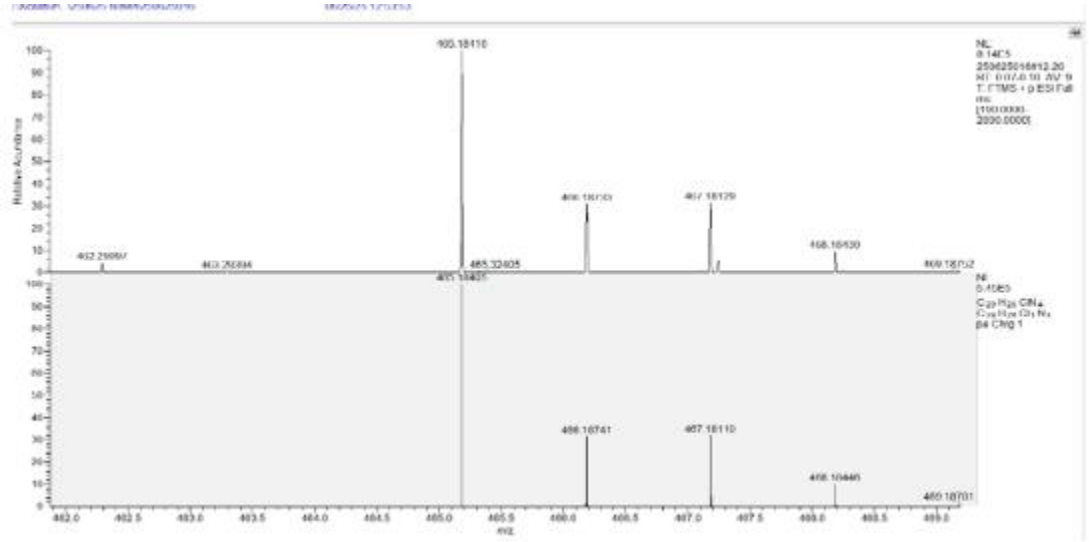

Figure 173: HRAM/MS Chromatogram of 71. High Resolution Accurate Mass/Mass Spectrometry using positive mode ESI: [M+H]+ of [C29H25ClN4] = 465.18405 amu (top); observed = 465.18410 amu (bottom).

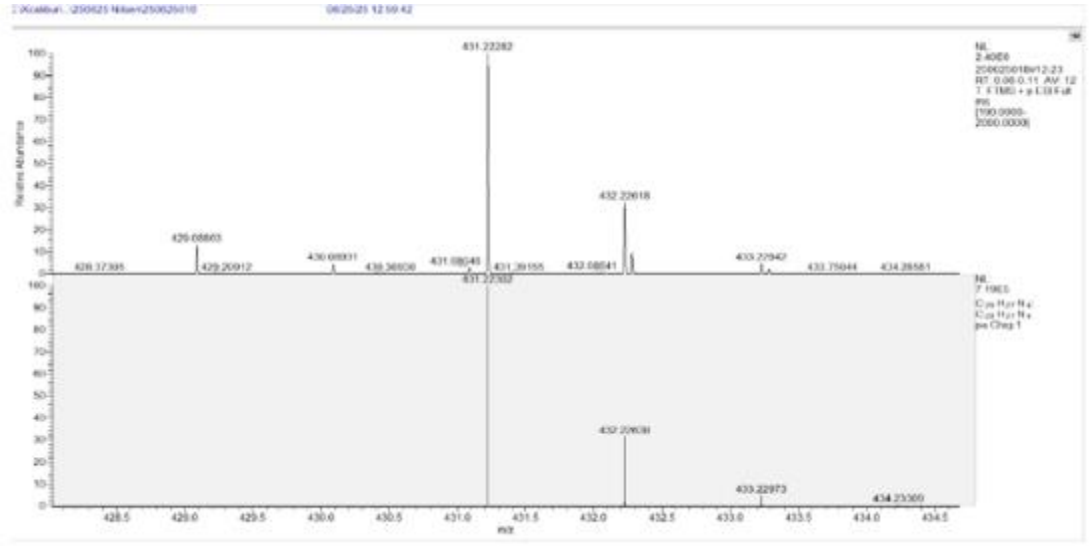

Figure 174: HRAM/MS Chromatogram of 72. High Resolution Accurate Mass/Mass Spectrometry using positive mode ESI: [M+H]+ of [C29H26N4] = 431.22302 amu (top); observed = 431.22282 amu (bottom).

F.5. High Performance Liquid Chromatography of Select Compounds Presented in Chapter 6

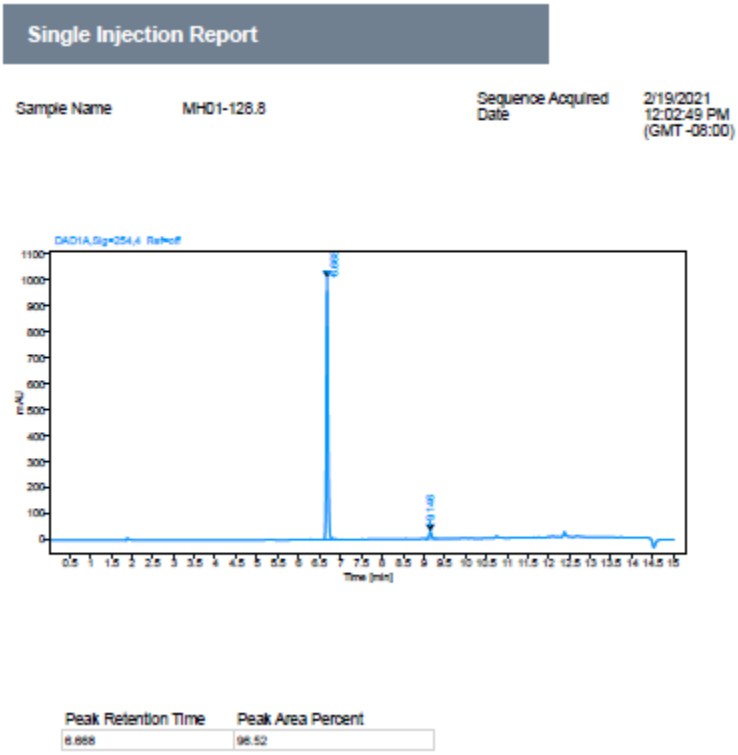

Figure 175: HPLC trace spectra of 17.

Single Injection Report

Sample Name	MH01-175.6_	Sequence Acquired Date	1/7/2022 3:41:12 PM (GMT -08:00)

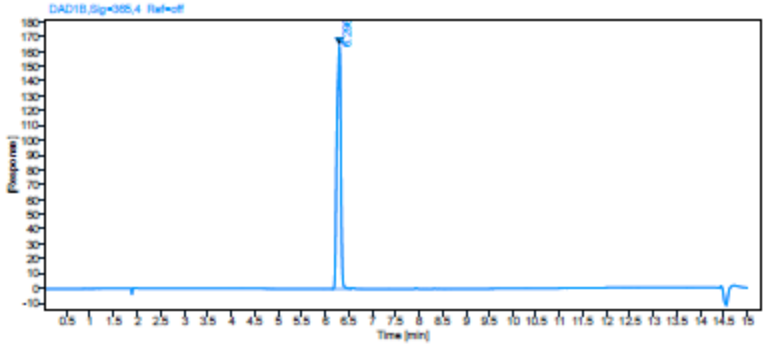

Peak Retention Time	Peak Area Percent
6.296	96.73

Figure 176: HPLC trace spectra of 20.

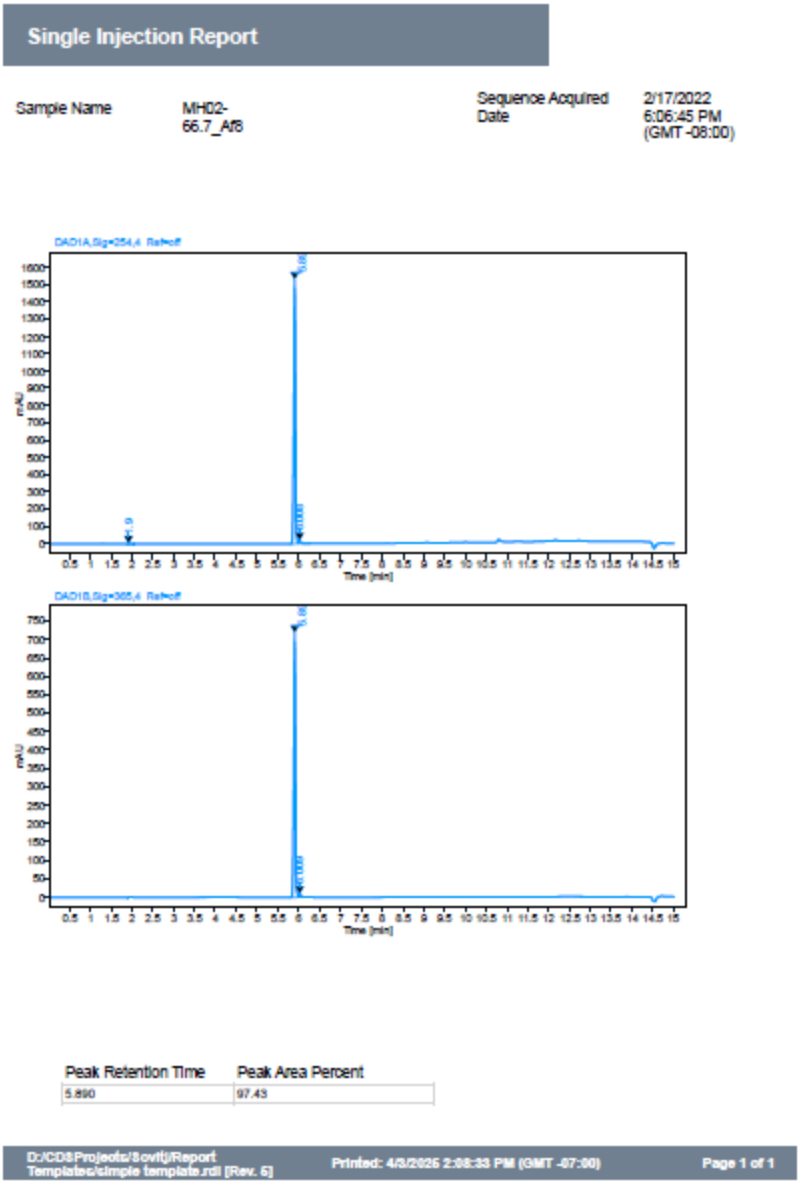

Figure 177: HPLC trace spectra of 31.

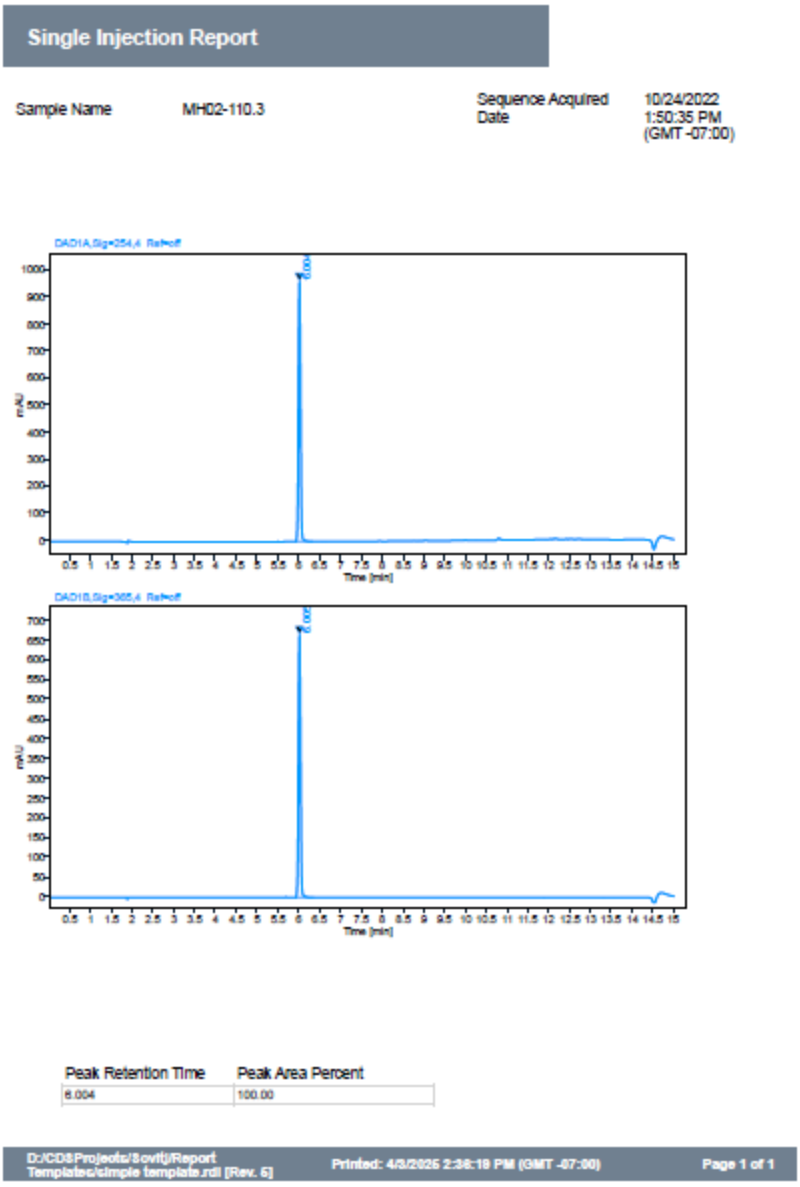

Figure 178: HPLC trace spectra of 35.

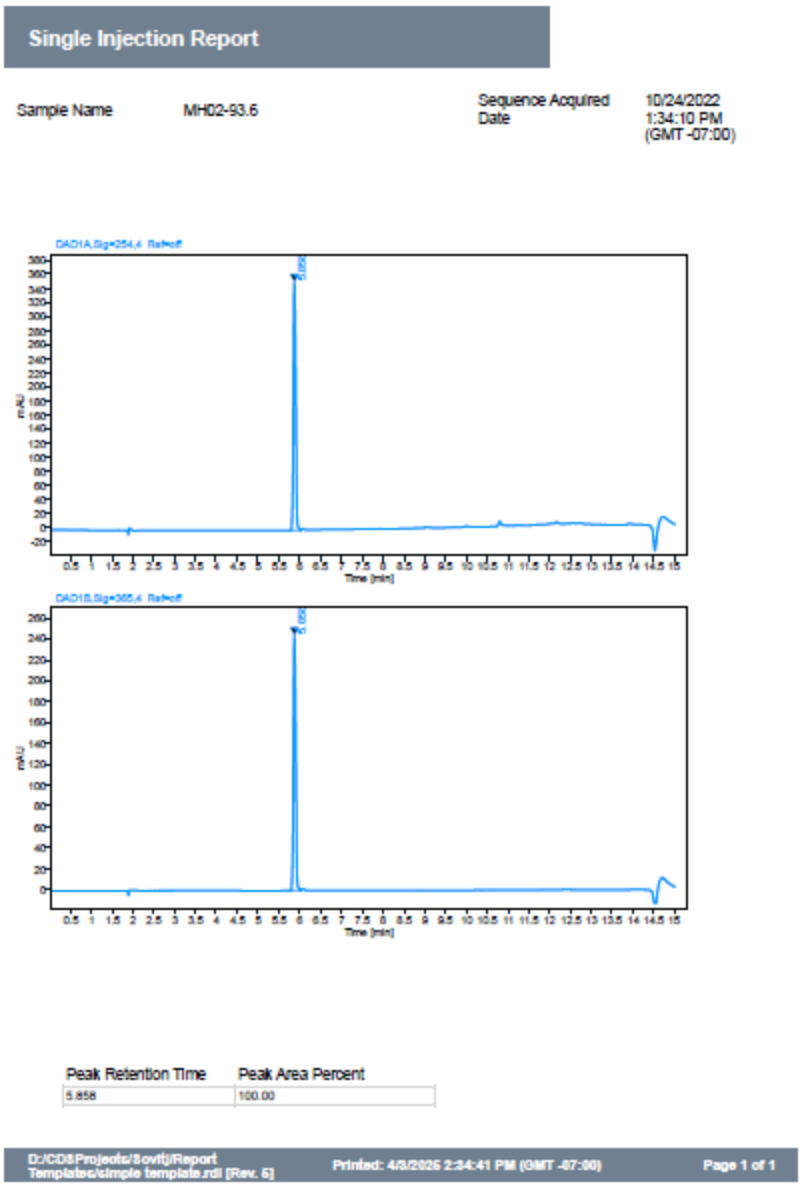

Figure 179: HPLC trace spectra of 40.

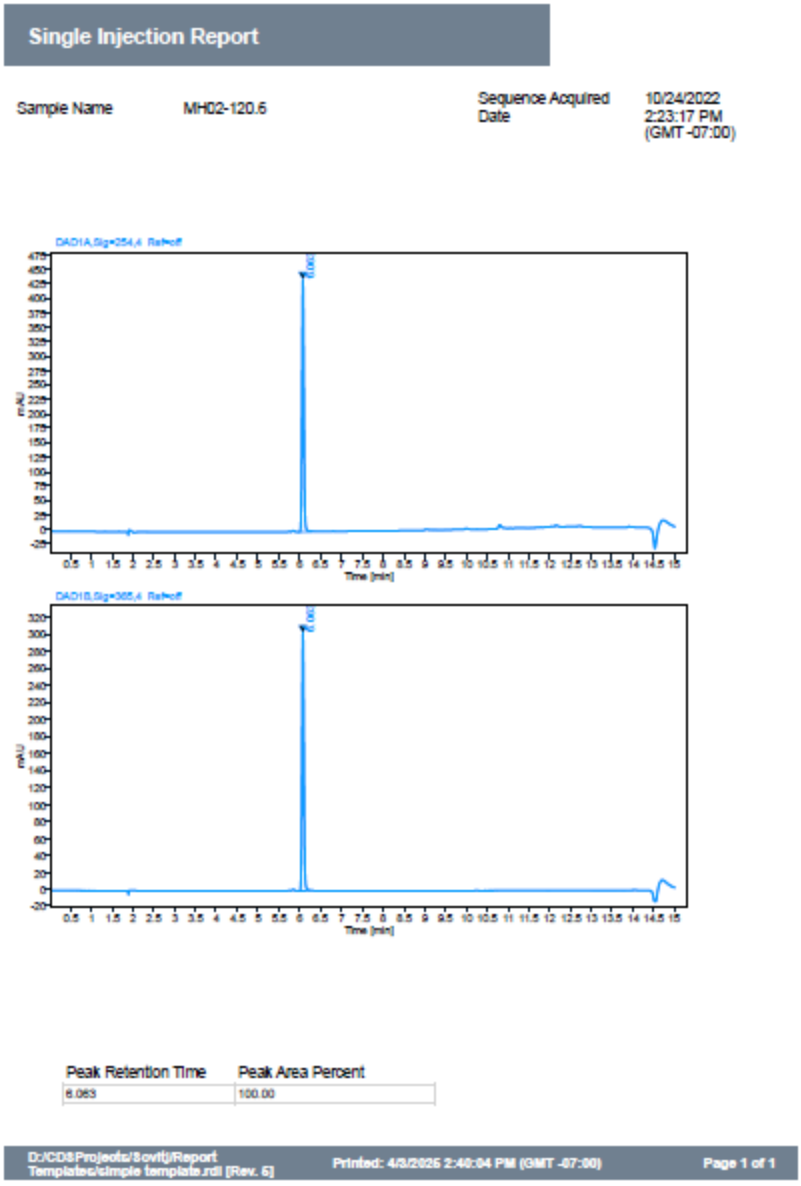

Figure 180: HPLC trace spectra of 41.

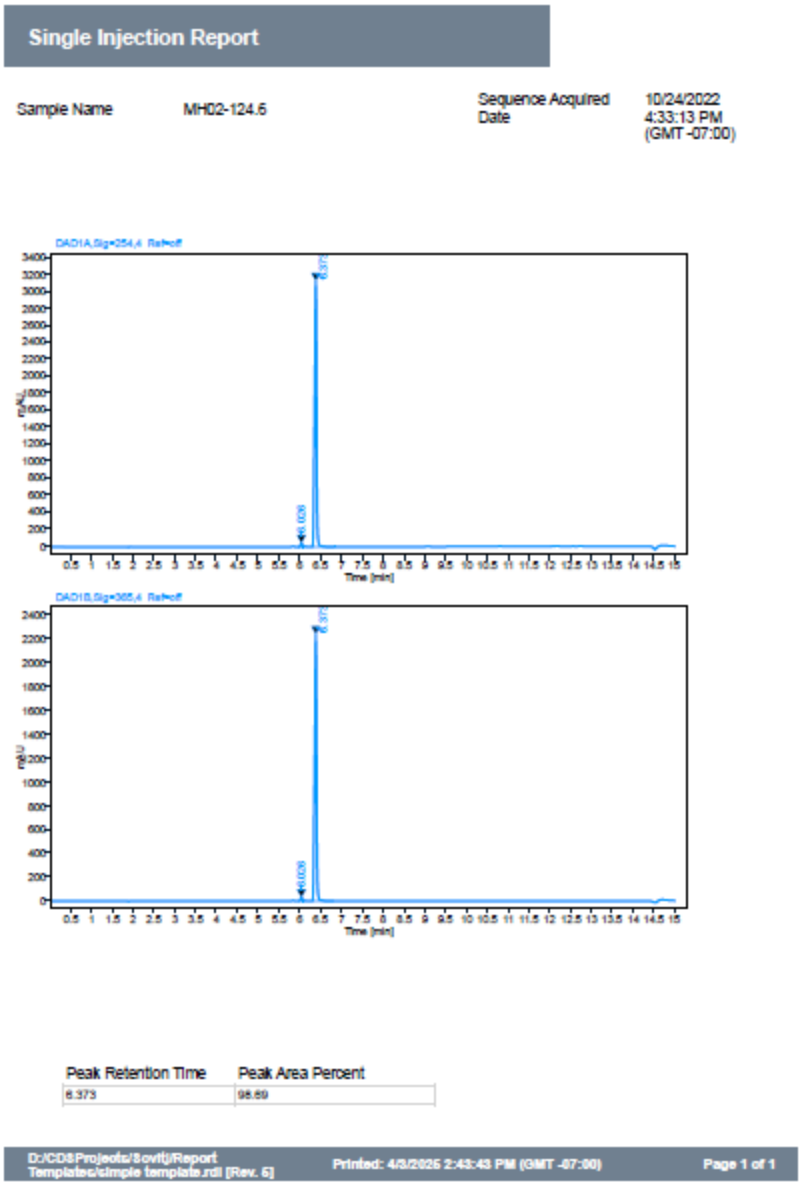

Figure 181: HPLC trace spectra of 42.

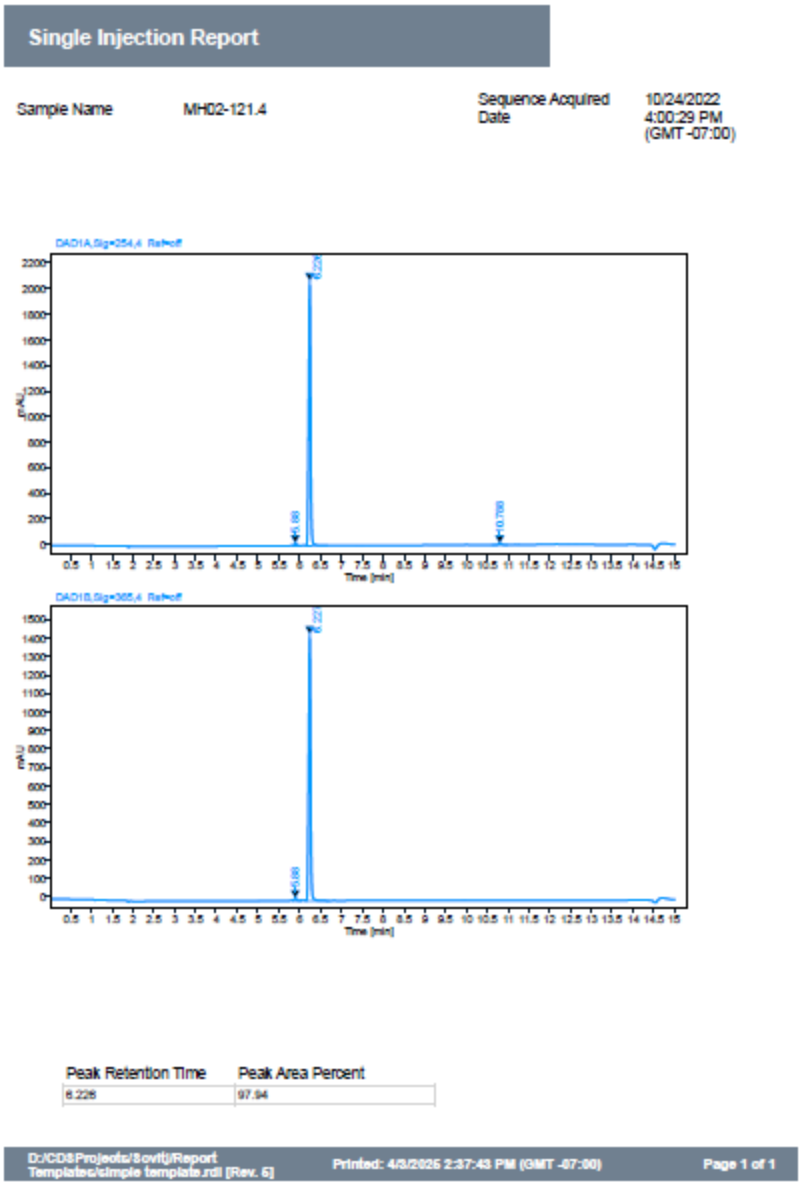

Figure 182: HPLC trace spectra of 43.

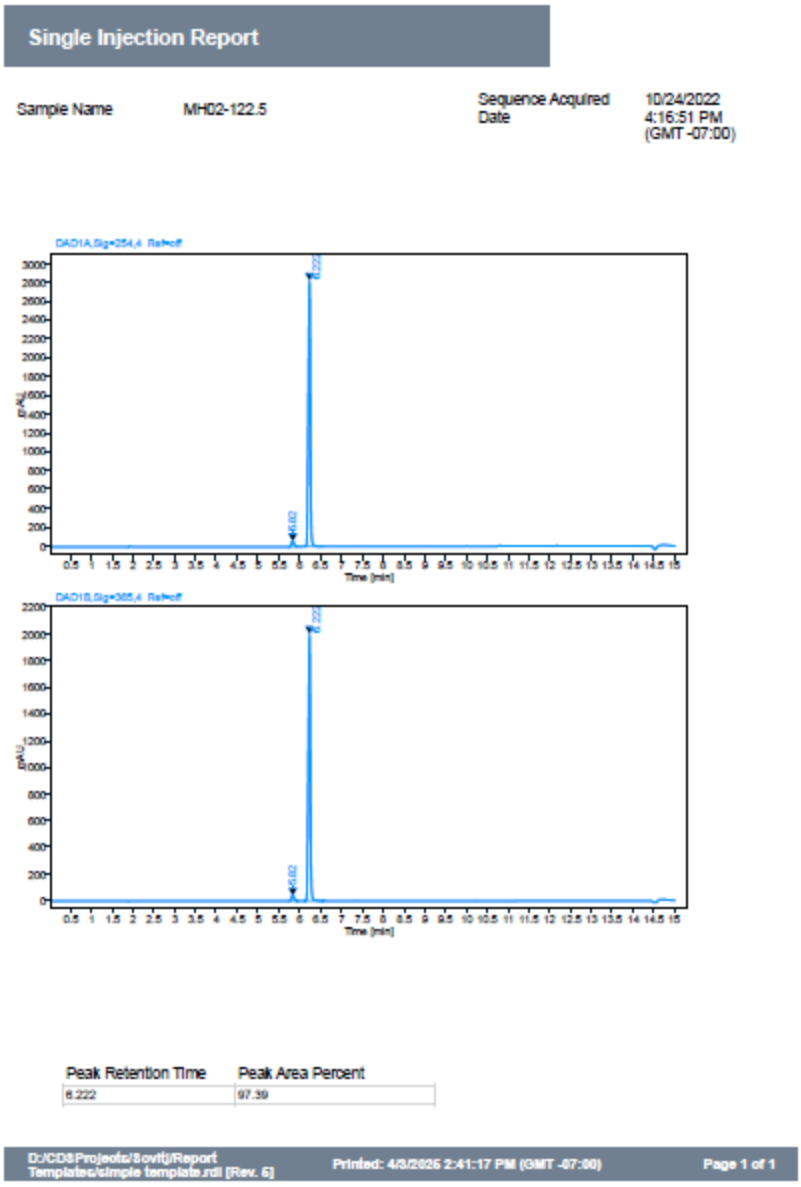

Figure 183: HPLC trace spectra of 44.

Single Injection Report

Sample Name	MH02-140_	Sequence Acquired Date	5/30/2025 2:27:40 PM (GMT -07:00)

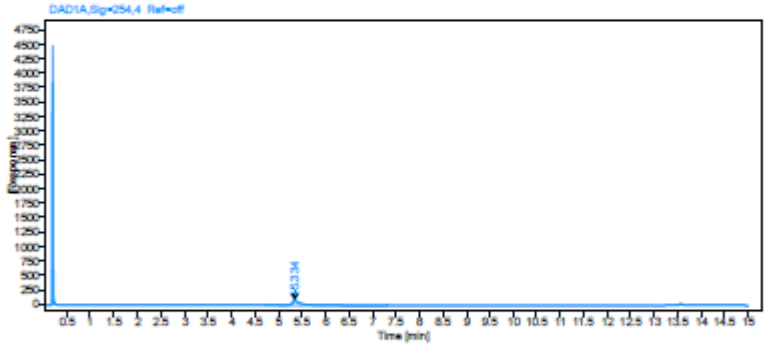

Peak Retention Time	Peak Area Percent
5.334	100.00

Figure 184: HPLC trace spectra of 45.